INDIAN JOURNAL OF PHYSICS
VOL. XXII (1948)

CONTENTS

PART I

Contents

Contents

PART VII

AUTHOR INDEX

SUBJECT INDEX

NOTICE

TO INTENDING AUTHORS

Manuscripts for publication should be sent to Mr. A. N. Banerjee, Assistant Editor, 210, Bowbazar Street, Calcutta.

The manuscript of each paper should contain in the beginning a short abstract of the paper.

All references to published papers should be given in the text by quoting the surname of the authors followed by the year of publication within braces, *e.g.*, Sen (1942). The actual references should be given in a list at the end of the paper according to the following specimen :

Sen, B. K., 1942, Volume rectification of crystals, *Ind. J. Phys.*, 16, 329.

The references should be arranged alphabetically in the list.

All diagrams should be drawn on thick white paper in Indian ink, and letters and numbers in the diagrams should be written in pencil.

Annual Subscription Rs. 12 or £ 1-2-6

USE OF BRIGHT PLATINUM ELECTRODES FOR MEASUREMENT OF ELECTROLYTIC RESISTANCES

By KRISHNADAS CHOUDHURI

ABSTRACT. On account of certain difficulties with platinised electrodes, it is desirable to use bright electrodes in measurements of electrolytic resistances. It has been shown that the Wheatstone's bridge method gives as satisfactory results with bright electrodes

In designing the cell for strong electrolytes, the underlying idea is that the greater the ratio of the area of the electrodes to that of the cross-section of the current-carrying part of the solution, the less pronounced will be the effect of polarisation. For the solution of KCl, the form of the cell is that shown in Fig. 1. The area of each electrode is one sq., cm. whereas the

USE OF BRIGHT PLATINUM ELECTRODES FOR MEA-SUREMENT OF ELECTROLYTIC RESISTANCES

By KRISHNADAS CHOUDHURI

ABSTRACT. On account of certain difficulties with platinised electrodes, it is desirable to use bright electrodes in measurements of electrolytic resistances. It has been shown that the Wheatstone's bridge method gives as satisfactory results with bright electrodes as with platinised electrodes by using a two-electrode cell and

(1) an a. c. galvanometer of the wattmeter or of the dynamometer type through an amplifier,

(2) a low impressed voltage,

(3) a shunted capacitance in the R-arm and by making the ratio arms of equal resistance.

INTRODUCTION

After Kohlrausch introduced the use of alternating currents and electrodes coated with platinum black for the determination of electrolytic resistances, his method is almost invariably used for the purpose. The platinum black coating, although it effectively eliminates the disturbing effect of polarisation, has, however, certain inherent disadvantages, the notable among which are the following :—

(1) it adsorbs the solute molecules and so it is necessary to stir the solution from time to time (in order to keep the strength of the solution between the electrodes constant) and to clean the cell carefully when changing the solution ;

(2) it acts as a catalyst in the oxidation of certain substances, particularly dye-stuffs.

Attempts have, therefore, been made from time to time to avoid the coating altogether. Notable amongst the works in this line is that of Shedlovsky (1930), who recommended the use of multiple electrodes in the same cell. His final recommendation is, however, to platinise the electrodes slightly for the sake of consistency and constancy.

The present paper is an attempt in this direction using two-electrodes only.

DESIGN OF THE CELL

In designing the cell for strong electrolytes, the underlying idea is that the greater the ratio of the area of the electrodes to that of the cross-section of the current-carrying part of the solution, the less pronounced will be the effect of polarisation. For the solution of KCl, the form of the cell is that shown in Fig. 1. The area of each electrode is one sq., cm. whereas the
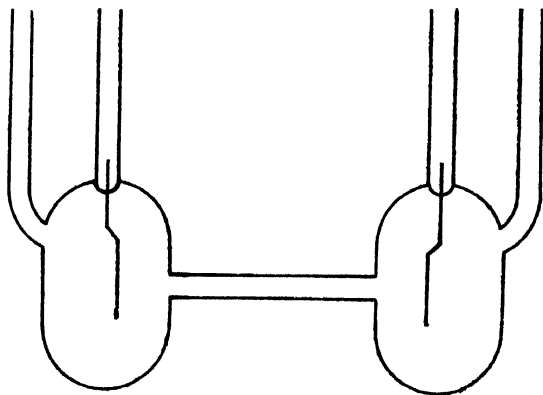
FIG. 1

area of the cross-section of the connecting tube is 0·07 sq. cm. The approximate resistance of normal KCl solution in this cell is 200 ohms. Since in the method employed the resistance of the diagonal arm containing the detecting instrument is practically $\propto$, (*i.e.* $G \sim \propto$), this cell can be used up to a strength as low as N 500 (*i.e.* up to a resistance of about 10' ohms) with the same degree of accuracy.

ARRANGEMENT OF APPARATUS

The arrangement of apparatus is shown in Fig. 2. It is the usual Wheatstone's bridge arrangement in which an amplifier is used in the galvanometer or telephone arm. The detecting instrument is the vertical wattmeter devised by Mukherjee (1930, 1938). This instrument is composed
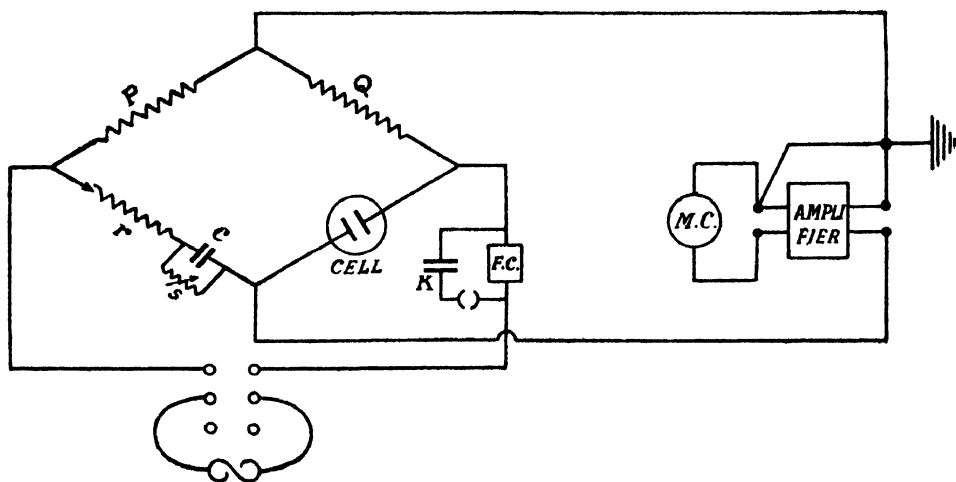
FIG. 2

of two systems of coils of which the fixed system produces the magnetic field and the moving system is deflected by the field. The former is put in

the battery arm of the bridge and the latter in the out-put side of the amplifier. The ratio arms are of equal resistances so that their inductances are also the same. In the third arm, there is, in series with a resistance r, a condenser shunted by a variable resistance s. The effective resistance and reactance of the system composed of the condenser and the shunt are respectively $\dfrac{s}{1+s^2c^2p^2}$ and $-\dfrac{s^2cp}{1+s^2c^2p^2}$, where $p = 2\pi$ times frequency. Therefore, when $V_t = V_b$, the resistance of the Ac-arm, namely,

$$r + \frac{s}{1+s^2c^2p^2} = R \quad \dots \quad \dots \quad \dots$$

is equal to the resistance of the solution and the reactance, $-\dfrac{s^2cp}{1+s^2c^2p^2}$, balances the polarisation reactance of the solution as well as the residual inductive reactance of the Ac-arm.

METHOD OF FINDING THE BALANCE POINT

In detecting instruments of the wattmeter or dynamometer type, the deflection is given by

$$\delta = A I_f \, I_m \cos \psi$$

where I_f, I_m are the r.m.s. currents in the fixed coils and moving coils respectively and ψ, the phase-difference between them. The deflection is, therefore, zero when

(1) I_f or $I_m = 0$,

or   (2) $\cos \psi = 0$ i.e., $\psi = \dfrac{\pi}{2}$.

The balance corresponding to condition (1) is called the true balance. In practice, the null point corresponding to condition (2) is easily obtained. If, however, the phase of the current through the fixed coil with respect to the current through the moving coil is altered by introducing a condenser, K, in parallel with the fixed coil, the null point is disturbed and there is deflection one way or the other according as I_f is in advance of, or behind, I_m.

The procedure for finding true balance, is as follows:—

Keeping $s = 0$, a null point is obtained by adjusting r, when the condenser K is off the circuit. Then the direction and extent of deflection are observed when K is introduced. The shunt is then given an arbitrary value and after obtaining the null-point by adjusting r with K off, the direction and extent of deflection are again observed with K on. Proceeding in this manner a condition is attained when null point will not be disturbed by introducing K. This condition corresponds to the true balance.

EARTHING

In working with alternating currents it is important to select the point which should be earthed. The question of earthing has been very elaborately

the amplifier due to a defect in its make up, that current would only pass through the moving system and not through the fixed system. On the otherhand, to produce a deflection of the moving system, it is necessary that both the fixed and the moving systems must be traversed by currents from the same source.

Another feature was the use of very low voltage between the electrodes.

REFERENCES

Jones, G., 1935. *J. Amer. Chem. Soc* , **57**. 272.
Mukherjee, H., 1930, *Zeit. f. Phys.*, **64**, 286; 1931, *ibid*, **67**, 702.
Mukherjee, H , 1938, *Ind J. Phys.*, **12**, 195.
Shedlovsky, T., 1930, *J Amer. Chem. Soc.*, **52**, 1800,
Warburg E., 1899, *Wied .Ann* , **67**, 493.
Warburg, E , 1901, *Drude Ann. Physik* , **6**, 125.
Wien, M , 1896. *Wied. Ann.*, **58**, 37.
Wien, M., 1902, *Drude Ann. Physik.*, **8**, 372.

ELECTRICAL PROPERTIES OF INDIAN MICA
III. THE EFFECT OF PRE-HEATING

By P. C. MAHANTI* and S. S. MANDAL

ABSTRACT   The power-factor of Bengal ruby and Madras green muscovite micas of different qualities has been measured after their heat treatment at different temperatures for different periods It is found that their power-factor attains a minimum value after their heat treatment for half-an-hour at 200°C.

INTRODUCTION

The effect of temperature on the electrical properties of micas, presumably of different geographical origins, has been studied by several workers, notably, by the British scientists. Dannatt and Goodall (1931) investigated the effect of temperature on the power-factor and permittivity of ruby, green and amber micas over a range covering the working conditions met with in electrical engineering practice. They made measurements at several temperatures up to a maximum of 130°C. The power-factor of each kind of mica was found to increase with temperature, while the variation of permittivity was too small to be of any account. Hartshorn and Rushton (1939) also studied the effect of temperature over the range of 25°C to 90°C on the power-factor and permittivity of typical samples of clear ruby mica, subjected to the action of an alternating voltage at frequencies of 50 to 4000 cycles per second. They observed that under low voltage gradients (less than about 2 kV/mm.), the power-factor increased considerably with rise of temperature while the temperature co-efficient of the permittivity was very small, in fact, of the same order as the co-efficient of linear expansion of the electrodes of the experimental condensers. Hackett and Thomas (1941) made a thorough investigation of the effect of temperature on the electric strength of ruby and amber micas. Using specimens of 0.1 mm thickness, the apparent electric strength (electric strength in air) was found to be substantially constant up to 500°C for dark amber mica and up to 300°C for clear green, clear ruby, stained ruby, light brown ruby and silver amber micas. Above these temperatures the apparent electric strength fell rapidly until 700°C was attained and tended to a constant value up to 900°C. They also studied the effect of pre-heating on the electric strength of muscovite mica in air and observed no significant change in its value. It was, however, noticed that when a sample of muscovite mica was subjected to one hour's pre-heating at 150°C, there was a marked increase in its electric strength

* Fellow of the Indian Physical Society.

when tested in nitrobenzene at 20°C, where its premature breakdown is known to occur. This increase was greatest for light brown (96%) and least for the stained ruby (19%), with the result that pre-heating caused the apparent electric strength to be of the same order for all the muscovites. In view of the possible practical application of this effect, it was thought of interest to study it in detail. It may be noted here that the effect of pre-heating on other electrical properties of muscovite mica has received no attention as yet. The object of the present investigation was, therefore, to study the effect of pre-heating on the power-factor of different kinds of muscovite mica available in India, so that after suitable heat-treatment they might be efficiently employed in electrical industries where a low power-factor is very essential. Data were obtained to show the effect of the period of pre-heating at a particular temperature as well as of the effect of pre-heating temperatures on their power-factor.

<center>E X P E R I M E N T A L</center>

For the purpose of our investigation, the two varieties of muscovite mica, namely, the Bengal ruby and the Madras green, available in abundance in in the mica mines of Bihar and Madras respectively, were chosen. Each variety consisted of typical samples of the following qualities, *viz.*, (*i*) Clear, (*ii*) Stained   and   (*iii*) Stained and slightly spotted. For each quality of mica several test pieces, approximately 2 cm. by 1 cm. and of thickness varying from 2 to 3 mils were carefully cut or split from blocks kindly supplied by the Geological Survey of India. They were then examined carefully under a microscope and only those possessing uniformity in texture, colour and transparency without any pit or loose layer were chosen for test. The selected pieces were then devided into several lots, each lot containing not less than ten such pieces. At each pre-heating temperature, two or more such lots were used, one to study the effect of the period of pre-heating at that temperature and the other to study the effect of pre-heating temperatures in the range 100°C to 900°C on the power factor of a definite quality of ruby and green micas under investigation. For the latter purpose a pre-heating period of half-an-hour at each temperature was chosen.

An electrically heated muffle-furnace was used to pre-heat the test pieces to a desired temperature by adjusting its heating current to a suitable value with the help of an external rheostat. The temperature of the furnace was recorded by means of a calibrated platinum platinum-rhodium thermocouple. It was only when the temperature was found to be steady at a desired value that the mica test pieces were introduced into the furnace and kept there for a desired period. At the end of this period the test pieces were removed to a desiccator containing anhydrous calcium chloride and fitted with a thermometer and were allowed to cool down to the room temperature. With

each test piece, a test condenser was prepared after the method described in previous papers (Datta, Sen Gupta and Mahanti, 1943 ; Mahanti, Mukherjee and Roy, 1945). All such test condensers were then stored in another similar desiccator until measurements were made on them.

Measurements of power-factor and capacity of the test condensers were made by the method of substitution using the same standard condenser and the same Schering bridge as previously described (*loc. cit*). It has been shown that the true power-factor, ϕ_T, of a test condenser is obtained from the relation

$$\phi_T = (C_s/C_T) \phi'_T,$$

where ϕ'_T = the effective diluted power-factor of the test condeser, C_s = capacity of the bridge standard condenser in the third arm of the bridge before the substitution of test condenser, C_T = capacity of test condenser. The accuracy of measurements was checked from time to time by measuring the power-factor and permittivity of a standard sample of polyvsterene.

Curve	1	Pre-heating temp		100°C
,,	2	,,	,,	200°C
,,	3	,,	,,	300°C
,,	4	,,	,,	400°C
,,	5	,,	,,	500°C
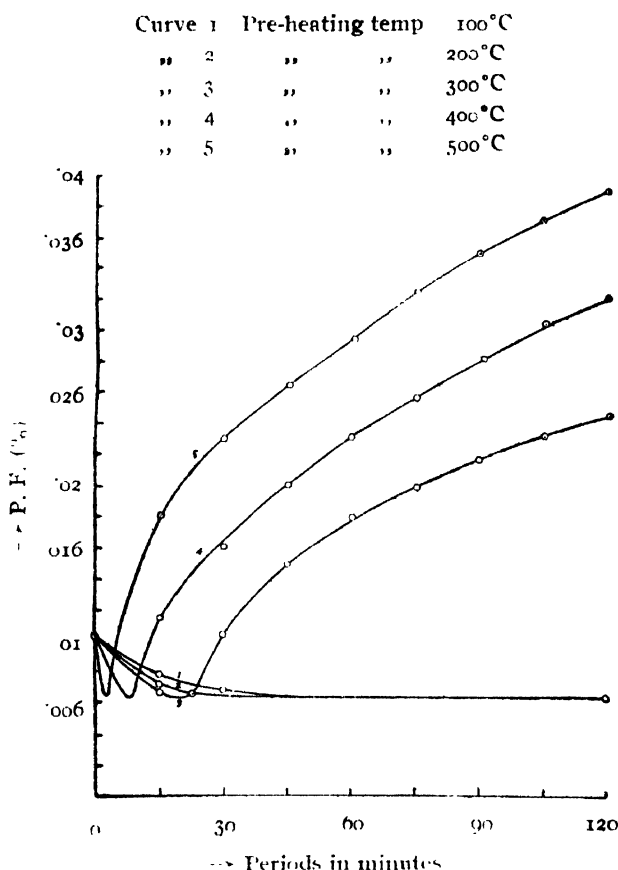
FIG. 1

Effect of Pre-heating Period on the Power-factor of mica
Bengal Ruby Red (Clear)
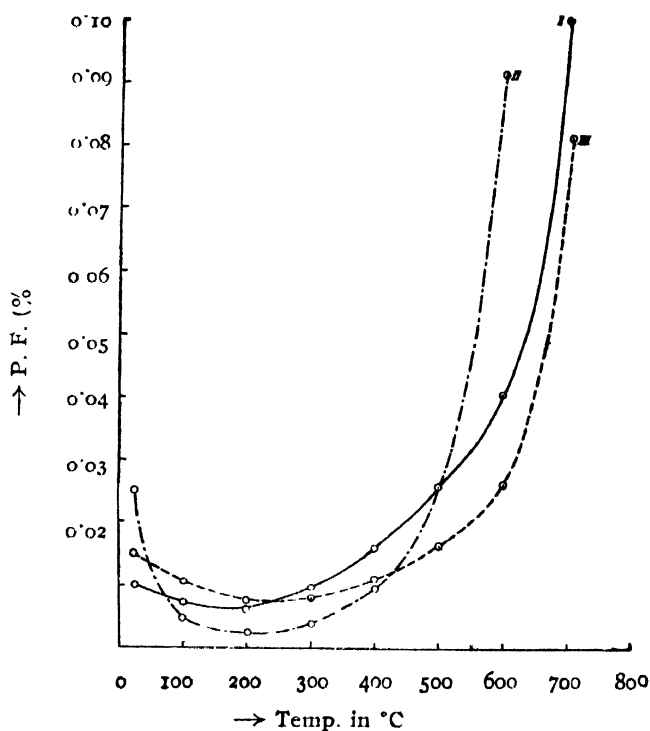
FIG. 2

Bengal Ruby Mica
I—Clear
II—Stained
III—Stained and spotted.

Typical data showing the effect of the period of pre-heating at a number of temperatures on the power-factor of Bengal ruby mica of the clear quality are given in Table I, and represented graphically in Fig. 1. In Tables II and III are included respectively the data of power-factor at various pre-heating temperatures for each quality of the Bengal ruby and Madras green mica and in Figs. 2 and 3, they are shown graphically. Value of power-factor recorded in each table is the average value of several measurements made on several test condensers at each pre-heating temperature.

It may be noted here that a visual inspection of the test pieces after their heat-treatment at different temperatures revealed no change in their colour, condition of surface, texture and transparency up to 500°C for Bengal ruby and up to 400°C for Madras green micas. Beyond these temperatures they were found, however, to lose gradually their transparency and develop silver-white patches on their surface. Finally these patches extended over the whole surface and changed in colour to light straw yellow. Their texture got loose, so much so, that even very fine laminations could be separated very easily out of them. Above 700°C, the test pieces began to swell and at 900°C, they were so delicate that even with a soft touch, they could be easily turned to dust. It was not possible to measure the power-

I—Clear II—Stained III—Stained and slightly spotted
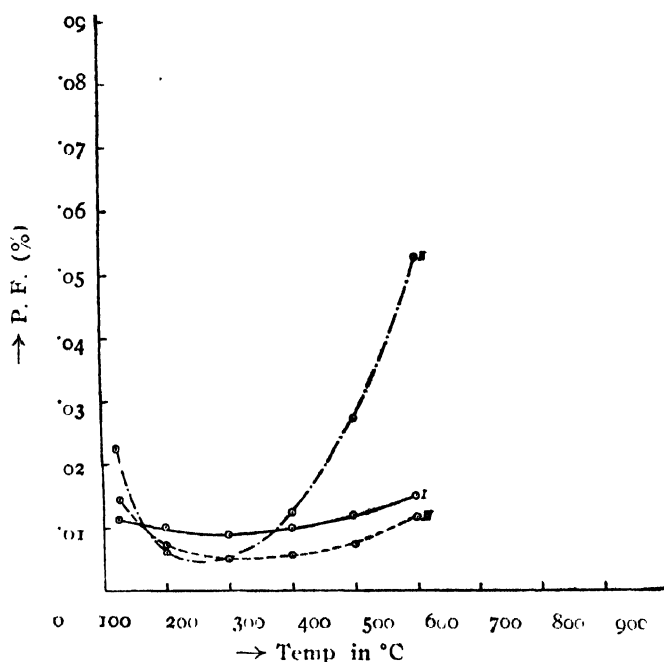
Fı . 3

Madras Green Mica

factor of any quality of Madras green mica above 500°C and of Bengal ruby mica above 700°C. The stained quality of the latter variety showed too high a power-factor even at 600°C and at 700°C, no measurement could be made.

TABLE I

Bengal Ruby Mica (Clear)

Thickness 2 mils

Average power-factor before pre-heating 0.0104%.

Pre-heating period in minutes	Average power-factor (%)				
	100°C	200°C	300°C	400°C	500°C
1 0	0 0102	0.0102	0.0102	0.0098	0 0094
2 5	0.0098	0 0096	0 0095	0.0085	0.0062
5.0	0 0094	0 0090	0 0088	0.0073	0.0098
7.5	0.0090	0 0086	0 0082	0 0062	0 0130
10 0	0.0085	0.0080	0.0074	0 0080	0 0152
15.0	0.0078	0.0072	0.0066	0.0114	0.0180
30.0	0 0068	0 0062	0.0104	0.0160	0.0230
45 0	0 0062	0 0062	0.0148	0 0200	0.0264
60.0	0 0062	0 0062	0.0178	0 0230	0.0294
75.0	0 0062	0.0062	0.0198	0.0256	0 0324
90.0	0.0062	0.0062	0 0216	0 0280	0.0348
105.0	0.0062	0.0062	0.0230	0.0302	0.0370
120 0	0 0062	0.0062	0.0244	0.0320	0.0388

TABLE II

Bengal Ruby Mica

Period of pre-heating 30 mins.

Pre-heating Temperature (°C)	Average power-factor (%)		
	Clear	Stained	Stained and slightly spotted
Room Temp.	0 0104	0.0252	0 0152
100	0.0 68	0.0050	0 0105
200	0 0062	0 0038	0.0075
300	0 0101	0.0047	0 0089
400	0.0158	0.0099	0.0118
500	0 0255	0.0255	0 0162
600	0.0408	0.0919	0 0261
700	0.1036		0.0816

TABLE III

Madras Green Mica

Period of pre-heating 30 mins.

Pre-heating Temperature (°C)	Average power-factor (%)		
	Clear	Stained	Stained and slightly spotted
Room Temp	0 0116	0 0225	0.0145
100	0.0101	0.0061	0.0075
200	0 0083	0 0051	0.0050
300	0.0107	0.0125	0 0055
400	0.0120	0 0275	0.0075
500	0.0150	0 0530	0 0120

CONCLUSIONS

An inspection of the data in Table I or of the curves in Fig. 1 reveals the following interesting features :

(i) Irrespective of temperatures up to 500°C the power-factor of muscovite mica at first decreases from its value before heat-treatment with increasing period of pre-heating.

(ii) Between 100°C and 200°C, the power-factor first decreases and then attains a constant value after about half-an-hour heat-treatment at 200°C The lower the temperature of pre-heating, the larger is the period of heat-treatment after which the power-factor attains a constant value. At 200°C after about half-an-hour's heat-treatment the power-factor becomes constant.

(*iii*) Above 200°C and up to 500°C, and beyond which the muscovite mica becomes unsuitable for use after heat-treatment, the power factor although decreases at first, tends to increase with increasing period of pre-heating. The higher the temperature of heat-treatment, the smaller is the period during which the power-factor decreases.

From Tables II and III or from Figs. 2 and 3, it is evident that when the pre-heating temperature is increased, the power-factor of either variety of muscovite mica decreases from the value before heat-treatment to a minimum at about 200°C irrespective of the quality of mica and then increases rather rapidly to a very high value. From the present data, one is therefore led to conclude that to improve the power-factor of muscovite micas for their use in the manufacture of radio condensers, they should undergo a heat-treatment preferably at 200°C for a period not exceeding half-an-hour.

The above behaviour of mica is probably due to the presence of moisture which is completely driven off at 200°C. It is well known that micas usually include a small percentage of interlaminar water and water of crystallisation which can be expelled at and above the boiling point of water. This is distinct from the water of constitution which is only driven off from muscovite above 500°C. Hartschorn and Rushton (*loc. cit.*) are of opinion that the increase of power-factor with rise of temperature especially at low frequencies is due to the effects of dielectric absorption caused by the presence of moisture.

DIELECTRIC RESEARCH LABORATORY,
DEPARTMENT OF APPLIED PHYSICS,
UNIVERSITY COLLEGE OF SCIENCE & TECHNOLOGY,
CALCUTTA.

REFERENCES

Dannat, C., and Goodall, S. E. (1931), *J. I. E. E.*, **69**, 490.

Datta, S., Sen Gupta, J., and Mahanti, P C. (1943), *Ind. J. Phys*, **17**, 79.

Hackett, W , and Thomas, A. M. (1941), *J. I. E. E.*, **88**, 295.

Hartshorn, L , and Rushton, E. (1939), E. R. A. Report, Ref. L/Too.

Mahanti, P. C., Mukherjee, M. K., and Roy, P. B. (1945), *Ind. J. Phys.*, **19**, 88.

MELT VISCOSITY : PART III. PLASTICIZED SHELLAC

By SADHAN BASU

ABSTRACT   The presence of plasticizers in general brings about a lowering of activation
e nergy for viscous flow.

Plasticizers which are miscible with shellac increase the viscous volume while those
which are incompatible or immiscible lower it.

INTRODUCTION

In the two previous communications (Basu, 1947) it has been shown that
shellac and its constituent resins are greatly aggregated in the melted condi-
tion, and the contribution of the polar groups towards this aggregate formation
has been clearly brought out.   In the present paper an attempt has been
made to find out the effect of plasticizers on shellac in relation to its internal
structure as revealed by the previous measurements, and thus to get an
improved understanding of their action.

EXPERIMENTAL

To incorporate a plasticizer into shellac, it was found sufficient to hot
roll it with shellac for five minutes at 90°C ; the resulting mass was then
cooled, powdered and dried.   The melt viscosity measurements were done
with the same apparatus as described in the previous communication
(Basu, 1947a).

The temperature regulation was done by means of a Cenco bi-metallic
thermoregulator, which kept the temperature accurate within $\pm 0.5°C$ in
the range $50° - 125°C$.

RESULTS

The results of viscosity measurements on shellac in presence of various
plasticizers (10% of the weight of shellac) are summarised in Tables I and II
and the corresponding graphs given in Figs. 1 and 2.

The values of E_0' and $\lambda\lambda_2\lambda_3$ as calculated from the above data and
Figs. 1 and 2 are given in Table III.

DISCUSSION

A consideration of the values of E_0' as given in Table III shows that
the presence of plasticizers brings about a lowering of the energy of activa-
tion.   This can be easily understood, since the presence of plasticizers,
usually substances having high dielectric constants, lowers the intermiceller
forces, which appear to be of electrical origin.

TABLE I

$f - 5.495 \times 10^{-3}$ dynes/cm²

Plasticizer	$1/T \times 10^3$	Viscosity η (in poise)	$\log \eta$
Diamyl phthalate	2 84	8,809.10	3.9449
	2.72	3,411 45	3 5329
	2.64	1,511.05	3.1793
	2.56	868.05	2.9385
Tributyl phosphate	2.84	8,005.35	3.9034
	2.72	3,954 45	3 5970
	2.62	1,929.00	3.2853
	2.56	1,125 25	3 0512
Castor oil	2.82	20,929 65	4.3207
	2.72	10,609 50	4 0257
	2.62	4,147.35	3 6177
	2 52	1,864.70	3.2706
Sextone "B"	2.72	1,993.30	3 2995
	2.62	1,189 55	3.0788
	2 58	868 05	2.9386
	2.52	610.85	2.7859
Santicizer 17	2.84	4,661.75	3.6686
	2.72	1,736.10	3.2395
	2.62	830 75	2.9046
.	2.58	514.40	2.7113

TABLE II

Temp.	Plasticizer	f (dynes/cm²) $\times 10^3$	η (poise)	$\log \eta/f$
348°K	Diamyl phthalate	12.4875	4,372 40	−0.4559
		19.4805	2,443.40	−0.9017
		22.4775	1,768.25	−1.1042
356°K	Tributyl phosphate	11.4885	3,022 10	−0.5949
		20.9790	1,543 20	−1.1334
		25.4745	1,157.40	−1.3424
369°K	Castor oil	5 4950	4,661 75	−0.0633
		11.4885	1,186.20	−0.9863
		17 4795	1,125.25	−1.5731
353°K	Sextone 'B'	12.4875	4,211.65	−0.4722
		20.9790	2,118.35	−0.9959
		24.9750	1,736.10	−1.1581
352°K	Santicizer 17	5.4950	2,121.90	−0.4133
		12.4875	1,575 35	−0.8993
		20.4795	964.50	−1.3270

TABLE III

—	E_0' (K—cal)	$\lambda\lambda_2\lambda_3$ (in c.c.) $\times 10^{18}$
Diamyl phthalate	16.20	14.30
Tributyl phosphate	20.78	12.04
Sextone 'B'	10.35	13.78
Santicizer 17	16.89	15.43
Castor oil	25.90	3.51

The values of $\lambda\lambda_2\lambda_3$, however, present some interesting features. Thus for the first four compounds the values are much higher than the value for unplasticized shellac (Basu, 1947a) but in the case of castor oil it is comparatively low. To explain these we must first try to get a clear idea of the interaction between a polymer and its plasticizer. The recent idea of swelling and dispersion of polymers by liquids can give us some clue to that.

| 4.32.07 |
| 4 05.23 |
| 3.78.41 |
| 3 515.7 |
| 3 201.7 |
| 2.979.5 |
| 2 979.5 |

$\lambda log \rightarrow$

2.46   2.56   2.   2 76   2.85

$\rightarrow \frac{1}{T} \times 10^-$

⊙ —Diamyl Phthalate   △—Tributyl Phosphate
⊙′ Castor Oil   □—Sextone B
□′— Santicizer 17

FIG. I

(○)—Diamyl Phthalate   △—Tributyl Phosphate
(◐)'—Castor Oil   ☐'—Sextone B
☐'—Santicizer 17
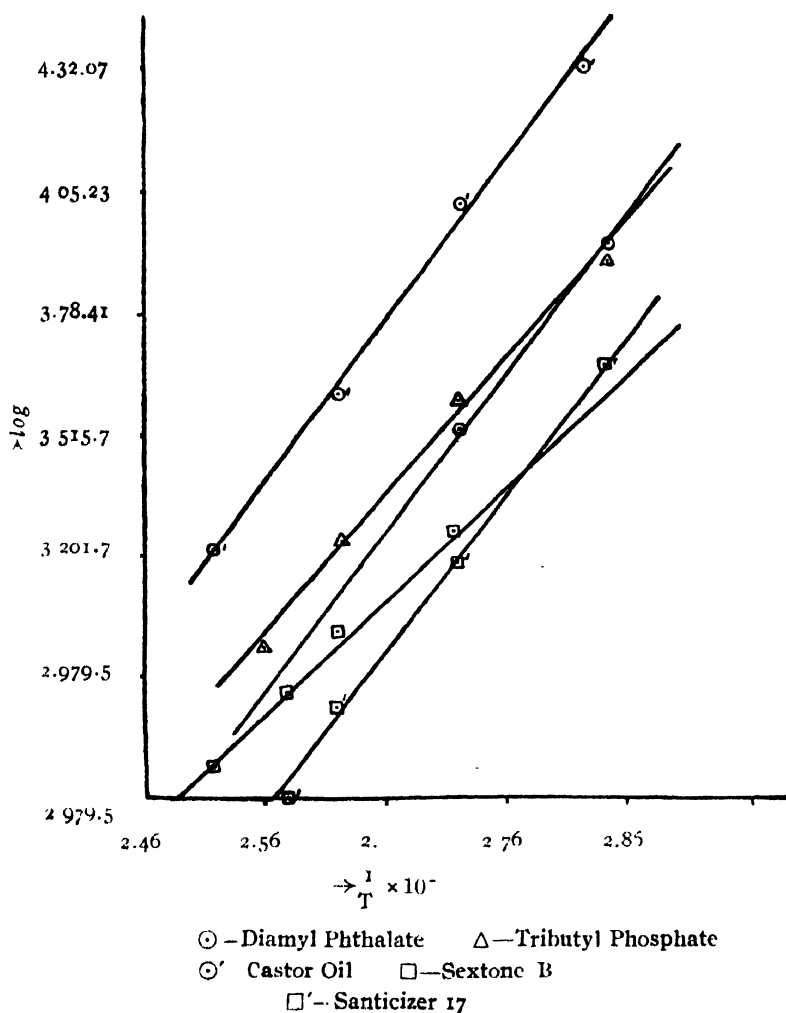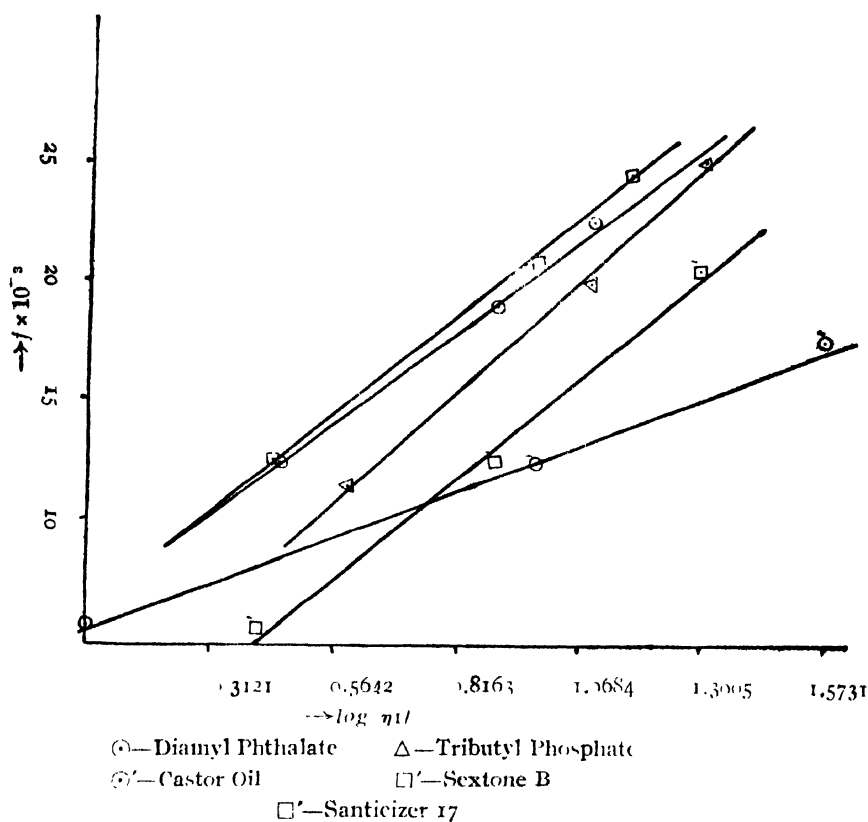
Fig. 2

The extents of interaction of shellac with plasticizers, as related to the dispersing capacity of the former, are summarised in Table IV.

TABLE IV

Plasticizer	Cold	Hot (75°C)
Tributyl phosphate	Swelling	Miscible (complete)
Diamyl phthalate	Swelling	Miscible (partial)
Sextone 'B'	Swelling	Miscible (complete)
Santicizer 17	Swelling	Miscible (partial) ; Sets to gel on cooling
Castor oil (anhydrous)	No action	No action

Mostly secondary types of forces are at play in the mixing processes involving a plasticizer and shellac. Since shellac is miscible (at least partly) with the first four plasticizers, it is to be expected that these should penetrate inside the shellac micelle, lowering the aggregation. Further the immobilisation of the plasticizer molecules inside the micelle causes the structure to become extended and mobile. The distance separating the polar groups is

thus increased and with that the distance jumped during the flow-process, which would account for the increased viscous volume.

The low viscous volume in presence of castor oil may be understood thus : castor oil is not miscible or compatible with shellac, it will therefore be non-homogeneously distributed with a relatively high concentration in the region between the clusters. The micelle will thus become dense and more compact. The distance separating the polar groups will be consequently reduced and, as a result the viscous volume also.

It may be added that by plasticizers we do not always mean solvent plasticizers. Non-solvents can be used in many cases as plasticizers for improving some physical properties, *e.g.*, water absorption, heat resistance, etc., of the plastic material. In the present case we are more interested in the flow properties of the plastic materials and it has been found that they are better affected by solvent plasticizers than non-solvent plasticizers. It is quite possible that non-solvent plasticizers may increase water absorption, elastic property, etc., but with that we are not interested at present.

REFERENCES

Basu, S , 1947*a*, *Ind. Jour. Phys.*
,,   ,,   1947*b*, *ibid.*, **21**, 83.

MEASUREMENTS ON THE EAST-WEST ASYMMETRY OF COSMIC-RAYS AT LAHORE, INDIA (22°N)

By OM PARKASH SHARMA and H. R. SARNA

ABSTRACT. A triple-coincidence counter telescope has been employed for the present study of east-west asymmetry at Lahore '22' N). Each Geiger-Müller tube (construction and filling details given fully) consists of a 0.194 mm diameter nickel wire anode and an oxidized cylindrical copper cathode (25 mm. thick) 2 5 cm in diameter and 35 cms. in length, sealed in a pyrex glass tube The counters are filled with ethyl alcohol (1.5 cm) and argon (9 5 cm) mixture to a total pressure of 11 cm of mercury. The telescope is mounted on a light wooden frame capable of rotation about horizontal as well as vertical axes, the angles being read accurate to ⅛th of a degree by pointers moving on graduated circular scales.

The asymmetry measurements have been made for a number of zenith angles The maximum of asymmetry occurs at 30° with respect to the zenith The results have been compared with those of other observers and it is suggested that the small apparent divergences might be due to differences in the angular cones subtended by the telescopes used by different observers

INTRODUCTION

The theory of motion of the electrically charged particles in the magnetic field of the earth has been developed by Störmer (1931) and by Lemaitre and Vallarta (1933). From this theory an asymmetric distribution of the cosmic ray intensity with respect to the magnetic meridian is to be expected if the radiations reaching a particular place, latitude and altitude specified, contained an electrically charged component of one sign in excess of the other.

Rossi (1930) was the first to point out that such an asymmetry should exist and that there would be greater intensity from the west if more of the particles were positively charged. However, his earlier experiments failed to show a difference between east and west intensities. The first experimental evidence of this directional asymmetry came with the experiments ◦ f Johnson and Street (1933) on the summit of Mount Washington (λ= 6°N) which was later confirmed by Johnson (1935) himself and others (Ehmert (1934), Gill (1940), Rossi (1934), Seidl (1941)) for different altitudes and latitudes. The unpublished results of Dr. P. S. Gill and Mr. Satya Pal show that the variation in the angular cone of the telescope does alter the value of the asymmetry.

From the most extensive survey of the east-west asymmetry by Johnson (*loc. cit.*), it is found that the asymmetry is maximum near the geomagnetic equator (15%) and decreases towards the higher latitudes, being 2-3% at

$\lambda = 50°$N at sea level. For tropical latitudes comparatively less work on east-west asymmetry seems to have been reported. Bhattacharya (1942) has found the east-west asymmetry at Calcutta $(\lambda = 12°N)$, $h = 80$ ft. and Darjeeling $(\lambda = 16.5°N)$ and $h = 7200$ ft.

In view of the above and as Prof. Vallarta (*loc. cit.*) has stated "The data obtained from such directional experiments, in particular the experimental value of east-west asymmetry at various angles to the vertical and at different azimuths may serve, as another basis in addition to the experimental value of the total intensity at different geomagnetic latitudes, for the energy analysis of the cosmic radiation" the following investigation on east-west asymmetry was carried at Lahore, India (22 N). The intensity measured is the total intensity as no lead absorbers were used.

GEIGER-MULLER COUNTERS

The G. M. counters used were of internally quenched type. The copper cylinder of the counter was made of .25 mm. thick copper sheet and a nickal wire (S. W. G. 36) was used for the axial wire. A pyrex glass envelope was used and tungsten leads were sealed out using $NaNO_2$ to clean the surface of the hot tungsten lead as usual. The copper cylinder was covered with a layer of copper oxide by heating it for about three hours at a temperature of about 350-400°C in an electric furnace after the cylinder had been cleaned successively with strong nitric acid, .1 N nitric acid and distilled water. The counters were first filled with alcohol vapour at a pressure of about 1.5 cm. of Hg, the vapour being obtained from a container cooled by ice and common salt (Collie and Roaf, 1940) and then with pure argon up to a final pressure of 11 cm. A number of counters were then simultaneously filled under similar conditions of pressure (which is very necessary for the counters to be used in coincidence experiments, as small difference in pressure changes the characteristics of the tubes) and after testing by oscillographic method, were carefully sealed. With a leaking resistance of .1 megohm the counters gave a plateau of 200 volts.

THE COSMIC-RAY TELESCOPE

The cosmic-ray telescope employed for the present study of the east-west asymmetry consists of three Geiger-Muller counters mounted in parallel positions on a light wooden frame-work, which is capable of orientation about an horizontal axis ; the actual inclination of the telescope being read accurately to 30 minutes of arc with the help of a sharp pointer moving on a graduated circular scale. The cathodes of the counters tubes are 2.5 cm. in diameter and 35 cm. in length. With a distance of 25 cm. between the extreme counters the triple train subtends an angle of 11.3° (Fig. 1) in the plane in which the telescope can rotate.

The high tension applied to the wires of the counters through a resistance of ·1 megohm, was obtained from a Street Johnson type of voltage regulator as modified by Evans (1934). The counter voltage remained independent of the fluctuations of the a.c. mains and could be controlled and kept constant at any value up to 2000 volts. The output voltage was read on a mircoammeter placed in series with a standard 2-megohm resistance.

The triple coincidences were recorded by a slightly modified form of the circuit recommended by Johnson (1938) (Fig. 2). The counters were used in the usual Rossi parallel connection. Before the final observations were started the circuit was thoroughly tested for discrimination against partial coincidences The counter train was connected as for normal operation but with the high voltage disconnected from one of the three counters. Under these conditions single and double pulses reach the circuit but no triple coincidences. If the discrimination is perfect, no count should be recorded on the recorder. It was found that no count was recorded in tests lasting three to four hours.

An important defect with the circuit of Johnson arises from the fact that the neon lamps employed are quite often light sensitive. The effect has been reported by Yeater (1945) and observed independently by us. It

Fig. 1

was noticed while making preliminary tests of the apparatus that in the course of daily observations the circuit practically used to stop working after 5 P.M., the rate of counting falling enormously. The counters were suspected to be photo-sensitive, but every precaution to shield them against light did not improve the matter. Suspecting the fault with the neon lamp, we directed a strong beam of light from a carbon arc on to the neon lamp whereby the number of counts increased by a factor of ten. On covering the neon lamp with a thick black paper no counts were recorded. To avoid this uncertainty in observations arising due to the neon lamp we had to discard its use and substitute a coupling condenser. Yeater (*loc. cit.*), however, met this difficulty by the direct method of putting extra lamps in the tent which housed the telescope to provide continuous diffused illumination, which in our opinion is a cure than prevention and we recommend the use of a condenser of correct value for coupling the plates of the amplifier tubes to the output valve. One disadvantage of this would be that the pulses reaching the grid of the output tube will not be equal in amplitude. However, this difficulty does not arise if the counters give pulses of equal amplitude.

Another test was applied to check the accuracy of the mechanical
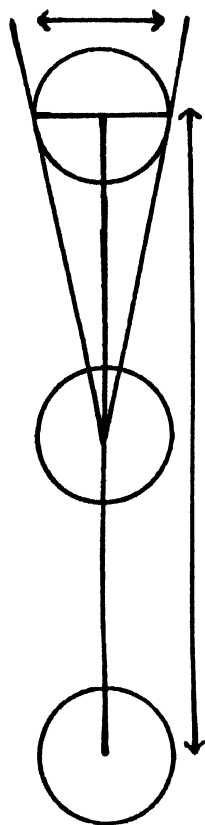
recorder, *i.e.*, to decide whether it missed any counts or not. (This recorder, which is operated by the plate current of the type 6L6 beam power tube, consists of a small electromagnet working the escapement wheel of a time piece). By this test we could also see that the pulses reaching the grid of the output tube were equal in amplitude. The coincidence pulse from the plate circuit of the 57 tube was also applied to the vertical plates of a cathode ray oscillograph through a small condenser of 25 $\mu\mu$F capacity. The triple coincidences, which could be very well differentiated from single or double ones (because they were of much greater amplitude), were visually counted on the oscillograph screen and also recorded on the clock recorder; the two counts were found to be exactly equal.

EXPERIMENTAL PROCEDURE

The counter telescope was set up in a small room in the Physics Laboratory, Government College, Lahore, under a single roof of a few inches of concrete. The axle of the frame work on which the counters are mounted
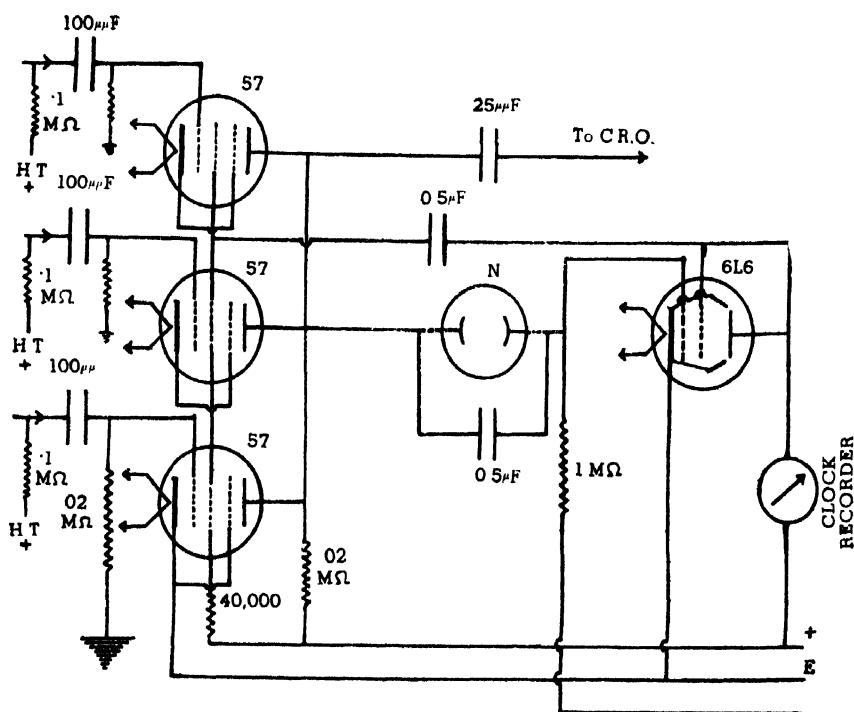
FIG. 2

was oriented magnetic north and south so that rotation would be in the local east-west plane. After testing the working of the circuit as above, the exploration of east-west plane was carried out by the following method. The telescope was oriented at a particular zenith angle to the west for a certain time and the counts recorded. The telescope was then rotated and oriented at the same zenith angle to the east for nearly the same time (30 minutes to an hour) and the counts recorded. This process was repeated a number of times and the total number of counts from east and west obtained. The readings

TABLE 1

Showing the East-West Asymmetry at Lahore 22°N

Zenith angle	Time (T) (minutes)	Total counts (N)	Counts per minute ± p.e	$\alpha = 2\dfrac{(I_w - I_e)}{I_w + I_e}$
12°	W = 471 E = 427	W = 1543 E = 1252	W = 3.276 ± 0.056 E = 2.932 ± 0.056	.1108 ± 0.0252
24°	W = 443 E = 431	W = 1202 E = 992	W = 2.716 ± 0.053 E = 2.304 ± 0.049	.1641 ± .0286
36°	W = 652 E = 593	W = 1610 E = 1237	W = 2.469 ± 0.041 E = 2.086 ± 0.040	.1682 ± 0.0252
36°	W = 633 E = 667	W = 1322 E = 1228	W = 2.088 ± 0.039 E = 1.841 ± 0.035	.1257 ± 0.0265
48°	W = 688 E = 695	W = 1163 E = 1065	W = 1.690 ± 0.033 E = 1.532 ± 0.032	.0981 ± 0.0285
60°	W = 623 E = 641	W = 678 E = 642	W = 1.088 ± .028 E = 1.002 ± .026	.0823 ± .0368

were taken after every interval of 12 and sometimes 6 degrees. (This method eliminates any error arising due to the changes in instrumental selectivity, short period changes or any other changes due to variations in barometric pressure or any magnetic disturbances.)

As Johnson (*loc. cit.*) has shown that the only systematic error which merits discussion is due to accidental counts. In all his readings the horizontal rate was less than 10% of the vertical rate and hence no correction for accidentals was needed. In our case it is less than even 6% and therefore we have not applied any correction.

The probable errors were calculated from the total number of counts, *viz.*,

$p = .67\sqrt{N/T}$ where N is the total number of counts in time T, and the

asymmetry calculated from the formula $\alpha = \dfrac{2(I_w - I_e)}{I_w + I_e}$ where I_w and I_e are

respectively the counting rates from west and east.

RESULTS AND DISCUSSION

The results of the present experiment on the east-west asymmetry at Lahore 22°N are given in Table 1 and graphically shown in Fig. 3. It is

East-West asymmetry curve (lines probable errors)
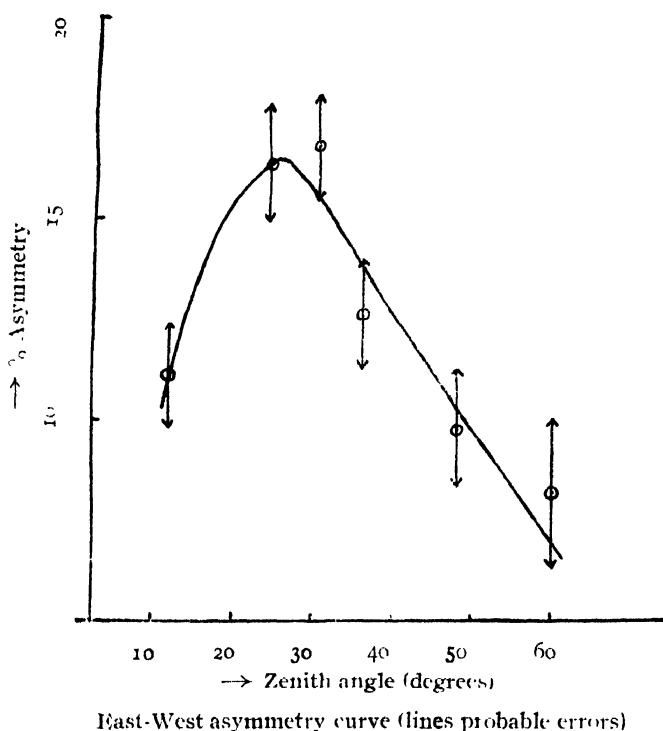
FIG. 3

evident that the asymmetry increases to its maximum value 16.82 at near about 30° and then decreases in conformity with the theoretical view of Swann (1935) and the experimental observations of others. The value of asymmetry (6.03%) at 60° has been measured by Gill (1941) *(loc. cit.)* at Lahore and ours is slightly different ; the difference might be due to the fact that Gill had used 10.2 cms. of lead in his experiments while we have not used any lead and also due to the difference in the angles subtended by our telescope.

According to Swann *(loc. cit.)* east-west effect increases with decrease of latitude at a given altitude. However, if we look at Johnson's results and compare with those of Gill *(loc. cit.)*, Bhattacharya *(loc. cit.)* and ours we find that there are divergences. The experimental values of asymmetry do not seem to follow the above law. These apparent divergences might, as we have already indicated, be due to different angular cones subtended by the telescopes used by different observers. It will be interesting, therefore, regarding the importance of this work for the analysis of the cosmic radiation, to carry on such measurements at different latitudes and altitudes with telescopes subtending equal angular cones.

SIGNIFICANCE OF EAST-WEST ASYMMETRY

According to Johnson (1938), Swann (1940) and Carlson and Schein (1941) the primary particles of cosmic rays can be supposed exclusively to be protons reaching the top of the atmosphere with a certain energy distribution, the lower limit being fixed by the considerations of the earth's magnetic field. During their passage through the atmosphere they generate various type of secondaries. As is generally known the softer secondaries, *i.e.*, electrons and positrons are equally balanced with regard to their sign of charge and so do not produce any asymmetry. The harder secondaries thus remain to produce the asymmetry as Hughes (1940) and Jones (1939) have shown that there is an excess of positive mesons throughout the energy spectrum, the ratio of positive to negative being 1.21 to 1.20. These mesons have sufficient energy to maintain the original direction of protons. However, as the rays are slowed by their passage through the atmosphere their path becomes more and more curved and when they reach the observers they have experienced a slight deflection from their original path or the direction they would have had, with the absence of energy losses. Johnson (1935) showed that no significant part of observed asymmetry can be accounted for by the deflection of the secondaries generated in the atmosphere. Hence there remains some uncertainty regarding the generation and absorption of the mesons.

The importance of the measurements lies, therefore, in the fact, that if taken at different altitude at each latitude, the data might give clues to the processes of creation, absorption and decay of mesons as they pass through the atmosphere.

REFERENCES

Bhattacharya, P. C., 1942, *Proc. Nat. Inst. Sci. India*, **8**, 263.
Carlson and Schein, 1941, *Phys. Rev.*, **59**, 840.
Collie, C. H. and Roaf, D., 1940, *Proc. Phys. Soc.*, **52**, 186.

Evans, R. D., 1934, *Rev. Sci. Inst.*, **5**, 371.

Ehmert , 1934, *Phys. Zeits* , **36**, 20.

Egelhaaf Von H., 1937, *Zeit fur. Phys.*, **108**, 19.

Gill, P. S., 1941, *Proc. Nat. Acad. Sci. India*, Vol. II, Part 2, p. 26.

Gill, P S., 1940, *Phys. Rev.*, **57**, 68.

Hughes, D J , 1940, *Phys. Rev* , **57**, 356.

Johnson, T. H , 1938, *Rev. Sci Inst.*, **9**, 221.

„   „   , 1935, *Phys Rev.*, **43**, 287.

„   „   , and Street, J C , 1933, *Phys Rev.*, **43**, 381.

„   „   , 1938, *Phys. Rev* , **54**, 385.

Jones, H., 1939, *Rev Mod. Phys.*, **11**, 235.

Lemaitre, G and Vallara, M. S , 1933, *Phys Rev.*, **43**, 87.

May, A. N., 1938, *Rep. Prog. Phys* , **5**, 390.

Rossi, B., 1930, *Phys Rev* , **36**, 606.

„   „   1934,   „   „   **45**, 212.

Seidl, F. G. P., 1941, *Phys. Rev* , **59**, 7.

Stormer, C , 1931, *Ergebnisse der Kosmischen Physik*, **1**, p. 1.

Swann, W. F. G., 1935, *Phys. Rev.*, **48**, 641.

„   „   1941,   „   „   **59**, 730.

Vallarta, M. S., 1933, *Phys Rev.*, **41**, 1.

Yeater, Max. L., 1945, *Phys. Rev.*, **67**, 74.

A STUDY OF RaE β-SPECTRUM FROM ABSORPTION MEASUREMENTS

By N. N. DAS GUPTA and A. K. CHAUDHURY

ABSTRACT. A new method for investigating the shape of the β-ray spectrum from absorption measurements has been described The β-ray spectrum of RaE has been studied with the help of this method It was found that RaE β-ray spectrum as deduced from absorption measurements agrees with the K. U form but deviates from the original Fermi distribution. This shows that the correction factor, that must be applied to the original Fermi expression in order to take into account the fact that RaE is a forbidden type of β-disintegration, is proportional to $(W_0 - W)^2$.

1 INTRODUCTION

The usual methods of investigation of β-ray spectra are with the help of either (a) magnetic spectrograph or (b) Wilson cloud chamber Both methods require fairly strong sources and long periods of careful observation. The cloud chamber method again suffers from the disadvantage of spurious curvatures due to various distortions discussed in detail by Das Gupta and Ghosh (1946). The number of scattered electrons is also a serious limitation of this method. On account of these defects, the magnetic spectrograph has mainly been used in the study of β-ray spectra.

In the present paper a new method of investigation of β-ray spectrum is described, by means of which it is possible to deduce from absorption measurements, the form of the differential spectrum of electrons from any β-ray source. Such a method is simple and has the additional advantage that it can be used with very weak or rapidly decaying sources. The experiments described below show that, with suitable precautions, the absorption method furnishes us with a very useful survey of the shape of the β-spectrum. Important conclusions can be drawn when we compare the experimental absorption curve of β-rays from any β-decaying source, e.g., RaE with the theoretical Fermi and K. U. forms of β distribution.

RaE β-spectrum has been used in this preliminary work because this spectrum is simple, unaccompanied by γ-rays and also a great deal of work has already been done on its shape with not very consistent results. Richardson (1934), investigating the shape with cloud chamber, detected a great number of slow electrons which did not fit in with the theoretical Fermi distribution.

Lyman (1937) investigated the β-ray spectrum of RaE by a magnetic spectrograph. He found agreement with the K. U. form for medium energies. But for energies greater than 1 Mev. the observed number of electrons was much less than that predicted by theory. However, in these early measurements, no great attention was paid to the thickness of the counter

window used in the detection of β rays. The result was that the low energy part of the spectrum was cut off by the window and not much reliance could be placed on such measurements. Langer and Whitaker (1937) first drew attention to the importance of reducing to a minimum the thickness of the counter window. They showed experimentally that the low-energy part of the RaE β-spectrum becomes more and more prominent as the counter window becomes thinner and thinner. They found that the shape of the RaE β-spectrum did not agree satisfactorily either with Fermi or K. U. theory. The deviation was greatest towards the high energy end of the spectrum. O'Conor (1937) used very thin counter windows and studied the shape carefully with the help of a magnetic spectrograph. His results were in general good agreement with K. U. theory and showed no peak in the energy distribution curve as expected for a K. U. form of spectrum (see Fig. 1). Alichanian and Zavelskij (1937) using a magnetic spectrograph, found agreement with K. U. theory down to the extreme low energy of 100 Kev. Below this energy limit there were, however, more slow electrons than one would expect from theory.

Flammersfeld (1937 and 1939) studied carefully the effect of counter window and of the source-backing layer on the observed shape of β-spectrum. Using very thin sources he found that between 25-1170 Kev. the shape does not agree with either Fermi or K. U. theory. Martin and Townsend (1939) using the same method came to the conclusion that the shape agreed neither with the original Fermi form (1934) nor with its K. U. modification (1935). In these experiments great care was taken to eliminate the effect of scattered electrons. Neary (1940) investigating RaE spectrum with specially thin counter windows and source plate found considerable deviation of the observed spectrum from K. U. form. His results when plotted against energy show a definite peak which is against K. U. form of β-distribution. The number of slow electrons observed were considerably lower than expected from theory.

From the foregoing resume of the previous experimental results, it will be apparent, that there is considerable difference of opinion regarding the correct form of the β-spectrum of RaE. In view of such discrepancies it was thought worthwhile to investigate the spectrum by means of an entirely different method which is described in the following sections.

2. EXPERIMENTAL DETAILS AND RESULTS

A source of RaE was deposited by electrolysis from a solution of crushed old radon needles. The mounting was a thin nickel foil ($\frac{1}{2}\mu$ thick) measuring about $\frac{1}{2}$ cm $\times \frac{1}{2}$ cm. This was placed in front of two rectangular box shaped counters in coincidence. The counters were provided with large grid windows $1'' \times 4''$ covered with thin mica foils. The total thickness of the three mica foils which a particle had to penetrate in order to produce a coincidence was about

15 mgm/cm^2 of mica. Additional aluminium sheets were placed between the 1st counter and the source and the rate of variation of counts with absorber thickness noted carefully.

The results of absorption measurements under these conditions are given in column (2) of Table II corresponding to the values of absorber thickness given in column (1) of the same table. In representing these results, the transmitted intensity at zero thickness of the absorber has been normalised to unity.

In order to compare the experimental results with theory, in the following sections we shall first deduce the differential spectrum N(W) from Fermi and K. U. theories. Next we shall calculate N(W) from absorption measurements and compare with theoretical N(W).

3. DETERMINATION OF DIFFERENTIAL SPECTRUM N(W) FROM FERMI AND K.U. THEORIES

Let the number of electrons having energy between the limits Wmc^2 and $(W + dW)mc^2$ be given by N(W)dW, where N(W) is the distribution function. The form of the distribution function as given by Bethe and Bacher (1936)

is

$$N(W)dW = \frac{|M|^2}{\tau_0} f(WZ)(W_0 - W)^k W^2 dW \qquad \ldots \quad (1)$$

where

$$f(WZ) = \left(\frac{Rmc}{\hbar}\right)^{2(s-1)} \frac{4}{(2s)!^2} \frac{2\pi\alpha Z}{1 - \exp\{-2\pi\alpha w(w^2 - 1)^{-\frac{1}{2}}\}} \{W^2(1 + 4\alpha^2 Z^2) - 1\}^{s-1}$$

and k = 2 or 4 according as we take Fermi or K. U. theory. In equation (1) M is the matrix element referring to the transition of the heavy particles, which is indeterminate and τ_0 is the half life of the β-disintegrating nucleus. Putting $|M|^2, \tau_0 =$ constant A and

$$n(W) = f(WZ)(W_0 - W)^k W^2 \qquad \ldots \quad (2)$$

the equation (1) reduces to

$$N(W)dW = An(W)dW \qquad \ldots \quad (3)$$

Since N(W)dW is a probability, we must have the integral of N(W) over all energies equal to unity. Hence

$$\int_1^{W_0} N(W)dW = A\int_1^{W_0} n(W)dW = 1 \qquad \ldots \quad (4)$$

where W_0 is the maximum total energy number. Equation (4) gives the value of the constant A, viz.

$$A = \frac{1}{\int_1^{W_0} n(W)dW} \qquad \ldots \quad (5)$$

where $\int_1^{W_0} n(W)dW$ is the area under the curve n(W) against W. n(W) was

calculated with the help of equation (1). The calculated values of n(W) are given in columns (2) and (3) of Table I. The areas under the curves n(W) corre-

sponding to Fermi and K.U. expressions were then calculated and found to be

$$\int_1^{W_0} n(W)_{\text{Fermi}} \; dW = 7.445; \quad \int_1^{W_0} n(W)_{\text{K.U.}} \; dW = 18.925$$

Hence, $A_{\text{Fermi}} = .134$; $A_{\text{K.U.}} = .053$ ... (6)

$n(W)$ given in columns (2) and (3) are then multiplied by corresponding values of A, giving $N(W)_{\text{Fermi}}$ and $N(W)_{\text{K.U.}}$ shown in columns (4) and (5) respectively.

TABLE I

Calculation of N(W) from Fermi and K.U. Theories.

W	$n(W)_{\text{Fermi}}$	$n(W)_{\text{K.U.}}$	$N(W)_{\text{Fermi}}$	$N(W)_{\text{K.U.}}$
1 00	4.87	25 8	.645	1 365
1.10	5 06	24.6	.679	1.302
1.25	5.27	22.4	.707	1.185
1.39	5.37	19.6	.721	1 037
1.59	5 25	15.4	.705	0 815
1.74	5 00	12.2	.671	0 646
1.98	4.37	7 6	.587	0.402
2.22	3.50	4.12	.470	0 218
2.70	1.42	.494	.191	0 026
2.96	.549	.079	.074	0 004
3 20	.053	.001	.007	0 00005
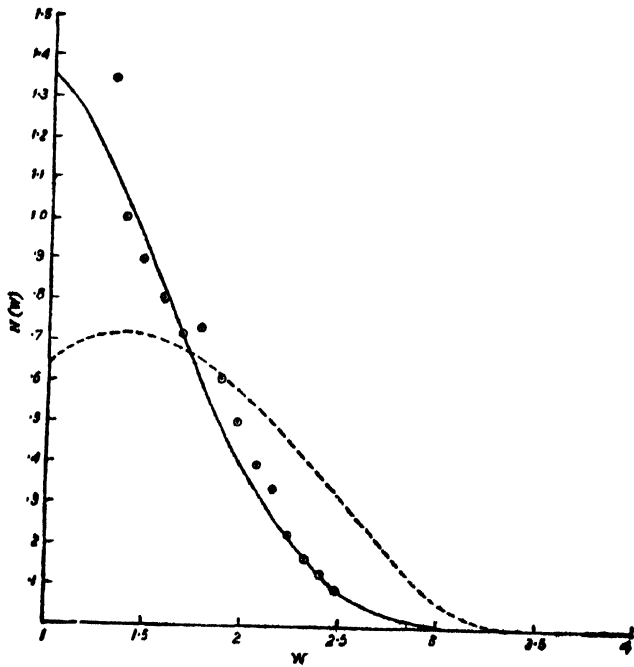
FIG. 1

Comparison of the theoretical Fermi and K.U. forms of β-distribution with the experimental results deduced from absorption measurements. —N(w) according to K.U. distribution, - - -N(w) according to Fermi distribution, ⊙ experimental N(w) deduced from absorption measurements.

A plot of the final values N (W) against W are shown in figure 1, where the dashed curve corresponds to the Fermi and the continuous curve corresponds to the K.U. theoretical spectrum.

4. DETERMINATION OF THE DIFFERENTIAL SPECTRUM N(W) FROM ABSORPTION MEASUREMENTS AND COMPARISON WITH THEORY

We assume that an electron having total energy Wmc^2 has a range R within any specified material. Hence we can as well think in terms of a continuous distribution N(R) of electrons against range R instead of a continuous distribution N(W) against energy number W. Let the number of electrons having range between R and R + dR be equal to N(R) dR. Provided R and W are the corresponding values, we have

$$N(R)dR = N(W)dW \qquad \dots (7)$$

Integrating (7) over all ranges of R and W, we have since the total number of electrons is the same in both cases

$$\int^{R_0} N(R)dR = \int^{W_0} N(W)dW = \qquad (8)$$

where R_0 is the maximum range for the heterogeneous beam of electrons corresponding to the maximum energy number W_0. From equation (7) we can find out the values of N(W) from the corresponding values of N(R) and *vice versa*.

Let us now consider the absorption of β-rays when an absorber of thickness x gms/cm² is placed in front of the source of β-rays which is RaE in our case. Only a fraction of the electrons will be transmitted through the absorber as a number of them will be scattered away or absorbed by the absorber when R is greater than x. This fraction will clearly be a function of x and R. Accordingly, calling this fraction $\phi(x, R)$, we have the total number of electrons transmitted through the absorber

$$A(x) = \int_x^{x_0} \phi(x, R)N(R)dR \qquad (9)$$

In equation (9) x/R is always less than unity and the upper limit x_0 of the integral is identical with the maximum range R_0 of the electrons. From physical considerations we see that the greater the thickness x of the absorber, the smaller is the value of function $\phi(x, R)$. Hence $\phi(x, R)$ is a monotonic decreasing function of x. Similarly $\phi(x, R)$ is a monotonic increasing function of R. Moreover, $\phi(x, R)$ must satisfy the following boundary conditions, *viz.,*

$$\phi(x, R) = 1 \text{ when } x = 0 \; ; \quad \phi(x, R) = 0 \text{ when. } x = R \qquad \dots (10)$$

Experiments on absorption of homogeneous β-rays by several workers (see Rutherford, Chadwick and Ellis, 1930) give definite evidence that $\phi(x, R)$ is a function of x/R and can be represented fairly accurately by a general expression of the form

$$\phi(x, R) = 1 + a\left(\frac{x}{R}\right) + b\left(\frac{x}{R}\right)^2 + c\left(\frac{x}{R}\right)^3 + \qquad \ldots \quad (11)$$

where the constant co-efficients a, b, c must satisfy the boundary conditions (10). To a first approximation, we write

$$\phi(x, R) = 1 - \frac{x}{R} \qquad \ldots \quad (12)$$

It is easily seen that equation (12) satisfies the boundary conditions (10). Combining equations (9) and (12) we have

$$A(x) = \int_x^{x_0} N(R)\,dR - x \int_x^{x_0} \frac{N(R)}{R}\,dR \qquad \ldots \quad (13)$$

and

$$\frac{dA(x)}{dx} = -\int_x^{x_0} \frac{N(R)}{R}\,dR \qquad \ldots \quad (14)$$

whence

$$\frac{d^2A(x)}{dx^2} = \frac{N(x)}{x} \ i.e., \ N(x) = x\,\frac{d^2A(x)}{dx^2} \qquad \ldots \quad (15)$$

With the help of equation (15) the values of $N(x)$ can be found directly from the experimental absorption curve $A(x)$. It is, however, difficult to obtain the second differential sufficiently accurately direct from the absorption curve. We have, therefore, adopted the following procedure which seems to be very satisfactory. Assuming that $A(x)$ can be represented by an expression of the type

$$A(x) = Be^{-Qx} \qquad \ldots \quad (16)$$

since $A(x)$ satisfies the boundary condition

$$A(x) = 1 \text{ at } x = 0 \qquad \ldots \quad (17)$$

we have $B = 1$, and

$$A(x) = e^{-Qx} \qquad \ldots \quad (18)$$

where

$$Q = -\frac{\ln A(x)}{x} \qquad \ldots \quad (19)$$
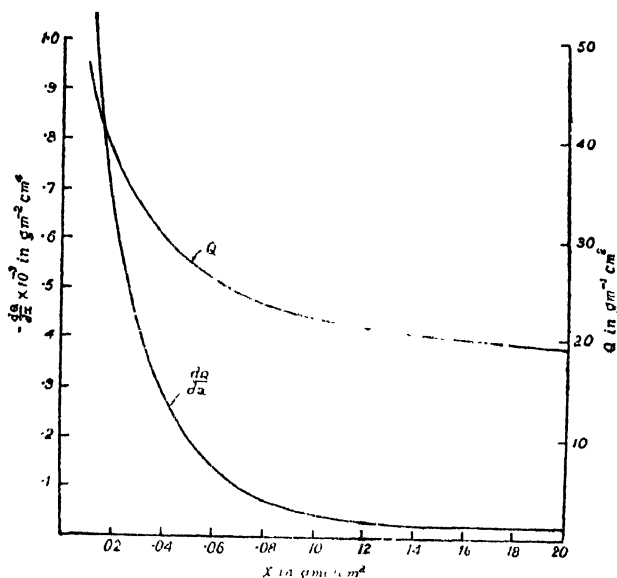
Variation of the calculated values of Q and $\dfrac{dQ}{dx}$ with x

FIG. 2

Q is not a constant quantity but is a function of x given by equation (19). It is high for small values of x and small for large values of x ultimately decreasing at a constant rate with x as can be seen from figure 2. Substituting the value of $\dfrac{d^2 A(x)}{dx^2}$ from equation (18), equation (15) can now be re-written in the form

$$N(x) = x A(x) \left\{ Q^2 + 2(Qx - 1)\frac{dQ}{dx} + x^2 \left(\frac{dQ}{dx} \right)^2 - x \frac{d^2Q}{dx^2} \right\} \qquad \ldots \quad (20)$$

Expression (20) was actually used for the calculation of N (x). dQ/dx and d^2Q/dx^2 were found by numerical analysis of the Q-x relation and taken from smooth curves. Figure 2 shows Q and dQ/dx against x graphically. Q could be found from (19) comparatively accurately and was taken from a smooth curve. The results found by these methods were seen to be more consistent than those calculated directly from relation (15). This is due to the fact that the main contribution to N(x) was from Q, the other terms within the double bracket in (20) serving rather as correction terms.

Columns (1) and (2) of Table II indicate the values of the absorber thickness x and the corresponding ordinates of the experimental absorption curve A(x). In column (3) is given the product $xA(x)$. The values of Q deduced with help of the relation (19) are included in column (4). As stated earlier it will be found that Q is not constant but decreases with x. The values of

dQ/dx deduced from numerical analysis of those of column (4) are given in column (5). These are also shown graphically in figure 2. The values of $\dfrac{d^2Q}{dx^2}$ deduced from those of column (5) are given in column (6). The expression within brackets in equation (20) can now be calculated. The calculated values are denoted by X and given in column (7) and those of N(x) based on equation (20) are given in the last column of Table II. The values of N(x) thus obtained were then converted to those of N(W) with the help of relation (7) by dividing N(x) with the corresponding values of dW/dx.

dW/dx was found by numerical analysis of the range-energy relation for homogeneous β-rays already investigated by several workers (see P. Curie 1935). The graph of dW/dR against R, writing R for x, is shown in figure 3, and the values are also listed in column (4) Table III, given below.
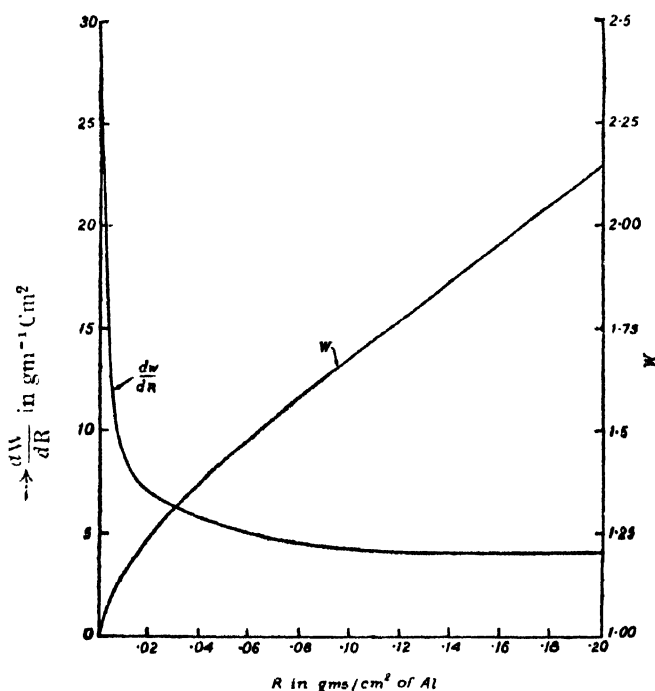
Variation of W and $\dfrac{dW}{dR}$ with R

FIG. 3

In columns (1) and (2) of Table III are given the values of R and the corresponding values of kinetic energy T of the electrons as obtained from the experimental range-energy relation. In the third column are given the values of W obtained from relation

$$W = \frac{T + mc^2}{mc^2}$$

TABLE II

Determination of Experimental N(x) from the
Absorption Curve A(x)

x in gms/cm^2 of Al	$A(x)$	$xA(x) \times 10^3$	$Q = -\dfrac{ln A(x)}{x}$	$\dfrac{dQ}{dx} \times 10^{-3}$	$\dfrac{d^2Q}{dx^2} \times 10^{-3}$	$X \times 10^{-3}$	$N(x)$
.01	62	6 2	47 8	−1.10	56.75	2.93	18.2
.02	.46	9 2	38.6	−.05	27.50	1 40	12.9
.03	.370	11.1	33 0	−.42	16.50	.752	8 30
.04	.300	12 0	30.0	−.28	10 75	.483	5.80
.06	.210	12.6	26 0	−.14	3.90	.350	4 50
.08	.150	12.0	23 7	−.075	2.40	.308	3 70
.10	.1 5	10 5	22.5	−.043	1.00	.297	3 12
.12	.076	8 7	21 8	−.029	30	.357	3 10
.14	.056	7 8	21 0	−.023	.30	.319	2.48
.16	.040	6.4	21.0	−.020	.00	.322	2.06
.18	.030	5 4	19 6	−.020	00	.297	1.60
.20	.022	4 4	19 1	−.020	.00	.261	1.41
.22	.017	3 7	18.7	−.020	.00	.244	.99
.24	.013	3 1	18 3	−.020	.00	.222	.688
.26	.010	2 6	17.0	−.020	00	.201	.523
.28	.08	2 2	17 5	−.020	.00	.181	.398

TABLE III

Determination of N(W) from Experimental values of N(R) given in Table II

R in gms/cm^2 of Al.	$T = K$ E. of electrons in 10^6 e v	W	$\dfrac{dW}{dR}$ gm $^{-1}$cm^2	N(R) from Table II	N(W) observed
.01	.090	1.16	8.6	18.20	2.12
.02	.130	1.25	7.0	12.90	1.84
.03	.160	1.31	6.3	8.30	1.33
.04	.190	1.37	5.7	5.80	1.02
.06	.245	1.48	5.0	4.50	.90
.08	.296	1.58	4.6	3.70	.80
.10	.344	1.67	4.3	3.12	.72
.12	.393	1.77	4.2	3.10	.74
.14	.440	1.86	4.1	2.48	.605
.16	.490	1.96	4.1	2 06	.502
.18	.539	2.05	4.1	1.60	.400
.20	.588	2.15	4.1	1.41	.344
.22	.630	2.23	4.1	.903	.220
.24	.672	2 31	4.1	.688	.168
.26	.714	2.39	4.1	.523	.127
.28	.756	2.48	4.1	.398	.097

The values of N(W) given in column (6) were obtained by dividing the values of N(R) given in column (5) by those of dW/dR given in column (4) of the Table III.

The experimental values of N(W) thus obtained are indicated in figure 1, along the theoretical Fermi and K. U spectra by ⊙ marks. From the figure it is quite evident that the experimental results are more in conformity with the K. U. form of β-ray spectrum and deviate unmistakably from the original Fermi form.

5. DISCUSSION

Our results indicate that RaE β-distribution follows a K. U form of spectrum closely and deviates markedly from the original Fermi distribution. Fermi theory is valid only for permitted β-decay. As RaE disintegration belongs to the forbidden class, straightforward Fermi theory should not strictly be applicable to it The difference between K. U. and Fermi forms is the single factor $(W_0 - W)^2$. Our results therefore indicate that the correction factor that has to be applied to Fermi theory in order to take into account the fact that RaE disintegration is forbidden is proportional to $(W_0 - W)^2$. With such a correction the modified Fermi theory should be applicable also to RaE β-disintegration.

The method of analysis of β-ray spectra, such as outlined above, is simple. Its successful application in the case of RaE spectrum shows that with the help of this method, a very useful survey of the form of the β-spectrum can be made. This method, is therefore a very valuable addition to the existing limited means of study of β-ray spectra. The spectra of a number of other radio-active substances are being studied with the help of this method and the results will be published in future.

Feather (1938) described a method by which some indication of the form of a β-spectrum could be obtained by comparing the absorption curve with that of a standard spectrum such as that of RaE. In the present paper, however, a method has been presented by which the differential β-spectrum can be obtained directly from analysis of the absorption curve. No comparison with the absorption curve of another standard substance is needed.

Our method suffers from the approximation given in equation (12) and that there are no adjustable constants which could take into account changes in experimental conditions. It is well-known that the absorption curve of a homogeneous beam of electrons may vary somewhat with the experimental set up. The analysis given above is limited to the case when the scattered electrons have been eliminated as far as possible and also the detector subtends as large a solid angle as possible at the source. Under such conditions it is contended that the absorption curve of homogeneous β-rays of different energies is given faithfully by the approximate relation (12).

However, when the experimental set up deviates a great deal from such ideal conditions, the general expression (11) may be used in the place of the approximate relation (12). The constants a, b, c etc., may then be adjusted to fit in the experimental conditions closely.

If we take the first three terms of equation (11), we have

$$\phi(x, R) = 1 + a\left(\frac{x}{R}\right) + b\left(\frac{x}{R}\right)^2 \qquad \ldots \ (21)$$

since $\phi(x, R)$ satisfies the boundary conditions (10), we have from equation (21)

$$1 + a + b = 0 \qquad \ldots \ (22)$$

In this case equation (13) changes over to

$$A(x) = \int_x^{x_0} N(R)dR + ax \int_x^{x_0} \frac{N(R)}{R}dR + bx^2 \int_x^{x_0} \frac{N(R)}{R^2}dR \qquad \ldots \ (23)$$

Using equation (22) we get from the equation (23) by differentiating $A(x)$ thrice

$$\frac{d^3A(x)}{dx^3} = \frac{(a+2b)}{x} \frac{dN(x)}{dx} + \frac{a}{x^2}N(x) \qquad \ldots \ (24)$$

which is a first order differential equation in $N(x)$ $\frac{d^3A(x)}{dx^3}$ can be determined

from the experimental curve $A(x)$ and the equation solved for $N(x)$. Taking the first four terms of equation (11) we get in a similar manner for $N(x)$

$$\frac{d^4A(x)}{dx^4} = -\frac{(a+2b+3c)}{x} \frac{d^2N(x)}{dx^2} + \frac{2(a+b)}{x^2} \frac{dN(x)}{dx} - \frac{2a}{x^3}N(x) \qquad \ldots \ (25)$$

which is a second order differential equation in $N(x)$. This again can be

solved for $N(x)$ provided $\frac{d^4A(x)}{dx^4}$ can be determined sufficiently accurately

from $A(x)$. The order of the differential equation in $N(x)$ increases as we take more and more terms in approximating for $\phi(x, R)$, and the solution becomes difficult. However, in view of the labour involved in the use of relation (24) or (25) and the uncertainty in the determination of the higher differentials of $A(x)$ it is thought worthwhile to use the simplest form of $\phi(x, R)$ given in (12) in analysing the results of the absorption measurements.

PALIT LABORATORY OF PHYSICS,
UNIVERSITY COLLEGE OF SCIENCE, CALCUTTA.

REFERENCES

Alichanian, A. I. and Zavelskij A. S , (1937), *Compt. Rendu. Acad. Sci. U S. S. R.*, **17**, 467.

Alichanian, A., Alichanov, A and Dzelepow, B. S., (1938), *Compt Rendu. Acad. Sci. U. S. S. R* , **19**, 5, 375.

Bethe, H A. and Bacher, R. F., (1936), *Rev. Mod. Phys* , **8**, 193.

Curie Madame, P . (1935), " Radioactivite " (Herman & Co. Paris), p 294.

Das Gupta, N. N. and Ghosh, S. K., (1946), *Rev Mod. Phys* **18**, 225.

Feather, N , (1938), *Proc. Camb Phil. Soc* , **34**, 599.

Fermi, E., (1934), *Zs. f. Phys.*, **88**, 161.

Flammersfeld, A , (1937). *Phys. Zeits.*, **38**, 973.

Flammersfeld, A , (1939), *Zs f. Phys.*, **112**, 727.

Konopinski, E J , and Uhlenbeck, G. E , (1935), *Phys. Rev.*, **48**, 7.

Konopinski, E. J., (1943), *Rev. Mod. Phys* , **15**, 209.

Langer, L. M. and Whitaker, M. D , (1937), *Phys. Rev.*, **51**, 713.

Lyman, E M , (1937), *Phys. Rev.*, **51**, 1.

Martin, L. H, and Townsend, A. A., (1939), *Proc. Roy. Soc.*, **170A**, 190.

Neary, G J., (1940), *Proc. Roy Soc.*, **175A**, 71.

O'Conor, J S , (1937), *Phys Rev.*, **52**, 303.

Richardson, H O. W., (1934), *Proc Roy. Soc.*, **147A**, 442

Rutherford, E , Chadwick, J , and Ellis, C D., (1930), " Radiations from Radioactive substances " (Cambridge Univ. Press), p. 414.

Watase, Y , and Itoh, J., (1938), *Proc Phys. Math. Soc. Japan*, **20**, 809.

ON THE SIZE OF MICELLES IN JUTE FIBRE OF DIFFERENT QUALITIES AND OF KNOWN STRENGTH

By S. K. CHOWDHURY and S. C. SIRKAR

Plate I

ABSTRACT. The halfwidths of reflections from (002), (020) and (120) planes in the X-ray diffraction patterns due to samples of jute fibre of nine different qualities have been determined with the help of blackening-log intensity curves. The values of m_1, m_2 and m_3, which denote the number of times the unit cell is repeated in the micelle along the a, b and c axis respectively have been determined in each case by Laue's method. The average strengths of the fibre in the samples cut from adjacent portions of the samples used for the X-ray investigation have also been measured. It is observed that the value of m_1 is almost constant and is about nine in the case of eight of the nine samples studied, while in the remaining case it is seven. The values of m_2 vary from 7 to 12 for the different qualities of the fibre studied and these values seem to be proportional to the strength of the fibre. The values of m_1 also vary from 5 to 8 for the different varieties studied, but there seems to be no correlation between the value of m_1 and the strength of the fibre.

INTRODUCTION

The size of micelles in a few different varieties of unbleached jute fibre was first determined by Sirkar and Saha (1946), employing Laue's (Laue, 1926) method. The (020) reflections were almost masked by continuous blackening, because the slit used was not very fine, and so the reflections from (002), (031) and (120) were used for the determination of m_1, m_2 and m_3, which denote the number of times the unit cell is repeated along a, b and c-axis respectively. The present authors (Sirkar and Chowdhury, 1946) used narrower slits and determined the half widths of reflections from (002), (120) and (020) reflections in the case of five varieties of jute fibre, both in the raw and bleached states. The strengths of the fibres used for the X-ray investigation were not, however, known accurately, and although m_2 was determined directly from the half width of (020) reflection by Laue's method, and the value of m_2 was found to be the largest and about 15 in the case of high quality Tossa jute fibre which has generally a very large tensile strength, a general conclusion cannot be drawn from these results that the greater the value of m_2 larger is the strength of the fibre. It was, therefore, thought worthwhile to determine the value of m_1, m_2 and m_3 by the Laue's method in the case of a large number of different varieties of jute fibre of known strengths.

EXPERIMENTAL

Small narrow bundles, each containing about a dozen strands of raw jute fibre of a particular trade quality were selected and two samples from adjacent portions of the length of each such bundle were cut off. One of these two samples of each quality was selected for X-ray analysis and the other was sent to the Director, Technological Research Laboratories of the Indian Central Jute Committee for the measurement of the strength of the fibre. The strengths of jute fibre of fourteen different qualities were kindly supplied by him, but the half widths of reflections from (002), (020) and (120) planes were measured in the case of only nine of these varieties. The camera used was the same as that used by the present authors previously (Sirkar and Chowdhury, 1946). In each case two photographs of the X-ray diffraction pattern were obtained, one with such a moderately short exposure that the (002) reflection was not over exposed, and the other with a longer exposure to get sufficient blackening due to the (020) reflection. It was also necessary to draw two blackening-log intensity curves, one with densities ranging from .04 up to .54 and the other from, 0.2 up to 2.2 in order to measure the half widths of the (020) and (120) reflections which are faint and of the (002) reflection which is very intense. The microphotometric records were taken with a Kipp and Zonen type self-recording microphotometer and on each record the deflections corresponding to infinite density and the unexposed portion of the film were recorded. The intensity at any point in the spot was determined by first determining the total intensity at that point and then subtracting from it the intensity of the background with respect to the unexposed portion of the film. The observed half widths on the microphotometric record were reduced to radians by taking into account the magnification in the microphotometer (seven in this case), the value of the Bragg angle for the particular reflection and the distance of the film from the irradiated sample.

The values of m_3, m_2 and m_1 were then determined from the values of the half widths, of the (002), (020) and (120) reflections respectively by using the Laue's formula (Laue, 1926),

$$B \cos \frac{\chi_m}{2} = {}_0\lambda \left[\frac{\dfrac{h^2}{m_1^2 a^4} + \dfrac{k^2}{m_2^2 b^4} + \dfrac{l^2}{m_3^2 c^4}}{\dfrac{h^2}{a^2} + \dfrac{k^2}{b^2} + \dfrac{l^2}{c^2}} \right]^{\frac{1}{2}}$$

where B is the halfwidth of $(h\,k\,l)$ reflection in radian and λ_m is the angle between the incident and reflected X-rays. This formula reduced to the following forms for different values of $h\,k\,l$:

$$\text{For (002)}, \quad m_3 = \frac{.1777}{B_3},$$

PLATE I

J 815   J 864   J 823   285   J 801

(002)

(I20)

(020)
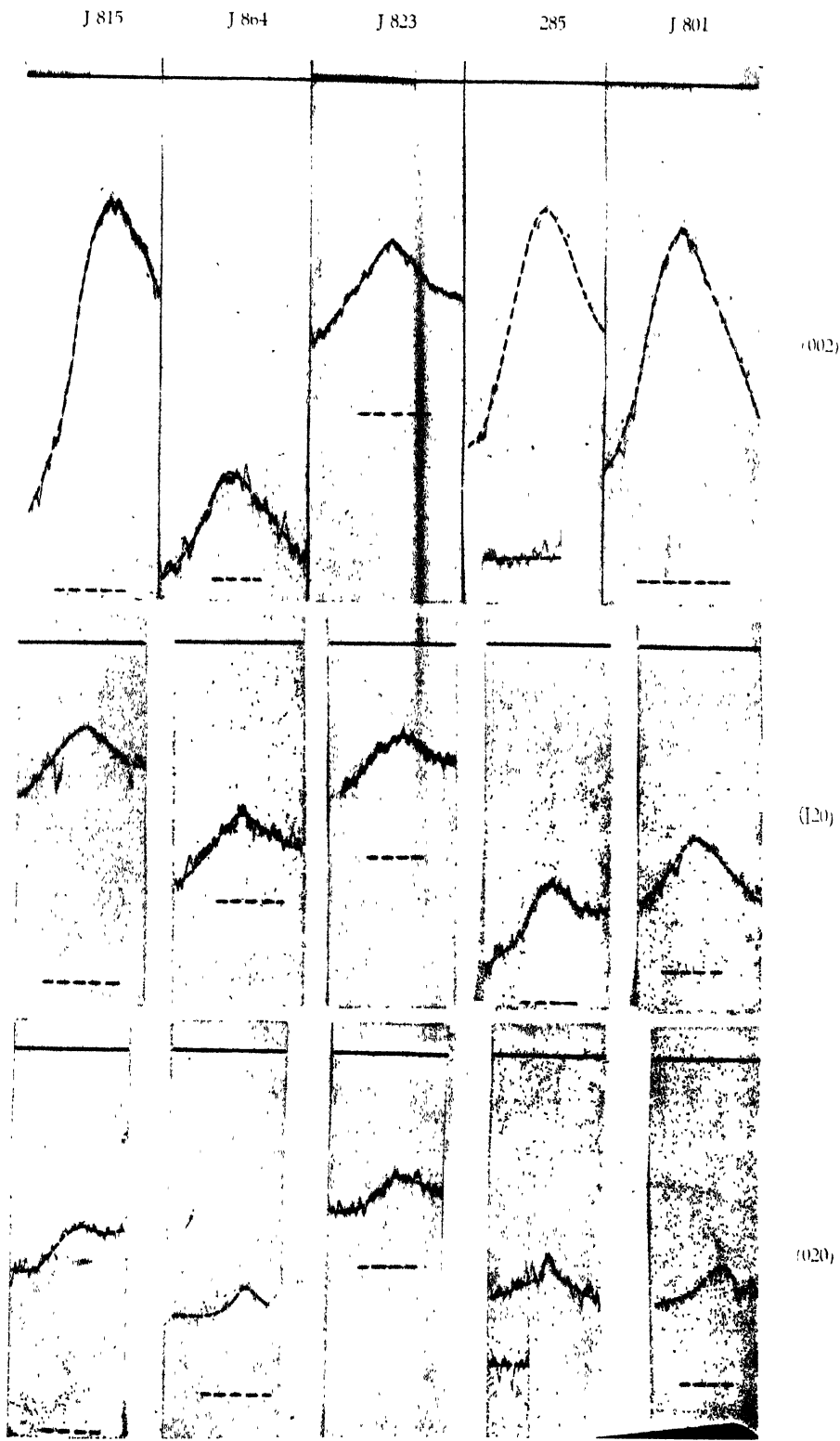
MICROPHOTOMETRIC RECORDS OF X-RAY REFLECTIONS FROM JUTE FIBRE

$$\text{for (020)}, \quad m_2 = \frac{\cdot 1361}{B_2},$$

$$\text{and for (120)}, \quad \frac{B_1^2}{38\cdot 23} - \frac{3\cdot 553 \times 10^{-4}}{m_2^2} = \frac{2\cdot 058 \times 10^{-4}}{m_1^2}$$

where, B_1, B_2 and B_3 are the values of B for these reflections.

RESULTS AND DISCUSSION

Some of the microphotometric records from which the values of the half widths of the reflections from (120), (020) and (002) planes were determined are reproduced in Plate I. The curves were smoothed out while these half widths were determined. These smoothed curves are shown by dotted lines in ink. The results are given in Table I in the last column of which the strength of the fibre is given in terms of breaking load divided by mass per unit length.

TABLE I

Trade Quality	B_3	m_3	B_2	m_2	B_1	m_1	Strength $F/M \times 10^6$
J 823	.022	8	.020	7	.021	7	1.89 ± .17
J 864	.020	9	.014	10	.021	5	3.9 ± .29
J 285	.020	9	.011	12	.016	7	4 55 ± 21
J 803	.020	9	.020	7	.022	6	2.15 ± 14
J 815	.025	7	.019	7	.024	5	2.69 ± .06
J 310	.019	9	.014	10	019	6	3.69 ± .18
J 801	.023	8	.014	10	016	8	3 26 ± .18
J 816	.020	9	.017	8	.020	6	2.92 ± .14
Chinsura green	.022	8	.019	7	.020	8	2.52 ± 09

It can be seen from Table I that except in the case of J 815, the value of m_3 is almost constant, being 8 in three cases and 9 in the remaining five cases. It is difficult to say whether the value 7 observed in the case of J 815 is due to some local defect in the film, because, no attempt has been made to repeat the experiment. The value of m_2 on the other hand varies widely from quality to quality being almost proportional to the strength expressed in terms of breaking load divided by mass per unit length and given in the last column of Table I. The values of m_1, again, varies widely from quality to quality, but there seems to be no correlation between the values of m_1 and the strength of the fibre. Thus the results seem to point to the general conclusion that the

strength of the fibre is partly determined by the length of the micelle along b-axis and the longer chain corresponds to the higher strength.

ACKNOWLEDGMENT

UNIVERSITY COLLEGE OF SCIENCE,
    CALCUTTA.

REFERENCES

Laue, M. V. (1926), Z. Krist. 64, 115.
Sirkar, S. C., and Chowdhury, S. K. (1946), Ind J. Phys. 20, 31.
Sirkar, S C. and Saha N. N. (1946), Proc. Nat. Inst. Sc., India, 12, 151.

CONCERNING THE USE OF A 920 DOUBLE PHOTO-CELL IN A CURRENT AMPLIFIER AND STABILIZER

By B. M. BANERJEE* and S. K. SEN

ABSTRACT. The characteristics of a gas-filled double photo-cell G. E. 920 as a translator element in a current stabilizer circuit has been studied. The characteristics are explained in the light of ionization in the residual gas in the common envelope. The characteristics differ from, and are inferior to that of two separate photo-cells or a vacuum double photo-cell. Gas-filling results in a deterioration rather than an improvement, of the characteristics of the tube as a translator element of a current amplifier or stabilizer.

INTRODUCTION

The 920 photo-cell is commonly used in a translator† circuit of the type given below. In a circuit of this type, it is frequently found that so long as $B = B'$, the system operates with the light shining mainly or wholly on one
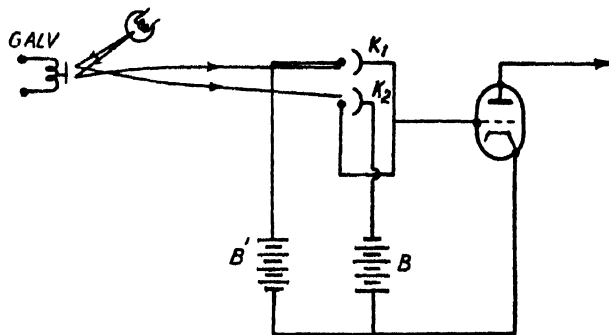
FIG. 1.

A commonly used galvanometer photo-tube translator circuit.

photo-cathode. In extreme cases the system refuses to function altogether. It is also found that the system may be made to function properly by making B' somewhat smaller than B.

* Fellow of the Indian Physical Society.

† A current amplifier consists of the following parts :—

(a) A translator which converts current variations into voltage variations sufficiently large to actuate a vacuum tube d.c. amplifier.

(b) A vacuum tube d c amplifier of a maximum current output equal to that specified for the current amplifier.

(c) A network for feeding back a portion of the amplified output current in opposite phase to ensure linearity and to stabilize the amplification to the desired level.

The translator usually consists of a galvanometer whose light spot shines on a double photo-cell in a circuit of the type shown in the figure. This arrangement was first utilised by Gilbert (1936).

EXPERIMENTS AND RESULTS

This observation points to the existence of an assymmetry in the sensitivities of the photo-cathodes, resulting out of its peculiar connection in this particular circuit.

The characteristics of the photo-cell in this circuit has, therefore, been studied thoroughly—the result of which is given in the curves of Figs. 2 and 3.

Fig. 2 represents the current voltage characteristics of all the electrodes in the photo-cell—Fig. 2(a) with the light shining wholly on cathode 1—the cathode at the lowest potential and Fig. 2(b) with the light shining wholly on cathode 2—the cathode at the intermediate potential. Experimental arrangement is indicated in the figure.
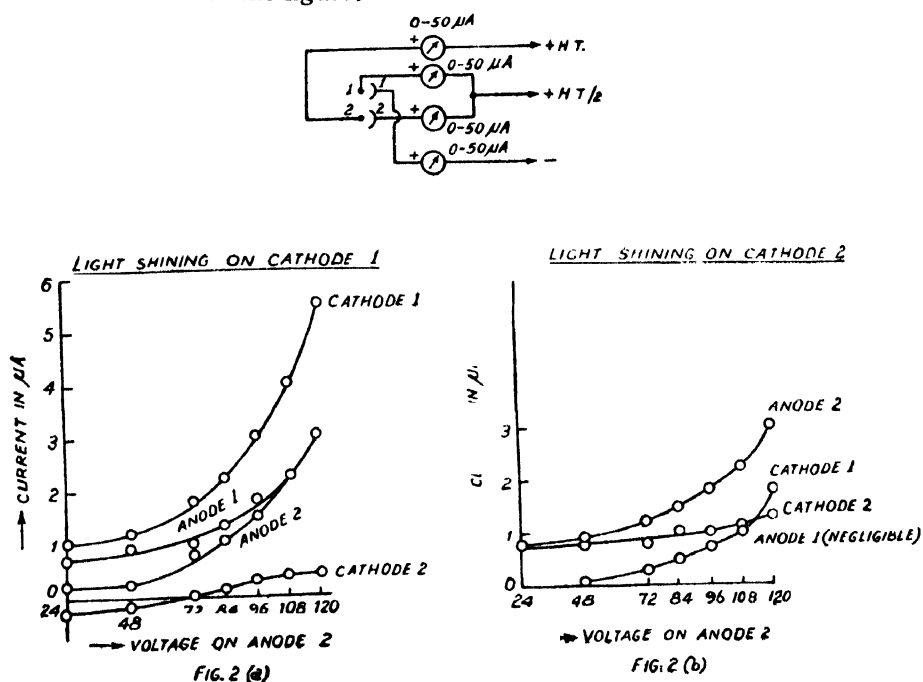
Current-Voltage characteristics of a 920 double photo-cell.

The following observations require particular mention :

1. The electrodes of both the photo-cells pass current even when light shines wholly on one photo-cathode.

2. The magnitudes of the currents passed by the different electrodes are greater when light shines on the photo-cathode at the lower potential.

3. The difference in the magnitude of the currents with light shining wholly on one or the other photo-cathode increases with the total voltage applied on the photo-cell.

Fig. 3 gives what may be called the *translation* characteristic—output voltage *vs.* light spot position of the photo-cell. As the position of the light spot depends upon the galvanometer current—galvanometer current is plotted

as the abscissa of the points in the curves. With no current in the galvano-meter, illumination on both the photo-cathodes are the same.
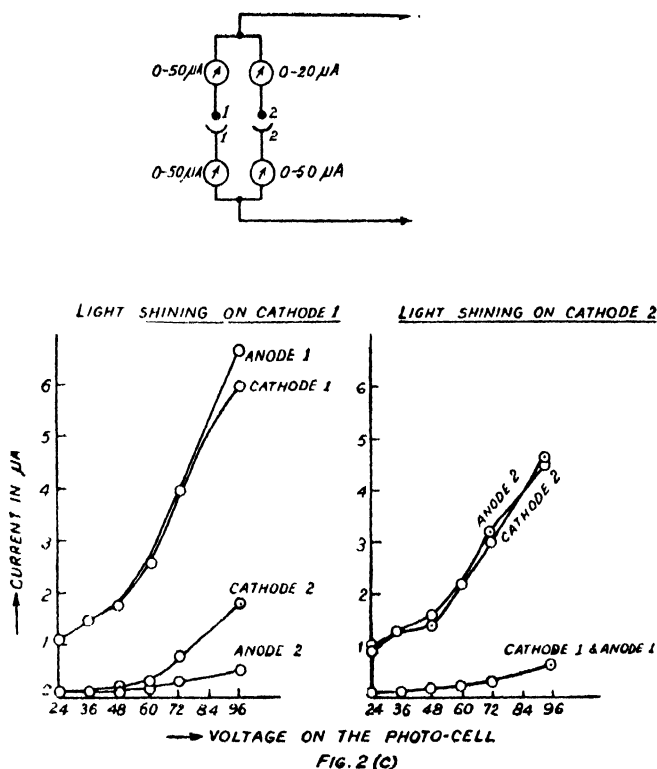
FIG. 2 (C)

The measurement of the "Output Voltage" of the photo-cell is a difficult problem. This voltage lies in the range of 20-70 volts. The photo-cell circuit is a high resistance circuit—inasmuch as only a few micro-amperes are passed
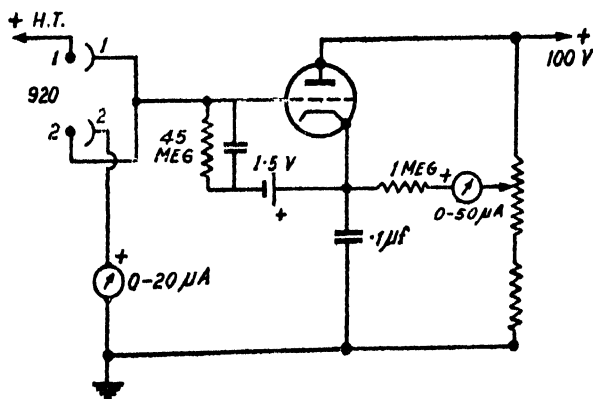
FIG. 3.

Experimental arrangement for obtaining the translation characteristic of a 920 double photo-cell. The voltmeter tube is a 6C6 connected as atriode. The filament voltage is reduced to 4.8 volts in order that the tube may have a high i_n put resistance.

by the photo-cell elements at considerable voltages.   A vacuum tube voltmeter
of high input resistance, which can measure positive voltages in the range of
20-70 volts, is therefore necessary.   The solution is found in the circuit of
Fig. 3.   This valve voltmeter has an input resistance approximately equal to
μ Rg which is about 800 megohms.   The grid leak of 45 megohms together
with a bias of 1.5 volts is necessary as otherwise the pointer of the   indicating
50 μA-meter moves out of scale when the light spot moves away from both the
photo-cathodes.   A condenser of .002 μf capacity bypasses the ripples picked
up by the grid of the valve-voltmeter.

The curves in Fig. 3 point towards the following observations.—

1.   The centre voltage of the curves is not necessarily equal to half the
photo-cell supply voltage—being usually considerably greater than half the
supply voltage.
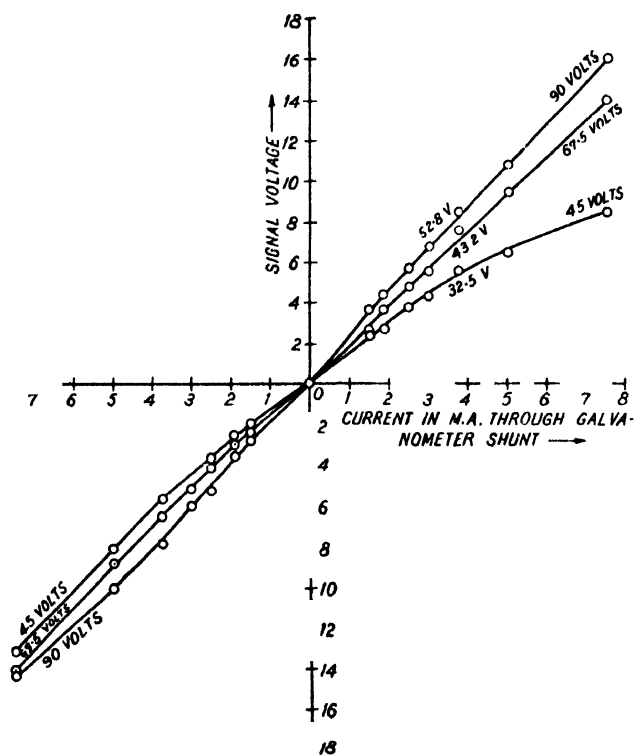
FIG. 3 (a)

Translation characteristics of a 920 double photo-cell translator.   The voltage
applied across the 920 photo-cell as well as the centre voltage is written down at the
side of each characteristic.   The ordinates give the signal voltage, output voltage being
obtained by adding this amount to the corresponding centre voltage.   The extreme points—
with 7.5 m.A. through the galvanometer shunt—represent points when the light shines
wholly on one cathode; the centre point with light equally on both cathodes.   The spot of
light is of diamond shape being obtained by reflection from the mirror of same shape of a
Rubicon Portable spotlight galvanometer.   The lamp is a 6.3 volt, 1 Ampere incandescent
lamp—running at 7 volts.   Light is collected through a small double convex condenser lens.

2.   The range* of output voltage is a small fraction of the supply voltage. With two separate photo-cells or with a vacuum double photo-cell it would almost equal the supply voltage in magnitude†. With the reduction of the supply voltage this fraction improves.
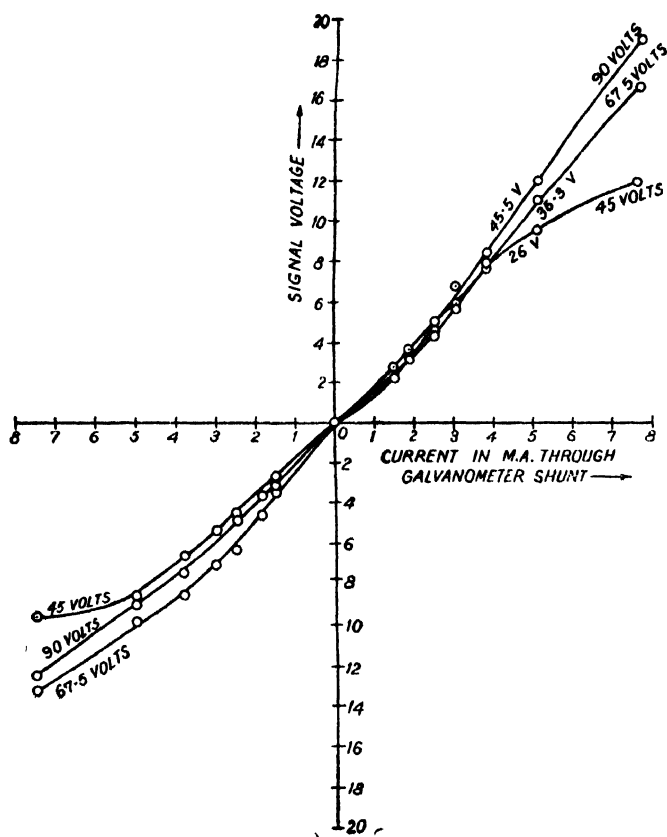
FIG. 3 (b)

The 67 5 volt characteristic of Fig. 3(b) crosses the 90 volt characteristic. This is somewhat abnormal. It is perhaps the result of a reduction in the intensity of light when the 90 volt curve was taken.

3.   The slopes of the characteristics diminish only slightly with decrease of the supply voltage. The absolute magnitude of the range of output voltages does not get much reduced even when the supply voltage is diminished considerably

The vacuum tube d.c. amplifier in the amplifier-stabilizer system operates over a limited range of input voltages. At the extremes of this range, the

*The output voltage is a maximum when light shines wholly on cathode 1 and a minimum when light shines wholly on cathode 2. With light shining on both cathodes, the output voltage may have any value between these two extremes. The range of output voltage is the difference between these two voltages.

†It is obvious that with two separate photo-cells or a vacuum double photo-cell the maximum output voltage will approach the supply voltage while the minimum will approach zero. As a result the range of output voltage almost equals the supply voltage.

output current is either zero or the saturated maximum value. The whole system may function only when the d.c. amplifier functions. So in order that the system may operate, the output voltage of the photo-cell must fall in this range. If the centre voltage of the photo-cell translator, coincides with the working range of the input voltage of the d.c. amplifier, the system operates in a balanced condition, *i.e.*, light shining equally on both photo-cathodes. Otherwise there is unequal illumination on the photo-cathodes. In this case variations in the intensity of the illuminating lamp will cause changes in the output voltage of the photo-cell and so changes in the output current of the amplifier stabilizer. This is undesirable. It defeats the advantages of using a double photo-cell translator. So arrangements must be provided in order that the centre voltage of the translator may be made to coincide with the working range of the input voltage of the d.c. amplifier. This may be accomplished by one or two potentiometers controlling the voltage on the photo-cells. Such adjustments will be found provided in some of the current stabilizers described in literature.* The authors of these articles however did not mention that such a provision of adjustment is inherently necessary to overcome the peculiarity of the 920 double photo-cell in this particular circuit. All of them appear to have overlooked that the centre voltage of a 920 translator is usually greater than half the supply voltage.

EXPLANATION OF THE OBSERVATIONS

The 920 photo-cell is a gas filled one. This gas therefore has to explain the observed peculiarities. A vacuum photo-cell cannot presumably show such characteristics.

Gas multiplication occurs due to the generation of ions by collision. This process takes place in the regions where there is a high field gradient, *i.e.*, near about the wire anodes. Positive ions move out from these regions to the two cathodes and constitute the major fraction of the cathode currents.

Curve 2(a)—Light shining wholly on cathode 1 (Fig. 2).

Electrons emitted from the photo-cathode 1 are captured by anode 1, anode 2, and also cathode 2, as all these are at a higher potential compared to the cathode 1. This explains the negative current registered by cathode 2, at low voltages where primary electrons constitute a good fraction of the currents. At higher voltages the collisional ions increase in number and the currents increase. At a particular value of the supply voltage, the positive ion current intercepted by cathode 2 equals the electron current received from cathode 1, and hence the cathode 2 current falls to zero. At still greater voltages, a greater number of positive ions are received by cathode 2 and so the cathode 2 current becomes positive.

As the collisional multiplication follows Townsend's (1915) exponential law, the currents of all the electrodes increase rapidly with voltage. Anode 2 rece⁻ s

---

* Chang. (1946) ; Lawson and Tyler (1939) ; T.R.E. Newsletter No. 3.

electrons from the ionized regions near about anode 1. As the ionization process is involved twice in the production of the anode 2 current, anode 2 current increases more rapidly than anode 1 current. Cathode 1 current is the largest of all the currents as cathode 1 receives most of the positive ions both from anode 1 and 2.

Curve 2 *(b)*—Light shining on cathode 2—the cathode at the intermediate potential.

Photo-electrons emitted by cathode 2 are captured only by anode 2. Positive ions generated at anode 2 move out and are captured by both cathodes. As the positive ions form a sheath around anode 2, the potential fall around anode 2 rapidly equals the potential difference existing between anode 2 and cathode 2, tending to approach the potential of cathode 1—the cathode at the lowest potential. Cathode 1 draws positive ions from this sheath of ions. As the supply voltage is increased more collisional positive ions are generated but the greater fraction is received by cathode 1 and so cathode 1 current increases rapidly. Cathode 2 current remains almost constant. Anode 1 current remains negligible as it is an electrode of small surface area, at an intermediate potential, situated out of the direct path of the positive ions.

When light shines on cathode 1-the cathode at the lowest potential, collisional multiplication takes place in the regions near about both the anodes. Whereas when light shines on cathode 2—the cathode at the intermediate potential collisional multiplication occurs near about one anode—(anode 2)—only. As a result the electrode currents in the first case are generally greater in magnitude than in the second case.

Curves in Fig. 2(c)—Confirm the above explanations. These are obtained with the electrodes of both the photo-cells at similar potentials. It is observed that a small current is passed by both the electrodes of the dark photo-cell This proves that some of the ions from the illuminated photo-cell stray into the region of the dark photo-cell.

It is not possible to derive the curves in Fig. 3 from those in Fig. 2. For that it is necessary to obtain current voltage characteristics with illumination on both photo-cathodes, as well as to obtain characteristics with differing voltages on anode 1 and cathode 2. However, curves in Fig. 2 are sufficient to indicate that the output voltage with equal illumination on both photo cathodes will not be half the supply voltage and also that the range of output voltage will not be as great as that of a translator using two separate photo-cells.

CONCLUSION

The operation of a gas filled double photo-cell like 920, as a translator element converting current variations into voltage variations, in current amplifier-stabilizer circuits is not so simple as is usually thought to be. As a result (a) the output signal voltage of the translator with equal illumination on both photo-cathodes is not equal to half the supply voltage and (b) the

range of output signal is a small fraction of the supply voltage. Now the vacuum tube amplifier which follows such a translator element in a current stabilizer circuit operates over a limited range of input voltages. For perfect functioning of the whole system, it is necessary that the working range of the input voltage of the d.c. amplifier falls at the centre of the translator output voltage. This can be achieved by suitable potentiometers balancing the photo-cell voltages. As a matter of fact such an arrangement is absolutely necessary.

A translator using two similar and separate photo-cells or a vacuum double photo-cell possesses a much greater range of output voltage. As a result it is more sensitive and less critical of adjustments. A vacuum double photo-cell translator would have of course a greater, but more constant internal resistance. This, however, is not a serious shortcoming inasmuch as it is quite possible to design the following d c. amplifier such that it possesses a sufficiently high input resistance.

In short, a gas filled double photo-cell translator requires careful adjustments and is less sensitive compared to two separate photo-cells or a vacuum double photo cell. A better translator tube would have resulted if the filling gas were not introduced.

PALIT LABORATORY OF PHYSICS,
UNIVERSITY COLLEGE OF SCIENCE, CALCUTTA.

R F ERENCES

Chang, W. Y. (1946), *Phys Rev* , **69**, 60.
Gilbert, R. W. (1936), *Proc. I. R. E.*, **24**, 1239
Lawson, J L., and Tyler, A. W. (1939), *R. S I.*, **10**, 304.
T R E., Newsletter, No 3.
Townsend, J S , Electricity in Gases, Clarendon Press, London

RAJ=DER=KAR & CO.

Commissariat Building,
HORNBY ROAD, FORT,
BOMBAY.

P R E S E N T S

From Stock

1. B. N, F. Jet Test Appratus
2. Tachometer, Tachoscope (Swiss)
3. Stop Watches (Swiss)
4. Spencer's Medical Microscope Model 33-MH.
5. Students Dissecting Microscope
6. Fortin's Barometer
7. Oertling Torsion Balance
8. Glass Metal Pumps
9. Metal Booster Pumps

CONTENTS

PAGE

NOTICE
TO INTENDING AUTHORS

Manuscripts for publication should be sent to Mr. A. N. Banerjee, Assistant Editor, 210, Bowbazar Street, Calcutta.

The manuscript of each paper should contain in the beginning a short abstract of the paper.

All references to published papers should be given in the text by quoting the surname of the authors followed by the year of publication within braces, *e.g.*, Sen (1942). The actual references should be given in a list at the end of the paper according to the following specimen :

    Sen, B. K., 1942, Volume rectification of crystals, *Ind. J. Phys.*, 16, 329.

The references should be arranged alphabetically in the list.

All diagrams should be drawn on thick white paper in Indian ink, and letters and numbers in the diagrams should be written in pencil.

THE EFFECT OF COLLISIONS ON THE CONTINUOUS ABSORPTION SPECTRA

By A. K. DUTTA and AMALENDU ROY

ABSTRACT   Continuous absorption spectra of polar molecules have been found to shift towards longer wavelength by collisions with both polar and non-polar gases. The change in absorption co-efficient is found to depend on the number of collisions suffered by a molecule with the foreign gas and reaches a maximum value with a definite proportion of the absorbing gas and foreign gas, irrespective of the polarity of the foreign gas. With inert foreign gas it appears that there is a sort of screening giving rise to a decrease in the absorption co-efficient value after the maximum is reached.

INTRODUCTION

It is accepted now, that molecules with atomic binding, break up on dissociation into two neutral atoms—one normal and the other excited, whereas those with ionic binding into two neutral atoms both of which are normal. The energies of dissociation in the two cases are thus, different and consequently the beginning of absorption also (Frank, 1927) Some work on the absorption limit of the hydrogen halides has been done to decide its type of binding. Some decision was in favour of the atomic type. Dutta (1932) concluded. on his investigations. that they corresponded to ionic binding.

In these works the effect on the absorption spectra due to collisions and intermolecular fields could not be detected. As it was observed by Goodev and Taylor, the Beer's law holds for these gases This tends to indicate that the pressure or the collisions have not got any effect on the probability of transition of the molecules. The hydrogen-halide molecules being polar, exert strong intermolecular electric influences on one another and it is probable that the energy levels in the molecules are, in some way, modified from absolutely free molecules. The spectra which we generally observe, are thus, not expected to be those of pure unaffected gaseous molecules, but should be due to molecules under various amount of intermolecular forces ranging from zero to a maximum. To know the absorption limit of unaffected gas molecules accurately and thereby to predict the type of binding we must know the quality and the quantity of this modification. It is with this point in view that the experiment had been undertaken.

EXPERIMENTAL

The absorption spectrum studied was that of HI and CCl_4 molecules. The total number of collisions suffered by a molecule was increased by adding a foreign gas. This, however, keeps the total number of collisions with similar molecules the same. But each molecule has suffered, besides, a number of collisions with the foreign gas introduced, according to its quantity. If the foreign gas has no absorption in the region studied, we can study only the effect of increased collisions on a molecule, some of which are with foreign polar and some with non-polar gases. These experiments have been

carried out both with a polar (HI) and a non-polar (CCl₄) gaseous substance, which primarily show a continuous absorption spectrum. The foreign gases selected were HCl gas as polar and argon as non-polar—none of which has any absorption in the regions where those of HI and CCl₄ begin.

HI gas was prepared by the action of distilled water on a mixture of 4 gms. of red phosphorus and 20 gms. of iodine crystals. The gas was purified by passing through glass beads with moist red phosphorus and a U-tube containing fused calcium chloride.

The vapour pressure of CCl₄ was sufficient for the purpose. HCl gas was prepared by the ordinary method of adding conc. H_2SO_4 on pure sodium chloride. Argon was taken from a storage cylinder. Different initial pressures of 1 cm., 2 cm. and 4 cm. of the absorbing gases were taken and increasing amounts of foreign gas added from time to time. After each addition photographs were taken of the absorption spectrum. The spectrograph used was an E_1 spectrograph with high dispersion.

Intensity measurements were carried out by means of a Zeiss photo-electric recording photometer and absorption co-efficients calculated. The spot of light of the photometer was allowed to run along the breadth of the different spectra along a particular wavelength. The absorption co-efficients at that particular wavelength were determined for the various spectra, each of which was modified to a different amount due to the presence of various amounts of foreign gases.
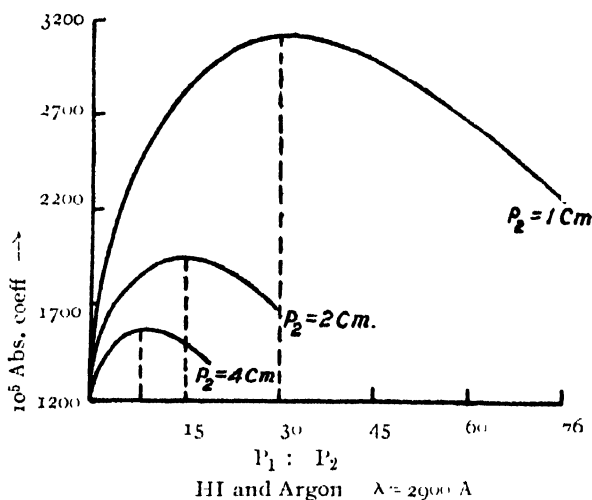
Fig. 1

RESULTS AND DISCUSSION

In the figure P_2 is the pressure of the absorbing gas and P_1 that of the foreign gas, so that P_1/P_2 denotes the ratio of the foreign gas quantity to the absorbing gas quantity.

It would be observed from the graph that in the case of mixtures of both HI and argon, and HI and HCl, the absorption co-efficient α increases

HI and HCl $\lambda = 2900$ Å
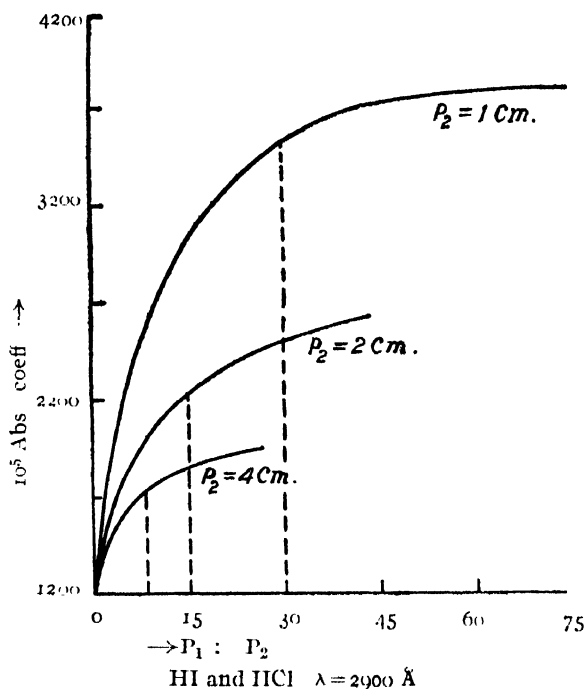
FIG. 2

with $P_1 : P_2$ value   , as the amount of the foreign gas is increased. One must remember here that the quantity of the absorbing gas is always the same along any one graph. To say that the absorption co-efficient increases at a particular wavelength is the same as saying that the absorption limit shifts towards the longer wavelength side. So the experimental results show (*vide* introduction) that collisions or electric field help in dissociation and give the amount of change suffered.

We find that with HI, the maximum with argon mixture or the saturation point with HCl mixture occurs at values of P_1/P_2 equal to 30, 15 and 7 when P_1 is equal to 1, 2 and 4 cms. This means that the maximum or the saturation point occurs at the partial pressure of the foreign gas equal to 30 cms. without any regard to the quantity of the initial gas present. It means that the number of collisions suffered by one absorbing gas molecule with the foreign gas molecules is a fixed quantity to give the maximum or the saturation point, no matter what the initial absorbing gas or the nature of the colliding partners may be. The total change in the absorption spectra which is determined by the perturbation suffered in the energy levels of a molecule is a quantity which is thus mainly determined by the number of collisions per sec. of each molecule with the foreign molecules. The maximum change in the absorption co-efficient in the case of the mixture HI and HCl is, however, greater than that in the case of the mixture of HI and argon. This is due to the fact that HCl is polar and argon is non-polar. One HCl molecule can, at the time of collision, disturb to a greater extent, the molecular equilibrium, due to its extra facility of possessing an electric

moment. We have further, observed that the P_1/P_2 curve becomes more and more steep as the pressure of the absorbing gas is decreased. For example, we have obtained for HI + HCl mixture that with $P_1/P_2 = 1$, the change in α-value (from that when $P_1, P_2 = 0$) becomes equal to 800×10^{-5} units for $P_2 = 1$ cm., 300×10^{-5} units for $P_2 = 2$ cms. and 100×10^{-5} units for $P_2 = 4$ cms. Thus the observed change in the absorption co-efficient for 1 cm. gas pressure is about double the change in absorption co-efficient for 2 cms. gas pressure (Figs. 1 and 2). Considering the fact that the absorption co-efficient or their changes have been obtained from the relation $\log I - \log I_0 = \alpha\, x.P_2$, we see that the change in α has also been obtained under the implied condition of division by P_2. Hence the total change introduced in the absorption co-efficient due to molecule tend to remain of the same value. It means that the molecular effect on the change of absorption co-efficient is not very widely variable with initial gas pressure. We have also to note here the peculiar characteristic of a maximum for 'α' with argon as foreign gas on HI. An HI molecule under collision with another HI molecule will be more influenced as compared to the case when under a collision with an argon molecule (due to polar nature of HI). The result indicates that due to large number of HI-argon collisions, some of the HI-HI collisions tend to become somehow ineffective and thus to decrease the absorption co-efficient value. The exact mechanism, however, cannot be clearly seen at present, for it goes against the principle of the kinetic theory. Lastly, considering the case of HI-argon with the hypothetical case of HI-HI, we note that if argon and HCl, by their collision, change the absorption co-efficient value, HI-HI collisions would also tend to change the α value. Let us consider that in 2 cms. of HI gas, 1 cm. acts as the absorbing material and the remaining 1 cm. only as colliding molecule, as with the cases considered in the present set of investigations. Since with 1 cm. HI and 1 cm. of any colliding gas like argon or HCl, the α value suffers a change from, say, 1200×10^{-5} units to about 1800×10^{-5} units, we should expect a value of the same order with HI colliding molecules also. But due to Beer's law, the total change in α-value must be from 1200×10^{-5} to 2400×10^{-5} units, so that we get that in the case of the pure gas like HI, a fairly large percentage of the absorption is due to collisional processes. Perhaps on a more detailed study, one can analyse the different contributing causes of Beer's law more quantitatively.

Results indicated that HCl has no effect on the absorption spectrum of CCl_4. Such results have also been observed by Harding (1936) and Schneider (1937) in the case of I_2 and O_2 which are also non-polar as CCl_4.

PHYSICS DEPARTMENT,
DACCA UNIVERSITY.

R E F E R E N C E S

Frank, F. C., 1927, *Zeits. fur. Physik*, **44**, 507.
Dutta, A. K., 1932, *Zeits. fur. Physik*, **77**, 404.
Harding. 1936, *Phil. Mag.*, **21**, 773.
Schneider. 1937, *Jour. Chem. Phys.*, **5**, 106.

ELASTO-VISCOUS EFFECT IN SHELLAC

By SADHAN BASU

ABSTRACT. Elasto-viscous properties of T. N. shellac as well as partially polymerised samples have been measured. The total extension has been found to be due to three distinct processes (1) true elastic deformation, (2) delayed elastic deformation and (3) a viscous flow Explanation of these various processes has been given by attributing an iso-colloidal structure to shellac. Calculation of the relaxation time has shown that the dispersed phase consists of micelles formed due to secondary forces between the molecules. The dispersion medium consists of monomeric particles

On partial polymerisation, the polymeric products have been found to form a part of the dispersion medium, increasing the viscosity of the same

The low value of extension has been explained as due to granular nature of the micelle.

INTRODUCTION

The deformation phenomenon under applied stress has aroused considerable interest in recent years owing to its great technical importance. This has been particularly so in the case of a number of natural and synthetic high polymers, *viz.*, rubber (Kolecko, Kuvshinsky and Gurevitch, 1937), cellulose and its derivatives (Heimann, 1937, 1938 ; Leaderman, 1941), methyl methacrylate (Robinson, Ruggy and Slautz, 1944), polyethylene and polyvinyl chloride-acetate resins (Diemes and Klemm, 1946), etc. The results obtained from measurements on these substances led to the conclusion that there is some sort of internal structure which may be either amorphous or polycrystalline, the individual peculiarities being due to the randomness of the orientation of the constituent units, the diversity of chemical composition and the effective forces between the molecules. In fact, deformation measurements have given us a new tool, though not fully developed yet, for studying the structure of these substances in the solid state. With a view to getting an insight into the structure of shellac in the solid state, deformation measurements have been done on this substance, the results of which are reported in the present paper.

THEORETICAL

Towards the beginning of the present century, it was recognised by Trauton and Rankine (1904) that the deformation in a plastic solid is very composite in nature, being made up of true elastic deformation, usually followed by a delayed elastic displacement and a viscous flow that increases linearly with time.

where F = the stress on the specimen, l and A respectively the length and cross section of the specimen and S = velocity of separation of the ends of the specimen. As the elongation is very small, being 1% at the utmost, change in cross section due to this may be neglected.

The activation energies for relaxation process and viscous displacement are obtained by multiplying the slopes of the curves $\log \tau - \frac{1}{T}$ and $\log \eta - \frac{1}{T}$ respectively, by 2.3R ($= 2.3 \times 1.8$) (Robinson, Ruggy and Slantz, *loc. cit.*).

APPARATUS

The necessary apparatus for this study was made in the Institute workshop. It consisted essentially of an iron frame. One end of the test specimen was clamped at the other end of the frame and another clamped to a small block with a hook for carrying weights. A sharp needle was attached to the lower end of the test specimens. The elongation of the specimen, when suitable weights were suspended from the hook, was noted by viewing the needle with a vernier microscope.

For measurements at different temperatures, the whole apparatus was placed inside an incubator with a glass door. (The temperature which was below 50°C was attained by means of suitable electric bulbs). The system was left in the incubator for 8 to 12 hours and when thermal equilibrium was established, suitable loads were applied and the movement of the pointer was observed through the glass door.

The most difficult part of the experiment was the clamping of the test specimen. Since shellac is very brittle, the specimen cracked during clamping and often quite a number of trials were necessary to get the specimen rightly clamped.

If the conditions for preparing the specimen remain the same, results obtained are reproducible within 5 to 10%. In view of the great difficulty of ensuring identical conditions in the preparation of the moulded specimens this amount of deviation may not be considered too much.

Preparation of the specimen.—The specimens were prepared in the form of thin strips having the following dimensions :

Length	...	... 11.5 cm.
Breadth	...	... 1 5 cm.
Thickness	...	... 0.1 cm.

Shellac was heated to 100° in a glycerine bath and kept at that temperature for 2 minutes, and then poured into a hot mould (80°C), having the above dimensions. The mould was then closed and 5 Kg. pressure applied for 1 minute. The strip was taken out after the mould had cooled to room temperature.

In making test pieces of polymerised shellac, strips were first prepared as above and, while still inside the mould, heated to some higher temperature

and kept at that temperature sufficiently long to bring about polymerisation. Great difficulty was encountered in taking out the polymerised strips, since they used to crack easily. It was found possible to prepare only two specimens with partially polymerised shellac by keeping the specimens at 110°C for 4 and 6 hours. Even then they often used to break easily. Strips made of shellac, polymerised in presence of chemical reagents, *e.g.*, ammonium chloride, tartaric acid, citric acid, oxalic acid, etc., had a notched blistery surface and hence were not used for deformation measurements. Further, it was not possible to prepare a strip with dewaxed shellac, hence T. N. lac was used throughout the work.

RESULTS

The results of elongation measurements with shellac strips at three different temperatures are given in Table I and the corresponding graphs in Fig. 2.

TABLE I

(Load 5 Kg.)

Time in min	Elongation in cm		
	22.5°C	32°C	35°C
0	0.050	0.081	0 106
1	0.063	0 144	0 179
2	0 069	0 194	0 256
3	0.077	0.235	0.321
5	0.086	0.289	0.393
10	0 096	0.347	0.463
15	0 106	0.407	0.544
20	0 119	0 463	0.618
25	0.132	0.519	0.691
30	0 142	...	0.764
35	...	0.564	...

As explained in the paragraph on " the method of calculation," these data were used in constructing Table II and the graph log $\delta - t$.

TABLE II

t (time in min.)		δ	$\log \delta$	τ (min.)
Temp. 22 5°C	0	0.025	-1.6021	..
	1	0.015	-1.8239	..
	2	0 009	-2.0458	5 26
	3	0 005	-2.2840	..
Temp. 32°C	0	0.16125	-0.7924	..
	1	0 09694	-1.0135	...
	2	0 05620	-1.2502	4 50
	3	0 03467	-1.4600	
Temp. 35°C	0	0 2257	-0.6463	.
	1	0.1291	-0.8890	..
	2	0 0747	-1.1267	4 12
	3	0.0413	-1.3844	

Relaxation times τ, as calculated from the slope of the $\log \delta - t$ curves, are also given in the above Tables. Log τ was then plotted against the reciprocal of absolute temperature, and from the slope of the curve so obtained activation energy for relaxation calculated.

TABLE III

Sample	Temp. (°C)	τ (min.)	η (pois) $\times 10^{-9}$	Activation energy (K-cal)	
				Relaxation	Viscous flow
Unpolymerised ...	22.5	5 26	10 520	...	..
	32.0	4.50	2 137	3 118	29 54
	35.0	4.12	1.327	...	..
Heated for 4 hrs. at 110°C	22.5	5 10	93.960		..
	35.0	4.66	10.790	3 410	34.85
	42.0	4.36	2.809	...	...
Heated for 6 hrs. at 110°C	22.5	4 60	187.800	...	...
	35 0	4.03	10.470	3.45	41 884
	42.0	3.80	2 719	..	...

In calculating the viscosity according to equation (3), S was determined from the constant slope line. The log of viscosity (Table VI) was then plotted against $1/T$ and the activation energy was calculated from the slope of the curve.

In the same way calculations were made by graphical method for specimens heated at 110°C for 4 and 6 hours respectively, the results being given in Table III.

DISCUSSION

The stress-relaxation phenomenon under applied external force may be understood from a consideration of the potential energy of the deformed system. In the deformed body the molecules are displaced from their normal positions against the molecular forces, as a result of which certain amount of potential energy is stored up in the system. Of the molecules so displaced, those which possess potential energy in excess over that of their neighbours are sometimes thrown out of their positions of greater potential energy into positions of smaller potential energy. If such a change of position, accompanied with loss of potential energy, occurs repeatedly, the energy of the whole system will diminish gradually, or in other words, elastic stress will relax. If the energy equilibrium requires a constant value of elastic stress, then under the action of constant external stress the relaxation of the internal stress will cause the deformation to proceed further and further, each stage of deformation corresponding to a position of new temporary equilibrium. In the case of polymeric substances where there is great heterogeniety in the nature of chemical forces, the probability of stress concentration at one particular type of bond or molecule is less and consequently the stress-relaxation will be an almost general phenomenon in these cases.

The molecular significance of this type of behaviour may be given as follows. The immediate effect of the application of a shearing stress is to bring about an extension of the Van der Waal's bonds between the units. After sometime, however, certain portions will yield under the applied stress and begin to move. The relaxation time of 5.26 minutes for shellac at 22.5°C under a force of 5 Kg. shows that the moving portions are fairly big. Presumably these consist of highly entangled clusters of molecules which are slowly disentangled and parallelised. This provides for the retarded elastic deformation. Superimposed on this type of deformation, there is a movement of certain loose and poorly organised portions, which greatly predominates when the disentanglement is complete. This process is responsible for viscous flow, finally leading to the rupture of the specimen.

To give a concrete shape to the above picture, we may attribute to shellac a sort of structure similar to that assumed for phenol plastics by Kozlov (1939). The resin, according to this view, may be supposed to consist of two phases, namely, a highly aggregated dispersed phase and a monomeric

dispersion medium. The slow motion of the dispersion medium under applied stress through and past the micelle (aggregated dispersed phase) is responsible for viscous flow, while the extension of Van der Waal's bonds between the clusters and the disentanglement of the same are responsible for true and retarted elastic deformation. Activation energy of 3.118 K-cal/mole only for disentanglement suggests that the aggregation is due to secondary type of forces. In other words, shellac may be looked upon as a loosely knotted system, giving a three dimensional structures due to secondary force, soaked in a highly viscous liquid.

Coming to the case of polymerised shellac, it is remarkable that while the effect of polymerisation on viscosity and activation energy for viscous flow is quite considerable the effect is but slight on the relaxation time and the activation energy for disentanglement. This can be explained on the assumption that there is a equilibrium between the monomeric dispersion medium (M) and the aggregated dispersed phase (M*)

$$M \rightleftharpoons M* \ ,$$
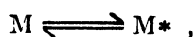
the course of polymerisation being

$$M \rightleftharpoons M* \rightarrow Mp,$$

where Mp is the polymerised product.

As the substance polymerises the reaction proceeds from left to right, and as a result more of the monomer aggregates to form clusters. If therefore the polymerised specimen may be supposed still to consist of a dispersion phase and a dispersed phase, the first phase containing the monomers and the polymers, and the second phase the aggregated clusters, it would follow that the disentanglement process would remain practically the same and hence also the time of relaxation. The inculsion of the polymerised product in the dispersion medium would result in an increase in the viscosity of the dispersion medium. When, however, polymerisation is allowed to proceed much further than has been attained in the present experiment, three-dimensional structure develops, the study of which would call for entirely new types of measurements.

As is seen from Table III the temperatnre co-efficient of viscosity is greatly increased on polymerisation. This may be attributed to a difference in the intermolecular forces between the monomer and the polymer, the bonds of which, being of the secondary type, are broken easily due to increased thermal agitation.

REFERENCES

Alexandrov and Lazurkin, 1940, *Acta Physicochemia*, **12**, 647.

Diemes and Klemm, 1946, *J. App. Phys.*, **17**, 467.

Helzmütter and Jenkel, 1940, *Zeit. f Physik Chem* , A**186**, 359.

Herman, 1937, *Kolloid-Z.*, **81**, 143 ; 1938, *ibid.*, **83**, 71.

Kistler, 1940, *J. App. Phys* , **11**, 773

Kolecko, Kuvshinsaky and Gurevitch, 1937, *Tech Phys. U S S.R.*, **4**, 622.

Kozlov, 1939, *Trans. Symp on Organ. Chem of Acad. Sci* , *U S S R.*, p 91

Leaderman, 1941, *Textile Research*, **11**, 171.

Maxwell, 1868, *Phil. Mag.*, **5**, 1934.

Robinson, Ruggy and Slautz, 1944, *J. App. Phys* , **15**, 343

Simha, 1943, *J. Phys. Chem* , **40**, 416

Taylor and ors., 1937, *Soc Glass Tech.*, **21**, 61

Trauton and Rankine, 1904, *Phil Mag* (**6**) **9**, 538

RAMAN SPECTRA OF SUBSTITUTED ARSENIC ACIDS

By JAGANNATH GUPTA and MRITYUNJOYPROSAD GUHA

ABSTRACT. The effect of progressive substitution of oxygen atoms in the arsenate ion $[AsO_4]'''$ by methyl groups has been studied. The spectrum of methyl arsenate ion $[(CH_3)AsO_3]''$ reveals that a tetrahedral skeleton is maintained, the symmetry being C_{3v}. The spectra of normal and secondary arsenates have been re-examined. The spectra of the secondary arsenate ion $[(OH)AsO_3]''$ and of the methyl arsenate ion $[(CH_3)AsO_3]''$ show similar structural symmetry. Approximate force constants have been calculated according to the central force system. Bond strengths of As—C and As—O appear to be alike in the substituted arsenates.

INTRODUCTION

The present work was undertaken some time ago to study the effect of suitable and progressive substitution of the oxygen atoms in the arsenate ion $[AsO_4]'''$ by units of masses virtually equal to that of oxygen itself (Guha, 1941), but had to be abandoned for the present before completion owing to unfavourable circumstances. It was, however, realized that some new and interesting data, together with a solution of apparently conflicting reports on arsenates in some older publications have been obtained, which are therefore reported in the present communication notwithstanding their evidently limited scope.

Striking differences are observed in the results reported by several workers on the Raman spectrum of the simple arsenate ion $[AsO_4]'''$, as can be seen from the following comparison :—

Authors	Raman frequencies of sodium arsenate (solution)
Nisi (1929)—	837
Ghosh and Das (1932)—	349, 462
Fehér-Morgenstern (1937)—	342(*w*), 398(*m*), 810(*s*)
Mitra (1939)—	348(*w*), 460(*w*), 837(*s*), 876(*vw*)

It was thus thought desirable at the outset to re-examine the spectra of normal arsenate and secondary arsenate (also known commercially as arsenate) with some care. The results, it will be seen, have generally confirmed the work of Fehér and Morgenstern. Substitution of oxygen by methyl group (CH_3) was then introduced, giving methyl arsinic and cacodylic acids respectively, whose relative acid strengths are comparable to that of

arsenic acid itself. The main subject of study was the nature of changes in the skeletal vibrations and their significance, taking the CH_3 group as an approximate mass point nearly equal in weight to that of an oxygen atom. These skeletal vibrations, in view of the large mass of the central atom, are all to be expected below 1000 cm^{-1}, the larger ones being either valence or bending vibrations of hydrogen atoms against heavier nuclei.

EXPERIMENTAL

The solutions of the different substituted arsenic acids and their respective salts were prepared as detailed below. Mercury 4358Å was utilized as the exciting line and the spectra were recorded on Ilford Golden Isozenith plates with an exposure of about 40 hours in each case.

Methyl arsenic acid, (CH_3) $AsO(OH)_2$—This was prepared by heating a mixture of methyl iodide and an alkaline solution of sodium arsenite according to the method of Quick and Adams (1922). The product so obtained was carefully purified by dissolving in a small bulk of water and reprecipitating by alcohol. A 25% solution in conductivity water was prepared and repeatedly filtered through quantitative filter paper until the solution was optically clear.

A 30% solution of sodium methyl arsenate was obtained by dissolving the acid in two equivalents of sodium hydroxide solution and then repeatedly filtering through a quantitative filter paper.

Dimethyl arsenic acid (cacodylic acid), $(CH_3)_2AsO(OH)$—A 50% solution was prepared by dissolving Merck's pure sample of the acid in conductivity water and then filtering as before.

A 50% solution of potassium dimethyl arsenate was obtained by dissolving the acid in one equivalent of potassium hydroxide.

Secondary and normal arsenates, K_2HAsO_4 and K_3AsO_4—A saturated solution of secondary potassium arsenate was obtained by dissolving Merck's pure sample in conductivity water. The normal arsenate solution was prepared by carefully neutralizing the solution of the secondary arsenate with the calculated amount of potassium hydroxide.

An experiment was then arranged to qualitatively determine the polarization of the lines. Sodium methyl arsenate and dimethyl arsenic acid solutions were examined. The mercury arc and the condenser were placed at a distance of about 2 ft. from the Wood's tube to reduce error due to obliquity of the incident beam. The plane window of the Wood's tube was coated with black paint leaving a rectangular aperture measuring 5mm × 2mm in the middle. The image of this window was then focussed on the slit of the spectrograph and a Wollaston double-image prism was interposed to vertically separate the image. The polarization photographs were taken with an exposure of about 40 hours on Ilford Golden Isozenith plates.

The results are shown in the Table I.

TABLE I

Methyl arsenic acid (25% soln.)	Dimethyl arsenic acid (50% soln.)	Sodium methyl arsenate (30% soln.)	Potassium dimethyl arsenate (50% soln.)	K_2HAsO_4 (sat. soln.)	K_3AsO_4 (soln.)
107 (½)					
	218 (3)D		220 (4)		
235 (1)	256 (2)	250 (1)D	273 (1)	315 (3)	328 (1)
				380 (3)	400 (1)
353 (½b)	332 (2b)D	367 (2)D	353 (2b)		
	619 (10)P	613 (5)D	615 (10)		
643 (5)	663 (5) D		656 (5)	697 (1)	820 (8b)
	754 (2)p		833 (2)	830 (10)	
803 (3b)	888 (2)p	810 (5b)p	892 (2)		
	1290 (1)		1288 (2)		
1442 (6)	1421 (3)D	1460 (10b)	1417 (3)		
2950 (1)	2950 (4)P	2925 (2)P	2950 (4)		
3030 (½)	3030 (2)D	3010 (1)	3022 (1)		

P—polarized, *p*—partially polarized, D—depolarized. (Figures within brackets indicate the relative intensities of the Raman lines).

DISCUSSION

It will be seen from the Table that the results obtained for both secondary and tertiary arsenates confirm generally those reported by Fehér and Morgenstern. Apparently a confusion might have been made between sodium arsenate of commerce, which is in fact the secondary salt Na_2HAsO_4 giving rise in solution to $[(HO)AsO_3]''$ ions, and the tertiary salt Na_3AsO_4, which, being deliquescent and highly soluble in water, cannot be easily crystallized and is best prepared in solution by direct neutralization.
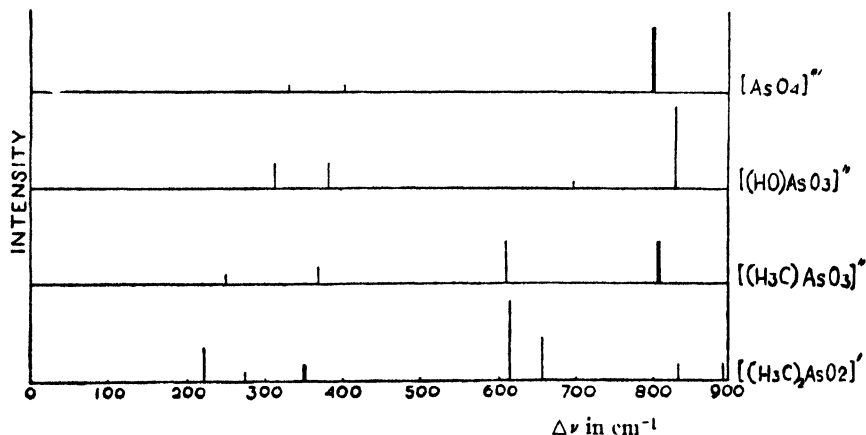
FIG. 1

Graphical representation of Raman frequencies below 1000 cm^{-1}

The presence of only *three* lines instead of *four* in the spectrum of the tetrahedral $[AsO_4]'''$ ion is believed by the present authors to arise from accidental degeneracy of the ν_1 and ν_3 frequencies. The degeneracy is theoretically derivable for a tetrahedral molecule XY_4 in the case where $m_X \gg m_Y$ (Hibben, 1939).

It will be evident from a comparative study of the skeletal vibrations in the Fig. 1 that a replacement of one of the oxygen atoms by an (OH) group forming the secondary arsenate ion $[(HO)AsO_3]''$ disturbs the symmetry with consequent change in the spectrum. The presence of only *four* frequencies with a similar, if not the same, distribution of relative intensities indicates that the tetrahedral structure of the ' skeleton ' remains intact and the symmetry is C_{3v}. In the methyl arsenate anion $[(H_3C)AsO_3]''$, the involved reduction of symmetry is similar, though opposite in the sense that the group (CH_3), unlike (OH), is lighter than oxygen which it replaces. Its spectrum, instead of being that of a symmetrical top having *six* frequencies, shows only four Raman lines of which all but one are depolarized, leading to the conclusion that the tetrahedral skeleton is still maintained, the symmetry again C_{3v}, and that the relative bond strengths of As—C and As—O bonds are essentially the same.

For the purpose of comparison, an approximate calculation of the valency and deformation forces of the anions $[AsO_4]'''$, $[(HO)AsO_3]''$ and $[(H_3C)AsO_3]''$ has been made using the central force system as applied to tetrahedral molecules of the type XY_4. It has been assumed that for normal arsenate, $\nu_1 = \nu_3 = 800$, $\nu_2 = 328$, $\nu_4 = 400$; for secondary arsenate, $\nu_1 = 830$, $\nu_3 = 697$. $\nu_2 = 315$, $\nu_4 = 380$. The results are given below, along with those for sulphate and similarly substituted anions derived from sulphate for comparison (Gupta and Majumdar, 1941).

Ion	$f \times 10^5$	$f' \times 10^5$	Ion	$f \times 10^5$	$f' \times 10^5$
$[AsO_4]'''$	3.5	0.6	$[SO_4]''$	4.6	1.1
$[(HO)AsO_3]''$	3.0	0.9	$[(HO)SO_3]'$	4.5	1.5
$[H_3C_1AsO_3]''$	3.1	0.8	$[(H_2N)SO_3]'$	4.9	1.3

The effect of introduction of the second methyl group is much more pronounced, as is shown in the spectrum of the cacodylate ion $[(CH_3)_2AsO_2]'$. A tetrahedral molecule of the type AX_2Y_2 (symm : C_{2v}) has nine frequencies, all supposed to be Raman-active, of which three are polarized. As usual, all the nine frequencies could not be recorded. But the spectrum of the cacodylate ion shows that out of the seven lines recorded, three are polarized, the rest completely depolarized as required by the theory.

ACKNOWLEDGMENT

REFERENCES

Fehér and Morgenstern, 1937, *Z. anorg. Chem.*, **232**, 169.
Ghosh and Das, 1932, *J. Phys Chem.*, **36**, 589.
Guha, 1941, *Science and Culture*, **7**, 315.
Gupta and Majumdar, 1941, *J Ind. Chem. Soc* , **18**, 457.
Hibben, 1939, Raman Effect and its Chemical Applications, p 102
Mitra, 1939, *Ind. J. Phys.*, **13**, 391.
Nisi, 1929, *Japan J. Phys.*, **5**, 119.
Quick and Adams, 1922, *J. Amer. Chem Soc.*, **44**, 805

A SPECIFIC GRAVITY BALANCE

By P. C. MAHANTI* and S. P. BHATTACHARYYA

ABSTRACT. The paper describes the details of a balance designed to indicate directly up to the 4th place of decimal the specific gravity of liquids and solutions The balance is as quick in operation as a common hydrometer used in industrial practice

INTRODUCTION

It is well known that the common hydrometer in different forms is universally used in industrial practice for the determination of specific gravity of liquids and solutions because of its simple construction and quick operation. It is, however, limited in its accuracy and in most cases it indicates the specific gravity correctly up to only the second place of decimal. If higher accuracy is desired, the stem of the hydrometer has to be made sufficiently long even for a narrow range of specific gravity commonly occurring. The object of the present investigation was therefore to design a specific gravity balance which would admit of greater accuracy in such determinations without sacrificing the advantages of a common hydrometer.

CONSTRUCTIONAL FEATURES AND WORKING

The specific gravity balance which has been designed is based on the principle of variation of weight of a sinker of constant volume when immersed in different liquids and solutions. The main features of the balance, shown in the accompanying figure, are the following : The longer arm of the balance, which is of uniform cross-section, is marked off in ten equal divisions from the fulcrum with the help of a travelling microscope. It has at its end a plated steel knife edge on which rests the stirrup carrying the hook. From the hook a glass sinker is suspended by means of a fine platinum wire to minimise the error due to surface tension. The sinker is weighted by the introduction of mercury into it. The shorter arm of the balance is provided with three adjustable screws for obtaining the equilibrium of the balance during adjustment when a sinker of a given weight is suspended from the other. At the end of this arm a pointer is attached which in its turn is placed against a mirror with an index mark over it. The fulcrum of the balance rests upon a beam which can be raised or lowered by means of an

eccentric wheel, attached to the bottom side of the base, which is also fitted with three levelling screws. The balance is enclosed in a suitable case in the usual way.

(a)

Scale ⅛"=1" Full Size
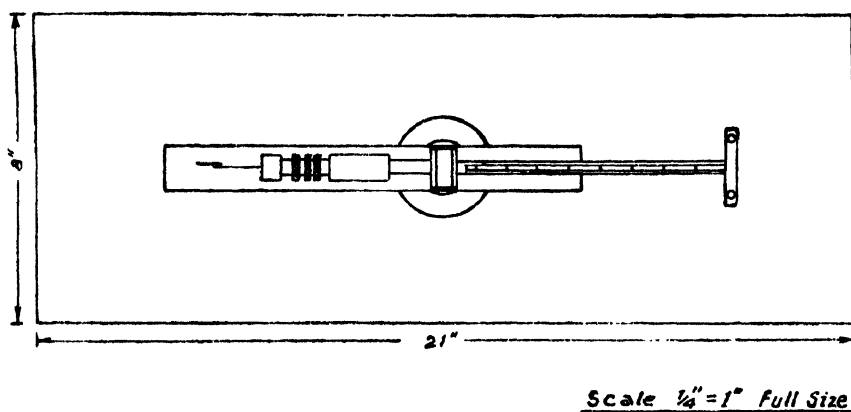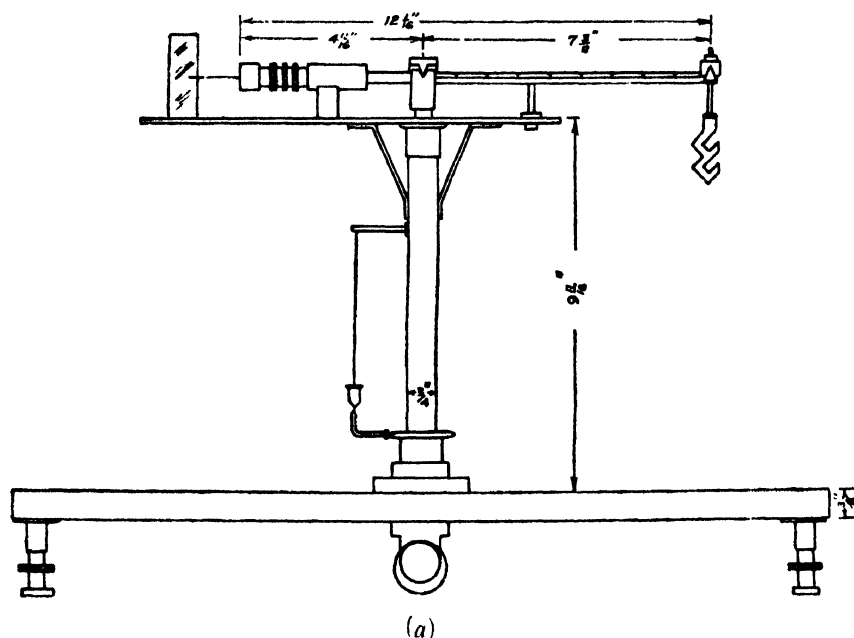
(b)

FIG. 1

Specific gravity balance (a) Elevation (b) Plan

The balance is provided with a set of four riders, namely R_1, R_2, R_3 and R_4 of German silver wire. Their weights are so chosen that R_2/R_1, R_3/R_1 and R_4/R_1 have values of o.1, o.o1 and o.oo1 respectively. With the help of these riders and with the given weight of the sinker, the specific gravity up to a value of unity can be measured by the balance. A duplicate of the heaviest rider (R_1) is, however, necessary if the value of specific gravity lies between 1 and 2. It may be noted here that if it is necessary to measure

specific gravity of still higher values, the above sinker is to be replaced by another having the same volume but different weight.

The actual value to be assigned to each rider is of importance and forms the special feature of the balance. In order that the positions of the riders on the longer arm of the balance when in the equilibrium condition, may indicate directly the specific gravity of a liquid in which the sinker is immersed, the heaviest rider (R_1) should have its weight in grammes numerically equal to the volume of water in c.c. displaced by the sinker when immersed in distilled water up to a predetermined mark at a given temperature. Thus once the weight of the rider R_1 is ascertained, it is very simple to fix the weight of the other riders. In the present balance we have the following data—

Weight of the sinker ... ... 9.2304 gm.

Volume of water displaced by the sinker at a room

temperature 32°.4.C ... ... 6.0800 c.c.

Hence $R_1 = 6.0800$ gm. ; $\qquad R_2 = 0.6080$ gm.

$R_3 = 0.0608$ gm. ; $\qquad R_4 = 0.00608$ gm.

All weighings were done on a set of accurate balances available in the institute. The sinker and the heavier riders were weighed on an accurate chemical balance having a sensitivity of 0.00001 gm., while the lighter riders on a micro-balance.

The equality of the interval between successive scale marks on the longer arm of the balance and the correctness of the weights of the different riders were checked from the principle of moments. For the first purpose, three additional riders, two of weights $2R_2$ each and one of weight $5R_2$ were prepared. The rider R_1 was placed successively at each scale mark from the fulcrum. For each position of the rider R_1, the equilibrium condition of the balance was first obtained with R_1 in position and then by removing R_1 and placing riders of suitable multiple weights of the rider R_2 at the terminal knife edge. Besides ensuring the equality of the divisions, it also proved the correctness of the weight of riders R_1 and R_2. A similar procedure was adopted to check the weight of the other riders.

It is evident that at the above temperature the true specific gravity of a liquid will be indicated correctly by the balance. But when the temperature during observation is different from the above temperature, a correction is necessary to take into account the change in volume of the sinker. If S_1 and S_t be respectively the specific gravity indicated by the balance and true specific gravity of a liquid at $t°c$ and if V_t be the volume of the liquid displaced by the sinker at $t°c$, then

$$S_1 = \frac{\text{weight of the volume of liquid displaced by the sinker at } t°c}{\text{weight of the volume of liquid of unit density displaced}}$$

by the sinker at 32°.4C.

$$= \frac{V_t\, S_t}{6.08 \times 1}.$$

$$\therefore\ \ S_t = \frac{6.08}{V_t}.S_1$$

$$= \frac{6.08}{6.08[1 + \gamma(t - 32.4)]}.S_1$$

$$= [1 - \gamma(t - 32.4)].S_1$$

where γ is the co-efficient of cubical expansion of glass and may be taken to be 24×10^{-6}.

Thus the true specific gravity of a liquid at any temperature can be calculated from the above equation whenever higher accuracy is desired.

TEST DATA

In order to check the working of the balance and the accuracy obtainable, the specific gravity of a number of pure organic liquids and solutions of a few inorganic salts in water at varying concentrations were measured with its help as well as by means of a specific gravity bottle. In the latter case all weighings were done with the chemical balance which was used previously to measure the weight of the sinker and the heavier riders. During each observation the temperature of the liquid or solution used was noted and their specific gravity as indicated directly by the balance was corrected, if necessary, to obtain their true specific gravity. The value of their specific gravity obtained by the specific gravity bottle method was also corrected for temperature. The two sets of values are included in the following tables for comparison.

TABLE I

Organic Liquids and Oil

Name of Sample	Temp. (°C)	True specific gravity by		Error
		Sp. gr. bottle	Sp. gr. balance	
Aniline	32	1.0230	1.0231	+0.0001
Amyl acetate ...	32	0.8596	0.8597	+0.0002
Transformer Oil ...	32	0.8447	0.8449	+0.0002

TABLE II

Potassium Bromide Solutions of different concentrations

Samples	Temp (°C)	True specific gravity by		Error
		Sp. gr. bottle	Sp. gr balance	
1	34 0	1.3626	1 3624	−0.0002
2	34.0	1 3050	1.3048	−0.0002
3	34.0	1 2828	1.2826	−0.0002
4	34.0	1 2146	1.2147	+0.0001
5	34.0	1 1950	1 1948	−0.0002
6	34.0	1 1833	1 1835	+0.0002
7	29.6	1.1025	1.1026	+0.0001
8	29.6	1.0978	1.0976	−0.0002
9	29.6	1 0641	1.0639	−0.0002
10	29.6	1.0286	1.0288	+0.0002

TABLE III

Copper Sulphate Solutions of different concentrations

Samples	Temp. (°C)	True specific gravity by		Error
		Sp. gr. bottle	Sp gr balance	
1	33 6	1 1994	1 1992	−0.0002
2	33 6	1.1713	1.1715	+0.0002
3	33 6	1 1305	1.1303	−0.0002
4	33 6	1.0961	1 0962	+0.0001
5	34 0	1 0230	1 0228	−0.0002

It is easily seen from the above tables that in no case the value of specific gravity found with the help of the present balance differs by more than ±0.0002 from its value determined by the specific gravity bottle method. On the other hand it does not take more than a few seconds to complete the measurement with this balance, which can be easily constructed and set up in any laboratory.

INSTRUMENTS DESIGN LABORATORY,
DEPARTMENT OF APPLIED PHYSICS,
UNIVERSITY COLLEGE OF SCIENCE AND TECHNOLOGY,
CALCUTTA.

CHANGES IN THE ORIENTATIONS OF THE PRINCIPAL MAGNETIC AXES OF SINGLE CRYSTALS OF THE IRON GROUP OF SALTS WITH VARIATION OF TEMPERATURE*

By AKSHAYANANDA BOSE

ABSTRACT In most of the crystals studied by the author the orientations of the principal magnetic axes were found to change very little with temperature In a few cases the changes were large and are obviously to be attributed to changes in the relative orientations of the different paramagnetic groups present in the unit cell of the crystal, due to the fact that the binding between such groups is comparatively weak The individual members of the paramagnetic groups are bound much more firmly so that these groups persist even in the state of solutions and in consequence the electric field axes associated with each group do not change.

INTRODUCTION

In the course of the investigations on the magnetic behaviour of single crystals of the salts of the iron group it was observed that in a few of the crystals the principal magnetic axes had a tendency to change their orientations when the crystals were subjected to a variation of temperature. Such variations have earlier been observed also by Bartlett (1932) who worked within a limited range of temperatures from about $+50°$ to $-50°C$, for almost all the crystals studied by him. Though a very large number of crystals were investigated by the present author over a large range of temperature and also later by some of his colleagues, they never found any such change for crystals in which the position of the principal magnetic axes are fixed uniquely from crystal symmetry such as the tetragonal, trigonal, hexagonal or rhombic classes as is only to be expected. Even in the triclinic crystal $CuSO_4,5H_2O$ (Krishnan and Mookherji 1938) no such change was observed. Appreciable changes were found only in a few exceptional cases of monoclinic crystals and the present paper deals with the nature and the probable cause of these variations.

METHOD AND RESULTS

The method of observing the settings of the crystal in a magnetic field and their variations is the same as has been used in this laboratory in connection with the measurements of anisotropies of single crystals (Krishnan,

---

* Part of a thesis approved for the D.Sc. degree of the Dacca University.

Mookherji and Bose, 1939). It is obvious that when a crystal is suspended in a homogeneous horizontal magnetic field with a fine quartz fibre from a torsion head, with one of its principal magnetic axes vertical, the other two principal axes will tend to set along and perpendicularly respectively, to the magnetic field, and will actually do so when the torsion head has been adjusted so that there is no torsion on the fibre.

To observe the variations of the orientations of the horizontal axes of the crystal with temperature it was put in a cryostatic device in which any temperature between 300°K and 80°K can be attained and maintained steady (Bose, 1940, 1946). The changes of the orientation of the crystal were noted with the help of an index attached near the middle part of the suspending system, just outside the cryostat chamber, as has been described in these papers. When such changes were observed at different temperatures the torsion head was turned until on putting on the magnetic field there was again no torsion on the fibre, *i.e.*, the crystal had again freely set with its new position of the maximum susceptibility axis along the field. The amount of rotation on the torsion head gives us the change of orientation of the axis. The observations on ten monoclinic crystals were taken by the author at various temperatures between 300°K and 80°K and the results are tabulated in the following tables. The notations adopted are the same as in our earlier papers. The results are for suspensions of the crystals with " *b* " axis vertical.

TABLE I*

For changes of setting in the Magnetic Field

Crystal	Total change in the direction ψ, of χ_1 on passing from 300°K to 80°K
$NiSO_4$, $(NH_4)_2SO_4$, $6H_2O$	$-14°$ to $-19°.25$
$NiSO_4$, K_2SO_4, $6H_2O$	$-12°5$ to $-13°5$
$NiBeF_4$, $(NH_4)_2BeF_4$, $6H_2O$	$-14°.3$ to $-13°.3$
$CoSO_4$, $(NH_4)_2SO_4$, $6H_2O$	$-43°2$ to $-41°.2$
$CoSO_4$, K_2SO_4, $6H_2O$	$-15°.5$ to $-13°.5$
$CoBeF_4$, $(NH_4)_2BeF_4$, $6H_2O$	$-38°1$ to $-31°.6$
$Cs_2 CoCl_4$ (Orthorhombic)	Nil
$FeSO_4$, $(NH_4)_2SO_4$, $6H_2O$	$-54°5$ to $+52°.5$
$FeSO_4$, K_2SO_4, $6H_2O$	$+58°.3$ to $+60°.3$

* The initial angle and the changes are measured in sexagesimal degrees.

A. Bose

TABLE II *

$CuSO_4$, A_2SO_4, $6H_2O$

Salts	Initial angle ψ at 300°K	Change in the direction of χ_1 axis with temp as compared with that at 300°K										
		280°	260°	240°	220°	200°	180°	160°	140°	120°	100°	80°
A = K	−77°.5	−1 1	−.9	−9	−.8	−.6	−5	−4	−3	−.2	0	0
A = NH₄	+77°.5	+3 7	+2 3	+1 3	+.8	+.7	+.5	+5	+.3	0	0	0

In the orthorhombic crystal of Cs_2CoCl_4 no changes in the orientation occurred. In addition to these the author observed in an earlier measurement (Krishnan, Mookherji and Bose, *loc. cit.*) no change in orientation in the trigonal crystals of $NiSO_4$, $6H_2O$ and $NiSeO_4$, $6H_2O$, the monoclinic crystals of $MnSO_4$,$(NH_4)_2SO_4$,$6H_2O$ and $Gd_2(SO_4)_3$,$8H_2O$. In the monoclinic crystal of ammonium chromium oxalate, however, with suspension along " b " axis a very large change of " ψ " by about 78° was observed between 303°K and 90°K.

DISCUSSIONS

In the paramagnetic crystals that we are considering, the electric field in the neighbourhood of the paramagnetic ion, which profoundly affects its magnetic behaviour, is known to arise from the negatively charged atoms surrounding the paramagnetic ion (Van Vleck, 1932 ; Bethe, 1929 ; Penney and Schlapp, 1932, etc.). It can be seen in a general way that when the atoms are densely packed, as they are in these crystals, the field should be predominantly cubic in its symmetry. Representing the potential, V, of the electron in this crystalline field as a Taylor's series about the centre of the paramagnetic ion, it can be shown that when the field is accurately cubic in symmetry the first non-vanishing terms in the series can be expressed in the convenient form,

$$V = D(x^4 + y^4 + z^4) + 3Dr^4 \qquad \ldots \quad (1)$$

in which the last term corresponding to the spherically symmetric part of the field can be omitted for convenience, since it does not disturb the relative separations of the energy levels, with which alone we are concerned here. On the other hand, if the field deviates from cubic symmetry by having a small rhombic field superposed on the cubic, the first non-vanishing terms in the expansion will be the square terms of the type,

$$V = Ax_1^2 + By_1^2 + Cz_1^2 \qquad \ldots \quad (2)$$

where $C = -(A + B)$, since every term in the potential should satisfy Laplace's equation.

* The initial angle and the changes are measured in sexagesimal degrees

In general, the x, y, z axes of this rhombic part and those of the cubic part of the field will not coincide, though for our purposes, since the field is predominantly cubic, it would be convenient and sufficient to assume that the principal axes of the two coincide. If any lower type of symmetry is specifically required to explain experimental data we shall have to construct such a field by suitably orienting the two sets of axes.

There is also another factor which complicates the problem, namely, that the unit cell of the crystal will in general, contain more than one paramagnetic ion, and the crystalline field axes, associated with the different paramagnetic ions in the unit cell, will be oriented with respect to one another. These orientations cannot be always calculated since, detailed data regarding the dispositions of the atoms round the paramagnetic ions in the unit cell, are generally unavailable.

Now, the crystalline field axes associated with each paramagnetic ion will be uniquely determined by the dispositions of the negative charges in its neighbourhood and will remain unaffected if these dispositions are not disturbed. Actually, the paramagnetic ion and the neighbouring charged atoms form a closely bound group, due to the existence of strong binding forces between them, nearly as strong as in chemical bindings; as is evidenced by the large over-all separations, of the order of 20,000 cm.$^{-1}$ of the energy levels of the paramagnetic ions, produced by the electric fields due to those surroundings charged atoms. It is natural to think that such closely bound groups and, in consequence, the large electric fields round the paramagnetic ion might persist even in the state of solution and would thus offer a satisfactory explanation of the large deviations from the "free ion" behaviour observed in the aqueous solutions of many of the salts of the iron group,-- deviations which are not only as large but of nearly the same magnitude as in the solid state.

The bindings between different such groups in the unit cell, however, may be relatively much weaker and there may, therefore, be appreciable changes in their relative positions with change of temperature. Even such changes should be very small as shown by the small thermal co-efficient of expansion of the crystals, of the order of 10^{-4} per degree, and in any case be in conformity with the symmetry requirements of the unit cell. The changes in the position of the atoms bound to the paramagnetic ion, due to changes of temperature, should be much smaller still.

Indeed, the magnetic observations themselves should offer a sensitive test of any such changes. Where the principal magnetic axes of the crystal are not determined uniquely by the symmetry of the crystal, as for example, the magnetic axes of a triclinic crystal, or the two axes in the (010) plane of a monoclinic crystal, any changes in the positions of these axes will give us a measure of the changes in the relative positions and orientations of the different paramagnetic groups in the unit cell. Experimentally it is found in the crystal of copper sulphate pentahydrate, which is triclinic and whose

unit cell contains two molecules of $CuSO_4, 5H_2O$), there is hardly any change
in the directions of the principal magnetic axes of the crystal in the tempera-
ture range studied. Again, in most of the monoclinic Tutton salts studied
by us, containing two paramagnetic ions in the unit cell, there is very little
change in the directions of the two principal magnetic axes χ_1 and χ_2 lying
in the (010) plane, on passing from room temperature to about 80°K, as will
be seen from the Tables I and II. Copper ammonium and copper potassium
sulphates, nickel ammonium sulphate and cobalt ammonium fluoberyllate are
the few exceptions where an appreciable change in the directions of χ_1 and χ_2
occurs, mostly at temperatures above 150°K. For the first three crystals
Bartlett (1932) also finds such changes of axes nearly of the same magnitude
as ours, between $+50°C$ and $-50°C$.

In those cases where the magnetic axes of the crystal do not change at
all, as actually happens in most of the crystals, one can safely conclude that
in the range of temperature noted the crystalline electric fields in the neigh-
bourhood of the paramagnetic ions are practically unaffected by the changes
in temperature. This is further corroborated by a detailed calculation of
the crystal field constants which are found to remain practically independent
of temperature in such cases as six co-ordinated nickel salts and four co-
ordinated cobalt salts, where the conditions are particularly favourable for
such a calculation.* Even when a considerable change in the magnetic axes
of the crystals is observed, it may not indicate any change either in the
magnitude or the asymmetry of the electric field associated with any particular
paramagnetic ion. It may merely be due to the axes, associated with the
different paramagnetic ions in the unit cell, changing their relative orienta-
tions, and this is presumably the reason for observed changes in the χ_1 and χ_2
axes of the few salts noted previously.

Detailed calculations of the crystalline field constants for nickel salts
referred to above, further show that they not only are independent of the
temperature, but also are of nearly the same magnitude in the different
nickel salts, in which the immediate neighbours surrounding the nickel ion
are the same ; for example in all the Tutton salts of nickel or the highly
hydrated sulphates and selenates of nickel, in which each Ni^{++} ion is
surrounded by six water molecules occupying the corners of an octahedron
with the Ni^{++} ion at the centre. From this point of view, it is not only the
predominant cubic part of the field that will be determined by these immediate
neighbours, but also the feeble rhombic part ; the fields due to the distant
atoms are regarded as negligible in comparison with even the feeble rhombic
fields due to the immediate neighbours. We are aware that some of the
earlier workers have attributed the large cubic part to the immediate neigh-
bours and the feeble rhombic part to the influence of the distant atoms. But

---

* These will be published in later papers and may also be referred to in the memoir
published by the author (1946).

there is already considerable evidence, especially, from the magnetic behaviour of these ions in aqueous solution, that the asymmetry of the electric field required to account for such behaviour is due to the immediate neighbours, and it may be presumed from the similarity of magnetic behaviour that this should be so in crystals also.

In any case, the assumption of the same crystalline fields in all the nickel salts, for example, or in all the cobalt salts, when the paramagnetic ions are surrounded by the same immediate neighbours, apart from its great plausibility considerably simplifies the discussions. It is, therefore, desirable to adopt this view unless we are forced by the experimental data to discard it. We may mention immediately that no experimental evidence available at present is inconsistent with this assumption.

It may be mentioned, finally, that there may also be another cause of this change in the orientation of the magnetic axes in addition to the changes caused by relative orientation of the different paramagnetic groups in the unit cell, as evidenced by the exceedingly high change in the value of "ψ" obtained in the crystal of ammonium chromium oxalate. It should be noted that this crystal as mentioned in the earlier papers has a very feeble paramagnetic anisotropy of only about $\frac{1}{2}\%$ and of the same order of magnitude as its diamagnetic anisotropy. In view of this not only the large change in ψ but also the small increase of anisotropy $\chi_1 - \chi_2$ as actually observed, are to be expected, since the large diamagnetic part of the anisotropy will be independent of temperature and the value of ψ will not be the same for the diamagnetic and the paramagnetic parts. From the nature of the variations at high temperatures it appears also that there is a critical point for these variations where they became maximum.

Further investigations at high temperatures are in progress at this laboratory to elucidate the nature of these changes in the magnetic axes of paramagnetic crystals.

INDIAN ASSOCIATION FOR THE
CULTIVATION OF SCIENCE, CALCUTTA.

REFERENCES

Bartlett, B W , 1932, *Phys. Rev* , **41**, 818

Bethe, H , 1929, *Ann der Phys* , **3**, 133

Bose, A , 1940, *Proceedings of the Indian Science Congress*

    ,,   1946, Paramagnetism of Single Crystals of the Salts of the Iron Group of Elements at Low Temperatures *(Hindusthan Printing Works,* Dacca

Jordahl, O. M., 1934, *Phys Rev.,* **45**, 87

Krishnan, K. S and Mookherji, A., 1938, *Phys. Rev.,* **54**, 533, 841.

Krishnan, K. S , Mookherji, A, and Bose, A , 1939, *Phil Trans. Roy. Soc (A* , **238**, 125.

Penney, W G , and Schlapp, R., 1932, *Phys. Rev.,* **41**, 194.

    ,,   ,,   ,,   **42**, 666

Van Vleck J H., 1932, The Theory of Electric and Magnetic Susceptibilities. (Oxford).

    ,,   1932, *Phys. Rev.,* **41**, 208.

ON NUCLEAR ENERGETICS AND β-ACTIVITY. III.
THE GROUPS I=21 TO I=55.

By SUKUMAR BISWAS and AMBUJ MUKHERJEE

ABSTRACT The present paper is a summary of a work to be published shortly containing a detailed discussion of nuclei included in the isotopic groups I=21 to the end I 55. The object of this paper is to correlate the observed energy releases in β^-, β^+ and K-capture processes with the modified Weizsäcker-Bethe mass defect formula having an additional spin-dependent term, proposed by Prof M N. Saha and A. K Saha (1946). The authors have calculated the energy release in β^- and β^+ emissions according to Weizsäcker-Bethe formula for the nuclei in these groups and compared them with the observed energy releases so as to observe the effect of the spin dependent term. A general agreement with the newly proposed formula is found though the available data is too meagre for many groups specially in the rare-earth region. The probable activities and energetics of still unknown nuclei are predicted in the light of newly proposed formula together with their methods of production It is, however, found that a varying value of β in the mass defect formula is much more satisfactory than a constant value and an empirical curve of β as a function of I is derived.

1. INTRODUCTION

This paper is in continuation of two previous papers on "Nuclear Energetics and β-activity" by Prof. M. N. Saha and A. K. Saha (1946) (Paper I) and A. K. Saha, Ghoshal and Das (to be published shortly) (Paper II). In the first paper Prof. Saha and Saha (Jr.) modified the Weizsäcker-Bethe mass defect formula by an additional spin-dependent term and observed energy-releases were explained satisfactorily for groups $I= -1$ to $I=6$ in Paper I and $I=7$ to $I=20$ in Paper II. The present paper is a summary of a large work to be published shortly containing a systematic and critical study of β-activity and K-capture process for groups $I=21$ to $I=55$. The nuclei have been arranged in isotopic groups in the Nuclear Chart* (Fig. 1), from which certain β-stability rules (Saha, Sirkar and Mukherjee, 1940) can be studied. In the first section the observed energy releases in β-activities are discussed element by element, of which only two elements are included in this summary. In the next section the β-instability of the nuclei

---

* Since the completion of this work, a number of new isotopes, radio-active as well as stable, have been discovered. These are to be supplemented in the Nuclear Chart. These are : La^{138}, stable, o89% abundance [Inghram et al, 1947, Phys. Rev. **72**, 967]; Bi^{204}, 12hr. (K-capture) ; Bi^{206}, 6.4d (K-capture) ; Po^{206}, 9d (K-capture & α) ; Po^{207} 5 7h (K-capture & α) ; Po^{208}, ~3yr(α). [Templeton et al, 1947, Phys. Rev. **72**, 768, 758]; Bi^{210} (RaE) α Ti^{206} (4 23m) [Broda & Feather, 1947, Proc Roy Soc. **A190**, 20].

is discussed in order of different I groups. The energy releases of the nuclei are calculated according to Weizsäcker-Bethe formula and these are given in form of A^- and A^+ curves for different I groups. The energetics of known and unknown nuclei are studied according to the new formula.

The notations and symbols used are same as in Paper I and Paper II.

2. DISCUSSION OF ENERGY-RELEASES

Out of the discussion of 47 elements, $_{50}$Sn to $_{96}$Cm, we select in the present extract the following elements, $_{55}$Cs and $_{93}$Np as the typical illustration of the method of study followed.

$_{55}$Cæsium.

(Tables 1.1 and 1.2)

Cs^{125} : Not yet produced. May be obtained from .094% Xe^{124} (p, γ) Cs^{125} (d, n)

reaction. The very low frequency of the target and the difficulty of using a gaseous target renders the possibility of carrying out the experiment rather remote.

Cs^{126} : Not known. Cannot be produced by usual reactions.

Cs^{127} : Not yet produced. May be produced by .088% Xe^{126} (p, γ) Cs^{127}. (d, n)

The difficulties of production are the same as with Cs^{125}.

Cs^{128} : Not yet produced. May be produced by .101% Ba^{130} $d, \alpha)$ Cs^{128} The yield will be very low due to low abundance of the target.

Cs^{129} : Not yet produced. May be produced by reaction, 1.9% Xe^{128} (p, n) $(d, 2n)$

TABLE 1.1

Production Table of Cs.

	Target		Reaction	Product		Half-life
	Element	Isotopes		Element	Isotopes	
1	Cs	133	(n, γ)	Cs	134	3h(−), 1 7y(−)
2	Ba	130, 132, 134, 135, 136, 137, 138	(n, p)	Cs	130, 132, 134, 135, 136, 137, 138	33m(−)
3	Cs	133	(d, p)	Cs	134	3h(−), 1.7y(−)

TABLE 1.2

Cs

Nucleus	Half-life	Assignment class	E_β (Mev)	E_γ (Mev)	Energy-release E (Mev)
Cs^{125}	...				
Cs^{126}	×				
Cs^{127}	..				
Cs^{128}	...				
Cs^{129}	. .				
Cs^{130}	...				
Cs^{131}	10 d (K)	A		.145 (? .031	
Cs^{132}	...				
Cs^{133}	Stable (100%)				
Cs^{134}	3h (−)	A	1.0	.	1 0
	1 7y (−)	A	658, ∼.09	568, .002, .794	2 054
Cs^{135}	>2.5×10⁴y (−)	A	.	...	...
Cs^{136}	13d (−)	B	.28	1.2	1.48
Cs^{137}	33y (−)	A	.5, .8	7	...
Cs^{138}	33m (−)	B	2 6	1 2	3.8
Cs^{139}	7m (−)	A	...	...	...
Cs^{140}	40s (−)	B	...		...
	Short (−)	A			
Cs^{141}	Short (−)	B	...	...	...
Cs^{142}	∼1−2m (−)	B	...	...	...
Cs^{143}	Short (−)	A	.	...	..
Cs^{144}	Short (−)	A	..	...	...
Cs^{145}	Short (−)	B	..	..	...

Cs^{129}. The above-mentioned difficulties are present in the production of this nucleus.

Cs^{130} : Not yet produced. Should be obtained from the reaction, 100% I^{127} (α, n) Cs^{130}, provided α-particles of sufficient energy are available.

Cs^{131} : This nucleus is interesting as it shows consecutive K-capture process. A 10d (K) activity obtained from 11.7d K-active Ba^{131} is assigned to Cs^{131} as reported by Yu, Gideon and Kurbotov (1947). It emits .145 Mev γ-rays that are strongly converted (97%) giving .112 Mev electrons. X-ray of 30 Kev energy is also reported. Katcoff (1947)

studied this nucleus and found no γ-ray associated with 10.2d Cs¹³¹. The X-ray energy was measured as 30.8 Kev. The mass assignment is made unique by him with the help of critical absorption measurements by Finkle (1947).

Cs¹³² : Not yet produced. May be produced by the reaction 26.96% Xe¹³²
(p, n) Cs¹³². The fairly good frequency of Xe¹³² renders the possibil-
(d, 2n)
ity of the reaction quite good.

Cs¹³⁴ : Activities of 3h(−) and 1.7y(−) are uniquely assigned to Cs¹³⁴. Kalbfell and Cooley (1940) obtained a 1 Mev β-ray associated with the 3h(−) activity and a .9 Mev β-ray with 1.7y(−) activity by absorption method. Presence of γ-rays associated with the latter activity is reported but no measurement has been done by him. Eliott and Bell (1947) studied 1.7yr. Cs¹³⁴ with magnetic lens spectrometer together with coincidence techniques and obtained two β-spectra having end-energies of .658 Mev and ∼.090 Mev. Three γ-rays of energies .568, .602 and .794 Mev were obtained. According to the level-scheme suggested by him, energy-release, E⁻ comes out as 2.054 Mev. This is in agreement with the values of Siegbahn and Deutsch (1947) who observed major disintegration by ˙645 Mev β-rays followed by two γ-rays of .584, .776 Mev, the total energy-release being 2.005 Mev. For the 3h(−) period energy release E⁻ may be taken as ∼1 Mev.

Cs¹³⁵ : Produced so far only in fission having a period >2.5 × 10⁴y(−). May be obtained from the reaction, 10.54% Xe¹²⁴ (p, γ) Cs¹³⁵. No
(d, n)
measurement of β-energy has yet been done. The identification is in agreement with Saha-Saha theory as the nucleus is on the flank of the group of stable nuclei in the group I = 25.

Cs¹³⁶ A 13 d(−) activity obtained from fission and decaying to stable Ba is assigned vaguely to Cs¹³⁶. It is difficult to assign properly the activity from fission and the reactions, 100% La¹³⁹ (n, α) Cs¹³⁶ and 8.95% Xe¹³⁶(p, n) Cs¹³⁶ should be tried. Finkle et al (1946) determined Eβ− ∼ 0.28 Mev by absorption in Al and Eγ = 1.2 Mev by absorption in Pb. E⁻ may be taken as ∼1.48 Mev.

Cs¹³⁷ : A 33y(−) activity obtained so far only in fission-chain is uniquely assigned to Cs¹³⁷. May be produced also by reaction, 11.32% Ba¹³⁷
(n, p) Cs¹³⁷.

According to Plutonium Project Report (1946) the mass-assignment has been done mass-spectroscopically. Glendenin and Metcaff (1946) observed two β-rays of energies 0.5 Mev (50%) and 0.8 Mev (50%) by absorption in Al, using Feather's relation. Both β-transitions

are of 3B class. A γ-ray of energy .75 Mev has also been obtained by them by absorption in Pb. Metcalf et al (1944) previously obtained values of o.8 Mev and ∼o.4 Mev for β-rays and o.7 Mev for γ-ray. With the available data it is not possible to arrive at a satisfactory level-scheme and possibly another γ-ray is missing. This requires further investigation.

Cs^{138} : A 33 m(−) activity is obtained from reaction (2) and also from fission. Since Ba has a number of stable isotopes nothing definite about mass can be said from this one reaction and none in the fission-chain definite.

Glasoe and Steigman (1940) measured E_B = 2.6 Mev by absorption in Al. Glendenin and Metcalf (1946) measured $E_\gamma = 1.2$ Mev by absorption in Pb. E¯ may be taken as 3.8 Mev.

Cs^{139} : It has so far been obtained only in fission having 7m(−) activity uniquely assigned. It cannot be produced by usual reactions. No energy measurement is done yet.

Cs^{140} : One 40s(−) activity obtained so far only in fission is assigned to Cs^{140}. No chain could be established for the activity and the assignment is vague. A "short" (−) activity descendant of 16s Xe^{140}, is assigned to Cs^{140} uniquely. No energy measurement has been done for either activity.

Cs^{141} : A short (−) activity obtained from fission, as descendant of 3s (−) Xe^{141}, is ambiguously assigned to Cs^{141}. None in the chain is definite and this cannot be produced by usual reactions. No energy measurement has been done yet.

Cs^{142} : A 1-2m (−) activity obtained from fission only, is assigned vaguely to Cs^{142} as none in the chain definite. Cannot be produced by usual reactions. No energy measurement has been done.

Cs^{143} : A short (−) activity obtained from fission is uniquely assigned to Cs^{143}. No energy measurement has been done yet.

Cs^{144} : A short (−) activity is obtained from fission-chain. This has been uniquely assigned to Cs^{144}. No energy measurement has been done.

Cs^{145} : A "short" (−) activity obtained from fission as descendant of 8s (−) Xe^{145} is assigned to Cs^{145}. None in the chain is definite and this cannot be produced by usual reactions. No energy measurement has been done.

₉₃Neptunium

So far, six isotopes of Np are reported by Seaborg (1946). Some of them are produced by bombardment with 22 Mev deutrons and 44 Mev α-particles obtained from Berkeley Cyclotron. With such high energy interesting reactions viz., (d, 3n), (d, 4n), (α, p3n), (α, p4n), (α, 3n) etc. are found to occur.

(TABLES 2.3 AND 2.2)

Np^{232} : This is not yet known. May be produced by the reactions U^{233} $(d, 3n)$ Np^{232}, since U^{233} has now been produced and isolated in $(d, p4n)$

weighable amounts. This is expected to be $β^+$-active.

Np^{233} : This is not yet known. May be produced by the reactions U^{235} $(d, 4n)$ Np^{233} and U^{233} $(d, 2n)$ Np^{233}. Probable activity of this $(α, p3n)$

isotope is K-capture or $β^+$ emission.

Np^{234} : This 4.4 d period K-capturing isotope was prepared by the following reactions : U^{235} $(d, 3n)$ Np^{234}; Pa^{231} $(α, n)$ Np^{234}; and U^{235} $(α, p4n)$ Np^{234}. A $γ$-ray has been detected from this nucleus, but the energy is not measured. The K-capture process is in agreement with the stability rules.

Np^{235} : A 240 d K-capturing isotope has been prepared by the following reactions : U^{235} $(d, 2n)$ Np^{235} and U^{235} $(α, p3n)$ Np^{235}. No energy measurement has been yet done. This activity is also in agreement with the theory.

TABLE 2.1

Production Table of Np.

	Target		Reaction	Product		Half-life
1	U	235	(d, n)	Np	236	20h (−)
2	U	235	(d, 2n)	Np	235	240d (K)
3	U	238	(d, 2n)	Np	238	2d (−)
4	U	235	(d, 3n)	Np	234	4.4d (K)
5	U	238	(d, 4n)	Np	236	20h (−)
6	Pa	231	(α, n)	Np	234	4.4d (K)
7	U	235	(α, p)	Np	238	2d (−)
8	U	235	(α, p2n)	Np	236	20h (−)
9	U	235	(α, p3n)	Np	235	240d (K)
10	U	238	(α, p3n)	Np	238	2d (−)
11	U	235	(α, p4n)	Np	234	4 4d (K)

TABLE 2.2

Nucleus	Half-life	Assignment Class	E_β (Mev)	E_γ (Mev)	Energy-release E (Mev)
Np²³²	...	...			
Np²³³	...	...			
Np²³⁴	4.4d (K)	A			
Np²³⁵	240d (K)	A			
Np²³⁶	20h (—)	A			
Np²³⁷	2.25 × 10⁶y(α)	A			
Np²³⁸	2d (—)	A			
Np²³⁹	2.3d (—)	A	.47	.22, .27	
Np²⁴⁰	...	...			
Np²⁴¹	...	...			

Np²³⁶ : A 20 h (—) activity is associated with Np²³⁶. This was prepared by the following reactions: U²³⁵ (d, n) Np²³⁶; U²³⁸ (d, 4n) Np²³⁶; U²³⁵ (α, p2n) Np²³⁶. No measurement of β-energy is done yet.

Np²³⁷ : Np²³⁷ is an α-active nucleus of 2.25 × 10⁶y half-life being the descendant of 500 y (α) Am²⁴¹. This is the most stable isotope of Np. This has been isolated in weighable amounts and is used as target.

Np²³⁸ : This is the second transuranic nucleus obtained by Seaborg in 1940. A 2.0 d β-active Np²³⁸ is obtained from the following reactions: U²³⁸ (d, 2n) Np²³⁸; U²³⁹ (α, p3n) Np²³⁸ and U²³⁵ (α, p) Np²³⁸. Nothing is reported about β-energy.

Np²³⁹ : The 23d (—) Np²³⁹ is the first transuranic element discovered by McMillan and Abelson (1940) as the decay product of 23m (—) U²³⁹ which was formed by U²³⁸ (n, γ) reaction. They measured β⁻-energy as .47 Mev. and γ-energies as .22 and .27 Mev by β-spectrograph. The energy-release E⁻ comes out as .96 if the γ-rays are assumed to be in cascade being genetically related to the β-emission. This value of E⁻ is higher than expected from Saha-Saha theory and more definite information about E⁻ is required.

Np²⁴⁰ : Not yet known. May be obtained by the rare reaction U²³⁸ (α, pn) Np²⁴⁰.

Np²⁴¹ : Not yet known. May be prepared from U²³⁸ (α, p) Np²⁴¹ reaction.

This discussion of Np shows that the stability rules hold good also in the transuranic region.

3. DISCUSSION OF A⁻ AND A⁺ CURVES

In this section the observed energy-releases are compared with the A⁻ and A⁺ curves. These curves are drawn with the formulae given in Paper I. These are enlisted below for easy reference.

$$\Delta M = \alpha A - \beta \frac{I^2}{A} - \gamma A^{\frac{2}{3}} - \delta \frac{Z^2}{A^{\frac{1}{3}}} + \chi(Z, A)$$

$$E^-(Z, A) = A^-(Z, A) + \chi(Z + 1, A) - \chi(Z, A)$$

where

$$A^-(Z, A) = .766 + \frac{4\beta(I - 1)}{A} - \frac{.58(A - I + 1)}{A^{\frac{1}{3}}} \cdot \text{Mev.}$$

β is taken as 19.5, 18.9 or 17.4 Mev.

$$E^+(Z, A) = A^+(Z, A) + \chi(Z - 1, A) - \chi(Z, A)$$

where

$$A^+(Z, A) = -1.788 - \frac{4\beta(I + 1)}{A} + \frac{.58(A - I + 1)}{A^{\frac{1}{3}}} \text{ Mev.}$$

$$E^k = E' + 2m - \tfrac{1}{2} m \alpha'' Z^2$$

$$\simeq E' + 2m$$

I = even

For Z = even, N = even ... $E^- = A^- + \chi(Z+1, A) < A^-$

$E^+ = A^+ + \chi(Z-1, A) < A^+$

For Z = odd, N = odd ... $E^- = A^- - \lambda(Z, A) > A^-$

$E^+ = A^+ - \lambda(Z, A) > A^+$

I = odd

$E^- \simeq A^-$

$E^+ \simeq A^+$

Out of the discussion of 35 I groups, three groups, two odd and one even, are included here as typical illustration.

$$I = 21.$$

This group extends from Kr^{93} to Eu^{147} with several gaps and many undiscovered nuclei as seen in the Nuclear Chart (Fig. 1). The stable region includes Sb^{123} to Xe^{129}. The nuclei in the left flank of Sb^{123} are β⁻-active while those on the right of Xe^{129} show K-capture or β⁺activity. The stability rule of Saha, Sirkar and Mukherjee (*loc. cit.*) is thus obeyed in this group. The gaps indicate that the corresponding nuclei cannot be obtained with known reactions except by fission. The energetics of the nuclei are discussed below one by one.
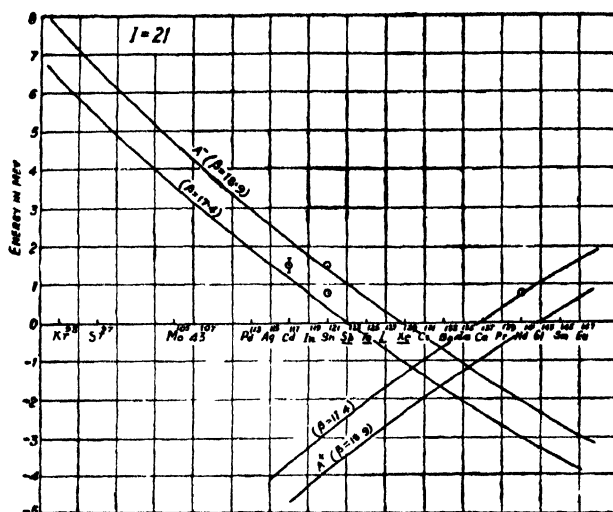
FIG. 2

Kr^{93}, Sr^{97}, Mo^{105}, 43^{107} :

These short-lived β^--active nuclei have been obtained in fission; but their energy releases have not yet been measured. They will decay with high energy releases as given in A^- curve, since $E^-\simeq A^-$. As discussed below, A^- curve with $\beta=17.4$ is more suitable that the other curve.

Cd^{117} :

A 2.8h (−) activity is uniquely assigned to Cd^{117}. The energy is given as 1.3 to 1.7 Mev. and nothing is reported about γ-rays (Lawson and Cork, 1940). Energy-release, E^- is $\simeq 1.5$ Mev. or greater. This point falls somewhat below the A^- curve with $\beta=18.9$, but is closer to $\beta=17.4$ curve and is in fair agreement with the latter.

Sn^{121} :

Two activities 62h (−) and 130d (−) are ambiguously assigned to Sn^{121}. Corresponding values of E^- are .76 Mev and $\simeq 1.5$ Mev. The 130d (−) activity may belong to Sn^{123}. Now $E^-=.76$ Mev agrees well with A^- curve with $\beta=17.4$; and $E^-=1.5$ Mev agrees with A^- curve having $\beta=18.9$ in $I=21$, but if this is assigned to Sn^{123} it agrees well with A^- curve with $\beta=17.4$ in $I=23$. In this region $\beta=17.4$ being more satisfactory, from other considerations, 62h (−) and 130d (−) activities most probably belong to Sn^{121} and Sn^{123} respectively.

Sb^{123}, Te^{125}, I^{127}, Xe^{129} :

These stable nuclei are expected to occur in the region where both A^- and A^+ are negative (A^+ lying between −1.02 and 0, however, includes the possibility of K-capture). The A^- and A^+ curve with standard value of $\beta=18.9$, flagrantly violates this condition. It is found that a lower value of $\beta=17.4$,

justifies the positions of the stable nuclei and is in agreement with the measured energy-releases in this group.

Cs^{131} :

Recently a K-capture activity of this nucleus has been reported (Yu, et al, 1947)). The value of A^+ is -1.0 Mev with $\beta = 17.4$ curve, and A^+ is equal to -2.0 Mev if $\beta = 18.9$ curve is considered. So K-capture process is possible with $\beta = 17.4$ curve while $\beta = 18.9$ definitely excludes K-capture energetically. Thus $\beta = 17.4$ value is in good agreement with observed fact. The absence of any γ-ray as observed by Katcoff (1947) follows from the theory since energy-release, E^k is comes out as very small.

Ba^{133} :

A K-capture process is definitely assigned to Ba^{133}. A $^+$ curve with $\beta = 18.9$ makes this process improbable whereas A^+ curve with $\beta = 17.4$ makes K-capture quite possible since $A^+ = -.65$ in this case.

La^{135} :

A K-capture activity is probable for this still unknown nucleus.

Ce^{137} :

This isotope is expected to show K-capture or small β^+ activity.

Pr^{139} :

A β^+-activity is more probable than K-capture for this nucleus.

Nd^{141} :

This uniquely assigned nucleus shows β^+ activity and the energy-release, E^+ is .78 Mev. This point is in good agreement with A^- curve having $\beta = 17.4$.

The nuclei on the right side of Nd^{141} are all expected to be β^+-active.

Thus we see that the agreement with Saha-Saha formula is good with the value of $\beta = 17.4$ but not with the value of $\beta = 18.9$. Such a smaller value of β is found satisfactory for a few groups in this region. This variation of the value of β with I is of much importance and will be discussed at the end of the present paper.

$$I = 25.$$

This group extends from Cd^{121} to Yb^{165} with a solitary nucleus Kr^{97} obtained from fission, in the extreme left. The stable nuclei are included between Ba^{137} to Eu^{151} with the exception of Ce^{141}, Pr^{143} and 61^{147} which show β^--activities. These three nuclei violate Saha, Sirkar and Mukherjee stability rule as their assignments, being arrived at mass-spectroscopically, are unique. The nuclei on the left of Ba^{137} show β^--activity.
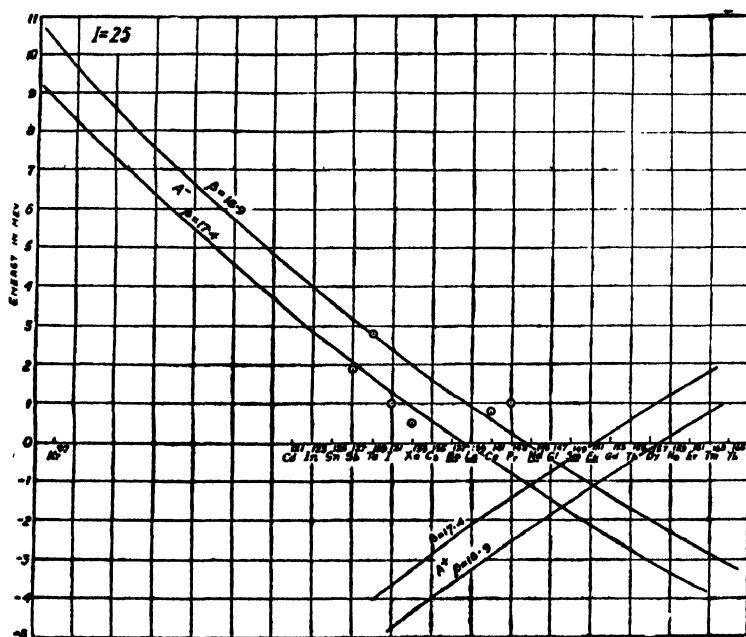
F.G. 3

Sb[127] : The E⁻ value for this uniquely assigned nucleus is 1.87 Mev. This point falls much below the A⁻ curve (β = 18.9). This value is, however, in good agreement with A⁻ curve having β = 17.4.

Te[129] : The value of E⁻ for this uniquely assigned nucleus is ≃ 2.88 Mev. This value is in agreement with A⁻ curve having β = 18.9 and falls much above the shifted curve (β = 17.4).

I[131] . The energy-release E⁻ for this uniquely assigned nucleus is 1.042 Mev. This point being far below the A⁻ curve with β = 18.9, agrees well with the shifted curve with β = 17.4.

Xe[133] : This nucleus is uniquely assigned. The energy-release E⁻ = .489 Mev. This value is much smaller than the A⁻ value with β = 18.9, but agrees well with the shifted curve with β = 17.4.

Ba[137]. La[139] : The position of these two stable nuclei cannot be justified with A⁻ curve with β = 18.9. since A⁻ is highly positive. The shifted curve with β = 17.4, however, justifies their stability.

Ce[141] : The assignment is unique. The value of E⁻ = .86 Mev. The activity of this nucleus is a violation of stability rule as evident from its position.

Pr[143] . This β-active nucleus is uniquely assigned. E = 1.0 Mev. This activity of Pr[143] is a violation of stability rule.

Thus we see that A⁻ curve with β = 18.9 do not satisfy Saha-Saha theory at all. The A⁻ and A⁺ curves with β = 17.4 is in good agreement with theory for all the nuclei whose energies have been measured excepting Te[129]. The

stable nuclei starting from Ba^{137} and ending in Eu^{151} fit fairly well with the curves with $\beta = 17.4$.

$$I = 28.$$

This group extends from Sb^{130} to Ta^{174}. This group exhibits some exceptions to Saha, Sirkar and Mukherjee stability rules. Xe^{136} is an even-even nucleus and is stable. The following even-even nuclei, $_{56}Ba^{140}$ and $_{58}Ce^{144}$, expected to be stable are both β^--active. Of these Ba^{140} is uniquely assigned and is very well-studied since Hahn's pioneer work on fission. The other one Ce^{144} is also uniquely assigned. All the remaining nuclei obey stability rules. Now we discuss the nuclei whose energy values are available, one by one.
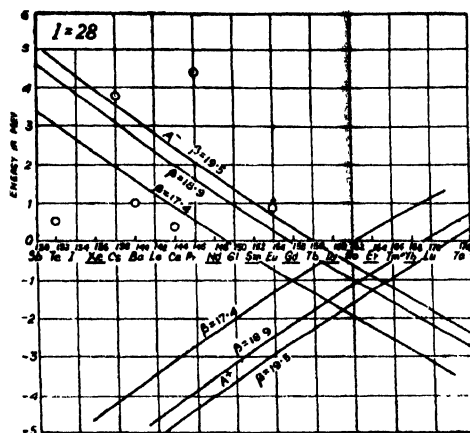
FIG. 4

Te^{13} The assignment is vague. This nucleus being even-even, shows β^--activity since it falls further left. The A^- value is so large that even a large subtraction of χ-term cannot make E^- $-ve$. A small E^- value .5 Mev. is an interesting and good agreement with Saha-Saha theory. Hence the assignment may be taken correct.

Cs^1 The assignment is vague. The value of E^- is 3.8 Mev. This point falls somewhat above A^- curve ($\beta = 18.9$) as expected for odd-odd nuclei.

Ba^{140} This uniquely assigned nucleus is an exception to the stability rule, as we have mentioned above. The energy release E^- is 1 Mev which, however, falls below the A^- curve satisfying the characteristic feature of radio-active even-even nucleus.

La^{142} .   The energy-measurement of this vaguely assigned nucleus is incomplete. It is expected to give a high energy-release, being much greater than A^- value.

Ce^{14} :   This uniquely assigned nucleus gives an energy release of .348 Mev. This point falls much below the A^- curve ($\beta = 18.9$) satisfying the

characteristic condition for radio-active even-even nucleus, given by the theory.

Pr^{146} : The assignment is vague. $E^- \simeq 4.4$ Mev which comes much above the A^- curve ($\beta = 18.9$), in agreement with the theory. Hence the assignment is most probably correct.

Eu^{154} : The energy-measurement of this vaguely assigned nucleus is incomplete. Since the γ-ray energy is not known, E^- will be greater than .9 Mev. This is in agreement with the theory.

Now we discuss the nuclei with isobaric stable nuclei on either side.

$$I = \begin{cases} 30 & \text{ONd} & \text{OSm} & \text{OGd} & \text{ODy} \\ 28 & \text{O61} & \wp\,\text{Eu} & \delta\,\text{Tb}^? & \text{OHo} \\ 26 & \text{OSm} & \text{OGd} & \text{ODy} & \text{OEr} \end{cases}$$

$$A \rightarrow \qquad 150 \qquad 154 \qquad 158 \qquad 162$$

61^{150} : Assuming that both transitions take place from the same level of the nucleus in question, $E^+ - E^- = A^+ - A^-$. $E^+ - E^- = -3.15 - .91 = -4.06$. So it is expected that 61^{150} will be β^--active having energy release $E^- \sim 3.5$ Mev if $\chi(61, 150)$ is of the same order as $\chi(59, 146)$. However, we have seen that on the spin-dependent term of Pr is much larger than that of average nuclei. β^+-activity, too, can occur if $E^- > 4.06$ Mev which is rather improbable ; if E^- lies between 3 and 4 Mev, K-capture can take place. So dual activity is expected under above condition.

Eu^{154} : $E^+ - E^- = -2.47 - .25 = -2.72$ Mev. We know that $E^- > .9$Mev. If E^- comes out > 2.72, positron activity also, becomes a possibility ; if $1.7 < E^- < 2.7$, K-capture can take place. This nucleus demands further investigation.

Tb^{158} : $E^+ - E^- = -1.81 + .3 = -1.51$ Mev. The suggested positron-activity of this nucleus is not very probable. β^--activity should exist and only if E^- is > 1.5 Mev, β^+-activity may accompany β^--activity. K-capture process is a probable one since it can occur if $E^- > .5$ Mev. This requires further investigation.

Ho^{162} : $E^+ - E^- = -1.15 + 1.02 = -.13$. This undiscovered nucleus is very interesting since both β^- and β^+-activities and K-capture are expected from this nucleus.

Tm^{166}, Lu^{170}, Ta^{174} : These three nuclei are expected to show β^+-activity, or K-capture, or both.

Thus we see that this group agrees well with Saha-Saha theory, though there is some anomaly about the activities of Ba^{140}, and Ce^{144}. These exceptions can be interpreted as follows. For $_{52}Te^{132}$ and $_{54}Xe^{136}$, the spin-dependent terms $\chi(53, 132)$ and $\chi(55, 136)$ are large and of the same order so that E^- for $_{52}Te^{132}$ is small +ve and E^- for $_{54}Xe^{136}$ is −ve. But spin-dependent

terms of $_{56}Ba^{140}$, and $_{58}Ce^{144}$, $\chi(57, 140)$, $\chi(59, 144)$ are of same order but are smaller than previous values. This makes them β^--active instead of being stable but E^- much smaller than A^- $(\beta=18.9)$. This is shown below.

	Te¹³²	Xe¹³⁶	Ba¹⁴⁰	Ce¹⁴⁴
A⁻ in Mev.	4.23	3.45	2.67	1.95
E⁻ in Mev.	.5	−ve	1.0	.35
-χ(Z+1, A)	3 73	>3.45	1 67	1.65

Similar anomaly has been found in group $I=8$. After stable $_{20}Ca^{48}$, three even-even nuclei $_{22}Ti^{52}$, $_{24}Cr^{56}$ and $_{26}Fe^{60}$ do not occur as stable isotopes. This has been discussed in details by Saha and Saha (1946) in paper I.

4. DISCUSSION OF β-VALUE

From the discussion of all the I groups, of which three are given above, a general agreement of the proposed formula is obtained qualitatively with the data available at present although there are some anomalies for a few nuclei. The important point in the study of energetics in the present paper, as well as in Paper I and Paper II, is the value of β in the mass defect formula. In the conclusion of three papers we observe that different values of β besides the standard value, 18.9 are found to be satisfactory for different regions of I groups, as given below.

$$I = -1 \text{ to } I = 6 ; \quad \beta = 19.5 \text{ Mev.}$$
$$I = 7 \text{ to } I = 20 ; \quad \beta = 18.9 \text{ Mev.}$$
$$I = 21 \text{ to } I = 26 ; \quad \beta = 17.4 \text{ Mev.}$$
$$I = 27 \text{ to } I = 50 ; \quad \beta = 18.9 \text{ Mev.}$$
$$I = 51 \text{ to } I = 55 ; \quad \beta = 19.5 \text{ Mev.}$$
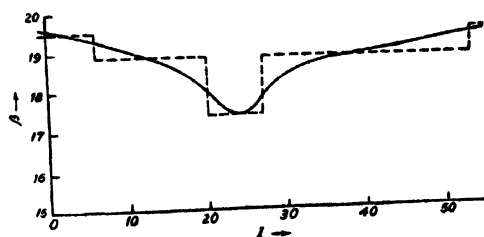
FIG. 5

Thus an approximate continuous curve of β can be plotted against 1 (Fig. 5) which passes through a minimum in the central region. This indicates that the value of β is not constant but is a function of I given by the above type of curve. The expression for the function is yet to be obtained.

ACKNOWLEDGMENTS

REFERENCES

Elliott and Bell, 1947, *Phys. Rev.*, **72**, 979.

Finkle 1947, *Phys Rev.*, **72**, 1260.

Finkle, Engelkemeir and Sugarman, 1946, *Rev. Mod. Phys.*, **18**, 513.

Glasoe and Steigman, 1940, *Phys. Rev* , **88**, 1.

Glendenin and Metcalf, 1946, *PPR, Rev Mod. Phys.*, **18**, 513.

Kalbfell and Cooley, 1940, *Phys. Rev.*, **58**, 91.

Katcoff 1947, *Phys. Rev.*, **72**, 1160.

Lawson and Cork, 1940, *Phys. Rev.*, **57**, 982.

McMillan and Abelson, 1940, *Phys. Rev.*, **57**, 1185.

Metcalf, Rubinsou, Seiler, Steinberg and Winsberg, 1946, *PPR, Rev. Mod.Phys.*, 18, 513.

Saha, M. N. and Saha A K., 1946, *Trans. Nat. Inst. Sci. Ind.*, II, 7, pp. 193-220.

Saha, A., Ghosal and Das, *Trans. Nat. Inst. Sci. Ind.* (In course of publication).

Saha, M. N. Sirkar and Mukherjee, 1940, *Proc. Nat. Inst. Sci. Ind.*, 6, 45.

Seaborg, 1944, *Rev. Mod. Phys.*, **16**, 1.

Seaborg, 1946, *Science*, **104**, 379.

Siegbahn and Deutsch, 1947, *Phys. Rev.*, **71**, 483.

Yu, Gideon and Kurbatov, 1947, *Phys. Rev.*, **71**, 382.

We are now manufacturing :

* Soxhlet Extraction sets of 100 cc, 250 cc and 1000 cc capacity
* B. S. S. Pattern Viscometers
* Kipp's Apparatus of 1 litre and $\frac{1}{2}$ litre capacity
  Petri Dishes of 3″ and 4″ diameter

and

ALL TYPES OF GRADUATED GLASSWARE
such as Measuring Flasks, Measuring
cylinders, Burettes, Pipettes
etc. etc.

Manufactured by

INDUSTRIAL AND
ENGINEERING APPARATUS CO., LTD.

CHOTANI ESTATES, PROCTOR ROAD, BOMBAY 7.

The following special publications of the Indian Association for the Cultivation of Science, 210, Bowbazar Street, Calcutta, are available at the prices shown against each of them :—

Subject	Author	Price Rs. A. P.
Methods in Scientific Research	Sir E. J. Russell	0 6 0
The Origin of the Planets	Sir James H. Jeans	0 6 0
Separation of Isotopes	Prof. F. W. Aston	0 6 0
Garnets and their Role in Nature	Sir Lewis L. Fermor	2 8 0
(1) The Royal Botanic Gardens, Kew.	Sir Arthur Hill	1 8 0
(2) Studies in the Germination of Seeds.	,,	
Interatomic Forces	Prof. J. E. Lennard-Jones	1 8 0
The Educational Aims and Practices of the California Institute of Technology.	R. A. Millikan	0 6 0
Active Nitrogen A New Theory.	Prof. S. K. Mitra	2 8 0
Theory of Valency and the Structure of Chemical Compounds.	Prof. P. Ray	3 0 0
Petroleum Resources of India.	D. N. Wadia	2 8 0
The Role of the Electrical Double layer in the Electro Chemistry of Colloids.	J. N. Mukherjee	1 12 0

A discount of 25% is allowed to Booksellers and Agents.

RATES OF ADVERTISEMENTS

Third page of cover	...	...	...	...	Rs. 32,	full page
do. do.	...	...	...	...	,, 20,	half page
do. do.	...	...	...	...	,, 12,	quarter page
Other pages	...	...	...	...	,, 25,	full page
do.	...	...	...	...	,, 16,	half page
do.	...	...	...	...	,, 10,	quarter page

15% Commissions are allowed to *bonafide* publicity agents securing orders for advertisements.

CONTENTS

the adjustment of the exposure time. Reducing the slit width to a minimum, a series of photographs were taken varying the exposure time from 1 to 30 minutes. Ilford Special Rapid plates were used. Sensitisation was found necessary to record the F_3-system completely. Better contrast was obtained with smaller times of exposure. Under these conditions the spectra were taken with the Hilger medium as well as the Littrow quartz instruments. A substantial extension towards the short wave-lengths was obtained in both F_1 and F_3-systems, (Plate II(A)) on the medium quartz spectrograms, the continuous spectrum at the violet end of the F_1-system being reduced to a minimum. Bands at the red end of the F_3-system which in the earlier work appeared broad could now be distinctly resolved into several components as can be seen on the Littrow quartz spectrograms. (Plate II(B))

F_1 System.—A complete catalogue of the band heads of this system is given in Table I. They are the mean of measurements made on two medium quartz spectrograms of exposure times 5 and 20 minutes. Plate II is a reproduction of the spectrum with the longer exposure. The table contains for comparision the data reported earlier by Ramakrishna Rao and K.R.Rao (1946). At the violet end of this system there is little or negligible overlapping with the bands of the F_2-system, but on the red side the bands continue to be intense even up to the mercury resonance line beyond which the bands might have been obliterated by the high intensity of the F-system. About fifty bands, in all, are ascribed to this F_1 system. This has enabled the autother to suggest a new and complete vibrational analysis.

· An examination of the spectrum (Plates IIA) has at first indicated the existence of two long and intense progressions, one at the violet end and the other at the red end of the system. The order of the intervals between the successive members in each of these progressions and their variation suggested that the first of these is a v' progression and the second a v'' progression; the transition from the v' to the v'' progression is seen from the increase in the spacing of the intense heads. This v'' progression is identical with that suggested by Rao and Rao although different quantum numbers had to be assigned now. The next feature which has helped in arriving at the analysis is the unmistakable appearance of discrete sequences, with but slight over-lapping, associated with each member chiefly of the more intense v'' progression. This sequence appearance was also noticed by Rao and Rao. With the aid of these sequences and the two above mentioned long progressions, the entire vibrational structure could be formed. The classifications of the bands are given in the last column of Table I. The value of $\omega'(=90.8)$ obtained with this classificatian is less than the value of $\omega''(=125.6)$ and is consistent with the observed red-degradation of the bands; it thus removes the anomaly in the scheme proposed by Rao and Rao, namely a sequence degradation to the violet among red-degraded bands. The band heads (represented by their intensities) are arranged in a diagonal array in Table II.

TABLE I

Mercury Iodide Bands, F_1-System

Wavelength (Int.)		Wave-number	Classification
Rao and Rao	Author		
	2450.24 (2)	40799 9	(8,0)
	2453.03 (1)	40753 6	(9,1)
2454 97 (00)	2454 74 (2)	40725.1	(7,0)
	2455.94 (0)	40705 3	(10,2)
	2457.58 (1)	40678.1	(8,1)
2460.03 (0)	2459.75 (3)	40642.3	(6,0)
	2464.64 (2)	40561.6	(5,0)
	2464 93 (2)	40556.8	(8,2)
2470.47 (0)	2469 61 (4)	40479.9	(4,0)
	2472.39 (2)	40434.5	(5,1)
2475.23 (0)	2474.73 (4)	40396.3	(3,0)
2476.76 (00)	2477.10 (3)	40357.5	(4,1)
	2479.86 (2	40312.6	(2,0)
	2482.72 (1)	40266.2	(3,1)
	2484.23 (0)	40241.8	(8,4)
	2484.72 (1)	40233.8	(4,2)
2485 94 (0)	2485.39 (1)	40223.0	(1,0)
	2486.72 (0)	40201.5	(5,3)
	2487 37 (3)	40191.0	(—)
2487.97 (1)	2487.60 (5)	40187.2	(2,1)
	2489.46 (0)	40157.2	(7,4)
	2490.29 (0)	40143.9	3,2
	2491.17 (0)	40129.6	0,0
	2492.18 (1)	40113 3	4,3
	2493 13 (5)	40098.1	1,1
	2494.14 (2)	40081.9	5,4
	2495.22 (3)	40064.5	2,2
	2497.47 (2)	40028.5	3,3
	2499.10 (0)	40002.3	4,4
2500.87 (2)	2500.61 (5)	39978.2	1,2
	2502.28 (1)	39951.5	2,3
	2503.24 (2)	39936.2	—
	2504.45 (2)	39916 9	3,4
2506.28 (5)	2506.08 (6)	39891.0	0,2
2508.56 (2)	2507.95 (3)	39861.1	1,3
2510.22 (4)	2509.91 (5)	39830 0	2,4
	2511.77 (2)	39800 6	3,5
2513.61 (8)	2513.6 (0)	39771.6	0,3
	2515.25 (3)	39745.5	1,3
2517.52 (3)	2517.18 (4)	39715.1	2,5
	2518.82 (2)	39689 2	3,6
2519.01 (3)	2519.36 (2)	39680.6	—
	2520.22 (0)	39667.1	4,7

TABLE I (contd.)

Mercury Iodide Bands, F₁-System

Wavelength (Int.)		Wave-number	Classification
Rao and Rao	Author		
2521.13 (7)	2520.96 (o)	39655.4	0,4
	2522.74 (2)	39627.5	1,5
2523.37 (oo)	2523.50 (2)	38615.6	
2526.21 (3)	2525.86 (3)	39578.5	3,7
	2527.16 (1)	39558.2	
	2527.53 (1)	39552.9	4,8
2528.50 (3)	2528.29 (4)	39540.5	0,5
2530.08 (3)	2529.79 (4)	39517.1	1,6
	2531.26 (1)	39494.1	2,7
2532.83 (6)	2532.73 (6)	39471.2	3,8
	2533 84 (6)	39453.9	4,9

TABLE II

v'' / v'	0	1	2	3	4	5	6	7	8	9
0	0	—	6	8	7	4				
1	1	5	5	3	3	2	4			
2	2	5	3	1	5	4	—	1		
3	4	—	0	2	2	2	2	3	6	
4	4	3	1	1	0	—	—	0	1	6
5	2	2	—	—	2					
6	3									
7	2									
8	2	1								
9	—	1								

There is a fall in intensity near the (0,0) band ; the intensity distribution is what is usually obtained for heavy iodide molecules.

F₃-System.—As in the F₁-system, a much larger number of band heads have been obtained than in the earlier work. The strong bands referred to by Rao and Rao (*loc. cit.*) as complexes of several bands are resolved in the Littrow picture
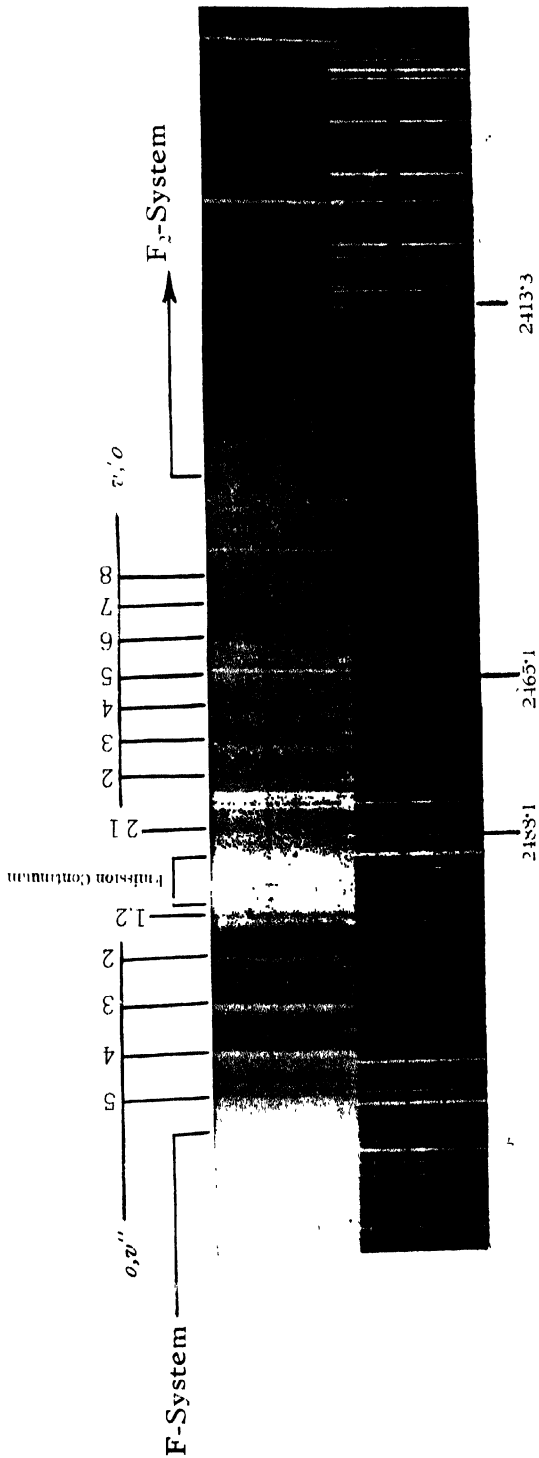
Fig. (1)   F-System of Murcury Iodide Bands and Iron Arc comparison.

Fig. 2. Mercury Iodide Bands — F₃ System.

(a) Medium Quartz and (b) Littrow Quartz Spectrograms.
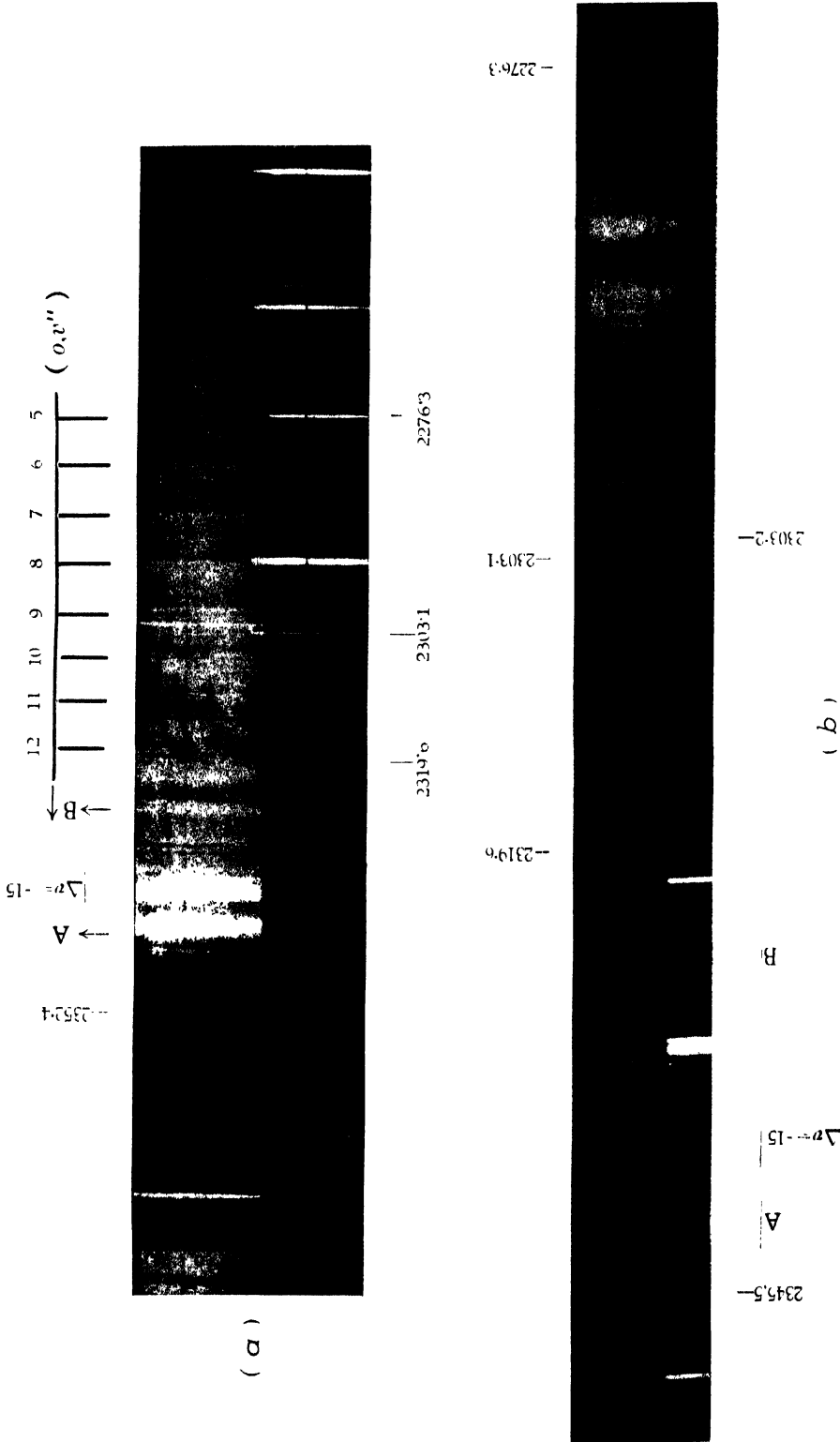
(Plate IIB). The measurements of bands, about 80 in all, are given in Table III. These are mean values from two Littrow plates. The wavelengths of the thirteen diffuse bands reported by Rao and Rao are also given in the same table. Quite a large number of bands are recorded below $\lambda2320$, chiefly because the photographic plate was oil-sensitised. These bands formed an extension of the violet end of the F_3-system. They are quite sharp and definitely degraded to the red unlike those at the long wavelength end. It is these bands which formed into long progressions that gave the key to the analysis. A preliminary analysis indicated that each one of the patches at the red end, only partially resolved on the medium quartz spectrograms, must be a sequence of bands. The high dispersion (2A per m. m.) obtainable on the Littrow pictures supported this view. From these considerations the vibrational scheme is built up. Two or three long v'' progressions could be formed but further assignment became difficult as a particular band could alternatively be placed.

TABLE III

Bands head of the F_3-system

Wave-length		Int.	Wave-number Obs	Classifica-tion.	Wave-number Cal.
Earlier work	Author				
	2265.8	0	44121	(1,4)	
	2267.3	0	44092	(2,5)	
	2269.2	0	44055	(3,6)	
	2271.4	0	44012	(0,4)	
	2272.1	0	43999	(1 5)	
	2273.5	0	43971	(2,6)	
	2276.5	0	43923	(0,5)	43909 4
	2278.3	1	43879	(1,6)	43878.8
	2282.14	2	43804.9	(0,6)	43795.1
	2284.14	1	43766.6	(1,7)	43766.4
	2285 77	0	43735.3	(2,8)	43739.2
	2288.18	2	43689.3	(0,7)	43682.7
	2290 14	2	43651.9	(1,8)	43656.0
	2291 03	1	43634.5	(2,9)	43629.8
	2293.89	00	43580.6	(4,11)	43578.5

Note.—The first eight bands were measured on the Hilger Medium Quality plates

TABLE III (*contd.*)

Wave-length		Int.	Wave-number Obs.	Classification.	Wave-number Cal.
Earlier work	Author				
	2294.17	1	43575 2	0,8	43572.5
	2295.47	1	43550.5	1,9	43547.5
	2296.92	0	43524 5	2,10	43523.3
	2298 02	1	43502.5	3,11	43499.4
	2299.14	0	43481.0	4,12	43475 8
	2299.97	3	43465 3	0,9	43463.8
	2301.26	2	43441.1	1,10	43441.0
	2302.05		43426.1	2,11	43418.8
	2303.43	1	43399 5	3,12	43396.9
	2304.67	1	43376.8	4,13	43375 3
	2305.71	2	43357.2	0,10	43357.3
	2306.74	2	43337.9	1,11	43336.5
	2307 87	2	43316.6	2,12	43316.2
	2308.90	1	43297.3	3,13	43296.2
	2309 47	1	43286.6	—	—
	2310.03	1	43276.1	4,14	43276.0
	2310 70	2	43263.6	-	—
	2311.49	2	43248.8	5,15 and 0,11	43252.8
	2312 34	2	43232 9	1,12	43233.9
	2313.30	3	43215.0	2,13	43215.6
	2314.31	1	43196.1	3,14	43197.6
	2314.56	?	43191.5	—	—
	2315.14	1	43180 6	4,15	43180.0
	2315 77	1	43168 8	—	—
	2316.24	1	43160 1	5,16	43162 7
	2316.98	3	43146 3	0,12	43150 2
	2317.64	1	43134.0	1,13	43133.3
	2318.13	4	43124.9	—	—
	2318.70	1	43114.3	2,14	43116.9

TABLE III (*contd.*)

Wave-length		Int	Wave-number Obs.	Classification	Wave-number Cal.
Earlier work	Author				
	2319.57	3	43098.2	3,15	43100.9
	2320.19	3	43086.6	4,16	43085.2
	2320.87	.	43074.0 ⎫	5,17	43069.9
	2321.36	2	43064.9 ⎭		
	2321.69	6	43058.8 ⎫	6,18	43055.0
2321.97 (5)	2321.98	5	43053.4 ⎭		
	2322.33	1	43047.1	0,13	43049.6
	2322.66	0	43040.6	7,19	43040.5
	2323.00	3	43034.5	1,14	43034.6
	2323.60	3	43023.4	2,15	43020.2
	2324.18	3	43012.7 ⎫	3,16	— 43206.1
	2324.79	4	43001.4 ⎭		
	2325.24	3	42993.1	4,17	42992.4
	2325.60	6	42986.4	—	—
	2326.15	0	42976.2	5,18	42972.1
2326.76 (6)	2326.79	0	42964.4	6,19	42966.1
	2327.44	0	42952.4	7,20	42953.5
	2327.71	3	42947.5	0,14	42950.9
	2328.17	4	42938.8 ⎨	8,21 and 1,15	42941.2 42937.9
	2328.90	2	42925.5	2,16	42925.5
	—	—	—	3,17	42213.4
2320.05 (4)	2330.12	6	42903.0	4,18	42901.6
2331.13 (2)	2331.10	6	42884.0 ⎨	5,19 6,20	42890.2 42879.2
2332.23 (0)	2332.04	5	42867.7	7,21	42868.6
	2332.88	2	42852.3	0,15	42854.2
	2333.24	2	42845.7	1,16	42853.2
2333.60 (2)	2333.78	4	42835.7	2,17	42832.7
2384.68 (3)	2334.82	6	42816.7 ⎨	3,18 4,19	42822.5 42812.8

TABLE III (*contd.*)

Band heads of the F_3-System

| Wave-length | | Int. | Wave-number Obs. | Classi-fication | Wave-number Cal. |
Earlier work	Author				
2335 64 (2)	2335 72	5	42800.2	5,20	42803.8
	2336.33	4	42789.0	6,21	42794.3
				7,22	42785.6
2336 ç2 (5)	2336.92	6	42778.2	8,23	42777.2
	2338.71	2	42745.5	1,17	42750.4
				2,18	42741.9
2339 53 (1)	2339.55	1	42229.4	3,19	42783.3
				4,20	42725.9
	2340.10	1	42720.1	5,21	42718.0
2340 92 (7bd)	2540.69	10	42692 8	9,25	42692.2
	2342.42	2	42677.8	11,27	42680.7
2342.56 (2)	2342.67	1	42673 2	12,28	42675.4
				26,42	42644.8
2344.51 (2)	2244.47	2	42640 4	4,21	42640.9
2345.49 (0)	2345.30	—	Mercury line		
2346.35 (00)	2346.34	2	42606.5	12,29	42606.2
2647 36 (00)	2347.21	1	42590.7	20.37	42595.6
—	—	—	—	0,18	42576.9

in more than one place. The method adopted in arriving at the classification was to derive the vibrational constants of the lower state using the data of band heads for which there is very close agreement between different sets of measurements. These are found to be in conformity with the ground state constants known from other systems. But the upper state constants could be determined only approximately from the above progressions. These values are finally fixed up by a method of successive approximation by comparing the calculated and observed values for bands and sequences such as $\Delta v = -10$ and $\Delta v = -11$ which are sufficiently well-resolved. The table of wave-lengths shows the observed and calculated values for all the bands and the general agreement between them. The discrepancies in the case of some are indeed found to be large. Perhaps an additional term in the formula may be necessary but on account of the nature of the bands such a term was not estimated. Table IV shows the intensity distribution in

this system which is totally different from that in the F_1-system. Long progressions and the tendency to sequence formation only at a point very remote from the origin are the chief characteristics. There are no bands representing the low v'' levels o to 3.

<div align="center">

TABLE IV

Intensity distribution in the F_3-system

</div>

v'/v''	4	5	6	7	8	9	10	11	12	13	14	15	16	17	18	19	20	21	22	23	24
0	0	0	2	2	1	3	2	2	3	1	3	2									
1	0	0	1	1	2	1	2	2	2	1	3	4	2	2							
2		0	0		0	1	0	1	2	3	1	3	2	4	2						
3		0						1	1	1	1	3	4	–	6	1					
4									0	1	1	1	3	3	6	6	1	2			
5													1	2	0	6	5	2			
6															5	0	6	4			
7																0	0		4		
8																		3	–		6
9																					

Special mention may be made of the classification of the last few bands in the system, chiefly of 42590.7 and perhaps of 42640.4, as they illustrate the somewhat rare feature of head-formation in sequences of band-heads (*cf.* Jevons, 'Report,' page 93). The band, 42590.7 is considered as the head of the sequence, $\Delta v = -17$, there being no alternative way of classifying it, it cannot be a member of the $\Delta v = -18$ sequence as the calculated position of its first member, (o,18), is at v 42576.9. The band at v 42640.4 can be considered either as (4,21) or as the sequence-head of the $\Delta v = -16$ sequence, which is expected at v 42644.8.

Mercury Isotope Effect.—The system shows bands involving very large v'' values *e.g.*, (3,15), (5,21) etc., in which the isotope effect may be appreciable. An actual estimate, however, indicates that these shifts (*e.g.*, ⁻7.2 cms $^{-1}$ for $Hg^{198}I^{127}$ in the case of (5,21) band) are approximately of the same order of magnitude as the sequence intervals, tending to make the bands appear diffuse when the resolution is not very large. The character of the bands at the red end justifies this view. A clear detection of the isotopic heads was not obtained even with the dispersion of the Littrow instrument.

VIBRATIONAL CONSTANTS AND ELECTRONIC
TRANSITION

The constants derived for the two systems F_1 and F_3 are collected in Table V which also shows those for the G- and H-systems. All the systems have a common ground state.

TABLE V

Table of Constants

System	F_1	F_3	G	H
Region	$\lambda\lambda 2530\text{-}2450$	$\lambda\lambda 2350\text{-}2265$	$\lambda\lambda 2234\text{-}2165$	$\lambda\lambda 2161\text{-}2115$
νc	40152.3	44530.6	45542.4	47110.2
ω''	125 6	126.1	125 7	125.3
$x''\omega''$	1.12	0.98	1.2	1.15
ω'	90.8	85.5	88.4	97.1
$x'\omega'$	0.93	0.8	0.2	1.65

The constants for both the states of the F_1-system are derived from the curves shown in Fig. 1 and are considered to be fairly accurate. The upper state vibrational constants for the G- and F_1-systems suggest that they
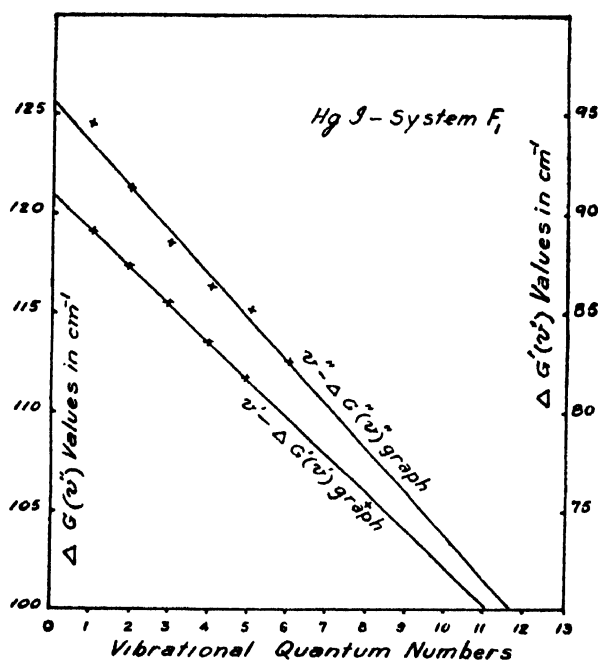
FIG. 1

are perhaps identical within the possible limits of error. The anharmonic constant $(x'\,\omega')$ for the G-system might be unreliable in view of the irregular variation of the $\Delta G'\,(v')$ values for this system (Ramasastry, and K. R. Rao, 1947).

The ν atom obtained for the F_1-system is of the same order of magnitude as the wave-number of the mercury resonance line at $\lambda 2537$. The values of the constants and the character and appearance of the bands of the F_1-and G·systems suggest that they may be due to a $^2\pi - {}^2\Sigma$ transition with the $^2\pi$ interval of 5490 cm^{-1}.

ACKNOWLEDGMENT

Physics Department
Andhra University

REFERENCES

Ramakrishna Rao and K. R Rao, 1946, *Ind. J. Phys* , **20**, 148
Ramasastry and K. R. Rao, 1947, *Ind J Phys.*, 21, 143.
Ramasastry, 1947, *Ind. J. Phys.* (communicated).

ON THE ANOMALOUS ABSORPTION OF GAMMA-PHOTONS

By P. K. SEN CHAUDHURY *

ABSTRACT. The absorption co-efficient of RaC gamma-rays penetrating through more than 16 cm. and up to 20 cm of lead was experimentally measured with Geiger-muller counter. The counter was placed in different distances from the source and in vertical and horizontal positions in order to investigate the nature of secondary radiations. The results obtained show that the heterogeneity of the photon beam and the secondary radiation combined together has two opposite effects on the apparent absorption co-efficient obtained by gradually increasing the thickness of absorber One predominates over the other depending on the position of the counter When the counter is nearer to the absorber surface the apparent absorption co-efficient increases with increasing thickness of Pb and when further away it decreases with increasing thickness These investigations may, therefore, have some significance in Rossi transition curve for cosmic-rays When the counter is at a distance 45 cm. away from the source both for horizontal and vertical positions of the counter the absorption co-efficient of gamma-rays filtered through 19 cm Pb is $416 \pm .028$ cm ^{1} which is more than 10% less than the theoretical minimum absorption co-efficient for gamma-rays in Pb. It is concluded that so much difference may be mainly due to positron annihilation radiation. Incidentally it is pointed out that since a slow positron gains in energy by capturing an electron the subsequent annihilation quanta may be partly responsible for the backward radiations in cosmic-rays and for the excess of low energy Compton electron associated with a cascade.

Another interesting fact noticed in the last experiment is that with the source in proper position the background rate of counting which remains nearly steady after 24.8 cm of Pb is about double to that due to cosmic-rays alone. This may be merely due to some multiple scattered quanta but the possibility of these residual radiations being partly meson-like or neutron-like is not excluded.

INTRODUCTION

Since the discovery of gamma-rays, its absorption in different materials had been investigated by many workers and a nice summary of all the earlier works is given by Rutherford, Chadwick and Ellis (1932). In all these experiments, electroscopes and ionisation-chambers of comparatively large dimensions were used for the measurement of intensity and the absorption of gamma-rays from Ra (B + C) and ThC in lead, mercury, aluminium, etc., was studied under various experimental devices to eliminate the effect of so-called degraded radiations of secondary origin. These degraded radiations are secondary gamma-rays of longer wave length produced in the material

* Fellow of the Indian Physical Society.

when a beam of gamma-rays passes through it and their effect is to increase the absorption co-efficient μ defined by the well-known exponential relation $I = I_0\, e^{-\mu d}$. But the numerical values for the absorption co-efficient obtained by various workers were rather conflicting and on analysis it was found that the absorption co-efficient depends mainly on two factors, *e.g.*, (1) degree of filtration and (2) the geometry of experimental arrangements. Factor (1) is due to the fact that we can never isolate strictly mono-chromatic gamma-ray source and the softer component of heterogeneous beam generally used is gradually cut out as the absorber thickness increases. As for example if we consider RaC gamma-rays, with which most of the experiment has been done, then, according to Ellis and Aston as mentioned by Rutherford, Chadwick and Ellis (*loc. cit.*) only 7.3% of the emitted gamma-rays are of energy 2.22 Mev and the rest are distributed over widely different energies. Skobelzyn (1927) obtained the evidence of a very feeble intensity of gamma-rays of energy 3 Mev. According to more recent investigation by Alichanow, Latyshev and others (1947) the hardest fraction of RaC gamma-rays is of energy 2 42 Mev. Similarly their investigations also showed that ThC gamma-rays of which the bulk of radiations are of energy 2.65 Mev, also contain a fraction roughly 25% of energy about 1.5 Mev to 2.2 Mev. Nowadays comparatively homogeneous gamma-rays are also available from the artificially radioactive element like sodium, etc., but even a homogeneous beam in passing through the matter becomes heterogeneous. In cosmic-rays also when a large burst or shower is generated by an energetic particle, we get a heterogeneous beam of photons partly due to Bremsstrahlung and partly due to positron annihilation radiations. Of course the intensity is comparatively small. The dependence of absorption co-efficient on the geometry of experimental arrangement is due to the mechanism of gamma-ray absorption as will be clear from the following brief discussion on the theory of gamma-ray absorption.

In recent years the inter-action of photons with matter has been thoroughly investigated from theoretical point of view and the results obtained have been very fruitful in explaining interesting cosmic-ray phenomena. In the region of gamma-photons it is now well-known that the absorption consists of three different processes namely, (1) photoelectric process, (2) Compton scattering and (3) pair formation and in higher energy region the latter two processes alone are important. The probability of Compton scattering was calculated by Compton, Dirac and finally by Klein and Nishina (1927) according to relativistic quantum mechanics. The probability of a photon of energy K_0 being scattered at an angle θ as a degraded quanta of energy K is given by the formulae.

$$d\phi = \frac{\gamma_0{}^2}{2}\, d\Omega\, \frac{K^2}{K_0{}^2}\left(\frac{K_0}{K} + \frac{K}{K_0} - \sin^2\theta \right) \qquad \cdots \quad (1)$$

$$K = \frac{K_0 \mu}{\mu + K_0 (1 - \cos\theta)}$$

μ is the rest energy of an electron and $d\Omega$ the element of solid angle. Now if the crossection (1) is integrated over all angles the total probability of a photon being lost by scattering per electron is obtained and in the higher energy region it is of the form

$$\varphi = \varphi_0 \frac{3}{8} \frac{\mu}{K_0} \left(\log \frac{2K_0}{\mu} + \frac{1}{2} \right) \qquad \ldots \quad (2)$$

which shows that the probability of Compton scattering decreases as the energy of the quantum increases. On the other hand the probability of pair formation is proportional to the square of atomic number and rapidly increases as the energy of the photon increases. Therefore due to these two opposite effects gamma-photons have a minimum absorption co-efficient and as calculated by Heitler (1944), the minimum absorption co-efficient in lead is .475 cm^{-1} for energy about 3 Mev. The minimum is rather flat and there is very little change in the value of absorption co-efficient from energy 5 mc^2 up to 10 mc^2. The theoretical values of absorption co-efficient have been experimentally verified by several workers, *e.g.*, Meitner and Hupfeld (1930), Chao (1930), Tarrant (1930) and others. But though all of them used adequate precaution to eliminate the effect of secondary radiations they did not use sufficient filter thickness to cut out the softer components. Only 6 or 7 cm. lead was used as the filter thickness. The presence of softer component at this thickness would appreciably increase the absorption co-efficient.

Recently Cork and Pidd (1944) measured the absorption co-efficient of gamma-rays in different materials and for radio-active sodium gamma-rays of energy about 2.8 Mev they found a value much lower than the theoretical value in lead and copper up to about 10 cm. thickness. They concluded that Klein-Nishina formulae for Compton scattering are not valid. Cork (1945) confirmed his result in a subsequent paper. We came across this paper when we had finished our experiment and our results are also similar to that of Cork only under certain experimental condition. But the conclusions of Cork and Pidd about the inefficiency of Klein-Nishina formulae have been contradicted by Gerhart Groet-Zinger and Lloyed-Smith (1945) who measured the absorption co-efficient of radio-sodium gamma-rays with a twofold coincident counter arrangements. The counter thickness was such that only Compton electron of energy more than 2 Mev can pass through both the counters. They found complete agreement with theory. Their results, therefore, show that the anomaly is due to some secondary softer radiation.

EFFECT OF SECONDARY RADIATIONS

Now let us make a brief analysis to what extent different secondary radiations may effect the experimentally determined absorption co-efficient

depending on the geometry of experimental arrangement. Firstly, the probability of Compton scattering as given by (1) for energetic quanta is maximum in the forward direction and so some of the photons, which are presumed to be lost by scattering, may still pass through the measuring instrument and thus reduce the absorption co-efficient. The presence of softer secondaries in the original beam itself, however, would increase the absorption co-efficient.

Secondly corresponding to each photon lost by pair formation we get a positron electron pair emitted within a solid angle approximately $\frac{mc^2}{K_0}$ where K_0 is the energy of the photon. The positron, however, gains in energy by capturing an electron before annihilation. As a matter of fact a slow positron has a negative energy absorption co-efficient and therefore its absorption at low energy will be quite different from that of an electron. The positron may annihilate emitting two photons in the backward and forward directions or a single photon in the forward direction. Dirac (1930) calculated the probability of two quanta annihilation of a positron and showed that it is maximum when the positron is at rest. In general, however, the positron annihilation radiations will have a continuous energy distribution. Experimentally also the disappearance of fast positron in Wilson chamber photographs has been observed by some workers. According to Heitler (*loc. cit.*) again the probability of positron annihilation is maximum when its K. E. is about mc^2. Therefore the total energy of positron electron system plus the K. E. of the positron will be about 1.5 Mev. Since the energy of the quanta emitted in the backward direction is generally of the order mc^2 the quanta emitted in the forward direction will be of energy about 1 Mev. The whole energy may also be emitted as a single quanta in the forward direction but the probability of one quanta annihilation as calculated by Heitler (*loc. cit.*) is only 20% to that of two-quanta annihilation. This two-quanta annihilation was roughly verified by Klemperer (1933), Thibaud (1933), Joliot (1934) and others. The excess scattering of photons of energy mc^2 in the forward direction, as observed by Gray and Tarrant (1932), is an indirect evidence of two quanta annihilation. Similarly the upward radiation produced by cosmic-rays at higher altitude as observed by Korff and Clarke (1939) by placing a lead block below the counter may be partly due to upward positron annihilation quanta, for whenever a shower is produced in lead, positrons are generated and these by two-quanta annihilation emit corresponding number of photons in the upward direction. The same positron annihilation photon may also produce excess of low energy Compton electron associated with a shower.

Now the extent to which these positron annihilation radiations can effect the absorption co-efficient, provided the measuring instrument is within the solid angle of pair emission, will depend on what fraction of these can come out of the absorber without scattering or re-absorption. The probability of

absorption for one Mev photon is rather high. But recently Ruark (1945) and others have suggested that when a positron captures an electron the annihilation of the positron electron system is not instantaneous. He also refers to a paper by Wheeler (1946). The name Electro-meson itself suggests that the system can penetrate a large thickness of matter as a cosmic-ray meson before annihilation. If this idea is theoretically sound it is of particular significance in penetrating cosmic-ray cascades and in the absorption of hard gamma-rays capable of generating pair. The effect will be to reduce the absorption co-efficient. Dr. Bhabha, however, is of opinion that such a system can only form an unstable atom and if it is of sufficient K. E. the process will be immediately ionised. But there it will again capture an electron and it will continue till the annihilation.

Thirdly if the pair formed be of sufficient energy they can multiply as in cascade process worked out by Bhabha and Heitler (1927) and others. The effect will be to reduce the absorption co-efficient. But in the gamma-ray region if any quanta are produced by radiation loss it will be of low energy. The critical energy for Pb. is about 10 Mev. Moreover cascade-effect is confined to first few cm. of Pb only.

EXPERIMENTAL PROCEDURE AND ARRANGEMENTS

We repeated Russel's (1913) experiment at higher thickness of lead with gamma-rays from a radon capillary in equilibrium with RaB, RaC, etc. As is well known the penetrating component is only RaC gamma-rays and the rest are cut out at much lower thickness of absorber. Russel measured the absorption co-efficient in mercury up to about 20 cm. for gamma-rays from a 300 mc., radon capillery in equilibrium. A large electroscope was used for the measurement and he found the same absorption co-efficient from about 3 cm., up to about 20 cm. of mercury. From the mass absorption co-efficient of mercury he also deduced the absorption co-efficient for lead to be about .5 cm.$^{-1}$ But afterwards his homogeneous absorption co-efficient up to 20 cm. of mercury and lead was doubted by Rutherford, Chadwick, Ellis (loc. cit. and others due to the complexity of gamma-ray spectra revealed by the study of recoil electrons. As stated above the high degree of heterogeneity in the RaC gamma-ray itself has been recently confirmed by Latyshev (loc. cit.) and others. Further due to the large dimension of the electroscope and experimental arrangements the secondary effect was too large. Moreover the electroscope he used was of such sensitivity that a fraction less than 2×10^{-6} of the total intensity could not be detected. Now for 300 mc. of radon there will be about 10^{10} disintegrations per second and consequently this much sensitivity is rather too small. We therefore repeated Russel's experiment with a much more sensative Geiger-Muller counter placing it at different

distances from the absorber surface in order to investigate the nature of secondary effect.

FIG. 1

FIG. 2
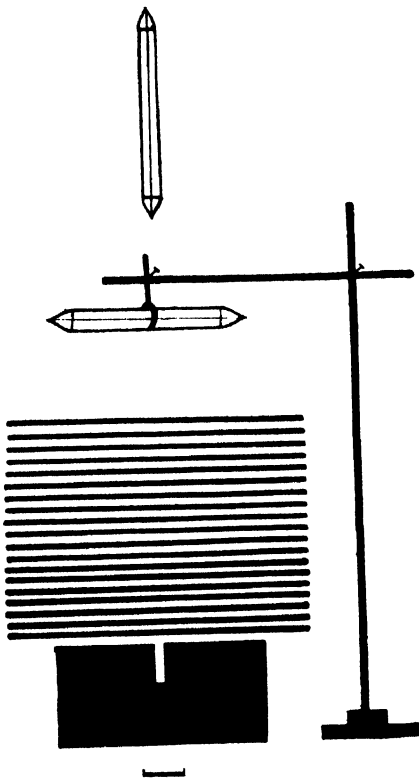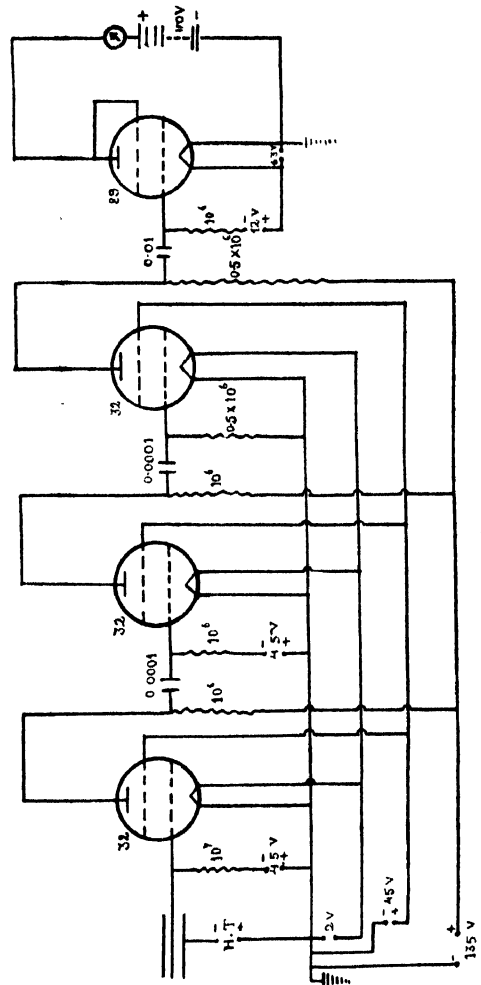
The experimental arrangement is shown in Fig. 1. A small radon capillary of length about 5 mm. was placed vertically in a hole of diameter about 5 mm. and depth 4 cm., drilled at the centre of a lead block of diameter 21 cm. and thickness 10 cm. Then successive numbers of lead plates of dimension 12″ × 12″ × 1/8″ were placed on the hole symmetrically up to a height about 20 cm. The object of the hole is to give a canalising effect and eliminate as far as possible the effect of an extended source. The corresponding intensity under each thickness of absorber was studied with two Geiger-Muller counters placed horizontally and vertically above the absorber and at different

TABLE 1

Distance of the counter above the source = 30cm.

Counter voltage = 1500 volts.

Amount of Radon	Thickness of Pb. absorber in cm.	No. of count per 2mt. ↓	No. of count per 2mt ↑	Average No. of count per 2 mt.	Absorption co-efficient	Range
56 mc.	24.77	208	197	202 5		
	20.33	297	278	287.5		
	20.01	280	293	286.5		
	19.69	301	305	303 0		
	19.37	312	333	322.5	.48 cm.⁻¹	19.7 & 18.7 cm.
	19.06	312	347	344.5		
	18.74	388	375	381.5		
	18.42	416	390	403.0	.52 ,,	19 1 & 17.8 cm.
	18.10	410	135	437.5		
	17.79	480	475	477.5		
	17.47	520	515	533 5		
	17.15	584	567	575 5	.43 ,,	17.8 & 16 5 cm
	16.83	622	617	619.5		
	16.52	656	695	675.5		
	16.20	768	817	792.5	.40 ,,	17.2 & 15 9 cm.
	15.88	855	835	845.0		

TABLE II

Distance of the Counter above the source = 40 cm.

Counter voltage = 1500 volts.

Amount of Radon	Thickness of Pb. absorber in cm.	Average No. of count per 2 mt.	Absorption co-efficient	Range
110 mc.	24.77	204		
	20.33	326		
	20.01	351		
	19.69	362	.43 cm.⁻¹	20.33 & 19.10 cm.
	19.37	394		
	19.06	414	.40 cm.⁻¹	19.7 & 18.7 cm.
	18.74	436		
	18.42	490	.47 cm.⁻¹	19.10 & 17.80 cm.
	18.10	521		
	17.79	586		
	17.47	647	.49 cm.⁻¹	17.47 & 17.15 cm.
	17.15	725		
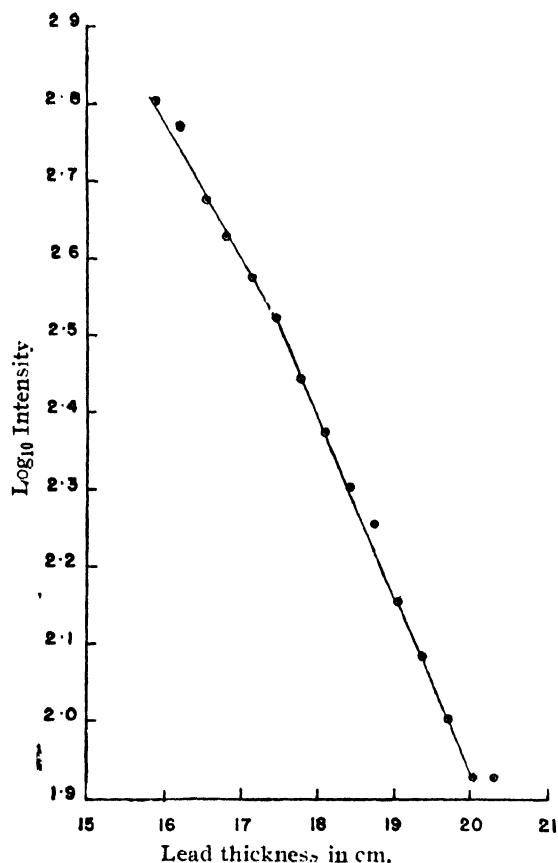
FIG. 3

distances away from the source in order to investigate the nature of secondary radiations. The results obtained are represented in the tables above. The data of Tables I and II were obtained by the same counter placed horizontally at a distance 30 cm. and 40 cm. respectively away from the source. The counter is of diameter 3.5 cm. and the length of the copper tube in glass is 15 cm. The data of Table III were obtained by a more sensitive and stable counter placed vertically above the source with the bottom of the tube at a distance 45 cm. away from the source. This counter was of diameter 2.7 cm. and length 15 cm. The circuit designed by us with the available valves is shown in Fig. 2. The mechanical counter was a Cenco counter capable of counting at the rate of about 10 per sec. and the resolving time was much less than what is necessary for the high rate of counting used in these experiments. Data of Table I and Table II are plotted in logarithmic scale against the absorber thickness in Fig. 3 and Fig. 4 respectively.

TABLE III

Counter No. 2 held vertically.

Distance of the bottom of the counter above the source—45 cm.

Pb filter thickness—19 cm.

Amount of Radon	Thickness of Pb. absorber in cm.	No of counts per 2 mts.									Absorption Co-efficient
		↓	↑	↓	↑	↓	↑	↓	↓	↑	
150 mc.	27 31	300	285		295		290			288	
	24.77	307	300	321	305	323	296				$416 \pm .028$ cm^{-1}
	20.33	399	410	135	395	424	405	433	408	426	
	19.00	510		500		510		518	500		
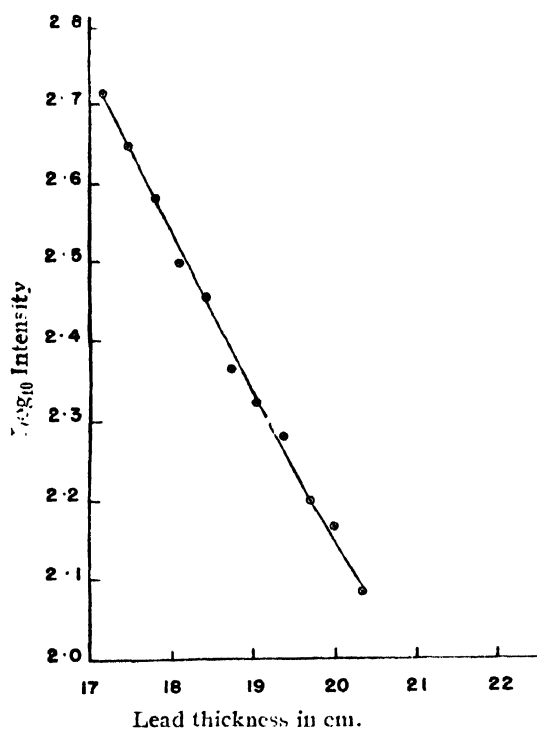
Fig. 4

RESULTS AND DISCUSSION

Table I shows that starting from about 16 cm. thickness of absorber the apparent absorption co-efficient is at first less than the theoretical minimum absorption co-efficient in lead and then gradually increases with the increasing thickness of absorber up to 19.1 cm. The absorption co-efficient between 19.7 and 18.7 cm. is again slightly less and may be due to fluctuation. In order to visualise the effect of fluctuation we repeated the experiment more than once and finally observed the rate of counting when increasing the absorber and then again when decreasing the absorber with a large number of thin lead sheets. From the data it appears that although some error is unavoidable at least the qualitative nature of the result is correct. The logarithmic plot of the data in Fig. 3 also shows that at least two, if not three, different st. lines can be drawn. In this position the counter was 30 cm. above the cylinder surface and due to slight curvature of the lead sheets when the absorber thickness was 20.33 cm., the counter was at a distance about 5 cm. above the absorbing surface and in this position the absorption co-efficient is practically the same as that obtained by Russel. As a matter of fact Russel's experimental condition was such that the absorber itself formed the bottom of the electroscope.

When the counter is 40 cm. above the cylinder surface Table II shows that allowing for some unavoidable fluctuation, the absorption co-efficient steadily decreases with increasing thickness of the absorber as is expected from gradual elimination of the remaining trace of softer radiations. The logarithmic plot

of the data in Fig. 4 also shows a distinct change in slope towards higher thickness. An approximate calculation from the relative intensity distribution of RaC gamma-rays as given by Aston and Ellis (*loc. cit.*) and the theoretical absorption co-efficient shows that even after 16 cm. thickness of absorber about 10% of 1.8 Mev gamma-rays remain. The absorption co-efficient of the fraction of gamma-rays between 18.7 to 20.33 cm. of lead fluctuates between .40 cm.$^{-1}$ and .43 cm.$^{-1}$.

It is therefore clear from the absorption co-efficient measurement in these two positions that as a combined effect of heterogeneity of photon beam and secondary radiation there are two opposite effects on the absorption co-efficient obtained by gradually increasing the absorber thickness. One predominates over the other depending on the geometry of experimental arrangement. When the counter is nearer to the absorbing surface the absorption co-efficient increases with increasing thickness of absorber. As referred by Rutherford, Chadwick, Ellis (*loc. cit.*) similar evidence was obtained by Oba and Bastings. When the counter is further away the absorption co-efficient decreases with increasing thickness. This may be the reason why Russel obtained the same absorption co-efficient from 3 cm. up to 20 cm. of mercury, although RaC gamma-rays are highly heterogeneous. Similarly in other experiments the apparent agreement with theory may be purely due to the balancing of these two opposing effects or due to incomplete filtering.

Further it may be pointed out that in large cosmic-ray showers and bursts we get similar heterogeneous beams of photons and as various geometry of counter arrangements are used to study the shape of transition curves and other cosmic-ray phenomena this experiment may have some indirect significance in those experiments also.

Now as the Table 2 shows that the average absorption co-efficient for gamma-rays filtered through about 18 cm. of lead is .415 cm.$^{-1}$, which is more than 10% less than the theoretical minimum absorption co-efficient in lead, we therefore more thoroughly studied the absorption of gamma-rays filtered through 19 cm. of lead with a more sensitive and stable and smaller counter placed vertically at a distance 45 cm. above the source. The number of counts per two minutes was observed several times at random extending over two hours under 19.06, 20.33, 24.77 and 27.31 cm. of lead absorber. The observations at the two latter thicknesses were to notice if there were any fluctuations in the back-ground immediately before and after the measurement under the two former thicknesses. The experimental data are represented in Table III along with the calculated absorption co-efficient and the standard deviation. The absorption co-efficient is .416 ± .028 cm^{-1} which is the same as the average absorption co-efficient obtained in the previous experiment by placing the counter horizontally at nearly the same distance away from the source. This shows that the lower value is not due to scattered photons as in that case there would have been appreciable difference in absorption co-efficient measured at two different orientations of the counter. As stated above Cork and Pidd

(*loc. cit.*) obtained a value of absorption co-efficient .405 cm.$^{-1}$ for 2.8 Mev gamma-rays which is practically the same as that obtained by us for 2.4 Mev gamma-rays of RaC. Theoretically the minimum absorption co-efficient changes very slowly with energy, and therefore there is very little difference in value for this much difference of energy between 2.8 and 2.4 Mev. As we, and particularly Cork and Pidd, have used a highly canalised beam there can be little error due to scattering from an extended source. Cork and Pidd further state that after certain filter thickness an equilibrium is reached between the scattered and the unscattered radiations and the scattered radiations are present in the same ratio both in the incident and in the emergent beam and therefore they cannot affect the value of absorption co-efficient. They do not give any theoretical proof of their statement but our experiment, with the counter in vertical and horizontal position, and their own experiment at lower energy gamma-rays support this statement. With the same geometry of arrangements Cork and Pidd found almost complete agreement or very little difference with the theoretical value for 1.14 and 1.30 Mev gamma-rays, although these photons have also maximum probability of being scattered in the forward direction as that of 2.4 or 2.8 Mev photons. On the other hand their assumption that Klein-Nishina formulae is insufficient, is found to be untenable by the experiment of Gerhert-Groetzinger and Lloyed-Smith (*loc. cit*). who verified the Klein-Nishina formulae by confining their measurement only to high energy photons. From all these as well as from the fact that the disagreement with theory becomes appreciable only for higher energy photons when the pair formation begins it can be reasonably concluded that this anomally is due to pair-formation. From the total absorption co-efficient curves for gamma-rays in lead, as plotted by Heitler (*loc. cit.*), it appears that for 2.4 Mev gamma-rays about 1/5th of it is due to pair-formation and 4/5th due to Compton scattering and a negligible fraction due to photoelectric absorption. When a pair is formed both the positron and the electron will have only 1.2 Mev energy and as such they cannot come out of the absorber nor can they emit any radiation of appreciable energy as in a cascade. But since a positron gains in energy by capturing an electron before annihilation therefore positron annihilation radiation is likely to be the main cause of disagreement with the theory. Cork further states that in copper the pair formation is negligible and as the disagreement exists there also it is not due to pair formation. But if the value of absorption co-efficient calculated by them for pair formation in copper is subtracted from the total theoretical absorption co-efficient the experimental value is brought much nearer to the theoretical value and moreover, if Wheeler's idea of electro-meson is true, then the annihilation radiation from the filter may also affect the result. Of course, as kindly pointed out by Professor S. N. Bose, at higher energy the probability of multiple scattering will increase but just as scattering cannot effect the absorption co-efficient measurement similarly multiple scattering which is of still higher order may

not affect the absorption co-efficient appreciably. We hope to further investigate this point in future.

Another interesting fact, observed in the last experiment, was that when the radon source was placed in the cavity the background rate of counting, which practically remained steady after 24.77 cm. of lead absorber, was nearly double to that due to cosmic-rays alone when the source was not there. As shown from Table III the background count per 2 mt. is nearly 300, whereas the average background rate of counting, observed for about 15 minutes immediately before placing the source and just after its removal, is 157 ± 8. We carefully searched for any contamination in lead sheets, radon carrier, etc., but this was completely absent. We did not notice this in the two previous experiments and we took the rate of counting after 24.77 cm. of lead as the natural background. This might be partly due to the fact that we were not so careful and partly due to the fact that comparatively smaller amount of radon was used in those experiments. the difference of the last experimental conditions from the two previous ones was that (1) the counter was held vertically, (2) a strong radon source was used and (3) the source was enclosed by another platino-iridium tube. Although we are not sure of its chemical composition, it is as tested by a magnet not a very light element so that neutron may be emitted by photo disintegration of the nucleus. Moreover the counter was an ordinary copper glass counter filled with argon and petroleum-ether and therefore its probability of neutron counting was very small. Therefore this excess of background may be merely due to some multiple scattered photon reaching the counter other than through the absorber or due to some meson type of radiation emitted by the source or the container. Now the minimum thickness of lead that a photon will have to traverse in coming out of the cylinder is about 7 cm. at the bottom and 11 cm. by the side of the cylinder and then it will have to suffer back reflection and multiple scattering in order to reach the counter and as such its probability is very small. We cannot be, however, sure of it unless more lead sheets are used at the bottom and by the sides of the cylinder. As we have exhausted all the lead sheets we could acquire at present it is not possible to further elucidate this point. But the probability of the residual counting being due to some meson-like emission by the source or the container may not be impossible. We hope to investigate this point further in near future. But it should be mentioned that even if this double background is due to some scattered quanta reaching the counter other than through the absorber it cannot effect the absorption co-efficient calculated with this steady background.

supplying the lead sheets, and to Dr. S. D. Chatterjee, D.Sc., of Bose Institute, Calcutta, for supplying the glass copper assembly of the second counter.

TATA MEMORIAL HOSPITAL,
RADIUM DEPARTMENT, BOMBAY.

REFERENCES

Alichanow and Latyshev (1947), *Rev. Mod. Phys.*, **19**, p. 132.

Bhabha and Heitler (1937), *Proc. Roy Soc.*, **159A**, 132

Chao (1930), *Phy. Rev.*, **36**, 1519.

Cork and Pidd (1944), *Phy. Rev.*, **66**, 227.

Cork (1945), *Phy. Rev.*, **67**, 53.

Dirac (1930), *Proc. Camb. Phil. Soc.*, **26**, 361

Gerhart Groet-Zinger and Lloyed-Smith (1945), *Phy. Rev*, **67**, 53.

Gray and Tarrant (1932), *Proc. Roy. Soc*, **136**, 652

Heitler (1944), The Quantum Theory of Radiation, 2nd Edition, p. 215

Joliot (1934), *C. R.*, **198**, 81.

Klein and Nishina (1929), *Zeit. f. Phys.*, **52**, 853.

Klemperer (1933), *Proc. Camb. Phil Soc*, **30**, 347.

Korff and Clarke (1939), *Phy. Rev.*, **56**, 704.

Meitner, L. and Hupfeld, H. (1930), *Zeit. f. Phys.*, **67**, 147

Ruark (1945), *Phy. Rev.*, **68**, 278.

Russel (1913, *Proc. Roy. Soc.*, A, **88**, 72.

Rutherford, Chadwick and Ellis, 1932, Radiation from Rodio-active Substance

Skobelzyn (1927), *Zeit. f. Phys*, **43**, 354, (1929), **58**, 595.

Tarrant (1930), *Proc. Roy. Soc.*, **128**, 348.

Thibaud (1933), *C. R.*, **197**, 1629.

Wheeler (1946), *Ann., New York, Acad. Sci.*, **48**, 219.

ULTRA-VIOLET BANDS OF ZINC IODIDE—PART III.

By C. RAMASASTRY

Plate III

ABSTRACT. The band system E of the zinc iodide molecule, lying between $\lambda\lambda 2450$-2250 is photographed on the Hilger Littrow quartz spectrograph. Each band consists of three component heads, which are shown to be due to the three isotopic molecules $Z^{64} I^{127}$, $Zn^{66} I^{127}$ and $Zn^{68} I^{127}$, thus confirming the existence of the isotope 68 of zinc for the first time from the study of bands. Vibrational analysis of the bands gave the following constants; for $Zn^{64}I^{127}$.

$$\nu = 44114.5 \qquad \omega' = 142.0 \qquad x' \omega' = 3.0$$
$$\omega'' = 225.6 \qquad x'' \omega'' = 1.0$$

The diffuseness of the bands with $v' > 2$ is considered as evidence of predissociation in the upper state between the vibrational levels $v' = 2$ and $v' = 3$.

INTRODUCTION

The emission spectrum of zinc iodide was investigated by Wieland (1929) along with other allied halides. He gave the analysis of an intense and violet-degarded system lying between $\lambda\lambda$ 3392.6-3257.8 and derived the vibrational constants

$$\nu = 30117.6 \qquad \omega' = 248.2 \qquad x' \omega' = 0.70$$
$$\omega'' = 223.4 \qquad x'' \omega'' = 0.75$$

In addition, he reported the existence of two more groups of bands, one in the vicinity of 2400A and the other in the visible; but no measurements were given. Later, Oeser (1935) studied the spectra of the halides of zinc and cadmium both in absorption and in fluorescence. He could not obtain any banded absorption for zinc iodide but listed about fourteen fluorescence bands in the visible region. In an attempt to find the second component of the Wieland system, which was suggested by Howell (1943) to be one component of a doublet electronic system due to the transition $^2\pi - {}^2\Sigma$, Tiruvenganna Rao and K. R. Rao (1946) reinvestigated the spectrum of zinc iodide in emission and established the predicted component system in the set of ten diffuse bands lying to the violet side of the Wieland's main system, with the upper state constants $\omega' = 211.7$, $x' \omega'' = 2.5$ and $\nu_e = 30506.3$.

The doublet width of 370 cm.$^{-1}$ so obtained is of the expected magnitude. They also confirmed the existence of bands in the $\lambda 2400$ region and designated them as system E. The present paper deals with a detailed study of this system E.

EXPERIMENTAL

The experimental set up for this investigation is the same as that previously employed by the author in similar investigations and described in detail elsewhere. The spectrum is excited in the electrodeless H. F. discharge and also by a 1/4 K. W. transformer. For a complete development of this system E, it is found that the excitation with an H. F. oscillator is more favourable than that with a high voltage transformer. Considerable difficulty was experienced in obtaining a good photograph of the bands, due to the general continuum overlying the entire spectrum of the molecule. The system C between $\lambda\lambda 3400$-3250, analysed by Wieland, is the one most readily obtained owing to its high intrinsic intensity. A study of the various conditions in the discharge tube indicated that the overlapping continuum is probably not wholly due to the zinc iodide molecule itself, but most of it may be due to the continuous spectrum of free iodine (Ramasastry, 1947) formed as a decomposition product. After a number of attempts, it was found that the continuous spectrum could be reduced to a minimum and bands are brought out prominently by using the salt in a pure and dry condition, with optimum heating and minimum exposure in a very sharply focussed spectrograph having a fine slit. The colour of the discharge is beautiful golden yellow due, perhaps, to an emission continuum in the yellow region of the spectrum. The tube is to be heated until the salt just begins to sublime and the discharge shows this characteristic yellow colour. To maintain the temperature, intermittent heating is essential, chiefly, just at the instants when the discharge shows a tendency to become less yellow and more white, for this condition represents an excessive partial vapour pressure of iodine. Initially, the tube gives some trouble because of the presence of traces moisture that are invariably present in the salt owing to the highly hygroscopic nature of zinc halides. When long exposures of about four hours duration are required, heating should be done more systematically, say for about $1\frac{1}{2}$ seconds in every 5 seconds.

The Hilger small, medium and Littro quartz spectrographs of dispersions of 15, 5 and 2 A.U. per mm. in this region are employed for photographing the bands. Ilford Special Rapid and Selo-Chrome plates are used. Some of the plates are sensitised with fluorescent oil. The system could be obtained practically with no continuous spectrum within about 5 minutes, 20 minutes and 3 to 4 hours respectively on the three instruments. Measurements are made with a Hilger comparator taking the iron arc lines as standards.

An examination of the spectrogram revealed that each band is not single but consisted of just three heads of decreasing intensity ; the fainter components occurring on the short wave-length side of the strongest or the main head. The relative intensities of the three heads, as estimated visually, remained almost the same from band to band. This has led to the consideration that the component heads are, probably, of isotopic origin rather than details of rotational structure. Reference to the table of isotopes showed an agreement between the relative percentage abundance (50.9, 27.3, 17.4) of the three isotopes 64, 66, and 68 of zinc and the estimated ratio of the intensities of the three component heads. The three components are thus attributed to the isotopes of zinc as iodine, the other constituent of the molecule is known to have but a single isotope of mass number 127. Keeping this feature in view, the vibrational analysis is worked out. The picture (Plate III b) presents prominently four pairs of intense bands with sharp heads between $\lambda 2359$ and $\lambda 2327$. The wave-number differences between corresponding members of adjacent pairs are about 215 cm^{-1} which is of the order of the ground state frequency ($\omega'' = 223.4$) and it gradually decreases as one goes towards the longer wave-length side. Considering these successive members as forming ground state progressions, they could be extended both ways to include as many as twelve members in each ; the intensity in each progression rises to a maximum and then falls off gradually, as is expected. The appearance of distinct pairs, however, does not continue (Plate III a) very far. As the long wave-length end is approached, a sufficiently intense band is found to occur between the pairs. These intermittent bands, about six in number, could be formed into a third ground state progression with a smaller value of v'. Almost all the intense band heads in this manner formed members of three v'' progressions with $v' = 0$, 1 and 2. About a dozen bands towards the violet end, which are bread, diffuse and faint, have alone remained to be classified. The measurement of these bands is uncertain by as much as 0.5 A. U. corresponding to about 10 wave-numbers in this region. The very diffuse nature of these bands suggests the setting-in of predissociation in the upper state after the vibrational level $v' = 2$. On this basis they could be grouped into two progressions with $v' = 3$ and $v' = 4$. The uncertainty in the measurements of these bands on account of their diffuseness may be expected to account for the large discrepancies in the ΔG (v) values. The vibrational scheme thus derived is presented in Table I.

Table II gives details of the wave-length, wave-number data of the bands. The last column gives the assignment. The measurements are the mean values of four independent settings on the medium as well as Littrow Hilger quartz instruments. The symbol M indicates measurements only on the medium quartz plates. The intensities are visual estimates.

TABLE I

ZnI Bands—Vibrational Analysis of the E-System

$v'' \backslash v'$	0	1	2	3	4	$\Delta G(v)$
0				—	—	
1				44254 (0)	44391 (0)	
2		43773 (1)	43883 (1)	44039 (1)	44170 (1)	
3		43336.5(1)	43672 (1)	43823 (2)	43954 (2)	
4		43336.5(1)	43469 5(2)	43598 (2)	43737 (1)	
5		43118 5(2)	43242 5(2)	43382.5(1)	43514 (1)	217.5
6		42902.5(3)	43028 5(3)	—	43297 (1)	215.9
7	42540.5(1)	42688.0(5)	42816 0(2)	42955.3(1)	43082.0(0)	213.3
8	42329.5(2)	42476.5(5)	42605.0(3)	42731.5(1)	42868,0(0)	211.5
9	42126.0(4)	42267.0(4)	42398 5(4)	42522.0(1)	42652.5(0)	206.8
10	41924.5(4)	42060.0(4)	42192.0(4)			205 0
11	41723.5(1)	41852.0(3)	41986.5(3)			204 8
12	41525.5(2)	41646.5(2)	41783 5(2)			202.2
13	41332.0(0)	—	41580.5(2)			195.7
14	—	—	41380.0(1)			—
15	40927.0(0)	41059.0(1)	41181.5(0)			200.5
16	40734.0(0)	40872.5(1)				
$\Delta G(v)$	136.0	130.0				

TABLE II

Zinc Iodide Bands—System E

Wave-length	Int.	Wave-number	Assignment	
			$(v'.v'')$	Zn Isotope
2458.05	0	40670.0M	(1,17)	64
2454.2	0	40734 0M	(0,16)	64
2445 9	1	40872 5M	(1,16)	64
44.7	0	892.5M		
2442.65	0	40927.0M	(0,15)	64
2434.80	1	41059.0M	(1,15)	64

TABLE II (*contd.*)

Wave-length	Inst.	Wave-number	Assignment	
			$(v'. v'')$	Zn Isotope
2427.55	o	41181.5	(2,15)	64
2426.6		41197.0		
2425.4		41217.5		
2418.7	0	41332.0	(0,13)	64
2417.85	o	41346.0		
2415.9	1	41380.0	(2,14)	64
14.3	0	406.5		66
13.7	0	418.0M		67 ?
13.0	o	430.0M		68
2410.9	1	41466.0	(1,12) ?	64
2410.05	o	41480.5		
2407.45	2	41525.5	(0,12)	64
05.58	1	552.5		66
			(0,12)	68
2404.25	2	41580.3	(2,13)	64
02 65	0	607.5		66
01.45	0	629.0		68
2400.45	2	41646.5	(1,12)	64
399.5	1	662.5		66
98.1	o	687.0M		68
2396.0	1	41723.5	(0,11)	64
94.45	0	750.5		65
93.35	0	761.0		67 ?
93.05	0	775.0		68
2392.55	2	41783.5	(2.12)	64
91.3	1	805.0		66
90.1	0	826.0		68
2388.65	3	41852.0	(1,11)	64
88.2	0	860.0		
87.35	1	874.5		66
86.7	0	886.0		67
86.0	0	898.0		68
2385.1	0	41914.5		
2384.5	4	41924.5	(0,10)	64
83.1	2	949.0		66
81.85	0	971 5		
2381.0	3	41986.5	(2,11)	64
79.85	1	2007.0		66
78.65	0	028.0		68
2376.85	4	42060.0	(1,10)	64
75.75	2	079.0		66
74.75	1	097.0		68
2373.1	4	42126.0	(0,9)	64
71.75	2	150.5		66
70.5	0	171.5		68

TABLE II (*contd.*)

Wave-length	Inst.	Wave-number	Assignment	
			$(v'. v'')$	Zn Isotope
2369.4	4	42192.0	(2,10)	64
68.4	2	210.0		66
67.95	0	217.5		67
66.85	1	237.0		68
2365.2	4	42267.0	(1,9)	64
64.1	2	286.0		66
63.1	1	304.5		68
2361.7	2	42329.5	(0,8)	64
60.5	1	350.5		66
59.86	0	362.5		67
59.9	1	378.5		68
2357.85	4	42398.5	(2,9)	64
56.7	2	419.5		66
56.2	0	428.5M		67
55.6	1	439.0		68
2353.5	5	42476.5	(1,8)	64
52.6	3	493.5		66
51.65	1	510.0		68
2351.0	od	42522.0	(3,9)	64
50.3	od	534.5		
2350.0	1	42540.5	(0,7)	64
47.9	0	577.0		68
2346.4	3	42605.0	(2,8)	64
45.3	1	625.0		66
44.0	0	642.5		68
2343.8	od	42652.5	(4,9)	64
42.9	od	667.5		
2341.9	5	42688.0	(1,7)	64
41.0	2	705.0		66
40.2	1	718.0		68
2339.5	1	42731.5	(3,8)	
38.9	0	752		
38.0	0	758.5		
2334.85	2	42816.0	(2,7)	64
33.90	1	834.0		66
32.95	0	851.0		68
2332.00	0	42868.0	(4,8)	
31.20	0	883.0		
2330.15	3	42902.5	(1,6)	64
29.35	2	916.5		66
28.75	1	927.5		68
2327.35	1	42953.5	(3,7)	64
26.55	0	968.5		
25.95	0	980.5		

TABLE II (*contd.*)

Wave-length	Int.	Wave-number	Assignment	
			(v', v'')	Zn Isotope
2323.3	3	43028.5	(2,6)	64
22.55	2	043.5M		66
21.95	1	057.5		68
2320.45	1	43082.0	(4,7)	
19.40	0	108.0		
2318.5	2	43118.5	(1,5)	64
17.9	1	129.0		66
17.5	0	136.0		68
2311 95	2	43242.5	(2,5)	64
11.3	1	252.0		66
10.85	0	260.5		68
2308.9	1	43297.0M	(4,6)	
07.35	1	326.5		
2306.8	1	43336.5	(1,4)	64
05.9	0	354.0		66
2304.35	1	43382.5	(3,5)	
03 8	0	393 5		
03.1	0	405.5		
2300.1	0	43463M		
2299.75	2	43469.5	(2,4)	64
99.3	1	478.9		66
2297.4	1	43514M	(4,5)	
2295.5	1	43550 M	(1,3)	
2293.0	2	43598 M	(3,4)	
2289.1	1	43672 M	(2,3)	
2285.7	1	43737 M	(1,4)	
2283.8	1	43773	(1,2)	
2281.2	2	43823 M	(3,3)	
2278.1	1	43883 M	(2,2)	
2274 4	2	43954 M	(4,3)	
2270.0	1	44039 M	(3,2)	
2263 3	1	44170 M	(4,2)	
2259.0	0	44254 M	(3,1)	
2252.0	0	44391 M	(4,1)	

The vibrational constants for the upper states had to be determined only from the two intervals 136 and 130 involving the levels $v' = 0$, 1, and 2. Examination of the data indicates that even of these two values o

(130) is reliable. The difference 136 is obtained as a mean of about eight values which show large discrepancies. It may be significant to note that there is a steady decrease in the values, probably it arises from errors involved when the band heads instead of the band origins had to be measured. On account of such discrepancies the adopted values $\omega' = 142$, $x'\omega' = 3.0$ should be considered only as approximate.

For the determination of the constants of the ground state a graphical method is employed. The differences formed from bands, on which the settings are doubtful, are discarded. Averages of the remaining reliable ΔG (v) values are plotted as ordinates against equal divisions on the abscissae and a curve is drawn (Fig. 1) passing through as many points as possible. By extrapolation the ω'' value of 223.9 is obtained which agrees with the
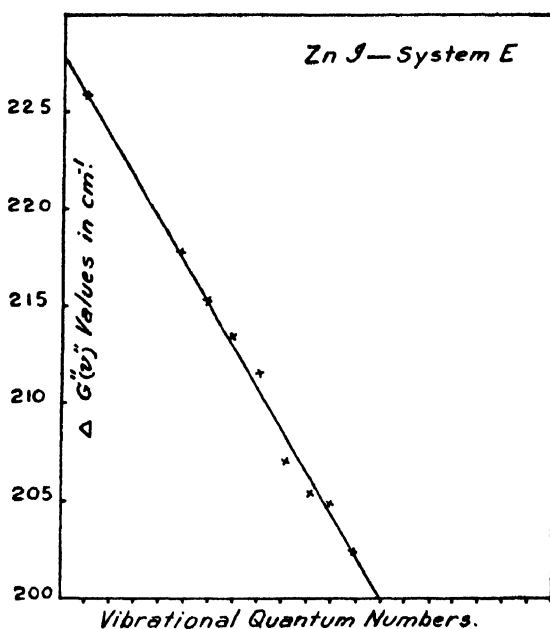
FIG. 1

value 223.4 reported previously by Wieland and is consistent with the view that all the v'' vibrational levels, beginning from $v'' = 0$, are represented among the bands, *i.e.*, starting with the assignment of the two bands of wave-numbers 44254 and 44391 as (0,3) and (0,4) bands respectively.

With the above vibrational constants and the quantum number assignments a confirmation of the scheme is attempted with the help of the isotope shifts. This has revealed a systematic divergence between the calculated and the observed isotopic shifts. A satisfactory agreement could finally be arrived at when the ground state vibrational quantum numbers are increased by 1. It meant starting with the assignment of the two bands $v44254$ and $v44391$ as (1,3) and (1,4) instead of as (0,3) and (0,4) respectively; this also involved an increase in the value of ω'' from 223.9 to 225.6. Though there will be no

Fig. 4. Zinc Iodide Bands (E System).

(a) Medium Quartz and (b) Quartz Littrow Spectrograms
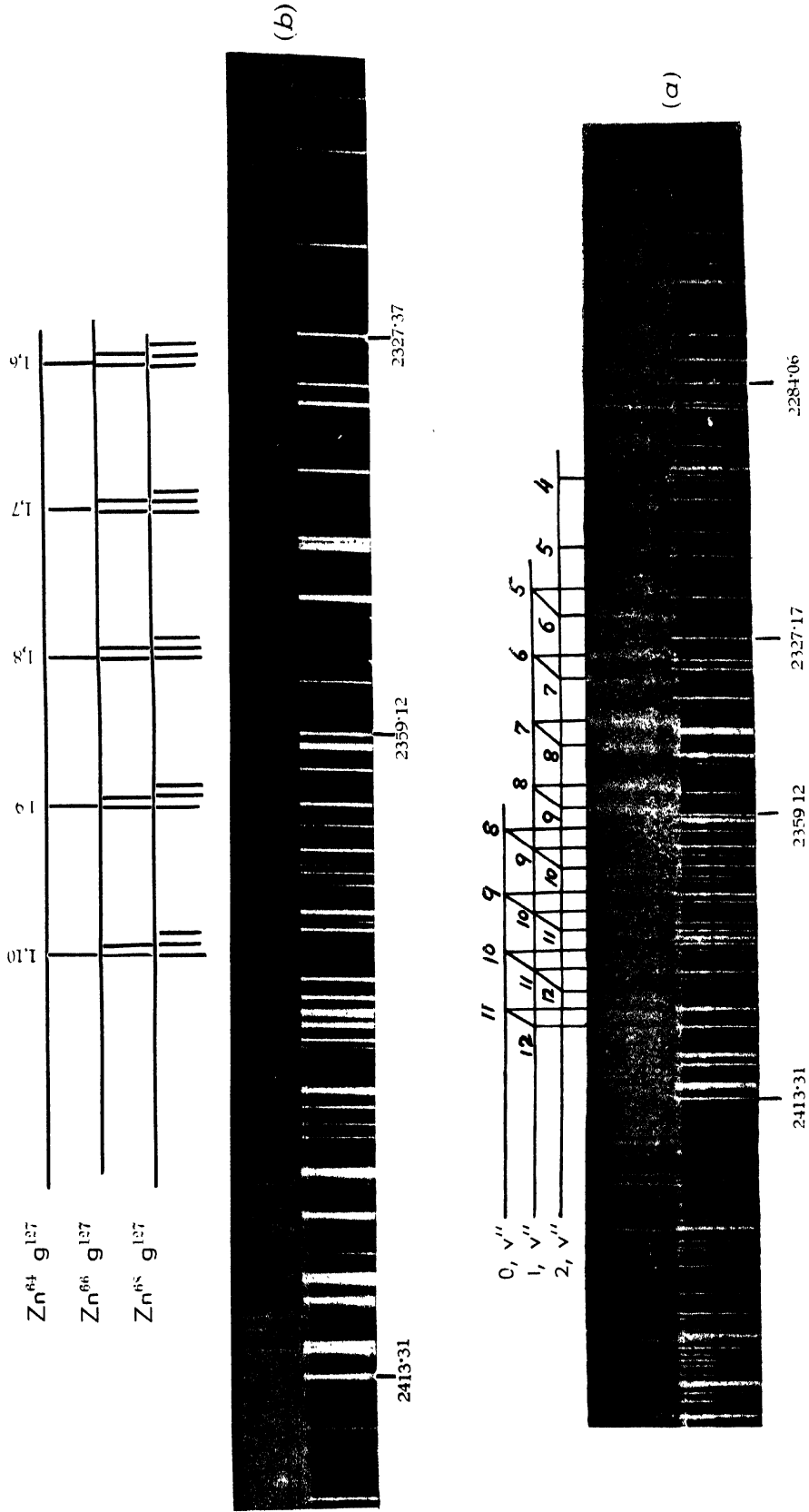
bands to represent the $v''=0$ level, it is this assignment of quantum numbers that is finally adopted and is shown in Tables I and II. The agreement between the observed and calculated isotope shifts in the case of all bands, where the measurements could be made with some degree of certainty, is seen from Table III and Table IV is a collection of all the constants used in the calculation.

TABLE III (*Isotopic Shifts*)

v''/v'	0		1		2	
	obs.	cal.	obs.	cal	obs.	cal.
4					8.5	7.3
					—	14.6
5			10.5	11.1	9.5	9.6
			17.5	22.2	18.0	19.2
6			14.0	13.6	14.0	12.1
			29.0	27.2	29.0	24.2
7	—	17.3	17.0	16.0	18.0	14.5
	36.5	34.0	30.0	32.0	35.0	29.0
8	21.0	19.8	17.0	18.5	20.0	17.0
	—	39.6	33.5	37.0	37.5	34.0
9	24.5	22.1	19.0	20.8	21.0	19.3
	45.5	44.2	37.5	41.6	40.5	38.6
10	24.5	24.5	19.0	23.2	18.0	21.8
	—	49.0	37.0	46.4	45.5	43.6
11	27.0	27.0	22.5	25.7	20.5	24.2
	51.5	54.0	46.0	51.4	41.5	48.4
12	27.0	29.4	—	28.1	21.5	26.7
	55.0	58.8	40.5	56.2	42.5	53.4

TABLE IV

$$v_e = 44114.5$$

$$\omega'_e = 142.0 \qquad \omega_e'' = 225.6$$

$$x'_e\omega'_e = 3.0 \qquad x'''_e\omega''_e = 1.0$$

Molecule	$\rho-1$	ρ^2-1
$Zn^{66} I^{127}$	—.01	—.02
$Zn^{68} I^{127}$	—.02	—.04

Three characteristic features of this system of zinc iodide bands may be emphasised in conclusion, which are not observed in the system C, analysed by Wieland.

(a) For the first time, evidence of the isotopes of zinc 66, 68 (and probably also of 67) has been distinctly obtained. The relative magnitudes of the ω' and ω'', the large v'' values involved in the band system, and the direction of degradation of the bands proved favourable for the detection of the isotopic

components, whereas in the C-system the isotopic heads corresponding to mass 66 only are resolved.

(b) Predissociation in the upper electronic state which is in evidence not by an abrupt absence but by the sudden diffuseness of all the bands after the vibrational level, $v' = 2$.

(c) Long ground state progressions, rather than long sequences while the sequence appears, are predominent on the C-system.

All these features are found also in yet another system of the zinc iodide which the author has succeeded in photographing. This system (which may be designated as D_i) was not measured or even mentioned by any of the previous workers. It consists of about eighty bands between $\lambda 3000$ and $\lambda 2700$. The bands are degraded to the red. A preliminary analysis gave two long progressions but the presence of a third one could not as yet be established definitely owing to the crowding and considerable overlapping of the main heads and the isotopic heads. The analysis of this system of bands will be presented in a later communication.

REFERENCES

Howell, 1943, *Proc. Roy Soc.*, **182**, 95.
Oeser, 1935, *Zeit. f. Phys.*, **95**, 699.
Ramasastry, 1947, *Ind. J. Phys.*, Communicated.
Tiruvenganna Rao and K. R Rao, 1946, *Ind. J. Phys.*, **20**, 49.
Wieland, 1929, *Helv. Phys. Acta.*, **2**, 46 and 77.

ELECTRICAL CHARGES IN LAYER-LATTICE SILICATES IN RELATION TO IONIC EXCHANGE

By R. P. MITRA AND K. S. RAJAGOPALAN

ABSTRACT. Many layer-lattice silicates, *e.g.*, the micas and the clay minerals, show, especially in finely divided states, a marked capacity to exchange some of the exposed ions of the silicate lattice for similarly charged ions of a 'contact' solution. The mechanism of this ionic exchange and in particular, the nature and the origin of the (surface) charges which hold the exchangeable ions in the liquid phase at some distance from the surfaces of the crystallites has been discussed. The weakness of a purely colloidchemical explanation of these charges in terms of what are known as 'primarily absorbed ions' on the surface has been pointed out, and our existing knowledge of the atomic structures of these crystals has been shown to provide a more real and reliable basis for discussions on the exchange reaction and the surface charge. The most polar ions (and, in some cases, groups) on the surface of the crystallites interact with the dipoles of the 'contact' liquid which makes them execute a certain type of oscillatory motion about mean positions in the liquid phase at some distance from the surface, and it is these ions which under suitable conditions, are exchanged for similarly charged ions present in the liquid phase. The mechanism of this ion-dipole interaction and its electrochemical consequences, especially, in regard to the exchange behaviour of the crystallites have been discussed, taking the mica-water system as a model The nature of the so-called 'broken bonds' developed on the lateral surfaces of the caystals and the role frequently attributed to them in determining the ion-exchange properties of these systems has also been discusssd The acidic and basic character of hydroxyl groups present in these silicates has been examined.

Many crystalline silicates, *e.g.*, the clay minerals and the micas, have a layer-lattice structure (Pauling, 1930). The characteristic structural element is a hexagonal network of O^{-2} ions co-ordinated tetrahedrally about Si^{+4} or Al^{+3} (Fig. 1). This network is joined through the unshared oxygen
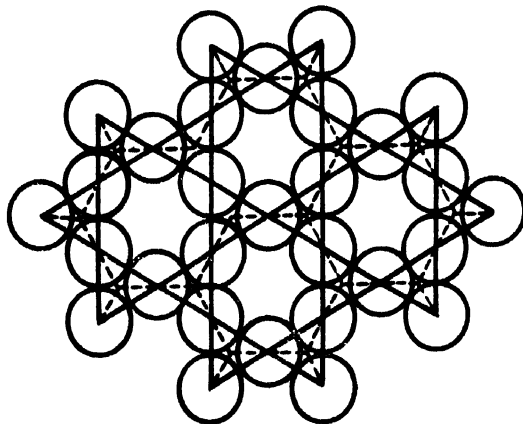
FIG. 1

Hexagonal network of linked Si(orAl)-O
tetrahedra in which all the tetrahedra
point in the same direction.

of each tetrahedral unit to groups of O^{-2} and OH^{-1} ions arranged octahedrally around ions like Al^{+3}, Mg^{+2} and Li^{+1}. Fusion of the tetrahedral and octahedral layers gives the unsymmetrical packet, $Al_2Si_2O_5(OH)_4$ (Fig.2a), found in clay minerals of the kaolin group. A symmetrical packet having the composition $Al_2Si_4O_{10}(OH)_2$ (Fig. 2b) is formed when a second tetrahedral layer is attached to the octahedral sheet from the other side and it occurs in the mineral pyrophyllite and, with some ismorphous replacement of the Si and/or Al by cations having a smaller positive charge, in the micas and clay minerals of the montmorillonite and illite groups. Both the 2-layer and the 3-layer silicates can and do take up cations (or bases) from solutions in exchange for cations already present in the silicate lattice. Anions, as a rule, do not have much preference and even when taken up are much less eagerly retained. Exception is made in the case of certain anions the most important of which is PO_4^{-3}.

The fact that the silicate crystal can take up cations and anions from solutions shows that it contains potentially active negative and positive centres

KAOLINITE

PYROPHYLLITE
MONTMORILLONITE (IDEAL CASE)
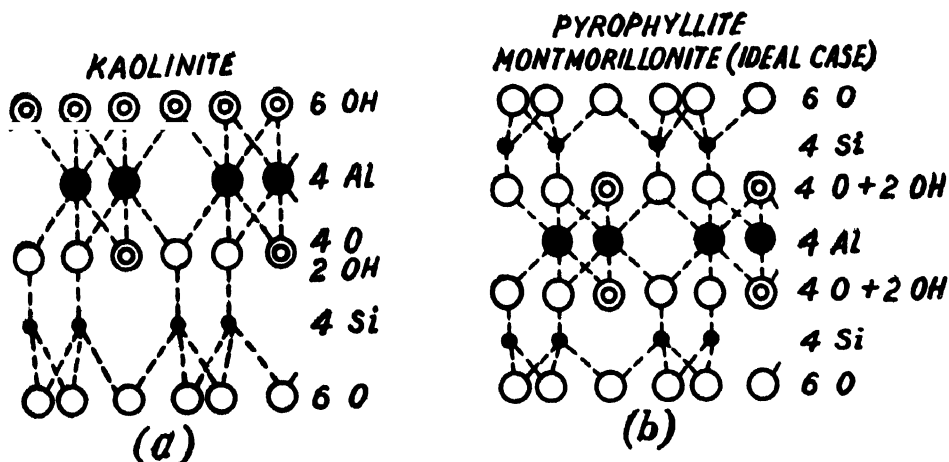
FIG. 2

in the lattice. Clay crystallographers believe that the exchangeable ions of clays are constituents of the silicate lattice being held opposite such potential centres of charges and yet accessible to the ions of a contact solution (Hendricks, 1945). The existence of these 'charge centres' is also indicated by the electro-kinetic behaviour of clays in ionising media. Depending on its own constitution and its ionic environment in the medium, the clay crystal migrates towards one of the electrodes at a definite rate, the exchangeable ions—they are the *gegenions* or counter ions of Pauli, moving towards the opposite electrode.* In a stable

---

* A simultaneous discharge of cations as well as anions takes place when aqueous suspensions of the clays are electrodialysed. The clay appears to suffer a hydrolytic cleavage, the H^+ and OH^- of water taking the places of the cation and the anion respectively.

suspension of the clay in an ionising solvent, the exchangeable ions, like all other counter ions, show quite definite and measurable conductivity and activity co-efficients (Wiegner and Pallmann, 1929; Mitra, 1936, 1940, Marshall., 1942,) properties which are, however, lacking in the clear ultrafiltrate of the sol (Mitra, *loc. cit.*). The existence of charge centres on the surface of the clay crystal which hold the exchangeable ions in the liquid phase at some distance from the surface is thus beyond doubt. But how do these (surface) charges come about? According to the well-known theory of Mukherjee (1920-21) and Fajans (1921) one would refer these charges to a primary adsorption (*i.e.*, adsorption by chemical or valence forces) of ions on the surface of the clay particles. Mukherjee and his co-workers (1933, 1937, 1945) have used this theory to great advantage in their discussions on the electrical properties of colloids including hydrosols of hydrogen (or, acid) clays. While the merits of the adsorption theory as a convenient working hypothesis for purposes of qualitative discussions on several aspects are beyond question, its limitations become obvious coming down to details and individual systems. For instance, identification of the 'primarily adsorbed' ions is far from easy in most cases, and the difficulty becomes almost insurmountable when one has to deal with endless sheets of co-ordinated ions as obtain in the clay minerals and other layer-lattice silicates. Fortunately, our knowledge of ion lattices in general and of the lattice-structure of platy silicates including the clays in particular, has developed to an extent as would make it unnecessary to invoke any adsorption hypothesis to account for the surface charges in these silicate crystals. Taking, for instance, the muscovite structure which is now so well understood mainly from the work of Jackson and West (1931) the K-ions in the interior of the lattice are known to

FIG. 3

The structure of Muscovite projected on (010) (After Jackson and West).

The heights of the atoms above the face of the unit cells, as measured along the axis of projection, are indicated by the numbers. An atom on the lower face of the unit cell is indicated by o, on the top face by 100, and intermediate heights are given accordingly.

be co-ordinated by electrostatic bonds to twelve O^{-2} ions (Fig.3) and yet these same K ions are readily exchanged when brought to the surface by cleavages

of the crystal perpendicular to the c-axis.* Each exposed K ion will now be co-ordinated to six oxygen ions if the cleavage has been perfect and it would be unnecessary to take recourse to any adsorption mechanism to account for the presence of the K^+ ions on the surface. The crystal chemist can probe deeper into the crystal and find a reason for the bonding (or co ordinating) power of the oxygens for the potassiums. He can trace this bonding power to unsatisfied oxygen valencies arising from a tetrahedral co-ordination of the oxygen ions around Al^{+3}'s in addition to the Si^{+4}'s, one in every four silicons having been replaced isomorphously by an Al^{+3}. Cations in the octahedral layer may similarly be replaced by others having a smaller positive charge—Mg^{+2} for Al^{+3} is the major replacement in the montmorillonites (Marshall, 1935) and the crystal chemist has been able to offer a very plausible explanation of the negative charges within the lattice on the basis of such replacements. The exchangeable cations only serve to balance these negative charges. Very fair agreement between the observed cation exchange power of montmorillonite and that calculated from isomorphous replacements has been obtained (Nagelschmidt, 1935, Marshall, *loc. cit.*). The balancing cations in this mineral can be exchanged for large organic cations (Giescking, 1939, Nelson and Hendricks, 1943). Different organic cations have been found to give different values of the basal spacing (001) which, combined with a knowledge of the sizes of the organic cations, definitely shows that the balancing (or exchangeable) cations in montmorillonite are held between the three-layer packets in much the same manner as the potassiums in muscovite.

While the above explanation of the negative charges seems to work quite well for most layer-lattice silicates having the 2:1 or symmetrical lattice†, it breaks down in the case of the 1:1 or unsymmetrical silicates, *e.g.*, kaolinite where isomorphous replacement is rather the exception than the rule, and the two-layer packets are practically neutral being made up in most cases almost exclusively of Si-O tetrahedra and Al (or Mg)—O(or OH) octahedra. There are no multi-co-ordinated large metal cations in the lattice (required for balancing negative charges arising from isomorphous replacements) which can be exchanged for those of an added electrolyte and yet finely ground kaolinite has been reported to take up cations from solutions to the extent of 100.5 milliequivalents per 100 gms. of the solid (Kelley and Jenny, 1936). To what is this cation binding power due? One answer to this question, which has been frequently given, is that the cations are held on the lateral surfaces of the sheets where unsatisfied negative charges or valencies are developed as a result of lattice termination (Hendricks, *loc. cit.*). The lateral surface increases on grinding which produces fractures

---

* Tetrahedral Al^{+3} being absent in the analogous platy mineral pyrophyllite, $Al_2Si_4O_{10}$ $(OH)_2$, there are no unsatisfied oxygen valencies to hold multi-co-ordinated large cations such as K^+ which become exchangeable on being brought to the surface by cleavages perpendicular to the c-axis.

† Chief exceptions are pyrophyllite and talc.

parallel to the *c*-axis by breaking valence bonds between Si and O, and between Al and O (or, OH). The fact that the cation binding power of kaolinite increases on grinding (Kelley and Jenny, *loc. cit.*) is, on this theory, to be attributed to an increase in the number of the broken bonds. This explanation has been critically examined in a recently published paper (Mitra, 1946) where it has been pointed out that if a cation's combining power is at all to be attributed to the broken bonds, an anion's binding capacity due to the same cause has to be simultaneously recognised, *i.e.*, the mineral must be considered amphoteric and not merely acidic. This follows directly from the "principle of microscopic neutrality" which requires that potentially positive and negative ends or poles be produced simultaneously and in equivalent numbers by the rupture of the ionic bonds. The finely ground solid would therefore tend to take up equivalent amounts of cations and anions from a contact-solution and not merely cations. Failure to appreciate this fundamental aspect of the broken ionic bond has been responsible for much of the confusion which exists in discussions of the relationship of the cation exchange capacity of clays to their crystal structure. One might refer in this connection to the criticism made by Kelley and Jenny (*loc. cit.* against a suggestion of Hofmann, Endell and Wilm (1934) according to which the exchangeable cations in clays are held by broken bonds on the edges of the Si-O planes. Kelley and Jenny ask, "If the broken bonds should bind cations from the solution, what would happen to the remaining anions in solution?" They argue that "if their (Hofmann *et al's*) hypothesis is valid, then when the clay fragments were removed from the solution more anions than cations would be left in the solution but such a system cannot exist, for it violates the law of electro-neutrality." They realise that "a solid cannot adsorb cations from solutions without an exchange process or an equivalent adsorption of anions" but fail to see that in the broken bond a cause for an equivalent adsorption of anions exists just as surely—theoretically at least—and for the same reason as it does for an adsorption of the cations. The 'broken bond theory' may or may not be true but the argument which Kelley and Jenny use to reject it is not quite convincing. Their criticism would be certainly valid if only a cation's binding power were attributed to the broken bonds as, indeed, appears to have been done by Hofmann *et al* and, more recently, by Hendricks (*loc. cit.*). Actually, however, the broken bonds would tend to bind—it is not claimed that they will actually do so—both cations and anions, *i.e.*, they would give a potentially amphoteric character to the comminuted solid—an aspect to which no reference is found in the writings of the above investigators

Let us now examine the more fundamental question : Is the broken bond theory at all plausible, that is, will the broken bonds in clay crystals and, for the matter of that, in any insoluble ionic crystal at all remove cations and anions from a contact solution? We might also put the question like this : will the act of comminution at all give rise to positive and negative

ends or poles which can exert sufficiently strong resultant positive and nega-
tive electrical fields external to the crystal so as to be able to remove cations
and anions from a contact solution by electrostatic attraction? The strengths
and separations of the oppositely charged poles appear to be the most im-
portant factors which have to be considered for answering this question.
This is, of course, true in so far as the ionic wall is concerned. Factors like
the size, valency, polarisability and state of hydration of the ions of the
contact solution would also matter but not unless there are strong enough
electrostatic fields beyond the crystal surface. We believe that with most
ionic crystals made up of closely packed oppositely charged ions, the odds
will be very much against the spacings between the positive and negative
poles being large enough to admit of the creation of sufficiently strong
negative and positive electrical fields external to the crystal which can attract
cations and anions from a contact solution and fix them to the solid wall.
It must be remembered that of the poles developed by comminution, con-
tiguous ones will carry dissimilar rather than similar charges in a statistical
sense. Let us take the case of the endless sheet of linked Si-O tetrahedra.
In breaking this sheet numerous Si-O-Si bonds will be ruptured. When
any two linked tetrahedra are torn apart, the oxygen through which they
were linked can evidently go with only one of the silicons giving it a nett
negative charge, a positive charge being left with the other silicon. Suppose,
now, a circular disc is taken out from the sheet and we then fix our atten-
tion on the peripheral silicons of this disc (Fig. 4). We shall find that
if a particular Si has been forced to part with one of its linked oxygens (e.g.,
the oxygen marked 1) in favour of the other part of the sheet giving a silicon-
oxygen configuration having the composition $(SiO_3/_2)$ and carrying one unit
of positive charge, then the silicon on the disc contiguous to it will have
completely appropriated to itself an oxygen ion (the oxygen marked 2 in
the figure) which has been torn off the other part of the sheet giving an Si-O

OXYGEN
ATOM

SILICON
ATOM
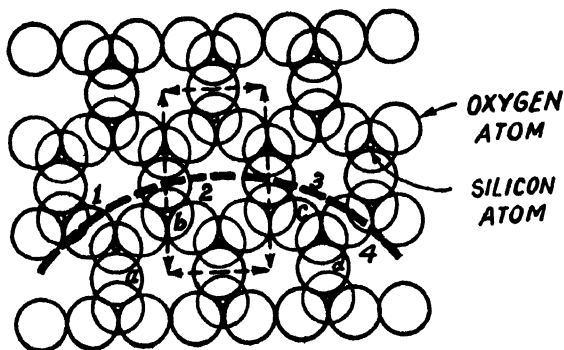
FIG. 4

assemblage with the composition $(SiO_3/_2)$ and carrying one extra unit of
negative charge. This is a physical necessity in as much as the positive
charge gained by the Si which has lost one linked oxygen will, by electros-

tatic attraction, try to win for the contiguous Si a complete oxygen ion taken from the other part of the sheet so that the positive charge may be balanced. The ionic crystal must be, to put it in Hendricks' language, "statistically neutral *on the smallest possible scale*" (Hendricks, 1945, *loc. cit.*). This should be so for the surface just as well as for the interior. The sheet can break only according to this plan. The act of comminution cannot chalk out an atomic line of demarcation just anyhow and anywhere through the sheet. The question, now, is, will the two peripheral contiguous $(SiO_3/_2)^{+1}$ and $(SiO_5/_2)^{-1}$ groups act as discrete centres of positive and negative charges towards the anions and cations of a contact solution with forces strong enough to bind them to the solid wall? Or, will there be a spatial rearrangement of the oxygens around the peripheral silicons so as to annul any possible external effect of contiguously situated oppositely charged poles created by comminution? The odds, we believe, are in favour of the second possibility which, in effect, amounts to a mutual cancellation of the positive and negative fields of contiguous poles so as to inhibit, or, even completely destroy a possible amphoteric character of the solid wall giving a substance akin to the socalled "Aquivalenz Korper" of Fajans.

Hydroxyl groups in layer-lattice silicates are often considered as the principal ionogenic groups capable of giving rise to positive as well as negative charges by dissociating as OH groups or as H ions, the ionic composition of the medium, especially, its p_H, determining which type of dissociation will occur. According to Kelley and Jenny *(loc. cit.)*, the acid character, *i.e.*, the cation exchange power of the minerals kaolinite and pyrophyllite is entirely due to the OH groups of the lattice. Kaolinite has two types of OH planes (Fig. 2,a), one made up entirely of OH groups and forming the exposed surface of a lattice packet and the other, a composite (O,OH) plane imbedded within a hexagonal network of oxygen ions.[*] Only the subsurface OH groups are present in pyrophyllite (and other clay minerals having a 3-layer lattice). This difference would lead one to expect that hydrogen kaolinite should be dibasic (Mitra, 1941-42), while a monobasic acid character is shown by pyrophyllite.[†] Hydrogen montmoril-lonite usually behaves as a monobasis acid (Mitra, Mukherjee and Mitra, (1946). Its acid character is due mainly to the H ions on the surface of the 3-layer packets derived from an exchange of the balancing cations of the lattice. Being at a considerable distance from the centres of nega-tive charges which in montmorillonite are mainly located in the octahedral layer, these H ions are expected to be more dissociable than the hydrogens of the OH groups. The usually observed monobasic acid character of hydrogen montmorillonite is to be attributed to a neutralisation of these

---

[*] OH groups belonging to the subsurface (O, OH) plane are also accessible through the hexagonal rings in the superimposed oxygen network provided, of course, the incoming ion has a diameter smaller than that (3Å) of the hexagonal ring.

[†] Unpublished work of K. S. Rajagopalan

readily dissociable H ions. The expected second stage of dissociation due to the hydroxylic hydrogens, is perhaps too weak for detection (as in the case of the third stage of dissociation of phosphoric acid), a contributing factor being the tendency of the first stage of dissociation to suppress the second.

A polybasic acid character of the layer-lattice silicates might be expected on other grounds. These become evident when the different possible types of isomorphous replacements in the lattice are considered. Such replacements may occur in tetrahedral as well as octahedral layers. The separation of the negative charge from the H ions on the surface of the lattice packet will be different in the two cases and consequently the strength of the electrostatic bond holding them will also be different. The H ions will, therefore, have different energies of dissociation. The fact that hydrogen montmorillonite usually shows a monobasic acid character is consistent with the current notion that in montmorillonite isomorphous replacement is almost entirely confined to the octahedral layer. The characteristic replacement in the micas is of Al^{+3} for tetrahedral Si^{+1}. The seat of the negative charge is nearer to the surface than in montmorillonite and consequently mica should behave as a weaker acid than montmorillonite.* It would indeed be interesting from the point of view of the crystal chemistry of these silicates to follow up the electrochemical consequences of various types of isomorphous replacements expressed in terms of such features as the conductivity and activity coefficient of the gegenions, the nature of titration curves with bases and the magnitude of the free acid to the total neutralisable acid of hydrogen, or, acid systems. Investigations on these lines are being carried out in this laboratory.

A good case for the basic character of the planar OH groups in kaolinite seems to have been made on the basis of the interaction of this mineral with phosphoric acid, or, acid phosphates. This reaction is more and more favoured as the p_H of the phosphate solution diminishes and at a sufficiently low p_H, Stout (1939) found a complete replacement of the planar OH groups in finely ground kaolinite by PO_4^{-3} ions. The subsurface OH groups being not accessible to the large PO_4^{-3} ions through the hexagonal rings of oxygens were naturally left unreacted upon. The planar OH groups, however, are all accessible as their complete replacement indicates. But the kaolinite structure is such that an exposure of all the planar OH groups necessarily entails an opening up of all the subsurface OH groups of the lattice as well. These latter OH groups can react with such ions in solution as have a diameter smaller than the hexagonal rings of oxygens within which they are embedded. For example, they can react with the strong bases. Assuming then that the OH groups in kaolinite, planar as well as subsurface, have a potentially acid character, a high value of the cation binding power comparable to the phosphate fixing capacity would be expected in alkaline solutions. Actually, however, Stout's data indicate a much smaller cation binding power, the

---

* Unpublished work of K. S Rajagopalan appears to substantiate this view.

value 78.0 m e. per 100 gms., recorded at as high a pH as 11.0, representing only about 5 o per cent of the total amount (1,550 m e.) of OH groups in 100 gms. of the mineral.

One way out of the above inconsistencies would be to give up the idea that OH groups in kaolinite are responsible for its acid character. Other ways also exist. For instance, it might be argued that a complete replacement of the planar hydroxyl by PO_4^{-3} ions does not necessarily indicate that all of them had been lying exposed from the very beginning. The individual packets in kaolinite are held by fairly strong hydrogen bonds and the mineral, even when finely ground, would hardly be expected to give single-packet platelets. It is just possible, however, that with progressive intake of PO_4^{-3} ions, more and more OH groups open up and are made available to the action of the phosphate. This would no doubt happen if the phosphated kaolinite separated out as a second solid phase. Stout's observation (Stout, *loc. cit.*), that finely ground kaolinite, when phosphated, becomes amorphous to X-rays, seems to support the assumption that a second solid phase is formed.

The same line of reasoning may be followed to see what happens when a strong acid like HCl reacts with kaolin. As before, hydroxyls will be replaced by Cl's, however, the Cl being a misfit in the crystal mainly because of a much larger diameter than OH, has to keep out of the solid kaolin phase. On the other hand, the lattice energy of $AlCl_3$ is not large enough to admit of the formation of a separate solid phase under the existing conditions. The Cl, therefore, remains in a diffusible, or, dissociated condition imparting a positive charge to the surface. This positive charge hampers the dissociation of further OH groups and may thus make inoperative even such amongst them as are lying on the exposed surfaces of the lattice packets. Remembering that a very large number of the OH groups are likely to be blocked within the multi-packet particles, it follows that a very small fraction of the kaolinitic OH's will react with the acid at moderate concentrations. It is only at very high concentrations of the acid that the basic character of kaolinite will be expected to have its full play. Under these conditions, every Al^{+3} ion will have its full complement of 3 Cl^- ions and the kaolinite lattice will break up into $AlCl_3$ and silicic acid.

A similar state of affairs would be expected in the interaction of kaolin with an alkali. The neutralisation of some of the OH groups would give a greater negative charge to the surface* and make the dissociation (and neutralisation) of further OH groups difficult for this reason and since the sodium salt does not form a separate solid phase a much smaller number of OH groups will be attacked by the alkali than by phosphate ions in an acid medium as Stout's results definitely show. In strongly alkaline solutions, however, the lattice will break up into sodium silicate and sodium aluminate.

---

* This follows from the fact that the sodium salt of a weak acid is more strongly dissociated than the acid itself.

The break-up of the lattice as a result of the dissolution of the reaction product, or, the formation of a second solid phase is an extreme case of the charging or discharging process associated with an ionic reaction of the silicate crystal. Of much greater interest are the milder reactions which leave the silicate lattice virtually intact and effect only an exchange of ions between the surface layers of the crystal and the liquid phase with a corresponding variation of the surface charge. Let us follow up such an ionic reaction of finely ground muscovite suspended in water. The K ions on the surface dissociate giving a nett negative charge to the platelets. A simple mechanism of the dissociation suggests itself. The K ions on the surface carry a residual positive charge being bonded to the solid phase by only six out of the required number of twelve oxygen ions. Being centres of positive charges, the surface potassiums orient and attract water dipoles with the negative polarities of the latter directed towards them and in doing so are themselves drawn by the dipoles towards the liquid side. The average amplitude of vibration of the surface K's will, for this reason, be greater than what it is in the body of the crystal and, in this sense, the K ions on the surface will exist partly in the liquid phase surrounded by water dipoles. They are not truly dissolved K-ions free to occupy any part of the liquid phase for as soon as they dissociate the surface gets a nett negative charge and the electrostatic attraction which is set up prevents a further outward journey of the K ions. Attention must here be drawn to one essential aspect. It must be clearly understood that when a muscovite crystal is split along the potassium-bearing plane the K ions distribute themselves equally between the two parts. On now directing our attention to the cleavage surface of *one of the platelets* (Fig. 5 *a*) we shall find that only a half of its exposed hexagonal rings of oxygens is occupied by K-ions and the other half is vacant. There will be an accumulation of 0.5 unit of (excess) positive
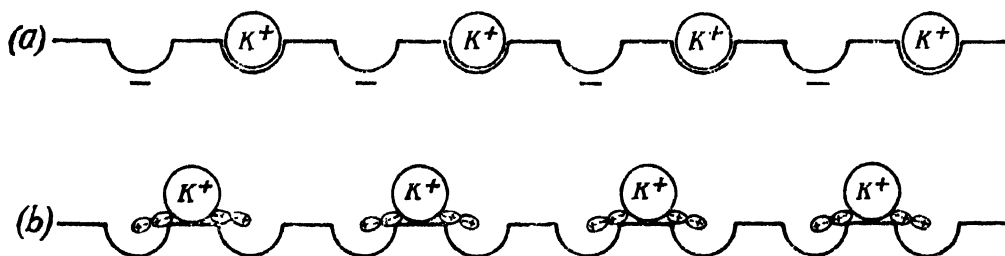
FIG. 5

charge in the region of an occupied ring while a vacant one will have 0.5 unit of negative charge focussed at its centre. The principle of microscopic neutrality will require that an occupied ring has as its immediate neighbour a vacant one in a statistical sense. In other words, positive and negative charges, each 0.5 unit in strength, will be distributed on the surface with

contiguous centres of charge carrying dissimilar charges. The muscovite crystal seeks to get rid of these local concentrations of opposite charges by interaction with the water dipoles in a manner such that the exposed potassiums are pulled out of their hexagonal cavities, or, rings and made to take up positions in between contiguously situated rings as roughly depicted in Fig. 5b. Such a redistribution of the surface potassiums following on their interaction with the water dipoles serves to make the surface statistically neutral on a smaller scale compared with the dry crystal, and to minimise the potential energy of the system—as it should in order that it may pass on to a stabler state of equilibrium. Each K-ion carrying one unit of positive charge now balances two 0.5 units of negative charge situated at the centres of adjacent hexagonal rings. Actually, the potassiums execute oscillations between these centres but taking the time average of this oscillatory motion, they may be looked upon as occupying mean positions between the centres as shown in Fig. 5b.

When a foreign electrolyte, *e.g.*, LiCl is added to such a system, the kinetic motion of the Li⁺-ions will sometimes take them within the space between the negatively charged surface and the positively charged K⁺-ions. As positive charges cannot crowd together, the K⁺-ions will be displaced (or exchanged) to pair with the diffusible anion, Cl,⁻ in the bulk of the liquid phase. The Li⁺-ions which displace K⁺-ions become bonded to the surface by quite similar forces as their predecessors. Like the K's they will also register their activity on a reversible Li electrode. In the language of the colloid chemist, they are the mobile ions in a diffusible double layer. In the above discussion, however, hypotheses, inherent in a purely colloid chemical treatment, have been altogether circumvented. In particular, we have avoided invoking the primary adsorption of any anion to balance the positive charge of the dissociated K ions and give neutral "ion pairs" on the surface. The formulation of such ion pairs and their identification in individual systems constitute the very essence of the adsorption method of approach to problems relating to the electrochemistry of disperse systems. However, it would be unnecessary and even futile to try to single out such ion pairs in the case of the silicate crystal just as surely and for the same reason as it would be impossible to pick out neutral molecules in any ionic lattice, either in its interior or on the surface. Representation of these surface reactions in terms of primarily adsorbed ions and ion pairs on the surface may be sufficient for purposes of their qualitative discussion, but the basis of a quantitative theory can only be laid on a detailed knowledge of the structure of the crystallites, especially, of their surface layers. A complete quantitative theory will emerge only when in addition to this knowledge accurate information regarding the nature and the magnitude of the interaction between the ions on the surface of the crystallites, the ions of the contact solution and the molecules of the solvent is available.

CHEMICAL LABORATORIES,
DELHI UNIVERSITY
DELHI.

REFERENCES

Fajans, 1921, *Zeit Physik. Chem.*, **97**, 478.

Gieseking, 1939, *Soil Sci.*, **47**, 1.

Hendricks, 1945, *Ind. Eng Chem.*, **37**, 625

Hofmann, Endel and Wilm, 1934, *Z. Angend Chem* , **47**, 539

Jackson and West, 1931, *Z. Krist.*, **716**, 211.

Kelley and Jenny, 1936, *Soil, Sci.*, **41**, 367.

Marshall, 1935, *Z. Krist.*, **91**, 433.

     ,,   1942, *Jour. Phys., Chem*, **42**, 1077.

Mitra, J., 1936, *Ind. Jour Agri. Sci.*, **6**, 556.

     ,,   1940, *ibid.*, **10**, 317

     ,,   1941-42, *Ind Soil Sci.*, Bulletin, 4, 41

     ,,   1946, *Ind. Chem Soc* , **23**, 386.

Mukherjee, 1920-21, *Trans Fard. Soc.*, **16**, 103

     ,,   1933, *Koll Zeit*, **62**, 257.

     ,,   1937, *Trans. Net Inst. Sci* (India), 1, 227

     ,,   1945, *Nature*, **155**, 268.

Mukherjee and Mitra, 1946, *J Coll. Sci*, 1, 141.

Nagelschmidt, 1935, *Min Mag.*, **28**, 140.

Nelson and Hendricks, 1943 *Soil Sc.* **56**, 285.

Pauling, 1930, *Proc. Nat. Acad Sci, U.S.A.*, **16**, 123, 578

Stout, 1939, *Pig Soil. Sci. Amer.*, **4**, 177.

Wiegner and Pallmann, 1929, *Verp d Zwei Komm Int Bodenk, Ges*, 92

INFLUENCE OF TEMPERATURE AND CONCENTRATION OF REACTING SOLUTION ON MERCERISATION OF RAW JUTE-FIBRE*

By N. N. SAHA

(Plates IVA and IV B)

ABSTRACT. Raw jute fibres were treated with caustic soda solutions of various concentrations (5% to 50%) at different temperatures (−10°C to +60°C), washed with water and dried, and the products thus obtained were analysed by studying X-ray diffraction photographs which revealed three distinct types of patterns, e.g., (i) some due to native cellulose (ii) some due to partially mercerised cellulose and (iii) the rest due to completely mercerised cellulose. The results obtained have been given graphically It is pointed out that the results obtained with raw jute fibre differ considerably from those obtained in the case of cotton by Sisson and Saner, especially in the higher concentration-region, e.g, concentration between 40% and 50% and temperature range −10°C to +40°C An attempt has been made to explain these differences in the two cases.

INTRODUCTION

It is well known that when caustic soda solution reacts with pure cellulose, soda cellulose is formed and on washing the product with water and drying it a final product is obtained which has the same chemical constitution as that of cellulose but has a crystal structure quite different from that of native cellulose. This product is called hydrated cellulose. The percentage of cellulose thus changed depends however on the concentration and temperature of the reacting alkali solution. This problem was first investigated in the case of cotton cellulose by Sisson and Saner (1941). It was shown recently by Sirkar and Saha (1947) that the crystal structure of the hydrated cellulose obtained similarly from raw jute fibre is different from that of the hydrated cellulose obtained from cotton. Also for a particular concentration of the solution at a particular temperature the percentage of hydrated cellulose formed in this way in the case of jute fibre seemed to be different from that observed in the case of cotton fibre by Sisson and Saner. It was therefore thought worth-while to investigate the problem more thoroughly with raw jute fibre as the starting material and by using NaOH solutions of different strengths at different temperatures to see if there is any influence of the high percentage of lignin present in raw jute fibre on the mechanism of mercerisation. The X-ray analysis of the hydrated cellulose can give the information

* Communicated by Prof. S. C Sirkar.

whether the sample consists wholly of hydrated cellulose or partly of some native cellulose, because the positions of 101 and 101 reflections in the former case is quite different from those in the latter. Hence this method has been employed in the present investigation and the results which have been discussed later are found to be different from those observed in the case of cotton cellulose by Sisson and Saner.

EXPERIMRNTAL

Raw jute fibres cut to small lengths (about 7 cm.) were first cleaned and dipped into about 10 c.c. of caustic soda solution of known strength in a test tube previously brought to the desired temperature by keeping the test tube partly immersed in a water bath hot or cold, or in a freezing mixture as the case might be. No tension was applied during the treatment. After treatment at a definite temperature for about 10 minutes the sample was taken out and washed for about an hour with water at the same temperature. When the temperature of NaOH solution used was below $0°C$ the washing was effected with ice-cold water. The sample of fibre was then dried in air for about two days. X-ray photographs of these samples were taken after making all the strands parallel by pressing them mildly and holding taut during the exposure in a specially designed camera used previously by Sirkar and Saha (1947). The photographs were taken with a very fine slit of 0.5 mm. bore and 5 cm. in length using $CuK\alpha$ radiation from a Hadding tube. The patterns were examined visually and by noting the absence or presence of 101 and 101 reflections of the native cellulose, it was ascertained whether native cellulose was absent or partially present in the sample. The results observed in this way are given in Table I and they are represented graphically in Fig. 1. Some of the diffraction patterns are reproduced in Plates IVA and IVB.

RESULTS AND DISCUSSION

The hatched portion in Fig. 1 corresponds to reactions which produce cent per cent hydrated cellulose, the dotted portions represent the conditions under which the product contains some percentage of native cellulose besides hydrated cellulose, the clear portions represent the conditions under which the reacting solution had no effect on the native cellulose. Owing to experimental difficulties it was not possible to use solutions at temperatures lower than $-10°C$. For comparison the curve obtained with raw cotton fibre by Sisson and Saner (1941) is reproduced in Fig. 2.

It can be seen from Table I that the degree of mercerisation depends in a peculiar way on the temperature and concentration of the solution used. Further, the results of the present investigation, given in Table I and graphically represented in Fig. 1, differ appreciably from those obtained in case of cotton by Sisson and Saner, as can be seen from a comparison of the curves
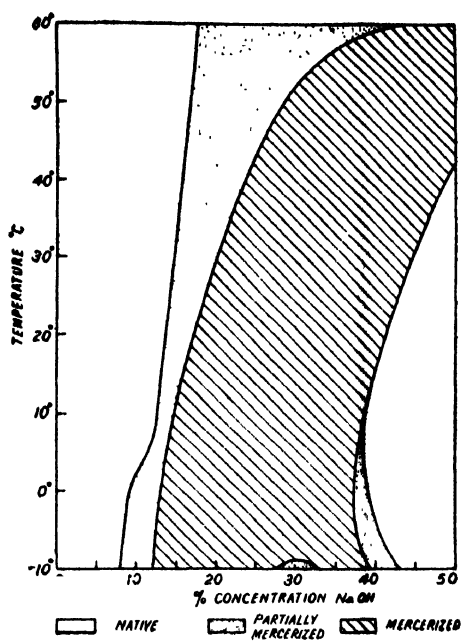
FIG. 1
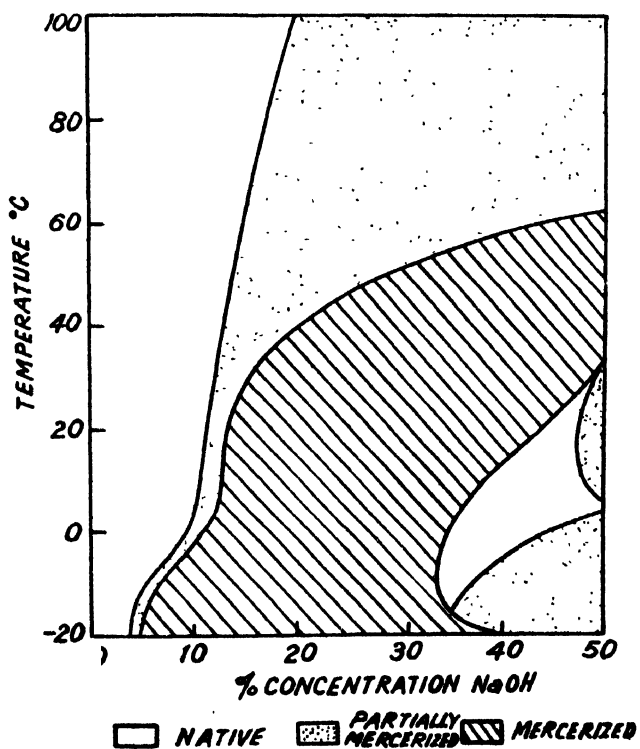
FIG. 2

TABLE I

Strength of NaOH Soln.	Temp. of the solution in °C	Degree of mercerisation	
		Present author	Sisson and Saner
50%	60°	Complete	Complete
50%	40°	Native	Complete
50%	20°	Native	Partial
50%	0°	Native	Partial
50%	−10°	Native	Partial
45%	60°	Complete	Complete
45%	10°	Complete	Complete
45%	20°	Native	Native
45%	0°	Native	Native
45%	−10°	Native	Partial
40%	60°	Partial	Partial
40%	40°	Complete	Complete
40%	20°	Complete	Complete
40%	10°	Native	Native
40%	0°	Native	Native
40%	−10°	Partial	Partial
35%	60°	Partial	Partial
35%	40°	Complete	Complete
35%	15°	Complete	Complete
35%	−10°	Complete	Native
30%	60°	Partial	Partial
30%	40°	Complete	Complete
30%	15°	Complete	Complete
30%	−10°	Partial	Complete
20%	50°	Partial	Partial
20%	25°	Complete	Complete
20%	15°	Complete	Complete
20%	−10°	Complete	Complete
10%	5°	Native	Partial
10%	0°	Partial	Partial
10%	−10°	Partial	Complete
5%	0°	Native	Native
5%	−10°	Native	Partial

in Figs. 1 and 2. For instance, Fig. 1, shows that the range of complete mercerisation at a low temperature of about −10°C extends from 12% to 38% with a small hump of partial mercerisation at 30% NaOH solution, whereas in cotton cellulose (Fig. 2) it was found to extend from 7% to 34%. The range of partial mercerisation (Fig. 1) which is preceded by the complete mercerisation zone and followed by a native zone begins from 8% to 9% at −10°C whereas in case of cotton it begins from 5% at the same temperature. Sisson and Sauer obtained the mercerisation of cotton at 20°C when the concentration of the alkali used was about 13% to 14%, but in the case of jute fibre only partial mercerisation is observed with this strength and for complete mercerisation at 20°C the strength of the NaOH solution required is about 18%. It is evident from Fig. 1 that in the reactions at low temperature the concentration of the alkali solution required for complete mercerisation is higher than that in the case of cotton and below a strength of 12% of the solution it is not possible to obtain completely mercerised sample of jute fibre even when the temperature of the reacting solution is −10°C, but in the case of cotton even a 7% solution gives complete mercerisation at this temperature. It is thus seen that in the temperature range from −10°C to +40°C, the concentration required for obtaining totally mercerised sample from raw jute fibre at a particular temperature is higher than that required in the case of cotton. From 50°C up to about 60°C, however, both cotton fibre and raw jute fibre yield the same results.

It also appears from Fig. 1 that at higher concentration, e g., about 48% the complete mercerisation of raw jute fibre cannot be effected if the temperature of the solution used is below 40°C. In the case of cotton complete mercerisation with the same solution is obtained above 30°C. But while in this latter case the zone of partial mercerisation is larger than that of native cellulose reverse is true in the case of raw jute fibre at this high concentration range. It is found that with 40% and 45% NaOH solutions the temperature of the solution should be raised above 15°C and 30°C respectively for obtaining complete mercerisation in the case of raw jute fibre.

Again, the examination of Fig. 2 shows that in the case of cotton the mercerisation is complete with 20% solution in the temperature range between −20°C and +40°C, with 30% solution between −20°C and +52°C and with 40% solution the mercerisation does not begin below 16°C and from 16°C to about 58°C the mercerisation is complete, whereas in case of jute the corresponding temperature ranges for complete mercerisation are −10°C to +30°C, −8°C to +52°C, and +15°C to +59°C respectively.

From the results observed it is seen that the process of mercerisation is facilitated when the condition of the treatment is such that low temperatures are maintained when the concentrations of the NaOH solution used are low and high temperatures when the concentrations are high, though the complete mercerisation zone at high temperature and high concentration is small. It appears from above that concentration of alkali is not the only factor influ-

N. N. Saha

encing the process of mercerisation. It has been suggested by Sisson and Saner (1941) that in the case of cotton the failure of complete mercerisation in the reactions of high concentrations (above 40%) and low temperatures is probably due to the formation of sodium hydroxide hydrates which are unable to penetrate into the micelles. If this be true it would be more difficult for these hydrates to enter into the micelles when the latter contain cements of lignin. Thus the want of any change in the cellulose in jute fibre in reactions with concentrated NaOH solutions at temperature below 40°C, observed in the present investigation seems to support the hypothesis put forward by Sisson and Saner. But this hypothesis cannot account for all the results obtained. An alternative hypothesis, therefore, is being put forward below.

Mercerisation being an exothermic process, the formation of native cellulose with NaOH solutions of lower concentration at high temperature can be easily understood, because exothermic processes are not favoured by high temperatures according to Le Chatelier and Braun's Principle. But the absence of mercerisation with alkali solution of high concentration at lower temperature is not explicable by the above principle. It is probable that at higher concentrations of alkali an impervious surface-coating of the product is formed which prevents the diffusion (Saha, 1947) of the alkali inside the micelles. This coating may be dissolved when dilute solutions are used but it seems that it is dissolved only at higher temperature when a concentrated solution is used. The low range of mercerisation at this high concentration of alkali solution when the temperature is also high, is obviously due to the exothermic nature of reaction.

On comparison of Fig. 1 with Fig. 2 it is observed that both the partial and complete mercerisation zones at low concentration and low temperatures have shifted towards the higher concentration side. It is also observed that between concentration range of 45% and 50% the partial mercerisation zone present in cotton cellulose is totally absent in case of raw jute fibres. It appears that the differences in these two cases may be due to the presence of lignin in the raw jute fibre. In dilute solutions of NaOH, some portion of NaOH solution is spent up in reacting with lignin and therefore only a small fraction of cellulose is reacted upon. At high concentration it appears that lignin facilitates the formation of a more impervious coating on its surface and thus prevents the alkali solution to react with the cellulose. It seems that this coating is soluble at temperatures above 40°C and therefore complete mercerisation of the fibre is effected at higher temperatures.

Fig. 3

Fig. 4

Fig. 5

Fig. 6

Fig. 7
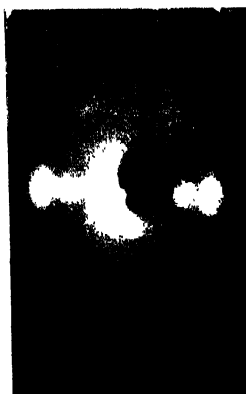
Fig. 8
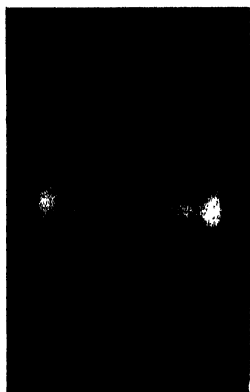
Fig. 9

Fig. 10

Fig. 11

X-ray diffraction patterns.

Fig. 12   Fig. 13   Fig. 14
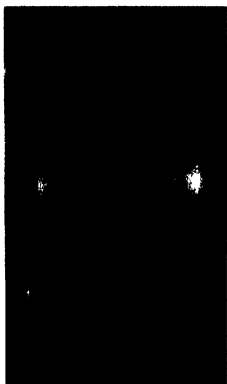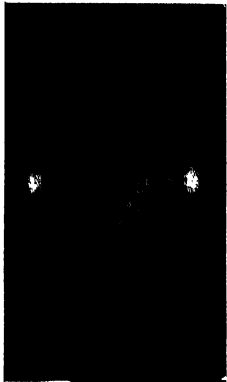
Fig. 15   Fig. 16   Fig. 17
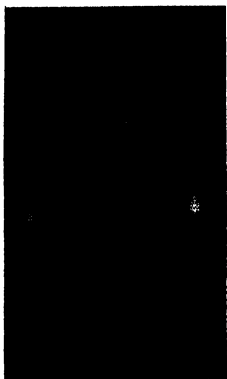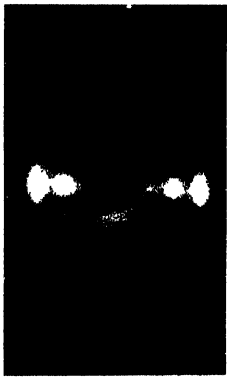
Fig 18   Fig. 19   Fig. 20

X-ray diffraction patterns.

The work was done under a scheme drawn up by Prof. M. N. Saha and financed by Indian Central Jute Committee.

PALIT LABORATORY OF PHYSICS,
UNIVERSITY COLLEGE OF SCIENCE, CALCUTTA.

REFERENCES

Saha, N. N., 1947, *Nat. Inst. Sc. India*, **13**, 339
Sirkar, S. C. and Saha, N. N , 1947, *Nat. Inst Sc. India*, **13**, 1.
Sisson and Saner, 1941, *J. Phys. Chem.*, **45**, 717.

EXPLANATION OF PLATES

Plate IV-A

Fig. 3.   Raw jute fibre.
Fig. 4.   Treatment with NaOH solution of 50% at   60°C.
Fig. 5.   ,,   ,   .,   50% at   40°C.
Fig. 6.   ,,   ,,   ,,   50% at   20°C.
Fig. 7.   ,,   ,,   ,,   50% at − 10°C.
Fig. 8.   ,,   ,,   ,,   45% at   0°C.
Fig. 9.   ,,   ,,   ,,   40% at   60°C.
Fig. 10.   ,,   ,,   ,,   40% at   10°C.
Fig. 11.   ,,   ,,   ,,   40% at − 10°C.

Plate IV-B

Fig. 12.   Treatment with NaOH solution of 35% at − 10°C.
Fig. 13.   ,,   ,,   ,,   35% at   60°C.
Fig. 14.   ,,   ,,   ,,   30% at   60°C.
Fig. 15.   ,,   ,,   ,,   30% at   10°C.
Fig. 16.   ,,   ,,   ,,   20% at − 10°C.
Fig. 17.   ,,   ,,   ,,   20% at   50°C.
Fig. 18.   ,,   ,,   ,,   10% at − 10°C.
Fig. 19.   ,,   ,,   ,,   10% at   0°C.
Fig. 20.   ,,   ,,   ,,   5% at   0°C

CONTENTS

NOTICE
TO INTENDING AUTHORS

Manuscripts for publication should be sent to Mr. A. N. Banerjee, Assistant Editor, 210, Bowbazar Street, Calcutta.

The manuscript of each paper should contain in the beginning a short abstract of the paper.

All references to published papers should be given in the text by quoting the surname of the authors followed by the year of publication within braces, *e.g.*, Sen (1942). The actual references should be given in a list at the end of the paper according to the following specimen :

Sen, B. K., 1942, Volume rectification of crystals, *Ind. J. Phys.*, **16**, 329.

The references should be arranged alphabetically in the list.

All diagrams should be drawn on thick white paper in Indian ink, and letters and numbers in the diagrams should be written in pencil.

CHARACTERISTICS OF THE SOUTHWEST MONSOON AIRMASS

By P. A. MENON

ABSTRACT. The main features of the southwest monsoon airmass, as derived from radiosonde ascents of Trivandrum, Madras and Calcutta for the year 1947, are summarised The mean temperature curves of the three stations plotted on a tephigram do not support the prevalent view that the monsoon air mass is a homogeneous current and has a saturated adiabatic lapse rate.

The southwest monsoon has been studied by various workers with the surface data and occasional upper air temperature data Since 1944 daily radiosonde ascents are being made at a number of stations in India and it is now possible to study the characteristics of the southwest monsoon in greater detail. In this note the main features of this airmass as derived from the data of Trivandrum, Madras and Calcutta for the year 1947 are summarised.

Trivandrum is located on the west coast of India about thirty miles from Cape Comorin This may be considered as the first station in India to be struck by the southwest monsoon after crossing the equator. At this stage the southwest monsoon is uninfluenced by any travel over land Madras is situated on the east coast of the peninsula and hence is very suitable for studying the characteristics of the monsoon air after it has crossed the Ghats (with associated lifting and subsidence) and also travelled over 400 miles of land Calcutta is located at the place of deflection of the southwest monsoon into a south-easterly current under the influence of the monsoon through over Gangetic plain and would thus give the characteristics of the deflected monsoon.
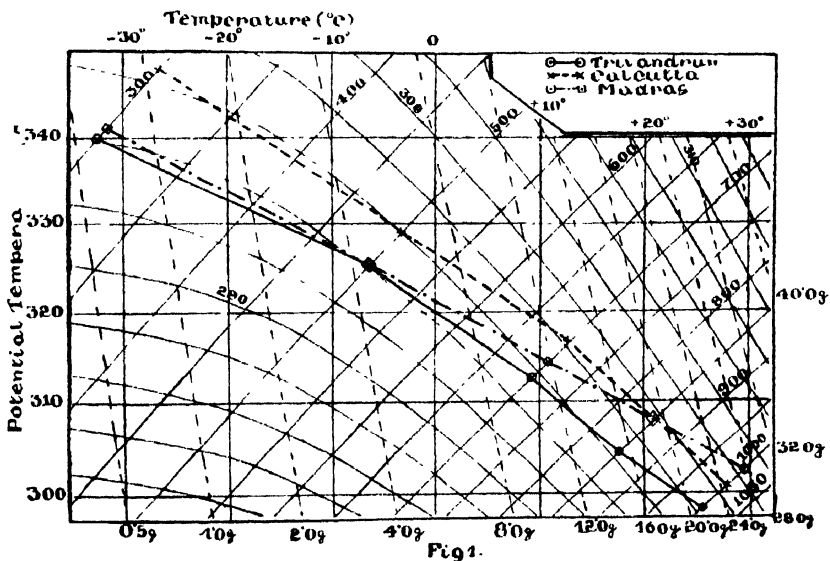
Fig 1.

FIG. 1

Table I gives the variation of temperature at various levels, and also the mean temperature and the average variability. The monsoon at Calcutta is warmer at all levels than at Trivandrum by 2 to 5°C. At ground level Madras is warmest and at 850 mb, the temperature is the same as that over Calcutta. But from 700 mb. onwards the mean temperatures at Madras and Trivandrum are almost identical. This shows that the effect of the land travel in reaching Madras is confined only to levels below 700 mbs. and the Trivandrum characteristics are preserved aloft.

In Fig. 1, the mean temperature curves for the three stations are plotted on a tephigram. It will be seen that the lapse rates at both Trivandrum and Calcutta are distinctly greater than the saturated adiabatic. This does not agree with the prevalent view that the monsoon air mass has a saturated adiabatic lapse rate. At Madras the lapse rate between 1000 and 700 mbs. is greater than either of the other two stations but aloft the curve is identical with Trivandrum.

TABLE I

(a) Ground level

Temperature (°C)	Trivandrum		Calcutta		Madras	
	No. of occasions	Frequency (%)	No. of occasions	Frequency (%)	No. of occasions	Frequency (%)
24	8	8.7	..	...	...	..
25	29	31.5	2	3.5	1	0.9
26	49	53.5	7	11.6	3	2.6
27	5	5.4	17	28.2	11	9.5
28	1	1.1	19	32.2	15	12.9
29	...	...	7	11.6	33	28.4
30	...	..	4	6.7	20	17.2
31	...	...	3	5.0	15	12.9
32	...	...	1	1.7	7	6.0
33	...	...	..	...	7	6.0
34	...	...	.	..	...	...
35	...	...	...	...	3	2.6
36	...	...	...	...	..	...
37	...	...	...	...	1	0.9
Total No of Observations	92		60		116	
Mean Temperature (°C)	25.6		27.9		29.6	
Average Deviation	0.6		1.1		1.6	

TABLE I (*contd.*)

(*b*) 850 mb. level

Temperature (°C)	Trivandrum		Calcutta		Madras	
	No of occasions	Frequency (%)	No of occasions	Frequency (%)	No of occasions	Frequency (%)
13	...	...	...	.	1	0.9
14	4	4 4	.	...	...	...
15	10	11.1	1	1.7	1	0 9
16	11	12.2	1	1.7	4	3.4
17	18	19.7	2	3 3	4	3.4
18	26	28 9	7	11.7	11	9.5
19	18	19 7	6	10 0	12	10 4
20	2	2.2	14	23.5	19	16.3
21	2	2.2	10	17.0	23	19 8
22			9	15 0	15	12.9
23	..		5	8.3	20	17.2
24	.	...	1	1.7	3	2.6
25	..	...	1	1 7	3	2.6
26	..		1	1.7	...	...
27		..	1	1.7	...	...
28		...	1	1.7	...	...
Total No. of Observations	91		60		116	
Mean Temperature (°C)	17 1		20 6		20.6	
Average Deviation	1.3		1.8		1 8	

TABLE I *(contd.)*

(c) 700 mb. level

Temperature (°C)	Trivandrum		Calcutta		Madras	
	No. of occasions	Frequency (%)	No of occasions	Frequency (%)	No. of occasions	Frequency (%)
3	1	1.1	..	...	...	...
4	..	...	..	...	1	0.9
5	3	3.4	...	...	6	5.5
6	6	6.7		..	4	3.7
7	6	6.7	1	1.8	6	5.5
8	7	7.9	1	1.8	14	12.9
9	23	26.0	1	1.8	18	16.6
10	11	12.4	9	16.4	22	20.2
11	22	24.8	4	7.3	18	16.6
12	7	7.9	14	25.4	14	12.9
13	3	3.4	9	16.4	2	1.8
14	...	...	14	25.4	1	0.9
15	...	...	2	3.6	1	1.8
16		...	.	...	2	1.8
Total No. of Observations	89		55		109	
Mean Temperature (°C)	9.4		12.2		9.6	
Average Deviation	1.6		1.4		1.8	

TABLE I (*contd.*)

(d) 500 mb. level

Temperature (°C)	Trivandrum		Calcutta		Madras	
	No. of occasions	Frequency (%)	No. of occasions	Frequency %	No. of occasions	Frequency (%)
0	2	2.5	3	6.2	...	...
−1	2	2.5	1	2 1	2	1.9
−2	2	2.5	9	18 8	3	2.9
−3	8	10.0	7	14 6	7	5.9
−4	5	6.3	11	22.9	9	7.9
−5	17	21.3	7	14.6	20	26.5
−6	8	10 0	9	18 8	14	13.2
−7	13	16.3	.	..	11	9.7
−8	8	10 0	1	2.1	9	7.9
−9	7	8 9	...		8	8 8
−10	1	1.2	...	.	5	4.7
−11	2	2.5			5	4.7
−12	1	1.2	..	...	2	1.9
−13	1	1 2	.	...	..	...
−14	2	2 5		.	...	.
−15	..	.			1	0.9
−16	.	...		...	..	...
−17	1	1.2	.	..	...	...
Total No. of Observations	80		48		105	
Mean Temperature (°C)	6.3		−3.8		6.3	
Average Deviation	2 3		1.5		2.1	

TABLE I (*contd.*)

(*c*) 300 mb. level

Temperature (°C)	Trivandrum		Calcutta		Madras	
	No. of occasions	Frequency (%)	No. of occasions	Frequency (%)	No of occasions	Frequency (%)
−19	.		1	3·7	...	...
−20	...			.	...	..
−21	..		1	3·7	...	.
−22	..		1	3·7	...	...
−23	..		.		1	1.5
−24	...		1	3·7		...
−25			5	18.5	1	1.5
−26	1	1 8	4	14.8	1	1.5
−27	4	7·4	4	14 8	6	8.9
−28	3	5.5	...	.	2	3.0
−29	3	5.5	7	25·9	4	6 0
−30	3	5·5	2	7 4	9	13 4
−31	10	18.5	1	3 7	14	20 9
−32	7	13 0	.		9	13 4
−33	6	11 2			9	13·4
−34	2	3 6	.		3	5 5
−35	6	10.9			5	7 5
−36	1	1.8	...		1	1.5
−37	4	7·3		.	...	...
−38	2	3·7			1	1 5
−39	1	1.8		...	1	1.5
−40					...	...
−41	.				...	...
−42	..				...	.
−43	1	1.8			.	...
Total No. of Observations	54		27		67	
Mean Temperature (°C)	−32 4		−26.6		−31.1	
Average Deviation	2.8		2 3		2 2	

The temperatures at ground level at Trivandrum are remarkably uniform, being on 85% of occasions either 25 or 26°C. This has given rise to the impression that the monsoon is a very homogeneous current. Table I, however, shows that *it is not so*. The temperatures at higher levels are not at all uniform, and vary between fairly wide limits. The average variability (which represents a measure of the degree of variation of temperature) steadily increases from o.6 at the ground level to 2.8 at 300 mb. level. Thus even at Trivandrum the southwest monsoon is not a homogeneous airmass at upper levels and shows appreciable temperature variations. The average variability for Calcutta is more than that for Trivandrum at ground level and 850 mb. but less than Trivandrum aloft. This shows that the air at Calcutta is less heterogenous than at Trivandrum at upper levels. The average variability at Madras is the highest at ground level and the same as at Calcutta at 850 mb. level. At 700 and 500 mb. it is nearly the same as at Trivandrum

which supports the view arrived at before that the air at Madras above 700 mb. is unmodified by the intervening land travel.

High relative humidity is an important property of the monsoon air mass. Table II gives the number of occasions when the relative humidity at 700 mb. level was less than 50%.

TABLE II

Station	No of ascents that reached 700 mb level	No. of occasions when relative humidity at 700 mb was less than 50%	Percentage of occasions when R H at 700 mb was less than 50%
Trivandrum	80	15	18%
Madras ..	100	9	8%
Calcutta ...	55	4	7%

Though at Trivandrum the monsoon is ' fresh ' from the source region of the moisture, the relative humidity there at 700 mb. level is less than 50% more frequently than either at Madras or Calcutta. This seems to be all the more strange when we take into consideration a special feature pertaining to the year 1947. During this year there were fairly prolonged break in the monsoon and as such one would naturally expect that Trivandrum, being located at the southernmost point of India, would be more frequently under the sway of genuine southwest monsoon current than Calcutta and hence should show greater occasion of high humidities at 700 mb. than at Calcutta. In spite of this we find that on significantly greater number of occasions Trivandrum had a lower relative humidity at 700 mb. level than Calcutta. As high humidity is the chief characteristic of the monsoon air mass, it may be concluded that the depth of the monsoon airmass at Trivandrum or Madras is less than at Calcutta.

An oft repeated statement is that the monsoon air, in crossing the Western Ghats and owing to any precipitation in its travel over Deccan, is denuded of moisture. Table III gives the mixing ratio (gm/kg) at Madras and Trivandrum at 850 and 700 mb. levels. Strangely the mixing ratio is greater at Madras than over Trivandrum. How the intervening land between Trivandrum and Madras acts as a source for moisture is a matter for further study.

TABLE III

Average mixing ratio at Station	850 mb.	700 mb
Madras ...	13.6	8 2
Trivandrum ...	12 1	7 0

TABLE IV

Station	No of inversions or isothermal layers	Total No. of observations
Trivandrum	22	92
Madras	21	116
Calcutta ...	4	60

The number occasions of occurrence of inversions or isothermal layers between 900 and 500 mbs. at the three stations is given in Table IV. Thus resistance to convection is more frequent at Trivandrum and Madras than at Calcutta.

Investigation of the monsoon characteristics at other stations and the significance of the day to day variations in temperature and humidity are in progress.

ACKNOWLEDGEMENTS

DIELECTRIC PROPERTIES OF SOME SOLID INSULATING MATERIALS AT 750 Mc/s

By S. K. CHATTERJEE

ABSTRACT Dielectric constants and power factors of solid insulating materials like mica, mycalex, plexi glass etc., have been measured at 750 Mc/s Loss factors and power dissipated in watts in the materials have also been calculated from observed results. A resonant line oscillator, having tuned concentric lines in the filament circuit, has been constructed for the purpose The detector, which is also of the resonant line type, has been constructed for voltage measurement.

INTRODUCTION

A considerable amount of work has been carried out by different workers in an endeavour to clarify the behaviour of solid insulating materials under alternating electric stress. When a solid material is subjected to ultra high frequency electric stress, various factors become operative within the body of the material depending on its physical and chemical complexities. This makes an understanding of the dielectric behaviour of solid insulating materials under high frequency stress, a difficult matter. The use of any material for the purpose of u.h.f. work presupposes a knowledge of the dielectric constant ϵ and conductivity of the substance at the particular frequency region. Conductivity for insulating materials varies widely at different frequencies and is controlled largely by the same molecular or ionic processes which determine the dielectric constant. So, in selecting any material for service at cm waves, both dielectric constant and conductivity should be considered together. The conductance phenomenon can be studied by measuring the loss-tangent (tan δ) of the substance.

A number of theories have been postulated to explain dielectric absorption and associated behaviour of dielectrics subjected to a.c. fields. Most significant amongst them are the inhomogeneity theory of Maxwell, extended by Wagner (1914), and the theory of polar molecular orientation by Debye (1929). Debye's theory provides well the necessary explanation for the observed dielectric behaviour of gases and especially liquids. The rotation of dipoles in a viscous medium gives rise to frictional heat loss, expressed as power factor, and also to a contribution to dielectric constant which vanishes when the dipoles are prevented from responding by too great viscosity or too high frequencies. This explanation may be accepted as correct for the case of liquids but is difficult of immediate acceptance in the case of solid insulating

materials as it is extremely difficult to attach a meaning to the term viscosity in the case of solids. An attempt to extend the dipole theory in the case of amorphous solids has been made by Gemant (1935). The conception of 'relaxing elasticity,' which is originally due to Maxwell, has been introduced by Gemant to explain the behaviour of solid bodies. But no complete theoretical explanation is as yet available for explaining the behaviour of solids under the influence of a.c. fields. Most of the important insulating materials are solids. Materials like ebonite, bakelite, mycalex, etc., are polyphasic systems containing some components in a microcrystalline form, others in the amorphous state. The experimental investigation, on the behaviour of solid insulating materials under h. f. electric stress, should therefore be continued in order to assist the eventual development of a satisfactory theory. A study of dielectric constant and loss factor, especially, at ultra high frequencies is essentially important, in view of the fact, that the subject of u. h. f. has gained considerable importance, in recent years, in its application to almost every branch of science. Construction of u. h. f. equipments and finally their efficient operation depends to a great extent on the evolution and commercial utilisation of various loss-free materials.

THEORETICAL

Dielectric Constant.—Dielectric constant has been determined by adopting a modification of Drude's (1895) Lecher wire method. Instead of, immersing the whole Lecher wire, in the dielectric as has been done by Drude, insulating materials in the form of thin slabs are interposed between the indicator at the sending end and the shorting bridge, so that the Lecher wire system immersed in an air-dielectric-air medium.
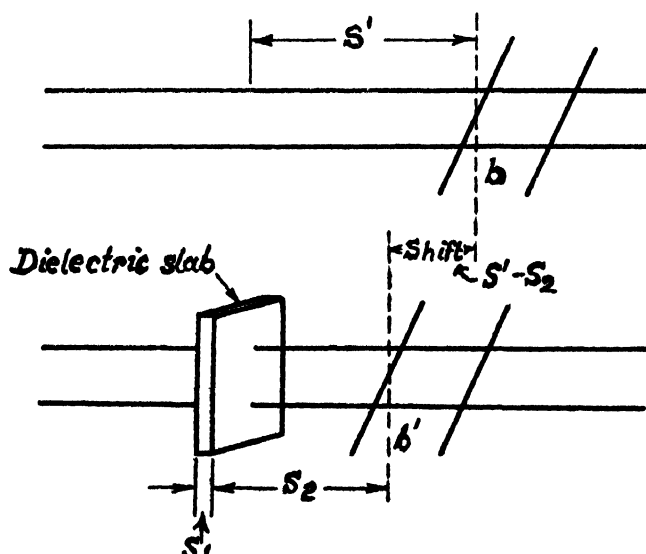
FIG. 1

In figure 1 *b* indicates the position of the short circuiting bridge for resonance, in case the Lecher wire is completely immersed in air, the position of the bridge

is to be moved to b' in order to restore resonance, when the slab is interposed between the indicator and the bridge. If the slab is moved from this position on either side, the resonance is disturbed and the bridge requires shifting to a new position to restore resonance. If the slab is moved gradually, and for each position the bridge shift is measured, the position of the slab for maximum bridge shift can be found. An expression for the refractive index n of the material in terms of the maximum bridge shift, the thickness of the slab (S_1) and wavelength of excitation (λ) has been deduced (King, 1937) to be

$$\tan \frac{\pi}{\lambda} (\text{Max. bridge shift} + S_1) = n \tan \frac{\pi n S_1}{\lambda}. \qquad \dots (1)$$

In the region of cm waves, the refractive index may be considered to be equal to the square root of the dielectric constant. So eqn. (1) may be written as

$$\tan \frac{\pi}{\lambda} (\text{Max. shift} + S_1) = \sqrt{\epsilon}. \tan \frac{\pi S_1}{\lambda}. \sqrt{\epsilon} \qquad \dots (2)$$

Hence, the experiment consists of finding the maximum bridge shift at a particular frequency and measuring the thickness of the material to find the dielectric constant.
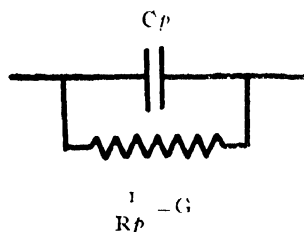
Fig. 2

Loss Angle.—The insulating slab may be represented (Fig. 2) as a parallel combination of capacitance and resistance. The admittance of the combination may be written as

$$Y = G + jB$$

where G and B represent conductance and susceptance of the material respectively. The power dissipated in the material under the influence of h. f. electric field is due to both conductance current and displacement current and may be expressed as

$$P = V^2 . C_p . \omega . \tan \delta$$

where $C_p \omega$ is the susceptance of the material. So the loss tangent can be written as

$$\tan \delta = \frac{1}{R_p . C_p . \omega} = \frac{G}{C_p . \omega .} \qquad \dots (3)$$

For a parallel wire transmission line of length l and propagation constant γ and terminated by impedances Z_t and Z_r, at the transmitting and the receiving

end of the line, the impedance Z_r at any point x from the transmitting end of the line can be deduced to be

$$\left\{ \sinh \gamma(l-x) + \frac{Z_r.\gamma}{Lp+R}.\cosh \gamma (l-x) \right\}$$

$$\frac{\gamma}{Lp+R} \left\{ \cosh \gamma(l-x) + \frac{Z_r.\gamma}{Lp+R}.\sinh \gamma(l-x) \right\}$$

where L, R, represent the inductance and resistance per unit length of the line respectively and p represents the Heaviside differential operator. The above expression of impedance may be written as

$$Z_x = \frac{Z_0 Y_r.\sinh \gamma(l-x) + \cosh \gamma(l-x)}{\frac{1}{Z_0} \left\{ Z_0 Y_r.\cosh \gamma(l-x) + \sinh \gamma(l-x) \right\}}$$

where Z_0 is the characteristic impedance, and

$$Y_r = \frac{1}{Z_r}$$

when $x = 0$, the input admittance of the line (Y), completely immersed in air, can be written to be

$$Y = \frac{1}{Z_0} \frac{Z_0 Y_r.\cosh \gamma l + \sinh \gamma l}{Z_0 Y_r \sinh \gamma l + \cosh \gamma l} \qquad \dots (4)$$

For a terminating link of zero impedance, the input admittance of the parallel wire, immersed in air (Eq. 4) may be written as

$$Y = \frac{1}{Z_0} \coth \gamma l.$$

After the material is inserted the total admittance of the system becomes

$$Y = G + jB + \frac{1}{Z_0} \coth \gamma l$$

$$\simeq G + j\left(B - \frac{1}{Z_0} \cot \beta l\right)$$

neglecting the attenuation constant compared to phase constant.
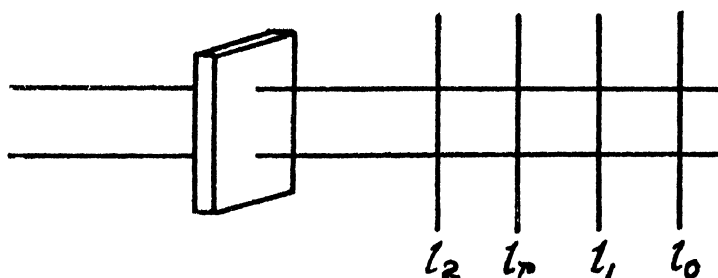
FIG. 3

If (Fig. 3) l_0 is the length of the Lecher wire at resonance when it is solely immersed in air and l_r is the length at resonance when the slab is interposed, it can be shown that

$$B = \frac{1}{Z_0} \tan \frac{2\pi}{\lambda} (l_0 - l_r) \qquad \dots (5)$$

and

$$G = Z_0 \frac{1}{\sqrt{q-1}} \left\{ \tan \frac{2\pi}{\lambda}(l_0 - l_r) - \tan \frac{2\pi}{\lambda}\left(l_0 - l_r - \frac{l_1 - l_2}{2} \right) \right\} \qquad \dots (6)$$

where l_1 and l_2 are the lengths so that

$$\left| \frac{V^2_m}{V^2} \right| = q$$

where, V_m is the voltage developed at the test object at resonance and V is the voltage developed at the test object for any position of the bridge other than resonance.

The resonant line voltmeter, described under experimental head, may be considered as a square law detector. So, if I_m and I represent the change in the plate current of the detector, corresponding to V_m and V, then

$$\frac{I_m}{I} = \left| \frac{V^2_m}{V^2} \right| = q$$

From Eqns. (3), (5) and (6),

$$\tan \delta = \frac{G}{C_{p\omega}} = \frac{1}{\sqrt{q-1}} \cdot \left\{ 1 - \frac{\tan \frac{2\pi}{\lambda}\left(l_0 - l_r - \frac{l_1 - l_2}{2} \right)}{\tan \frac{2\pi}{\lambda}(l_0 - l_r)} \right\}$$

If $I_m = 2I$, the above expression reduces to

$$\tan \delta = 1 - \frac{\tan \frac{2\pi}{\lambda}\left(l_0 - l_r - \frac{l_1 - l_2}{2} \right)}{\tan \frac{2\pi}{\lambda}(l_0 - l_r)} \qquad \dots (7)$$

So, the experimental method of determining loss tangent involves the determination of bridge shift $(l_0 - l_r)$ and also half the width $\left(\frac{l_1 - l_2}{2} \right)$ of the resonance curve where I_m/I equals q.

EXPERIMENTAL EQUIPMENTS

Oscillator.—The circuit diagram of the oscillator using 316-A tube is shown in Fig. 4. For efficient operation of the oscillator, tuning in the form of adjustable concentric lines, have been provided in each of the filament leg of 316-A. The concentric lines consist of copper tubes, silvered inside of bore diameter ½″, outer diameter 5/8″ and length 16″ with a solid silvered

brass rod of diameter ¼″ and length 16″, placed coaxially. One end of the rod
is soldered with a metal plug to one end of the outer tube. The other end
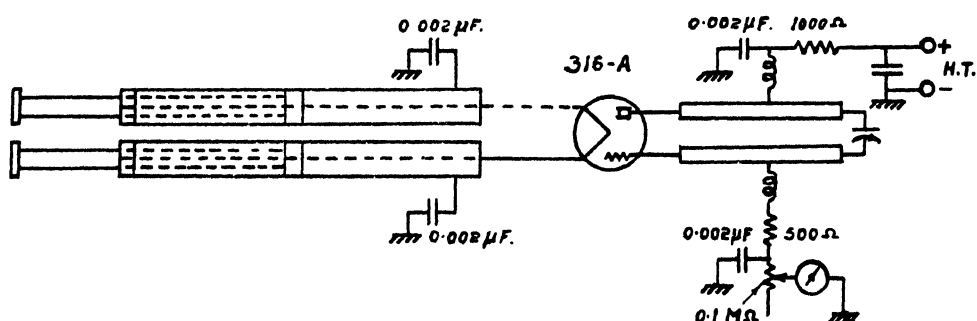
FIG. 4
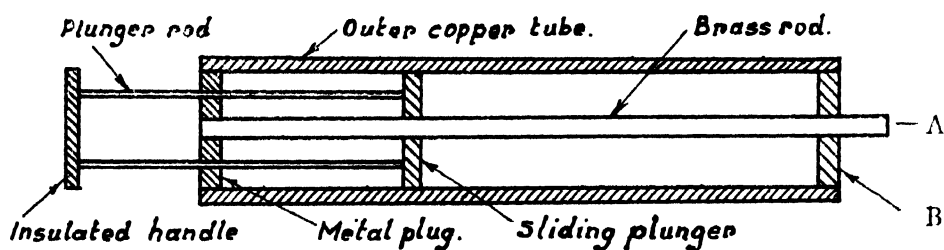
FIG. 4A.

A—To Filament,   B—Insulated bushing.

of the inner conductor passes through an insulated bushing and directly
connected to filament leg. For optimum operation, length of each of the
filament tuned line, should be about one quarter wavelength. The length
can be adjusted, at each frequency of operation, by means of, a close fitting
metal plug, which makes good contact, between the inside wall of the outer
tube and the rod, and which can be smoothly shifted by means of a plunger.
The construction of the filament tuning stub is shown in Fig. 4A. The
resonant lines between plate and grid consists of two tubes of diameter ⅛″
and length 2⅛″, with a small trimmer at the end for changing the frequency.
The r. f. chokes on the plate and grid circuit, consisting of 15 turns of
32 B & S copper wire and of length 1½″ wound on mycalex rod of ¼″ diameter
have been found to be satisfactory. A sheet of copper, 2′ × 6″ × 1/32″, has been
fixed underneath the bakelite chasis of oscillator to provide a reference ground
and all the bypass condensers from the plate, grid and filament circuits have
been directly connected to this reference gound.

The adjustment of the oscillator has been found to be critical, especially
with respect to the filament tuning. For each wavelength, the filament stubs
need adjustment. The two supporting bridges for these tuned lines are also
adjustable, so that they are easily placed at the points of minimum r. f.
voltage, in order that the power-loss due to dielectric absorption may be kept

at a minimum value. The positions of plate and grid supply leads are also adjustable, so that they can be connected to nodal points, as far as practicable. All the adjustments are made at low plate supply voltage for maximum grid current and then the full plate supply voltage of 300 volts is applied.

The oscillator works over a range of 40 cms to 50 cms wavelength. The oscillator is coupled loosely to the Lecher wire system and is also screened by a copper box from the rest of the system, so that the detector may not be susceptible to direct pick-up.
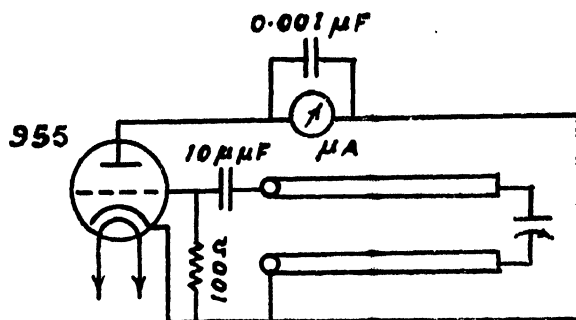
FIG. 5

Detecting Device.—The detecting device consists of a resonant line valve voltmeter using 955 (Fig. 5). The two resonant lines connected between grid and cathode consists of two silvered copper tubes of diameter 1 δ″ and length 2″. The trimmer shunted at the end of resonant lines is meant for tuning.

The experimental arrangement is shown in Fig. 6. For power-factor measurement, the insulating slab is placed at a voltage antinode, next to the short circuiting bridge, so that the line impedance at the position of the slab is practically infinite. The valve voltmeter fixed at right angles to the Lecher wire and placed on a movable truck is placed near the voltage antinode, next to that of the slab. This arrangement reduces to minimum the
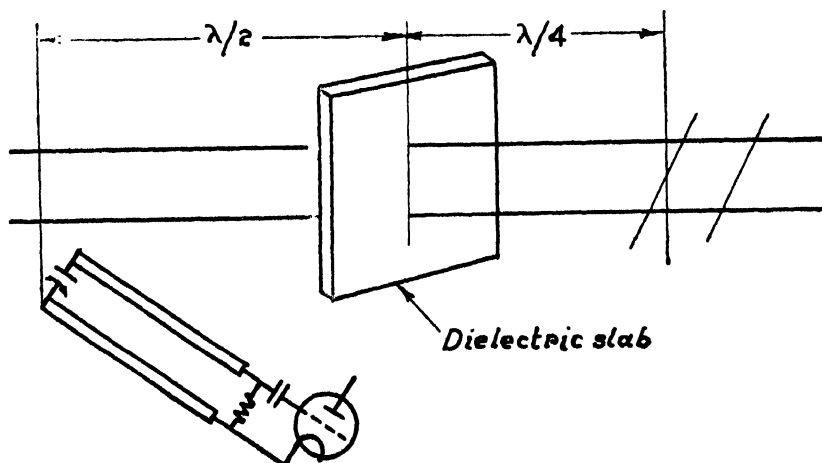
FIG. 6

loading effect on the main circuit and hence improves the accuracy of the determination of bridge positions. Moreover, the voltage measurement is not affected, as the half wavelengths long line, between the voltmeter and the slab, if assumed to have negligible attenuation, may be regarded as an unity ratio transformer. The short circuiting bridge is of tandem type.

RESULTS AND DISCUSSION

Table I shows the values of c and tan δ for four different materials as obtained experimentally. The expression (2) for dielectric constant is a transcendental equation. To calculate the values of c, Newtonian approximation Sanden and Jahnke's table have been used.

TABLE I

Frequency $= 750$ Mc's

Material	Thickness (S_1) (cms)	$(l_0 - l_1)$ (cms)	$\left(\dfrac{l_1 - l_2}{2}\right)$ (cms)	q.	ϵ	tan δ
Mycalex	0 07	3 0	0.2	1 8	4.2	.08
Plexiglass .	0 64	1.0	0.1	2	2.6	.02
Mica (Brown) .	0 63	2.0	0.15	2	4.2	.07
Ebonite	1 25	2 0	0.2	1.63	2.6	0.12

The power loss per unit volume of a dielectric is equal to $2\pi f E^2$ 0˙2244 $\times 10^{-12}$. watts per cu.

This may be written in this case as $= 106 \times 10^{-5}. E^2 . \epsilon \tau$ (8)

where $f =$ Frequency in c.p.s. $= 750 \times 10^6$ c.p.s.

$\qquad$ $E =$ Voltage gradient in dielectric (r.m.s. voltage per in.)

$\qquad$ $\tau =$ Power factor of the dielectric which may be taken as tan δ.

To measure the voltage gradient (E), the valve voltmeter is calibrated by means of a G. R. oscillator, type 857-A, and a thermocouple microammeter combination at 500 Mc/s, and the result involving plate current change and input voltage is plotted as shown in Fig. 7. The voltage gradient has been found from the change in plate current at resonance (I_m), spacing between Lecher wire and the curves in Fig. 7. From Table I and eqn. (8), power loss in watts for different materials have been calculated and given in Table II.

The rate at which heat is generated in a dielectric is proportional to $\epsilon \tau$, which is termed the loss factor of the dielectric. The loss factor is the best single criterion for the ability of a solid insulating material to withstand high r. f. voltages. From the above two Tables, it may be remarked that plexi
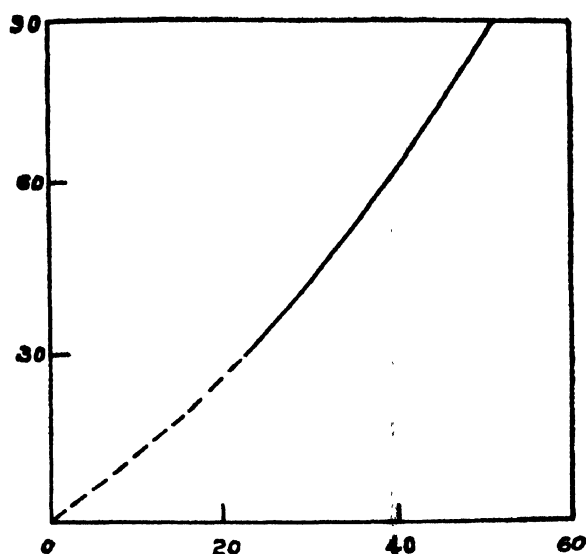
FIG. 7

TABLE II

Frequency = 750 Mc/s

Spacing between Lecher wire = 1 5″

Material	I_m μA	E Volts/in	Power loss in watts/ cu. in.	Loss factor $\tau.\ \epsilon$
Mycalex	60	24	.21	0.34
Plexi-glass	72	30	.05	0.05
Mica (Brown)	60	24	.18	0.29
Ebonite	65	26	.22	0.31

glass and mica, having lower loss, are more suitable for work like valve bases, insulating supports, coil formers etc., whereas mycalex and mica may be used for such work as necessitates insulating materials of high dielectric constants.

ACKNOWLEDGMENT

The author desires to express his grateful thanks to Dr. N. B. Bhatt, Head of the Department, for giving all facilities to carry out the above investigation. The author also wishes to make grateful acknowledgment to Miss Rajeswari, M.Sc., for assisting in setting up the equipment.

DEPARTMENT OF ELECTRICAL COMMUNICATION ENGINEERING,
INDIAN INSTITUTE OF SCIENCE,
BANGALORE.

REFERENCES

Debye, P., 1929, Polar Molecules, Chemical Catalog C ›

Drude, 1895, *Wied. Ann.*, **58**, 633.

Gemant, A , 1935, *Phil. Mag.*, XIX, 746.

King, R., 1935, *Proc. I. R. E.*, **23**, 885.

King R., 1937, *Rev-Sci-Inst.*, VIII, 201.

Wagner, K. W., 1914 *Arch. fur Elekts*, **2**, 3; 1

ON THE RAMAN SPECTRA OF A FEW NITRILES AT LOW TEMPERATURES

By B. M. BISHUI

Plate V

ABSTRACT. The Raman spectra of acetonitrile, propionitrile and benzonitrile have been investigated in the liquid and solid states and also the polarisation of the lines has been studied The line due to $C \equiv N$ deformation oscillation seems to be weakened and the frequency of the line due to $C \equiv N$ valence oscillation diminishes in the solid state. The lines due to $C - H$ valence oscillations also undergo changes in structure and intensity. No new line appears in the low-frequency region in the case of the two aliphatic nitriles but one such line appears in the case of benzo nitrile in the solid state. It is suggested that these changes in the Raman spectra may be due to formation of strongly associated molecules in the solid state.

INTRODUCTION

In continuation of the previous work by the present author in collaboration with Sirkar (1943, 1945, 1946a, 1946b) on Raman spectra of organic compounds in the solid state at low temperatures, the Raman spectra of three nitriles, *e.g.*, acetonitrile, propionitrile and benzonitrile have been studied in the solid state at low temperatures. It has already been observed that with the solidification of organic liquids at low temperatures, some changes in the Raman spectra take place. These three compounds have been chosen in the present investigation to find out whether the presence of the benzene ring has any influence on the appearance of the new lines in the low frequency region which have been observed in the case of benzene and some of its substituted compounds by previous authors and also by Sirkar and Bishui (1946). Further, the Raman spectra of these three liquids had been studied only by a few authors and the data regarding the polarisation of the Raman lines were not known for two of them. Hence this investigation was undertaken to study the Raman spectra in the liquid and solid states and also the polarisation of the Raman lines in all these cases, in order to understand the significance of the changes which are observed in the Raman spectra with the solidification of these liquids.

EXPERIMENTAL

Pure liquids were taken from Kahlbaum's original packings and were redistilled in vacuum. The technique used was almost the same as that developed for studying the Raman spectra of substances at low temperatures by

Sirkar and Bishui (1943), but slight modifications were introduced. The liquid distilled in vacuum was put in a long Pyrex tube passing through a cork which was fitted into the mouth of a transparent Dewar vessel of Pyrex glass placed in a vertical position. A narrow Pyrex glass tube, bent twice at right angles, the horizontal portion of which was double-walled and the annular portion of which had been evacuated and sealed previously was used for introducing liquid oxygen into this Dewar vessel. One of the vertical limbs of the tube was dipped into the liquid oxygen contained in a big metallic Dewar vessel and the other end passed through the cork fitting in the mouth of the transparent Dewar vessel. Another narrow glass tube bent at right angles was fitted in the cork in such a way that one of its ends lay about an inch below the cork, while the other end was connected through a stopcock and a reservoir to a Cenco Hyvac oil pump. When this vacuum pump was started and the stopcock was opened, the liquid oxygen from the metallic Dewar vessel came slowly and was collected in the lower part of the transparent Dewar vessel. The flow stopped as soon as the stopcock was closed. In this way an atmosphere of liquid oxygen vapour almost with a steady range of temperatures was maintained within the transparent Dewar vessel. A Pyrex tube containing the liquid was held with its bottom just above the surface of liquid oxygen. The apparatus is shown in figure 1. The advantage
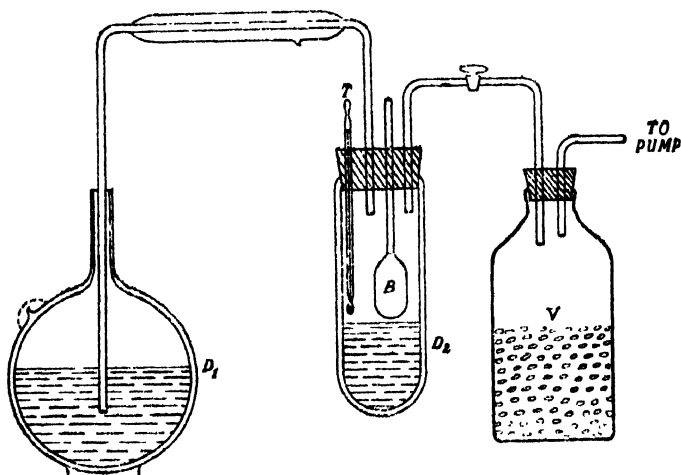
FIG. 1

of this method over the previous one was that this time the light was not absorbed by the liquid oxygen and consequently the time of exposure was much reduced. With this arrangement it was possible to continue the work during the rainy season even when the humidity was as high as 90%. In order to have a constant temperatures at a certain depth in the transparent Dewar vessel care was taken to maintain the level of the liquid oxygen in it at a particular height. A pentane thermometer was used to record the temperature of the solidified substance. The temperature was different at

Fig. 1

Fig 2

Fig 3

Fig. 4

Fig. 5

Fig. 6
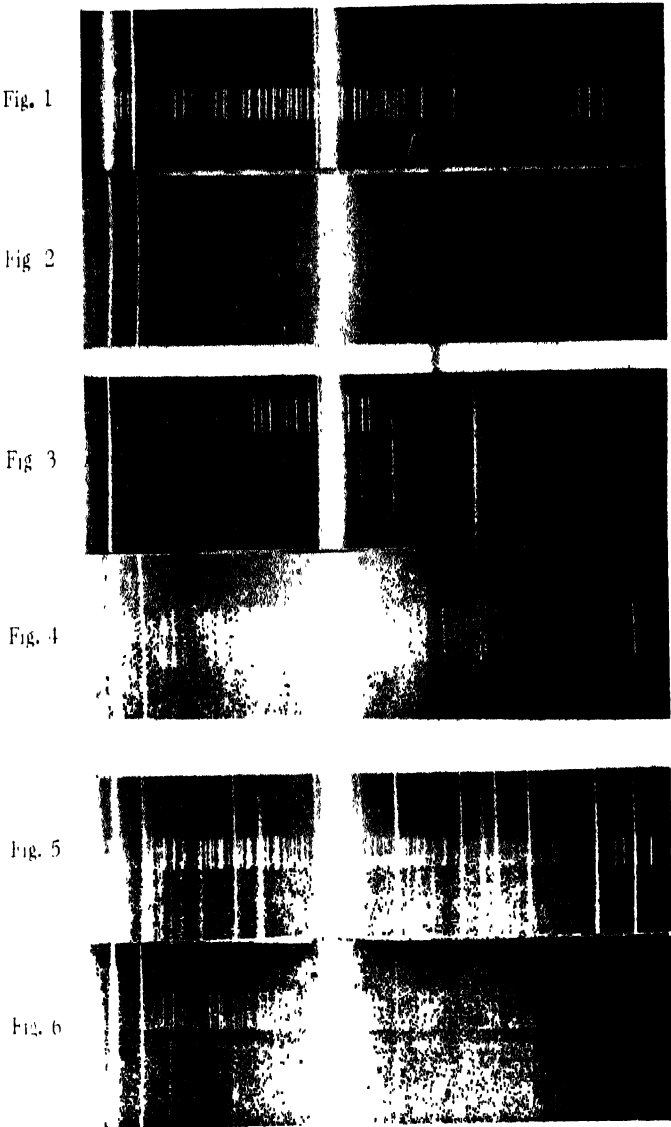
Fig. 1.   Acetonitrile at about + 30°C.
  „   2.   „   „   „   − 150°C.
  „   3.   Propionitrile „   „   + 30°C.
  „   4.   „   „   „   − 150°C.
  „   5.   Benzonitrile „   „   + 30°C.
  „   6.   „   „   „   − 150°C.

ifferent heights above the surface of the liquid oxygen and the mean was observed.

Suitable portions of the Dewar vessel were blackened and the substance was illuminated with two vertical mercury vapour lamps, the light being focussed with the help of two six-inch glass condensers. The scattered light emerged through a window on one side.

A Fuess spectrograph having optical parts of glass was used in the present investigation. It has dispersion of about 14 A.U. per mm. in the region of 4046 A.U. A blue-violet glass filter was placed in the path of incident light in order to diminish the intensity of the continuous background in the region on long wavelength side of 4358 A.U. The polarisation of the Raman lines due to the liquid state was studied in each case by photographing simultaneously the spectra of the vertical and horizontal components of the scattered light with the help of a double image prism. Light from a mercury arc focussed with the help of the condenser was used as the incident light in this case also. The spectrograms, therefore, only indicated whether any Raman line was partially polarised or completely depolarised and no attempt has been made to measure the absolute values of factor of depolarisation accurately. In the case of the lines which are totally depolarised, the horizontal component appears stronger than the vertical component because the latter is reduced in intensity due to reflections at the surfaces of the prism in the spectrograph, and this criterion helped to identify the totally depolarised lines.

RESULTS AND DISCUSSIONS

The results obtained are given in tables I, II, and III. The first column of each table contains the results reported by some of the previous workers. The letters P and D denote polarised and totally depolarised $(\rho = 6/7)$ respectively. The approximate visually estimated intensities are given in the parentheses. The data for the solid at about $-150°$ C obtained in the present investigation are given in the last column. Some of the spectrograms are reproduced in Plate V.

Acetonitrile.—The Raman spectrum of acetonitrile in the liquid state was studied formerly by Dadieu and Kohlraush (1929), Pal and Sengupta (1930), and Petrikaln and Hochberg (1929), but the polarisation was not studied before. The data reported by Magat (1934) have been inserted in the first column of Table I, for comparison. The frequencies of some of the lines reported by previous workers are a little lower than those observed in the present investigation. The lines at 2294 cm^{-1} and 2731 cm^{-1} observed in the present investigation were not reported by the previous workers. The line at 384 cm^{-1} due to C≡N deformation oscillation seems to be weakened, and the line at 2731 cm^{-1} due to C−H valence oscillation vanishes in the solid state at low temperature. The most intense line at 2256 cm^{-1} due to C≡N valence oscillation is accompanied by the weak satellite at 2294 cm^{-1}

in the liquid state. Although this satellite was not reported by earlier workers, it is definitely present in the spectrogram reproduced in Plate V. This line may be due to the formation of associated molecules through $C \equiv N$ bond and such association of molecules in the liquid state is probable in the present case, because the molecule is strongly polar and small in size. According to group theory CH_3CN molecule should yield four polarised and four totally depolarised Raman lines. The results obtained in the present investigation regarding the polarisation show that there are five polarised and three

TABLE I

Acetonitrile. C_2H_3N

Liquid at about 32°C		Solid at about −150°C Present author
Magat (1934)	Present author	
377 (3)	384 (5) e, k ; D	386 (od)
917 (3)	918 (4) e, k ; P	910 (ob)
1230 —		
1367 (2)	1370 (3b) e, k, P	1370 (1)
1417 (0)		
	1450(ob) e, k ; P	
2249 (3)	2256(10) e, i, o, p, q ; P	2243 (4)
	2294(1) e, k ; P	2290 (o)
	2731(1) e, k ; ?	
2941 (2)	2942 (10) e, i, k, o, p, q ; P	2937 (5s)
2996 (1)	3004(4b) c, k ;D	3004 (4s)

TABLE II

Propionitrile. C_3H_5CN

Liquid at about 32°C		Solid at about −150°C Present author
Howlett (1931)	Present author	
220 (F)	218(4' ±e, ± k ; D	118(1) 222(1) V
370 (?)	377(3b) e ; D	
540 f)	549 2) c, k ; P	552(o) e, k
	674(2) e, k ; P	674'2 e, k
840 (f)	84ɔ(5) e, k ; P	846'1) e, k
990 ..	......	.....
	1005(3) e, k ; P	1010 1) e, k
1080 (f)	1075(3) e, k ; P	1072(1) e, k
1260 (f)	1260(2) k ; P	1260(1) k
1310 (f)	1316(2) k, D	1316(1) k
1430 'f)	1432(3) e, k ; D	1424(1) k
1470 (f)	1472(3) e, k ; D	V
2240 if)	2250(10) e, k, o, p, q ; P	2242(3) e, k, o, p, q
2900 f)	2900(4) e, k, o, p, q ; P	2900(2) e, k, o, p, q
2950 (f)	2948(10) e, i, k, o, p, q ; P	2950(5X) e, i, k, o, p, q
		2970(3) e, k, o, p, q
3000 (f)	2997(4) e, k, o, p, q ; D	2993(3), e, k, o, p, q

TABLE III

Benzonitrile. C_6H_5CN

Liquid at about 32°C		Solid at about −150°C Present author
Magat	Present author	
170(8) 6/7	174(3b) e, D	94(4) k
380(2) 0.36	380(2) e, D	
	407(1) e k : ?	
460(6) ...	463(5) e, k ; P	459(1) k
549(5) ...	556(4) c, k ; D	555(0) e, k,
621(5) 6/7	630(5) e, k ; D	630'1)
752(3) 0.15	755(4) c, k : P	749(0)
765(5)	769(4) e, k ; P	764(0)
	809(1) e, k ; P	.. ..
	855(1) e, k ; ?	
998(5) 0.04	996(8s) e, k ; **P**	996 (5s)
1023(3) ...	1024(3) e, k ; P	
1178(8) ...	1172(2s) e, k ; D	1172 (2)
	1184(2s) e, k : P	1182 (2)
1190(8) 0.24	1197(3s) e, k ; P	V
1310(1) ..		
1353(0) ...		
	1430(1b) e ; D	
1447(1) ...	1453(1) e, k ; D	
1493(2) ...	1498'1) e, k, D	
	1540(0) e, k. ?	
1596(10) 6/7	1601(10) e, k ; D	1595 (5) e, k
	2176(1) e, k, P	
2225(12) 0.23	2232(10) c, k, p	2226(5) e, k
		3060(2) e, k
3068(8) 0.30	3070(1) e, k, p, q ; P	3068(4) e, k
3146(1) ...	3146(1) e, k ; P	3146(0) e
3196... ...	3197(1) e, k ; P	3197(0) e.

depolarised lines. Evidently one of the depolarised lines is too weak to be recorded and the line at 2294 cm^{-1} which is polarised is probably not due to the single molecule.

In the solid state at about −150°C the substance does not yield any new Raman lines in the low frequency region and it is observed that some of the prominent Raman lines of the single molecule undergo changes in frequencies and intensities at this low temperature. For instance, the lines at 918 cm^{-1}, 2256 cm^{-1} shift to 910 cm^{-1} and 2243 cm^{-1} respectively in the solid state. These lines being due to the C−C and C≡N valence oscillations this diminution of the frequencies shows the influence of intermolecular field in the solid state on these bonds. Another remarkable change observed is the enhancement of the intensity of the line 3004 cm^{-1} in the solid state. This line is due to the antisymmetric C−H valence oscillation.

Propionitrile.—The Raman spectrum of propionitrile in the liquid state was studied formerly by Dadieu and Kohlhaush (1930) and Howlett (1931). The results reported by the latter author have been included in the first column of Table II for comparison. The lines at 674 cm^{-1}, 1075 cm^{-1} were not observed by the previous workers. No satellite in the neighbourhood of C≡N vibration is observed in this case. There are six totally depolarised Raman lines in the Raman spectrum of propionitrile. Hence the molecule has a symmetry element which is probably a plane of symmetry.

In the solid state at about −150°C this substance also does not yield any new Raman lines in the low frequency region and it was observed that the line 377 cm^{-1} due to the C≡N deformation oscillation and 1472 cm^{-1} due to C−H deformation oscillation in the liquid state vanish completely in the solid state at low temperature. It can be seen from Table II that no other remarkable change takes place in the frequencies of the remaining prominent Raman lines, when the liquid is solidified at about −150°C, excepting the changes occurring in the C−H vibrations. The line at 2948 cm^{-1} due to the liquid is split up into two lines at 2950 cm^{-1}, 2970 cm^{-1} in the solid state at low temperature. This suggests that some change in the structure of the CH_3− group takes place in the solid state at low temperature, and this may be due to formation of a loose linkage through this group.

Benzonitrile.—The Raman spectrum of benzonitrile in the liquid state was studied by Kohlraush and Pongratz (1932) and Simons (1932). The results reported previously (Magat, 1934) have been included in the first column of Table III for comparison. The lines at 407 cm^{-1}, 809 cm^{-1}, 855 cm^{-1}, 1430 cm^{-1} and 2176 cm^{-1} due to the liquid observed in the present investigation were not reported by the previous workers. The presence of the satellite 2176 cm^{-1} of the C≡N vibration 2276 cm^{-1} has been verified by observing a satellite of the line 2276 cm^{-1} excited by 4046A. In this case also this line may be due to formation of associated pairs of molecules in the liquid state.

In the solid state at about −150°C the substance yielded a new Raman line at 94 cm^{-1} in the low frequency region and it was observed that some of

the prominent Raman lines of the single molecule undergo changes in frequencies and intensities at the low temperature. It was also observed that some of the lines due to the liquid completely vanish in the solid state at low temperature. The line at 380 cm^{-1} due to $C \equiv N$ deformation oscillation disappears in the solid state. The presence of the line at 2176 cm^{-1} in the solid state could not be definitely established.

Since the Raman line due to $C \equiv N$ valence oscillation appears in the solid state with undiminished intensity while the intensity of the line due to the $C \equiv N$ deformation oscillation is practically absent in the solid state, it seems that this oscillation is restricted in the solid state. As this line is totally depolarised its intensity cannot be diminished by transmission through the mass of the crystal. Thus this fact is definitely an example of restriction on certain mode of vibration in the solid state.

Thus three interesting facts emerge out from the study of the Raman spectra of these three nitriles. First, the line due to $C \equiv N$ deformation oscillation becomes extremely weak in the solid state and the frequency of $C \equiv N$ valence oscillation diminishes slightly in the solid state. Secondly, there appear no new lines in the low frequency region in the spectra of the two aliphatic nitriles in the solid state at low temperature, but in the case of benzonitrile one new line appears at 94 cm^{-1}. Thirdly, the $C-H$ valence oscillations either undergo changes in intensity or are split up into components in the solid state. From the investigations of the Raman spectra of aliphatic and aromatic organic compounds at low temperatures made by Sirkar and Bishui (1943, 1945, 1946a, 1946b) previously, it was observed that new lines appear in the low frequency region in the case of all benzene compounds without fail, whereas in the case of many aliphatic compounds these new Raman lines do not appear in the low frequency region in the solid state at low temperatures. This peculiar behaviour of benzene compounds may be due to the presence of double bonds which are not wholly saturated in the benzene ring. Probably there is some tendency for the formation of associated molecules even in the liquid state and when the benzene compounds are solidified at the low temperature the molecules come closer and closer and probably they finally form strongly associated groups of molecules. Thus the appearance of new Raman lines in the low frequency region in the case of all the benzene compounds may be due to the formation of such strongly associated molecules in the solid state through carbon bonds. The changes in the lines due to $C-H$ valence oscillations with the solidification of the two aliphatic nitriles studied may be due to the formation of such associated molecules through the hydrogen bond which may not yield sharp lines but may produce diffuse bands which are difficult to detect.

suggestions during the progress of the work and to Prof. M. N. Saha, F.R.S., for kindly providing facilities for work in the Palit Laboratory of Physics and to Council of Scientific and Industrial Research for financial assistance.

Palit Laboratory of Physics,
University College of Science,
92, Upper Circular Road, Calcutta.

REFERENCES

Dadieu, A , and Kohlraush, K W. F , (1929) *Wien. Ber* , **138**, 799.

Dadieu, A , and Kohlraush, K W. F , (1930), *Wien. Ber.*, **139**, 165

Kohlraush, K. W. F , and Pongratz, A , (~932), *Wiener Ber.*, KI, 11b, 142, 637.

Howlett, L E , (1931), *Canad. J of Res* , **4**, 8.

Magat, M., (1934), *Annual Tables of constants etc.*, pages 29.

Pal, N. N., and Sengupta, P. N , (1930), *Ind. J Phys* , **5**, 13.

Patrikaln, A., and Hochberg, J., (1929), *Z. f Phys. Chem. B*, **3**, 217.

Simons, L., (1932), *Soc. Sci Fenoica commentations Phys Math* , **5**, 13

Sirkar. S. C., and Bishui, B. M., (1943), *Proc. Nat. Inst. Sc. India* **9**, 287.

"   "   (1945), *Ind. J. Phys.*, **19**, 24.

"   "   (1946a), *Ind. J. Phys* , **20**, 33.

"   "   (1946b), *Ind. J. Phys.*, **20**, 111.

MULTIPLET SEPARATIONS IN COMPLEX SPECTRA
(OF d^3 AND d^1 CONFIGURATIONS)

By V. RAMAKRISHNA RAO and K. R. RAO[*]

ABSTRACT. Expressions for multiplet separations derived by Goudsmit for complex spectra arising out of equivalent electron configuration have been applied to the spectra of vanadium and columbium, which have been recently analysed extensively on the basis of Zeeman effect and hyperfine structure studies. The check-up between theoretical and experimental values have indicated a correspondence chiefly in the case of the deeper terms. The disagreement in columbium II is exceptionally large.

INTRODUCTION

Separations between multiplet levels, in line spectra, were characterised according to Lande by factors, designated as Γ, giving the displacement of each level from the centre of gravity of the whole multiplet. They are similar to Lande's 'g' factors, explaining magnetic separations and can be represented thus

$$\Gamma = \Sigma a_i l_i s_i \cos \overline{(l_i s_i)} \qquad \dots (1)$$

which gives the total interaction energy for several electrons. In the case of normal multiplets, the expression reduces to

$$\Gamma = A l s \cos (ls) = \tfrac{1}{2} A \left[j(j+1) - l(l+1) - s(s+1) \right] \qquad \dots (2)$$

where

$$A = \Sigma a_i \frac{l_i}{l} \overline{\cos(l_i l)} \frac{s_i}{s} \overline{\cos (s_i s)},$$

is the well-known separation factor. For a given multiplet the Γ-values of the different levels may be calculated in terms of A with the help of the above equation. It gives us the Lande interval rule.

An interesting property of these Γ-factors is, as pointed out by Lande, that the sum of the Γ-values, for a given value of m, is the same for a strong as well as a weak field—known as the Γ-permanance rule. Goudsmit made a further investigation of the properties of these factors and following Pauli's study of the building up of the 'g' values of an atom from those of the individual electrons enunciated a Γ-sum-rule, analogous to the g sum-rule concerning Zeeman separations. It states that, for a number of levels arising from a given electron configuration, the sum of all the Γ-values belonging to a definite value of m, is independent of the strength of the field. This Γ-sum rule was illustrated by the case of two equivalent 'p' electrons. The Γ-sum remains constant for all couplings provided it is taken for these levels which have equal j's, among terms of a given configuration.

An important application of Goudsmit's rule is, as shown by him, that it is possible to derive expressions for multiplet separations in general cases.

Such expressions are of great practical value in the analysis of the structures of complicated spectra. The validity of the method was illustrated by Goudsmit (1928) (for levels arising from equivalent electrons) by a comparison of the observed and predicted multiplet separations chiefly in the spectrum of singly-ionised titanium which was then the only one of that type almost completely known.

Some other spectra corresponding to equivalents electron configurations have since been analysed, based extensively on evidence from Zeeman effect data and hyperfine structure observations and application of X-ray laws to iso-electronic systems and it would be of interest to examine how far predictions made on Goudsmit's method would be in accord with the actual analysis. Among the spectra considered in this paper are those due to d^3 and d^4 equivalent electron configurations, particularly of vanadium, columbium and chromium.

RESULTS AND DISCUSSION

TABLE I

Multiplet Separations for Equivalent d Electrons

Configuration	Multiplet	Total Separation	Separation factor, A
d^3	⁴F	7 2a	1 3a
	⁵P	4 3a	1 3a
	²H	11/10, a	1 5a
	²G	27, 20a	3, 10a
	²F	−7 12a	1 6a
	²D ⎫ ²D ⎭	5/ 6a	1/3a
	²P	a	2/3a
d^4	⁵D	5 2a	1/4a
	³H	11/10a	1/10a
	³G	27 20a	3 20a
	³F ⎫ ³F ⎭	7 12a	1/12a
	³D	−5/12a	−1/12a
	³P ⎫ ³P ⎭	3/2a	1/2a

Table I is a part of the table derived by Goudsmit giving the total multiplet separations for equivalent d electrons (d^3 and d^4) expressed in terms of 'a'. It also gives the values of the separation factor Λ. For the method of deriving these values, reference may be made to Goudsmit's original paper (1928).

A notable feature in the table is the predicted inversion of the two terms (d^3) ^2F and (d^4) ^3D, for which the separations are negative.

Table II gives the observed and calculated multiplet separations in the iso-electronic spectra Ti II, (Bacher and Goudsmidt, 1932) V III, and Cr IV (Bowen, 1937) and in Zr II., for which the ground configuration corresponds to d^3. In each case the constant 'a' is estimated from the ^2H separation,

TABLE II

Separations in Spectra of d^3 Configuration

Term	Spect.	$j-5\tfrac12$ obs	calc	$4\tfrac12$ obs	calc	$3\tfrac12$ obs	calc	$2\tfrac12$ obs	calc	$1\tfrac12$ obs	calc	$\tfrac12$ obs	calc	Over-all separation obs	calc
^4F	Ti II			128.4	133.2	103.1	103.6	75.8	74.1					307.6	310.9
	V III			244	211	194	165	145	117					583	493
	Cr IV			390	345	310	268	237	192					949	805
	Zr II			458.0	511	404.0	398	322.8	284.0					1185.4	1193
^4P	Ti II							122.3	74.1	32.1	11.1			154.4	118.5
	V III							181	118	77	71			258	188
	Cr IV							200	192	119	115			418	307
	Zr II							180.7	181	275.0	170.4			115.0	451.7
^2H	Ti II	97.8	97.8												
	V III	155	155												
	Cr IV	253	253												
	Zr II	375.2	375.2												
^2G	Ti II			120.5	120.0										
	V III			221	192										
	Cr IV			349	311										
	Zr II			315.1	461.7										
^2F	Ti II					−59.9	−51.8								
	V III						−82								
	Cr IV						131								
	Zr II					−81.0	−199								
$^2D's$	Tr II							120.4							74.1
	V III							147							123
	Cr IV							—							192
	Zr II							734.4						1169.1	284
^2P	Ti II													125.0	88.9
	V III													180	141
	Cr IV													—	230
	Zr II													466.8	341

the term having the largest l value. For instance for V III, d^3 ^{2}H $\rightarrow 11a/10 = 155$ or $a = 140.9$. Hence the predicted overall separation for d^3 ^{4}F $= 7a/2 = 493$. The component separations are then,

$$^4F_{3\frac{1}{2}} - {}^4F_{4\frac{1}{2}} = 211$$

$$^4F_{2\frac{1}{2}} - {}^4F_{3\frac{1}{2}} = 165$$

$$^4F_{1\frac{1}{2}} - {}^4F_{2\frac{1}{2}} = 117$$

The other term separations are similarly calculated.

The agreement is good in certain cases chiefly in terms of higher l and j values. The largest deviations are in the ^{1}P and ^{2}P intervals. The higher stage iso-electronic spectra also indicate considerable departures. In general it is the overall separations, rather than the component intervals that give better agreement. Such disagreement may be partly due to the departure from the Russel-Saunders type of coupling.

TABLE III

Separations in Spectra of d^4 Configuration

Term	Spectrum	J-6		5		4		3		2		1		0		Overall Separations	
		obs	cal	obs	cal	obs	cal	obs	cal	obs	cal	obs	cal	obs	cal	obs	cal
^{5}D	V II							130.3	146.4	102.3	109.8	70.6	73.2	36.1	36.6	339.3	366.0
	Cr III							220	236.4	172	177.3	150	118.2	60	59	572	591
	Cb II							423.5	615.2	363.0	161.4	279.4	307.6	159	153.8	1221.9	1538.3
^{3}H	V II	84.6	87.6	76.4	73.0											161.0	161.0
	Cr III	136	142	124	118											260	260
	Cb II	373.9	369.1	302.0	307.4											676.8	676.8
^{3}G	V II			99.5	109.5	94.4	87.6									193.9	197.1
	Cr III			142	177	160	142									292	319
	Cb II			314.2	462	357.2	369.6									671.4	831.6
^{3}F's	V II					66.3	51.8									170.2	85.4
	Cr III					12.2	39.9									—	138
	Cb II					72	60									1574.4	359.1
						355.1	459.6										
						-24.5	884.2										
^{3}D	V II																
	Cr III							60	-219	24.3	-116					84.3	-365
	Cb II								-355	...	-236					.	-591
								-424.8	154.5	360.9	-102.6					-63.9	-256.5
^{3}P's	V II									393.5		219.3				233.6	219.0
	Cr III									-258.4		-120.8					
	Cb II									68		—					354.6
										1069.0		—					
										-512.0		630.1				979.9	923.0
												-207.2					

The inversion of the ^{2}F term in Ti II and Zr II are noteworthy ; a similar inversion in V III and Cr IV spectra may be confidently predicted.

The largest discrepancy in the ^{2}D interval sum of Zr II is 1169.1, as observed against a calculated sum of 284. Even the order of magnitude is very high. Perhaps the identification of the terms is uncertain.

Table III gives the results for the spectra of V II, (Meggers and Moore, 1940) Cr III (Bowen, 1937) and Cb II, (Humphrey and Meggers, 1948) corresponding to the d^4 configuration. Of these the analysis of V II and Cb II was carried out very extensively and based on evidence derived from the study of the hyperfine structure and Zeeman effect of a large number of lines. The agreement between the observed and calculated separation is close, for ^{5}D and ^{3}G levels of V II and Cr III and in particular of the overall intervals ; Cb II intervals show generally much larger deviations. For ^{3}F and ^{3}P, theory can predict only the sum of the intervals of each type of term, *i. e.*, Σ F and not of the terms separately. In V II the observed values for ^{3}F's is double the calculated value and the discrepancy is much larger for Cb II. The ^{3}P sum is consistent both for V II and Cb II, as well as the inversion of the ^{3}D term in Cb II. The identification of ^{1}D in V II may be uncertain.

From the foregoing study it would seem that the method of Goudsmit may well be taken recourse to in predicting the interval sums with a certain confidence only for the deeper set of terms of a given configuration.

The data for the various spectra referred to above are taken from the following references.

PHYSICS DEPARTMENT,
ANDHRA UNIVERSITY.

REFERENCES

Ti II
Zr II   } Bacher and Goudsmit, 1932 'Atomic Energy states' R 471, 535, and 495
V III

Cr III
Cr IV   } Bowen, 1937, *Phy. Rev.*, **52**, 1153.

Cb II   Humphreys and Meggers, 1945, *Bean,Suand I* , **34**, 477

V II   Meggers and Moore, 1940, *Ibid.*, **25**, 83.

        Goudsmit, 1928, *Phy. Rev.*, **31**, 946.

DIELECTRIC CONSTANTS OF SOME SOLID INSULATING MATERIALS AT ULTRA SHORT WAVES

By S. K. CHATTERJEE and MISS RAJESWARI

ABSTRACT. Dielectric constants of several insulating materials in the form of thin slabs have been measured by the Lecher wire method over a wavelength range of 140 cms to 57 7 cms Dielectric constants in the case of materials under investigation have been found to vary with wavelengths. In the case of solid paraffin, dielectric constants have been found to increase with wavelengths becoming shorter In other cases dielectric constants show a decreasing tendency with wavelength decreasing.

INTRODUCTION

The behaviour of insulating materials under electric stress is a matter of fundamental importance to communication engiiers. The uncertainties of dielectric behaviour of solids arise from the fact that under high frequency excitation various factors become operative within the body of the material depending on its physical and chemical constitution. Hartshorn (1926) stressed on the need of a thorough investigation of various causes responsible for the uncertain dielectric behaviour. The use of any material as a dielectric in the region of cm. waves presupposes a knowledge of the dielectric constant and loss factor of the material in the particular band of frequencies. Various methods have been evolved for the study of the dielectric behaviour of different materials. The frequency variation of an oscillator, due to the insertion of the material in the tank condenser, has been utilised by Niven (1911), Hyslop and Carman (1920), Kerr (1926) and in a modified form by Wyman (1930) etc. to determine the dielectric constants of various materials. Capacitance variation method has been employed by Hartshorn and Ward (1936) to determine the dielectric constant of various ceramic materials. The difference in the wavelength of standing waves produced by resonance on parallel wires with the wires being first wholly immersed in air and then in the dielectric has been utilised first by Cohen (1891) and later on more extensively by Drude 1895), Rudop (1913) etc. Instead of parallel wires, concentric tubes have been used by Drake, Pierce and Dow (1930). The standing wave method has been suitably modified by King (1937) to measure dielectric constants of a thin slab of materials. Theoretical and experimental development of resonator systems suitable for the determination of dielectric constant has been achieved by Horner and others (1946). The measurement of 'Q' of a resonator has been utilised by Dakin and Boggs (1944) and England (1944). Wave-guide properties have been used by Lamont (1940) for such measurements. A new technique has been developed by MacLean (1946) for dielectric

loss measurements. The object of the present investigation is to measure dielectric constants of thin slabs of insulating materials over a wide band of ultra short waves by employing a week source of oscillation and following the method outlined by King.

<div align="center">T H E O R E T I C A L</div>

The velocity v of a sinusoidal current in the steady state on two parallel wires, immersed wholly in air, is $v = \omega/\beta$ where, β is the retardation angle per unit length of the line and ω is the angular velocity of the impressed e. m. f. in radians per second. If the parallel wires are immersed in medium of dielectric constant ϵ, the velocity v_ϵ, is given by $v_\epsilon = v/\sqrt{\epsilon}$, the frequency $\omega/2\pi$ of the wave being constant. Or, we can write $\lambda_\epsilon = \lambda\sqrt{\epsilon}$. This amounts to, as if, the length of the wire has been shortened from λ to $\lambda.\epsilon$ due to the insertion of the dielectric. If instead of immersing the parallel wire wholly in the dielectric, a thin slab of the dielectric is interposed, then calculating the input admittance (King, 1937) of the whole system from the telegraphist's line equation at ultra high frequencies, it can be shown that

$$\tan \tfrac{1}{2} \beta \, (s^1 - s_2) = n \tan \tfrac{1}{2} \, n\beta s_1$$

or, $$\tan \tfrac{1}{2} \beta \, (\text{max. shift} + s_1) = n \tan \tfrac{1}{2} \, n\beta s_1 \qquad \ldots \quad (1)$$

where, $s^1 - s_2 = $ maximum shift due to the introduction of the slab,

$s_1 = $ thickness of the slab,

$n = $ refractive index of the material.

The retardation angle β is given by (Drake and Pierce, 1930)

$$\beta = \frac{\omega}{c_1} . \sqrt{\epsilon} . (1 - \eta s)^2 . f(h)$$

where, $$\eta = \frac{l}{l\omega} \text{ and } s = \frac{g}{c\omega} \text{ and }$$

$$f(h) = \left[\frac{(1 + h^2)^{\frac{1}{2}} + 1}{} \right]^{1/}$$

where, as shown by Pierce (1922),

$$h = \frac{rc\omega + gl\omega}{lc\omega^2 - rg}$$

where, r, c and $l =$ resistance, capacity, and inductance respectively per loop unit length of a smooth line,

$c^1 = $ velocity of electromagnetic waves in vacuum,

$g = $ leakage conductance per unit loop length of the line.

Then the velocity $$v_\epsilon = \frac{\omega}{\beta} = \frac{c^1}{\sqrt{\epsilon} . (1 - \eta s)^{\frac{1}{2}} f(h)}$$

or $$\frac{c^1}{v_\epsilon} = \sqrt{\epsilon} . (1 - \eta s)^{\frac{1}{2}} f(h) = \frac{\lambda}{\lambda}$$

But the ratio of wavelength in vacuum to that in the dielectric is the index of refraction n. Therefore

$$n = \sqrt{\epsilon} \cdot (1 - \eta s)^{\frac{1}{2}} \cdot f(h)$$

For a short and well insulated line, g may be considered to be negligibly small. Moreover, at cm. waves ω is very high. So,

$$lc\omega^2 \gg rg \text{ and } rc\omega > gl\omega$$

Therefore,

$$h = \frac{rc\omega + gl\omega}{lc\omega^2 - rg} \doteq \frac{r}{l\omega}$$

and

$$(1 - \eta s)^{\frac{1}{2}} = \left(1 - \frac{rg}{lc\omega^2}\right)^{\frac{1}{2}} \doteq 1$$

The expression for the index of refraction, therefore, at ultra short waves for a short well insulated line, reduces to

$$n = \sqrt{\eta \epsilon} \qquad \qquad \dots \quad (2)$$

So by finding out the maximum bridge shift for a certain material, the refractive index and hence the dielectric constant of the material can be calculated with the help of the equations (1) and (2).

EXPERIMENTAL

The experimental technique mainly consists of the following :

1. The wavelength of the oscillator along the Lecher wire, when the latter is wholly immersed in air is determined by finding bridge positions for three consecutive maxima of the indicator reading. The bridge then being placed in its first position of maxima, the oscillator is moved in its truck parallel to the Lecher wire till the indicator shows its maximum. The oscillator is kept fixed in this position throughout the experiment.

2. The optimum position of the slab is determined so that the bridge shift $(s^1 - s_2)$ may be a maximum. This procedure minimises the error in the determination of ϵ. The slab is provided with two holes at the centre, the diameters of the two holes being almost of the same size as that of the wires, so that the contact between slab and wires is properly ensured, while at the same time the slab can be moved smoothly and snugly along the wires. The slab is placed between the indicator and the bridge. The bridge is moved till the indicator reads maximum. Then moving the slab towards the bridge,

step by step, the bridge shift at each step is measured. Fig. 1 shows the relation between bridge shift and the slab position for one of the materials.
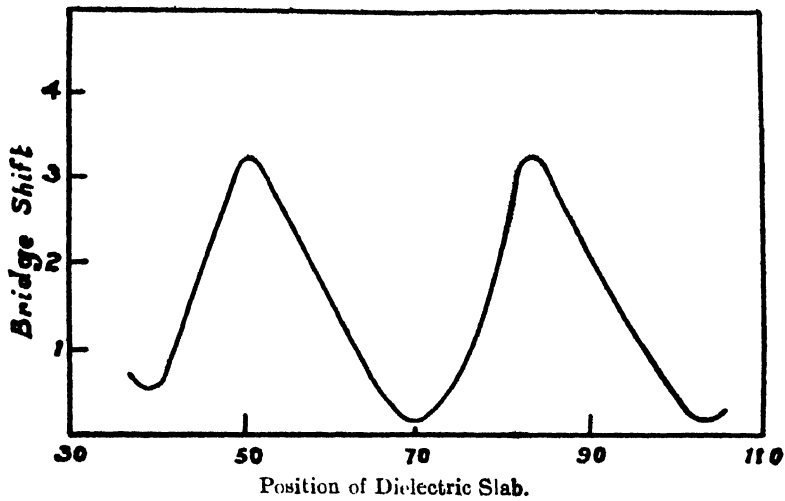
Fig. 1

3. The wavelength of excitation being varied from 140 cms to 57.7 cms maximum bridge shift $(s' - s_2)$ at each step corresponding to the optimum position of the slab is noted. The wavelength of excitation is checked before and after each observation.

4. The thickness of the material is measured.
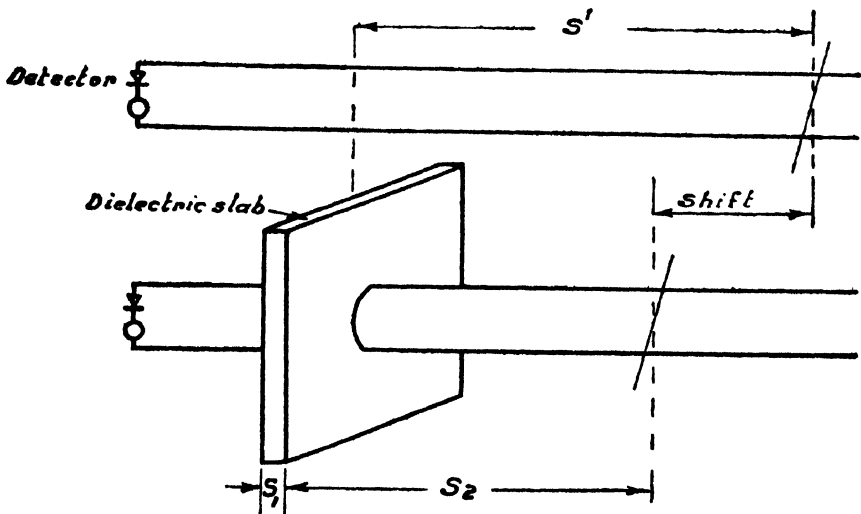
Fig. 2

The above procedure is repeated for ten different materials, in the form of thin slabs. The experimental arrangement is shown in figure 2.

The oscillator used is of the resonant type with two 955 tubes in parallel. Two oscillators have been used. One of them covers a range of 142 cms to 96 cms. The other covers a range of 98 to 56 cms. The resonant

lines of the first oscillator are 9 cms in length and 0.3 cms in diameter and spacing between lines is 0.43 cms. The filament chokes for the oscillator consists of air cored coils of 50 turns and diameter 0.4 cms made from
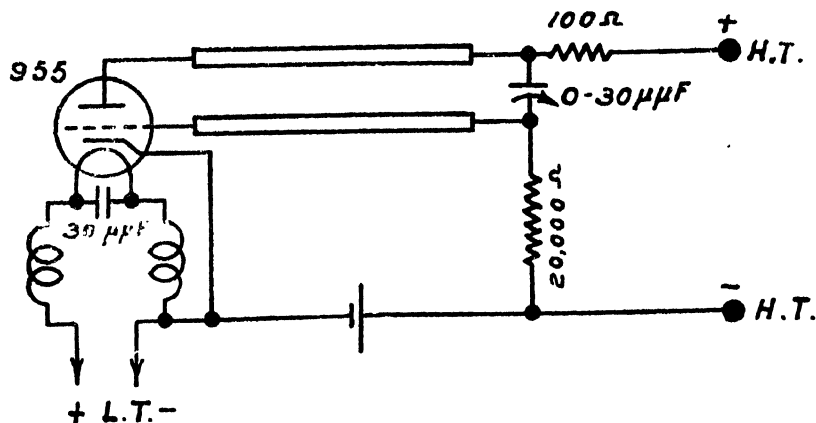
FIG. 3

26 S.W.G. enamelled copper wire. For the second oscillator, the resonant lines are of length 3.6 cms., diameter 0.3 cm. and spacing 0.5 cm. The filament chokes of diameter 0.3 cm. consists of 40 turns made from the same gauge of wire as above. The frequency of the oscillators is varied by changing the spacing between resonant lines and also by adjusting the trimmer shunting the end of the resonant lines. The oscillator circuit diagram is shown in Fig. 3.

The indicator used consists of a crystal detector-micro-ammeter combination fixed at one end of the Lecher wire line 1.

The diameter of the Lecher wires 0.326 cm. and the spacing 5 cms. from centre to centre have been chosen to satisfy the requirements of the parallel wire theory with regard to the ratio of the wire diameter to the wire separation *viz.* $(d/a)^2 \ll 1$.

The experimental results for the different materials are tabulated as follows. In order to calculate the refractive index from the equation 1 Newtonian approximation Sanden and Jahnkes tables have been used.

TABLE I

Material	λ (cms.)	Max. Shift (cms.)	ε	Material.	λ (cms)	Max. Shift (cms)	ε
Celeron (Thickness $S_1 = 1.33$ cm)	140.0	5 7	5.3	Bakelite (Thickness $S_1 = 0.96$ cm)	140 0	4.5	5.7
	120.0	5 7	5.3		120.0	4 4	5.6
	111.1	5.5	5.2		111.1	4 3	5.5
	100.0	5.6	4 7		100.0	4.3	5.5
	88.2	5.3	4 5		88.2	3 3	4.5
	78.9	5 3	4.5		78 9	3 3	4.5
	71.4	4 5	3.9		71 4	2 7	3.8
	65.2	4 0	3 6		65 2	2 6	3 8
	60 0	4.0	3.6		60.0	2 4	3 5
	57.7	4.0	3.6		57 7	2.0	3.1

TABLE I—(contd.)

Material	λ (cms)	Max. Shift (cms)	ε	Material	λ (cms)	Max. Shift (cms)	ε
Mycalex (Thickness S₁=0.97 cm)	140.0	4.1	5.2	Mica (Brown) (Thickness S₁=0.63 cm)	140.0	2.6	5.0
	120.0	3.9	4.9		120.0	2.2	4.3
	111.1	4.0	5.1		111.1	2.5	4.9
	100.0	4.0	4.5		100.0	2.5	4.9
	88.2	4.3	5.5		88.2	2.4	4.8
	78.9	4.4	5.6		78.9	2.4	4.7
	71.4	4.5	5.7		71.4	2.4	4.8
	65.2	4.5	5.7		65.2	2.5	4.9
	60.0	4.0	5.2		60.0	2.2	4.5
	57.7	4.3	5.5		57.7	2.2	4.5

Material	λ (cms)	Max. Shift (cms)	ε	Material	λ (cms)	Max. Shift (cms)	ε
Micanite Thickness 0.02 cm	140.0	3.7	4.9	Ebonite Thickness 1.25 cm	140.0	3.6	3.8
	120.0	3.7	5.0		120.0	3.5	3.8
	111.1	3.7	5.0		111.1	3.5	3.8
	100.0	3.7	5.0		100.0	3.0	3.4
	88.2	3.5	4.8		88.2	2.9	3.3
	78.9	3.2	4.5		78.9	3.0	3.4
	71.4	3.2	4.4		71.4	3.0	3.4
	65.2	3.4	4.7		65.2	3.0	3.4
	60.0	3.2	4.5		60.0	3.0	3.4
	57.7	3.2	4.5		57.7	3.0	3.4

Material	λ (cms)	Max. Shift (cms)	ε	Material	λ (cms)	Max. Shift (cms)	ε
Fibre Thickness 0.64 cm.	140.0	2.1	4.2	Bees Wax Thickness 2.02 cms	140.0	2.6	2.0
	120.0	2.0	4.0		120.0	2.5	2.2
	111.1	2.0	4.0		111.1	2.3	2.1
	100.0	1.8	3.8		100.0	2.3	2.1
	88.2	2.2	4.4		88.2	2.5	2.2
	78.9	2.0	4.1		78.9	2.5	2.3
	71.4	1.8	3.7		71.4	2.6	2.3
	65.2	2.0	4.1		65.2	2.1	2.0
	60.0	1.8	3.8		60.0	1.8	1.9
	57.7	2.1	4.3		57.7	1.8	1.9

Material	λ (cms)	Max. shift (cms)	ε	Material	λ (cms)	Max. Shift (cms)	ε
Paraffin Wax Thickness 2.13 cms	140.0	2.1	2.0	Plexiglass (Methyl-metha Crylate) Thickness 0.64 cm	140.0	1.35	3.0
	120.0	2.2	2.0		120.0	1.20	2.8
	111.1	2.2	2.0		111.1	1.30	2.9
	100.0	2.0	2.1		100.0	1.10	2.9
	88.2	2.1	2.3		88.2	1.10	2.7
	78.9	2.1	2.0		78.9	1.30	2.9
	71.4	2.3	2.1		71.4	1.00	2.9
	65.2	2.4	2.1		65.2	1.00	2.5
	60.0	2.5	2.2		60.0	1.00	2.5
	57.7	2.5	2.2		57.7	1.00	2.5

DISCUSSION

The nature of variation of bridge shift with different position of dielectric slab, as shown in Fig. 1, can be shown to agree with that obtained theoretically from the equation (Lamont, 1940)

$$n \cot \beta_1 s_1 (\cot \beta s^1 - \cot \beta s_2) + \cot \beta s^1 \cot \beta s_2 + n^2 = 0$$

where, $s_2 = s^1 - (s_1 + \delta), \quad \delta = \text{shift}$

This shows that the shift is a function of the absolute position of the slab. From the stand point of optical analogy, this result seems to be unexpected. In optical problems, such results are encountered due to the interference of two separate travelling waves. In the present case, interference occurs at the boundaries of the dielectric between the incident wave and a portion of it reflected. It has been pointed out by Lamont, that under resonant conditions reflections take place at the dielectric boundaries and at the bridge in such a manner that the resulatant stationary waves show little change of intensity at the boundaries but exhibit a definite phase change, depending on the position of the dielectric slab. This variation of phase change is considered to be responsible for different amounts of bridge shifts with different dielectric slab positions with respect to the original standing wave system.

From the experimental results, dielectric constants for all the above cases of materials, except solid paraffin wax, have been found to decrease with the wavelength. As reported by Hormell (1902), the dielectric constant of paraffin of different densities varied from 2.13 to 2.22 and from 2.16 to 2.25 at wavelengths of 81.68 cms. and 61.32 cms. respectively. In the present investigation dielectric constants of paraffin (solid) at 78.9 cms. and 60 cms. have been found to be 2.0 and 2.19 respectively.

The frequency dependence of dielectric constants may be explained by molecular process or by a mechanism of interstitial conduction which requires the presence of adsorbed ions on the surface of structural units as suggested by Murphy and Lowry (1930). When an e.m.f. is applied to the dielectric, a polarised distribution of these ions takes place, due to a surface mobility, but after the source of excitation is removed the ions return to their normal distribution. The electrical effect of the adsorbed ions is, therefore, similar to that of a dipole and they produce a kind of dielectric polarisation. The structural unit with its adsorbed ions can be represented by an equivalent electrical circuit, where each layer of adsorbed ions is represented by a capacity in series with a resistance. Both the capacities and the resistances become smaller, the greater the distance from the interface of the layers of ions to which they refer. In figure the equivalent electrical circuit c_m represents the capacity due to the dielectric polarisation of molecules; $c_1, c_2 \ldots \ldots c_{n-1}, c_n$ represent the capacities due to redistribution of adsorbed ions on the surface of the micelles; $R_1, R_2, \ldots \ldots R_{n-1}, R_n$ represent the series resistances

equivalent to frictional resistances which hinder the process of formation of a polarised distribution of adsorbed ions and R_d is the D.C. resistance. By an
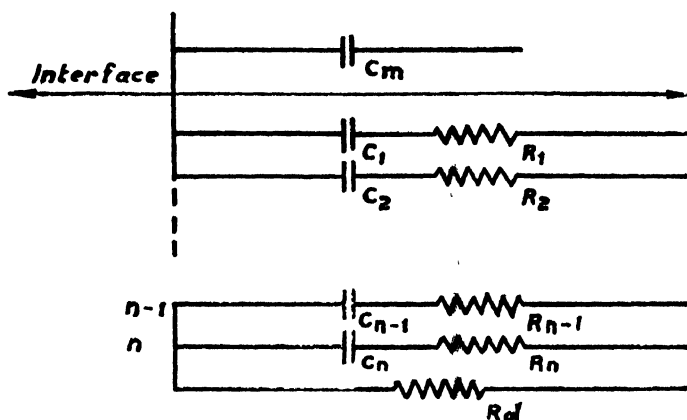
FIG. 4

analysis of the circuit, it can be shown that the equivalent parallel capacity decreases with decreasing wavelength. At very high frequency, the capacity term due to the adsorbed ions, or similar process involving long relaxation time, becomes zero, the only capacity that remains is that due to the polarisation of the charges within the molecules. In this connection, it is interesting to note that Debye (1912) suggested that if the system is compared with a pure capacity C and a resistance R in series, the following relations hold good.

$$\epsilon' = \frac{c/c_0}{1 + R^2 \omega^2 c^2}$$

$$\epsilon'' = \frac{c}{c_0}\left(\frac{R\omega c}{1 + R^2 \omega^2 c}\right)$$

where, ϵ', ϵ'', etc. have their usual significance.

Most of the solid dielectrics, for instance, ebonite, fibre, mycalex etc., investigated above, may be classed as either amorphous or of a crystalline type containing many lattice irregularities and impurities. Part of the dielectric constant of these materials may be regarded as due to the presence of dipoles and (or) ions in the dielectric. The electrical dipoles are either due to the polar groups existing in the molecules building up the amorphous substance or to the occluded or impurity molecules, which are more or less subjected to restricted rotation. The ions may be considered to originate from or belonging to the substance itself or formed by electrolytic impurities, which can both travel over certain distances through the structure of the amorphous solid, along crystal flaws or irregularities. The positions of a dipole, which is originally bound to certain position by the molecular field of the surroundings, can only be altered if a certain amount of energy is supplied. Similarly the displacement of the ions also needs a certain amount of energy. The amount

of activation energy needed for reorientation or rotation will be different for different dipoles or ions according as the solid is of amorphous or crystalline type.

On the assumption of a statistical scattering of the activation energies determining the progressive or rotational diffusion of ions or dipoles, Gevers and Pre' (1946) have worked out a theory which explains the dielectric properties of amorphous dielectrics. It has been concluded from this theory that, as a first approximation, contribution to the dielectric constant is made only by those ions and dipoles whose relaxation times (τ) exceed the value $\tau = 1/\omega$, where ω is the angular frequency of the alternating field or the part of the dielectric constant which is dependent on the frequency is a function of the activation energy corresponding to $\omega\tau = 1$.

ACKNOWLEDGMENT

DEPARTMENT OF ELECTRICAL TECHNOLOGY,
    INDIAN INSTITUTE OF SCIENCE,
        BANGALORE.

REFERENCES

Cohen, U. Heerwagen, 1891, *Wied. Ann.*, **43**, 343
Debye, 1912, *Phys. Zeit.*, **13**, 97.
Drake F. H., Pierce G. W., etc., 1930, *Phys. Rev.*, **36**, 613.
Drude, 1895, *Wied. Ann.*, **55**, 637.
Dakin, Boggs, 1944, *A. I. E. E. Tech. paper*, **44**, 161.
England, C. R., 1944, *Bell. Sys. Tech. Jour.*, **23**, 114,
Gevers, M., Pre' F. K., 1946, *Trans. Far. Soc.*, **42A**, 17.
Hartshorn, L., 1926, *J. I. E. E.*, **64**, 1152.
Hartshorn, L. and Ward, W. H , 1936, *J.I.E.E.*, **79**, 597.
Horner,. F., Tailor, T A., 1946, *J. I. E. E*, **93**, 53.
Hormell, W. G., 1902, *Phil. Mag* **3**, 52.
Hyslop and Carman, 1920, *Phy. Rev.*, **15**, 243.
King, R., 1937, *Rev Sci. Inst.*, **8**, 201.
Kerr, 1926, *Jour. Chem. Soc.*, **128**, 2796.
Lamont, H.R.L , 1940, *Phil. Mag.*, **30**, 1.
Lamont, 1940, *Phil. Mag*, **29**, 521.
MacLean, W.R., 1946, *Jour. App. Phys.*, **17**, 558.
Murphy, E. J., Lowry, H. H., 1930, *J. Phy. Chem.* **34**, 598.
Niven, 1911, *Pro. Roy Soc.*, **85A**, 139.
Pierce, G. W., 1922, *Am. Acad. of Arts and Science*, **57**, 180.
Rudop, 1913, *Ann. der. Physik.*, **42**, 489
Roberts, S, Hippel., A V., 1946, *Jour. App. Phy* , **17** 610.
Wymann, J., 1930, *Phys. Rev.*, **35**, 623.

MULTIPLET SEPARATIONS IN COMPLEX SPECTRA— PART II

By V. RAMAKRISHNA RAO and K. R. RAO*

ABSTRACT. Expressions, derived by Goudsmit and Humphreys for multiplet separations in complex spectra, have been applied to the observed multiplets of d^3s and d^3p configurations in Zr I, Cb II, and Ti I, V II and Cr III. A comparison between the theoretical and the experimental values of the separation factors indicated agreement in the deeper terms and chiefly of the d^3s configuration. The method is expected to give only the order of magnitude of the separations when it is used for the purpose of predicting unknown structures.

INTRODUCTION

In a previous paper, by the authors (Rao and Rao, 1948) expressions for multiplet separations derived by Goudsmit (1928) for complex spectra due to equivalent electron configurations have been applied to certain spectra of vanadium, columbium, etc., which have been recently analysed extensively from a study of Zeeman effect and hyperfine structures of a large number of lines. The comparison indicated good agreement for the deeper terms; the spectrum of columbium II showed exceptionally large deviations. A similar comparison is attempted in this paper for the multiplet separations of terms arising from the general configurations such as d^3s and d^3p. For such configurations Goudsmit and Humphreys (1928) have derived formulæ for the separations of normal multiplets on the fundamental assumptions that they are due to the interaction energy between spin and orbital magnetism of the electrons. The interaction energy is expressible in the form,

$$\Gamma = Als \cos (ls) \qquad \ldots \quad (1)$$

in which

$$A = \sum_i a_i \frac{l_i}{l} \cdot \cos (l_i l) \frac{s_i}{s} \cos (s_i s)$$

The method of deriving the factor A in the case where we have a number of equivalent electrons was shown by Goudsmit, and referred to in the previous paper. For other configurations, Goudsmit and Humphreys (*loc. cit.*) have shown, that the interaction energy may be found in the terms of that of the equivalent group and the interaction energy of the addded electron, provided the quantum vectors of the initial configuration remain unchanged.

* Fellow of the Indian Physical Society

They have shown that, if the co-efficients A′ and a_2 refer to the original multiplet and the added electron the factor A of the resultant term may be written as,

$$A = A'\left(\frac{l'}{l}\right)\cos (l'l)\frac{s}{s}\cdot\cos (s's) + a_2 \frac{l_2}{l}\cos (l_2 l)\frac{s_2}{s}\cos (s_2 s)$$

where s is the resultant of the vectors s' and s_2. Hence by substitution for the cosines it was derived that

$$= A'\cdot\frac{s(s+1)+s'(s+1)-s_2(s_2+1)}{2s(s+1)} \times \frac{l(l+1)+l'(l'+1-l_2(l_2+1)}{2l(l+1)}$$

$$+ a_2\cdot\frac{s(s+1)+s_2(s_2+1)-s'(s'+1)}{2s(s+1)} \times \frac{l(l+1)+l_2(l_2+1)-l'(l'+1)}{2l(l+1)} \qquad (2)$$

The application of this formula was illustrated by Goudsmit and Humphreys for the spectra of Fe and of ionised oxygen ; agreement was found in A′ values obtained from different multiplets. They expected this method to be useful in checking up the assignment of configurations and terms in complicated cases ; it should also be useful in predicting the magnitude of level separations, where they are not known.

RESULTS AND DISCUSSION

In the following section results are shown of a check-up, attempted in the iso-electronic spectra of Zr I and Cb II and of Ti I, V II and Cr III, for which the spectral data are known extensively. All the data are collected in Tables I and II below. The first column gives the spectrum and the configuration. The second contains the spectral term or terms due to the configuration and also the theoretical values of the separation factor calculated from the expression (2) by substituting the appropriate l and s values for the ion and of the added electron ; these latter values are indicated in the first column.

The observed spectral data are utilised in the following manner. Taking the example of Ti I (Table II) for each of the quintets and triplets due to the different configurations, the separation factor A is calculated (i) from adjacent levels using the general relation

$$\Gamma(j-1)-\Gamma(j) = Aj \qquad \ldots (3)$$

and (ii) from the total separation, by dividing this total by the sum of all j values except the lowest. The mean of all these values of A is shown in column (5). A′ is then calculated from this mean, by the help of the expressions in column (2) and shown in column (6). For the ion too the same procedure is applied by taking the mean value of the separation factor obtained both from adjacent levels and the total separation ; these are presented in the

last three columns. If agreement is perfect between theory and observation, the values of A′ from the various terms should be constant and identical with that derived from the ion data.

TABLE I

Separations in Zr I and Cb II

Electron configuration.	Equation (2)	Separation factor A calculated from			A′ calculated from A	A′ calculated from the ion data.		
		Adjacent levels	Total separation	Mean value		Adjacent levels	Total separation	Mean value
Zr II d^3	$^4F\ A = A'$					101.8 101.3 101.1	112.9	107.4
Zr I d^3s								
$l' = 3\ s' = 1\frac{1}{2}$ $^4F + s$	$^5F\ A = \frac{3}{4} A'$	69.7,72.9, 75.2,76.4	72.7	73.4	97.9			
$l_2 = 0\ s_2 = \frac{1}{2}$	$^3F\ A = \frac{5}{4} A'$	96.5,105.2	100.2	100.6	80.4			
d^3p								
$l' = 3\ s' = 1\frac{1}{2}$ $^4F + p$	$^5G\ A = \frac{9}{16}\cdot A' + a_2/16$	74 9,84.6, 92.7,113.7	88.2	90.8				
$l_2 = 1\ s_2 = \frac{1}{2}$	$^3G A = \frac{15}{16} A' - \frac{a_2}{86}$	84.4,70.4	78.2	77.7				
	$^5F A = \frac{11}{16} A' + \frac{a_2}{48}$	82.5, 76.2, 74 3 74.1	77.8	77.0				
	$^3F A = \frac{55 A'}{48} - \frac{a_2}{48}$	Partial Inversion	58.4	·58 4				
	$^5D A = A' - \frac{a_2}{12}$	74.3, 79.9, 85.2, 89.1	79.6	81.6				
	$^3D A = \frac{5 A'}{3} + \frac{a_2}{12}$	120.1, 129.8	115.9	115.3				
	G terms $\Sigma A = \frac{3 A'}{2}$			168.5	112.5			
	F ,, $\Sigma A = \frac{11 A'}{6}$			135.4	73.8			
	D ,, $\Sigma A = \frac{8 A'}{3}$			196.9	73.1			
	All quintets $\Sigma A = \frac{9 A'}{4}$			249.6	110.7			
	All triplets $\Sigma A = \frac{15 A'}{4}$			251.4	67.0			
	Total $\Sigma A = 6 A'$			501.0	83.5			

TABLE I (*contd.*)

Electron configuration	Equation (2)	Separation factor A calculated from			A' calculated from A	A' calculated from the ion data		
		Adjacent levels	Total separation	Mean value		Adjacent levels	Total separation	Mean value
Cb III d^3	^{4}F A = A'					169.5 188 5 206.8	184.7	187.4
Cb II d^3s	^{5}F	120.7,128.2	127.8	129.2	172.3			
	^{3}F	133.5,136.2 104.9,131.6	116.3	117.6	94 1			
d^3p	^{5}G	163 5,168.4 178.2,189 4	172.4	174.4				
	^{3}G	153.6,162 6	157 6	157 9				
	^{5}F	99.2,37 9, 138.1,115.5	92.3	96.6				
	^{3}F	195.2,265.1	225.2	228.6				
	^{5}D		99.3	99 3				
	^{3}D	344.1,317.3	333.4	331.6				
	G terms			332.4	221.6			
	F terms			325.2	177.4			
	D terms			430.9	161.6			
	Quintets			370 3	164.6			
	Triplets			718.1	191.5			
	Total			1088	181.4			

The separation factors from adjacent levels are given in the tables in order to examine, at once, how far Lande's interval rule is obeyed and hence the conformity of the atom to the normal R-S coupling. Where adjacent levels happen to be irregular, values from the total separation alone are shown.

A check is possible for each term of the d^3s configuration; for the terms of the d^3p state, only the interval sums such as "of all the G terms" or "of all the quintets", etc., could be used to estimate A', as the terms containing a_2 (which is not calculable) would then vanish.

Examination of the tables indicate a fairly close agreement in the spectra of titanium and an approximate one for chromium; the departures are large in the other spectra dealt with, *i.e.*, vanadium and columbium. In general, agreement is better for the deeper terms and terms of the d^3s configuration

TABLE II

Separations in Ti I, V II and Cr III

Electron con-figuration	Equation (2)	Separation factor Λ calculated from			Λ' calculated from Λ	A' calculated from the ion data		
		Adjacent levels	Total separation	Mean value		Adjacent levels	Total separation	Mean value
Ti II d^3	^4F Λ=A'					28 5, 29.5, 30.3	29.3	29.4
Ti I $d^3 s$	^5F	20.0, 20.4, 20.6, 20 5;	20.4	20.5	27.3			
	^3F	34.3, 36.0	35.0	35.1	28.1			
d^3p	^5G	22.9, 23.1, 23 2, 23.3;	23.1	23.1				
	^3G	27.1, 28.9	28.0	28.0				
	^5F	21.5, 21.4, 21.3 21.2,	21.4	21.3				
	^3F	33.1, 30.1	31 7	31.6				
	^5D	18.5, 26.3, 26.0, 26.1;	23.1	24.0				
	^3D	47.9, 53.7	50.2	50.6				
	G terms			51.2	34.1			
	F terms			53.0	28.9			
	D terms			74.6	28.0			
	Quintets			68.6	30.5			
	Triplets			110.2	29.4			
	Total			178.8	29.8			
VIII d^3 / VII d^3s	^4F Λ=A'					54, 56, 58	56	56
VII d^3s	^5F	38.9. 39.9, 40.5, 41.1	39.8	40.1	53.5			
	^3F	63.9, 67.2	65.3	65.5	52.4			
d^3p	^5G	48.4, 49.3, 50.2 51 0.	49.5	49.7				
	^3G	41.8. 42.4	42.1	42.1				
	^5F	40 4, 57.8, 81.9, 92.1	61.6	66.8				
	^3F	58.7, 64.6	61.2	61.5				
	^5D		33.0	33.0				
	^3D	54.6, 43.3	50.1	49.3				
	G terms			91.8	61.2			
	F terms			128.3	69.6			
	D terms			82.3	30.8			
	Quintets			149 5	66.4			
	Triplets			152.9	40 8			
	Total			302.4	50 4			
IIV d^3s	^4F A=A'					88,90.3,95	90.3	90.9
	^5F	64,66,67,68	65	66	88			
	^3F	108,114	110	111	89			
d^3p	^5G	84,85,87,88	86	86				
	^3G	65,65,	65	65				
	^5G	52,60,67,74	60	62				
	^3F	88,101	94	95				
	^5D	96,109,117	105	107				
	^3D	126,114	121	120				
	G terms			151	101			
	F terms			157	85			
	D terms			227	102			
	Quintets			255	113			
	Triplets			280	75			
	Total			535	89			

than for the others. The extent of the disagreement will indicate the measure of deviation from the Russel-Saunders type of coupling which is fundamentally assumed to be occurring in the atom, as is evident from equation (2).

As a method for the purpose of predicting the unknown structure of a spectrum, it may give us merely the order of magnitude of the separations and their approximate values, chiefly in terms of the d^3s configuration. It is hoped that guidance of this type would be of help in analysing complex spectra, in which Zeeman effect or other studies are difficult to carry out experimentally.

The data quoted in Tables I and II are taken from the references mentioned below.

PHYSICS DEPARTMENT,
ANDHRA UNIVERSITY

REFERENCES

Goudsmit, 1928, *Phy. Rev.*, **31**, 946.
Goudsmit and Humphreys, 1928, *Ibid* , 960.
Rao and Rao, 1948, *Ind. Jour. Phy.* (Communicated). **22**, 4, 173

ACKNOWLEDGMENTS

INDIAN ASSOCIATION FOR THE CULTIVATION OF SCIENCE

210, Bowbazar Street, Calcutta-12.

Applications are invited for the posts of :

(1-2) a Professor of Organic Chemistry and a Professor of Theoretical Physics, in the grade Rs. 800-40-1000, 1000-50-1250;

(3-4) a Research Officer in Physical Chemistry and a Research Officer in Optics, in the grade of Rs. 300-25-500. D. A. and Provident Fund in all cases.

Applicants for Professorships should be distinguished scientists having long experience of research, and will be required to organize and promote research and guide scholars in research work in their respective subjects. Experience of work on High Polymers is desirable.

Research Officers will have to carry out and organize research under the guidance of Professors. Applicants should ordinarily have a Doctorate Degree with long experience of research work in : Optics including Light-scattering and Raman Effect for (3), and Physical Chemistry, preferably Chemistry of High Polymers for (4).

Six copies of applications together with testimonials, statement of qualifications and age, and copies of original publications, should reach the Registrar on or before 1st August, 1948.

For candidates applying from overseas, abstracts of applications may be sent in advance by Air Mail.

CONTENTS

NOTICE TO INTENDING AUTHORS

Manuscripts for publication should be sent to Mr. A. N. Banerjee, Assistant Editor, 210, Bowbazar Street, Calcutta.

The manuscript of each paper contain in the beginning a short abstract of the paper.

All references to published papers should be given in the text by quoting the surname of the authors followed by the year of publication within braces, *e.g.*, Sen (1942). The actual references should be given in a list at the end of the paper according to the following specimen :

Sen, B. K., 1942, Volume rectification of crystals, *Ind. J. Phys.*, **16**, 329.

The references should be arranged alphabetically in the list.

All diagrams should be drawn on thick white paper in Indian ink, and letters and numbers in the diagrams should be written in pencil.

PARAMAGNETISM OF SINGLE CRYSTALS OF THE SALTS OF THE IRON GROUP OF ELEMENTS AT LOW TEMPERATURES—PART I—THE IONIC SALTS OF THE F-STATE IONS Cr+++ AND Ni++*

By AKSHAYANANDA BOSE

ABSTRACT. In the first few sections of the paper a critical discussion of the existing theories of paramagnetic salts and experimental data supporting the crystalline electric field theory of paramagnetic salts developed by Van Vleck, Bethe and Penney and Schlapp, are given In the latter parts, experimental data on the anisotropies and effective moments of several six-coordinated nickel salts at various temperatures, in the range of 300°K and 80°K, attained with a specially devised cryostat by the author, are given and discussed on the basis of the electric field theory. Assuming the electric field in these crystals to be predominantly cubic, with a small superimposed rhombic component, the basic $^3F_4$-state of the Ni++ ion splits up into a Stark-pattern, consisting of a singlet and two triplets with a mean separation of about 20,000 cm⁻¹ due to the cubic field; the components of the triplet being separated to a much smaller extent by the rhombic field. In the six-coordinated nickel salts the cubic field constant D, has a positive sign and in such a field the singlet level is the lowest lying in the Stark-pattern Consequently in such salts we should expect the Ni++ ion (1) to have approximately a 'spin only' value for the effective magnetic moment, (2) to obey the Curie Law of temperature variation of the susceptibility closely and (3) to have a feeble anisotropy. In the Ni++, however, the spin orbit coupling is fairly strong, about —335 cm⁻¹, and hence the effect of the crystalline field on the spin moments will be quite large by virtue of the coupling of the spin moments with the orbitals which are themselves strongly affected by these fields In addition to this the contribution from upper cubic levels will also be appreciable. With the help of our experimental data we have calculated the cubic and rhombic field constants for Ni++ salts and have made a detailed consideration of the relative contributions of the various factors towards the total effective magnetic moment The anisotropies and the effective moments and their temperature variations agree perfectly with the theoretical calculations of Penney and Schlapp The field constants calculated are found to be practically independent of temperature, as is to be expected in view of the strong binding between the Ni++ ion and its neighbouring co-ordination group. It is also possible to calculate the spin-orbit coupling constant λ, for Ni++ ion purely from magnetic data and these calculated values agree fairly with the spectroscopic value. A similar treatment for the Cr+++ ion which is in the $^4F_{3/2}$-state leads to the conclusion that here contributions from other sources than the spin moment towards the effective moment is of very much less importance and in consequence the salts have much less anisotropy and obey Curie Law almost perfectly

GENERAL THEORY OF PARAMAGNETIC BEHAVIOUR

1 Elementary Magnets Free

All theories of paramagnetism are based on the finding that the ultimate particles in the paramagnetic substances, namely the atoms, ions or molecules, as

* Part of a thesis approved for the D Sc. degree of the Dacca University.

It must be remembered, however, that the deviations from the Curie Law are more or less common among the paramagnetic substances, particularly in the solid and the liquid states, (Stoner, 1934) and it is only in a few cases like those considered above that the deviations can be explained on the basis of such "over-lapping" of the multiplet intervals. For example, the salts of the iron group of elements, in which the multiplet intervals for the free ions are moderately large, do show considerable deviations from the Curie Law even when allowance is made for the overlapping of the levels. We have, therefore, to invoke, in general, for the explanation of these deviations, the restrictions that would be imposed in these media on the freedom of rotation of the elementary magnets.

2. *The Weiss Law of Temperature Variation of Susceptibilities*

It is well-known that the temperature variation of the susceptibilities of many of these paramagnetic substances particularly at high temperatures is given by the relation,

$$\chi = \frac{C}{T - \theta} \tag{6}$$

where θ, is a small characteristic temperature for the substance ; which reminds us of the similar behaviour of the ferromagnetic substances above their Curie points. This suggests at first sight that in these paramagnetic substances also, the deviation from the Curie Law is due to the same type of "inner fields", which explain the behaviour of ferromagnetics both above and below their Curie temperatures and which has been since known to arise from the Heisenberg "exchange interaction" between the spin moments of the magnetic particles. This surmise, however, is not justified for the following reasons.

Firstly, large values of θ occur even in such highly magnetically dilute salts as Tutton salts in which the ferromagnetic interactions should be negligible. Secondly, in these paramagnetic substances both positive and negative values of θ are observed and further, ferromagnetism does not occur even below the value of θ, where positive, as deduced from measurements of susceptibilities at high temperatures.[*] Actually, at temperatures near about θ, the deviations from the Curie Law become quite complicated and is another reason against accepting the ferromagnetic "inner field" as the cause of these deviations.

Indeed, the validity of a law of the type (6) limited to high temperatures only, $T \gg \theta$, has not much significance, since then a small deviation from Curie Law, *whatever its origin*, can be expressed by the power series

$$\chi = \frac{C_1}{T} + \frac{C_2}{T^2} + . \tag{7}$$

---

[*] The ferromagnetism observed by Simon in some of the ordinary paramagnetics at very low temperatures of the order of 0.1 °K, is presumably due to the mutual influences of the elementary magnets, owing to their close proximity at such low temperatures, and is quite unrelated to the above large deviation from the Curie Law (1936, *Comptes Rendus*),

For large values of T, for which only Weiss Law is obeyed experimentally, the series reduces to a first approximation to

$$\chi = \frac{C_1}{T - \theta}, \quad \theta = \frac{C_2}{C_1} \dots\dots\dots \qquad \dots \quad (8)$$

Thus a proper experimental verification of the law of the type (6) can be made only at temperatures *comparable to* θ, and it is precisely here the law fails experimentally.*

Thirdly, an inner field of the exchange type cannot explain how in some salts, *e.g.*, Cr^{+++} and Ni^{++}, which closely obey the Curie Law and in which therefore the elementary magnets may be presumed to be free, the effective moments of the elementary magnets Cr^{+++} and Ni^{++} instead of being the free ion values, are experimentally found to be such as appear to arise—as has been pointed out by Sommerfeld (1923), Bose (1927) and Stoner (1929)—mostly out of the spin moments of the electrons ; as if the orbital moments have become in some way quenched. On the other hand, it is also to be noted that the deviations from the Curie Law are the largest where the effective magnetic moments have large orbital contributions, *e.g.*, in the salts of Fe^{++} and Co^{++}. Fourthly, the " inner field " theory fails also to give any explanation of the large magnetic anisotropy that is observed in many paramagnetic crystals, the variation of this anisotropy with temperature and its relation to the orbital moments.

Thus an " inner field " of the exchange interaction type cannot explain the observed deviations from the behaviour to be expected from the free magnetic particles, at any rate in the highly diluted paramagnetic salts ; though in substances like the anhydrous chlorides or oxides and similar compounds of the transition elements, due to high concentration of the magnetic particles, the exchange forces also may have an appreciable influence on the magnetic behaviour. (Starr, Bitter and Kaufmann, 1940)

3. *The Influence of the Crystalline Electric Fields on the Paramagnetic Behaviours*

It should be remembered that any alternative to the 'inner field' theory must explain the following outstanding experimental facts satisfactorily :

(1) The deviations from the Curie Law of temperature dependence which at low temperatures become complicated.

(2) The part played by the orbital angular momentum of the elementary magnets in connection with these deviations.

(3) The magnetic anisotropies of single crystals and their intimate relation with the deviations from the Curie Law.

(4) The relative contributions of the spin and the orbital moments towards the total effective moments of the magnetic particles.

---

* These failures have been referred to in the literature of the subject as 'cryomagnetic anomalies' (Stoner, 1934).

(5) The peculiar magnetic properties of the complex salts of the transition elements whose susceptibilities are in general much lower than those of the corresponding ionic salts and sometimes even diamagnetic.

In recent years the theoretical investigations of Bethe (1929, 1932), Van Vleck, (1932) Penney and Schlapp (1932) and others have thrown considerable light on the nature of the mechanism responsible for restraining the freedom of orientation of the elementary magnets ; and just such a mechanism as would explain the above facts has been found to exist in the strong and asymmetric electric fields that would obtain in the neighbourhood of the paramagnetic ions in the substances that we are considering.

Under the action of such an electric field the $(2J + 1)$-fold degeneracy, corresponding to any particular value of the total quantum number J, existing for an assemblage of free paramagnetic ions in the absence of a magnetic field, will be already removed, at least partially, even before the incidence of the magnetic field.

This will be in effect a Stark-splitting of the energy states of the paramagnetic ions. In many of the paramagnetic salts the electric field will be sufficiently strong to break down the L-S coupling and further to produce a large separation compared to kT, of the $(2L + 1)$ orbital levels ; $(2S + 1)$-fold spin degeneracy of each of these orbital levels will, however, be practically entirely left over. The result will be that when a magnetic field is put on, it is only the spin moments of the paramagnetic ions that will be capable of turning round in the magnetic field and contributing to the observed paramagnetism of the medium, whereas, the orbital part of the moment will be more or less completely *frozen*. But though the orbital moments are in this manner prevented from contributing to the effective magnetic moment of the ions, they will still have profound influence on the susceptibility of the medium in the following manner. Though the spin moments are to a first approximation unaffected by the crystalline electric fields, their freedom of orientation in the magnetic field, however, will be very much hampered indirectly through their coupling with the orbital moments, which are themselves strongly affected. This will in effect be equivalent to the imposition on the spin moments, of local restraining fields magnitude of which will depend on the orbital moments and the strength of the spin-orbit coupling. Such 'local fields' besides having an essentially different origin from Weiss 'inner fields', differ from them also in other important respects. Whereas, the 'inner field' in Weiss theory is proportional to the intensity of magnetization thus leading to an expression of the type, $\chi = C/(T-\theta)$, which should hold at *all* temperatures greater than θ, the local fields meant to replace the crystalline electric fields will be proportional to the intensity of magnetization as a rough approximation only at temperatures T much greater than θ. This is very satisfactory, since then the $\chi = C/(T-\theta)$ will be valid only at $T \gg \theta$ and will break down at low temperatures just as is required by experimental results.

It will be further seen that if we still choose to think in terms of formula (6), the value of C will be determined chiefly by the spin moment of the magnetic particles while the orbital moments will play an important role in determining θ. Thus, as we have mentioned earlier, the susceptibility of the medium which depends on C and θ, will depend not only on the spin moments which contribute to the effective moment but also on the orbital moments which are apparently frozen. The important role played by the orbital moment in determining the susceptibilities was missed in the earlier theories since its influence is confined nearly entirely to θ, the origin of which was previously ascribed to 'inner fields' the nature of which was not properly understood.

Again, the crystalline electric field cannot produce magnetisation by itself since its effect ultimately is merely to quench directly the orbital moments and introduce indirectly large restrictions in the form of local fields on the spin moments. These fields, therefore, cannot lead to the development of ferromagnetism like the 'inner fields' contemplated in Weiss theory.

Lastly, these local fields, intended to replace the asymmetric crystalline fields, will naturally partake of the symmetry of these latter fields and will account for the observed magnetic anisotropies in crystalline media, whereas, the exchange forces are incapable of producing any anisotropy.

So far we have considered the splitting of the energy levels by the crystalline electric fields which are sufficiently strong to break the spin-orbit coupling, but not strong enough to break the Russel-Saunders coupling altogether which is the case for the ionic salts of the iron group with which we are mainly concerned in the present paper. But it should be mentioned here that many cases are known, as for example, some of the complex salts like potassium ferricyanide, potassium ferrocyanide, etc. in which, owing to the close proximity of the negative charges surrounding the paramagnetic ion much closer than in the ordinary ionic salts, the electric fields become sufficiently large to break even the Russel-Saunders coupling and all the l-moments as well as the s-moments of the electrons in the incomplete shell of the individual paramagnetic particles responsible for their magnetism, will be quite independent of each other. Under the influence of the electric field, $(2l + 1)$-fold degenerate energy level occupied by the electrons will be split up into as many different levels, each with a two-fold spin-degeneracy and the various electrons in the incomplete shell of the magnetic particle will be accommodated in these levels, of course in accordance with the Pauli Exclusion Principle. The effective magnetic moment will evidently depend on the relative separation of these levels, which ultimately will be determined by the magnitude and asymmetry of the crystalline field involved.

Cases also are known, for example, in the rare-earth salts in which owing to the screening effect of outer completed shells of electrons, the influence of the electric fields on the inner incomplete $4f$-shell responsible for paramagnetism of these salts is not strong enough to break down completely even the $L-S$

coupling. In such a case we cannot separate out for discussion the spin and orbital degeneracies but will have to regard the energy levels as having a $(2J+1)$-fold degeneracy, *some* of which will be removed by the crystalline field and whatever degeneracy is left over will be removed on the application of a magnetic field. This would account for the deviations from normal paramagnetic behaviour.

4. *Earlier Experimental Evidence for the General Validity of the Electric Field Theory*

The electric field theory has received considerable support from magnetic studies especially those made recently on the crystals of the salts of the rare-earth and the iron group of elements with the latter of which we are concerned.

(1) For the S-state ions, where there are no orbital moments to be quenched, the splitting of the spin levels under the influence of the electric fields will be extremely small. The three principal susceptibilities of the single crystals should then conform, as Van Vleck and Penney (1934) have shown, to expressions of the type,

$$\chi_i = \frac{C}{T}\left(1 + \frac{\theta_i}{T}\right), \quad i = 1, 2, 3 \qquad \dots \quad (9)$$

where θ's are very small, of the order of $0.1^\circ K$ and the sum of the three θ's should be equal to zero. The mean susceptibility will therefore conform almost accurately (*i.e.* upto $1/T^2$ terms at least) to the simple Curie Law, and even for the three principal susceptibilities the deviation from the Curie Law will be very small. These results are verified experimentally in the case of salts of Gd^{+++} ion ($^8S_{7/2}$-state) and Mn^{++} and Fe^{+++} ions ($^6S_{5/2}$-states) in the powdered state (Stoner 1934 ; Leiden Comms.) as also in the state of solution (Bose 1935). It is further found experimentally that the single crystals of these salts have very small but finite magnetic anisotropies as required by (9) and correspond to splitting of the spin levels of the order of $0.1^\circ K$ (Krishnan and Banerjee, 1936) which can also be obtained independently (Kürti and Simon, 1935) from specific heat measurements of these salts at low temperatures and also from experiments on cooling produced in them by adiabatic demagnetization. Further, at all ordinary temperatures the anisotropy varies as $1/T^2$ as required by (9) (Krishnan, Mukerji and Bose, 1939).

As has been already mentioned, the indirect influence of the crystalline electric fields on the spin moments, through their coupling with the orbital moments which are themselves strongly affected, is evidenced by the deviations from the Curie Law or by the anisotropies exhibited by the single crystals of these substances, which should therefore be a measure of the strength of the spin-orbit coupling. It has been actually possible to calculate the

strength of the coupling in Ni^{++} salts (Krishnan and Bose, 1938, 1939) where conditions are favourable for such calculations.

A particularly striking achievement of the electric field theory (Van Vleck, 1932 ; Penney and Schlapp, 1932 ; Görter 1932) lies in the finding (*a*) that in a given field the Stark-pattern for Co^{++} ion ($^4F_{9/2}$ — state) is inverted with respect to that of Ni^{++} ion ($^3F_1$-state) and (*b*) that as one passes from tetrahedral four-coordinated to octahedral six-coordinated salts the potential at the central paramagnetic ion changes sign which is equivalent to an inversion of the Stark-pattern. From this point of view the magnetic properties of six-coordinated Co^{++} and Ni^{++} salts should be very different from each other and further the four-coordinated Co^{++} salts should behave similarly to the six-coordinated Ni^{++} salts and vice versa. These results have been verified experimentally with the six-coordinated Co^{++} and Ni^{++} salts as also with the four-coordinated Co^{++} salts Cs_2CoCl_4 and Cs_3CoCl_5 (Krishnan and Mukherji 1938).

Again, in the case of single crystals of $CuSO_4$, $5H_2O$, from the known X-ray fine structure of the crystal, (Beevers and Lipson, 1934) it is possible on the basis of the electric field theory to locate the directions of the principal magnetic axes in the crystal, and to predict that though the crystal is triclinic it is nearly uniaxial magnetically. Both these predictions are fulfilled (Krishnan and Mukherji 1936, 1938).

Further, these large internal electric fields required by the theory are consistent with the known distribution of the charged atoms immediately surrounding the paramagnetic ions in the solid state (Hoffmann, 1931 ; Beevers and Lipson, 1934 ; Hendricks and Dickinson, 1927 ; Chrobak, 1934) and fields of the same magnitude can even exist in the liquid or solution state. For, according to a well known theorem of Jahn and Teller (1941) the distribution of the charged atoms immediately surrounding a given ion is conditioned by the quantum state of the ion itself and has to be such that the resulting electric field should remove wholly the orbital degeneracy of the ion. This would explain satisfactorily the large deviations from the Curie Law of the same order as in solids, observed for paramagnetic salts in aqueous solutions (Stoner, 1925). Evidence for such large Stark-splittings of the energy levels of the paramagnetic ions in aqueous solutions are forthcoming from the observations on the absorption spectra (Spedding, 1937,38 ; Freed, 1938 ; Bose, 1938,39) and the large magnetic birefringence (Chinchalkar etc. 1931-35) of these solutions.

EXPERIMENTAL METHOD
1. Cryostat

For the purpose of experimental investigations on magnetic behaviour of single crystals at low temperatures a suitable cryostat was devised by the author, a detailed description of which has already been given in an earlier paper (Bose, 1948). The cryostat was of the gas flow type, the cryostat

chamber being cooled by a flow of cold air through it. The efficiency of cooling and uniformity and steadiness of temperature in the chamber were very high due to the combined action of several factors namely : (1) a proper exchange of heat between the flowing gas and the walls of the chamber by making the flow of the gas turbulent by its passage through a series of suitably arranged perforated copper discs, (2) a thorough conduction of heat by making the walls and the discs of copper sheet and providing a large surface of contact between the gas and these copper surfaces, (3) a suitable thermal capacity of the chamber (4) an efficient automatic relay system for regulating the flow of cold gas through the chamber, controlled by a sensitive constant volume air thermometer incorporated in the chamber. Thus the temperature inside the crystal chamber could be maintained steady to about $0.01°K$ at any desired value between $300°K$ and $80°K$ over long periods, to enable magnetic measurements to be made.

2. *Notations Adopted for Magnetic Measurements*

We adopt here the same notations as used by Krishnan and his co-workers (1932-39) for denoting the magnetic constants of crystals.

In monoclinic crystals the two principal susceptibilities in the (010) plane are denoted by χ_1 and χ_2 respectively, χ_1 being the greater of the two, and the inclinations of the χ_1 axis to 'c' and 'a' axes are given by ψ and $\beta - \psi$ respectively, where β is the obtuse angle between 'a' and 'c'. Further, we denote the angle between χ_2 and 'a' axes by θ, so that $\beta = \pi/2 + \theta + \psi$. The susceptibility along the 'b' axis is denoted by χ_3. In the orthorhombic crystals the three principal magnetic axes will evidently be the crystallographic axes 'a', 'b' and 'c' axes and the principal susceptibilities measured along these axes will be denoted by X_a, X_b and X_c respectively. In the tetragonal, hexagonal and trigonal systems the crystallographic symmetry axis 'c' will evidently be also an axis of rotational magnetic symmetry and we shall denote the susceptibility along this axis by $\chi_{||}$ and that in the perpendicular plane by $X_{\perp}$.

Our magnetic measurements consist of firstly, locating one of the magnetic axes if it is not already known from crystal symmetry, from which the direction of the other two can be easily found out, and then determining the principal anisotropies $\chi_1 - \chi_2$ and $\chi_1 - \chi_3$, from measurements on anisotropies in any two known planes in the crystal. For the uniaxial crystals evidently, only one such measurement is needed to determine $X_{||} - X_{\perp}$. Secondly, the absolute susceptibility along any known direction of the crystal is determined, which combined with the anisotropy measurements, gives us the values of all the three principal susceptibilities.

3. *The Measurement of Magnetic Anisotropics*

The principle underlying these measurement is the same as in our earlier works and the details of the actual technique are given in the paper

mentioned in a previous section. The crystal is suspended in a horizontal homogeneous magnetic field with a fine quartz fibre suspension from a torsion head and so adjusted that the torsion on the fibre is zero. Starting with this position the torsion head is rotated through a critical angle α_c and the crystal follows through a smaller angle $\pi/4 + \sigma_c$, such that the equilibrium of the crystal in the field becomes unstable and the crystal turns round suddenly. It can then be shown that the anisotropy, $\Delta\chi$, of the crystal in the horizontal plane is given by

$$\frac{1}{2} \cdot \frac{m}{Mc} \cdot H^2\Delta\chi = X \text{ (say)} = \frac{\alpha_c - \pi/4 - \sigma_c}{\cos 2\sigma_c} \qquad \dots \quad (10)$$

where $\sin 2\sigma_c = 1/2\lambda$.

In the above equation m is the mass of the crystal, M its gm. molecular weight, H the magnetic field, and c the torsion constant of the fibre. For low temperature work the crystal is suitably suspended within the cryostat chamber and its anisotropy measured as above, at different temperatures. In the present measurements the crystals were usually chosen to have a large degree of geometric symmetry and the magnetic field being also highly homogeneous the effect due to the anisotropy of shape is negligible. The measurements of anisotropies of orthorhombic crystals were made by suspending the crystal successively with two of the principal axes vertical, observing the direction of setting in the magnetic field, and determining the difference between the maximum and minimum susceptibilities in the horizontal plane. For monoclinic crystals one suspension with 'b' axis vertical enables us to determine the directions of the principal susceptibilities χ_1 and χ_2 in the plane (010) *i.e.*, the angles ψ and θ between χ_1 and 'c' axes and between χ_2 and 'a' axes; and also the difference $\chi_1 - \chi_2$. Measurement with one other suspension will give $\chi_1 - \chi_3$ also. In general, since the (001) plane in the crystals used by us were well developed, this measurement was made either with the 'a' axis vertical, which gives

$$|\Delta\chi| = \pm [(\chi_1 - \chi_3) - (\chi_1 - \chi_2) \sin^2\theta] \qquad \dots \quad (11)$$

or with (001) plane horizontal, which gives

$$|\Delta\chi| = \pm [(\chi_1 - \chi_3) - (\chi_1 - \chi_2) \cos^2\theta] \qquad \dots \quad (12)$$

the positive or negative sign being chosen in the equations according to as the 'b' axis sets perpendicular or parallel to the magnetic field in the above suspensions. Occasionally, the second measurement of anisotropy was made with the well developed ($\bar{2}$01) plane vertical and 'b' axis horizontal. With each suspension the measurements of anisotropies of the crystals were made from room temperature down to about 80°K and back again to room temperature at intervals of about 25°, thus providing a check.

4. *Measurement of Absolute Susceptibilities*

The absolute susceptibilities were measured by suspending the crystal in an inhomogeneous magnetic field with a vertical gradient, from one arm of a

sensitive torsion microbalance of special design (Bose, 1948) and measuring the vertical force on the crystal with the balance. As shown in the earlier paper

$$\frac{F_T}{F_\Theta} = \frac{\chi_T}{\chi_\Theta} \left[1 + {}^{\epsilon}a\Theta\right]\left[1 + \gamma\Theta\right)\left(1 - \frac{\Theta}{T}\right) \tag{13}$$

where F_T and F_Θ are the vertical forces on the crystal at any temperature T and room temperature Θ respectively, temperatures being measured on the absolute scale, χ_T and χ_Θ are the corresponding gram molecular susceptibilities of the crystal along the direction of the field, which in this region is horizontal; $k_{a\Theta}$ the volume susceptibility of air and k_Θ that of the crystal in the field direction both at room temperature ; and γ is the coefficient of thermal volume expansion of the crystal. Thus if the forces at different temperatures are measured, knowing the absolute susceptibility of the crystal in the direction concerned at room temperatures, the values at other temperatures can be calculated. In actual practice, the crystal was suspended from one arm of the torsion balance within the cryostat chamber, placed in the inhomogeneous magnetic field and the angle of torsion on the balance fibre necessary for balancing the magnetic force was noted at various temperatures.

5. *Experimental Results*

The values of anisotropies $\chi_1 - \chi_2$ and $\chi_1 - \chi_3$ at intervals of $20°C$ as obtained from graphical interpolation from actual experimental values are given in the Table II and plotted in Figs. 1-3.

Knowing the anisotropies of the crystal in this temperature range, the determination of absolute susceptibility along any one convenient direction in the crystal, at different temperatures in the same range, will serve to give uniquely all the three principal susceptibilities of the crystal at these temperatures. These principal susceptibilities are then corrected for the diamagnetism of the salt and the effective moments of the paramagnetic ion in the crystal for the three principal directions are calculated therefrom using the formula

$$\chi_i = \frac{N p_i^2 \beta^2}{3kT}, \ i = 1, 2, 3 \qquad \dots \tag{14}$$

where χ_i is the corrected principal susceptibility per gm. ion, and p_i is the effective moment per ion in the direction concerned, expressed in terms of the Bohr magneton. The values of the effective moments thus calculated are given in Table III and plotted in the insets of Figs. 1-3. The variations of the effective moment represent uniquely the deviations from the 'free ion behaviour' and therefore form suitable basis for discussion of the observed paramagnetic behaviour of crystals on the crystalline electric field theory. Since, the variations of the effective moments were not very large and no singularities or discontinuities were observed in the magnetic behaviour for any of the crystals

studied here, a determination of the absolute susceptibilities at three different temperatures was sufficient to give the temperature variations of the effective magnetic moments within this range correctly.

Table I gives the values used for the diamagnetic corrections.

TABLE I

Ion or molecule	K_2SO_4	$(NH_4)_2SO_4$	SO_4^{-2}	$(NH_4)_2BeF_4$	$6H_2O$	BeF_4^{-2}	Cs_2Cl_4	$Fe^{++}, Co^{++}, Ni^{++}, Cu^{++},$
Value of Diamagnetic correction $\times 10^6$	-70.2	-77.8	-33.6	-66.7	-77.7	-32.6	-162	-13.0

TABLE II

For Principal Anisotropies of Crystals with Different Suspensions

$NiSO_4$ $(NH_4)_2 SO_4 6H_2O$ Monoclinic ; $\beta = 107°4'$ $a:b:c = 0.7370:1:0.5032.$				$NiSO_4. K_2SO_4. 6H_2O$ Monoclinic ; $\beta = 105°0'$ $a:b:c = 0.7379:1:0.5020.$				$NiBeF_4. (NH_4)_2BeF_4. 6H_2O$ Monoclinic ; $\beta = 106°40'$ $a:b:c = 0.737:1:0.491.$			
(1) '*b*' axis vertical (2) '*a*' axis vertical '*b*' axis normal to field.				(1) '*b*' axis vertical (2) '*a*' axis vertical '*b*' axis normal to field.				(1) '*b*' axis vertical, (2) '*a*' axis vertical, '*b*' axis normal to field.			
Temp °K.	Angle* between '*a*' axis & χ_2 axis $= \theta$	$\chi_1 - \chi_2$ $\times 10^6$	$\chi_1 - \chi_3$ $\times 10^6$	Temp °K.	Angle * between '*a*' axis & χ_2 axis $= \theta$	$\chi_1 - \chi_2$ $\times 10^6$	$\chi_1 - \chi_3$ $\times 10^6$	Temp °K.	Angle * between '*a*' axis & χ_2 axis $= \theta$	$\chi_1 - \chi_2$ $\times 10^6$	$\chi_1 - \chi_3$ $\times 10^6$
303.1	31	110.0	106.2	303.1	27	158.0	152.6	299.1	31	107.0	103 4
280	32	120.0	116.9	280	27	174.0	166.4	280	30.5	114.5	110.1
260	32 5	130 0	126.9	260	27	190.3	181.3	260	30	124 3	119.0
240	32.75	143.0	139.1	240	27	209.9	199.8	240	30	136.7	131.8
220	33	158.2	154.7	220	27	233.8	223.4	220	30	152.6	147.8
200	33 25	177 6	173 7	200	27	263.2	252.9	200	30	172 1	168.2
180	34.5	203 0	200.6	180	27	301.7	291.8	180	30	195.2	195.1
160	35.5	236 0	235.4	160	27	350.9	340.8	160	30	234.2	230.2
140	36	281.1	281.7	140	27	426.7	406.9	140	30	282.4	279.7
120	36.25	349.3	350.1	120	28	545.1	501.4	120	30	354.6	353 2
100	36.25	454.4	453.7	100	28	717.4	672.8	100	30	454.5	446.7
90	36.25	533.5	533.3	90	28	813.4	772.7	......	...	...	...
86.6	36.25	565.8	564.3	86.6	28	857.8	812.8	84.7	30	547.0	531.3

*Angle measured in degrees.

TABLE III

For the Gm. Molecular Principal Susceptibilites and the Squares of the Effective Magnetic Moments. (*Corrected for Diamagnetism*).

Crystal	Crystal suspension and the direction along which the susceptibility is measured, i.e. the direction setting along field	Temp °K.	$\chi_1 \times 10^6$	$\chi_2 \times 10^6$	$\chi_3 \times 10^6$	p_1^2	p_2^2	p_3^2	p^2
NiSO$_4$(NH$_4$)$_2$ SO$_4$, 6H$_2$O	'b' axis vertical, 'χ_1' axis along field	297 5	.1315	.1202	.1206	10 34	10 07	10.08	10.16
		167.9	7520	7298	7300	10 17	9.870	9 872	9.971
		86 6	14412	13846	13848	10.06	9.661	9.663	9.795
NiSO$_4$K$_2$SO$_4$, 6H$_2$O	(001) plane horizontal 'a' axis along field.	297.1	1350	.1188	.1191	10 42	10.03	0 05	10.17
		173 4	7471	7155	7165	10 43	9 993	0. 01	10 14
		86 6	14633	13775	1382	10 21	9.610	9.642	9 821
NiBeF$_4$(NH$_4$)$_2$, BeF$_4$,6H$_2$O	'b' axis vertical, 'χ_1' axis along field	297.4	4354	.4246	.4250	10 43	10.17	0.18	10 26
		172.2	7391	7180	7183	10.25	9 959	9 963	10.06
		84.7	14777	14230	14246	10.08	9.709	9.721	9 837

DISCUSSION OF RESULTS

1. The Directions of the Principal Magnetic Axes in Relation to Asymmetry of the Crystalline Electric Field

In the paramagnetic crystals that we are considering the paramagnetic behaviour, as we have seen, is largely affected by the electric field acting on the paramagnetic ion, arising from the surrounding negatively charged atoms. It has been shown by Van Vleck (1932), Bethe (1929), Penney and Schlapp (1932) and others, that in most cases the deviation of the paramagnetic ion from 'free ion' behaviour may be explained by the simple postulate of a predominantly cubic field with a small rhombic component superposed upon it, acting on the paramagnetic ion. Thus the potential V, of the electron in this crystalline field may be represented as a Taylor series, about the centre of the paramagnetic ion, the non-vanishing terms in which are given by

$$V = Ax_i^2 + By_i^2 - (A+B)z_i^2 + D(x^4 + y^4 + z^4) + 3Dr^4 \qquad \dots \quad (15)$$

in which the squared and fourth power terms represent the rhombic and the cubic parts of the field respectively. The last term need not be considered further, since it represents the spherically symmetric part of the field and does not change the relative separations of the levels in the Stark-pattern produced by the field.

In general the x, y, z axes of the rhombic and the cubic parts do not coincide each to each, though for our purpose it is found to be enough to assume that they do coincide. Whenever experimental data make it necessary to have a field of lower symmetry we can construct it by suitably orienting the two sets of axes.

A further complication in the analysis of the behaviour of paramagnetic ion arises due to the fact that the unit cell of the crystal will in general

contain more than one ion with their field axes oriented with respect to one another and a knowledge of these orientations is generally not available. The crystalline field axes associated with each ion are uniquely determined by the dispositions of the surrounding negatively charged atoms and presumably will not change since the paramagnetic ion is strongly bound to the neighbouring charged atoms, as evidenced by the large over-all Stark separation of the energy levels of the order of 20,000 cm^{-1}. Further evidence of such strong binding is obtained from the persistence of such ionic groups even in the state of solutions which explains the large deviations from the 'free ion' behaviour observed in the aqueous solutions of many of the salts of the iron group.

The binding between the different ionic groups may, however, be relatively much weaker and the groups may therefore change their orientations with respect to one another as temperature changes, causing an appreciable change in the position of the magnetic axes of the crystal where they are not already fixed by crystal symmetry. Actually such changes have been observed by us though these are very small except in a few cases. A detailed account of these has been published in an earlier paper (Bose, 1947).

In any case it may be safely concluded that the electric field in the neighbourhood of the paramagnetic ions are practically unaffected by the changes in temperature. This is further corroborated by a detailed calculation to be given later, of the crystal field constants in such favourable cases as the six-coordinated nickel salts and the four-coordinated cobalt salts. A further point which emerges from these considerations is that not only the predominant cubic part of the field but also the feeble rhombic part will be determined by the immediate neighbours, the effect of more distant charged atoms being negligible. This point of view apart from its plausibility considerably simplifies the problem of correlating the magnetic behaviours of the *ion* and the *crystal*.

2. *Nature of Stark-pattern under Crystalline Field for Different Ground States and its Effect on the Magnetic Behaviour*

In the iron group of elements we are concerned with the S, D and F-state ions only, in which the coupling between the orbital and the spin momenta of the 3d electrons, responsible for the paramagnetism of the ions, is of the Russel-Saunders type. The crystalline fields involved in the *ionic salts* of these ions are sufficiently strong to break the *l-s* coupling but not strong enough to break the *l-l* or the *s-s* couplings, so that we can discuss the effect of the crystalline fields upon the L and S moments of the ions separately. Since the spin moments are not much affected by the crystalline fields, the behaviour of the S-state ions *e.g.*, Mn^{++} and Fe^{+++}, where the entire magnetic moment is due to the spins, will be simple as has been already mentioned in a previous section.

General behaviour of the other ions of the iron groups will be evident from what follows. Neglecting for the present any effect of the crystalline

fields upon the spin energy levels of the ions, the Stark-pattern of the ions in these electric fields would correspond to the removal, either partly or wholly, of the $(2L + 1)$-fold orbital degeneracy. How complete is the removal of the orbital degeneracy will depend upon how asymmetric the field is. For example, in a field of cubic symmetry the D-state splits up into a doubly degenerate and a triply degenerate level ; and an F-state into a singlet and two successive triply degenerate level. With the large cubic fields involved in these crystals, the over-all separation of the above cubic Stark-patterns will be of the order of 10^4 cm^{-1}. A small rhombic field superimposed on the cubic field will naturally separate the components of the individual doublet or triplet but to a much smaller extent than the cubic separations. Each one of these various levels will, in the absence of a strong spin-orbit coupling, retain its $(2S + 1)$-fold spin degeneracy, which can be removed by the application of the magnetic field and will lead to the magnetization of the medium. In general, however, though the spin moments are very little affected by the electric fields directly,* still owing to the coupling of these moments with the orbital moments, there will be an appreciable separation of the spin components also, by the rhombic field. The width of this spin Stark-multiplets will depend upon the strength of the rhombic field and the spin-orbit coupling.†

Since the Stark-pattern of the F-state corresponds to two adjacent triplets and a singlet, the energy of the singlet state should be either the highest or the lowest in the pattern. Which it is will depend upon the nature of the cubic part of the crystalline field. This point is of great interest and will be discussed in a part of the paper to be published later on. If the singlet level is the lowermost, since the triplets will be far removed from it, cubic separation being of the order of 10^4 cm^{-1}, practically the singlet level alone will be occupied at all ordinary temperatures.‡ Since this level retains almost all its $(2S + 1)$-fold spin degeneracy in the crystalline field, the ion will behave very nearly like S-state ions, in having a feeble anisotropy, nearly spin only value of the effective moment and small deviation from the Curie Law.

In the D-state ions on the other hand, the lowest state in the cubic field has to be either the doublet or the triplet, the separation between the components of either of which, being produced by the feeble rhombic field, will be comparable to kT and the population of the upper components of the lowest level will be quite appreciable. The magnetic behaviour of these ions will

---

* Here we should not forget the very small 2nd order Kramers splitting of the spin-levels due to the direct effect of the electric fields on the spin moments.

† It should be mentioned here that when the number of electrons in the incomplete shell is odd, there will be a two-fold Kramers spin degeneracy that will always be left over, however large the spin-orbit coupling may be.

‡ We shall see later on that the populations of the upper levels are not negligible and these levels also contribute appreciably to the total magnetisation through the temperature-independent " high frequency" terms.

not therefore be so simple as that of the F-state ions with the singlet level lying lowest. In general, the behaviour of the F-state ions with the triplet lying lowest and the D-state ions will be complicated and will be dealt with in subsequent parts of the paper.

3. *Ionic Salts of* Cr^{+++} *and* Ni^{++}

In the six-co-ordinated salts of Cr^{+++} and Ni^{++} ions, of which the ground states are $^4F_{3/2}$ and $^3F_4$ respectively, the singlet level is the lowest. This corresponds, as shown by Van Vleck (1932) and Görter (1932) to the cubic field constant D in the expression (15) being positive. It has been shown (1) that the crystalline field in these salts may be usually represented by a predominant cubic part with a superimposed small rhombic component such that the principal axes of the former are coincident, respectively, with those of the latter, so that the field potential may be represented by

$$V = D\ (x^4 + y^4 + z^4) + Ax^2 + By^2 - (A + B)z^2. \qquad \dots \ (16)$$

It is assumed further (2) that the crystal field axes for all the paramagnetic ions in the crystal are parallel to one another.* Penney and Schlapp (1932) have calculated the principal susceptibilities of the crystal in terms of the field constants and the spin-orbit coupling constant λ, for the free ion, obtained from the over-all multiplet width for the free ion (Laporté, 1928),

$$W = \lambda.S(2L + 1). \qquad \dots \ (17)$$

The three principal susceptibilities of the crystals, evidently measured along the co-ordinate axes x, y, z, and the corresponding effective magnetic moments may be given by

$$\chi_i = \frac{N\beta^2}{3kT}\ p_i{}^2, \quad i = 1, 2, 3 \qquad \dots \ (18)$$

where according to Penney and Schlapp

$$p_i{}^2 = p_0{}^2\left[1 + 8\lambda\alpha + \frac{\Delta_i\lambda^2}{kT} + \dots\dots - 3kT\alpha\right], \qquad \dots \ (19)$$

where $p_0{}^2 = 4S(S + 1)$, p_0 being the 'spin only' value of the moment and related to the corresponding susceptibility by

$$\chi_0 = \frac{N\beta^2}{3kT}\ p_0{}^2 ; \qquad \dots \ (20)$$

also,

$$\Delta_1 = \tfrac{2}{3}(\alpha_2 + \alpha_3 - 2\alpha_1) \qquad \dots \ (21)$$

and two similar expressions for Δ_2 and Δ_3. The α's are functions of crystalline field constants D, A and B. The mean susceptibility of the crystal

---

* This will be the case when the unit cell of the crystal contains only one paramagnetic ion. Though assumption (2) is not explicitly stated by Penney and Schlapp, it is at the basis of all their calculations.

is given by

$$\lambda = \frac{N\beta^2}{3kT}\,p^2, \qquad \qquad \dots \ (22)$$

where $p^2 = \frac{1}{3}(p_1{}^2 + p_2{}^2 + p_3{}^2) = p_0{}^2[1 + (\alpha_1 + \alpha_2 + \alpha_3)(\frac{8}{3}\lambda - kT)].$ $\dots$ (23)

4. *Magnetic Behaviour of Nickel Salts; Calculations of Spin-orbit Coupling and Field Constants*

Calculations of the field constants D, A, B and α's in various Ni^{++} salts, from magnetic data at room temperature by Krishnan and Mukherji (1938), gives us an idea regarding the relative importance of the effects of the cubic and rhombic parts of the field on the magnetic behaviour.

Taking for the Ni^{++} ion the spin-orbit coupling constant $= -335$ cm^{-1} calculated from its over-all multiplet width 2347 cm^{-1} as given by Laporte and values of α's given by us in Table V, we have calculated the values for the different terms in the expressions (19) for the effective moments along the three principal axes, for the crystal of $NiSO_4(NH_4)_2SO_4$, $6H_2O$ as an example, to exhibit the relative importance of the different terms. At room temperature, namely 303.1°K :

$$p_1{}^2 = p_0{}^2\left[1 + 8\lambda\alpha_1 - 3kT\alpha_1 + \frac{\Delta_1\lambda^2}{kT} + \dots\dots\right]$$

$$= 8[1 + .2268 + .0527 + .0054] = 10.28$$

and similarly,

$$p_2{}^2 = 8[1 + .2064 + .0480 - .0028] = 10.01 \qquad \dots \ (24)$$

$$p_3{}^2 = 8[1 + .2066 + .0480 - .0027] = 10.02$$

It will be seen at once that the last terms in the above expressions are quite negligible at room temperature and indeed vanishes altogether for the mean square moment. Of the others, the temperature independent terms, namely, $1 + 8\lambda\alpha_i$ greatly predominate, since the term $3kT\alpha_i$ is less than 5% of $1 + 8\lambda\alpha_i$. Thus, it will be seen at these temperatures : ( ) that

$$\frac{p_1{}^2 - p_0{}^2}{p_0{}^2} \sim 8\lambda\alpha_1 - 3kT\alpha_1 \sim \cdot23 + \cdot05 = \cdot28, \qquad \dots \ (25)$$

i.e., for a nickel salt the square of the effective magnetic moment in any particular direction, say $p_1{}^2$, and hence the principal as also the mean susceptibilities may be as much as 28% higher than the 'spin only' value ; (2) on the other hand $p_1{}^2$ will change little with temperature and hence the three principal susceptibilities of the crystal and *a fortiori* their mean will conform closely to the Curie Law ; (3) lastly, since the three α's differ from one another by only about 10% and the terms involving the α's account for less than a fourth part of the moments, the anisotropy of the crystal, $(\chi_1 - \chi_2)/\chi = (p_1{}^2 - p_2{}^2)/p_2{}^2$ should be only 2 or 3% and thus quite feeble.

From the expressions (19) for $p_i{}^2$ it will be seen that, of the two terms $-3kT\alpha_i$ and $\frac{\Delta_i\lambda^2}{kT}$ involving temperature the first is positive since α_i is

negative, and decreases with temperature for all the three principal moments, whereas, the second is positive for $p_1{}^2$ but negative for $p_2{}^2$ and $p_3{}^2$ and increases in magnitude with decrease of temperature for all the Ni^{++} salts studied by us. Thus $p_1{}^2$ goes on diminishing as the temperature falls, but at a decreasing rate as the last term becomes more and more important, until at a temperature somewhat below 80°K, the value of $p_1{}^2$ reaches a minimum and then increases again. The values of $p_2{}^2$ and $p_3{}^2$ on the other hand, go on falling at gradually increasing rate as temperature decreases. Though, unfortunately our data could not be extended below 80°K to verify these interesting calculations in all details, the experimental values fit in extremely well within the present range of temperatures with those theoretically calculated, as will be seen from Table III and the graphs for $p_1{}^2$ for the three Ni^{++} salts.
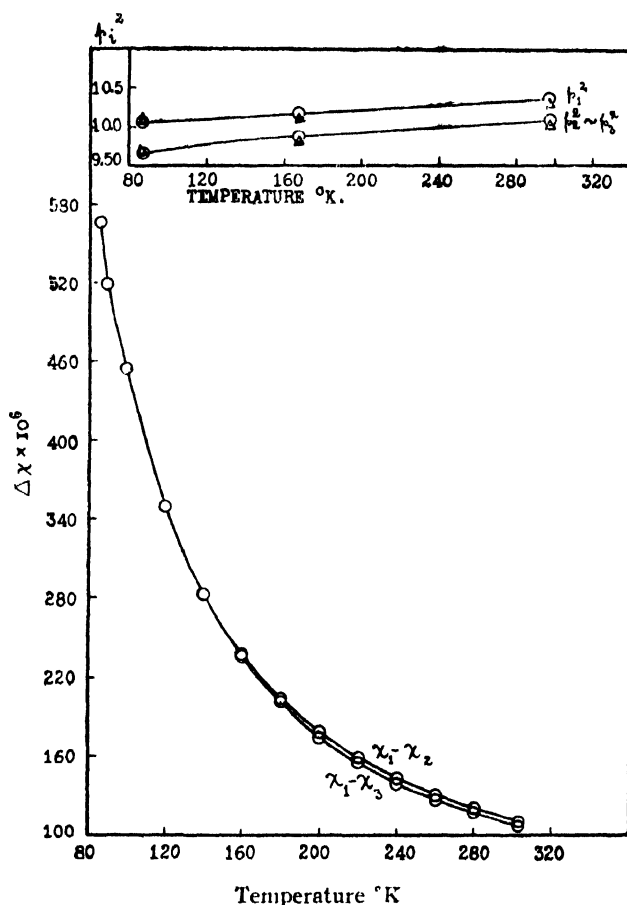
Fig. 1

Temperature Variation of Principal Anisotropies and Effective Moments of NiSO$_4$(NH$_4$)$_2$SO$_4$.6H$_2$O

Reverting to the expression (19) it will be seen that the excess of the effective magnetic moment over the ' spin only ' value, is mainly due to two

causes. A small part of this excess is due to the term $-3kT\alpha_i$, which corresponds to the temperature independent part of the susceptibility, and can
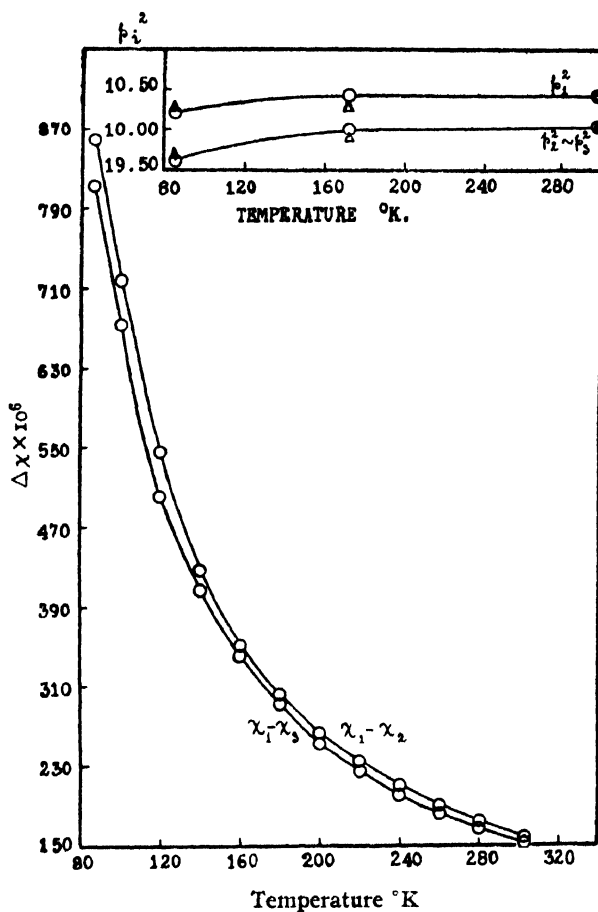
FIG. 2

Temperature Variation of Principal Anisotropies and Effective
Moments of $NiSO_4.K_2SO_4.6H_2O$

be traced ultimately to the influence of the upper levels in the Stark-pattern. But the bulk of it, represented by the term $8\lambda\alpha_i$, can be traced to the indirect effect on the spin moments of the electric field, through the spin-orbit coupling, and thus dependent on the value of λ. At low temperatures of course, the value of the second order spin term $\dfrac{\Delta_i\lambda^2}{kT}$, becomes also highly important; but in the present range it is more or less negligible.

Conversely, it should be possible, from these deviations from " spin only " value, to calculate the constant of spin-orbit coupling λ, purely from magnetic data, since the field constants α, may be regarded as practically independent of temperature, for reasons previously stated, and may thus be eliminated using data at different temperatures. Since in the expression for $p_i{}^2$ or p^2 the term involving λ is fairly large, about 23% of the other terms, it might appear at first that the variations of the effective moments with temperature

should serve us conveniently to eliminate the α's. It is, however, found that this is not so, since the term involving λ, though large, is independent of the
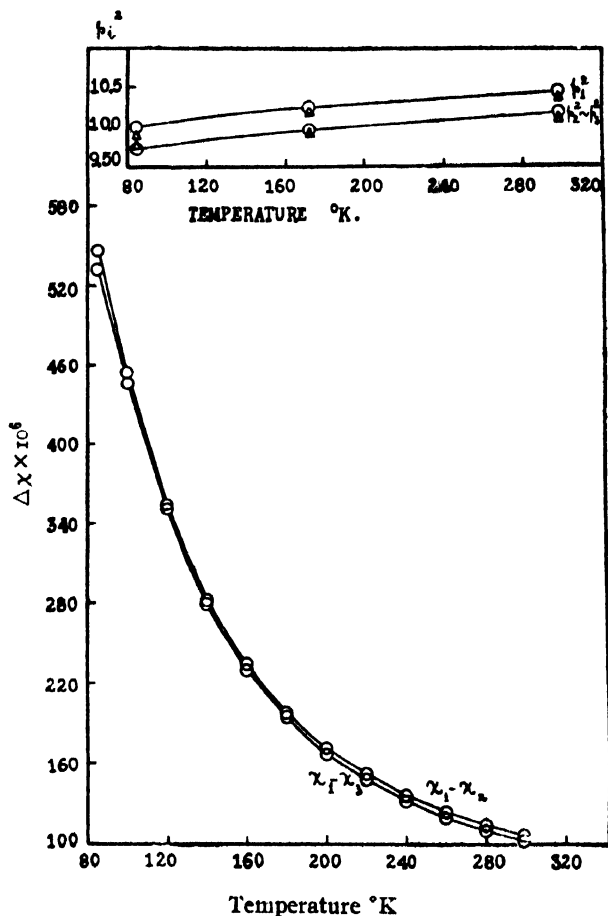
Temperature °K

FIG. 3

Temperature Variation of Principal Anisotropies and Effective
Moments of $NiBeF_4(NH_4)_2 BeF_4.6H_2O$

temperature. On the other hand, in the expression for anisotropy Δ^χ, for any selected plane in the crystal, namely,

$$\frac{\Delta X}{X_0} = \frac{\Delta p^2}{p_0^2} = \left[8\lambda - \frac{2\lambda^2}{kT} - 3k'T \right] \Delta\alpha, \tag{26}$$

where $\Delta\alpha$ will be a constant depending on the crystalline field and the crystal plane chosen, the temperature independent last term in the *absolute susceptibility* will be largely suppressed. For example, for Ni^{++} at room temperature 300°K say, all the three terms are negative and are respectively, of the order of -0.026, -0.010 and -0.006. The λ^2 term is not negligible as in the expression for effective moment. Indeed, even at room temperatures it is nearly twice the term independent of λ and at 80°K becomes about 25 times this term and comparable in magnitude with the temperature indepen-

dent first term in the *anisotropy*. Thus the measurement of anisotropy at different temperatures is more suitable for the calculation of λ.

In a previous paper (1938-39) we obtained in this manner from anisotropy measurements of the salts $NiSO_4,6H_2O$ and $NiSeO_4,6H_2O$ the values of $\lambda = -330$ cm^{-1} and -340 cm^{-1} respectively, agreeing satisfactorily with the spectroscopic value of -335 cm^{-1}. In the Table IV will be found the values of λ, for various other nickel salts studied by us, fitting with the anisotropy measurements over the whole range of temperature. The mean value of λ, for different crystals and different crystal planes is found to be about -350 cm^{-1}, agreeing fairly well with the spectroscopic value and is indeed gratifying.

It may be mentioned here that though the temperature variations of the effective moments are not so suitable as those of the anisotropies for calculating λ, they are still fairly consistent with the values of λ, calculated in the latter manner.

TABLE IV

Ratio of $\Delta\chi$ at temperatures T to that at room temperature ($303.1°K$)

Salts	$NiSO_4, (NH_4)_2SO_4, 6H_2O$		$NiSO_4K_2SO_4, 6H_2O$		$NiBeF_4(NH_4)_2BeF_4, 6H_2O$	
Ratio obtained from anisotropies	$\chi_1-\chi_2$	$\chi_1-\chi_3$	$\chi_1-\chi_2$	$\chi_1-\chi_3$	$\chi_1-\chi_2$	$\chi_1-\chi_3$
Values of λ	-315 cm^{-1}	-348 cm^{-1}	-370 cm^{-1}	-360 cm^{-1}	-345 cm^{-1}	-360 cm^{-1}
Temperature °K	Ratio		Ratio		Ratio		Ratio		Ratio		Ratio	
	obs.	calc.	obs.	calc.	obs.	calc.	obs.	calc.	obs.	calc.	obs.	calc.
303.1	1.000	1.000	1.000	1.000	1.000	1.000	1.000	1.000	1.000	1.000	1.000	1.000
240	1.300	1.298	1.310	1.310	1.328	1.316	1.309	1.313	1.289	1.308	1.287	1.313
200	1.614	1.614	1.636	1.640	1.665	1.654	1.658	1.648	1.624	1.638	1.643	1.648
160	2.145	2.144	2.217	2.194	2.221	2.229	2.234	2.213	2.210	2.191	2.248	2.213
100	4.131	4.127	4.273	4.289	4.539	4.398	4.410	4.349	4.288	4.278	4.362	4.349
90	4.850	4.828	5.021	5.036	5.147	5.171	5.064	5.111	—	—	—	—

The agreement between the observed and calculated values entered in Table IV, shows that for a given crystal and crystal directions a single value of λ, fits well over the whole range of temperature. This result may be taken to confirm the assumption on which these calculations are based, namely, that the magnitude and asymmetry of the crystalline field should be independent of temperature, which was made from considerations regarding the strong binding between the paramagnetic ion and its immediate neighbours and the consequent

approximate non-variance of their positions with changes of temperatures. A direct calculation of the three α's at different temperatures, from the three principal susceptibilities of the nickel salts studied by us, also leads to the same conclusion, namely, that the α's are practically independent of temperature as will be seen from the Table V.

TABLE V

For the crystal Field Constants α_1, α_2 and α_3 for Ni^{++} Salts

Crystal	Temp. °K	$-a_1 \times 10^6$	$-a_2 \times 10^6$	$-a_3 \times 10^6$
$NiSO_4(NH_4)_2SO_4 . 6H_2O$	297.5	85.7	78 0	78.3
	167.9	85.4	77.8	77.9
	86 6	82.7	75 2	75.2
$NiSO_4K_2SO_4 . 6H_2O$	297.4	88.2	77.2	77.5
	173.4	94.7	83.4	83.8
	86.6	86.4	75.0	75.6
$NiBeF_4(NH_4)_2BeF_4.6H_2O$	297 4	89.2	81.8	82.1
	172 2	88.9	81.4	81.6
	84 7	84.9	77.9	78.1

It may be mentioned here that these calculations of α's are not merely the converse of that of λ, which would have been then a trivial result. The information conveyed by these two calculations are quite different not only because the measurement of *principal susceptibilities*, from which α's are calculated, are independent of the measurements of *anisotropies*, from which λ is calculated, but also the relative importance of the terms corresponding to the oth, 1st and 2nd powers of λ, involved in these two calculations are quite different.

5. Chromic ion : Close Approximation to S-State Ions Regarding Magnetic Properties.

For the Cr^{+++} ion with three electrons in the $3d$ shell, λ is positive, unlike Ni^{++} with 8 electrons in the $3d$ shell and its numerical value calculated from the over-all multiplet width of $912\ cm^{-1}$ (Laporte, 1928), is $\lambda = +87\ cm^{-1}$, much smaller than for Ni^{++} ion. These two factors together completely alter the relative importance of the different terms in the expression for p^2, as compared to that of Ni^{++}. Taking α's to be of the same order of magnitude as in the ionic salts of nickel, we obtain for the mean susceptibility at $300°K$.

$$p^2 = p_0^2[1 + (\alpha_1 + \alpha_2 + \alpha_3)(\tfrac{8}{5}\lambda - kT)] = 15[1 - .058 + .052] \quad \ldots \quad (27)$$

Here the last two terms, which represent the deviation of the effective magnetic moment from its 'spin only' value, are both small, of comparable magnitudes

and of opposite signs.* Hence the deviation from the 'spin only' value becomes very small, being about $\frac{1}{2}\%$ smaller at room temperature and about $4\frac{1}{2}\%$ at 80°K.

Our measurements for chromic salts refer to room temperature only, where 'spin only' value is approximately obtained (Krishnan, Mukherji and Bose, 1939).

We should further expect from the theoretical expressions, the anisotropy of the crystal to be smaller and the conformity to Curie Law much closer than even in the nickel salts. Indeed, the anisotropies of the chromic salts are nearly of the same magnitude as the anisotropy of the diamagnetic part of the susceptibility of these crystals, as will be seen from the table VI by comparison of the data for the isomorphous salts, ammonium chromium oxalate and potassium aluminium oxalate the latter being diamagnetic. In view of this it becomes difficult to verify even the $1/T^2$ law, deduced theoretically for the temperature variation of the paramagnetic part of the anisotropy.

TABLE VI

Anisotropies at 303.1°K

Anisotropies × 10^6	$(NH_4)_3$ Cr$(C_2O_4)_3$, $3H_2O$ $a : b : c = 0.983 : 1 : 0.387$	$K_3Al(C_2O_4)_3$, $3H_2O$ $a : b : c = 0.999 : 1 : 0.395$
$\chi_1 - \chi_2$	4.3	7.9
$\chi_1 - \chi_3$	-10.3	13.9
ψ	29°	19°

Further, approximate calculations for the value of λ, for the Cr^{+++} ion from the above experimental data agree in order of magnitude with the spectroscopic value. A more detailed experimental investigation on Cr^{+++} salts is in progress in this laboratory in view of the inadequacy of existing experimental data.

INDIAN ASSOCIATION FOR THE CULTIVATION OF SCIENCE,
CALCUTTA

* That these two terms in Cr^{+++} are of comparable magnitudes and of opposite signs, and that neither of them can be neglected, needs to be emphasised here in view of the fact that in the expression given by Penney and Schlapp (*loc. cit.*) the kT term is neglected, whereas a term proportional to λ^2, which indeed should vanish in the expression for the mean square moment, is retained.

REFERENCES

Beevers, C. A. and Lipson, H., 1934, *Proc. Roy. Soc. (A)*, **146**, 570.

Bethe, H., 1929, *Ann. der Phys.*, **3**, 133.

——— 1932, *Zeits. f. Phys.*, **60**, 218.

Bose, A., 1935, *Proc. Ind. Acad Sci.*, I. **No. 9**, 605.

——— **No. 10**, 754.

——— 1947, *Ind. Jour. Phys.* **21**, 277.

———1948, ——— **22**, 76

Bose, D. M., 1927, *Zeits. f. Phys.*, **43**, 864.

——— and Mukherji, P. C., 1938, *Phil. Mag*, **26**, 757.

——— ——— 1939, *Ind Jour. Phys.*, **13**, 219.

Cabrera, B. and Duperier, A, 1925, *Jour. de Phys*, **6**, 121.

Chinchalkar, S. W., 1935, *Phil. Mag.*, **20**, 856.

Chrobak, L, 1934, *Zeit. f. Krist*, **88**, 35.

Debye, P., 1926, *Ann. der Phys.*, **81**, 1154.

Frank, A., 1932, *Phys. Rev.*, **39**, 119.

Freed, S. and collaborators, 1938, *Jour. Chem. Phys.*, **6**, 297 and 651

Giauque, 1927, *Jour. Amer. Chem. Soc.*, **49**, 1864.

Görter, C. J, 1932, *Phys. Rev.*, **42**, 137.

de Haas and Görter, C. J., *Leiden Comms.*, **208c** and **210d**.

Haenny, C., 1931, *Comptes Rendus*, **193**, 931.

——— 1932, ——— **195**, 219

Hebb, M H., and Purcell, E M., 1937, *Phys. Rev.*, **45**, 346

Hendricks, S. B. and Dickinson, R, G., 1927, *Jour. Amer Chem. Soc.*, **49**, 2149.

Hoffmann, 1931, *Zeits f Krist.*, **78**, 279.

Howard, 1935, *Jour. Chem. Phys*, **3**, 813

Jackson, L. C., 1933, *Proc Roy. Soc. (A)*, **140**, 695

Jahn and Teller, 1937, *Proc. Roy. Soc. (A)*, **161**, 220.

——— ——— 1938, ——— **164**, 117.

Kramers, H, 1929 *Proc Amster. Acad.*, **32**, 1176.

Krishnan, K. S. 1939 *Nature* **143**, 600.

——— and Mukherji, A., 1938, *Phil Trans. Roy Soc. (A)*, **237**, 135

——— and Bose, A., 1938, *Nature*, **141**, 329

——— Mukherji, A. and Bose, A., 1939, *Phil. Trans. Roy. Soc. (A)*, **238**, 125.

——— and Mukherji, A, 1936, *Phys Rev.*, **50**, 860

——— ——— 1938, ——— **54**, 533.

——— ——— 1938, ——— **54**, 841.

——— and Banerji, S., 1941, *Phys. Rev.*, **59**, 770.

——— ——— 1936, *Phil. Trans. Roy. Soc (A)*, **235**, 343.

——— ——— and Chakravarty, N. C, 1933, *Phil. Trans Roy. Soc (A)*. **232** 99

Kürti and Simon, 1935, *Proc. Roy. Soc. (A)*, **149**, 152.

Laporte, O., 1928, *Zeits. f. Phys.*, **47**, 761.

Leiden Communications, **122a**, **129b**, **140d**, **167b** **167c**, **168a**, etc.

Penney, W. G. and Schlapp, R, 1932, *Phys. Rev.*, **41** 194.

——— ——— 1932, ——— **42**, 666.

Sommerfeld, A. 1923, *Phys. Zeits.* **24**, 360.

——— 1923, *Zeits f. Phys.* **19**, 21.

Spedding, F. H. and collaborators, 1937, *Jour. Chem. Phys* **5**, 191, 316 and 416.

——— ——— 1938, ——— **6**, 297.

Starr, C., 1940, *Phys. Rev.*, **58**, 984.

———, Bitter, F. and Kaufmann, A. R. 1940 ——— **58**, 977.

Stoner, E. C., 1929, *Phil. Mag* **8**, 250.

——— 1934 "Magnetism and Matter" (Methuen) also the earlier book "Magnetism and Atomic Structure" Methuen).

Van Vleck, J. H. 1932 The Theory of Electric and Magnetic Susceptibilities (Oxford)

——— 1934, *Phys. Rev.* **41**, 208.

——— and Penney, W. G., 1934, *Phil. Mag.* **17**, 961.

——— and Frank, A., 1929, *Phys. Rev.* **34**, 1494 and 1625.

CATHODO-LUMINESCENCE SPECTRA OF INDIAN FLUORITES

By B. MUKHERJEE

Plates VIA and VIB

ABSTRACT. The cathodo-luminescence spectra of some chemically decomposed speci-mens of Indian fluorite in the visible and in the ultra violet region were studied using a direct-vision spectrograph and a Fuess quartz spectrograph. For the examination of rare earths in fluorites, when they were converted into oxides, the luminescence exhibited was so bright that an exposure of 5–10 mins. was quite sufficient for taking a spectrogram. On inspection of the line-like bands in the luminescence spectra, it was ascertained that the activators for luminescence of decomposed specimens were Sm, Dy, Eu, Er, Nd, Gd and Tb. The rare-earths with even atomic number were the chief activators for lumines-cence with the exception of Eu of odd atomic number. For the strong activating ability of the above rare-earths, the presence of Pr could not, however, be ascertained definitely. In all specimens Sm acted as the chief activator for luminescence. It was concluded that, though Mn was present in all the specimens, the characteristic Mn-band in the visible region was suppressed in the luminescence spectra by the strong activating action of rare-earths, when present in optimum quantity for strong activating ability. The natural colour of fluorite was in no way connected with the varieties of rare-earths contained in it.

INTRODUCTION

The fluorides of rare-earths being highly insoluble the majority of natural fluorites contain rare-earth metals as minor constituents from below the range of detection to $0.1\% - 0.2\%$. Such fluorites are in large numbers charac-teristically coloured and exhibit fluorescence or phosphorescence under the action of ultraviolet radiation, temperature elevation, cathode rays and X-rays.

Crookes (1883) observed by the action of cathode-rays on natural calcium compounds the appearance of citron yellow band in the luminescence spectra which he ascribed to yttrium; this was, however, proved by Urbain to be due to dysprosium. Urbain (1909) investigated on the cathodo-luminescence of coloured and uncoloured fluorites, particularly the specimen named as 'chlorophane,' remarkable for its green luminescence and found in the spectra the appearance of bands of Sm, Dy, Tb and Gd. The identi-fication of observed bands was carried out referring to the spectra shown by the synthetical mixture of calcium fluoride and the pure rare-earths. The cathodo-luminescence spectra consisted of sharp line-like bands superimposed on broad diffuse bands; the wave-lengths of these lines of rare-earths were affected by the nature of base materials. Tanaka (1924) investigated on the cathodo-luminescence of 17 fluorites and found Sm as the chief active agent, other active agents being Y, Dy, Er, La, Ce and probably Yb. Wick (1924) found in 5 fluorites of England, in confirmation with Urbain's data, Sm, Dy, Gd and also Eu. According to Urbain La, Ce, Y and Yb, whose salts are colourless and devoid of absorption spectra, were found not to exhibit any such luminescence. Nichols and Howes (1926) studied various cases of the dominance and suppression of one activator

over another and concluded that the luminescence of Nd is suppressed by minute traces of either Sm or Pr and traces of Sm will suppress the luminescence due to traces of Pr, when the dilution is of the same order but that when Pr greatly preponderates, the Sm-bands are suppressed. They also observed that in a solution where Tb predominates the Dy bands disappear and in a solution in which Dy predominates both spectra appear. Yoshimura (1934) found in 10 Japanese fluorites chiefly Sm, Eu, Tb, Dy and in few Pr, Nd, Gd and Er as activators for cathodo-luminescence. These investigations showed that the presence of Sm, Eu, Tb, Dy, Nd, Pr, Er, that is, the coloured earths and also Gd is characterised by intense luminescence phenomenon by the action of cathode rays.

About the colouration of natural fluorites Yoshimura considered that the colour of fluorite was almost independent of the varieties of rare-earths contained in it and it was not possible to point out a special colour to be produced by the presence of certain definite element.

The object of the present investigation was to determine the rare-earths present in different specimens of Indian fluorite which were effective as activators for the luminescence and to trace the influence of other impurities present in fluorites on the luminescence spectra.

EXPERIMENTAL

The qualitative arc spectrographic analysis of the fluorites was carried out at 10 amps. 220 volts with a E_1 quartz spectrograph. The presence of rare-earths could not, however, be detected in any of the specimens. It was found that all the specimens of fluorite contained a measurable quantity of Mn. The method of cathodo-luminescence was then applied for the study of rare-earths in fluorites. The method of excitation for the specimens was by cathode rays obtained in a tube, designed according to Urbain (Fig. 1).
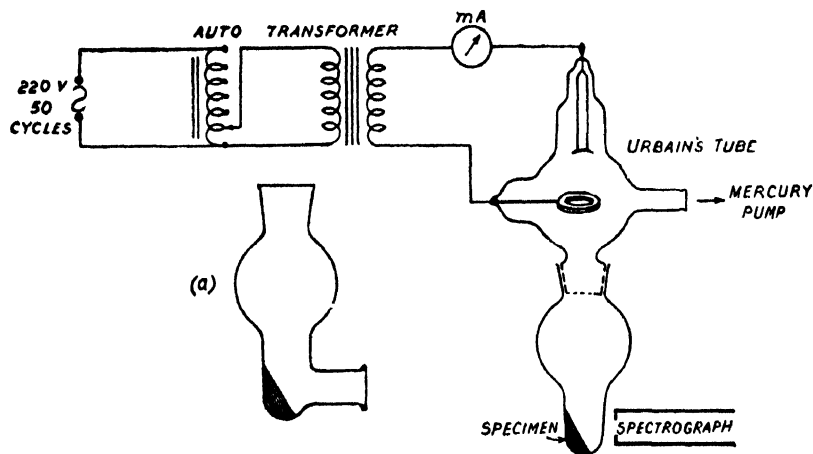
FIG. 1.

The vacuum in the cathode ray tube was maintained by one stage mercury pump run by a Cenco oil pump. A transformer with an auto-transformer was used as the source of excitation. The best condition for

excitation of the specimens was at 4000 volts. It was found necessary to keep the pump running continuously, otherwise the pressure in the tube increased slowly. This phenomenon was due to gases produced from the luminescent substance by the bombardment of the cathode rays. The intensity of luminescence was found to be maximum for all the specimens examined when the current in the tube was kept at 3.5 m A. The stop-cock connecting the tube with the mercury pump was constantly regulated in order to keep the current steady at 3.5 m A. The slight fluctuation in the current was found to be very effective for intense luminescence. The tube was cooled by an air-blower.

The intensity of luminescence exhibited **by** the fluorites was generally weak. In order to increase the luminescence chemical treatment of the fluorites was necessary. Urbain found that for the examination of rare-earths in fluorites when they were converted into sulphates the luminescence exhibited was more bright than when converted into oxides. In the present investigation it was found that the fluorites when converted into oxides the luminescence exhibited was so bright that an exposure of 5 mins. was quite sufficient for taking the spectrogram. Fluorite was powdered and then attacked with H_2SO_4 (analar) so as to remove HF and the excess H_2SO_4 was removed by slowly heating till no more fumes came out. The residual sulphate was dissolved by heating with 1 : 8 HCl (analar). Filtered and the filtrate was digested with liquor ammonia and $(NH_4)_2CO_3$ in excess so that they were all transformed into insoluble carbonate. The precipitate was washed free from SO_4^{--} with a dilute solution of $(NH_4)_2CO_3$ in dilute ammonia; then filtered, dried and ignited at nearly 800°C for 15 mins. in a muffle furnace. This oxide was exposed to cathode rays in the tube just after the heat treatment. The effect of the heat treatment at high temperature was that the intensity of the line-like bands was increased while that of the continuous background was decreased

For the study of the visible spectra, a direct-vision spectrograph was used. The spectrograph was fitted with an arrangement for photographing a graduated scale which served as a reference wave-length scale. The scale was calibrated with the lines of spectra of Li, He, Na, Ca, Tl, Sr, Cs, and iron arc spectrum. Before taking a spectrogram of the cathodo-luminescence spectrum, the mark 50 in the scale was always adjusted to coincide with the Na-line 5896 Å or 5890 Å. For the study of the ultraviolet spectra, the lower tube which contained the specimen was replaced by another, fitted with a quartz window at the side. The quartz plate was attached to a narrow prolongation of the sample holder with ' pecein ' (Fig. 1.a). A Fuess quartz spectrograph was used and a Cu-arc spectrum was always taken along with the luminescence-spectrum of the specimen. The diaphragm had two slots, arranged as in Hartmann's diaphragm, of which the length of one was equal to the vertical height of the quartz window. After an exposure of the luminescence spectrum of the specimen, the slot of the diaphragm was

changed. The cathode tube was removed sideways and a quartz 90° prism was properly placed in front of the slit. The light of the Cu-arc was sharply focussed on the slit after passing through a quartz lens and the 90° prism.

The time of exposure for photographing the luminescence spectra in both spectrographs was 5-10 mins., panchromatic plates (31°) being used. The identification of the line-like bands in the spectra of different specimens, observed under a 'comparator' of nearly 10-times magnification, was carried out referring to Urbain's data for the different system of rare-earth oxide in calcium oxide $(R_2O_3 - CaO)$. As a preliminary work, synthetic mixtures of nearly 1.0% Sm, Pr and Gd oxides in CaO were prepared and their cathodoluminescence spectra were photographed (time of exposure 5 mins.) which were almost identical with that of Urbain. The vacuum in the cathode ray tube being sufficiently high only a few faint lines of the discharge were recorded in the spectrum which were, however, eliminated from the tables. A standard mixture of 0.01% MnO_2 in CaO was prepared and its cathodoluminescence spectrum was photographed. In order to get an idea of the relative intensities of different lines in the luminescence spectra of the specimens, photometric records of the spectrum plates were taken with a Moll Microphotometer. The wave-lengths of the Gd-lines in the ultra-violet spectrum were accurately measured with a 'comparator' of nearly 20-times magnification.

TABLE I

Rare-earths contained as activators in the chemically decomposed specimens of Indian fluorite

No. of specimen	Locality	Colour of specimen	Colour of cathodo-luminescence	Rare-earths contained as activators
*6251	Nandgaon and Khairagarh States, E.S.A.	Violet and green	Pink, blue tinge	Sm, Dy, Eu, Er (Tb).
*6688	Malhan, Jubbulpore, C. P.	Deep violet	Orange-yellow	Sm, Dy, Eu, Er, and Mn.
**1	Nandgaon, C.P.	,,	White, light orange-yellow tinge	,,
**2	,,	Green	Violet, yellow tinge	Sm, Dy, Eu, Er, Nd, Tb, Gd,
*3	Bastar State, Bhopalpatnam.	Violet	White, yellow tinge	Sm, Dy, Eu, Er, Nd, Gd (Tb).
*4	Jaipur State, Rajputana	Green	Violet, orange tinge	Sm, Dy, Eu, Er, Nd, Tb, Gd,
*5	Chitral.	White, light green tinge	White, blue-violet tinge	Sm, Dy, Eu, Er, Nd, Gd (Tb).

* Specimen from Dr. A. K. Dey of Geological Survey of India.
** Specimen from Dr. H. K. Mitra of Tata Iron and Steel Co.

TABLE II

Wave-lengths of the line-like bands in the visible region observed in the luminescence spectra of chemically decomposed specimens. λ in 1.Å.

6251	6688 & 1	2	3	4	5	Rare-earths in CaO Urbain's data
6663 m	*6603 m	6663 m	*6603 m	6663 m	*6603 m	6660 Sm
*6603 s	6474 f	*6603 s	6474 f	*6603 m	6474 f	6605 Sm
6474 m	6336 m	6474 f	6336 s	6474 f	6336 s	6470 Sm
6336 s	6264 s	6336 s	6261 ss	6336 s	6264 s	6310 Eu, 6330 Tb
6264 s	6243 s	6261 s	6243 ss	6264 s	6148 ss	6265 Sm
6243 s	6148 s	6264 s	6264 ss	6243 s	6051 ss	6245 Eu, 6240 Tb
6148 ss	6051 s	6243 s	6148 ss	6148 ss	5934 m	6150 Sm, 6155 Eu
6120 f	5931 s	6148 ss	6051 ss	6051 ss	5850 ss	6128 Eu
6051 ss	5850 s	6051 ss	5934 s	5934 s	5763 ss	6052 Sm
5934 s	5826 s	5934 s	5852 s	5850 s	5684 ss	5930 Eu
5875 s	5763 s	5875 s	5826 s	5826 s	5598 m	5877 Dy, 5878 Tb
5850 s	5684 s	5850 ss	5763 ss	5763 ss	5556 m	5848 Dy, 5843 Tb
5826 s	5598 f	5826 s	5684 ss	5684 ss	5406 m	5830 Dy
5763 ss	5556 f	5763 ss	5598 m	5658 m	5328 f	5762 Sm
5684 ss	*5482 f	5684 ss	5556 m	5598 f	5184 m	5683 Sm
5658 m		5658 m	5492 m	5556 s	4938 m	5603 Er
5598 m		5598 m	5406 f	5526 m	4896 m	5601 Sm
5586 f		5556 m	5328 f	5492 m	4846 m	5550 Er, Tb
5556 s		5526 m	528 f	5106 m	4818 m	5527 Eu, 5521 Tb
5526 m		*5482 f	5184 f	5398 f	4792 m	5495 Er, Tb
5492 f		5406 s	5136 f	5328 f	4766 f	5480 Sm
*5482 s		5184 m	5064 f	5280 f	4748 f	5105 Eu, 5400-5390 Tb
5406 f		5136 m	5043 f	5226 f	4726 ff	5330 Er
4896 m		4946 f	4916 f	5184 f	4690 f	5280 Er, Eu
4846 m		4938 m	4896 f	5136 f	4656 f	5225 Tb
4818 f		4896 s	4846 m	5064 m	4606 f	5180 Eu
4392 f		4846 m	4818 f	5043 m	4572 f	5130 Eu
*4376 m		4818 m	4572 f	5004 m	4512 ff	5063 Dy
4350 f		4792 s	4170 ff	4946 m	4470 ff	5015 Nd
4336 f		4766 m	4155 ff	4938 f	4455 ff	5000 Dy
		4748 m	4100 ff	4896 m		4935 Dy
		4726 m		4846 s		4910 Eu, 4900-4882 Dy
		4690 m		4818 s		4895 Tb
		4656 f		4792 m		4815 Dy, 4855 Tb
		4606 f		4766 f		4815 Dy, 4825 Tb
		4572 ff		4748 f		4797 Dy
		4516 ff		4690 m		4760 Er
		4512 ff		4656 f		4755 Eu
		4170 f		4606 f		4718 Dy
		4155 f		4572 f		4718 Dy, 4720 Eu
		4100 f		4524 f		4690 Nd, Er
		4392 f		4512 f		4685 Eu
		*4376 m		4170 m		4660 Nd, 4690-4665 Dy
		4350 m		4155 m		4655 Eu
		4335 m		4100 m		4610 Nd
				4392 f		4590 Er
				*4376 m		4575 Nd
				4350 m		4550 Er
				4335 f		4510 Dy
						4500 Er
						4515 Nd
						4490 Eu
						4472 Tb
						4166 Eu
						4160 Er
						4455 Tb
						4400 Nd, 4410 Tb
						4395 Tb
						4370 Tb
						4350 Tb
						4330 Eu

The intensities of the line-like bands are expressed by the symbols, ss = very strong ; s = strong ; m = medium ; f = faint : ff = very faint,

* These lines were coincident with faint lines of discharge

The calibration of the scale in the direct-vision spectrograph due to small dispersion

TABLE III

Wave-lengths of the line-like bands in the ultraviolet region observed in the luminescence spectra of chemically decomposed fluorites and corresponding maxima of gadolinium in calcium oxide. λ in 1.A.

Specimen of fluorite				0.08% Gd_2O_3 in CaO	Urbain's data for (Gd_2O_3-CaO)
2	3	4	5		
3159 m	3159 s	3159 m	3159 m	3159 s / 3155 s	3158.5 / 3155.5
3153 s	3153 ss	3153 s	3153 s	3153 ss	3153 0
3150 s	3150 m	3150 s	3150 s	3150 ss	3150 5
3146 s	3147 ss	3147 ss	3147 } 3143 } s	3147 ss	3147 0
3143 ss	3143 s	3143 s		3144 ss	3144 0
3140 f	3140 f	3140 f	3140 f	3140 ss	3140 5 / 3138.0
3135 m	3135 s	3135 f		3135 s	3136 0 / 3134 0
3130 m	3130 m			3130 m	3130.0
				3094 m	3094.0
				3088 f	3088.5
				3085 f	3085.0

INTERPRETATION OF RESULTS

The cathodo-luminescence spectrum of 0.01% MnO_2 in CaO (orange-yellow luminescence) was found to be broad banded (from 6340 Å to 6150 Å and 6050 Å to 5560 Å) as to be practically continuous. All the specimens of fluorite contained traces of Mn. In specimen Nos. 1 and 6688 the line-like bands of rare-earths were superimposed on a strong background due to Mn which proved that the content of rare-earths in the two specimens not being the optimum quantity for strong activating ability, Mn also acted as an activator along with the rare-earths. The luminescence spectra of all other specimens consisted of strong line-like bands of rare-earths superimposed on very weak background. From this consideration, it may be concluded that when the rare-earths were present in optimum quantity for strong activating ability, the characteristic spectrum of Mn was totally suppressed leaving only the line-like bands produced by the activating action of different rare-earths.

The calcium carbonate acting as a diluent contained traces of Mn and so exhibited, when converted to oxide, orange luminescence. Urbain (1911) found that there was no chemically pure calcium salt free from Mn and so

Visible spectra of decomposed specimens.

No. of Specimens

6688

6251

1

2

3

4

5

0.01%
MnO₂ in CaO

$$\lambda \text{ IN } 1.A°$$

Photometric curve of Luminescence spectrum of chemically decomposed specimen No. 6251.
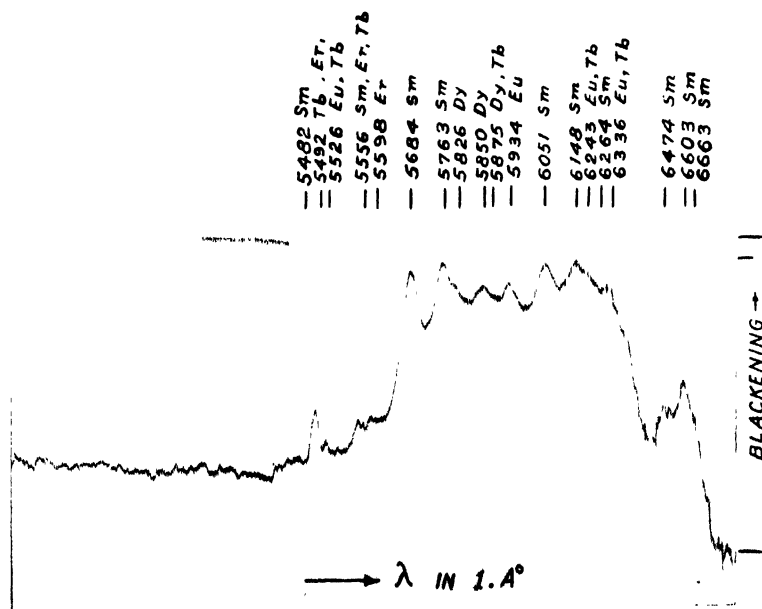
Ultra-violet spectra of decomposed specimens.
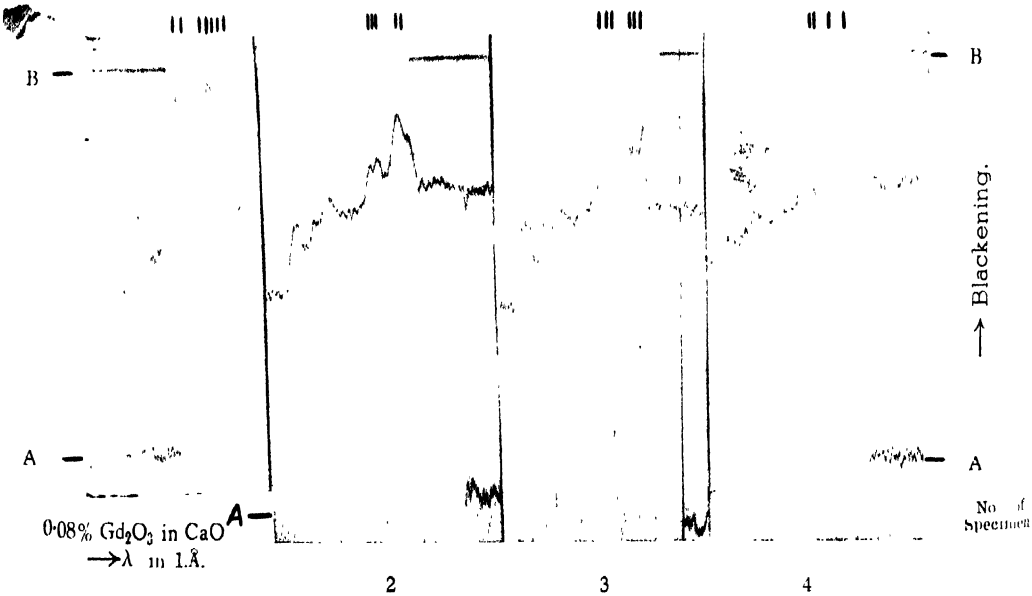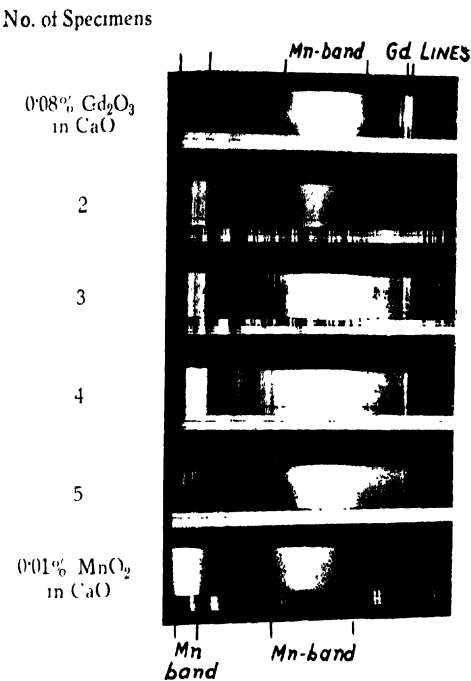
Photometric Records of Gd - Lines

always exhibited bright orange to pale red luminescence according to the proportion under cathode rays. Urbain and Bruninghaus, however, after three months daily crystallisation obtained lime cathodically pure, that is, free from luminescence. In the present investigation the cathodo-luminescence spectra of all the specimens examined showed a continuous band in the ultraviolet region, from 4000 Å to 3400 Å approximately with maximum intensity in the region 3850 Å to 3500 Å. This characteristic strong band was also observed in the standard spectra of o.o8% Gd_2O_3 in CaO and of o.o1% MnO_2 in CaO. It is concluded that this characteristic band was not due to lime but due to the presence of Mn in the base material CaO and in the specimen. It was also found that while the characteristic Mn-band in the visible region was suppressed by the strong activating action of rare-earths, the characteristic band of Mn in the ultra-violet region appeared in the luminescence spectra of all specimens. From these facts, it is to be concluded that while Mn was present in all the specimens, the Mn-band was suppressed only in the visible spectra by the strong activating action of rare-earths, when present in optimum quantity.

The activators for luminescence in the specimens were Sm, Dy, Eu, Tb, Er, Nd and Gd. The characteristic line-like bands of Tb being faint, it is, probable that Tb (65) acted as a weak activator. It can be ascertained that rare-earths with even atomic number (Nd 60, Sm 62, Gd 64, Dy 66, Er 68) were the chief activators for luminescence with the exception of europium (Eu 63) of odd atomic number. The presence of Pr (59) of odd atomic number could not, however, be ascertained definitely because of the activating ability of the above rare-earths.

DISCUSSION

Yoshimura (*loc. cit.*) exposed natural fluorites to cathode rays and the time of exposure for taking a spectrogram was about 30-40 hours. Moreover, the cathode ray tube was frequently shaken in order to expose a fresh surface of the powdered sample as the intensity of luminescence was weak and decreased gradually by prolonged excitation of cathode rays. In the present investigation all the specimens of fluorite, when converted into oxides by chemical treatment, exhibited so bright a luminescence that an exposure of 5-10 minutes was quite sufficient for taking a spectrogram. Yoshimura (1934) also observed that green fluorites contained, in general, quite numerous rare-earths and the fluorites of the colours other than green contained a few of them. In the present investigation, the author found that the natural colour of fluorite was in no way connected with the varieties of rare-earths contained in it (Table I).

About the geochemical significance of the luminescence phenomenon, it was a point of much discussion whether Sm and Eu could be obtained primarily in the bivalent form or only in the presence of the reducing action of radioactive radiation. It was probable that the naturally fluorescing

B. Mukherjee

fluorites were always radioactive or that radioactive radiations had influence on them. (Gmelins, 1938). Goldschmidt showed that tetravalent uranium and thorium could replace isomorphously the bivalent calcium in fluorspar. According to Goldschmidt, the fact that Eu was enriched in many minerals the same replacement might occur in the case of fluorspar. It was also long known that in certain minerals (*e.g.*, parisite, cordylite, yttrocerite and yttrofluorite) the fluorides of calcium, barium and the rare-earth elements were present in isomorphous mixture (Vogt, 1914). From all these facts, the author is rather inclined to believe that an isomorphous replacement of the bivalent form in question occurred in the case of fluorites.

In the previous note of the author (Mukherjee and Sarkar, 1947) the luminescence spectra of chemically decomposed specimens of fluorite was mentioned. The associated white mineral in specimen No. 6688 examined was barite and in the cathodo-luminescence spectrum of this decomposed specimen only Mn (no rare-earths) acted as activator for luminescence.

REFERENCES

Crookes, W., 1883, *Phil. Trans.*, **174**, 891.

Gmelins, 1938, *Handbuch der anorg chemie.*, **39**, 45.

Mukherjee, B, and Sarkar, P. B, 1947, *Science and Culture*, **13**, 209

Nichols, E. L, and Howes, H. L, 1926, *J Opt Soc. Am*, **13**, 573.

Tanaka, T., 1924, *J. Opt. Soc. Am.*, **8**, 501.

Urbain, G., 1909, *Ann. Chim. Phys* (8), **18**, 222.

            1911, Spectrochimie, 169

Vogt, T, 1914, *Jahrb Min.*, **11**, 9.

Wick, F. G., 1924, *Phys. Rev.*, (2), **24**, 272.

Yoshimura, J., 1934, *Sc. Pap I.P.C.R.*, (Japan), **23**, 224,

ABSORPTION OF U. H. F. WAVES IN SALT SOLUTIONS

By S. K. CHATTERJEE and B. V. SREEKANTAN

ABSTRACT. Percentages of absorption of u h f waves (300-500 Mc/s.) in aqueous solution of sodium chloride for different concentrations, have been measured by optical method. Attenuation coefficients and hence absorption indices have been calculated for different frequencies. Values of reflexion coefficients at different frequencies have also been calculated. Values of ionic relaxation time as obtained experimentally for different concentrations of the solution have been compared with the values calculated from Debye-Falkenhagen theory. Values of dielectric constant and loss tangent, as deduced from experimental results, have been compared with those calculated theoretically from Debye-Falkenhagen theory. Values of dipole conductivity and molar conductivity have been calculated from experimental results and their variation with frequency studied. It has been found that the position of maximum absorption shifts towards higher concentration for higher frequencies. The product of wavelength corresponding to maximum absorption and the normality of the solution expressed in gm. equivalent per litre has been found to be 16 64 a constant

INTRODUCTION

The greater part of wireless communication being conducted over sea, an exact determination of the absorption coefficient of sea-water and its variation with frequency is important. Conductivity of different samples of sea-water has been measured by Hill (1907) in the audio frequency range and by Van der Pol (1918) in the medium and long wave band. Electrical properties of sea-water has been studied by Smith-Rose (1933-34) up to 10 Mc/s and by Drysdale (1920) up to 1 Mc/s. For u.h.f. waves transmitted over sea, the absorption of energy by sea-water being considerable and field intensity measurements over sea being difficult, it has been thought worth-while to carry out the measurement in the laboratory in order that the effect of sea water on the propagation of u.h.f. waves, may be more definitely ascertained. Chemical composition of sea-water being liable to variation in its salt content from 0.18 to 4.15, it has been decided to study first the absorption and other associated properties of individual salt solutions that compose average sea-water (Dorsey, 1940) and then the solution as a whole, over a frequency range of 300-500 Mc/s. Electrical properties of potassium chloride solution has been measured at lower radio frequencies by Drake,

Pierce and Dow (1930) and of sodium chloride solution by Cooper (1946), over a frequency range of 0.95-13 Mc/s and 690-4320 Mc/s.

Besides the interest of wave propagation, the absorption of u.h.f. waves in salt solutions is of basic importance in the study of the problems of molecular structure. With liquids or solutions, the tendency of an applied e.m. field to orient molecular dipoles is resisted by molecular inertia and by the viscous forces of the environment, resulting in a lag between the application of the field and the rotation with consequent absorption of energy. The maximum loss takes place at an angular frequency ω given by the reciprocal of the relaxation time τ of the molecule or polar group, where the relaxation time is a function of molecular dimensions, viscosity and absolute temperature. In the case of salt solution, if an ion moves through the solution on the application of an e.m. field, the ions surrounding it will be continually changing their distribution to maintain equilibrium distribution. The result is that in the neighbourhood of the ion there exists an excess of ions of opposite sign. The variation of electric intensity within the ionic atmosphere during its formation is characterised by a relaxation time Θ according to the well known Debye-Falkenhagen theory (Falkenhagen, 1934).

$$\Theta = \frac{8.85 \times 10^{-11} \cdot D_0}{\Delta_\infty \cdot \gamma^*} \qquad \dots \quad (1)$$

where Δ_∞ = equivalent conductivity of solution

D_0 = dielectric constant of water = 80

γ^* = concentration of solution expressed in gm. equiv. per litre.

The object of the present paper is to study the absorption and reflexion of e.m. waves over a frequency range of 300-500 Mc/s., by aqueous solution of sodium chloride of different concentrations.

PRINCIPLE OF THE METHOD

A small aerial connected to an u. h. f. oscillator (G. R. Type No. 857A) and placed at the principal focus of a cylindrical parabolic reflector A serves as a source of radiation giving out a parallel beam. The beam after being reflected by a plane aluminium reflector B passes through the liquid contained in the glass cell E, (15 cms × 7.5 cm × 7.5 cms.) and then strikes the detector aerial D which is placed horizontally underneath the glass cell. The detector unit C is enclosed completely by means of a thick aluminium box, excepting for a small hole at the top through which the detector aerial is taken out. This screen reduces to minimum the stray reflection pick-up by the detector unit, as it is desired that the detector should pick-up only the beam which has passed through the cell. The detector microammeter placed just outside the screened box, is connected to the detector with a short twisted screened flex. The arrangement is shown in Fig. 1.

FIG. I
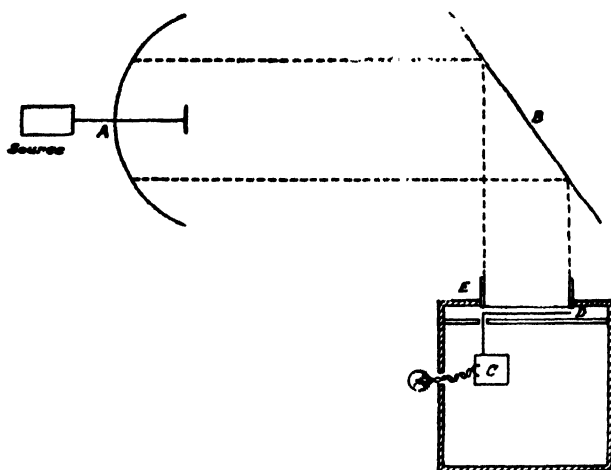
Initial intensity I received by the detector in absence of the cell is measured. Then placing the cell with liquid of uniform thickness x in the path of the beam, transmitted intensity $I_{t r}$ is measured. Changing the thickness of the liquid to a new value x' and keeping the cell in the same position, the transmitted intensity $I'_{t r}$ is measured. Assuming that the reflected intensities remain the same in both cases, and also assuming that the attenuation of the glass cell itself remains unchanged, in the presence of the liquid the attenuation coefficient α can be deduced as follows

$$T = \text{Transmission factor} = \frac{\text{Power transmitted}}{\text{Power received}} = \frac{I_{t r}}{I} = e^{-\alpha x}$$

Similarly,

$$\frac{I'_{t r}}{I} = e^{-\alpha x'}$$

So,

$$\alpha = \frac{1}{2.3(x'-x)} \cdot \log_{10} \frac{I_{t r}}{I'_{t r}} \qquad \ldots \quad (2)$$

The absorption index k can be found from the following relation :

$$\alpha = \frac{2\pi n k}{\lambda} \qquad \ldots \quad (3)$$

involving refractive index n and wavelength λ. The reflextion coefficient R has been calculated from the following relation (Baz, 1939)

$$R = \frac{(n-1)^2 + k^2}{(n+1)^2 + k^2} \qquad \ldots \quad (4)$$

EXPERIMENTAL

Detector deflexion is a measure of the energy incident on it, so it is desirable that the detector plate current change should bear a linear relation

with energy incident on it. Detector used is of resonant line type (Fig. 2).
Characteristics of detector is shown in Fig. 3.
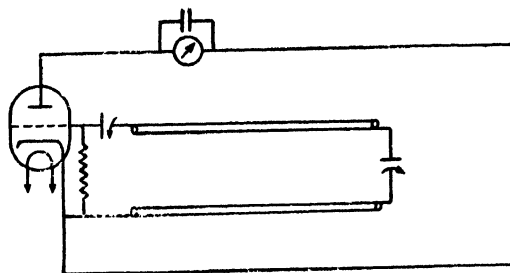
FIG. 2
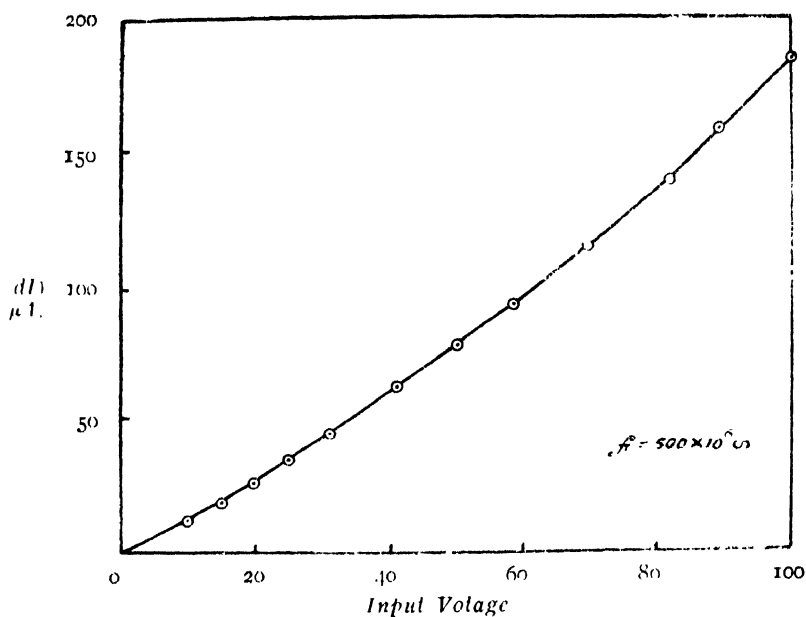
FIG. 3

Characteristic of the Detector

Percentages of transmission for different normalities (N/2 to N/16) of the
solution at different frequencies and for different depths of liquids have been
measured, and the results for 2 mm. depth of liquid have been reported in
Table I.

In order to calculate the attenuation coefficient, at different frequencies,
relation (2) may be used, if the transmission takes place directly, *i.e.*, without
suffering any reflexion within the liquid which may be considered true, if
the liquid depth is very small compared to the wavelength used. To be more
accurate, attenuation coefficients have been determined from the slope of the
average of the envelopes of the curves, one of which is represented in Fig. 4.
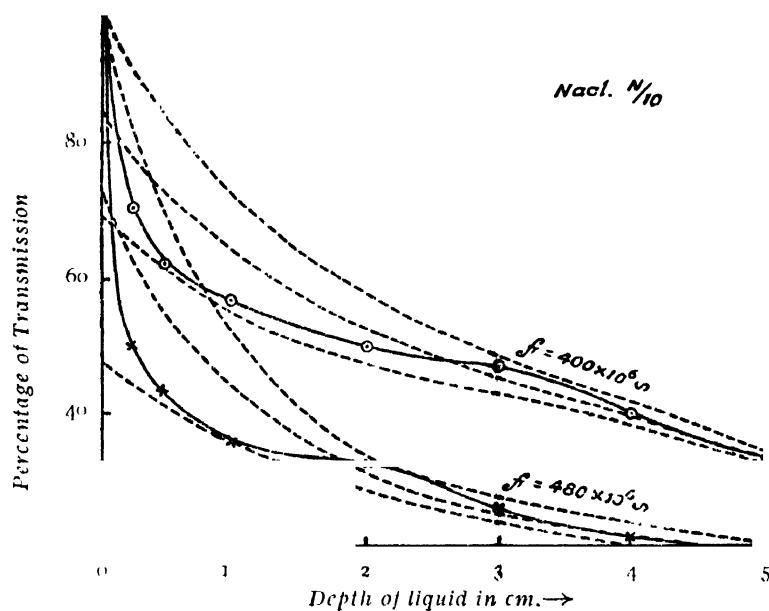
Fig. 4

Values calculated from different portions of the average curve will be different. So two values of attenuation coefficients α_1 and α_2 corresponding to two different slopes $1-2$ cms and $2-3$ cms have been calculated for different frequencies and normalities, out of which values for three different normalities have been represented in Tables II, III and IV.

TABLE I

Frequency in Mc/s	% of transmission through a depth of 2 m.ms of liquid						
	N/2	N/3	N/4	N/5	N/6	N/8	N/16
300	92	100	93	84	80	85.3	88.8
320	83.3	100	90 9	91.6	93.2	85 2	90 0
340	77.2	80	75.8	58.3	58.3	76.6	73.0
380	...	87 5	96 0	96 3	90 6	81.4	100 0
400	71 4	88 0	100 0	82 3	96.4	98.5	100 0
420	79 4	96 3	76 4	...	..	90 9	...
460	79.4	62 0	70.0	89 3	..	88.8	...
480	78.9	54.4	50 3	63 0	0	56.8	75.4
500	64.7	51 3	52 5	56 0	.	68 7	75 0

Substituting values of n from Tables VIII to X in column 3 values of k_1 and k_2 have been calculated With the values of n and k_2, values for reflexion

coefficients have been calculated from Eq. 4..The values of k_2 corresponding to α_2 have been selected, as it has been found that they agree more closely with the values calculated theoretically. Variation of percentages of absorption with different normalities for different frequencies have been shown in Fig. 5 for 2 mms depth of liquid.

TABLE II

Normality = N/2

Frequency in Mc/s	α_1	α_2	n	k_1	k_2	R
360	0 084	0.101	9.063	0.1238	0.1523	0.6427
400	0.099	0.062	9.059	0.2380	0.0842	0.6419
440	0.089	0.078	9.055	0 1023	0.0943	0.6414
480	0.045	0.015	9.051	0.0486	0.0169	0.6419

TABLE III

Normality = N/5

Frequency in Mc/s	α_1	α_2	n	k_1	k_2	R
360	0.118	0.180	8.986	0.175	0.266	0.6397
400	0.183	0.108	8.980	0.243	0.144	0.6393
440	0.177	0 148	8.976	0 213	0.178	0.6393
480	0.163	0 052	8 973	0.181	0 057	0.6395

TABLE IV

Normality = N/10

Frequency in Mc/s	α_1	α_2	n	k_1	k_2	R
360	0.1503	0.1057	8.956	0.2224	0 1568	0.6387
400	0.0936	0 045	8.954	0.0991	0.0675	0 6386
440	0.1039	0.082	8.952	0.1260	0.0997	0.6386
480	0.182	0.113	8.952	0.2032	0.1234	0.6386
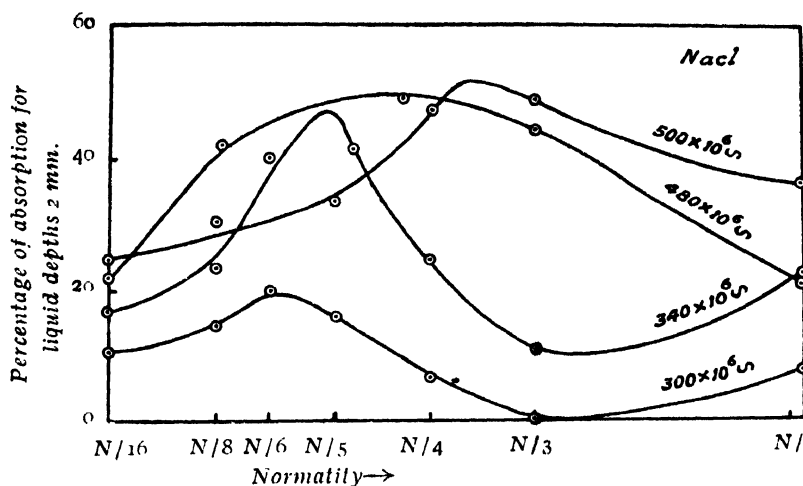
FIG. 5

DISCUSSION

It will be observed from Fig. 5 that the normalities for which the absorption is maximum for frequencies 300, 340 and 480 Mc/s are 0.166 N, 0.20 N, 0.25N respectively. The product of the normality γ expressed in gm. eq. per litre and the wavelength λ_{max}, corresponding to the frequency of maximum absorption is found to be a constant equal to 16.64 for aqueous solution of sodium chloride as shown in Table V.

TABLE V

γ in gm. eq per litre	λ_{max} cms	$\gamma \times \lambda_{max}$	Average
0.166 N	100 0	16.66	
0 20 N	88.2	17.64	16 64
0.25 N	62 5	15 62	

This value agrees fairly with 16.45, the value given by Forman and Crisps (1946).

From Tabels II, III and IV it will be observed that reflection coefficients for different cases do not vary much.

Several mathematical theories have been postulated to explain the frequency dependence of dielectric properties. Though different theories present different mechanisms of absorption, they all suggest some form of relaxation function. Therefore the relaxation time corresponding to the frequency of maximum absorption is of interest. From Debye's (1929)

expression for the generalised dielectric constant

$$\epsilon = \epsilon' - j\epsilon''$$ (5)

it may be deduced that ϵ'' is a maximum, when

$$\omega\tau = \frac{\epsilon_\infty + 2}{\epsilon_0 + 2}$$ (6)

For solutions of normalities o. 166 N, o. 20 N, o. 25 N, ϵ_∞ may be assumed to be equal to the dielectric constant of water at u. h. f. which is 80. Values of dielectric constant (ϵ_0) at the audio frequencies for sodium chloride solution, for different concentrations have been calculated from the following relation (Falkenhagen,) *loc. cit.* and the result is given in Table VI.

$$\epsilon_{\omega=0} - \epsilon_s = \frac{1.97 \times 10^n |z_1 z_2| \{|z_1| + |z_2|\}^{1/2}}{2\epsilon_s^{1/2} T^{3/2}. (1 + 1/\sqrt{q})^2}.(q.\gamma^*)^{1/2}$$ ... (7)

where, $z_1 =$ valence of Na ion $= 1$

$z_2 =$ valence of Cl ion $= 1$

$T = 300°$ A

$\epsilon_s =$ dielectric constant of water $= 80$

$q = 0.5$ for Nacl.

$\gamma^* =$ concentration in gms. eq. per litre.

Substituting proper values Eq. (7) reduces to

$$\epsilon_{s=0} - \epsilon_s = 3.536\sqrt{\gamma^*}$$ (8)

TABLE VI

Concentration	$\epsilon_{\omega=0} - \epsilon_s$	$\epsilon_{\omega=0}$	Concentration	$\epsilon_{\omega=0} - \epsilon_s$	$\epsilon_{\omega=0}$
N	3 536	83.536	N/8	1 250	81.250
N/2	2 497	82.497	N/10	1.116	81.116
N/3	2.028	82.028	N/16	0.884	80.884
N/4	1 768	81.768	N/32	0.625	80 625
N/5	1 581	81 581	N/64	0 442	80 442
N/6	1.443	81.443	N/128	0.313	80.313

From Table VI and Eq. (6), values of τ for three different concentrations have been calculated and given in Table VII. Values of τ for the same concentrations have also been calculated by using Deby-Falkenhagen relation (Eq.1) and given in the same table for comparison.

In the expression for ϵ (Eq.5), values of ϵ' and ϵ'' may be evaluated from the following relation

$$\epsilon' = \epsilon_\infty + \frac{\epsilon_0 - \epsilon_\infty}{1 + x^2} \qquad \dots \text{(9)}$$

$$\epsilon'' = \frac{\epsilon_0 - \epsilon_\infty}{1 + x^2} x$$

where, x given by

$$x = \omega\tau \left[\frac{\epsilon_0 + 2}{\epsilon_\infty + 2} \right]$$

varies with frequency as well as τ. When the concentration is varied, dielectric constant varies and there is a variation of τ also in accordance with Falkenhagen theory. It is only when the dielectric constant is assumed to remain constant, independent of concentration, and only τ varies, the relation $x = 1$, gives the frequency of maximum absorption. For ϵ'' to have maximum value, $\dfrac{\partial \epsilon''}{\partial x} = 0$

But,

$$\frac{\partial \epsilon''}{\partial x} = (\epsilon_0 - \epsilon_\infty) \frac{\partial}{\partial x} \left(\frac{x}{1 + x^2} \right) + \frac{x}{1 + x^2} \frac{\partial}{\partial x} (\epsilon_0 - \epsilon_\infty) \qquad \dots \text{(11)}$$

It is only when second term (Eq. 11) is assumed to be zero, that ϵ'' is a maximum, when $x = 1$. But when the variation of the dielectric constant is taken into consideration, it is extremely difficult to determine the value of x for which ϵ'' is a maximum. While we have assumed, the constancy of the dielectric constant for determining the frequency of maximum absorption, the variation of dielectric constant has been taken into consideration, in calculating the values of ϵ'' for different frequencies and concentrations (Tables VIII-IX). It follows, therefore, that the frequency of maximum absorption, for a particular concentration, as determined by :

1) keeping the frequency constant and varying the concentration, or
2) keeping the concentration constant and varying the frequency is not the same.

In both cases ω_{max} is given by

$$\omega_{max} = x . \frac{\epsilon_\infty + 2}{\epsilon_0 + 2} . 1/\tau$$

where ϵ_0, ϵ_∞ and τ are the same in both cases, but in the first case $x \neq 1$ and, in the second case, $x = 1$. Hence, for determining τ, for a particular frequency, it is preferable, to keep the concentration constant and vary the frequency, since in that case x is unity. But in following this method there are certain experimental drawbacks, *viz*:

(*i*) It is more difficult to have a wide range of frequency variation than concentration.

(*ii*) It is difficult to have constant intensity of oscillation for all frequencies. Apart from this consideration, the higher observed values of τ in

TABLE VII

Concentration	Cal τ in secs. $\times 10^{10}$	Obs. τ in secs. $\times 10^{10}$
0.25 N	2 632	3.245
0.20 N	3.291	4.591
9.166 N	3.967	5.212

TABLE VIII

Normality $= \dfrac{N}{4}$; $(\epsilon_0)_{N/4} = 81.768$; $\epsilon_\infty = 80.0$, $\tau = 3.245 \times 10^{-10}$ sec ;

$$\epsilon_0 - \epsilon_\infty = 1.768$$

Frequency in Mc/s	$\omega\tau$	$\epsilon' = n^2$	ϵ''	$\tan \delta$	$\dfrac{\triangle k}{\text{(mho/cm.)} \times 10^1}$
300	0.6117	81.272	0.795	9.781×10^{-3}	1.324
360	0.7313	18.132	0.849	1.02×10^{-2}	1.697
420	0.8505	81.020	0.876	1.08×10^{-2}	2.015
480	0.9959	80.884	0.884	1.093×10^{-2}	2.357
500	1 020	80.847	0.881	1.091×10^{-2}	2.417
600	1.224	80.690	0.862	1.069×10^{-2}	2.876

TABLE IX

Normality $= \dfrac{N}{5}$; $(\epsilon_0)_{N/5} = 81.581$; $\epsilon_\infty = 80$; $\epsilon_0 - \epsilon_\infty = 1.581$;

$$\tau = 4.591 \times 10^{-10} \text{ sec.}$$

Frequency in Mc/s	$\omega\tau$	$\epsilon' = n^2$	ϵ''	$\tan \delta \times 10^3$	$\dfrac{\triangle k}{\text{mho/cm.}}$
200	0.5769	81.176	0.6908	8.59	7.674×10^{-4}
250	0.7211	81.029	0.7548	9.31	1.048×10^{-4}
300	0.8654	80.889	0.7843	9.696	1.307×10^{-4}
340	0.9855	80.790	0.7905	9.783	1.493×10^{-4}
400	1.154	80.664	0.7800	9.672	1.734×10^{-4}
500	1.442	80.499	0.7350	9.131	2.042×10^{-4}

Table VII, may be ascribed to the fact that Falkenhagen expression for τ is based on the assumption of Debye's, theory, which is primarily applicable to more dilute solutions, than those employed in the present investigation. The change of conductivity and viscosity of the solutions, if there is a temperature rise due to passing of e.m. wave, along with the first cause, may be responsible for the observed higher values of τ. But the temperature change being negligible, in the present experiment, due to very weak source employed, the possibility of second cause is ruled out.

In order to determine the frequency dependence of dielectric constant ϵ' and loss tangent $\tan \delta = \epsilon''/\epsilon'$ for the above three concentrations, Eqns. (9) and (10) and values of τ from Table VII have been utilised. The results are given in Tables VIII to X.

TABLE X

Normality $= \dfrac{N}{6}$; $(\epsilon_0)_{N/6} = 81.443$; $\epsilon_\infty = 80.0$; $(\epsilon_0 - \epsilon_8) = 1.443$

$\tau = 5.212 \times 10^{-10}$ sec.

Frequency in Mc/s	$\omega\tau$	$\epsilon' = n^2$	ϵ''	$\tan \delta \times 10^3$	Δk mho/cm
200	0.655	80.99	0.6661	8.22	7.401×10^{5}
250	0.819	80.85	0.7094	8.77	9.849×10^{-6}
300	0.982	80.721	0.7215	8.94	1.202×10^{-4}
360	1.118	80.591	0.7098	8.81	1.419×10^{-4}
400	1.311	80.520	0.6920	8.60	1.539×10^{-4}
500	1.629	80.382	0.6368	7.92	1.708×10^{-4}

Values for absorption conductivities Δk for different frequencies and concentrations have been calculated from the following relations (Sharbaugh, etc., 1947)

$$\Delta k = \frac{(\epsilon_0 - \epsilon_\infty)\nu^2/\nu_c^2}{(1 + \nu^2/\nu_c^2) \times 1.80 \times 10^{12}} \qquad (12)$$

where,

$$\nu_c = \text{critical frequency} = \frac{\epsilon_\infty + 2}{\omega\tau(\epsilon_0 + 2)}$$

Variation of loss factor ϵ'' and dipole conductivity with frequency for different concentrations are shown in Figs 6 and 7 respectively. It will be observed that the loss factor maxima shifts towards higher frequencies, as the concentrations become greater. It may also be noted that the rate of variation of dipole conductivity with frequency becomes greater, the higher the concentration.
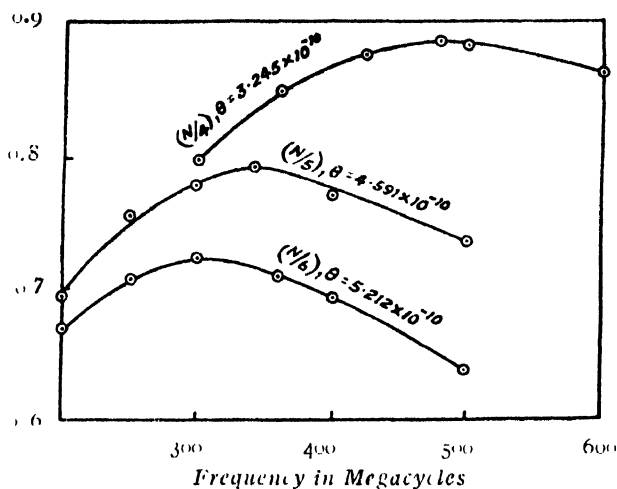
Fig. 6

Variation of ϵ'' with frequency.
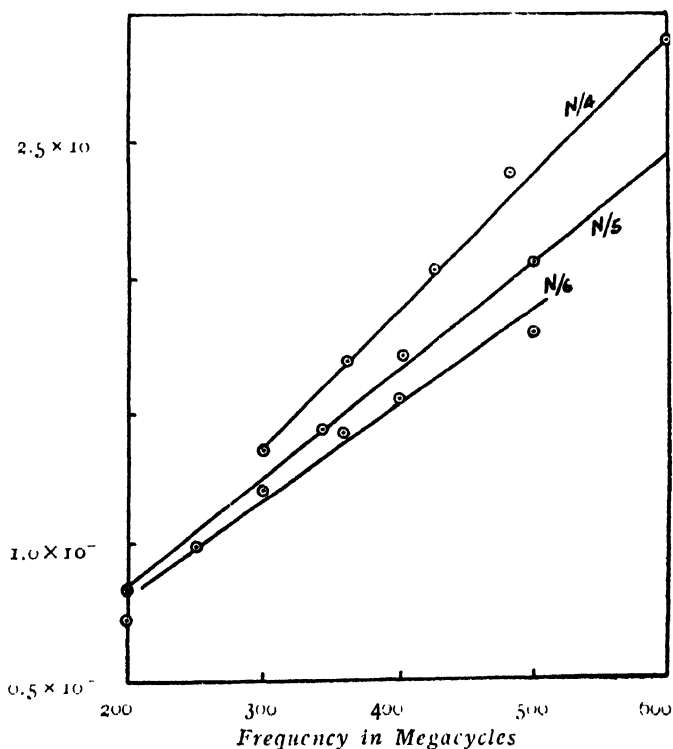
Fig 7.

Variation of Dipole Conductivity with frequency.

Dispersion of conductivity with frequency for strong electrolytes, may be explained in the following way (Falkenhagen, *loc. cit*). When an ion moves under the application of a stationary electric field, the charge distribution loses its symmetry. Disappearance of the unsymmetrical charge distribution

in the ionic atmosphere is governed by a law similar to that which determines Θ, the time of relaxation of the whole ionic atmosphere. When an e. m. field of angular frequency ω acts upon the solution, each ion will describe (apart from its Brownian movement) a to-and-fro motion. If $\omega \ll 1/\Theta$ the unsymmetrical charge distribution, in the ionic atmosphere, at any moment will correspond to the instantaneous velocity of the ion $i.\ e.$ the relaxation force will be the same as in the stationary field case. Whereas, if $\omega > 1/\Theta$ there will not be enough time for the formation of any unsymmetrical charge distribution and hence the retarding relaxation force will be reduced to minimum. The conductivity, therefore, increases with frequency. The conductivity at a frequency ν, $(\omega = 2\pi\nu)$ may be written as

$$\frac{\Lambda\omega}{\Lambda 10} \quad \Lambda_\omega = \Lambda_\infty - \Lambda_{I\omega} - \Lambda_I \tag{13}$$

where, $\Lambda_\infty =$ Conductivity at infinite dilution

$\Lambda_{I\omega} =$ the part due to the relaxation effect.

$\Lambda_{II} =$ the part due to electrophoretic effect

$\quad = 50.5 \sqrt{\gamma^x}$ for univalent system like NaCl.

The molar conductivity under steady electric field is given by :

$$\Lambda_0 = \Lambda_\infty - \Lambda_{10} - \Lambda_{11} \tag{14}$$

From Eqs. (13 and 14), it may be written

$$\Lambda_\omega - \Lambda_0 = \Lambda_{10} - {}_{1\omega} \tag{15}$$

For sodium chloride solution

$$\Lambda_{10} = 0.224 \Lambda_\infty . \sqrt{\gamma^*}$$

where, $\Lambda_\infty = 108.99$ for NaCl solution.

In order to find the variation of molar conductivity with frequency for three concentrations (N/4, N/5, N/6), the following procedure has been adopted. Two curves $\Lambda'_{I\omega}/\Lambda_{10}$ against $\omega\Theta$ and $(\epsilon_\omega - \epsilon_s)/(\epsilon_{\omega=0} - \epsilon_s)$ against $\omega\Theta$ have been plotted in Fig. 8 From these two graphs, variation
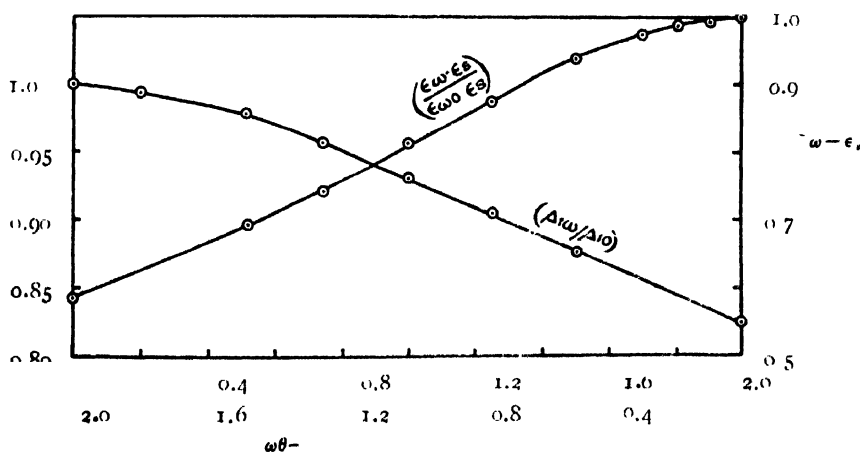
FIG. 8

Variation of conductivity and Dielectric constant with $\omega\theta$

of $(\epsilon_\omega - \epsilon_s)/(\epsilon_{\omega=0} - \epsilon_s)$ and $\Lambda_{1\omega}/\Lambda_{10}$ with frequencies for different normalities have been prepared (Fig. 8- 9). From these latter curves, variation
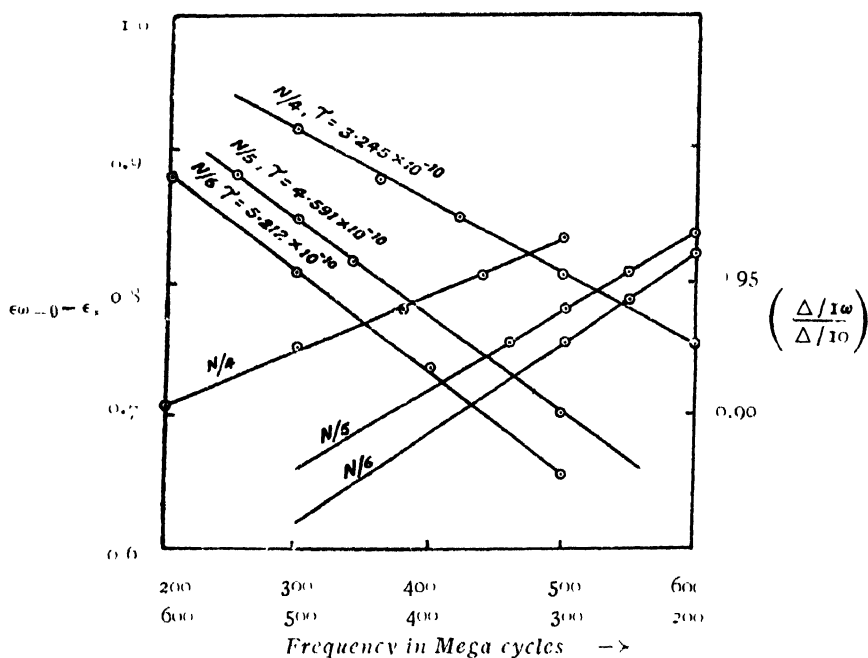
FIG. 9

of molar conductivities with frequency for three normalities have been computed and the results are plotted in Fig 9. It will be observed that the molar conductivity increases with frequency and that the rate of variation with frequency is less with higher concentration.

ACKNOWLEDGMENT

REFERENCES

Bäz, G., 1939, *Phy. Zeit.* 40, 394.

Cooper, R. 1946, *J. I. E. E.*, 93, Part III, 69.

Drysdale, C V , 1920. *J. I. E. E.*, 58. 572

Dorsey, N. E., 1940 'Properties of ordinary water substance'. Reynold Publishing Corporation, 654.

Drake, Pierce and Dow,. 1930, *Phys., Rev* ., 35, 613.

Debye, P., : 1929, Polor Molecules, Chemical Catalog Co., New York.

Falkenhagen, II., 1934, Electrolytes, p. 100, 176.

Forman and Crisp., 1946, *Trans. Far. Soc.* 42A, 187.

Hill, E G., 1907, *Proc. Roy.Soc. Edin* , 27, 233.

Smith--Rose, R. L , 1933 34, *Proc. Roy. Soc. A*, **143**. 135.

Sharbaugh A. H., Eckstrom, H. C., and Kraus, C. A., 1917, *J. Chem. Phys*, **18**, 56.

Van der Pol, B., 1918, *Phil Mag.*, **36**, 88.

ON THE STRUCTURE AND PROPERTIES OF NITROCELLULOSE FROM JUTE FIBRE*

By N. N. SAHA

Plate VII

ABSTRACT. X-ray diffraction patterns of the products obtained by nitrating raw and delignified jute fibres with a mixture of nitric and sulphuric acids have been studied. It has been found that the spacing of the most intense reflection is 7. 26 Å. U. in both these cases; but in the latter case the reflection consists of a ring indicating almost random orientation of the micelles in the product. The structure of the products seems to be different from that of nitroramic in both the cases. The inflammability and solubility of the products obtained from delignified jute fibre have been found to be different from those of the product obtained from raw jute fibre.

INTRODUCTION

Of all inorganic esters of cellulose, nitrate is the most important, but due to its high inflammability it is gradually being replaced by non-inflammable cellulose acetate. The widespread uses of nitrocellulose covering a wide range of nitrogen are well-known.

The number of hydroxyl groups available for esterification in each C_6 unit is three. When all the hydroxyl groups are reacted upon during nitration a homogeneous product corresponding to cellulose trinitrate is found. Theoretically the completely nitrated cellulose should contain 14.16 per cent of nitrogen but in practice this value has not been obtained. The solubility and other properties which permit its uses in various fields of application depend on the nitrogen content of the nitrated sample.

Cotton, in which cellulose in its purest form is available, is generally used for preparing nitrocelluloses. Miles and Craik (1930), Trogus and Hess (1931), and others have studied thoroughly with the help of X-rays the course of reaction during nitration of cellulose using ramie fibres, the crystallites of which are large and well-oriented, as the source of cellulose. According to Mark (1932 *loc. cit.*) the nitrogroups are distributed statistically along the chains. Trogus and Hess considered the process of nitration as a heterogeneous micellar reaction. Both cotton and ramie fibres contain very high percentages of cellulose but very negligible amount of lignin It is not known, however, whether the product obtained by treating raw jute fibre which contains large percentages of lignin with a mixture of nitric and sulphuric acids is identical

with that obtained from cotton fibre. Nitration is generally effected by acid mixtures e.g. mixture of nitric and sulphric acids ; and mixture of nitric acid and phosphoric acid, etc. It is quite likely that the lignin is not wholly removed by the action of mixtures of these acids.

The object of the present investigation is to study with the help of X-ray analysis the structure and properties of such a product obtained from jute fibres, and especially to study the influence of lignin present in the fibre on the formation and properties of the end product.

EXPERIMENTAL

Jute fibres cut into small lengths and cleaned by thorough combing were soaked in water for a few minutes. The bundle of fibres was then made free from water by pressing it between filter papers. Concentrated nitric acid about forty times the weight of the fibre was taken in a beaker and then concentrated sulphuric acid of the same volume was added slowly with constant stirring. The bundle of fibres previously soaked in water was then completely immersed in the acid-mixture. After about three minutes the bundle was removed and immersed in a sufficient volume of cold water. Finally the treated sample was washed thoroughly in a stream of running water until it was free from acid. The nitrocellulose thus obtained was pressed between filter papers and allowed to dry. In this method of nitration the fibrous form of raw jute fibre was not destroyed. Cotton and delignified jute fibres were also nitrated by the same method. Delignification of jute fibres was effected by chlorine peroxide. No tension was applied to the fibres during the treatment.

The product obtained from raw jute fibre was light yellow in colour but that from delignified jute fibres was as white a- nitrocotton and its fibrous nature was destroyed completely. The sample of nitrojute from raw jute fibre was found to be more inflammable than that obtained from delignified jute fibres, but it was just as inflammable as nitrocotton.

Nitrojute from delignified jute fibre and nitrocotton gave clear solutions in acetone. But when nitrojute from raw jute fibre was dipped in acetone a jelly-like mass was obtained which, when allowed to evaporate on a smooth surface, gave a thin film. The edge of this film was yellowish in colour whereas, the central portion was almost white. It appeared that the latter contained the product from cellulose and the former that from lignin.

Each of these samples was studied with the help of X-rays. Diffraction patterns of nitrated jute and cotton were photographed after making all the strands parallel by pressing them mildly with fingers and holding them taut during the exposure. The X-ray photograph of nitrocellulose from bleached jute fibre was taken using a very thin sheet of the substance, because the product was almost a powder. The photographs were taken in a camera with a very fine slit of 0.5 mm. bore and 5 cm. in length using Cu Kα radiation from a Hadding tube and they are reproduced in Plate VI.

The exposure required to obtain the photographs of the diffraction patterns of these nitrated samples was longer than that required for the untreated jute fibre.

RESULTS AND DISCUSSION

In Plate VI, figure 1 represents the diffraction pattern of untreated jute fibre, figure 2 represents that of nitrojute from raw jute fibre, figure 3 corresponds to nitrocotton and figure. 4 is due to nitrojute from delignified jute fibre. For comparison an X-ray photograph of nitroramie obtained by Trogus and Hess (*loc. cit.*) is reproduced in figure 5. In Table I are given the spacings of the reflections on the equatorial line of these samples and that of fully nitrated cellulose. These reflections are marked A_1, A_2 and A_3 respectively, starting from the innermost one.

It can be seen from figure 2, that the (101) and $(10\bar{1})$ reflections characteristic of the diffraction pattern due to raw jute fibre (fig. 1) are totally absent in those of nitrated compounds, but a very sharp equatorial reflection of 7.26 Å.U. spacing has appeared. Miles and Craik (*loc. cit.*) have shown that when the nitrogen content of nitroramie is 7.5% or below, the X-ray diagram indicates the presence of hydrated cellulose but with the increase of nitrogen content, the samples give quite different X-ray patterns. The spacing of (002) reflection in raw jute fibre is 3.92 ÅU and that in case of hydrated cellulose from jute fibre as obtained by Sirkar and Saha (1947) is 4.03 ÅU. On careful examination of figures 2, 3, and 4 due to nitrated raw jute, cotton and delignified jute fibres respectively, it is observed that the position of the most intense reflection in all these cases is exactly the same and the spacing of this reflection has been found to be 7.26 ÅU in comparison to 7.41 ÅU in the case of fully nitrated ramie. In the case of hydrated cellulose this ought to have been 7.96 ÅU. Further the sharp reflection from the $(10\bar{1})$ plane of hydrated cellulose was not visible in the patterns obtained with nitrojute.

The X-ray pattern due to nitroramie, (Fig. 5) shows that the most intense equatorial spot is followed by another medium sharp spot and between these two reflections there is a diffuse broad band. According to Miles and Craik (*loc.cit.*), the most intense equatorial spot in the pattern is not constant in position from one sample to other but shows definite shifts corresponding to an increase in spacings as the nitrogen content increases. It appears that the nitrojute obtained in this investigation may be classified into that group containing 10.5% or more of nitrogen and the constant position of the equatorial spot indicates that the degree of nitration in these three cases is same.

It can further be seen from figures 2, 3 and 4, that in the case of nitrocellulose from jute fibre there is no second sharp spot in the equatorial line as in nitroramie (Fig.5) but there are two diffuse bands of spacings 5.05 ÅU and 4.07 ÅU due to amorphous portion in the nitrated samples.

Though the spacing of Λ_1 reflection in these three cases have been found to be the same there is much difference as to the length and nature of the arc. The length of the arc is greater in case of nitrocotton (Fig.3) than that in the nitrojute (Fig.2), while in the case of nitrojute from delignified jute fibre (Fig. 4), a complete circle is obtained. From this it seems that the orientation of micells in nitrojute (Fig. 2) along the axis of the fibre is of much higher degree than that in nitrocotton. It further appears that the micelles in the product from delignified jute fibre orient themselves almost in a random manner so that the fibrous nature of the product is completely destroyed.

<div align="center">TABLE I</div>

<div align="center">Spacings in Å.U of spots in equatorial line</div>

Sample	Λ_1	Λ_2	Λ_3
Untreated jute fibre	6.05	5.15	3.92
Hydrated (jute)	7.96	1.42	4.03
Nitrojute (Raw)	7 26	5.05 (Band)	4 07 (Band)
Nitrocotton	7.26	5 05 (Band)	4.07 (Band)
Nitrojute (delignified)	7.26	5.05 (Band)	4.07 (Band)
Fully nitrated Ramie	7.41	4 23 (Band)	3.75

The results show that although some properties of nitrojute such as inflammability, solubility and retention of fibrous nature are different from those of nitrocellulose from bleached jute fibre, the X-ray patterns of both the products are identical. Hence lignin does not enter into micells of cellulose-nitrate giving the X-ray patterns. The results are different from those observed in the case of cellulose acetate (Saha, 1947) because the structure of the cellulose acetate obtained from delignified jute fibre was found to be different from that of the same compound obtained from raw jute fibre. It can also be seen from Table 1 that nitrojute approaches more towards fully nitrated cellulose than hydrated one and the X-ray photographs show no indication of the presence of hydrated cellulose or native cellulose.

So the present investigation leads to conclusion that the nitration is a homogeneous type of reaction though at the beginning the reaction is of micellar surface type as in acetylation of cellulose. The process of nitration as found in this investigation is much quicker than that of acetylation.
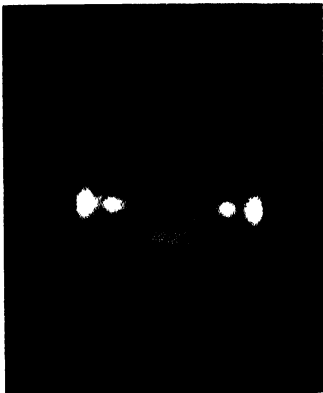
Fig. 1
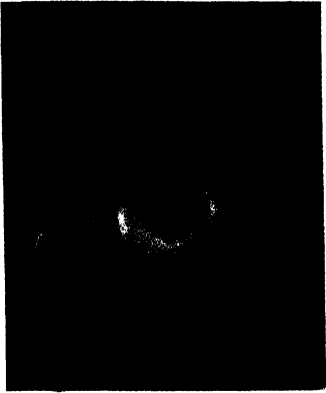
Fig 2
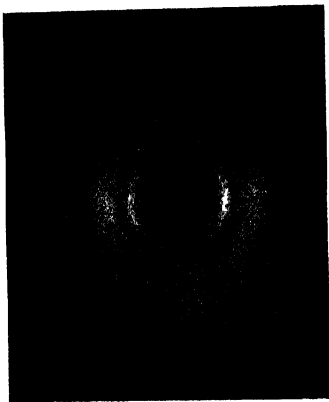
Fig. 3
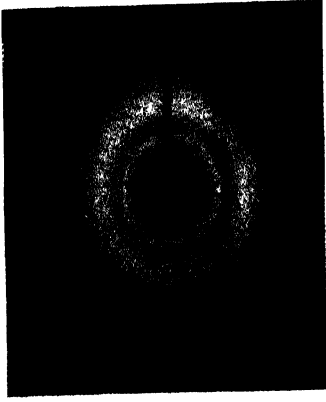
Fig. 4
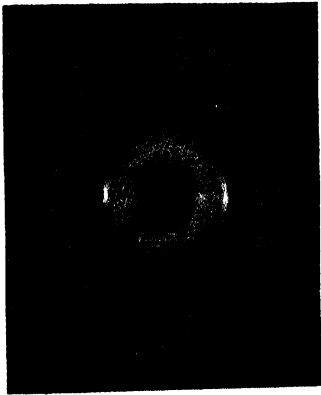
Fig. 5

X-ray diffraction patterns.

According to Herzon and Naray Szabo (1927) the diffraction patterns of samples containing 11% to 13% of nitrogen are due to the mixtures of trinitrate and unaltered cellulose. The X-ray diagrams obtained here do not indicate the presence of reflections due to unaltered cellulose. So the results of the present investigation do not support the mixture theory postulated by Herzog, *et al.* It appears that the samples containing about 11-13% of nitrogen are the product of homogeneous nitration.

ACKNOWLEDGMENTS

PALIT LABORATORY OF PHYSICS
UNIVERSITY COLLEGE OF SCIENCE,
    CALCUTTA.

REFERENCES.

Herzog, R. von, and Naray Szabo, S, von, 1927, *Z. Physik Chem. (1)*, **130**, 616.

Mark, H , 1932, *Physik and Chemie der Cellulose, Springer, Berlin*, 263.

Miles, F. D. and Craik, 1930, *J. Phys. Chem.*, **34**, 2607.

Saha, N. N., 1947, *Proc Nat. Inst. S. C India*, **13**, 339.

Sirkar, S C and Saha, N. N , 1947, *Proc. Nat. Inst. Sc. India*, **13**, 1.

Trogus, C. and Hess, K., 1931, *Z. Physik Chem. B)*, **12**, 268.

INDIAN ASSOCIATION FOR THE CULTIVATION OF SCIENCE

210, Bowbazar Street, Calcutta-12

Applications are invited for the posts of :

(1-2) a Professor of Organic Chemistry and a Professor of Theoretical Physics, in the grade Rs. 800-40-1000, 1000-50-1250 ;

(3-4) a Research Officer in Physical Chemistry and a Research Officer in Optics, in the grade of Rs. 300-25-500. D. A. and Provident Fund in all cases.

Applicants for Professorships should be distinguished scientists having long experience of research, and will be required to organize and promote research and guide scholars in research work in their respective subjects. Experience of work on High Polymers is desirable.

Research Officers will have to carry out and organize research under the guidance of Professors. Applicants should ordinarily have a Doctorate Degree with long experience of research work in : Optics including Light-scattering and Raman Effect for (3), and Physical Chemistry, preferably Chemistry of High Polymers for (4).

Six copies of applications together with testimonials, statement of qualifications and age, and copies of original publications, should reach the Registrar on or before 1st August, 1948.

For candidates applying from overseas, abstracts of applications may be sent in advance by Air Mail.

The following special publications of the Indian Association for the Cultivation of Science, 210, Bowbazar Street, Calcutta, are available at the prices shown against each of them :—

Subject	Author	Price Rs. A. P.
Methods in Scientific Research	Sir E. J. Russell	0 6 0
The Origin of the Planets	Sir James H. Jeans	0 6 0
Separation of Isotopes	Prof. F. W. Aston	0 6 0
Garnets and their Role in Nature	Sir Lewis L. Fermor	2 8 0
(1) The Royal Botanic Gardens, Kew.	Sir Arthur Hill	1 8 0
(2) Studies in the Germination of Seeds.	,,	
Interatomic Forces	Prof. J. E. Lennard-Jones	1 8 0
The Educational Aims and Practices of the California Institute of Technology.	R. A. Millikan	0 6 0
Active Nitrogen A New Theory.	Prof. S. K. Mitra	2 8 0
Theory of Valency and the Structure of Chemical Compounds.	Prof. P. Ray	3 0 0
Petroleum Resources of India	D. N. Wadia	2 8 0
The Role of the Electrical Double layer in the Electro Chemistry of Colloids.	J. N. Mukherjee	1 12 0

A discount of 25% is allowed to Booksellers and Agents.

RATES OF ADVERTISEMENTS

Third page of cover	...	...	...	...	Rs. 32, full page
do. do.	...	...	...	...	,, 20, half page
do. do.	...	...	...	...	,, 12, quarter page
Other pages	...	...	...	...	,, 25, full page
do.	...	...	...	...	,, 16, half page
do.	...	...	...	...	,, 10, quarter page

15% Commissions are allowed to *bonafide* publicity agents securing orders for advertisements.

CONTENTS

NOTICE
TO INTENDING AUTHORS

Manuscripts for publication should be sent to Mr. A. N. Banerjee, Assistant Editor, 210, Bowbazar Street, Calcutta.

The manuscript of each paper should contain in the beginning a short abstract of the paper.

All references to published papers should be given in the text by quoting the surname of the authors followed by the year of publication within braces, *e.g.*, Sen (1942). The actual references should be given in a list at the end of the paper according to the following specimen :

    Sen, B. K., 1942, Volume rectification of crystals, *Ind. J. Phys.*, **16**, 329.

The references should be arranged alphabetically in the list.

All diagrams should be drawn on thick white paper in Indian ink, and letters and numbers in the diagrams should be written in pencil.

ON THE SCATTERING OF FAST PARTICLES OF SPIN 1 BY ATOM NUCLEI

By K. C. KAR

ABSTRACT. The wave-statistical theory of scattering due to spin spin interaction discussed in the previous paper has been further extended for spin 1.

In a previous paper (Kar, 1947) the wave-statistical theory of scattering of fast particles of spin $\frac{1}{2}$ by atom nuclei was developed and the well-known Mott (1929) formula was derived. The formula derived for electron-electron scattering is, however, different from that of Möller (1932) in the general case although at the limiting cases for which the velocity is too low or too high, the two formulæ completely agree.

The object of the present paper is to further extend the wave-statistical theory to the case of scattering of fast particles of spin 1.

It may be seen without difficulty (Kar, *loc. cit.*) that on neglecting the spinorbit interaction, we have for the differential equation satisfied by the first order scattering function

$$\Delta(\lambda_1\chi_1) + k^2(\lambda_1\chi_1) = \frac{4\pi^2}{h^2c^2} \chi_0 \left[2\mathrm{E}V + 2\mathrm{E}V_{s-s} - V^2 \right] \qquad \ldots \ (1)$$

where V_{s-s} is the spin-spin interaction. It is apparent that the contributions of the terms $2\mathrm{E}V$ and $-V^2$ are same as in the previous paper (Kar, *loc. cit.*). The contribution of the remaining term is, however, different as the interaction potential V_{s-s} is different in the present case. Let us suppose that the scattering nucleus has $\frac{1}{2}$ spin. Thus the interacting particles have unequal spins and so the exchange factor 2 should be dropped from the spin-spin interaction potential. We have then

$$V_{s-s} = \pm S_1 S_2 \frac{Ze^2}{r} \qquad \qquad . \ (2)$$

where the upper sign denotes that the coulomb force is repulsive

On using the above interaction potential and proceeding in the usual manner we have for the first order scattering function.

$$\lambda_1\chi_1 = \mp S_1 S_2 \frac{Ze^2}{2m_0c^2} (1 - \beta^2)^{\frac{1}{2}} \mathrm{cosec}^2\tfrac{1}{2}\theta \, \cos k'r_0 A \, \frac{e^{ikr}}{r} \qquad \ldots \ (3)$$

As in the previous paper *(loc.cit.)* $\lambda_1 X_1$ should be multiplied by the spin and relativity factors, in order to get the complete scattering function due to spin-spin interaction. Now, it has been shown in the paper just referred to that the probability that there is no change in the sign of spin $\frac{1}{2}$, after scattering, is unity and is given by

$$D_s = P_{+\frac{1}{2}}^{-\frac{1}{2}}(\theta) P_{-\frac{1}{2}}^{+\frac{1}{2}}(\theta) e^{-i\frac{1}{2}\phi} e^{+i\frac{1}{2}\phi} = 1 \qquad \ldots \text{(4.1)}$$

whereas, the probability that there is change of sign after scattering, is given by

$$D_s = P_{+\frac{1}{2}}^{+\frac{1}{2}}(\theta) P_{+\frac{1}{2}}^{-\frac{1}{2}}(\theta) e^{+l\frac{1}{2}\phi} e^{-i\frac{1}{2}\phi} = \cos\theta \qquad \ldots \text{(4.2)}$$

where $P_{\frac{1}{2}}^{\frac{1}{2}}(\theta),\ldots$etc. are Legendre functions for $|m| = \frac{1}{2}$, $|n| = \frac{1}{2}$. The corresponding probabilities for the observer are obtained by putting $\pi - \theta$ for θ. Hence the total probability for the observer is evidently

$$\delta_R = 1 - \cos\theta \qquad (4)$$

which is the spin factor by which the scattering function (3) should be multiplied in order to get the total scattering.

We have now to decide whether the corresponding spin factors (δ) for spin 1 should involve Legendre functions of the type $P_1^1(\theta)$, $P_1^{-1}(\theta),\ldots$etc. It is evident that these Legendre functions cannot represent spin 1, because in that case Legendre functions of the type $P_1^{\frac{1}{2}}(\theta)$ cannot be interpreted. The only other course left to us for representing spin 1 by Legendre functions would be to represent it by squares of $\frac{1}{2}-$ integral Legendre functions. Thus the probability in the present case corresponding to (4.1) should be

$$D_R = \left\{ P_{+\frac{1}{2}}^{-\frac{1}{2}}(\theta) \right\}^2 \left\{ P_{-\frac{1}{2}}^{+\frac{1}{2}}(\theta) \right\}^2 e^{-i1\phi} e^{+i1\phi} = 1 \qquad \ldots \text{(5.1)}$$

while corresponding to (4.2) it should be

$$D_R = \left\{ P_{+\frac{1}{2}}^{+\frac{1}{2}}(\theta) \right\}^2 \left\{ P_{+\frac{1}{2}}^{-\frac{1}{2}}(\theta) \right\}^2 e^{i1\phi} e^{-i1\phi} = \cos^2\theta \qquad \ldots \text{(5.2)}$$

The physical significance of taking squares is that the ultimate unit of spin is $\frac{1}{2}$. The spin 1 is developed due to the simultaneous existence of two component $\frac{1}{2}-$ spins. The probability of this simultaneous happening is obtained by taking squares according to the usual law of probability. Now, in the case of spin $\frac{1}{2}$ we took the spin factor with respect to the observer of the scattered wave *(vide* Eq. 4) by putting $\pi - \theta$ for θ. In the present case of spin 1 because we have to take squares we should take the geometric mean

for the observers situated with the incident and scattered waves facing the scatterer. Consequently (5.2) should be $-\cos^2\theta$ being the product of $\cos(\pi-\theta)$ and $\cos\theta$. It should be noted that if one takes the geometric mean (5.1) remains unaffected. Thus the spin factor becomes

$$\delta_\kappa = 1 - \cos^2\theta = \sin^2\theta \qquad \dots \quad (6)$$

It should be noted that the results in (5.1) and (5.2) may also be obtained in the following way :

$$D'_\kappa = \left\{ P_{+\frac{1}{2}}^{-\frac{1}{2}}(\theta) P_{-\frac{1}{2}}^{+\frac{1}{2}}(\theta) \right\} \left\{ P_{+\frac{1}{2}}^{-\frac{1}{2}}(\theta) P_{-\frac{1}{2}}^{+\frac{1}{2}}(\theta) \right\} e^{-i_1\phi} e^{+i_1\phi} = 1 \qquad \dots \quad (7.1)$$

corresponding to (5.1) and

$$D'_\kappa = \left\{ P_{+\frac{1}{2}}^{+\frac{1}{2}}(\theta) P_{+\frac{1}{2}}^{-\frac{1}{2}}(\theta) \right\} \left\{ P_{+\frac{1}{2}}^{+\frac{1}{2}}(\theta) P_{+\frac{1}{2}}^{-\frac{1}{2}}(\theta) \right\} e^{+i_1\phi} e^{-i_1\phi} = \cos^2\theta \qquad \dots \quad (7.2)$$

corresponding to (5.2). Taking into account these two different ways, it is evident that the spin factor should be normalised by dividing by 2. Accordingly the spin factor should be $\delta_i = \frac{1}{2}\sin^2\theta$ (*vide Eq. (6)*).

Next we consider the relativity factor. From its definition already given and remembering that in taking squares we should take the geometrical mean as in the case of the spin factor.

$$\delta_{r\,e} = \frac{1-\beta^2-1}{1} \cdot \frac{1-(1-\beta^2)}{1-\beta^2} = -\frac{\beta^4}{1-\beta^2} \qquad \dots \quad (8)$$

Hence we have for the total scattering function, neglecting the effect of $-V^2$ term in (1).

$$\lambda_1 X_1 = \mp \left(\frac{Ze^2}{2m_0 v^2} \right)(1-\beta^2)^{\frac{1}{2}} \operatorname{cosec}^2 \tfrac{1}{2}\theta A^{-} \cos k'r_0 \left\{ 1 - \tfrac{1}{2}S_1 S_2 \frac{\beta^4}{1-\beta^2}\sin^2\theta \right\} \quad (9)$$

Hence the relative intensity of scattering becomes

$$I = \left(\frac{Ze^2}{2m_0 v^2} \right)(1-\beta^2) \operatorname{cosec}^4 \tfrac{1}{2}\theta \cos^2 k'r_0 \left\{ 1 - S_1 S_2 \frac{\beta^4}{1-\beta^2}\sin^2\theta \right\} \quad \dots \quad (10)$$

Since the weights for anti-parallel to parallel spins are as 2:1 and since $S_1 = \frac{1}{2}$, $S_2 = 1$, we have for the total intensity of scattering

$$I = \left(\frac{Ze^2}{2m_0 v^2} \right)^2 (1-\beta^2) \operatorname{cosec}^4 \tfrac{1}{2}\theta \cos^2 k'r_0 \left\{ 1 + \tfrac{1}{6}\frac{\beta^4}{1-\beta^2}\sin^2\theta \right\} \quad \dots \quad (11)$$

which is the formula obtained first by Massey and Corben (1939) in a different way.

It may be mentioned in conclusion that in the above formula we have considered the interaction between spin $\frac{1}{2}$ of the nucleus and spin 1 of the scattered particle. If, however, the nucleus has also spin 1, there is the exchange effect. And so the spin-spin interaction potential should be multiplied by the numerical factor 2. But because of the nuclear spin 1 there should be the additional weight factor $\frac{1}{2}$, which neutralises the exchange effect of 2. Thus it may be easily seen, remembering that $S_1 = 1$, $S_2 = 1$, that the intensity should be [*vide* Eq. (10)]

$$I = \left(\frac{Ze^2}{2m_0v^2} \right)^2 (1 - \beta^2) \operatorname{cosec}^4 \tfrac{1}{2}\theta \, \cos^2 k'r_0 \left\{ 1 + \tfrac{1}{3} \frac{\beta^4}{1-\beta^2} \sin^2\theta \right\} \quad \ldots \quad (12)$$

which is slightly different from Massey and Corben's formula (11) in as much as the numerical factor in the second term is $\frac{1}{3}$ instead of $\frac{1}{6}$.

PHYSICAL LABORATORY,
PRESIDENCY COLLEGE,
CALCUTTA

REFERENCES

Kar, K. C., 1947, *Ind. Jour. Phys*, **30**, 69
Massey and Corben, 1939, *Proc. Camb. Phil. Soc.*, **35**, 463.
Moller, 1932, *Ann. d. Phys*, **14**, 531.
Mott, N. F., 1929, *Proc. Roy. Soc.*, **124**, 425.

POLARISATION OF RAMAN LINES OF ETHYLENE DIBRO-
MIDE IN SOLUTION AND INTENSITIES AT
DIFFERENT TEMPERATURES *

By B. M. BISHUI

Plates VIII A and VIII B

ABSTRACT. The polarisation of the Raman lines of solutions of ethylene dibromide in methyl alcohol. benzene, toluene, carbon tetra-chloride and hexane has been studied It is observed that the line 1056 cm^{-1} is totally depolarised in the case of the solutions in all the solvents except in hexane. In the latter case the line 1056 cm^{-1} is observed to be only partially polarised The ratio of the intensities of the lines 551 cm^{-1} and 660 cm^{-1} of ethylene dibromide in the liquid state at about 12°C, 30°C and 95°C has also been determined experimentally. It is observed that this ratio remains almost the same as the liquid is cooled down from the room temperature up to 12°C and it diminishes slightly when the temperature is raised to 95°C. It is pointed out that these facts are contradictory to the hypothesis put forward by Mizushima and co-workers regarding the origin of the line 551 cm^{-1} and can be explained by assuming the existence of strongly associated molecules in the liquid.

INTRODUCTION

The Raman spectra of pure ethylene dichloride and dibromide in the liquid state at room temperature and in the solid state at low temperatures were studied previously by Mizushima et al (1934, 1936) and the results were explained on the hypothesis that in the solid state all the molecules are in the trans configuration and in the liquid state there are two forms—one trans and other as having no centre of symmetry. The lines 1056 cm^{-1} and 1440 cm^{-1} were expected to be polarised according to their hypothesis. Sirkar and Bishui (1945) repeated the investigations and on studying the polarisation of the Raman lines pointed out that the two lines mentioned above are actually totally depolarised and therefore the explanation offered by Mizushima and Morino (1938) was not satisfactory. They further suggested that in the liquid state some of the ethylene dibromide molecules might be in an associated state forming thereby groups having the symmetry C_{2v} and in the solid state the group might change to one having a symmetry D_{2h}.

Later Bishui and Sanyal (1947) studied the relative intensities of the lines 660 cm^{-1} and 551 cm^{-1} of the ethylene dibromide dissolved in different solvents. On comparing the results with those published earlier by Mizu-

* Communicated by Prof. S. C. Sirkar.

shima, Morino and Higasi (1934) regarding this intensity ratio and the permanent electric moment of the molecule it was concluded by them that the results could not be explained by assuming the presence of two types of single molecules of ethylene dibromide having different symmetry elements in the solutions. They tried to explain the results by assuming the presence of associated molecules having only a plane of symmetry in the pure liquid. If the associated molecules break up into single molecules when ethylene dibromide is dissolved in any solvent, it is expected according to the hypothesis put forward by Sirkar and Bishui (1945) that the line 1056 cm^{-1} due to C-C valence oscillation should not be totally depolarised in the case of such a solution. In order to investigate this question the polarisation of the Raman lines of ethylene dibromide dissolved in benzene, toluene, carbontetrachloride, hexane and methyl alcohol has been studied in the present investigation. Since some of the prominent lines due to carbon-tetrachloride, benzene and toluene are totally depolarised, by comparing the depolarisation of these lines with that of the line 1056 cm^{-1} it is also possible to ascertain easily whether the line 1056 cm^{-1} of ethylene dibromide dissolved in these solvents is actually totally depolarised or not. Hexane has been chosen as one of the solvents because Mizushima *et al* (1934) and later Bishui and Sanyal (1947) observed that the line 551 cm^{-1} of ethylene dibromide diminishes in intensity when the liquid is dissolved in hexane.

If the hypothesis put forward by Mizushima *et al* that the relative proportion of molecules of trans and other configuration present in the liquid is dependent upon temperature be true it is expected that the ratio of the intensities of the lines 551 cm^{-1} and 660 cm^{-1} will increase at high temperature. In order to test the hypothesis, the Raman spectra of ethylene dibromide in the liquid state have been studied at three different temperatures, *e.g.*, at 12°C, *i.e.*, two degrees above melting point, at the room temperature and at about 95°C. These results also have been discussed in the light of the hypothesis put forward by previous workers.

<center>E X P E R I M E N T A L</center>

Kahlbaum's pure ethylene bromide was available from old stock in the laboratory for the present investigation. The solvents also were taken from Kahlbaum's or Merck's original packings. All the liquids had to be redistilled in vacuum in order to get rid of fluorescence. The molecular concentrations of ethylene dibromide in the solutions used were as follows: in methyl alcohol 0.19, in carbon tetrachloride 0.35, in benzene 0.35, in toluene 0.55 and in hexane 0.43 and 0.37. The purity of the solvents was tested by photographing their Raman spectra. The Fuess Spectrograph used in the previous investigations was employed in the present investigations also.

In order to study the polarisation of the Raman lines the light from a mercury arc was focussed on the Wood's tube containing the solution and the vertical and horizontal components of the scattered light were photo-

graphed simultaneously. It was easy in the case of solutions to find out whether a particular line was totally depolarised or not by comparing the relative intensities of its horizontal and vertical components with those of a known totally depolarised Raman line of the solvent. The convergence of the incident light and the weakening of the vertical component during passage through the spectrograph only made the horizontal component stronger, but the comparison mentioned above was not rendered difficult by such an increase in the intensity of the horizontal component. The comparison was made by taking microphotometric records of the horizontal and vertical components of the Raman lines with the help of a Moll's self recording microphotometer.

In order to study the relative intensities of the lines 551 cm^{-1} and 660 cm^{-1} at different temperatures, a Wood's tube of Pyrex glass provided with a flat thin window was surrounded by a jacket of Pyrex glass. Water cooled in a reservoir by melting ice up to about 12°C was circulated with the help of a pump through the jacket throughout the exposure and the Raman spectrum of pure ethylene dibromide, sealed inside the Wood's tube and maintained at a temperature of 12°C, was photographed using the spectrograph mentioned above. Next the Raman spectrum of the liquid at the room temperature (about 30°C) was photographed on a plate taken from the same packet. Finally steam was passed continuously through the jacket and the Raman spectrum of the liquid thus kept at a temperature of about 95°C was photographed on another plate taken from the same packet. The microphotometric records of the lines 551 cm^{-1} and 660 cm^{-1} were taken in all the three cases. Ilford ' Selochrome ' plates were used in the present investigation. The relative intensities of the lines 551 cm^{-1} and 660 cm^{-1} were determined with the help of a blackening log-intensity curve drawn by taking intensity marks using a tungsten filament lamp and different widths of the slit of the spectrograph.

RESULTS AND DISCUSSION

The microphotometric records of the horizontal and vertical components of the Raman spectra of solution of ethylene dibromide in carbon tetrachloride and hexane are reproduced in figures 1 and 2, Plate VIIIA and the spectrograms for all the solutions are reproduced in Plate VIIIB. It will be observed from Fig. 1 that the line 314 cm^{-1} of carbon tetrachloride, which is totally depolarised, has got both the horizontal and vertical components almost equally intense in the arrangement used for photographing them In fact the horizontal component is slightly weaker than the vertical component. At the same time the horizontal and vertical components of the line 1056 cm^{-1} of ethylene dibromide in the solution are of the same intensity. This definitely proves that this line of ethylene dibromide is totally depolarised because the factor of depolarisation of the line 314 cm^{-1} of carbon tetra-

chloride is about 0.8. The spectrograms reproduced in the Plate VIII B also show that this line is totally depolarised in solutions in benzene, methyl alcohol, and toluene. On the other hand from Figure 2, Plate VIII A, it appears that the horizontal component of the line 1460 cm^{-1} is about twice as intense as the vertical component while the horizontal component of the 1056 cm^{-1} line is only slightly more intense than the vertical component in the arrangement used to photograph this Raman spectrum. Hence if the line 1460 cm^{-1} be totally depolarised the line 1056 cm^{-1} is only partially depolarised.

Hence as the molecules of ethylene dibromide are dissolved in hexane not only the intensity of the line 551 cm^{-1} but also the factor of depolarisation of the line 1056 cm^{-1} diminishes appreciably. If the line 551 cm^{-1} were due to the vibration of a molecule of the *gauche* configuration, as suggested by Mizushima *et al* (1942), the diminution of intensity of this line in the solution would indicate an increase in the number of molecules in the trans configuration in the solution, but the line 1056 cm^{-1} due to the C-C valence oscillation of the single molecule, either of the trans configuration or of any other rotational isomer, could never be totally depolarised. Hence the results cannot be explained on the hypothesis put forward by Mizushima *et al*. On the other hand if it is assumed that in the pure liquid the molecules are mostly associated and the group formed in this way has a plane of symmetry, as suggested by Sirkar and Bishui (1945), the line 1056 cm^{-1} is expected to be almost totally depolarised in the pure liquid. In the solution in hexane some of the associated groups probably break up into single molecules as indicated by the diminution of the intensity of the line 551 cm^{-1} and the number of single molecules thereby increases. Since the line 1056 cm^{-1} due to the C-C oscillation of a single molecule cannot be totally depolarised the value of factor of depolarisation of this line in solution is expected to be less than 6/7. Thus all these observed facts can be explained on the hypothesis put forward by Sirkar and Bishui and it is difficult to explain them on the hypothesis put forward by Mizushima *et al* (1934).

TABLE I

Temperature	$I_{660} : I_{551}$
12°C	100 : 17
30°C	100 : 18
95°C	100 : 15

The microphotometric records of the Raman spectra of ethylene dibromide at 12°C, 30°C and 95°C are reproduced in Fig. 8. As regards the relative intensities of the lines 551 cm^{-1} and 660 cm^{-1} at different temperatures the values estimated are given in Table I. The value for 12°C is only approximate because due to opalescence of the liquid at a temperature just above

Horizontal   Vertical

Fig. 1

Horizontal   Vertical
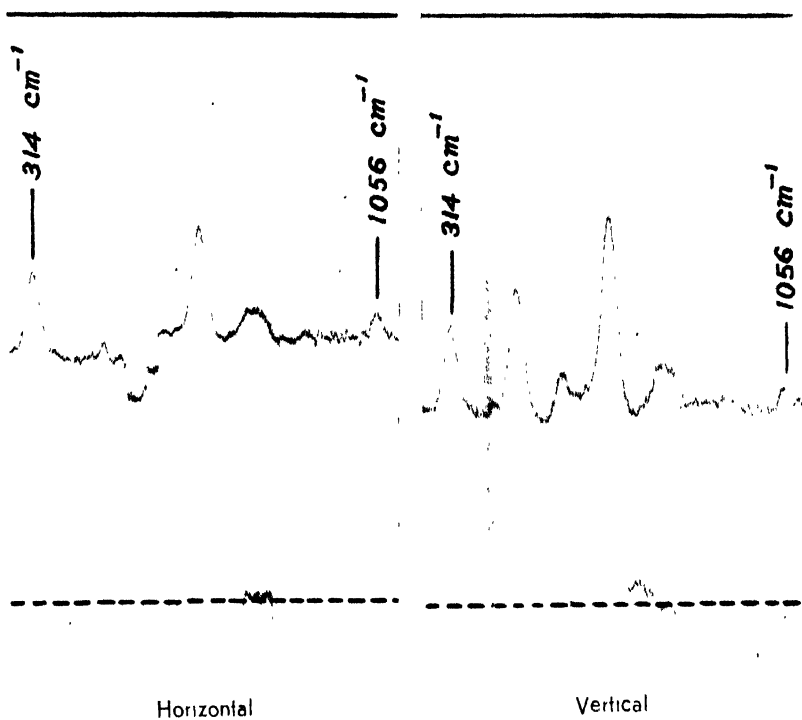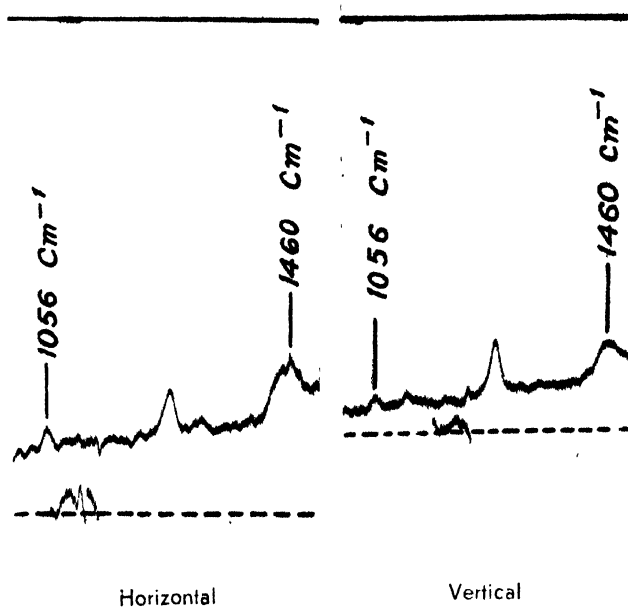
Fig. 2

Polarisation of Raman lines of ethylene dibromide in solution.
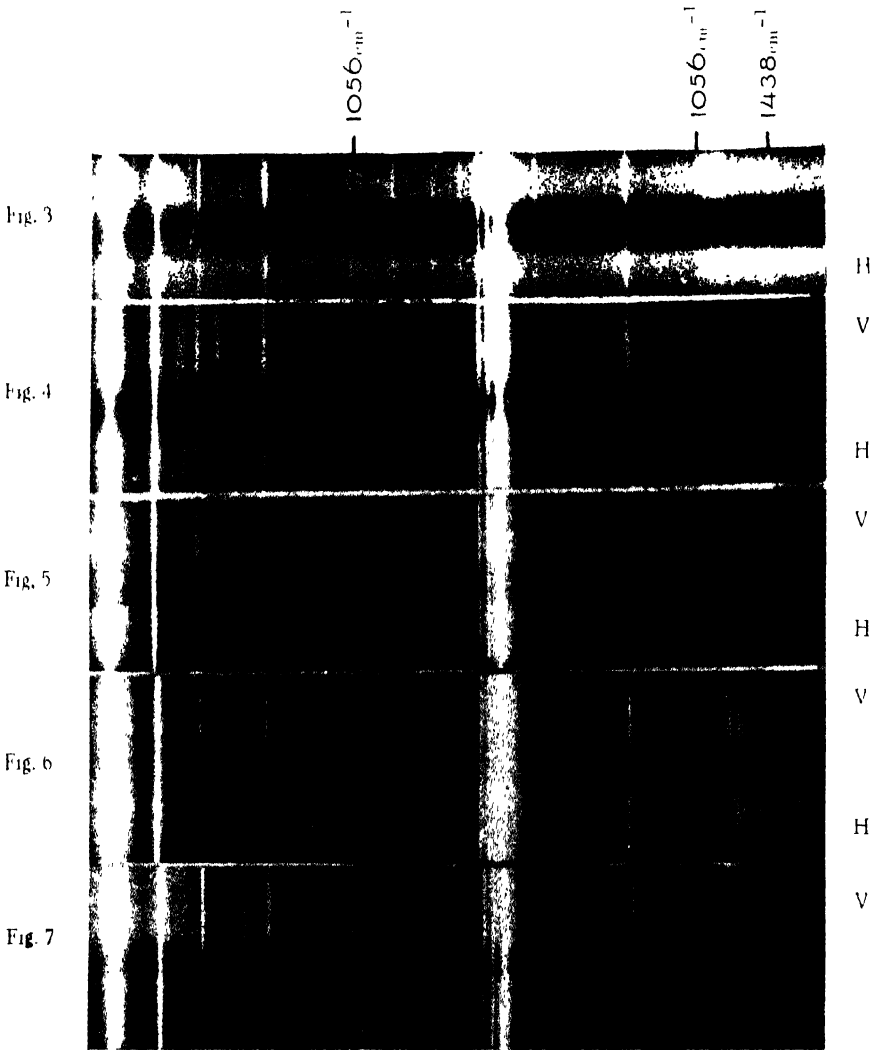
Polarisation of the Raman lines.

Fig. 3 $C_2H_4Br_2$ + C_6H_{14} – Molar Con. – 0·43.

Fig. 4.   „   + CC_4 –   „   „   = 0·35.

Fig. 5.   „   + C_6H_6 –   „   „   = 0·35.

Fig. 6.   „   + C_7H_8 –   „   „   = 0·55.

Fig. 7.   „   + CH_3OH –   „   „   = 0·19.

the melting point there was continuous background in the spectrum of the scattered light.
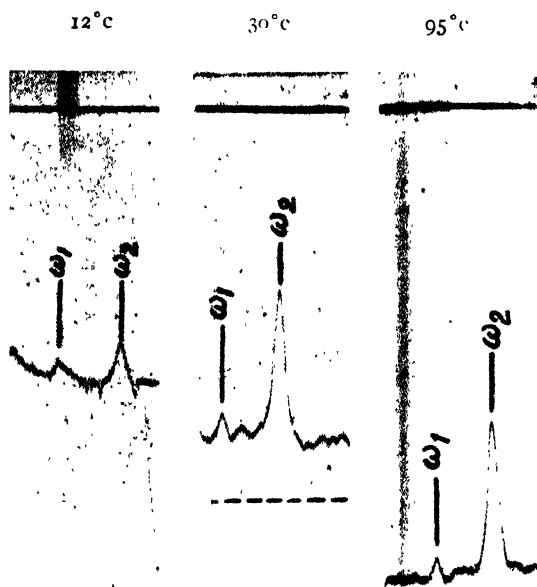
FIG. 8

Microphotometric records of Raman spectra of
ethylene dibromide

$\omega_1 = 551$ cm^{-1}

$\omega_2 = 660$ cm^{-1}

It can, however, be seen from Table I that the relative intensity of the line 551 cm^{-1} does not diminish remarkably at 12°C and also it does not increase at 95°C. This fact is contradictory to the hypothesis put forward by Mizushima *et ai* (1934, 1942) that this line is due to a configuration of the molecule other than trans and that the number of such molecules increases with increase of temperature of the liquid. The observed facts, can on the other hand be explained by assuming that the line 551 cm^{-1} is due to a vibration in the strongly associated molecule and that the number of such molecules diminishes with increase of temperature. In the case of vapour the number of such associated molecules is expected to diminish still further and thus the line 551 cm^{-1} is expected to diminish in intensity still further. It has actually been observed by Morino, Watanabe and Mizushima (1942) that the line 551 cm^{-1} is almost absent in gaseous ethylene dibromide. The results obtained by them in the case of the vapour therefore support the hypothesis put forward by Sirkar and Bishui that the line is due to the vibration of an associated molecule and are contradictory to the hypothesis put forward by Mizushima *el al* (1934) that it is due to a form of the molecule other than the trans configuration.

2—1674P—6

ACKNOWLEDGMENTS

REFERENCES

Bishui, B. M. and Sanyal. S B., (1947), *Ind. J. Phys.*, **21**, 233.

Mizushima, S. and Morino, Y., 1938 *Proc. Ind. Acad. Sci.*, **8**, 315.

Mizushima, S Morino, Y. and Higasi, K., (1934) *Sc. Pap., Inst. Phys. Chem Res (Tokyo)*, **25**, 159

Mizushima, S. Morino, Y. and Noziri, S 1936. *Sc. Pap., Inst Phys. Chem. Res. (Tokyo)*, **29**, 63.

Mizushima, S. and Morino, Y. (1936). *Sci. Pap., Inst. Phys Chem. Res (Tokyo)*, **29**, 188

Morino, Y., Watanabe I, Mizushima S. (1942). *Sc. Pap., I P C R.*, **39**, 401.

Sirkar, S. C. and Bishui, B. M (1945) *Ind. J Phys*, **19**, 23.

EFFECT OF MOISTURE CONTENT ON THE DIELECTRIC PROPERTIES OF SOME SOLID INSULATING MATERIALS AT U.H.F.

By S. K. CHATTERJEE

ABSTRACT. Variations of dielectric constant and power factor of ebonite and fibre with different moisture contents have been studied at frequencies of 214 Mc/s to 750 Mc/s Result shows increases of dielectric constant with increasing moisture content. Rate of increase of power factor with increasing moisture content is much greater at lower frequencies. Loss factor, temperature coefficient of dielectric constant and power lost in the dielectrics at several frequencies for different percentages of moisture content have been calculated.

INTRODUCTION

Presence of moisture, either inside or on the surface of dielectric materials, exercises a vitally important effect on their insulating properties. The importance of moisture can be very well marked in materials which contain, either as natural constituent or as accidental contaminants, electrolytic substances which may dissolve in water to form conducting solutions. Occluded air can also influence the dielectric behaviour, particularly, when the applied voltage becomes sufficient to cause ionisation of the gas. This ionisation produces an increase in the number of conducting particles and rapid increase in the D.C. conductivity and, possibly, in the power factor with voltage. Practically all commercially available solid insulating materials contain occluded air and are sensitive in greater or less degree to atmospheric moisture. It has, therefore, been thought worthwhile to study the effect of moisture content on the dielectric properties at u. h. f. for insulating materials like ebonite and fibre which are easily available in India.

EXPERIMENTAL

Experimental technique involves the determination of maximum wave shift with and without the materials placed along a Lecher wire system between the source and shorting bridge. For the determination of power factor, a knowledge of the width of resonance curve at half power points is necessary in addition to that of maximum shift. The following relation (King, 1937) has been utilised for calculating dielectric constant ϵ

$$\tan \frac{\pi}{\lambda} (\text{max. shift} + s_1) = \sqrt{\epsilon} . \tan \frac{\pi s_1 \sqrt{\epsilon}}{\lambda}$$

where $s_1 =$ thickness of the material in cms.

$\lambda =$ wavelength of excitation in cms.

The power factor tan δ has been determined from the following relation (Chatterjee, 1948) :—

$$\tan \delta = 1 - \frac{\tan \dfrac{2\pi}{\lambda}\left(l_0 - l_r - \dfrac{l_1 - l_2}{2}\right)}{\tan \dfrac{2\pi}{\lambda}(l_0 - l_r)}$$

where $l_0 - l_r =$ wave shift in cms.

$\dfrac{l_1 - l_2}{2} =$ half width in cms. of the resonance curve at half power points.

Experimental detail has been published elsewhere (Chatterjee and Rajeswari, 1948). In order to determine the effect of moisture the samples were soaked in water for 24 hours. Percentage of moisture content is determined from the difference in the weights of the sample in the dry and wet condition. The sample is then subjected to successive stages of heating and at each stage values of ϵ and tan δ have been determined. The sample is weighed before and after each experiment to find the effect of absorption of moisture from the atmosphere during the experiment. The average weights have been taken. Results of experiment for ebonite and fibre for some of the frequencies are given in Figs. 1 to 4.
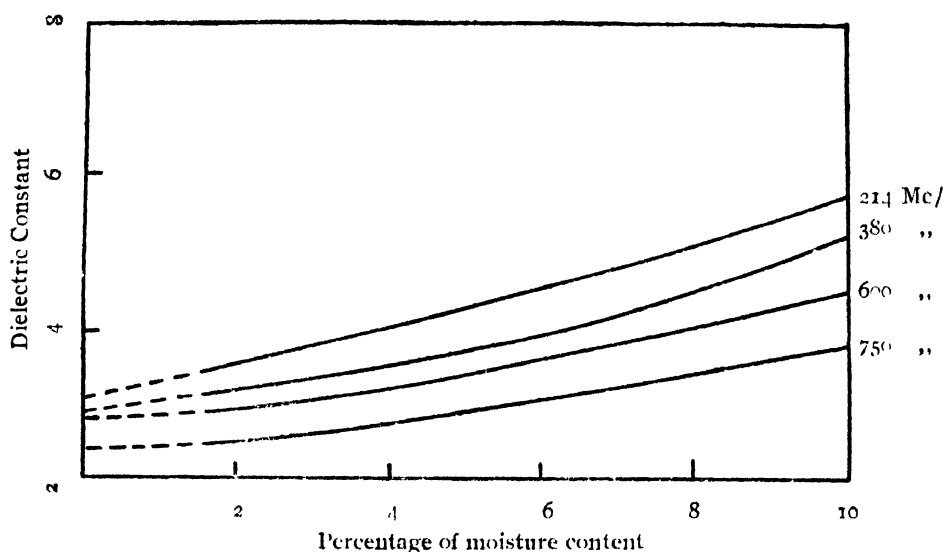
FIG. 1

Variation of dielectric constant of ebonite with moisture
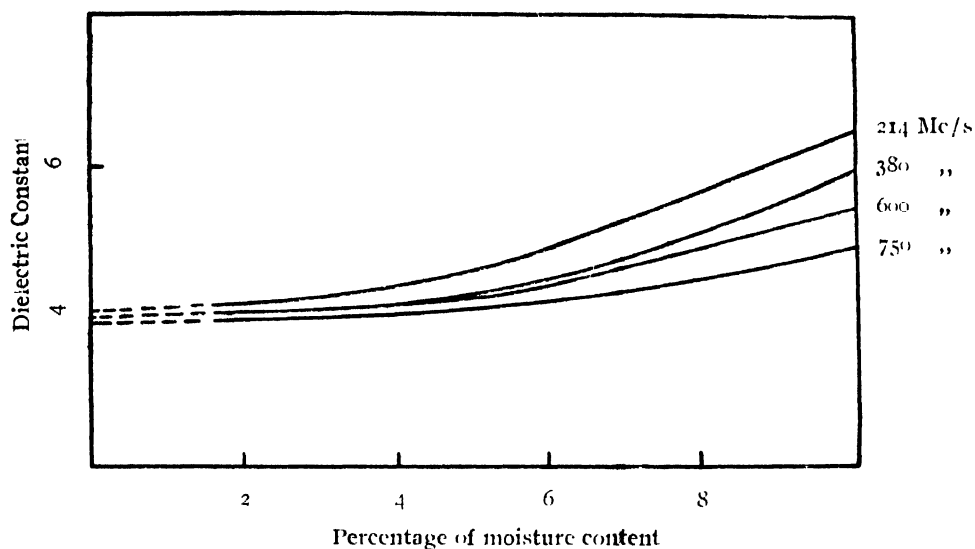
FIG. 2

Variation of dielectric constant of fibre with moisture
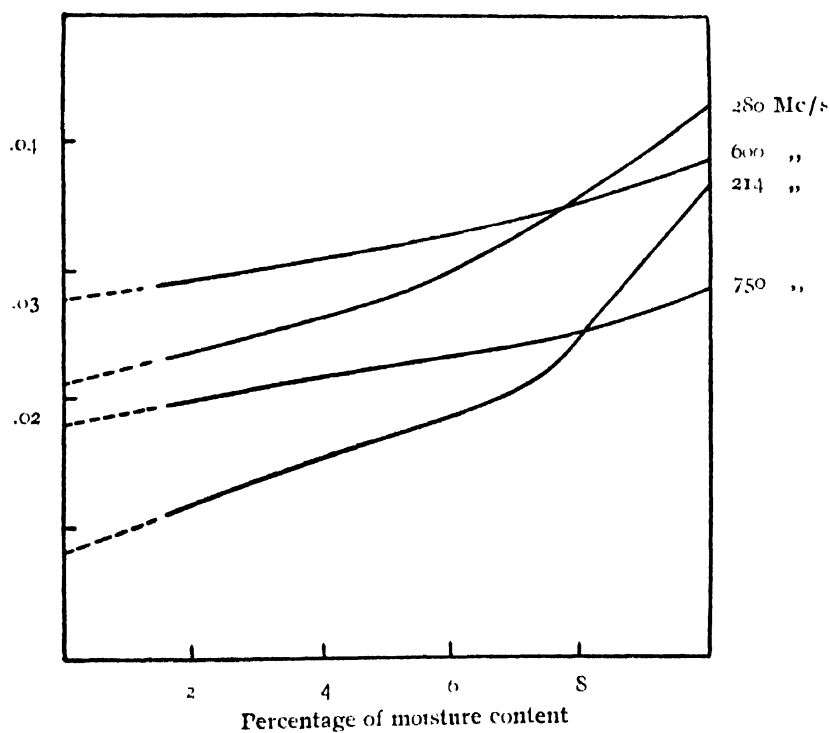
FIG. 3

Variation of tan δ of ebonite with moisture content
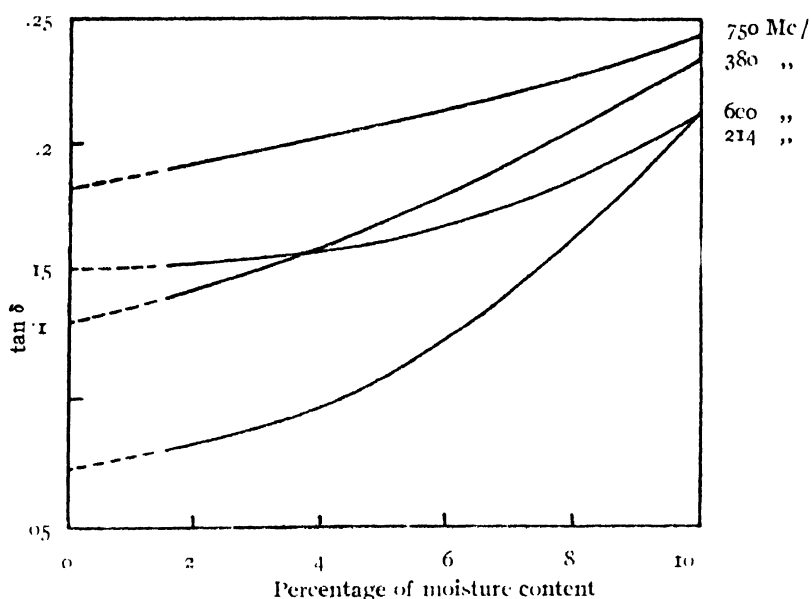
FIG. 4

Variation of tan δ of fibre with moisture content

DISCUSSION

It is observed from Figs. 1 and 2 that the dielectric constant increases with increasing moisture content. This is expected as the permittivity of water is high. The increase of ϵ with percentage of moisture content is much slower at higher frequency. Power factor increases sharply (Figs. 3 and 4) at the lower frequency end with increasing moisture content, but at the high frequency the increase is rather slow. Increase of power factor with moisture may be explained due to low resistivity of the material at high moisture content.

Values of loss factor ϵ. tan δ for both the materials at four frequencies and for different percentage of moisture content have been computed (Table I) from Figs. 1 to 4.

TABLE I

Material : Ebonite

Frequency in Mc/s.	ϵ. tan δ at different % moisture content				
	1.6	3.2	5 3	7.6	10.0
214	.037	.053	.071	.106	.202
380	071	085	.106	.143	.214
600	.084	.090	.106	.129	.167
750	.046	055	.064	.077	.104

TABLE I *(contd.)*

Material : Fibre

Frequency in Mc/s.	ε.tan δ at different % moisture content				
	1.6	3.2	5 3	7 6	10.0
214	3.28	.378	506	.81	1 32
380	.56	615	.731	98	1.33
600	60	656	.672	.816	1 11
750	.741	.80	86	.95	1.15

The power loss in watts (Table II) at different frequencies for varying degrees of moisture content have been calculated from Table I and following relation (Hoch, 1922) :—

Power loss in watts per cubic inch
$$= 2\pi f E^2 . \epsilon . \tan \delta \times 0.2244 \times 10^{-12}$$

where,

f = frequency in c. p. s.

E = voltage gradient in dielectric r m. s volts per inch

= 20 volts per inch

TABLE II

Material : Ebonite

Frequency in Mc/s.	Power loss at different % moisture content × 10^5				
	1.6	3.2	5 3	7.6	10
214	4.5	6 1	8.6	12.8	21.1
380	15.2	18.2	22.7	30.0	45.8
600	28.1	30 1	35 8	43 6	56 1
750	19.5	23 3	27 1	32 0	11 0

Material : Fibre

214	39.7	45.7	61.2	98.0	159.7
380	119.8	131.6	156.4	209.7	284.6
600	202.8	221.7	227.1	285.9	375 2
750	313.4	338.4	363.8	401.9	486.5

ACKNOWLEDGMENTS

The author expresses his grateful thanks to the Actg. Head of the department for giving facilities to carry out the investigation. The author desires to acknowledge with thanks the assistance rendered by Miss Rajeswari, in setting up the equipment.

DEPARTMENT OF ELECTRICAL COMMUNICATION ENGINEERING,
INDIAN INSTITUTE OF SCIENCE, BANGALORE

REFERENCES

Chatterjee, S , 1948, *Ind J Phys.*, **22**, 157
Chatterjee, S and Miss Rajeswari, 1918, *Ind. J. Phys.*, **22**, 180
Gevers, M and Pre., 1946, *Trans Far. Soc* , **42**, 47
Hoch, E T , 1922, *Bell. Sys. Tech. Jour* , **1**, 110
King, R , 1937, *Rev Sci. Inst.*, **8**, 201

ON THE VARIATION OF A.C. PERMEABILITY OF TRANSFORMER SHEET STEELS WITH   C. MAGNETIZATION

By B. M. BANERJEE*

Plate IX

ABSTRACT. An experimental study of the variation of A C. permeability of transformer sheet steels with D.C. magnetization is reported. The experiments indicate that the inverse of the A.C. permeability varies almost linearly with the D C. magnetization Oscillographic study of the hysteresis loops shows that they are always symmetrical and the tips of the loops bent in the direction of the H-axis The bending of the tips increases with D.C. magnetization. The implications of the measurements are the following :—

(1) The admittance of an iron-cored reactor without air-gap increases linearly with D.C. magnetization.

(2) The current passed by such a reactor always contains appreciable amounts of odd harmonics.

INTRODUCTION

While studying the variation of the reactance of certain saturable core transformer, it was noticed that the current passed by the A.C. coils, with constant † A.C. voltage impressed on them varies linearly with the current passed through the D.C. coil. Since the current through a reactor is given by the expression

$$I = \frac{E}{Z} \simeq \frac{E}{X}$$

$$= \frac{E}{pL}$$

$$= \frac{E}{p \cdot 4\pi n^2 A l \mu \cdot 10^{-9}} \qquad \qquad \dots \ (1)$$

the resistance of the coil being small in comparison to the reactance

where   I = A.C. current.

E = A.C. voltage impressed on the coil.

$p = 2\pi f$, $f =$ frequency of A.C.

$n = N/l$, N being the total number of turns in the A.C. winding.

* Fellow of the Indian Physical Society.
† Constant amplitude.

A = Area of cross section of the limbs carrying the A.C. magnetic flux.

l = Length of A.C. flux path.

μ = A.C. permeability of the core material.

It is to be concluded that $1/\mu$ varies linearly with the D.C. current. The constant A.C voltage (E) on the coils, keeps the core magnetized at a constant A.C. flux density (B) given by the expression,

$$E = N. B. A. f. 4. 44. 10^{-8} \qquad (2)$$

The D.C. magnetization is proportional to the current in the D.C. coil. The expression connecting the magnetomotive force H with the current flowing through the D.C. coil being

$$H = \frac{4\pi N' i}{l'.10} \text{ oersteds} \qquad (3)$$

where   N' = number of turns in the D.C. coil.

i = D.C. current in amperes.

l' = length of D.C. flux path.

The observation that the A.C. current varies linearly with the D.C. current therefore points to the following conclusion :

The inverse of the A.C. permeability at constant A.C. flux density varies linearly with the D.C. magnetization

A knowledge of the variation of A C. permeability with D.C. magnetization is necessary in order to make designs of reactors or transformers that must carry a D.C current. The above mentioned observation shows that a simple relation may exist between the A.C. permeability and D.C. magnetization. The importance of such a relation inspired the author to undertake a series of measurements on several samples of transformer sheets (Stalloy) over a wide range of D.C. magnetization and A.C. flux-density. These are reported in this paper. It will be observed that the relation is approximate. Nevertheless the approximation considerably simplifies the design problem and leads to designs close enough to the specified values to be of practical and commercial utility.

EXPERIMENTAL ARRANGEMENTS

The experimental arrangements used for obtaining data reported herein are represented in Fig. 1:—

The 110 volt winding of the 220V : 110V transformer T_2 applies a constant A.C. voltage across the winding S containing the sample. The number of turns in the winding is known. The A.C. current flowing through the

winding is registered by the current ranges of an Avometer—a rectifier type A.C. current meter fed through a current transformer. The anode current
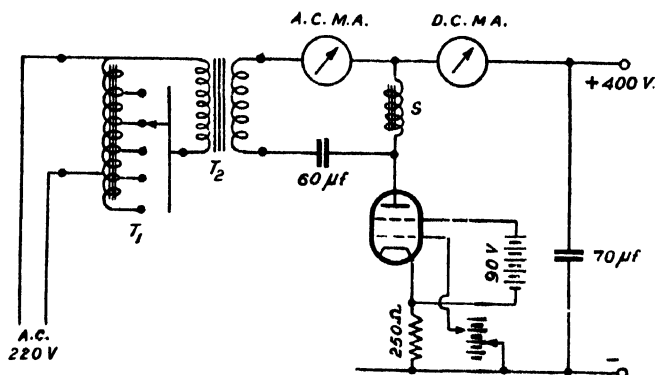
FIG. 1

Experimental arrangement for plotting the A.C. permeability vs D.C. magnetization curves.

of the tetrode power tube (or power tubes) T produces the D.C. magnetization. This is adjusted by varying the grid bias of the tube T. This current is made to flow through the sample winding S. The 60 μf paper condenser blocks the alternative path through the 110 volt winding of T_2. The resistance of the transformer windings (5 ohms ; 12 ohms), the reactance of the 60 μf blocking condnser (50 ohms) and the resistance of the sample winding (20 to 200 ohms), are small compared to the reactance of the windings. These are neglected in the calculations which utilised Eq. (1), (2) and (3). The A.C. current passed by the tube T, because of the A.C. voltage impressed on it is negligible as the effective plate impedance* of the tube is very high (≈ Megohms). The current registered by the A.C. meter is only the current passed by the winding. The A.C. voltage applied across the sample winding may be adjusted to any value between 26 volts to 120 volts by means of the auto-transformer T_1. The A.C. flux-density B depends solely upon the A.C. voltage and is independent of the A.C. coil current. Hence the measurements refer to the condition of constant A.C. flux density. The A.C. flux-density may be varied over a range of 1000-8000 gauss. The D.C. magnetization is

---

* The plate impedance of the tube is of the order of 100 000 ohms The low screen voltage—90 volts only—assure this high plate impedance Besides, degeneration in the cathode resistance of 250 ohms increases it several times

There is little chance of the tube taking a measurable A.C current because of the fluctuating plate voltage. It cannot also generate an A C current because of "ripples" in the grid and screen supplies The battery supplies assure a complete freedom from "ripples" in these supplies and so the plate current.

That the A.C. current taken by the tube is negligible is proved by the fact that the readings obtained are independent of the type of tube 6L6, 6V6, 6F6 or 6K6—and depends only on the D.C. current passed through it

produced by the tubes T—a pair of 6L6's—taking a D.C. current from zero to 150 m.A., through the windings. This produced a D.C. magnetization up to 15 oersteds sufficient to reduce the A.C. permeability by ten times.

RESULTS OF MEASUREMENTS

Measurements were made on several samples of silicon steel transformer sheets. These formed the cores of some radio transformers of foreign and Indian manufacture. The samples investigated upon are believed to be essentially different from each other and come from different sources. Besides these transformer sheets, experiments were performed also on "black sheet" and a certain specimen of permalloy. This specimen of permalloy was supplied to us by an American manufacturer through the India Supply Mission. Its permeability is found to be unusually low, it was probably sent without heat treatment.
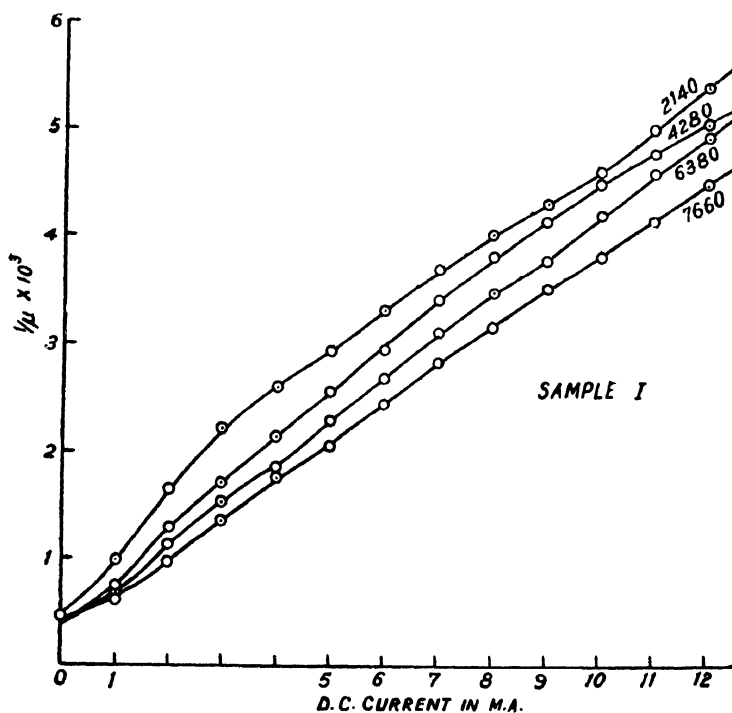
FIG. 2

A.C. permeability vs D.C. magnetization curves for a sample 1 of silicon steel sheet.

The sample experimented upon in Fig. 2 was in the form of a saturable core transformer of local construction. Details of this transformer may be obtained from the publication entitled "A circuit for the control of ionizing current by a saturable core transformer" (Banerjee and Mukherjee, 1947). The D.C. magnetization amounts to 1.7 oersteds per milliampere of D.C. current. The A.C. flux density in gauss is written down at the side of each curve.

The results of these measurements are represented in Figs 2,3, ... 9. It will be seen that the curves broadly verify the statement—"The inverse of the A.C. permeability at constant A.C. flux density varies linearly with the D.C. magnetization." It will also be seen that the slopes of the curves increase as the A.C. flux density diminishes—there being a greater change in A.C. permeability at low flux densities for a given change in the D.C. magnetization.

The departure from the straight line relation between the inverse of A.C, permeability and D.C. magnetization is more pronounced generally at low A.C. flux densities. It is evident from the curves that the exact relationship is quite complicated. So no attempt to formulate a mathematical expression which will take into account this departure from the simple relation will be made. A complicated mathematical expression is not of much help in simplifying the problem of practical designs.
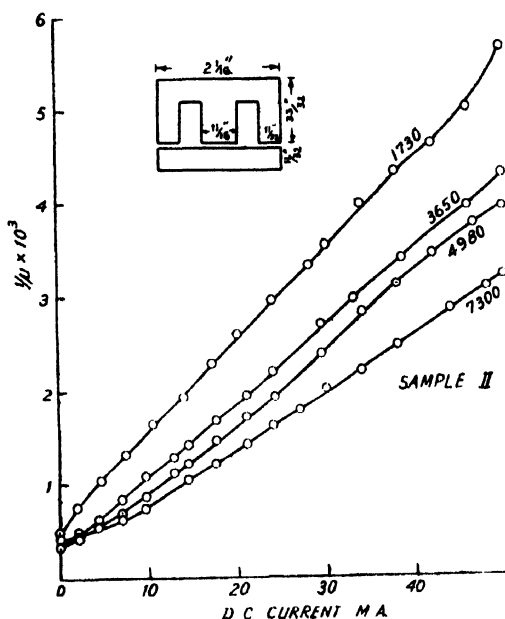
FIG. 3

Curves for sample II of silicon steel sheet

Details of Sample II are given below.

Thickness of core = 11/16″ inches; thickness of sheets = ·015″ ; number of turns in the winding, 2380 turns. The resistance of the winding is 200 ohms. The D.C. magnetization amounts to 0·285 oersteds per m.A. The number at the side of each curve indicates the A.C. flux-density in gauss for that curve.
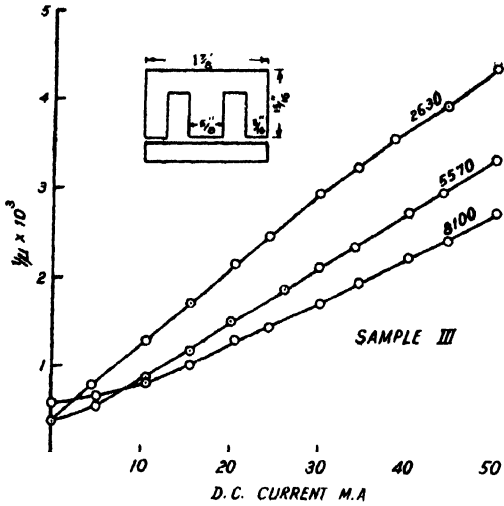
Fig. 4

Curves for sample III of silicon steel sheet.

Details of Sample III are given below.

Thickness of core $= \frac{5}{8}''$; thickness of sheets $= .018''$; 2000 turns in the winding ; resistance $= 200$ ohms. The D.C. magnetization amounts to 0.264 oersteds per m.A. The number at the side of the curve indicates the A.C. flux-density in gauss for that curve.
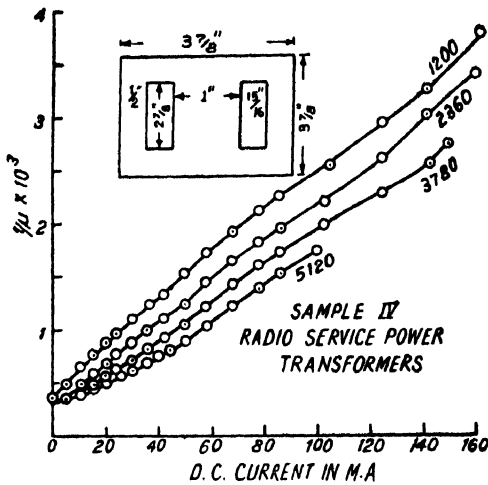
Fig. 5

Curves for sample IV "Stalloy" contained in a power transformer of Indian manufacture.

Details of Sample IV are given below.

Thickness of core $= 1\frac{1}{2}$ inches ; thickness of sheets $= .015''$; 1100 turns in the winding ; resistance $= 18$ ohms. The D.C. magnetization amounts to .056 oersteds per m.A. The numbers at the side of the curves indicate the A.C. flux-density in gauss.
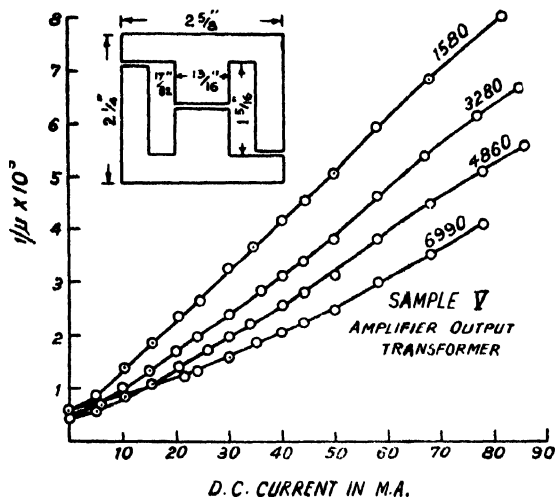
FIG. 6

Curves for sample V of silicon steel sheet.

Details of Sample V are given below.

Thickness of core $\frac{3}{4}''$; thickness of sheets $= .02''$; 2100 turns in the winding of 90 ohms resistance. The D.C. magnetization amounts to 0.195 oersteds per m.A. The numbers at the side of the curves indicate the A.C. flux-density in gauss.
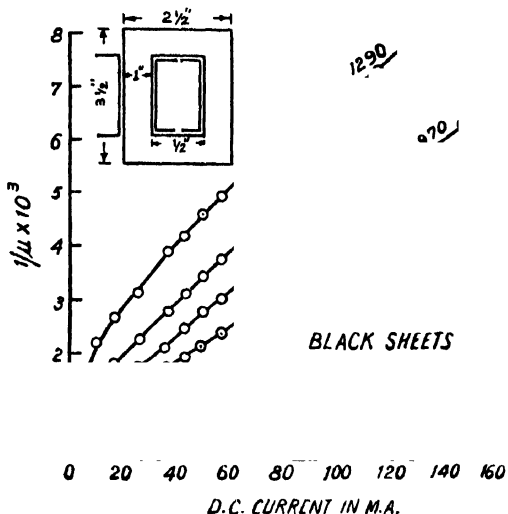
FIG. 7

Curves for a sample of "black-sheet"

Details of the Sample of ' black-sheet ' are given below.

Core thickness $= 1$ inch ; 32 sheets of $.02''$ thickness at each side. Two windings connected in series, each containing 1100 turns. Total resistance of the winding $= 130$ ohms. The D.C. magnetization amounts to 0.136 oersteds per m.A. The A.C. flux-density is written down at the side of each curve.
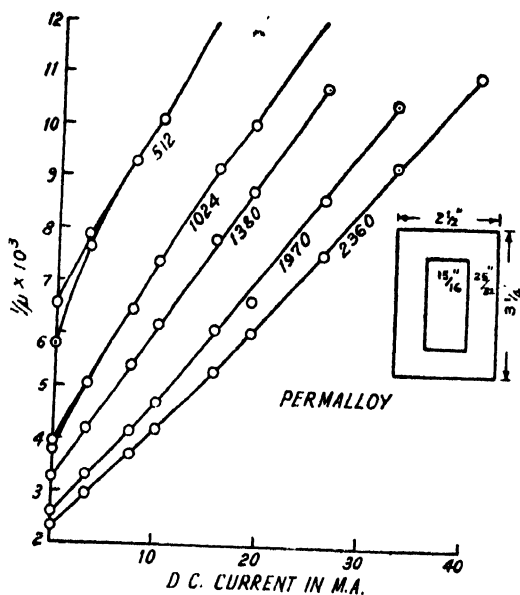
FIG. 8

FIG. 9

Curves for a certain sample of what is supposed to be permalloy.
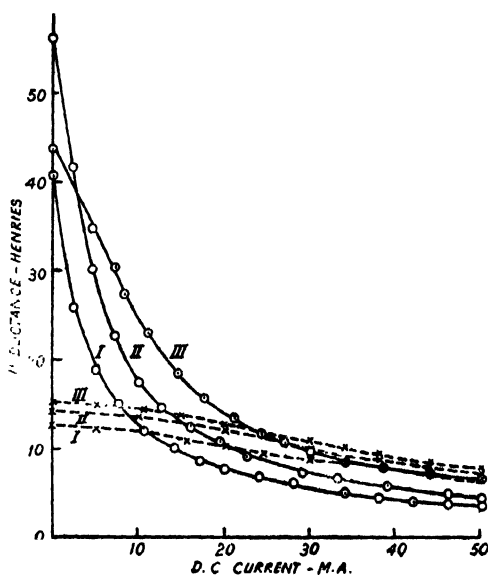
Inductance vs. D.C. current curves of sample II.

The permalloy sample in Fig. 8 was obtained from an American manufacturer in the form of a sheet ($.014''$ thick, $2\frac{3}{4}''$ wide) of considerable length rolled into a circle. It was cut by metal shears and assembled into a core of the form shown in the figure. Care was taken in assembling the core such that the flux-lines were along the length of the sheets. Two windings were put on the two longer limbs each containing 3000 turns. The total resistance of the winding was 370 ohms. The D.C. magnetization amounts to 0.354 oersteds per m.A. As usual, the A.C. flux-density is written down at the side of each curve. The low permeability figures indicate that the permalloy sample was sent without the heat treatment.

The full line curves represent the performance of the 2380 turn choke with no air gap in the core. The dotted line curves are for the same choke with a small air gap. It is to be seen that when there is a D.C. current flowing, introduction of an air gap sometimes increases the inductance. The air gap also greatly reduce the variation of inductance with D.C. current. Curves I correspond to an A.C. voltage of 26 volts on the winding and A.C. flux-density in the core of 1730 gauss; curves II corresponds to an A.C. voltage of 55 volts on the winding and an A.C. flux-density of 3650 gauss; curves III corresponds to an A.C. voltage of 110 volts and a flux-density of 7300 gauss.
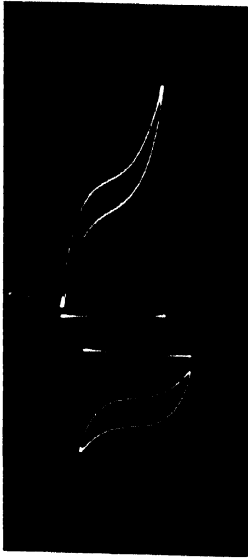
Fig. a   B — 7300 gauss

Fig. b

B = 3650 gauss
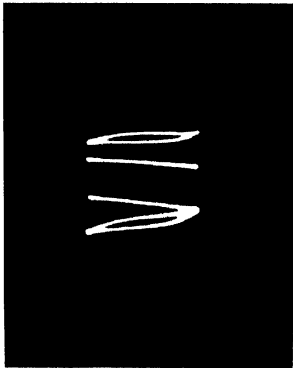
Fig. c   B = 1800 gauss
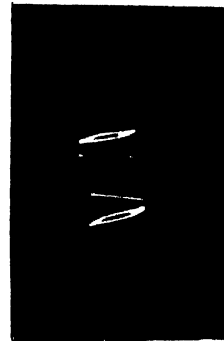
Fig. d   B = 900 gauss

Oscillograms of hysteresis loops with and without D. C. magnetization obtained with sample No. 2. The oscillograms were taken with a Cossor model 3391 double beam oscillograph The straight line by the side of the curves is the trace of the second beam which gives the B axis. The loop making a larger angle with the B axis is the one with D. C. magnetization. Note that the tips of the loops are bent in the direction of H axis and that the bending persists even upto a flux density as small as 900 gauss.

DISCUSSION ON THE METHOD OF MEASUREMENT

The measurements are essentially approximate and the author therefore does not claim precision. The errors arise from the following causes :—

(1) The equation utilised for the calculations assumes that the sample cores are uniformly magnetized throughout—they have a constant B and H everywhere. This is obviously not so with the samples utilised for the measurements.

(2) Equations (1) and (2) neglected the resistance of the sample winding and also the resistances and reactances of the transformer and the blocking condenser.

(3) The rectifier type A.C. milliammeter measures the average current and thereby limits the meaning of the measurements. A full understanding of the phenomenon is, however, not possible without the use of an oscillograph for studying the hysteresis loop or the waveform of the current.

The author did not adopt the 25 cm Epstein tests* recommended by the United States National Bureau of Standards. This testing method requires considerable quantities of sample material in the form of strips of 3 cm width and 28 cm length. As the sample materials were available to the author only in the form of cores of radio output and power transformers, he had to adopt the different arrangements of measurement as described here. The standard 25 cm Epstein test is superior to the method described here mainly in circumventing the effect of resistance of the windings. The arrangement described here is more suitable for rapid measurements with sample cores of small size in the range 1000-10,000 gauss induction with a D.C. magnetization.
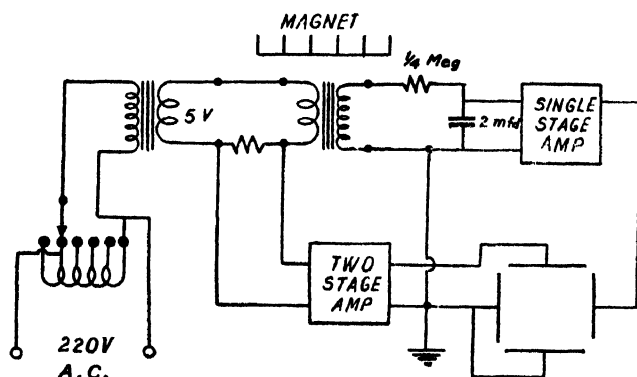
FIG. 10

Experimental arrangement for obtaining the hysteresis loops on an oscillograph.

* Sanford, R. L. Magnetic Testing, Circular of the National Bureau of Standards C 456.

OSCILLOGRAPHIC STUDY OF HYSTERESIS LOOPS

The experimental set up for an oscillographic study of the hysteresis loops with and without D.C. magnetization is indicated in Fig. 10. Sample No. 1—the saturable core transformer, sample No. 2—and sample No. 4 were subjected to this study. The saturable core transformer did not require the external magnet for D.C. magnetization which was effected simply by passing a D.C. current through the D.C. winding. With sample No. 4 D.C. magnetization was effected by passing a D.C. current through a third winding by means of a Pentode valve as in Fig. 1. Oscillograms of hysteresis loops for sample No. 2 are given in Plates IX A and IX B. They indicate the general nature of the phenomenon for silicon steels. The oscillograms were taken with a Cossor double beam oscillograph model 339A on Kodak blacktone bromide I, 15 plates. The straight line by the side of each loop is the trace of the second beam of the double beam tube which automatically trace out a line parallel to the B-axis. The slope of the straight line connecting the tips of the hysteresis loops with this line gives a ready idea of the A.C. permeability.

A critical study of the oscillograms reveals the following facts :—

(1) The hysteresis loops are symmetrical whether they are with or without D.C. magnetization.

(2) The angle of inclination of the straight line joining the tips with the B-axis is greater with a D.C. magnetization and is independent of the direction of magnetization.

(3) Even for quite small values of A.C. magnetization the tips of the loops are appreciably bent towards the direction of the H-axis. This bending of the tips of the small hysteresis loops becomes more pronounced with a D.C. magnetization.

CONCLUSION

The results of the measurements show that the variation of A.C. permeability at constant A.C. flux-density with D.C. magnetization of silicon steel sheets follow more or less closely a law which may be enunciated as "The inverse of A.C. permeability at constant A.C. flux-density varies linearly with the D.C. magnetization." Further the magnitude of the A.C. permeability becomes smaller and the variation more rapid as the A.C. flux-density diminishes. The oscillographic study of the hysteresis loops gives the following informations :—

(1) The hysteresis loops are symmetrical and have greater inclination with the B-axis with a D.C. magnetization which is independent of the direction of magnetization.

(2) Even for quite small values of A.C. magnetization, the tips of the loops are visibly bent towards the direction of the H-axis and this bending of the tips of the hysteresis loops is more pronounced with a D.C. magnetization. This latter information differs from the impression that may be gathered from text-books* dealing with the subject. The figures drawn in these text-books give the impression that there is no bending of the tips of the small hysteresis loops. The appreciable bending of the tips of the hysteresis loops mean that the no-load current of a transformer or choke employing these silicon steel sheets contain appreciable amounts of odd harmonics, even when operating at a small A.C. flux-density and that the amount of these odd harmonics increases with D.C. magnetization.

A knowledge of the variation of A.C. permeability with D.C. magnetization is necessary in the design of chokes and transformers which must carry a D.C. current. Assumption of the simple relation of variation which has been established here will enable the designer of these apparatus to make paper designs more easily and quickly. The bending of the tips of small hysteresis loops indicate that the output transformers and chokes of audio-frequency amplifiers do introduce appreciable distortion in the form of odd harmonics even when operating at a small A.C. magnetization and that this distortion increases with a D.C. magnetization. For reduction of these distortions it is not only necessary that the cores of these transformers operate at an A.C. flux-density much smaller than the usual 10, 000 gauss for power transformers, but that the no-load current be considerably smaller compared to the load current. In case there is a D.C. magnetization produced due to the flow of a D.C. current in one of the windings, an air gap must be introduced and it is recommended that it may profitably be somewhat greater than what may be necessary to secure the maximum inductance.

ACKNOWLEDGEMENT

REFERENCE

Banerjee, B. M and Mukherjee, A (1947), *Ind. Jour. Phys.*, **21**, 90.

* Terman, F. E Radio Engineering Handbook.

PARAMAGNETISM OF SINGLE CRYSTALS OF THE SALTS OF THE IRON GROUP OF ELEMENTS AT LOW TEMPERATURES. PART II. INVERSION OF THE STARK-PATTERNS FOR SIX-COORDINATED Ni^{++} AND Co^{++} IONS AND FOR FOUR AND SIX-COORDINATED Co^{++} IONS

By AKSHAYANANDA BOSE

ABSTRACT. The present paper deals with the magnetic behaviour of the salts of the Co^{++} ion which is in the $^4F_{9/2}$-state. It is well known that though both the Ni^{++} and the Co^{++} ions have F-ground states, there is a fundmental difference in the magnetic behaviours of their salts having similar structures. It is a particularly striking achievement of the crystalline field theory of Van Vleck, Penney and Schlapp, Goiter and others that it gives a simple explanation of the behaviour of the salts of Ni^{++} and Co^{++}. It is shown (a) that *in a given field* the Stark-pattern of the ground state of the Co^{++} ion is inverted with respect to that of Ni^{++} ion ; (b) that for octahedrally six-coordinated Ni^{++} salts the lowest lying state in the Stark-pattern is a singlet, whereas, for similar Co^{++} salts it is a triplet and (c) that as one passes from octahedral six-coordination to tetrahedral four-coordination the potential of the electric field at the central paramagnetic ion changes sign from positive to negative, which is equivalent to an inversion of the Stark-pattern. From this point of view it is evident that the six-coordinated cobalt salts studied here should show a complicated behaviour as against the simple behaviour of similar nickel salts dealt with in Part I of this paper. Further, the four-coordinated blue cobalt salt Cs$_2$CoCl$_4$ studied here should behave very similarly to the six-coordinated Ni^{++} salts. Temperature variation of the anisotropy and the effective moments of all these salts have been studied between 300°K and 80°K. The blue cobalt salt due to its similarity with nickel salts forms suitable material for calculating the spin-orbit coupling constant for Co^{++} ion, which agrees well with the spectroscopic value. The crystalline field constants for the blue cobalt salt have also been calculated and are found to be of nearly the same order of magnitude as in Ni^{++} salts and independent of temperature. The results for the six-coordinated cobalt salts serve to elucidate many of the obscure facts regarding the crystalline electric fields acting in these salts.

INTRODUCTION

In Part I of the present paper (Bose, 1948) we gave a general outline of the theory of the crystalline electric fields of Van Vleck (1932), Bethe (1932) and others and also some experimental results on the F-state ions Ni^{++} and Cr^{+++}, which are marked for their simplicity of behaviour and hence formed very suitable materials for a quantitative discussion on the merits of the theory. It was pointed out there, how even the nicer details of the theory, such as the small deviations from the Curie Law of the principal suscep-

TABLE I

For Principal Anisotropies of Crystals.

Cs_2CoCl_4; Orthorhombic; $a:b:c = 0.38:1:0.55$

(1) 'b' axis vertical, 'a' axis along the field.
(2) 'a' axis vertical, 'b' axis along the field.

Temp°K	$X_3 - X_2$ $\times 10^6$	$X_1 - X_3$ $\times 10^6$
297.1	327.0	254.0
280	413.9	268.0
260	449.8	291.3
240	497.1	315.1
220	543.0	348.0
200	601.9	382.1
180	676.4	432.8
160	769.8	492.3
140	898.9	577.6
120	1090.0	704.1
100	1373.0	890.6
90	1580.0	1014.0
83.8	1760.0	1126.0

$CoSO_4(NH_4)_2SO_4, 6H_2O$; Monoclinic; $\beta = 106°54'$; $a:b:c = 0.7392:1:0.4985$

(1) 'b' axis vertical.
(2) (001) plane horizontal, 'b' axis normal to field.

Temp°K	Angle between 'a' axis & X_2 axis $=\theta$	$X_1 - X_2$ $\times 10^6$	$X_1 - X_3$ $\times 10^6$
303.1	60	3023	1559
280	60	3604	1874
260	60	4204	2212
240	60	4922	2621
220	59.5	5794	3165
200	59	6880	3870
180	59	8241	4717
160	59	10080	5842
140	58.5	12600	7473
120	58	15950	9572
100	58	19960	12070
90	58	22150	13460
84.7	58	23380	14260

$CoSO_4K_2SO_4, 6H_2O$; Monoclinic; $\beta = 104°51'$; $a:b:c = 0.7404:1:0.5037$

(1) 'b' axis vertical.
(2) 'a' axis vertical, 'b' axis normal to field.

Temp°K	Angle between 'a' axis & X_2 axis $=\theta$	$X_1 - X_2$ $\times 10^6$	$X_1 - X_3$ $\times 10^6$
303.1	30.5	2532	1832
280	30.5	3015	2210
260	30.5	3478	2615
240	30.0	4038	3040
220	29.5	4709	3563
200	29.0	5521	4206
180	28.5	6563	5021
160	28.5	7863	6128
140	28.5	9638	7551
120	28.5	12030	9334
100	28.5	15340	11570
90	28.5	17580	12770
82.4	28.5	18500	13720

$CoBeF_4(NH_4)_2BeF_4, 6H_2O$; Monoclinic; $\beta = 106°46'$; $a:b:c = 0.740:1:0.485$

(1) 'b' axis vertical.
(2) 'a' axis vertical, 'b' axis along the field.

Temp°K	Angle between 'a' axis & X_1 axis $=\theta$	$X_1 - X_2$ $\times 10^6$	$X_1 - X_3$ $\times 10^6$
299.1	54.9	2930	1586
280	51.9	3324	2144
260	54.9	3809	2574
240	54.6	4402	3142
220	53.5	5140	3886
200	52.2	6053	4795
180	51.2	7216	6006
160	50.5	8690	7579
140	49.9	10830	9872
120	48.9	13750	12850
100	48.4	17210	15370
91	48.4	19250	18380
86.8	48.4	19930	19000

A. Bose

tibilities, the temperature variation of the anisotropies, the prediction of the strength of spin-orbit coupling, the great constancy of the crystalline electric fields and so on, were fully corroborated by our experimental results. The present paper deals with the Co^{++} ion which also is in an F-state and though the interpretation of the results here are less quantitative, they are none-the-less startling, as verifying one of the most interesting features of the electric field theory, namely, the fundamental difference in the behaviour of the Ni^{++} and Co^{++} ions, though both are in the F-state, as also that of the same Co^{++} ion but differently coordinated.

The mode of experimental procedure and the treatment of the experimental data have been already described in earlier papers (Bose, 1948) and it would be enough to tabulate here (Tables I and II) the final values of the principal anisotropies $\chi_1 - \chi_2$ and $\chi_1 - \chi_3$, the values of the principal gm. ionic susceptibilities χ_1, χ_2 and χ_3 corrected for diamagnetism, and the values for the principal and the mean effective moments p_1, p_2 and p_3 in terms of Bohr magnetons, all within the range of temperatures $300°K$ and $80°K$. Figs. 1 to 4 are also given to follow these temperature variations more effectively.

TABLE II

For the gm. molecular principal susceptibilities and the squares of the effective magnetic moments (*Corrected for diamagnetism*).

Crystal	Crystal suspension and the direction along which the susceptibility is measured, i.e., the direction setting along field	Temp °K	$\chi_1 \times 10^6$	$\chi_2 \times 10^6$	$\chi_3 \times 10^6$	p_1^2	p_2^2	p_3^2	p^2
Cs_2CoCl_4.	'a' axis vertical, 'b' axis along field	296.8	8515	8373	8118	20.36	20.02	19.41	19.93
		182.7	13596	13355	12935	19.88	19.54	18.91	19.44
		83.8	29269	28635	27509	19.57	19.14	18.39	19.03
$CoSO_4 (NH_4)_2$ $SO_4, 6H_2O$	(201) plane vertical, 'b' axis horizontal, normal to (201) plane along field*	296.0	11564	8370	9915	27.57	19.95	23.64	23.72
		185.2	19112	11238	14631	28.49	16.76	21.82	22.36
		84.7	42510	19130	28250	29.00	13.05	19.28	20.44
$CoSO_4 K_2SO_4$, $6H_2O$.	'b' axis vertical, 'χ_1' axis along field.	296.6	11885	9218	9949	28.40	22.03	23.78	24.74
		171.1	20455	13347	14978	28.19	18.40	20.65	22.41
		82.4	40585	22085	26865	26.95	14.66	17.83	19.81
$CoBeF_4(NH_4)_2$ $BeF_4, 6H_2O$.	'b' axis vertical, 'χ_1' axis along field.	296.7	11250	8262	9554	26.89	19.74	22.83	23.15
		185.8	18670	11822	13069	27.94	17.69	19.55	21.73
		86.8	39610	19680	20550	27.70	13.76	14.37	18.61

* Angle $(001) : (20\bar{1}) = 64°$.

DISCUSSIONS

1. *The difference in the Stark-pattern of Ni^{++} and Co^{++} ions under the same type of electric field and its effect on their magnetic behaviours.*

If we consider the various ions of the iron group in which the number of electrons, n, in the $3d$ shell, increases progressively from 0 to 10, the spin quantum number S, as is well known from Hund's rule, is equal to $n/2$ in the first half of the group and to $(10-n)/2$ in the second half, *i.e.*, the spin quantum number increases from 0 to $5/2$ and then diminishes, reaching 0 at $n=10$. On the other hand, the orbital quantum number L of the ion has zero values not only for $n=0$ and $n=10$, but also for $n=5$ as can be seen from the table below.

TABLE III

No. of $3d$ electrons = n	0	1	2	3	4	5	6	7	8	9	10
Ground state	$^1S_0$	$^2D_{3/2}$	$^3F_2$	$^4F_{3/2}$	$^5D_0$	$^6S_{5/2}$	$^5D_4$	$^4F_{9/2}$	$^3F_4$	$^2D_{5/2}$	$^1S_0$
Ions	K^+, V^{+5}	Sc^{++}, Ti^{+3}, V^{+4}	Ti^{++}, V^{+3}	V^{++}, Cr^{+3}, Mn^{+4}	Cr^{++}, Mn^{+3}	Mn^{++}, Fe^{+3}	Fe^{++}	Co^{++}	Ni^{++}	Cu^{++}	Cu^+, Ca^{++}

It is assumed as before that with the crystalline electric fields involved in the *ionic salts* of these ions the coupling between L and S is broken down but not those between the different l's that compound into L or the different s's that compound into S. As is well known, under such circumstances the effect of the electric field will be to give rise to a Stark-splitting of the ground state of the ion corresponding to a complete or partial removal of the $(2L+1)$-fold orbital degeneracy of the ion without much affecting the spin degeneracy, which latter will be completely removed only on the application of a magnetic field. The degree of removal of degeneracy and in consequence the nature of Stark-pattern will evidently depend upon how strong and asymmetric the electric fields are.

For the usual type of the ionic salts of the iron group, the most simple yet satisfactory electric field is one of which the potential is expressed by

$$V = Ax^2 + By^2 - (A+B)z^2 + D(x^4 + y^4 + z^4) \qquad \ldots \quad (1)$$

where the fourth power terms represent a predominant cubic field on which is super-imposed a small rhombic field represented by the squared terms. Under such a crystalline field an F-state will, in general, split up into a Stark-pattern consisting of a singlet and two adjacent triplets, each level of which will, in general, suffer a partial removal of the spin degeneracy corresponding to the effect of the spin-orbit coupling and to the second order

Kramers splitting, except when the number of electrons in the incomplete 3d
shell is odd, so that a two-fold Kramers spin degeneracy will be always
left over. The separation due to the cubic field will be very large, of the
order of 10^4 cm^{-1}, compared to the rhombic separation.

It has been shown by Van Vleck (1932) that in the Stark-pattern for the
F-state ion under the above type of electric field, since the singlet level must
always lie on one side, it may either correspond to the highest or the lowest
value of the energy in the pattern. Which it is will be decided by the sign
of the cubic field constant D, in the expression (1). If the singlet level is
lowermost, since the triplets will be far removed from it, cubic separation
being of the order of 10^4 cm^{-1}, practically the singlet level alone will be
occupied at all ordinary temperatures.* Since this level retains almost all
its $(2S+1)$-fold spin degeneracy in the crystalline field, the ion will behave
very nearly like S-state ions, in having a feeble anisotropy, a nearly spin only
value of the effective moment, and a small deviation from Curie Law. On
the other hand when the triplet level is lowermost, the separation between the
components of the triplet, being produced by the feeble rhombic field, will be
comparable to kT, and the population of the *upper components of the lowest*
level will be quite appreciable. The magnetic behaviour in such a case will
therefore evidently be much more complicated.

In the ionic salts of the iron group of elements, the electric fields in the
neighbourhood of the paramagnetic ion may arise either due to a distribution
of four equal negatively charged ions at the corners of a tetrahedron, or due
to six equal negative charges at the corners of an octahedron. Görter
(1932) has shown that the sign of D, the cubic field constant in the expression
(1) for the potential due to these charges, is negative in the first case and
positive in the second. An X-ray examination of the disposition of the
negatively charged atoms round the paramagnetic ion will therefore serve to
decide uniquely the sign of D.

In the iron group of elements, where the number of electrons n in the
3d shell increases from 0 to 10 from the beginning to the end of the group,
any atom or ion with $n = x \leqslant 5$, will have the same orbital quantum number L,
as one for which $n = 5 - x$ or $5 + x$ or $10 - x$, (Van Vleck, 1932). Hence,
in a given cubic field, *i.e.*, with the sign and the value of D determined, all of
the ions will have exactly the same Stark-pattern, except for the fact that
the patterns for some of the ions will be inverted with respect to those of the
others, and knowing the Stark-pattern for one, those for the others may be
uniquely determined. If we regard the pattern for $n = x$ as erect, then the
pattern for $n = 5 + x$, will also be erect, whereas the patterns for $n = 5 - x$ and

---

* In the final considerations, however, the populations of the upper levels cannot be
neglected and the contribution of these levels to the total magnetization, which is quite
appreciable, will come through the so called temperature independent "high frequency"
terms.

10 − x will be inverted. For example, if we regard the pattern for Cr^{+++} with $n = x = 3$, erect for a given sign of D, the pattern for Ni^{++} with $n = 8$, will also be erect, but those for Ti^{++} with $n = 2$, and Co^{++} with $n = 7$, will be inverted. Though it does not seem possible to decide from *a priori* considerations, whether in a cubic field with positive D, say, an *F*-state ion like Cr^{+++} will have its singlet level lowermost or uppermost, still it is possible to make this decision from other considerations; for example, from the magnetic behaviour of salts in which the distribution of the negative charges around the Cr^{+++} ion is known from X-ray data and hence the sign of D. In all the Tutton salts and in the hydrated sulphates, selenates, oxalates, etc., the distribution is known from X-ray data to be of the octahedral type, and hence D should be positive in these salts. The characteristics found in the magnetic properties of Cr^{+++} salts of this type, namely, the close conformity to the spin only value and to the Curie Law, and the low magnetic anisotropy, even when the crystal is not cubic, show that in these salts the singlet level should be the lowermost in the Stark-pattern of Cr^{+++}. *If we agree to call the Stark-pattern of the F-state ions erect when the singlet level is lowermost,* then we can conclude from the magnetic data for Cr^{+++}, that in a cubic field with positive D, the pattern for Cr^{+++} should be erect; from which using the inversion rule deduced above, we conclude that in the same field the pattern should be erect for Ni^{++} as well, but inverted for Co^{++} salts. The magnetic properties of both Ni^{++} and Co^{++} salts of the above type do confirm this conclusion.

2. *Simple magnetic behaviour of four-coordinated ionic Co^{++} salts as related to the inversion of the Stark-patterns.*

Now, since a change in the sign of D, from positive to negative or *vice versa*, will produce an inversion of the pattern (Van Vleck, 1932) we may conclude that when D has a negative sign, as will be the case when the distribution of the negative charges is tetrahedral, the pattern for Co^{++} will become erect, whereas the patterns for Cr^{+++} and Ni^{++} will be inverted. No four-coordinated ionic salts of trivalent chromium are known and the four-coordinated salts of Ni^{++} that are known are found to be square-coordinated and covalently, and are therefore diamagnetic. Ionic salts of Co^{++}, however, are available in which a tetrahedral four-coordination is known to occur, *e.g.*, the blue double chlorides Cs_2CoCl_4 and Cs_3CoCl_5. The structures of these two crystals have been analysed by X-ray methods by Powell and Wells (1935) and they find that each cobalt ion is surrounded by four negatively charged chlorine atoms, which occupy the corners of a tetrahedron, with the Co^{++} ion at the centre. Both these salts have been studied magnetically at room temperature by Krishnan and Mukherji (1938) and are found to have a much feebler anisotropy, about 4 to 6%, and the effective magnetic moments are much closer to

the 'spin only' value, than in the ordinary cobalt salts in which the Co^{++} ion is six-coordinated.

We have studied the temperature variation from room temperature down to 80°K, of the anisotropies and of the principal susceptibilities of one of them, namely, Cs_2CoCl_4 which is ortho-rhombic. The results obtained can be discussed in relation to the splitting of the energy levels in the crystalline field in the same manner as in octahedrally coordinated Ni^{++} and Cr^{+++} salts (Bose, 1948), to which the double chlorides of cobalt are analogous. The values of the three field constants α's for this crystal, calculated from the magnetic data, are given in the following table : —

TABLE IV

For the values of the crystal field constants
α_a, α_b and α_c for Cs_2CoCl_4

Temperature °K	$-\alpha_a \times 10^6$	$-\alpha_b \times 10^6$	$-\alpha_c \times 10^6$
296 8	200.7	191.1	171.0
182 7	205.7	195.5	177.8
83.8	211.3	200.8	182.2

It is remarkable that the α's are of nearly the same magnitude as in six-coordinated Ni^{++} salts (*loc. cit.*). Here again the α-values remain unaffected by changes of temperature, as is to be expected.

The effective magnetic moment along the χ_a axis say, will be given by the expression,

$$p_a{}^2 = p_0{}^2 \left[1 - 3kT\alpha_a + 8\lambda\alpha_a + \frac{\Delta_a\lambda^2}{kT} \right]$$

which, using the values of α above and the spectroscopic value of λ for $Co^{++} = -180$ cm^{-1}, becomes

$$= 15(1 + .1280 + .2966 + .0040) = 21.43$$

and similarly, we have

$$p_b{}^2 = 15(1 + .1217 + .2819 + .0008) = 21.07$$
$$p_c{}^2 = 15(1 + .1106 + .2564 - .0048) = 20.43$$

(3)

all at room temperature 297°K. The relative importance of the terms is thus roughly the same as for the six-coordinated nickel salts. The theoretically calculated values for the magnetic moments agree with the experimental values which are shown in Table II and Fig. 1. Here again as in nickel one can, using the measurements of the magnetic anisotropies at different temperatures, calculate the constant of the spin-orbit coupling λ, which agrees with the spectroscopic value of λ given above, as is evident from the data in Table V. These data further corroborate the already mentioned fact that the crystal field constants remain practically independent of temperature.

FIG. I
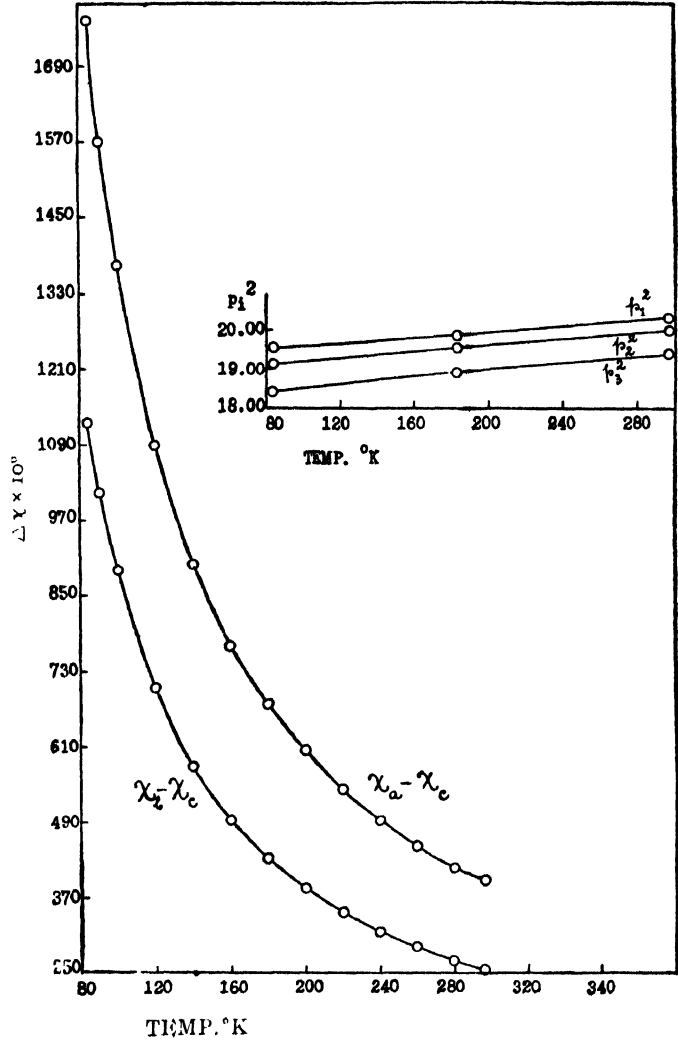
Temperature variation of principal anisotropies and
effective moments: Cs_2CoCl_4

TABLE V

For values of the ratio of $\Delta\chi$ at temperatures T
to that at room temperature (297.1°K)

Temperature°K.	$\lambda = -2.0$ cm^{-1}, Ratio obtained from		
	Calculation	$\chi_a - \chi_c$: Obs.	$\chi_b - \chi_c$: Obs.
297.1	1.000	1.000	1.000
263	1.140	1.133	1.113
200	1.500	1.516	1.504
160	1.933	1.939	1.938
100	3.504	3.459	3.506
83.8	4.472	4.433	4.433

3. *Complicated behaviour of the six-coordinated Cobalt salts.*

In the ordinary salts of cobalt like the hydrated sulphates, selenates, etc. in which the Co^{++} ion is octahedrally six-coordinated, the cubic field constant D will be positive, unlike in the blue cobalt salts considered previously and hence the singlet level will be the uppermost, whereas, the triplet level the lowermost in the Stark-pattern of the Co^{++} ion in the former crystals. With such a disposition of the Stark-pattern in which the lowermost level is a triplet, whose components have been separated to extents comparable with kT, by the rhombic part of the field, and the spin degeneracy of each component also slightly removed through the spin-orbit coupling, the calculation of the principal susceptibilities in terms of the crystalline field constants becomes complicated and laborious.

An approximate calculation, however, has been made by Penney and Schlapp (1932) on the simplifying assumption that $B = 0$ in the expression (1), so that $C = -A$, and further that D_q the cubic field constant used by Penney and Schlapp instead of D, is ~ 1200 cm^{-1}; nearly the same as in the nickel salts having similar coordination. They have made these calculations of the principal susceptibilities for two limiting cases for which $A = 40$ corresponding to a small value of rhombic field and $A = 200$, a very high rhombic field. For the first value, all the squares of the three principal moments $p_1{}^2$, $p_2{}^2$, $p_3{}^2$ are found to fall with lowering of temperature, slowly at first and rapidly at low temperatures. For the second value, $p_2{}^2$ and $p_3{}^2$ are found to diminish as before, whereas, $p_1{}^2$ rises slowly at first but rapidly at lower temperatures, reaching a maximum at very low temperatures. The theoretical curves for $p_1{}^2$, $p_2{}^2$, $p_3{}^2$, obtained by them for these two rhombic fields are given in their paper referred to above and are reproduced here in Figs. 5 and 6.

Experimentally, Bartlett's measurements (1932) on the principal susceptibilities of cobalt ammonium sulphate from $+50°C$, to $-25°C$, show a small rise in $p_1{}^2$, with lowering of temperature and appear to conform to the latter-field in this respect rather than to the former. On the other hand, there are serious difficulties, as pointed out by Penney and Schlapp, in accepting such a high rhombic field, as it leads to too high an anisotropy and too low values for the effective moments to fit with Bartlett's experimental results. For these and other considerations Penney and Schlapp are in favour of an intermediate value of the rhombic field, closer to the first than to the second.

Our present measurements extend to much lower temperatures than Bartlett's. They confirm the small increase in the $p_1{}^2$ values by Bartlett in cobalt ammonium sulphate, and a similar rise is observed also in cobalt ammonium fluoberyllate. In the crystal of cobalt potassium sulphate, however, the value shows a small fall instead of a rise (See Figs. 2 to 4).
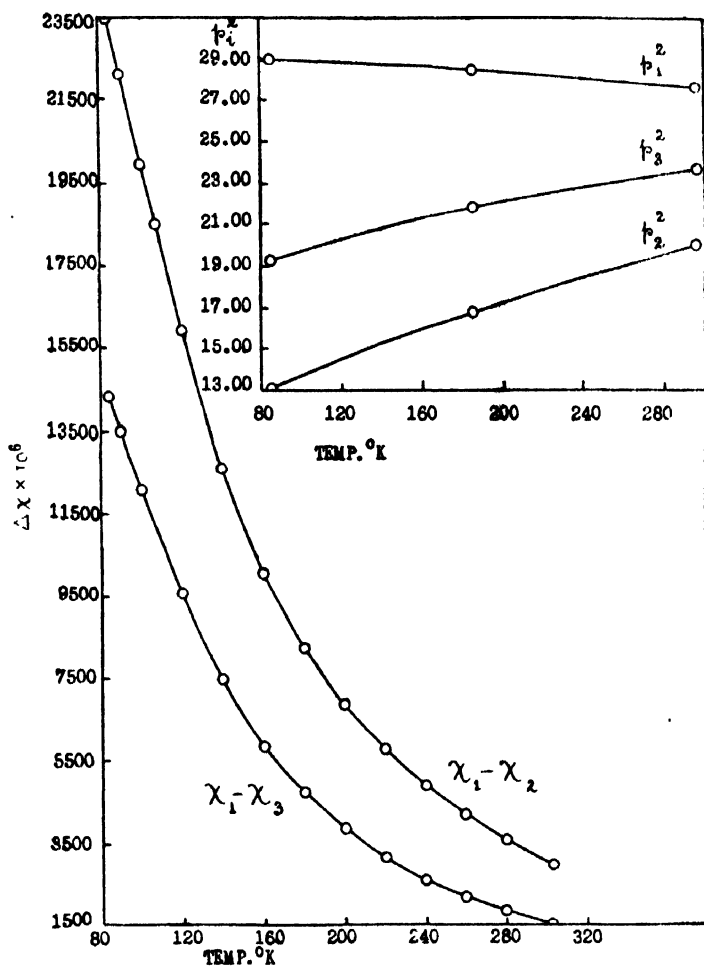
FIG. 2

Temperature variation of principal anisotropies and effective
moments : $Co(NH_4)_2(SO_4)_2, 6H_2O$

Since the crystalline fields in all the three crystals should be more or less
similar, one should not attach too much importance to the small rise in the
p_1^2 values in the two ammonium salts, in making the choice of the rhombic
part of the field. Apart from the difficulties pointed out by Penney and
Schlapp in choosing a high rhombic field, our low temperature values for the
three principal magnetic moments rule out the high rhombic field altogether.
Even a casual examination of the experimental results compared with
the theoretical values will convince one of this. To emphasise the point we are
giving below the experimental values for p_1^2, p_2^2 and p_3^2 at 80°K for
comparison with the theoretical values calculated from the two fields. The
observed values fit fairly closely with the lower rhombic field and in any case
completely rule out the higher field.
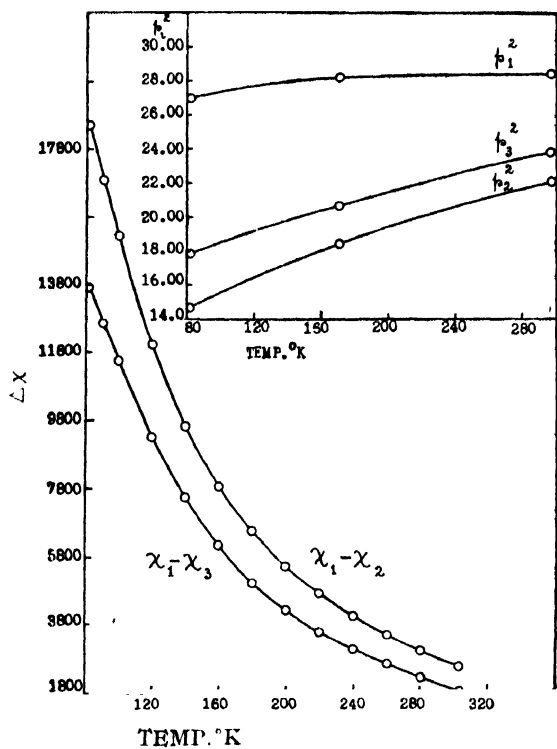
FIG. 3

Temperature variation of principal anisotropies and
effective moments. $CoK_2(SO_4)_2, 6H_2O$

TABLE VI

For observed and calculated values of p_1^2, p_2^2 and p_3^2 at $80°K$

Squares of principal moments		p_1^2	p_2^2	p_3^2
Observed	$CoSO_4(NH_4)_2SO_4, 6H_2O$	29.1	12.9	19.1
	$CoSO_4K_2SO_4, 6H_2O$	26.0	14.5	17.7
	$CoBeF_4(NH_4)_2BeF_4, 6H_2O$	27.9	13.1	13.9
Calculated	$\Lambda = 40$.	28.2	10.7	17.0
	$\Lambda = 200$.	41.0	1.8	16.6

We have further evidence in support of this choice from the measurements
made by Jackson (1924) on the magnetic anisotropies of cobalt ammonium
sulphate, which extend down to $14°K$. The magnetic data as given by
Jackson are however so improbable that Penney and Schlapp have been forced
to reject them altogether. Since then, however, an error has been found in
Jackson's calculation by Krishnan, Chakravorty and Banerji, (1933). On
correcting for this error it is found that in the temperature range overlapping
ours the values for the principal magnetic moments for cobalt ammonium
sulphate agree very well with our own, and hence we may presume that at
lower temperatures also, the recalculated values of Jackson are more or less
correct, The values of p_1^2, p_2^2 and p_3^2 for cobalt ammonium sulphate,
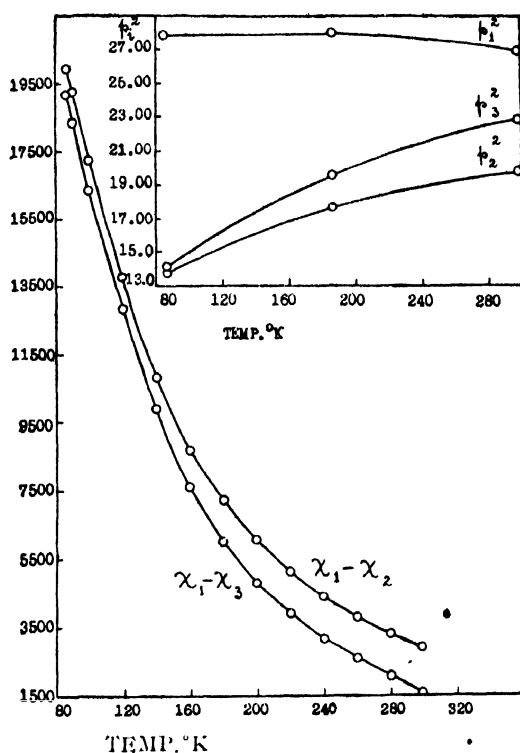
FIG. 4

Temperature variation of principal anisotropies and effective
moments: $Co(NH_4)_2(BeF_4)_2, 6H_2O$

TABLE VII

For effective magnetic moments of $CoSO_4(NH_4)_2SO_4, 6H_2O$ at different
temperatures by different workers.

Author	Temp°K	p_1^2	p_2^2	p_3^2
	328	28.19	21.37	25.13
	293	29.06	20.77	25 25
Bartlett	276	--	—	25.20
	269 5	29.29	20.49	—
	262	—	—	25.14
	253	29 72	20.19	25.37
	290	26.88	19.72	22.92
	77.2	27 71	11.65	18.84
Jackson	20.3	23.96	8.314	14.63
	16.7	24.00	7.508	11 34
	14 5	23.45	7.276	13.91
Present Author	296.0	27.57	19.95	23.64
	185.2	28.49	16.76	21 82
	84.7	29.00	13.05	19 28
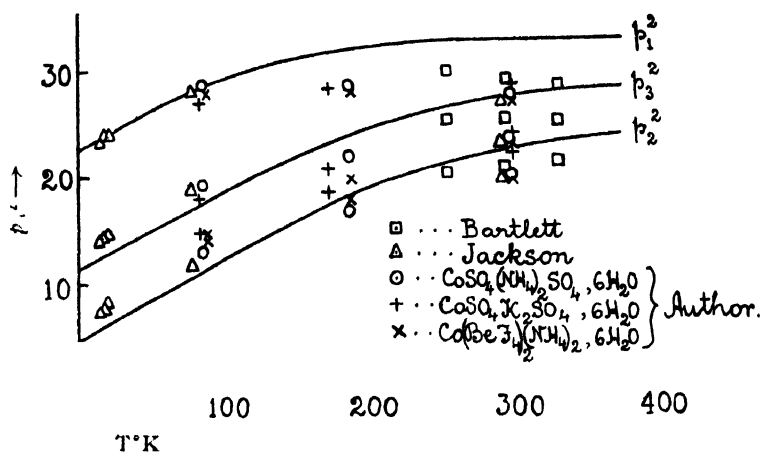
FIG. 5

Rhombic field small, A = 40
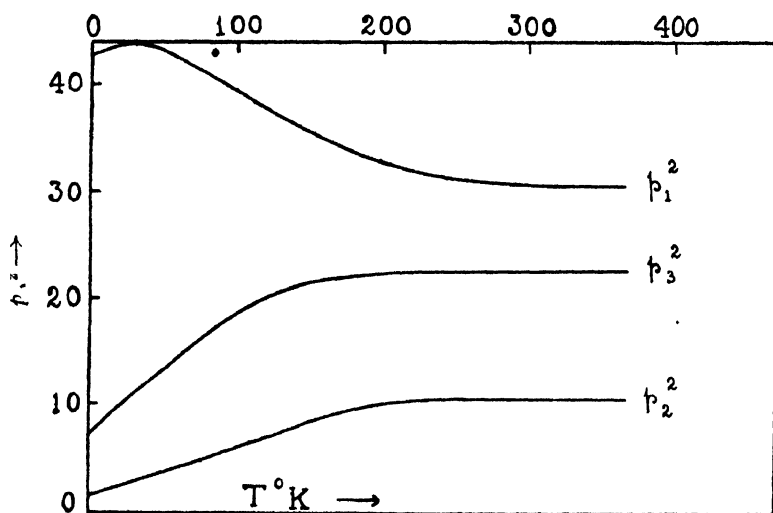
FIG. 6

Rhombic field large, A = 200

recalculated from Jackson's data, along with Bartlett's and author's data are given in Table VII and are further plotted in Fig. 5 for comparison. They agree well in the temperature ranges where they overlap. Thus Jackson's low temperature values also rule out completely the higher rhombic field and are in favour of the lower field.

Even when the most suitable value of A, has been selected, it is not to be expected, however, that the agreement between the theoretical and the experimental values will be close, when we remember that in Co^{++} the influence of the rhombic part of the field is very large. There are two reasons for this.

The choice of the rhombic field for discussion (Penney and Schlapp, loc. cit.) was guided by considerations of simplicity in calculation. The expressions for the principal susceptibilities besides depending on D_q,

involves in a complicated manner the two rhombic field constants $\sigma = \frac{1}{3}(A + B)$ and $\delta = \frac{1}{3}(A - B)$. Special choice by Penney and Schlapp of these constants amount to $\sigma = \delta = 20$ or 100, for the two limiting cases discussed above. These discussions may be regarded as merely demonstrating that σ and δ are of the order of 20. Any attempt at a closer fit with experimental data should aim now at finding the proper value of σ and δ *separately*, rather than find values for $\sigma = \delta$ other than 20, which would give a better fit, since no value of σ, if it is to be taken as equal to δ, can be expected to give a close fit.

There is another reason and a strong one, which would make even such attempts futile with our present incomplete knowledge of the fine structure of these crystals. The theoretical calculations were made on the tacit assumption that the electric field axes, associated separately with all the ions in the unit cell, are respectively parallel to each other, which is not generally true. The Tutton salts of cobalt contain two Co^{++} ions in the unit cell and are monoclinic, the principal axes of one of the ions thus being the mirror reflections of those of the other ion, in the (010) plane. Denoting the principal magnetic moments of the *ion* by P_1, P_2, P_3 respectively, to distinguish them from principal moments for the *crystal* p_1, p_2, p_3 it can be readily seen that

$$p_1^2 = P_1^2 \alpha_1^2 + P_2^2 \beta_1^2 + P_3^2 \gamma_1^2$$
$$p_2^2 = P_1^2 \alpha_2^2 + P_2^2 \beta_2^2 + P_3^2 \gamma_2^2$$
$$p_3^2 = P_1^2 \alpha_3^2 + P_2^2 \beta_3^2 + P_3^2 \gamma_3^2$$

$$\qquad \dots \quad (4)$$

where $\alpha_1, \alpha_2, \alpha_3$, are the direction cosines of P_1 ; $\beta_1, \beta_2, \beta_3$ of P_2 ; and $\gamma_1, \gamma_2, \gamma_3$ of P_3 respectively, with reference to the p_1, p_2, p_3 axes for the *crystal* as a whole. The theoretical calculations of Penney and Schlapp refer to P_1^2, P_2^2 and P_3^2 which, as will be seen from the expression given above, are not the same as p_1^2, p_2^2 and p_3^2 respectively. Unless we know the direction cosines defining the orientations of the three field axes associated with one of the paramagnetic *ions* in the unit cell, with reference to the three principal axes associated with the *crystal, i.e.*, in the absence of a detailed knowledge of the dispositions of the atoms surrounding the two paramagnetic ions, we cannot calculate the P's from the observed p's and hence cannot attempt the calculation of the field constants A and B.

These considerations thus also supply an explanation of the variation of the magnetic behaviour from crystal to crystal of the cobalt salts as observed experimentally (see Table II) ; since even if the field in the neighbourhood of the paramagnetic ions, which determines the P's are exactly the same in all the three crystals—not only as regards the cubic part but also the rhombic part—the relative orientations of the two paramagnetic groups in the unit cell may not be the same in the different crystals. Conversely, the observed fact that p_1^2 curves of the three cobalt salts differ from one another slightly, or the p_2^2 curves or the p_3^2 curves, should not be regarded as necessarily indicating a difference in the crystalline fields in the three crystals.

Though it is tempting to do so, such an explanation would be trivial, since we know definitely that the α's, β's and γ's should vary from crystal to crystal, as evidenced by the χ_j direction being different in the three salts. The variation of the α's, β's and γ's alone should be sufficient to produce all the observed differences in the curves for p_1^2 or p_2^2 or p_3^2 of these salts, since, the temperature variations of P_1^2, P_2^2 and P_3^2 for the cobalt ion in a given field are so different from one another.

INDIAN ASSOCIATION FOR THE CULTIVATION OF SCIENCE
210, BOWBAZAR STREET, CALCUTTA

REFERENCES

Barttlett, B. W , 1932, *Phys. Rev* , **41**, 818.

Bethe, H., 1929, *Ann. der. Phys.*, **3**, 133.

Bose, A., 1947, *Ind. Jour Phys.*, **21**, 277.

————— 1948, „   „   „   **22**, 76.

————— 1948, „   „   „   **22**, 195.

Görter, C. J , 1932, *Phys. Rev.* **42**, 437.

Jackson, L. C., 1924, *Phil. Trans. Roy. Soc. (A)*, **224**, 1.

Kramers, H., 1929, *Proc. Amster. Acad.*, **32**, 1176.

Krishnan, K S. and Mukherjee, A., 1938, *Phil. Trans Roy. Soc. (A)* **237**, 135.

——— ——— ——— and Bose, A., 1939, *Phil Trans. Roy. Soc (A)*, **238**. 125.

——— Banerjee, S. and Chakravorty, N C., 1933, *Phil. Trans Roy Soc (A)*, **232**, 99

Penney, W. G. and Schlapp, R., 1932, *Phys. Rev.*, **42**, 666.

Powell, H. M. and Wells, A F., 1935, *Jour. Chem. Soc.*, 359

Van Vleck, J. H , 1932, *Phys. Rev.*, **41**, 208.

Van Vleck, J. H., 1932, The Theory of Electric and Magnetic Susceptibilities *(Oxford)*

TOMMOROW'S INSTRUMENTS TODAY

RAJ-DER-KAR & CO.

COMMISSARIAT BUILDING

HORNBY ROAD

FORT

BOMBAY

OFFERS

FROM STOCK

GLASS METAL DIFFSION PUMPS, METAL BOOSTE
PUMPS OILS AMOILS OCTOILS OCTOIL,
BUTYL SABACATE

MANUFACTURED

By

DISTILLATION PRODUCTS
(U. S. A.)

SPENCER MICROSCOPE

CENCO HIGHVACS

BESLER EPIDIASCOPE

COMPLETE WITH FILM STRIP ARRANGEMENTS

Telephone 27304   Telegrams
    2 Lines   TECHLAB

CONTENTS

NOTICE
TO INTENDING AUTHORS

Manuscripts for publication should be sent to Mr. A. N. Banerjee, Assistant Editor, 210, Bowbazar Street, Calcutta.

The manuscript of each paper should contain in the beginning a short abstract of the paper.

All references to published papers should be given in the text by quoting the surname of the authors followed by the year of publication within braces, *e.g.*, Sen (1942). The actual references should be given in a list at the end of the paper according to the following specimen :

> Sen, B. K., 1942, Volume rectification of crystals, *Ind. J. Phys.*, **16**, 329

The references should be arranged alphabetically in the list.

All diagrams should be drawn on thick white paper in Indian ink, and letters and numbers in the diagrams should be written in pencil.

A STUDY OF THE ENERGY DISTRIBUTION OF SCATTERED X-RADIATION *

By HIRENDRA KUMAR PAL

ABSTRACT. An attempt has been made in this paper to study the intensity distribution of X-radiation scattered from various substances. Employing heterogeneous primary radiations extending over a wide range of wavelengths and making proper corrections, the ratio I_ϕ/I_{90} (where $I\phi$ means the intensity of the scattered radiation in a direction making an angle ϕ with the primary beam) has been determined experimentally for various angles from $\phi = 20°$ to $150°$. It has been found that in the backward direction the intensity of scattering from different substances agrees closely with that given by the quantum theory of Dirac, whereas in the forward direction, the observed scattering is complicated by interference effects.

INTRODUCTION

The energy distribution of the scattered X-radiation has been the subject of investigation for a long time past, and many theoretical as well as experimental investigations have been conducted.

Barkla (1908), and Barkla in collaboration with Ayres (1911), Owen (1911), and Crowther (1911), studied the energy distribution of scattered X-radiation for different radiators and different angles and they found that the experimental value $I\phi/I_{90}$ was in general agreement with the classical value $(1 + \cos^2\phi)$, except in the forward direction within a range of the order of $\phi = 30°$, in which case a marked preponderence over the classical value was observed, which they termed as "excess scattering." With a very hard radiation and a thin radiator of filter paper Owen (1911), obtained good agreement with the classical theory in the forward direction too. Barkla noticed a reduction in the value of I_{170}/I_{90} from 2 to 1.5 by increasing the hardness of the incident beam.

About a decade later Hewlett (1922) experimented upon the X-radiation scattered by solids such as carbon and lithium and liquids such as benzene, mesitylene and octane. For solids, the scattering curves depicted a number of maxima and minima, explained as due to interference, while for liquids there was only one maximum with indications of others unresolved. Prior to Hewlett, similar indications of interference of scattered X-rays from solid powders was simultaneously obtained by Debye and Scherrer (1917) and by Hull (1917).

---

* This forms a part of the subject matter of the thesis submitted and approved for the Ph.D. Degree of the Edinburgh University in 1937. This delay in the publication of the paper is due to some unavoidable circumstances.

Shortly after this, newer conceptions about the relation between waves and quanta began to develop. Breit (1926), Dirac (1926), Born and Waller (1928), and Gordon (1926) made theoretical approach to the subject and based their calculations on different methods and principles. They arrived at an identical expression for the scattered intensity which is given by

$$I_\phi = I_s \left(1 + \frac{h\nu}{mc^2} \text{ vers } \phi \right)^{-3},$$

where I_s = corresponding classical scattered intensity due to a single free electron, the other symbols having their usual significance. Klein and Nishina (1928) on the other hand, obtained a slightly modified scattering function on the hypothesis of electron spin. Another scattering function which was derived by Compton (1930) reads as

$$I_\phi = I_s \left\{ F^2 + \left(Z - \frac{F^2}{\sim} \right) \cdot 1 + \frac{h\nu}{mc^2} \text{ vers } \phi \right.$$

where $F = \int_0^\infty U(r) \cdot \frac{\sin kr \cdot dr}{kr}$, and $k = \frac{4\pi}{\lambda} \sin \phi/2$.

Woo (1931) subsequently introduced a correction term e^{-2M} in the expression of Compton to take account of the effect of temperature on scattering.

The above theoretical results, founded on the new wave mechanical conception gave a fresh incentive to reinvestigate the subject of the intensity distribution of scattered X-rays in all its bearings. Jauncey and Harvey (1931), and Coven (1931) reported a general agreement with the Dirac theory for angles not far from $\phi = 90°$. But Coven observed that in the forward direction, for angles $\phi = 30°$ to $60°$ the experimental ratio I_ϕ/I_{90} was below that predicted by the Breit-Dirac theory ; whereas Backhurst (1934) noticed an excess over the theoretical value in these directions—although the agreement with Dirac's theoretical value was satisfactory for angles $40°$ to $150°$. Chilinski's (1932) work, on the other hand, indicated a distinct excess for the experimental values in both the forward and backward directions.

Khubchandani investigated the effect on the scattering function of a progressive increase in the hardness of the heterogeneous primary incident beam. He employed three different wave-lengths, .7, .49, and .31 Å. U. and observed for three different scatterers (paraffin wax, carbon and filter paper) that (*i*) in the forward direction, the ratio I_{30}/I_{90}, while invariably showing an excess over the classical value and also over the Breit-Dirac value in most of the cases, gradually diminished with the increasing hardness of the beam, tending to approach the classical value and (*ii*) in the backward direction, the ratio I_{150}/I_{90} were approximately (within about 3%) equal for paraffin wax and carbon but less than 1.75, the classical value, for all the 3 wavelengths used and the first two of these values, *viz.*, those corresponding to wavelengths .7 and .49 Å. U. were in satisfactory

agreement with the Breit-Dirac values. For filter paper, however, the ratio increased with the increasing hardness of the incident rays; the smallest one agreeing with the Dirac-value and the biggest one with that given by the classical theory.

The conflicting character of the experimental results of different authors (as narrated above) together with the fact that, as yet there seemed to have been published no regular and systematic work on the dependence of X-ray scattering on the incident wavelength, in the light of the new quantum mechanics, called for a fresh and systematic investigation along these lines. It was with the object, if possible, of securing a foundation of facts regarding the distribution of scattered radiation, that the research embodied in this paper was undertaken.

EXPERIMENTAL

Description of the apparatus.

The X-ray tube was a watercooled, hot cathode, self rectified one, of the Müller type. The anticathode was made of tungsten. The tube was supported on a specially constructed wooden stand which could be rotated about a horizontal axis passing through the anticathode spot and perpendicular to the direction of the cathode stream, so that, by turning the stand through a right angle, the cathode stream could be made horizontal or vertical as desired. The horizontal axis of rotation was also the central ray in the primary beam. A cylindrical lead tube served as the outlet for the primary beam of X-rays, the exposure of which was controlled by a lead shutter.
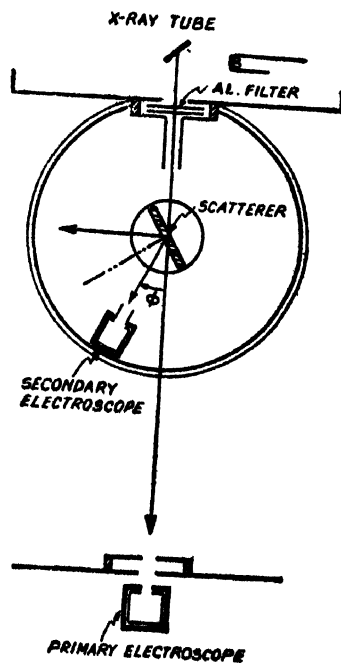
FIG. 1.

For measuring the intensity of X-rays the arrangement were of the usual type. Two gold-leaf electroscopes were used, one to standardise the primary beam and the other to measure the scattered secondary beam. The latter, on account of the comparatively feeble intensity of the scattered beam, was used in conjunction with a specially constructed ionisation chamber filled with the highly ionisable gas SO_2.

Five different scatterers were used, *viz.* (1) 70 sheets of filter paper, with a superficial density of each equal to .0064 gm/cm.^{2} (2) a paraffin sheet (thickness 1.8 cm.), (3) an aluminium sheet (thickness .8 mm.), (4) a carbon slab (thickness 6 m.m.), (5) a sulphur slab (thickness 1 m.m.).

Procedure

Heterogeneous primary radiations of various degrees of hardness were employed. They were obtained by first varying the applied H.T. by steps. from a minimum of 30 K. V. (peak) to a maximum of 100 K. V. (peak), and then progressively filtering with increasing thicknesses of aluminium.

When the X-ray tube had attained a steady condition at the proper voltage, the deflections of the secondary electroscope for $\phi = 90°$ and $\phi = \phi$ (say 30°) were alternately noted corresponding to a constant convenient deflection of the primary electroscope, the cathode stream being horizontal. The observations were repeated after turning the radiator through 180° and the mean of the values of $\delta\phi/\delta_{90}$ for the two cases taken. Any inequality of absorption in the two directions, by the material of the radiator was easily eliminated by following the method of Ayres and Barkla which requires the radiator to be placed so that the normal to its surface makes equal angles with the two directions.

Though the primary beam of X-rays was not monochromatic, yet an "equivalent or effective" wavelength could be assigned to each beam, defined by the wavelength of a homogeneous beam of X-rays which has the same mass-absorption coefficient $(\bar{\mu}/\rho)$ as for the heterogeneous complex beam in question,—a coefficient, determined arbitrarily from a 50% absorption in aluminium. The average or equivalent wavelength was obtained by interpolation from a calibration curve drawn with wavelength as abscissa and $(\bar{\mu}/\rho)$ as ordinate, the data for which were collected from "Spektroskopie der Rontgenstrahlen" by M. Siegbahn, page 231.

Corrections

The ratio of the observed deflections $\delta\phi/\delta_{90}$ does not give the real ratio of the intensities, $I\phi/I_{90}$ and certain corrections are to be applied, which are explained below :

(1) Correction due to stray effect :—A small fraction of the observed deflection $\delta\phi$ owes its origin to the combined effect produced by (a) scattering by air, (b) tertiary radiations (c) slight natural ionisation inside the electroscope, etc., and must therefore be subtracted from the observed deflection to get the real deflection. The correction was thus calculated.

Let $\delta\phi$ and δ_{90} be the observed deflections in a certain time, when the radiator is in position, and $a\delta\phi$ and $\beta\delta_{90}$ respectively, the corresponding deflections in the same time, when the radiator is removed. Then corrected

$$I\phi/I_{90} \cdot \frac{\delta\phi - a\delta\phi}{\delta_{90} - \beta\delta_{90}} = \frac{\delta\phi}{\delta_{90}} \cdot \frac{1-a}{1-\beta} = \frac{\delta\phi}{\delta_{90}}(1-a+\beta)$$

where a and β small.

The coefficients a and β could be easily measured and the correction factor $(1 - a + \beta)$ determined. It was found that in the backward direction, $\phi = 150°$, the correction was practically negligible. But in the forward direction, it was not generally so.

(2) Correction for the difference of absorb-abilities of the scattered radiation in different directions.

The ratio $I\phi/I_{90}$ is obtained from the observed $\delta\phi/\delta_{90}$ by multiplying the latter by the factor x_{90}/x_ϕ, which may be called the "relative absorbability" in the two directions $\phi = 90°$ and ϕ

Since over the range of wavelengths u   in these experiments, the absorptions in SO_2 and aluminium are proporti   l, we can replace x_{90}/x_ϕ by the corresponding quantity for a very thin l   er of aluminium of thickness Δt, which latter could be determined by a grap   al method.

(3) Correction due to obliquity.

Owing to the finite size of the aperture of the ionisation chamber, the rays entering it were not all parallel to the axis of the beam. This required a small correction to be applied to the value of $I\phi/I_{90}$; and estimated from the dimensions of the apparatus it was computed at about 1% of the whole. The observed value of $I\phi/I_{90}$ was to be increased by this amount.

(4) Correction for polarisation :—The theoretical expressions based both on the classical theory and on the wave-mechanical conceptions presuppose that the incident beam of X-rays is unpolarised. Practically, however, the primary beam is partially polarised.

Let us suppose that the partially polarised incident beam is made up of two parts :—

(1) an unpolarised part of intensity U and

(2) a plane polarised part of intensity P. Then if X and X′ represent the ratio $I\phi/I_{00}$ for the unpolarised beam and the observed partially polarised beam respectively, it can be shown that

$$X' = X + \frac{2P}{U} \cos^2\phi.$$

Or,
$$X = X' \quad \frac{2P}{U} \cos^2\phi.$$

The correction term can be calculated for any direction if the quantity P/U is determined. This could be easily done by placing the secondary electroscope at $\phi = 90°$ and measuring the ionisation for two distinct positions of the X-ray tube *viz.*, (A) with the cathode stream horizontal and (B) with the tube turned through a right angle so that the cathode stream was vertical.

The value of P/U was found to fall from about .1 to .013 as the applied H. T. increased from 30 K. V. to 100 K. V. and to increase from .013 to .045 as the beam at 100 K. V. was hardened more and more by progressive filtration. The maximum correction amounted to about 10% of the whole and that in the case of the softest radiation used.

EXPERIMENTAL RESULT

TABLE I

Angle $\phi = 150°$

Kilo Volt. (peak)	$\left(\dfrac{\bar{\mu}}{\rho}\right)_{Al.}$	Equiv. λ Å.U.	Scatterer	Uncorrected I_ϕ/I_{90}	Corrected I_ϕ/I_{90}	Dirac's theory.
30	6.55	.77	Paraffin	1.79	1.58	1 62
			Filter paper	1.785	1.61	
80 (filt. .54mm. Al.)[a]	1.88	.49	Paraffin	1.745	1 565	1.55
			Filter paper	1.75	1.56	
			Aluminium	1.67	1.56	
			Sulphur	1.65	1.57	
100 (filt. .54mm. Al.)	1.40	.44	Paraffin	1.72	1.54	1.53
			Filter paper	1.72	1 51	
100 (filt. 3.16mm. Al.)	.70	.34	Paraffin	1.725	1.44	1.47
			Filter paper	1.70	1.43	
100 (filt. 6.32mm. Al)	.45	.275	Paraffin	1.705	1.39	1.43
			Filter paper	1.68	1.40	
100 (filt. 9.48mm. Al.)	.37	.25	Paraffin	1.69	1.35	1 40
			Filter paper	1.615	1.37	
100 (filt. 15.8 mm. Al.)	.32	.225	Paraffin	1.65	1.28	1.36
			Filter paper			
80 (filt. 6.32mm Al.)	·65	.33	Carbon	1.72	1.49	·1.47

TABLE II

Angle $\phi = 30°$

Kilo Volt. (peak)	$\left(\dfrac{\bar{\mu}}{\rho}\right)_{Al.}$	Equiv. λ Å.U.	Scatterer	Uncorrected I_ϕ/I_{90}	Corrected I_ϕ/I_{90}	Dirac's theory.
30	6.55	.77	Paraffin	2.31	2.16	1.90
			Filter paper	3 11	2.94	
50	3.80	.635	Paraffin	2.05	2.04	1.93
			Filter paper	2.55	2.46	
			Aluminium	4.84	2.74	
80 (filt. .54mm. Al.)	1.88	.49	Paraffin	1.935	1.97	1.98
			Carbon	2.085	2.13	
			Filter paper	2.24	2.21	
			Aluminium	3.88	3.61	
			Sulphur	4.31	4.14	
100 (filt. .54mm. Al.)	1 40	.44	Paraffin	1.87	1.90	2.01
			Filter paper	2.165	2.16	
100 (filt. 3.16mm. Al.)	.70	.34	Paraffin	1.81	1.85	2.08
			Filter paper	1 985	1.98	
100 (filt. 6.32mm. Al.)	.45	.275	Paraffin	1.775	1.82	2.17
			Filter paper	1.875	1.89	
100 (filt. 9 48mm. Al.)	.37	.25	Paraffin	1.75	1.79	
			Filter paper	1.82	1.81	2.22
100 (filt. 15.8 mm. Al)	.32	.225	Paraffin	1.695		
			Filter paper	1.70	1.72	2.28
80 (filt. 3.16mm. Al.)	.92	.38	Aluminium	3.19	3.08	2.05

[a] This means that the primary radiation at 80 K. V. (peak) has been filtered by aluminium of thickness .54 mm.

TABLE III

Angle $\phi = 20°$

Kilo Volt. (peak)	$\left(\dfrac{\bar{\mu}}{\rho}\right)$Al.	Equiv. λ Å.U.	Scatterer	Uncorrected I_ϕ/I_{90}	Corrected I_ϕ/I_{90}	Dirac's theory
30	6.55	.77	Paraffin	3.275	3.04	2.05
			Filter paper	4.94	4.65	
50	3.80	.635	Paraffin	2.685	2.64	2.09
			Filter paper	3.94	3.80	
80 (filt. .54 mm. Al).	1.88	.49	Paraffin	2 365	2.40	2.14
			Filter paper	3.215	3.13	
80 (filt. 3.16 mm. Al.)	.92	.38	Paraffin	2.18	2.28	2.24
			Filter paper	2.785	2.83	
80 (filt. 6.32 mm. Al.)	.65	.33	Paraffin	2.125	2.23	2.29
			Filter paper	2.56	2.61	

DISCUSSION

$\phi = 150°$

According to the simple classical theory, the ratio $I\phi/I_{90}$ should be independent of the nature of the radiator and of the wavelength of the incident radiation.

Moreover, the ratio I_{150}/I_{90}, on the above theory has a value $(1 + \cos^2 150°)$ = 1.75. But Dirac's value of this ratio, which also is independent of the material of the scatterer, diminishes continually as the wavelength is shortened, the simple classical value being realised in Dirac's theory only in the limiting case when $\lambda = \infty$.

A survey of the results of experiment in Table I where Dirac's value is given in a seperate column for the sake of comparison, shows that, for any one radiation, the corrected values of the ratio I_{150}/I_{90} for the different scatterers are nearly equal and the mean of these agrees in general, remarkably well with the corresponding values given by Dirac's theory. This is illustrated by Fig. 2.

In the case of aluminium and sulphur, the two elementary radiators, only one radiation the most intense one ($\lambda = .49$ Å.U.) has been scattered, as the scattered rays in other cases were of extremely feeble intensity.

Dirac's theoretical value have, of course, been calculated here, on the assumption that the incident complex beam is analogous to a homogeneous one of a wavelength defined by what has been called "equivalent wavelength" and that, it is completely modified by the process of scattering. Indeed, for scattering substances consisting of light atoms, such as carbon, paraffin wax,

filter paper etc., the above assumption of a more or less complete modification, is not for truth, particularly when the primary beam is of a short wavelength.
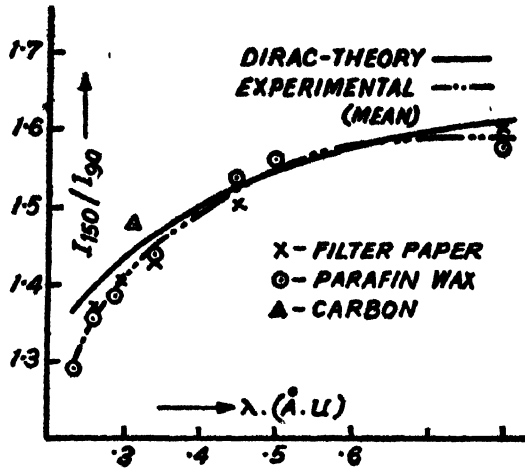
Fig. 2

It may be recalled that Backhurst, scattering monochromatic X-rays of wavelengths .395 and .31 Å. U. from beryllium and other substances, found in the backward direction as far as $\phi = 150°$ an agreement, within about 3%, with Dirac's theory, in every case.

In the present investigation, the experimental value of the relative intensity I_{150}/I_{90}, for paraffin wax, corresponding to the shortest wavelength $'\lambda = .225$ Å. U. falls short of the theoretical by about 6%. Such a discrepancy is greater than can be attributed to experimental error. The experimental values are generally smaller than theoretical value. This is more pronounced in the region of short wavelengths.

$$\psi = 30°$$
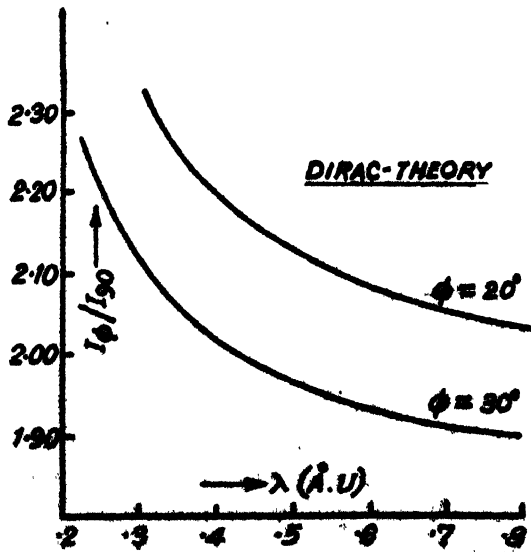
Fig. 3

The simple classical theoretical value of I_{30}/I_{90} is $(1 + \cos^2 30°) = 1.75$, and is a constant, as mentioned above, for all scattering substances and for radiations of all wavelengths. The quantum theory of Dirac, however, while retaining the scattering function unaffected by the nature of the scattering substance (under certain limitations), makes it dependent on the wavelength of the incident radiation. Dirac's relation between the scattered intensity and the incident wavelength has already been given in the introduction, from which it may be noted that $I\phi/I_{90}$ for $\phi < 90°$ decreased as the wavelength is increased, (Fig. 3) reaching the limiting classical value for $\lambda = \infty$.

The experimental results obtained by us in course of this investigation with different scattering substances, different radiations and different angles are completely at variance with the above two theories. In the first place, we have found that, for the same radiation and corresponding to the same angle of scattering, the ratio $I\phi/I_{90}$, depends in a large measure on the nature or physical constitution of the scattering substance. Employing the same incident radiation of equivalent wavelength .19 Å. U., we obtained for different scatterers the values of I_{30}/I_{90} indicated in the following table:—

TABLE IV

Scattering substance					Atomic number	I_{30}/I_{90}
Paraffin wax ...	...	.	...	...	$(< 6)^*$	1.97
Carbon ...	...	...	...	...	6	2.13
Filter paper ...	...	..	...	...	(> 6)	2 21
Aluminium ...	...	...	...	..	13	3.61
Sulphur ...	...	..	...	...	16	4.14

Thus the relative scattering certainly as far as these experiments go—


```
4.9   X - FILTER PAPER.
      ● - PARAFFIN WAX.
4.5   ▲ - ALUMINIUM.
      □ - CARBON.
4.1   ● - SULPHUR.
```
FIG. 4
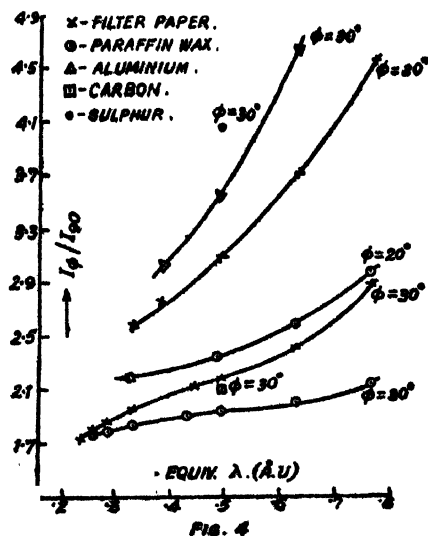
*For paraffin wax and filter paper which are not elementary substances, we can only suggest an "average" atomic number, calculated from their chemical composition.

increases with the atomic number of the scattering element. This dependence on the nature of the scattering substance, shown by radiations of other wavelengths also, is vividly brought out in Fig. 4, where the same order of succession, as above, has been maintained beginning from a wavelength of .77 Å. U. down to .225 Å. U.

Secondly, the value of I_{30}/I_{90}, was found always to be in excess of the simple classical value. This excess was also found to be the greater, the greater the wavelength of the incident radiation. All curves illustrated in Fig. 4, slope down from right to left, showing that with the progressive hardening of the incident rays, the ratio undergoes a continual diminution, for each scatterer approaching the classical limit 1.75. That in the case of filter paper and paraffin wax, this classical limit has been more or less realised, within experimental error, at the hardest end of the curves, is quite apparent from Fig. 4. But in the case of an aluminium scatterer, the extremely feeble intensity of the scattered rays, rendered it impossible to make reliable measurements corresponding to wavelengths shorter or longer than .38 and .635 Å. U. respectively. Nevertheless, the curve has manifestly a tendency to slope down, on the shorter wavelength side, so as to approach the simple classical limit. Such a result is, obviously, not in conformity with Dirac's theory, but it is in the opposite sense. In addition, the slopes of the curves indicate that aluminium is enormously more sensitive to changes of wavelength than paraffin wax, filter paper occupying an intermediate position.

$$\phi = 20°.$$

The simple classical value of I_{20}/I_{90} is equal to $(1 + \cos^2 20°)$, *i.e.*, 1.88 and is the same for all scatterers and for all radiations. Actual experiments, however, yielded results which have features precisely similar to those described in connection with $\phi = 30°$, showing thereby, that these features are not peculiar to any particular angle ϕ, but are probably true, in general, for all the small scattering angles. The difference is one of magnitude and not of kind. I_{20}/I_{90} was found to be very much greater than the corresponding value of I_{30}/I_{90}, but the relative positions of the different scatterers was unchanged.

With a view to determining how the excess scattering in the forward direction varies from angle to angle, for the same incident radiation and for the same scatterer, experiments were performed with filter paper (70 sheets) irradiated with radiation of equivalent wavelength .49 Å. U. In the following Table V, the experimental ratio (corrected) for different angles together with the corresponding values of $(1 + \cos^2 \phi)$ and also values predicted by Dirac's theory are recorded in different columns. The 5th and 6th column respectively shows the percentage excess of the experimental and Dirac's ratios over the simple classical value $(1 + \cos^2 \phi)$.

TABLE V

Angle ϕ	Exptl. $I\phi/I_{90}$	$1+\cos^2\phi$	Dirac. $I\phi/I_{90}$	% excess over $(1+\cos^2\phi)$	
				Exptl. I_ϕ/I_{90}	Dirac. I_ϕ/I_{90}
20°	3.13	1.88	2.14	66.5	13.8
30°	2.21	1.75	1.98	26.3	13.1
40°	1.78	1.59	1.78	11.9	11.9
60°	1.30	1.25	1.34	4.0	7.2
90°	1	1	1	0	0

The above results are illustrated in curves in Fig. 5.

FIG. 5.
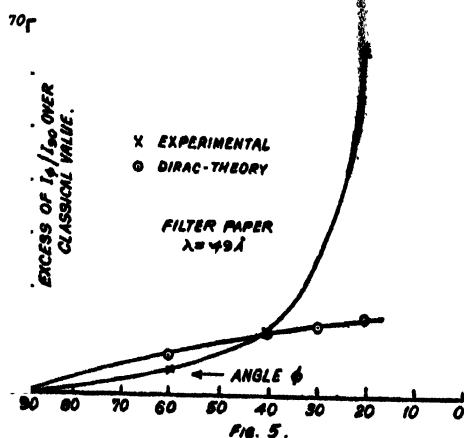
It is worth noting in this picture, that at a particular value of the angle ϕ, about 40°, the two curves intersect each other showing the experimental value of the ratio there to be coincident with Dirac's, whereas for angles smaller, the former is distinctly greater than the latter,—the more so, the smaller the angle. The curves are very close to each other through quite a big angular range, 40° to 90°, so that the difference between the experimental and Dirac's values of the ratio I_ϕ/I_{90} there, is small of the order of 3% of the whole. But that it represents nothing more than a mere accident for $\lambda = .49$ Å. U., can be shown from the following consideration. As the wavelength diminishes, the experimental curve moves down; whereas Dirac's curve—as can be shown from the Dirac's equation—moves up, increasing the above discrepancy between the two. With an increase in the wavelength, again, the experimental curve moves upwards and the Dirac's downward and the values of the ratio are again divergent for very long waves. For very short wavelengths, Dirac's values of the ratio become greater than the experimental, while for very long waves, the reverse holds. It is in a limited region of medium wavelengths only, that the difference between the values

of the ratio, experimental and Dirac's, becomes small, and that even for a short range of angles, depending on the scattering substance, and included in the forward direction, near $\phi = 90°$. In addition, as different substances show different amounts of excess scattering for the same incident wavelength and the same angle, the limited region of medium wavelengths is in all probability different and differently situated in the scale of wavelengths, for different scatterers.

In the light of these facts the experimental results obtained by Barkla and Ayres, Owen, Coven and Backhurst can be well understood.

To study the effect of the thickness of the scatterer, experiments were performed with thin and thick scatterers of the same substance —filter paper— and using two radiations, $\lambda = .49$ and $.44$ A. U., and they revealed that there is no appreciable difference in the value of I_ϕ/I_{90} (corrected) for $\phi = 150°$ and $\phi = 30°$. These results are in conformity with those of Crowther and Khubchandani, although showing some difference with those of Owen.

GENERAL CONSIDERATION

The Breit-Dirac theory of scattering has a restricted application in the sense that it takes no account of the existence of any coherent scattered radiation from different electrons within the atom or from different neighbouring atoms. It should, therefore, be more rigorously applicable to the case of monatomic gases, preferably the light ones, than to the case of solids or liquids, where the configuration of the electrons within the atom, the configuration of the atoms within the molecule and any special orientation of the molecules themselves, may produce interference effects which will, in general, be a function of (1) the atomic number of the scatterer, (2) the angle of scattering, (3) the wavelength of the radiation, as well as (4) atomic or molecular configurations.

In the backward direction, particularly for an angle as big as $150°$, the effect of interference is practically absent, and as such, such an angle forms a suitable direction for testing any theory, free from most of the complications. And along this direction, the Breit-Dirac theory, in general, has been found by us to be valid for all radiations (execpt probably for the shortest $\lambda = .225$ Å.U.) used in this investigation. This corroborates Backhurst's results.

In the forward direction, on the other hand, the effect of superposition of the scattered waves, agreeing in phase, is calculated to be great. Accordingly, if the observed excess scattering owes its origin to this superposition, then it should be of a greater magnitude, the closer the agreement in phase. The effect of phase-agreement becomes more marked as (1) the wavelength becomes longer, (2) the scattering angle becomes smaller and (3) the distance between the interfering sources becomes smaller. The

excess relative intensity should increase also with the atomic number of the scattering substance for the closer packing of the electrons inside the atom.

Let us now examine, on the basis of the above tests, how far the results of experiment in the forward direction are in conformity with the idea of interference. We have already seen that for the same radiator, the excess scattering is larger, the longer the wavelength and the smaller the angle. Also for the same wavelength and the same angle, the excess scattering increases with the atomic number : the excess scattering from sulphur (N = 16) is greater than that from aluminium (N = 13), and the excess scattering from aluminium is again greater than from carbon (N = 6). Although no definite atomic number, in the ordinary sense, can be assigned to paraffin wax and filter paper, yet the fact that filter paper yields a greater excess than carbon and paraffin wax less, is in general agreement with the idea. For, oxygen in filter paper and hydrogen in paraffin wax would contribute to the excess in precisely this way. The observed results thus fully endorse the idea of interference.

ACKNOWLEDGMENT

REFERENCES

Ayres and Barkla, C. G. (1911), *Phil. Mag.*, **22**, 187

Backhurst, (1934), *Phil. Mag.*, **42**, 129.

Barkla, C. G., (1908), *Phil. Mag* , **29**, 175.

Born and Waller, (1927, 1928), *Phil. Mag.*, **40**, 365.

Breit, (1926), *Phys. Rev.*, **27**, 362.

Chilinsky, (1932), *Phys. Rev.*, **42**, 153.

Compton, A.H. (1930), *Phys. Rev.*, **35**, 925.

Coven, (1931), *Phys. Rev.*, **38**, 1434.

Crowther, (1911), *Proc. Roy. Soc. A.*, **85**, 175.

Debye, P. and Scherrer, P., (1917), *Phys. Zeits*, **18**, 291.

H. K. Pal

Dirac, (1926), *Proc. Roy. Soc.* A., **111**, 406.

Gordon, (1926), *Zeits. f. Physik.*, **39**, 117.

Hewlett, (1922), *Phys. Rev.*, **12**, 688.

Hull, A. W., (1917), *Phys. Rev.*, **10**, 661.

Jauncey and Harvey, (1931), *Phys. Rev.*, **37**, 1203

Klein and Nishina, (1928), *Zeits. f. Physik.*, **52**, 582.

Owen, (1911), *Camb. Phil. Soc. Proc.*, **16**.

Woo, (1931), *Phys. Rev.*, **38**, 6.

CATHODO-LUMINESCENCE SPECTRA OF INDIAN CALCITES, LIMESTONES, DOLOMITES AND ARAGONITES

By BIBHUTI MUKHERJEE

Plates X-A and X-.

ABSTRACT. The cathodo-luminescence spectra Indian calcites, limestones, dolomites and aragonites in the visible and the ultraviolet regions were studied using a direct vision spectrograph and a Fuess quartz spectrograph. On inspection of the line-like bands, it was ascertained that the rare-earth activators for luminescence were in calcites Sm, Dy, Eu, and Er, in dolomites Dy and probably Sm, Eu, and in aragonites only Dy. The rare-earths with even atomic number were the chief activators for luminescence with the exception of Eu of odd atomic number. It was definitely ascertained that when rare-earths were present in calcite in optimum quantity for strong activating ability, the luminescence spectrum of Mn in the visible region was totally suppressed by the activating action of rare-earths. Below this optimum quantity both rare-earths and manganese acted as activators for luminescence. The position of the line-like band of rare-earth in the luminescence spectrum of calcite, dolomite and aragonite was the same as that in fluorite, which indicated that the limitations placed upon the activating rare-earth atoms by the neighbouring atoms were the same in all these minerals It was found that strontium and thallium showed no characteristic luminescence because of the strong activating ability of manganese when present in traces in CaO as diluent.

INTRODUCTION

The luminescence of calcites was known for many years (Gmelins, 1938). Becquerel (1889) at first found that the luminescence of calcites was due to manganese contained in them. Nichols, Howes and Wilber (1918) attributed the cathodo-luminescence of calcites to manganese present in traces. Tanaka (1924) studied the cathodo-luminescence of calcites and proved that the chief active agent for luminescence was manganese and the other active agents were thallium, dysprosium, samarium, yttrium. Yoshimura (1934) observed that the cathodo-luminescence spectra given by various calcites consisted of a broad band in the red to yellowish green region having two intensity maxima at 6050Å-5950Å and near 6310Å which is due to the presence of manganese, but no line-like bands due to rare-earths. Since the emissions due to rare-earths could not, however, be observed in the luminescence spectra the specimens were sufficiently ignited for several hours to convert them into oxides, and then the luminescence spectra of only two ignited specimens (out of five) showed the additional line-like bands due to rare-earths appearing overlapped on the broad band due

to Mn. The rare-earth activators for luminescence of these two ignited specimens were Pr, Eu, Dy and Tb.

Tanaka (*loc. cit.*) studied the cathodo-luminescence of limestones, dolomites, aragonites and found that the active agents for luminescence were Mn, Tl, Dy in limestones, Sr, Mn, Cu in aragonites and Mn, Dy, Y in dolomites. In the previous investigation on the cathodo-luminescence spectra of Indian flourites, the author (Mukherjee, 1948) pointed out that according to Urbain (1909) La, Ce, Y and Yb whose salts are colourless and devoid of absorption spectra were found not to exhibit any such luminescence. The author (1948) concluded that though Mn was present in all the chemically decomposed specimens of fluorite the characteristic Mn-band in the visible region was suppressed in the luminescence spectra by the strong activating ability of rare earths.

The object of the present investigation was to determine the activators for luminescence in calcites, limestones, dolomites, aragonites and to trace the influence of other impurities on the activating ability of rare-earths present in the specimens.

EXPERIMENTAL

The qualitative arc spectrographic analysis of calcites, limestones, dolomites and aragonites was carried out at 9 amps. 220 volts with a E_1 quartz spectrograph. The presence of rare-earths could not, however, be detected in any of the specimens. All the specimens contained traces of manganese. Traces of strontium was present in aragonite No. 6679. The method of cathodo-luminescence was applied for the study of rare-earths in these specimens.

In the experiment, the arrangement for generating the cathode rays and the method adopted for exciting the specimens in the tube was the same as that used in the previous investigation on Indian fluorites (Mukherjee, *loc. cit.*). Each of the specimens of calcite, limestone, dolomite and aragonite was powdered and heated for 5 minutes in a muffle furnace at nearly 800°C—1000°C. This ignited specimen was exposed to cathode rays in the tube just after the heat treatment. The best condition for excitation of the specimen was at 4000V, the current in the tube being kept at 4·5 mA. Direct vision spectrograph and Fuess quartz spectrograph were used for taking spectrograms both in the visible and the ultraviolet regions. The time of exposure in the direct vision spectrograph was 2·10 minutes, ultra-sensitive panchromatic plates being used. In the quartz spectrograph the time of exposure was 5·12 minutes.

The identification of the line-like bands in the luminescence spectra of the specimens, observed under a 'comparator' of nearly 10 times magnification, was carried out referring to Urbain's data for the different system of rare-earth oxide in calcium oxide (R_2O_3-CaO). Standard mixtures of

5684 Sm
5763 Sm
5860 Dy
5934 Eu
6051 Sm
6148 Sm
6264 Sm

CALCITE
PR 9609

CALCITE
PR 9610

CALCITE
4425

LIMESTONE
6074

DOLOMITE
6115

DOLOMITE
6093

DOLOMITE
6291

ARAGONITE
6679

·01 % MnO₂
IN CaO

·01 % SrO
IN CaO

Cathodo - Luminescence   Spectra.
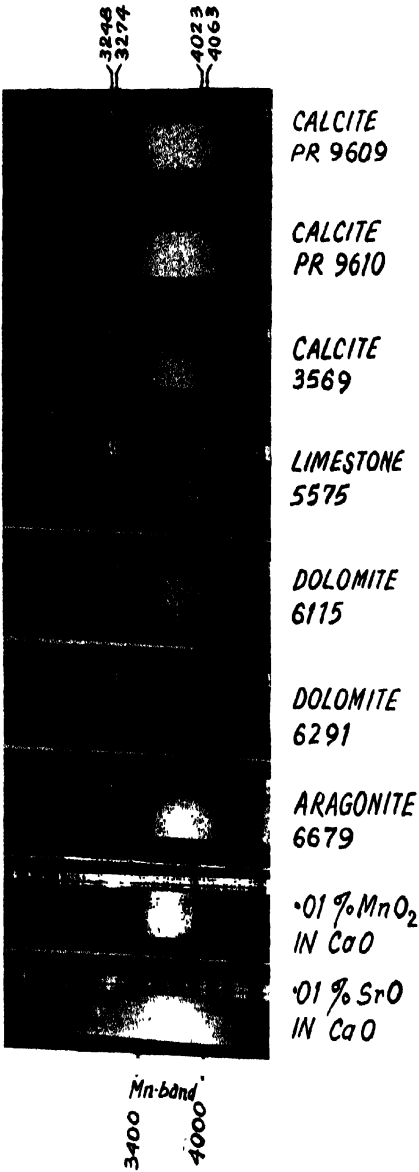
Cathodo - Luminescence Spectra.

nearly 0.01% manganese oxide in CaO, 0.01% strontium oxide in CaO and 0.01% thallium oxide in CaO were prepared and their cathodo-luminescence spectra were photographed using both the spectrographs.

TABLE I

Colour of luminescence of calcite, limestone, dolomite, aragonite and activators for luminescence.

No. of specimen	Locality	Colour of luminescence	Activators of luminescence
Calcite			
PR 9609	Giridih	Yellowish white	Sm*, Dy. (Eu), Mn
PR 9610	Udaipur	Greenish white	Sm, Dy, Eu, (Er)
PR 9602 (2)	Sinolu State	Orange yellow	No rare earths, only Mn
PR 9602 (4)	,,	,,	,,
3569	Beawar & Sendu Rly. Stn. B.B. & C.I. Rly.	,,	,,
11	Nr. Gadhagra	,,	,,
5530	Poonera, Ajmer Dt.	,,	,,
4425	2 miles W. of Barna, Kishengarh State, Rajputana,	,,	,,
4377	Mogok Sub. Div. Upper Burma	,,	,,
Limestone			
5387	Pentalgudi, Ramnad, Madura.	Deep orange	No rare-earths, only Mn
5413	Mankaria Village, Kekri Dt., Ajmer.	Yellow	,,
5575	Raipur, Gangpur State, Orissa.	Pale red, yellow tinge	,,
6074	Myli River, Palamaw, Lohardaga Dt, Bihar	Pale red, orange tinge	,,
6296	Salt Range, Punjab	,,	,,
7126	Someswar Range, Bihâr.	Organge-yellow	,,
Dolomite			
6115	Marble Rocks, Jubbulpore, C.P.	Yellowish white, Violet tinge	Dy*, (Sm), (Eu), Mn
6093	Nr. Saiduwali, Salt Range, W. Punjab.	Yellow	Dy, Mn*.
6291	From saline series, Salt Range, W. Punjab.	Orange-yellow	No rare-earths, only Mn
4727	Raipur, Gangpur State	Pale red	,,
1200	Jhanbeda hill deposits, Gangpur State	Orange-yellow	,,
Aragonite.			
6679	24 miles N.W. of Nokhundi, Baluchistan.	Yellowish-white	Dy, Mn

The * mark indicates the chief activator of luminescence.

<div align="center">

TABLE II

</div>

Wavelengths of the line-like bands in the visible region observed in the luminescence spectra of calcite, dolomite and aragonite. λ in 1 Å.

Calcite		Dolomite		Aragonite	Rare-earth-in CaO Urbain's data
PR 9609	PR 9610	6115	6093	6679	
6336 m	6336 s	6330 ⎰ s, b	5956 ⎱	5956 ⎱	6340 Eu
6264 s	6264 s	6240 ⎱	5875 ⎰ s, b	5875 ⎰ ss, b	6265 Sm
6148 ss	6148 s	6148 m	5850 ⎰	5850 ⎰	6245 Eu
6051 ss	6051 s	6051 s			6155 Eu
5934 s	5934 s	5956 ⎰ s, b			6150 Sm
5850 s	5850 s	5934 ⎱			6052 Sm
5763 ss	5763 s	5875 ⎰ s, b			5958 Dy
5684 ss	5684 s	5850 ⎱			5930 Eu
5556 f	5598 m	5826 s			5877 Dy
*5482 f	5556 m	5763 s			5848 Dy
	5492 ss	5684 m			5830 Dy
	*5482 f				5762 Sm
	5403 f				5683 Sm
	5358 f				5603 Er
	5178 f, b				5561 Sm
	4896 f				5550 ⎰ Er
	4850 m				5495 ⎱
	4718 f				5486 Sm
					5405 Eu
					5365 Eu
					5355 Er
					5180 Eu
					4900—4882 Dy
					4845 Dy
					4728 Dy
					4720 Eu

The intensities of the line-like bands are expressed by the symbols, ss = very strong ; s = strong ; m = medium ; f = faint ; b = broad. *Strong line of discharge.

The calibration of the scale in the direct-vision spectrograph due to small dispersion and broad width of the slit was subject to an error of 6Å. Some of these lines were also coincident with faint lines of discharge.

<div align="center">

INTERPRETATION OF RESULTS

</div>

Calcite.—The luminescence spectra of almost all calcites were found to be broad banded (from 6330 Å to 6150 Å and 6050 Å to 5560 Å). Such a broad band was observed in the luminescence spectrum of 0.01% manganese oxide in CaO (Mukherjee, 1948). The luminescence spectra of all calcites (PR 9609, PR 9610, 3569, etc.) also showed a broad band in the ultraviolet region (from 4000 Å to 3400 Å). This broad band was proved to be due to manganese acting as an activator in CaO as diluent (Mukherjee, 1948). It can, thus, be ascertained that Mn acted as strong activator for luminescence in calcites.

In the luminescence spectrum (visible region) of calcite No. PR 9609, it was observed that line-like bands of rare-earths were superimposed on the

broad band of manganese. In this calcite, rare-earths acted as activator for luminescence along with manganese. In the luminescence spectrum (visible region) of calcite No. PR 9610, only the line-like bands of rare-earths appeared, there being practically no broad band due to Mn. But the luminescence spectrum of this calcite in the ultra-violet region showed the characteristic broad band due to Mn, which proved that the Mn-band was suppressed only in the visible region by the activating action of rare-earths. From all these considerations, it is definitely ascertained that when rare-earths are present in calcites in optimum quantity for strong activating ability, the luminescence spectrum of Mn in the visible region is totally suppressed by the activating action of rare-earths. But below this optimum quantity (as in calcite No. PR 9609) both rare-earths and manganese act as activators for luminescence.

The rare-earth activators for luminescence in calcites were Sm (specially in specimen No. PR 9609), Dy, Eu; and probably Er also acted as activator.

Limestone.—The luminescence spectra of all limestones consisted of characteristic broad bands of Mn both in the visible and the ultra-violet regions. The Mn-band in the visible region was much stronger than that in the ultra-violet region. The line-like bands of rare-earths were not observed in the luminescence spectra of these specimens. Manganese alone acted as activator for luminescence in limestones.

Dolomite.—In the luminescence spectra of dolomites Nos. 6115 and 6093, Dy acted as the chief activator for luminescence along with Mn. In specimen No. 6115, Sm and Eu also appeared to act as activators. In the luminescence spectra of all specimens of dolomite (6115, 6093, 6291, etc.), the characteristic Mn-band in the ultra-violet region appeared strongly as was found in calcites.

Aragonite.—The luminescence spectrum of aragonite No. 6679, consisted of strong broad band of Mn in the visible region upon which was superimposed the characteristic line-like bands of Dy. The characteristic Mn-band in the ultra-violet region was also present. Thus it is ascertained that Dy acted as activator for luminescence in aragonite along with Mn.

It is interesting to note that rare-earths with even atomic number (Sm 62, Dy 66, Er 68) were the chief activators for luminescence of these minerals with the exception of europium (Eu 63) of odd atomic number. The presence of Gd could not, however, be ascertained in any of these minerals. The position of the line-like band of rare-earth in the luminescence spectrum of calcite, dolomite and aragonite was the same as it was found in fluorite (Mukherjee, 1948) which indicated that the limitations placed upon the activating rare-earth atoms by the neighbouring atoms were the same in all these minerals.

DISCUSSION

Tanaka (*loc. cit.*) ascertained that thallium also acted as activator for luminescence in calcite along with manganese and rare-earths. In the present investigation the luminescence spectrum of 0.01% thallium oxide in CaO was studied and it was found that only the characteristic Mn-bands appeared both in the visible and the ultra-violet regions. According to Urbain (1911) there was no chemically pure calcium salt free from manganese. Thus it can be ascertained definitely that in presence of even minute traces of Mn, thallium does not show any characteristic luminescence because of the strong activating ability of manganese in CaO as diluent.

Tanaka (1924) also ascertained that strontium and probably copper acted as activator for luminescence along with manganese in aragonites. In the present investigation the luminescence spectra of 0.01% and 0.1% strontium oxide in CaO were studied and it was found that only the characteristic Mn-band appeared both in the visible and the ultraviolet regions. Thus it is ascertained that strontium (though present in aragonite No. 6679) does not show any characteristic luminescence because of the strong activating ability of manganese (present always in traces) in CaO as diluent.

REFERENCES

Becquerel, E., 1889, *Comptes Rendus*, 107, 892.
Gmelins, 1938, *Handbuch der Anorg. Chemie*, 39, 45.
Mukherjee, B., 1948, *Ind Jour. Phys.* 22, 221.
Nichols, E. L., Howes, H. L. and Wilber, W. T., 1918, *Phys. Rev.*, 12, 35
Tanaka, T., 1924, *J. Opt. Soc. Am.*, 8, 411.
Urbain, G., 1909, *Ann. Chem, Phys.* (8), 18, 222.
Yoshimura, J., 1934, *Sc. Pap. I. P. C. R.* (Japan), 23, 240.

COINCIDENCE EXPERIMENTS ON 5.3y Co⁶⁰

By A. MUKHERJI and S. DAS

ABSTRACT. Coincidence experiments on 5 3y Co⁶⁰ showed that a β-ray is followed by two γ-rays in the transition Co⁶⁰→Ni⁶⁰. Absorption measurements with Cu foils indicated an average energy of the γ-rays to be 1.2 Mev. No angular asymmetry among the γ-rays was detected at different angles by γ−γ coincidence.

INTRODUCTION

The β-ray spectrum and the end energy of 5.3 year Co⁶⁰ were investigated in this laboratory by Das and Saha (1946). In continuation of that work, coincidence experiments were undertaken to arrive at a level scheme of the above nucleus. This nucleus has also been studied by Nelson, Pool and Kurbatov (1942) and Deutsch and Elliot (1942). Nelson *et al* found the end-energy of the β-ray spectrum to be $0.220 \pm .02$ Mev while Deutsch and Elliot found it to be $.300 \pm .006$ Mev. Das and Saha gave the end-energy as 0.23 Mev. According to the absorption measurements of Nelson *et al* each β-ray is followed by one γ-ray of energy $1.7 \pm .2$ Mev while according to Deutsch and Elliot each β-ray is followed by two successive γ-rays of energies $1.1 \pm .02$ Mev and $1.3 \pm .02$ Mev. The level schemes are given below.

$β−γ$ and $γ−γ$ coincidence experiments were undertaken in this laboratory to investigate this point further.

THEORY OF $β−γ$ AND $γ−γ$ COINCIDENCE EXPERIMENTS

The theory of $β−γ$ and $γ−γ$ coincidence experiments have been developed by Langer, Mitchell and McDaniel (1939). According to them, measurements of $β−γ$ coincidences per β-ray emitted and the $γ−γ$ coincidences per γ-ray emitted give the value of K, the average number of γ-rays per disintegration in the following way.

Let N be the number of disintegrations per sec. and K the average number of γ-rays per disintegration. Let $N_β$ and $N_γ$ be the rates of counting by two counters. Let $S_β$, $S_γ$ be the overall efficiencies (including solid angle) for two kinds of particles. In addition let $S_γ$ be essentially constant over the region of γ-ray energies investigated.

Therefore,

$$N_β = NS_β$$
$$N'_γ = NKS_γ$$

The number of $β−γ$ coincidences per sec. will be

$$N_{βγ} = NS_β KS_γ$$

The number of $\beta - \gamma$ coincidences per β-ray detected is

$$\frac{N_{\beta\gamma}}{N_\beta} = \frac{NS_\beta S_\gamma K}{NS_\beta} = S_\gamma K \qquad \qquad \dots (1)$$

The number of $\gamma - \gamma$ coincidences per sec. is given by

$$N_{\gamma\gamma} = N \frac{K^2(K-1)S_\gamma . S_\gamma}{2}$$

therefore, the number of coincidences per recorded γ-ray is

$$\frac{N_{\gamma\gamma}}{N_\gamma} = \frac{NK^2(K-1)S_\gamma^2}{2} \Big/ NKS_\gamma = \frac{K(K-1)}{2} S_\gamma \qquad \dots (2)$$

From eqns. (1) and (2) the ratio R of the two sets becomes

$$R = \frac{N_{\beta\gamma}}{N_\beta} \Big/ \frac{N_{\gamma\gamma}}{N_\gamma} = S_\gamma K . \frac{2}{K(K-1)S_\gamma} = \frac{2}{K-1} \qquad \dots (3)$$

so that
$$K = 1 + \frac{2}{R}.$$

EXPERIMENT

The sample examined has been prepared by the Co^{59} (d, p) reaction. The source was in the form of cobalt chloride soln. and for this experiment is mounted on a rectangular thin aluminium foil by evaporation on it.

For γ-ray detection G. M. counters, with oxidised copper cathodes and central wires of 3 mm. diameter, were used. The counter assembly was enclosed in Pyrex glass. The counters were filled with argon and etheyl ether at a ratio of 10:3 at a total pressure of 5 cm.

For the β-counter, the central wire of tungsten of 3 m.m. diameter was suspended at one end on a thin glass fibre drawn out in the form of a diameter of circular section of this end and at the other it is silver-soldered to a thick tungsten wire sealed to the counter envelope. The end having the glass fibre was open and was sealed with a brass cap which carried a window 0.5 cm. × 0.5 cm. This window was covered with a thin film of Perspex (3 mgm/cm^2) so that β-particles could pass through it without being appreciably absorbed. All the sealings were made leak-tight with Apeizon sealing-wax. The counter was filled with a mixture of argon and alcohol in the ratio of 7:3 at a total pressure of 5 cm. It carried a side-tube with a stop-cock so that it could be refilled when necessary.

For coincidence experiments the source and the counters were mounted on stands which could be slided on a bench carrying a scale, so that the distances between them could be adjusted and measured quickly.

The arrangement of the detecting and recording circuits were as follows.

The quenching circuits used were the Neher-Pickering (1938) circuits the output pulses being taken from the cathode. The use of the quenching circuits improved the plateau of the counters remarkably, extending the plateau to more than 300 volts.

The coincidence circuit was a conventional three-fold one using sharp cut off pentodes, 6SJ7.

The scaling circuit used was a scale of eight Don Devault (1941) type of circuit with slight modifications. Tubes used were 76.*

The recorder was a Cenco impulse counter counting 3,000 regularly spared pulses per min. driven by the current through a 6V6 tube which is normally biased to cut off positive pulses from the scaling circuit trips it.

The high-voltage stabilizer used to supply the cathode voltage of the G. M. counters was a modification by Banerjee (1942) of the Neher-Pickering's circuit (*loc. cit*).

All the circuits excepting the high-voltage stabilizer were run from a common power pack.
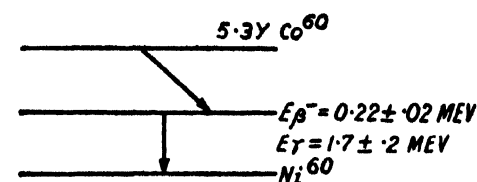
LEVEL SCHEME OF NELSON *et al*
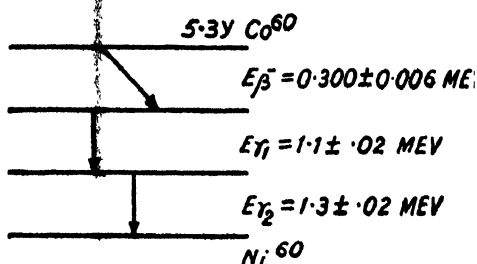
LEVEL SCHEME OF DEUTSCH AND ELLIOT.

Fig. 1
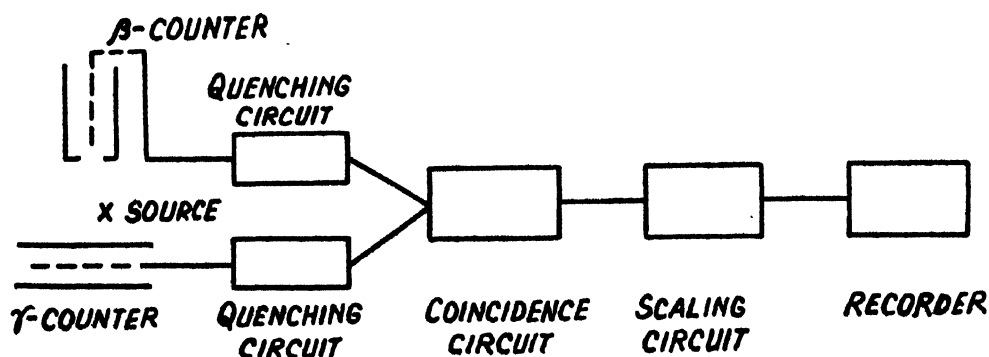
Fig. 2

For $\beta - \gamma$ coincidence the centre of the source, the centre of the window of the β-counter and the centre of the γ-counter were adjusted to lie in the same straight line. The β-counter and the γ-counter were placed symmetrically on both sides of the source, the dist. of the counters from the source being adjusted to give an optimum rate of counting.

For $\gamma - \gamma$ coincidence, the same arrangement was kept, only the β-counter was replaced by a γ-counter.

---

* The iron cored chokes used on the anodes of the 2nd valves of each stage being replaced by 25,000 Ω resistances.

TABLE I

Background counts of the β-counter in 5 min.	Counts recorded by β-counter with source in 5 min.	No of β-count per min.	Background counts of γ-counter in 5 min.	Counts recorded by γ counter with source in 5 min.	No. of γ-counts per min.	K
528.5	1078	109.9±3.142	520	1451	186.2±4.09	...

Background coincidence counts of β and γ counters in 15 min,	β−γ coincidence counts with source in 10 min.	True β−γ coincidence counts per min.	Background coincidence counts of γ counters in 15 min,	Coincidence counts of γ counters with source in 20 min.	True γ−γ coincidence counts per min.	K
5	67	6.368±.862	12	107	4.55±.702	1.844±.333

The background counts were taken at the beginning and at the end of the experiment.

For measuring the single β-counts and the single γ-counts, the same arrangement was kept only the coincidence circuit was switched off for single counts. Readings were taken for 5 mins. time interval.

The results are given in Table I. The value of K as may be seen is 1:8. Thus it may be concluded that two γ-rays are emitted per disintegration which agrees with the level scheme given by Deutsch and Elliot. For γ-rays energy, the absorption measurement with copper foil indicated the average mass absorption coefficient as .0468 cm^{-1} gm^{-1} corresponding to an average energy of the two γ-rays to be 1.2 Mev which is fairly close to the values of Deutsch and Elliot. We have tried to find the angular asymmetry of these the two γ-rays by placing two γ-counters equidistant from the source and their axes making angles of 45, 90 and 180 degrees successively. But we could not detect anything more than their symmetrical distribution.

REFERENCES

Banerjee, B M. (1942), *Ind. Jour. Phv.*, **16**, 87.

Das, S. and Saha, A K. (1946), *Proc. Nat. Inst Sci. Ind*, **12**, 227.

Deutsch, M. and Elliot, L. G. (1945), *Phy. Rev.*, **68**, 193

Don, De Vault (1941), *Rev. Sci. Inst.*, **12**, 83.

Langer L. M., Mitchell, A. C. G., and McDaniel, P. W. (1939), *Phy. Rev*, **56**, 422

Neher, H. V. and Pickering, W. H. (1938), *Phy. Rev.*, **53**, 316.

Nelson, M. E., Pool, M. L. and Kurbatov, J. D. (1942), *Phy. Rev*, **62**, 1.

LUMINESCENCE OF SOME ORGANIC COMPOUNDS UNDER X-RAY EXCITATION

By H. N. BOSE.*

Plates XI-A and XI-B

ABSTRACT. The luminescence spectra of uranyl nitrate, triphenyl-methane, naphthalene, diphenyl and mixtures of anthracene and naphthalene excited by X-ray have been reported in this paper. The spectra of naphthalene and diphenyl show a greater number of bands than were reported earlier. The mixtures of anthracene and naphthalene emit separate band systems of both the constituents, though shifts in position as well as changes in relative intensities are observed. Triphenyl-methane, which shows a measurable afterglow, has got no special feature in its luminescence spectrum distinguishing it from other molecular phosphors.

The results of investigations on the luminescence spectra of some of the well known molecular compounds have been reported in this paper, which include the repetition of some of the earlier works (Bose, 1945) with improved technique yielding increased intensity of luminescence and greater precision.

The luminescence spectra of organic compounds by X-ray excitation has attracted little attention up till now. Excitation in these cases takes place through the intermediary of photo-electron produced inside the crystal by the incident photons so that it is possible to assume a large number of photo-electrons of different energies inside the crystal at any instant ; besides, it is quite possible that in these cases emission takes place in molecules already ionised by the primary X-rays, which fact is expected to be reflected in the spectra. In ultra-violet excitation, direct excitation of the optical levels takes place ; difference in the probabilities of excitation of optical levels by photons and photo-electrons, if there be any, should tell upon the intensity distribution of the spectra. Moreover, the incident photons being of very high energy compared to that of the optical levels the intensity of different lines should depend only on the corresponding transition probabilities. These features are expected to make the study of X-ray luminescence spectra interesting and of important consequences.

RESULTS AND DISCUSSIONS

The results of the present measurement are shown in Table I the spectrograms and some of the microphotographs are given in plates XI-A and XI-B As expected the spectra in all cases consist of a number of bands ; the width

* Fellow of the Indian Physical Society.

of the bands are not same throughout and it is possible that some of them are composed of more than one component. The width in general increases perceptibly on the higher energy region. This can also be easily understood from our ideas about the energy states of these molecular crystals. In these crystals, optical transition takes place within the same molecular group, whose energy levels are very little affected by the crystalline field ; the levels remain rather sharp, observed breadth being due to either the thermal vibration of the lattice or superposition of one or more lines. In spite of the fact that the molecular character of the energy states are preserved in these crystals, the higher energy part of the spectra in which the higher energy levels are involved, will be comparatively more affected by surrounding neighbours.

TABLE I

Peaks of the luminescence spectra in ÅU

	(1)	(2)	(3)	(4)	(5)	(6)	(7)	(8)	(9)	(10)
Uranyl nitrate	6208	5913	5635	5370	5137	4962				
Triphenyl methane	6000	5780	5390	5250	4710	4620	4490	4290		
Naphthalene	6300	5900	5850	5410	5000	4640	4355	4135		
Diphenyl	6306	6210	6035	5700	5360	5160	4950	4580	4290	4150
Anthracene+10% of Naphthalene	6285	5830	5392	5073	4740	4560				
Naphthalane+10% of Anthracene	5720	5295	4945	4670	4465					

The emission due to uranyl nitrate (Plate XI-A f) consists of six almost equidistant well separated bands. These agree in position very closely with those obtained by ultraviolet excitation in the solid state and in solution. The emission thus takes place entirely within the molecular group UO_2 to which is attributed the optical behaviour of uranyl compounds. Excitation in the present case takes place through the intermediary of the photo-electrons which are produced by the incident X-rays inside the crystal in large number and of different energies. Absence of any afterglow in this case is also due to the same reason. There is, however, one important difference between ultraviolet and X-ray excitation. In former, fluorescence, though weak, is observed even in solution whereas in latter case fluorescence, ceases when the lattice breaks up in all substances. The existence of absorption and fluorescence under ultraviolet radiations indicates that the corresponding energy states of the molecular group remain intact, as is expected. This only indicates that photo-electrons produced inside the crystal can no longer excite the said electrons in the absence of the crystalline field, at least probability of such inelastic collisions is very much reduced. Whatever may be the reason, the presence of crystalline field greatly facilitates the inelastic colli-

sions of the photo-electrons moving through the crystal, with the optical electrons of the said molecular groups, which is necessary for emission; whenever the lattice breaks up, either on melting or in solution, the photo-electrons lose their energy mostly by other non-radiative processes (elastic collision, etc.).

The luminescence spectrum of tri-phenyl methane, shown in Plate XI-A (e) is similar to those of other molecular compounds and consists of a number of bands which extend throughout the entire visible region and (possibly in the ultraviolet region also) generally increase in width with frequency. Tri-phenyl methane is the only organic phosphor so far obtained, which shows a measurable afterglow under X-rays, which should make its study all the more interesting.

The spectra of naphthalene and diphenyl show a marked improvement in intensity and an increase in the number of bands ; the distribution of the bands throughout the visible region makes us believe that the spectra extend into the ultraviolet region.

The luminescence spectrum of anthracene with ten per cent of naphthalene dissolved in it and that of naphthalene with ten per cent. of anthracene dissolved in it are shown in Plate XI A (a) and (b), respectively. The two compounds in each case emit almost independently ; slight changes in positions and in intensity distribution take place. Absence of the weaker bands in each case does not indicate any characteristic quenching. The measurements reported by Pringsheim, in the case of ultraviolet excitation are also of the same nature (Pringsheim, 1939).

REFERENCES

Bose, H.N., 1945, *Proc. Nat. Inst. Sci.* **9**. 152.
Pringsheim, P., 1939, *Trans. Farad. Soc.* **35**, 28.
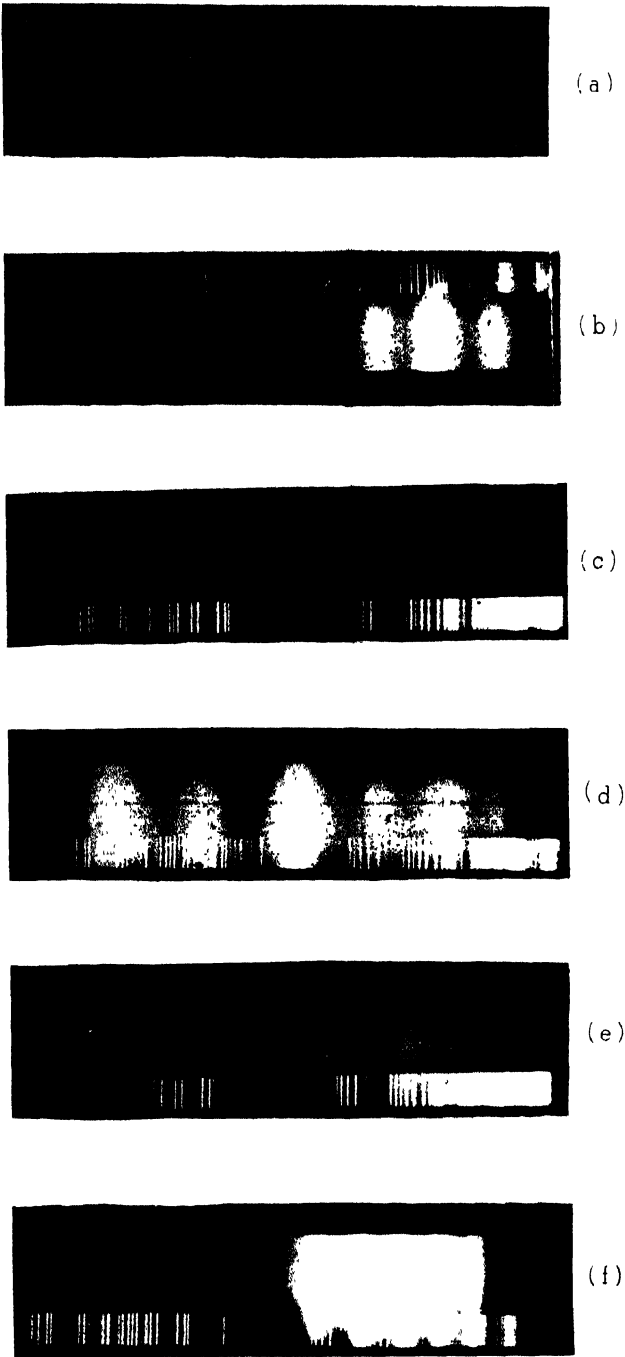
Fig. 1

Luminescence Spectra

(a) Naphthalene   +   10%   anthracene
(b) Anthracene   +   10% naphthalene
(c) Diphenyl   (d)   Naphthalene
(e) Triphenyl methane   (f) Uranyl nitrate.
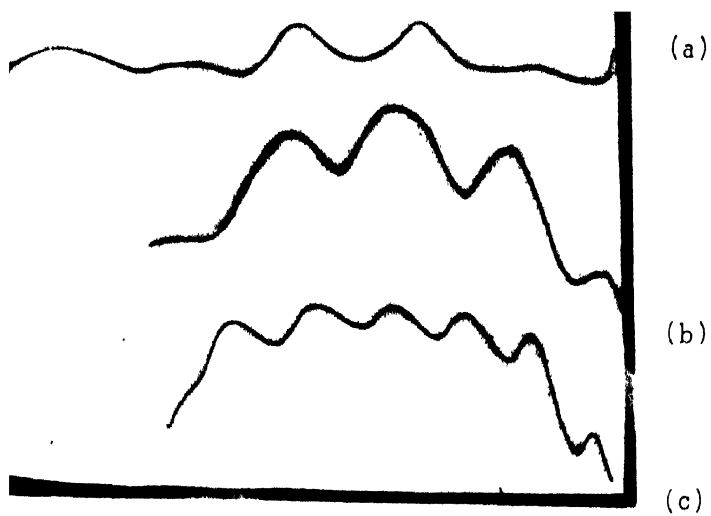
Fig. 2

Microphotometric curves of the luminescence spectra (reduced)

(a) Naphthalene + 10% of anthracene
(b) Anthracene + 10% of naphthalene
(c) Uranyl nitrate

THE RAMAN SPECTRA OF 1, 2- AND 1, 1-DICHLORO-ETHANES IN THE SOLID STATE *

By B. M. BISHUI

Plate XII

ABSTRACT. The Raman spectra of 1, 1- dichloroethane and 1, 2- dichloroethane in the solid and liquid states have been studied in order to test the hypothesis put forward by previous authors regarding the co-existence of rotational isomers in the case of 1-2 dichloroethane in the liquid state. It is observed that both the substances yield ten Raman lines having frequency shifts below 1100 cm^{-1} in the liquid state. Some of these lines of 1, 2-dichloroethane disappear when the substance is solidified, but in the case of 1,1-dichloroethane all these lines persist in the solid state. It is pointed out that these results do not support the hypothesis that the extra Raman lines in the liquid state are due to the co-existence of rotational isomers. It is pointed out that the results can be explained on the assumption that strongly associated molecules are present in these two liquids

INTRODUCTION

The Raman spectra of ethylene dihalides in the solid state were first studied by Mizushima et al (1936, 1938). They observed that some important lines disappear in the solid state and explained the phenomenon on the hypothesis that in the solid states the molecules are all in the trans state, while the liquid state contains the molecules of both the trans and gauche or cis configurations. Later, Sirkar and Bishui (1945) studied the Raman spectra of ethylene dibromide in the liquid and the solid state and also the polarisation of the lines due to the liquid state at room temperature, and criticised the hypothesis put forward by Mizushima et al showing that the two lines 1056 cm^{-1} and 1441 cm^{-1} of liquid ethyiene dibromide were totally depolarised, although according to their hypothesis these lines ought to have been polarised. An alternative hypothesis that in the liquid state some of the molecules might be in a strongly associated state, forming thereby groups having the symmetry C_{2v} and that in the solid state the group might change to one having a symmetry D_{2h} was put forward by Sirkar and Bishui (1945). Further, the results of investigations of the Raman spectra of ethylene dibromide dissolved in different solvents by Bishui and Sanyal (1947), of their polarisation and of the ratio of the intensities of the lines 551 cm^{-1} and 660 cm^{-1} of the pure ethylene dibromide at different temperatures by the present author (1948) seemed to support the view put forward by Sirkar and Bishui (1945). The sure test of the different hypotheses, however, lay in the study of the Raman spectra of dihalogen ethanes in which there can be no rotational

isomers. By comparing the Raman spectra of such disubstituted ethanes with those of similar molecules which may have rotational isomers one can definitely say whether the presence of rotational isomers is responsible for the presence of too many lines in the Raman spectra of these substances. For this purpose, the Raman spectra of 1, 2-dichloroethane and 1, 1-dichloroethane in the liquid and the solid state have been studied in the present · investigation and the results which are described below lead to the definite conclusion that the extra lines present in the Raman spectra of these substances in the liquid state are not due to the presence of rotational isomers.

<div align="center">EXPERIMENTAL</div>

The apparatus used in the present investigation for the study of the Raman spectra of the substances in the solid state at low temperatures was the same as that described earlier by Sirkar and Bishui (1943). Kahlbaum's pure substances distilled in vacuum were put in a double walled cylindrical pyrex glass tube held in a vertical position in the liquid oxygen contained in a transparent Dewar vessel. The interspace between the two walls of the container was evacuated with a Cenco hyvac pump, so that on pouring the liquid oxygen into the Dewar vessel to fill it up to a certain height from the bottom of the container, the temperature of the liquid was lowered very slowly, and consequently the process of solidification also was very slow. The frozen mass thus produced was transparent. The dry air was introduced afterwards into the interspace mentioned above and the temperature of the solid reached a steady value of about—170°C within an hour.

A Fuess glass spectrograph having a dispersion of about 14 A. U. per mm. in the region, 4046A was used. The liquid was illuminated by light from two vertical mercury arcs condensed by two six inch glass condensers placed on the opposite sides of the container. Cobalt-glass filters were placed in the path of the incident light to cut off continuous background in the blue-green region of the spectrum.

The polarisation of the Raman lines was studied qualitatively by photographing the horizontal and vertical components of the scattered light simultaneously on the same plate with the help of a double image prism as usual. The liquid was contained in a horizontal Wood's tube provided with a plane window. Light from a mercury arc focussed with the help of a condenser was used as the incident light in this case also. In the case of totally depolarised lines the horizontal component was more intense than the vertical component in this arrangement.

<div align="center">RESULTS AND DISCUSSION</div>

The spectrograms obtained for the liquid and solid states are reproduced in Plate XII.
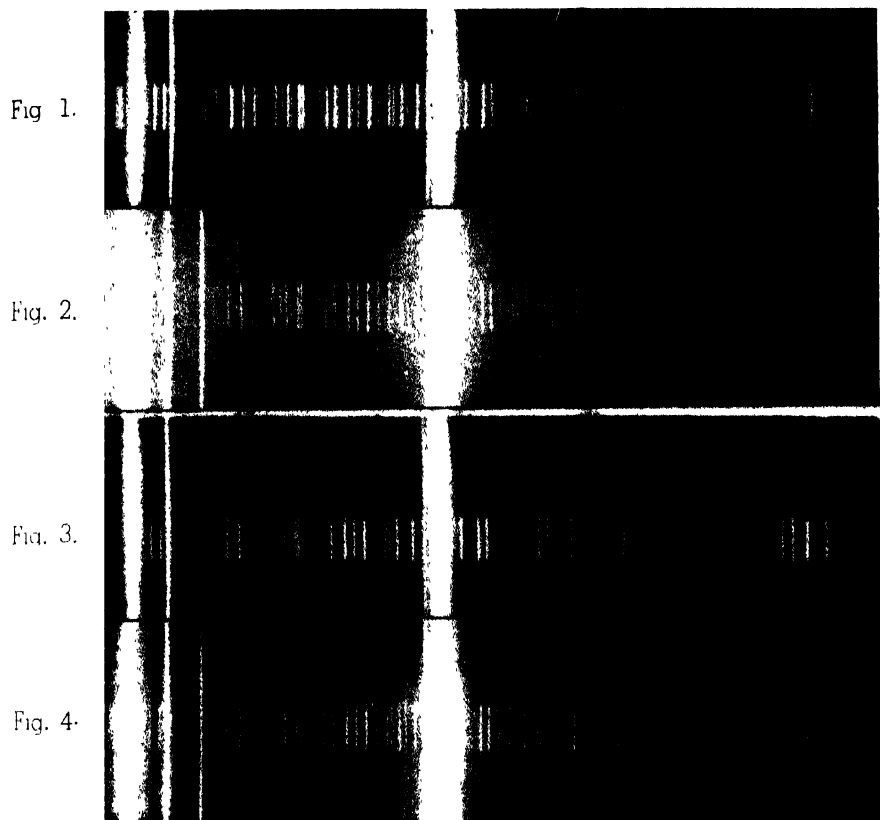
Fig 1.

Fig. 2.

Fig. 3.

Fig. 4.

Raman Spectra

Fig 1. 1, 2 - Dichloroethane at about + 30°C

Fig. 2. 1, 2 -   „   „ „   - 170°C.

Fig. 3 1, 1 - Dichloroethane at about + 30°C

Fig 4. 1, 1 -   „   „ „   - 170°C

The results are given in Tables I and II. The second column of each table contains the results reported by some of the previous workers. The letters P and D denote polarised and totally depolarised ($\rho = 6/7$) respectively. The approximate visually estimated intensities are given in the parentheses. The data for the solid obtained in the present investigation are given in the last column.

TABLE I

1, 2-dichloroethane $ClCH_2CH_2Cl$.

Liquid State		Solid State	
Present author.	Mizushima *et al* (1938).	Mizushima *et al* (1938) at about —140°C.	Present author at about —170°C.
—	—	53, k +	58 (2b). k
		74, k +	82 (1). k
128 (3b)e, k ; D	125 (5b)e ±, k ±	V	
265 (2)e, k ; P	265 (5)e ±, k, i	V	264 (2)e, k
301 (6)e, k ; P	300 (8)e ±, k, i	303 (5)e, k	300 (2)e, k
409 (2)e, k ; D	411 (5)e ±, k, i	V	—
654 (8)e, k ; P	654 (8)e ±, k, i, f	V	V
676 (3s)e, k ; D	677 (6b)e ±, k : i	V	
754 (10b)e, k ; P	- 754 (10b)e ±, k, i	748 (10)e, k, i, f, g	749 (8)e, k
833 (1)e, k ; D	881 (4)e, k	V	—
—	943 (5)e, k	V	
943 (3b)e, k ; P	989 (2)e, k	—	—
—	1031 (2)e, k	990 (3)e, k	—
1051 (3)e, k ; P	1052 (4)e, k	1058 (2)e, k	1057 (1)e, k
1122 (0)e, k ; ?	—	—	—
1150 ((2)e, k ; D	1145 (3)e, k	—	—
1205 (3)e, k ; D	1207 (5)e, k	—	
1270 (1)e, k ; D	1264 (3)e, k	1264 (2)e, k	
1298 (2)e, k ; P	1304 (6)e, k	1298 (3)e, k	1296 (3b)e, k
	1393 (1)e, k	1312 (1)e, k	—
1426 (3)e, k ; D	1429 (6)e, k	1437 (2)e, k	—
1443 (4b)e, k ; D	1445 (4b)e, k	1456 (2)e, k	1450 (1b)e, k
2840 (1)e, k ; P	2844 (3)e, k	—	—
2877 (2)e, k ; P	2874 (4)e, k	2870 (2)k	2880 (1b)e, k
2955 (10)e, k ; P	2957 (10)e, k, i	2965 (10)e, k, i, q, p, o	2960 (8)e, k
3004 (6b)e, k ; D	3005 (8b)e, k, i	3012 (6)e, k, p	3005 (2)e, k

It can be seen from Tables I and II that the number of lines having frequency shifts below 1100 cm⁻¹ is ten in the Raman spectra of both 1, 1-dichloroethane and 1, 2- dichloroethane. In the former case almost all the prominent lines persist in the solid state at low temperature and in the latter case some of the prominent lines disappear completely when the substance is solidified. As mentioned earlier this disappearance of the Raman lines of 1, 2- dichloroethane was first observed by Mizushima (1938) and explained on the hypothesis that the molecules having trans and other configurations coexist in the liquid state and the molecules are all of the trans type in the solid state. It was pointed out by Sirkar and Bishui (1945) that this explanation was not satisfactory and an alternative explanation based on the assumption that strongly associated molecules are present in the liquid and

<div align="center">

TABLE II

1, 1- dichloroethane $CH_3.CH_2.Cl_2.$

</div>

Liquid State		Solid State at about—170°C
Present author.	Magat (1934).	Present author.
—	—	70 (1) k
168 (1b)e; P	—	163 (1b) e, k
275 (4)e±k; P	276 (4)	277 (1) e, k
322 (2)e, k; P	—	322 (1) e, k
408 (3)e, k; P	400 (3)	408 (2) e, k
640 (6)e, k, i; P	642 (6)	640 (3) e, k
688 (3)e, k; D	687 (4d)	680 (2) e, k
905 (0)e, k; ?	978· (2)	977 (1b) e, k
977 (2)e, k; P	—	—
1054 (2)e, k; ?	1050 (0.5d)	1054 (0) e, k
1088 (2b)e, k; ?	1090 (1)	—
1255 (1)e, k; ?	1229 (0)	—
1270 (2)e, k; ?	1271 (1)	—
1352 (2)e, k; D	1353 (0.75d)	—
1442 (5)e, k; D	1438 (2d)	1442 (2) e, k
2930 (6)e, k; P	2929 (6)	2937 (5) e, k
2987 (8b)e, k; D	2985 (5)	2987 (4) e, k
—	—	2996 (3) e, k
3072 (5)e, k; P	3071 (0.25)	3072 (0) e; k

solid states was offered by the latter authors. In the case of 1, 1-.dichloroethane on the other hand there is hardly any probability of the exis-fence of two rotational isomers in the liquid state. Of course, we may visua-lise two different configurations of the molecule, one 'eclipsed' and the other 'staggered', as shown in Fig. 5, but only one such form is stable.

<div align="center">

Staggered   Eclipsed
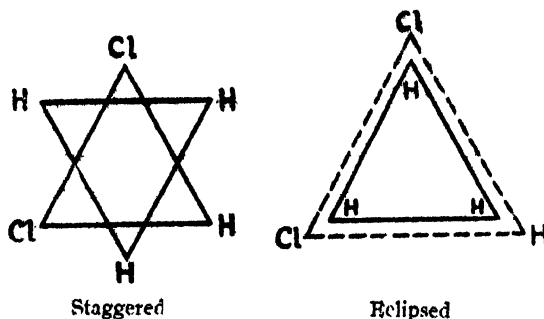
Fig. 5

</div>

This conclusion is drawn from the experimental results reported by Glockler and Sage (1941) in the case of CCl_3CHFCl. The single configuration of this molecule should yield 16 Raman lines according to group theory and only 18 such lines are also actually observed. From these results and from other evidences Glockler and Sage (1941) have concluded that probably the 'staggered' configuration is stable and the 'eclipsed' one is unstable

in these halogen substituted ethane compounds. Hence in the case of 1, 1-dichloroethane also probably the 'staggered' configuration is the stable one. Since some of the lines are totally depolarised the molecule has a plane of symmetry, but both the forms of the molecule have a plane of symmetry and therefore these data regarding the polarisation of the lines cannot indicate definitely which of the two configurations is actually present in the liquid.

The fact that all the Raman lines having frequency shifts below 1100 cm^{-1} observed in the liquid state are also present in the solid state at about -170° C clearly indicates that only one of two configurations is present in the liquid state. If there were two rotational isomers, would depend on the temperature, and at low temperatures one of the isomers would be converted into the other and consequently the Raman lines yielded by it would disappear at the low temperatures.

Hence the results obtained in the present investigation regarding 1, 1-dichloroethane clearly indicate that the presence of too many lines in the Raman spectrum of this liquid is not due to the presence of rotational isomers.

The disappearance of some of the lines of 1, 2-dichloroethane with the solidification of the substance has already been explained by Sirkar and Bishui (1945) on a hypothesis in which it was assumed that associated pairs of molecules having a centre of symmetry are formed in the solid state. The Raman spectrum of 1, 2- dichloroethane in the vapour state has been investigated by Morino, Watanabe and Midzushima (1942). They have come to the conclusion that the gauche molecules are more abundant than trans molecules in the liquid state and the opposite is true in the case of gaseous state. Previously Mizushima *et al* (1938) pointed out that in the solid state all the molecules are in the trans state and that when the substance melts and the molecules have freedom of rotation most of them assume the gauche form. It is, however, difficult to understand how in the gaseous state when such a freedom is greater the number of molecules of gauche form diminishes.

In the hypothesis in which the presence of associated molecules is postulated, these facts can be understood easily because in the vapour state most of the molecules become single and the lines due to single molecules become more intense than those due to the associated molecules. In the solid state some of the lines due to the associated molecules disappear because the resultant associated molecule has a centre of symmetry and the oscillations giving rise to these lines are antisymmetric to the centre of symmetry. Of course, from chemical point of view, there may be some difficulty in understanding the nature of the linkage which has been assumed to be responsible for the formation of the associated molecules by Sirkar and Bishui (1945), but the nature of the Raman spectra of the substance at the different states cannot be explained by assuming the co-existence of rotational isomers. There is probably no other alternative than to assume the existence of strongly associated molecules, because the results of present investigation show that

even when no such isomers can be present in the case of 1, 1-dicholoroethane, the number of Raman lines observed is too large for a single molecule.

The appearance of two lines at 58 cm^{-1} and 82 cm^{-1} in the case of 1, 2-dichloroethane and of one line at 70 cm^{-1} in the case of 1, 1-dichloroethane in the solid state is probably due to vibrations of the associated pairs of molecules in which single molecules, oscillate against each other. These lines are differentiated from those due to lattice oscillations because virtual chemical linkages are involved in these modes of vibrations.

ACKNOWLEDGMENT

REFERENCES

Bishui, B. M. (1948), *Ind. J. Phys.*, **22**, 251.

— and Sanyal, S. B., *Ind. J. Phys.* **21**, 233.

Glockler, G. and Sage C. (1941), *Jour. Chem. Phys*, **9**, 387 (1941).

Magat, M. (1934), *Annual Tables of Constants etc* Page 22.

Mizushima, S. and Morino, Y. (1938a) *Proc. Ind. Acad. Sc. A*, **8**, 315.

— and Morino, Y. and Norozi (1936) *Sci, Papers, Inst. Phys. Chem Research (Tokyo)* **29**, 63 and 188.

Morino, Y, Watanabe, I. and Midzushima, S. (1942) *Sc. Papers, Inst. Phys. Chem Research (Tokyo)* **39**, 401.

Sirkar, S. C. and Bishui, B. M. (1945), *Ind. J. Phys.*, **19**, 23.

— (1943), *Proc. Nat. Inst. Sc. of India*, **9**, 287.

ABSORPTION OF ULTRA HIGH FREQUENCY WAVES IN SALT SOLUTIONS

By S. K. CHATTERJEE AND B. V. SREEKANTAN

ABSTRACT. Percentage of absorption and reflexion suffered by a u h.f waves (300-480 Mc/s), in aqueous solutions of magnesium sulphate and calcium chloride have been determined. Absorption index, attenuation coefficients and reflexion coefficients for various frequencies at different concentrations of the solutions have been calculated. Experimental data have been utilised to calculate dielectric constant, loss tangent and absorption conductivity of the solutions at different frequencies and concentrations. Values of molar conductivity for magnesium sulphate have been calculated   Values of relaxation time obtained from experimental data have been compared with those calculated theoretically   Reflexion coefficient show very little variation for different concentration and frequency   Molar conductivity increases with frequency over the range in question

EXPERIMENTAL

The present paper forms a part of an investigation on the behaviour of sea water as a medium of propagation of u.h.f. waves. The object of the present investigation is to study the percentage of absorption and reflexion undergone by a u.h.f. wave while travelling through aqueous solution of magnesium sulphate and calcium chloride of different concentrations. Experimental detail involving description of equipments and principle of the method followed is under publication, (Chatterjee and Sreekantan, 1948 a). Observed percentage of absorption suffered by the wave in travelling through the solutions for different normalities at particular frequencies are recorded in Figs. 1 and 2.

· In order to determine the attenuation coefficient, values of percentage of transmission are plotted against various depths (up to 5 cms.) of solution for different concentrations and frequencies. The slope of the average curve between the two extreme envelopes gives the attenuation coefficient α (Chatterjee and Sreekantan, 1948 b). Values of α found from different portions of the curve will be different. Slope between 2 to 3 cms. of liquid give values for α which agree more closely with theoretical valves. The values of absorption indices k at different frequencies and normalities can be calculated from the following relation :—

$$\alpha = \frac{2\pi n k}{\lambda}$$

involving refractive index n and wavelength λ. The values of reflexion coefficients R for normal incidence can be calculated from the following relation :—

$$R = \frac{(n-1)^2 + k^2}{(n+1)^2 + k^2}$$

obtained from Fresnel's equation.

Values of α, k and R for both the solutions at four frequencies and three different concentrations have been given in Table I. Values of n used in the above calculation have been calculated from the values of ϵ' (Table V).

TABLE I

Normality $= 0.09N$ for $MgSO_4$ and $0.1N$ for $CaCl_2$

Frequency in Mc/s.	a		k		R	
	MgSO₄	CaCl₂	MgSO₄	CaCl₂	MgSO₄	CaCl₂
340	0.1081	0.0385	0.1654	0.059	0.6476	0.6418
400	0.1260	0.094	0.1646	0.125	0.6457	0.6393
440	0.1438	0.130	0.1711	0.164	0.6456	0.6415
480	0.1065	0.0804	0.1164	0.088	0.6439	0.6406

Normality $= (0.125\ N)$

340	0.0618	0.073	0.0934	0.129	0.6507	0.6431
400	0.2351	0.0967	0.3022	0.127	0.6486	0.6406
440	0.0849	0.1709	0.0996	0.205	0.6480	0.6412
480	0.811	0.0572	0.1100	0.063	0.6474	0.6409

Normality $= 0.166N$ for $MgSO_4$ and $0.2N$ for $CaCl_2$

340	0.0390	0.0495	0.0585	0.071	0.6562	0.6448
400	0.1086	0.0598	0.1391	0.078	0.6518	0.6424
440	0.1079	0.1189	0.1100	0.142	0.6500	0.6421
480	0.1361	0.047	0.1462	0.052	0.6486	0.6430

DISCUSSION

Figs. 1 and 2 show that absorption maxima generally shift towards higher concentration with increasing frequency. This is to be expected from the theoretical point of view. If the absorption maximum is regarded as taking place when $\omega\tau$ is unity, then shifting of absorption peak towards higher concentration, as the frequency becomes higher, should occur as the relaxation time τ is reduced with increasing concentration. It will further be observed that the concentrations at which maximum absorption occurs for $MgSO_4$ are 0.090 N, 0.111 N, 0.125 N and 0.166 N for frequencies 340, 440, 460 and 480 Mc/s respectively. Whereas for $CaCl_2$ the concentrations of maximum absorption are 0.105 N, 0.115 N, 0.18 N, 0.20 N and 0.21 N for

60

CALCIUM CHLORIDE.
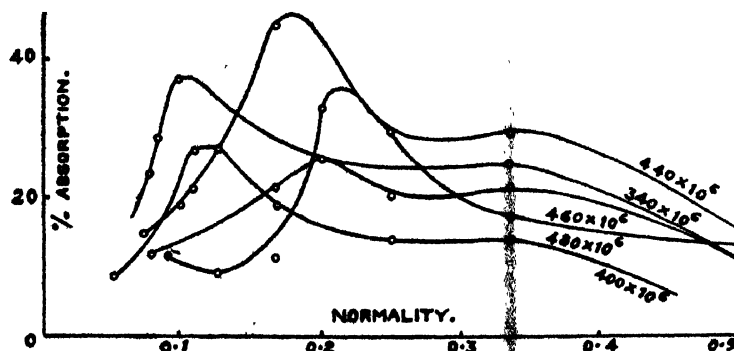
FIG. 1
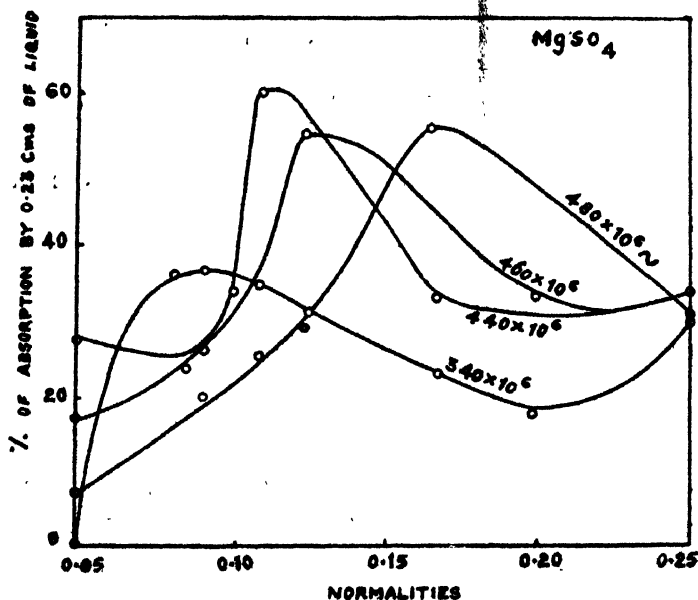
FIG. 2

frequencies 340, 400, 440, 460 and 480 Mc/s respectively. It will be evident from Table II that the product of wavelength λ and the corresponding concentration, γ^* at which the absorption is maximum, varies with frequency in both the cases. In case of $CaCl_2$ the product at 75 cm. wavelength is 8.625, whereas the value recorded by Forman and Crisp (1946) is 8.00 for 80 cm. wavelength.

Besides the interest of wave propagation, study of absorption leads to the insight of molecular structure. This may be gained from an investigation of dielectric behaviour of the solutions at different frequencies. This amounts

TABLE II

λ cms.	$\lambda.\gamma^*$	
	$MgSO_4$	$CaCl_2$
88.2	8.018	9.260
75.0	... ...	8.625
68 2	7.577	12.276
65.2	8.150	13.04
62.5	10.410	13.125

to a study of the frequency dependence of dielectric constant and loss tangent of the solution. Though different approach has been made by different authors to explain the mechanism of absorption, they lead to some form of relaxation function. Therefore, the time of relaxation giving a measure of the rate of restoration of random order after removal of the applied field is of interest.

The absorption maximum, or in Debye's notation ϵ'' maximum takes place when $\omega\tau = 1$, or more correctly, when

$$\omega\tau = \frac{\epsilon_\infty + 2}{\epsilon_0 + 2} \qquad \qquad \dots \quad (1)$$

which can be deduced from Debye's (1929) expression

$$\epsilon = \epsilon' - j\epsilon'' \qquad \qquad \dots \quad (2)$$

for generalised dielectric coefficient.

For the strengths of solution employed ϵ_∞ may be regarded as equal to the dielectric constant of water (80) at u.h.f. Values of dielectric constant ϵ_0 at low frequencies have been calculated (Table III) from the following relation given by Falkenhagen (1934) : —

$$\epsilon_{\omega=0} - \epsilon_s = \frac{1.97 \times 10^8 |z_1 z_2| \{ |z_1| + |z_2| \}^{\frac{1}{2}}}{2\epsilon_s^{\frac{1}{2}}.T^{\frac{3}{2}}. \left(1 + \frac{1}{\sqrt{q}} \right)}.(q^{\frac{1}{2}}) \qquad (3)$$

where z_1 = valence of Mg or Ca ion

z_2 = valence of SO_4 or Cl ion

$T = 300^\circ$ A

ϵ_s = dielectric constant of water (80)

$q = 0.5$ for Mg SO_4 and 0.421 for $CaCl_2$ respectively

γ^* = concentration in gm. eq. per litre

Substituting proper values, eq. (3) may be written as follows

$$\left(\epsilon_{\omega=0} - \epsilon_s\right)^{23°C}_{MgSO_4} = 28.95\sqrt{\gamma^*} \qquad \dots \text{(4)}$$

$$\left(\epsilon_{\omega=0} - \epsilon_s\right)^{23°C}_{CaCl_2} = 10.41\sqrt{\gamma^*} \qquad \dots \text{(5)}$$

TABLE III

MgSO₄		CaCl₂	
γ^*	$\epsilon_{\omega=0}$	γ^*	$\epsilon_{\omega=0}$
0.090 N	88.728	0.105 N	83.375
0.111 N	89.638	0.115 N	83.521
0.125 N	90.230	0.118 N	84.428
0.166 N	91.810	0.20 N	84.656
—	—	0.21 N	84.772

values of τ_{obs} for different concentrations (Table IV) have been calculated by using equation (1) and Table III. Values of τ_{cal} for same concentrations, have also been calculated by using the following Deby-Falkenhagen (1934) relation

$$\tau = \frac{8.85 \times 10^{-11}}{\Lambda_\infty . \gamma^*}$$

involving equivalent conductivity Λ_∞ of solution at infinite dilution, concentration of solution γ^* expressed in gm. eq. per litre and dielectric constant of water $\epsilon_s = 80$

TABLE IV

Frequency in Mc/s of max absorption.	MgSO₄		CaCl₂	
	$\tau_{cal} \times 10^{10}$ secs.	$\tau_{obs} \times 10^{10}$ secs	$\tau_{cal} \times 10^{10}$ secs.	$\tau_{obs} \times 10^{10}$ secs.
340	6.861	4.232	5.714	4.496
400	—	—	5.208	3.815
440	5.614	3.236	3.558	3.433
460	4.990	3.077	2.995	3.062

The frequency dependence of dielectric properties of the solutions can be studied by substituting the observed values of τ from Table IV in eq. (2), where ϵ' and ϵ'' are given by the following relation

$$\epsilon' = \epsilon_\infty + \frac{\epsilon_0 - \epsilon_\infty}{1 + x^2} \qquad \qquad \dots (6)$$

$$\epsilon'' = \frac{\epsilon_0 - \epsilon_\infty}{1 + x^2} \cdot x \qquad \qquad \dots (7)$$

where
$$x = \omega\tau \cdot \frac{\epsilon_0 + 2}{\epsilon_\infty + 2}$$

Values of ϵ' for different concentrations at different frequencies are given in Table V.

TABLE V

Values of ϵ' at different normalities

Frequency in Mc/s.	MgSO$_4$				CaCl$_2$		
	.090 N	0.11 N	0.125 N	0.105 N	0.115 N	0 18 N	0.20 N
340	84.364	86.034	86.616	81.688	82.045	82.709	83 010
400	83.631	85.278	85.825	81.415	81.760	82.425	82.652
440	83.324	84.819	85.291	81.262	81.593	82.214	82.430
460	83.055	84.608	85 114	81.192	81.517	82.164	82.330
480	82.890	84.401	84 897	81.128	81.443	82.021	81 320
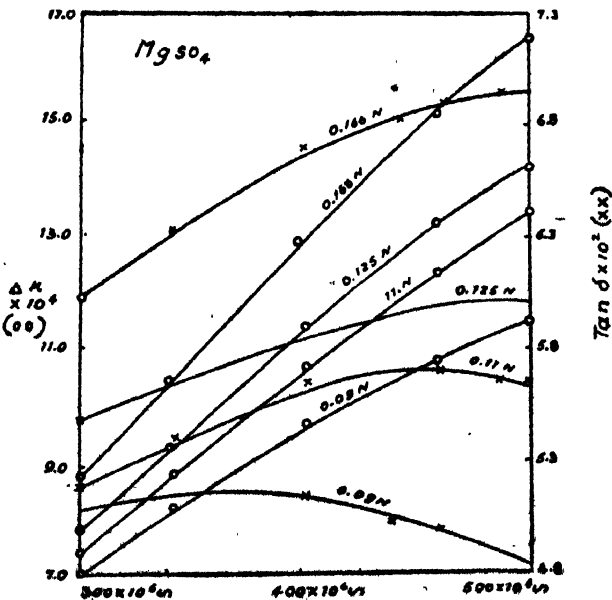
FIG. 3
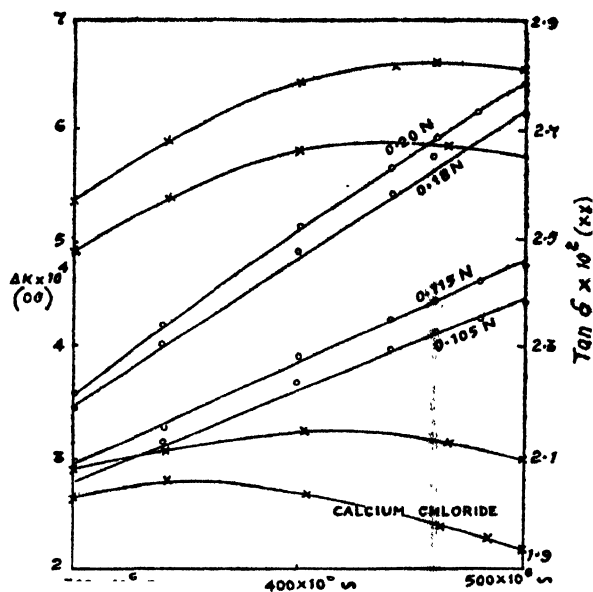
F IG. 4

Values of tan $\delta = \epsilon''/\epsilon'$, calculated from eqns. (6) and (7) are given in Figs. 3 and 4. Values for absorption conductivity Δk have been calculated from the following relation (Sharbaugh and others, 1947)

$$\Delta k = \frac{(\epsilon_0 - \epsilon_\infty).v^2/v^2{}_c}{1 + v^2/v^2{}_c) \times 1.80 \times 10^1}$$

where

$$v_c = \frac{\epsilon_\infty + 2}{\omega\tau(\epsilon_0 + 2)}$$

Variation of Δk with frequency for various values of concentrations (Figs. 3 and 4) shows an increase with frequency.

Variations of molar conductivity with frequency for both the solutions have also been studied with the help of the following relation (Falkenhagen, 1934)

$$\Lambda_\omega = \Lambda_\infty - \Lambda_{1\omega}\Lambda_{11}$$

The calculation shows an increasing value of conductivity with frequency increasing. The increase of conductivity with frequency may be explained in the following way. When an electrolyte is subjected to an alternating electric field, each ion will execute an oscillatory motion. When the exciting field frequency is low, the spherical symmetry of the steady state distribution will be disturbed and at any moment the symmetry of the charge distribution will correspond to the instantaneous velocity of the ion. If the frequency of the exciting field is great enough, so that the period of oscillation is comparable to relaxation time, the charge distribution of the ionic atmosphere will tend to correspond to the unperturbed state symmetry and hence the conductance will increase with increasing frequency. Or in other words, the part due to

relaxation force, given by (Falkenhagen, 1934) the following expression

$$\Lambda_{1\omega} = \frac{|e_1 e_2|}{3D_0 kT} . k^1 . \Lambda_\infty \times \text{Real part of } x,$$

decreases with frequency increasing and may vanish if the frequency of the impressed field is considerably high. In this case the expression for molar conductivity reduces to $\Lambda_\omega = \Lambda_\infty - \Lambda_{11}$. Or in other words, molar conductivity, within the frequency range in question, exceeds the low frequency value by $\Lambda_{1\omega}$

ACKNOWLEDGMENT

REFERENCES

Chatterjee, S. K. and Sreekantan B. V., 1948a, *Ind Jour. Phys.* **22**, 229.

Chatterjee S. K. and Sreekantan B. V 1948b, *ibid.*

Debye P., 1929, Polar Molecules, Chemical Catalog Co., New York.

Forman J., and Crisp D. J., 1947, *Trans. Far. Soc.*, "Dielectrics",

Falkenhagen H., 1934 "Electrolytes' p.219

    —do—   p.213

    —do—   p.191

    —do—   p.191

Sharbaugh A. H. etc., 1947, *Jour. Chem. Phys.* **16**, 56.

REVIEW

Electron and Nuclear Counters.—S. A. Korff, New York : Van Nostrand Co. ; London : Macmillan & Co. 1948, pp. IX, 212 illustrated, $ 3.25, 18 s.

Prof. Korff is the leading experimental investigator in the field of neutrons in Cosmic radiation. He has devoted considerable attention to the preparation of various types of counters in his laboratory which the reviewer had the opportunity of visiting in 1946.

This book contains an excellent account of the mechanism of counter action as far as it is known to-day. The first four chapters deal with the theory of operation of ionisation chambers, proportional counters, neutrons and Geiger-Muller counters. Chapter five contains a well illustrated discussion on the practical means of achieving the desirable characteristics in a Geiger-Muller counter. The last two chapters are devoted to a discussion of the errors and corrections to be applied in counter work and of auxilliary electronic circuits, *e. g.* scaling, recording and regulated high voltage circuits. There is also a collection of useful references at the end.

This volume will be very useful to all persons interested in experimental nuclear or cosmic ray physics. There is no other book at present that provides such useful information on counters.

INSTITUTE OF NUCLEAR PHYSICS,
CALCUTTA

N. N. DAS GUPTA

THEORY OF VALENCY AND STRUCTURE OF CHEMICAL COMPOUNDS

By

Prof. P. Rây

This Book, which is the outcome of the Cooch-Behar Professorship lectures at the Indian Association for the Cultivation of Science, deals with the development of the theory of valency from its origin to the latest quantum mechanical views on the subject. Specially suited to meet the requirements of teachers and students of advanced theoretical and inoraganic chemistry.

Extracts of reviews :

" The subject is discussed concisely, but the exposition is clear and interesting. Some of Prof. Rây's own work is dealt with, and there is a useful bibliography."

NATURE,

March, 27, 1948, Vol. 161.

" The quantum mechanical concepts are given with a minimum of mathematics with some helpful wave-pattern illustrations, and with mind-opening vigor......Complex (co-ordination) compounds predominate in the types of structures discussed in the book, since Prof. Rây made numerous original contribution in this field.. ...This little book should serve well to stimulate the interest of advanced students and teachers of chemistry in the subject."

Jour. of Chem. Education,

March, 1948, Vol. 25.

We are now manufacturing :

* Soxhlet Extraction sets of 100cc, 250cc and 1000cc capacity
* B. S. S. Pattern Viscometers
* Kipp's Apparatus of 1 litre and ½ litre capacity

Petri Dishes of 3″ and 4″ diameter

A N D

ALL TYPES OF GRADUATED GLASSWARE

such as Measuring Flasks, Measuring Cylinders, Burettes, Pipettes, etc., etc.

Manufactured by :

INDUSTRIAL & ENGINEERING APPARATUS CO., LTD.

CHOTANI ESTATES, PROCTOR ROAD, BOMBAY, 7.

The following special publications of the Indian Association for the Cultivation of Science, 210, Bowbazar Street, Calcutta, are available at the prices shown against each of them :—

Subject	Author	Price Rs. A. P.
Methods in Scientific Research	Sir E. J. Russell	0 6 0
The Origin of the Planets	Sir James H. Jeans	0 6 0
Separation of Isotopes	Prof. F. W. Aston	0 6 0
Garnets and their Role in Nature	Sir Lewis L. Fermor	2 8 0
(1) The Royal Botanic Gardens, Kew.	Sir Arthur Hill	1 8 0
(2) Studies in the Germination of Seeds.		
Interatomic Forces	Prof. J. E. Lennard-Jones	1 8 0
The Educational Aims and Practices of the California Institute of Technology.	R. A. Millikan	0 6 0
Active Nitrogen A New Theory.	Prof. S. K. Mitra	2 8 0
Theory of Valency and the Structure of Chemical Compounds.	Prof. P. Ray	3 0 0
Petroleum Resources of India	D. N. Wadia	2 8 0
The Role of the Electrical Double layer in the Electro Chemistry of Colloids.	J. N. Mukherjee	1 12 0

A discount of 25% is allowed to Booksellers and Agents.

RATES OF ADVERTISEMENTS

Third page of cover	Rs. 32, full page
do. do.	„ 20, half page
do. do.	„ 12, quarter page
Other pages	„ 25, full page
do.	„ 16, half page
do.	„ 10, quarter page

15% Commissions are allowed to *bonafide* publicity agents securing orders for advertisements.

CONTENTS

ON THE RAMAN SPECTRA OF n-PROPYL BROMIDE AND ETHYLENE CHLORHYDRIN IN DIFFERENT STATES*

By B. M. BISHUI

Plate XIII

ABSTRACT. The Raman spectra of n-propyl bromide and ethylene chlorhydrin in the liquid and solid states as well as the polarisation of the Raman lines of the liquids have been investigated. Some intense Raman lines are observed to disappear when n-propyl bromide is solidified as observed in the case of n-propyl chloride by previous workers, but such disappearance of some Raman lines in the case of ethylene chlorhydrin observed by those authors could not be confirmed. The hypothesis put forward by those authors that such a disappearance of the lines is due to the presence of only single molecules of one configuration in the solid state and of two different configurations in the solid state is shown to be unsatisfactory. An alternative hypothesis based on the assumption that the halogen atom of one propyl halide molecule forms a virtual bond with a carbon atom of a neighbouring molecule is put forward to explain the observed changes in the Raman spectra.

INTRODUCTION

The Raman spectra of n-propyl chloride and ethylene chlorhydrin were studied formerly by Mizushima, Morino and Nakamura (1940) and they observed that some of the prominent Raman lines due to the liquid state disappear completely when these substances are solidified. They explained the results on the hypothesis that the liquid state consists of two types of molecules, while the solid state contains only one type of molecules. It was, however, argued by them that since the lines disappearing in the case of n-propyl chloride are not analogous to those disappearing in the solid state in the case of ethylene chlorhydrin, the configurations of the molecules in the solid state of these two substances are different from each other.

They concluded that the solid ethylene chlorhydrin contains molecules of trans configuration and molecules of solid n-propyl chloride have their C-Cl group rotated through 120° from the trans configuration (gauche form). On the other hand, if the results observed with ethylene dichloride and n-propyl chloride are compared with each other it can be seen that analogous lines, e.g., the lines 654 cm⁻¹ and 649 cm⁻¹ due to the C-Cl valence oscillation disappear in the solid state in the two cases respectively. Therefore the configuration of the molecules which produces these lines should be the same in the two cases, i.e., if in the former case the Cl-C-C-Cl chain lies in one plane the C-C-C-Cl chain should also do so in the latter case. Since

Mizushima and Morino (1938) conclude that the ethylene dichloride molecules in the solid state are of trans configuration and Mizushima, Morino and Nakamura (1940) have pointed out that molecules of n-propyl chloride in the solid state are of gauche configuration—their explanation of these observed facts does not seem to be satisfactory. The question has therefore been re-investigated by studying the Raman spectra of n-propyl bromide and ethylene chlorhydrin at different temperatures and states. The Raman spectra of n-propyl bromide in the liquid state have also been studied at the room temperature and at about $-80°C$ to find out whether the disappearance of the lines in the solid state is a continuous process or it depends on the nature of the states alone, because according to the hypothesis put forward by Mizushima *et al* (1940) the intensity of the line 649 cm^{-1} should be dependent on temperature alone. Further, the Raman spectra of solutions of n-propyl bromide in n-hexane, carbontetrachloride, benzene and toluene have been studied in order to find out whether some of the lines undergo any change in intensity in the solution. The Raman spectra of ethylene chlorhydrin in the liquid state at the room temperature and in the solid state at about $-170°C$ have also been studied in order to verify the results reported by Mizushima, Morino and Nagamura (1940). The polarisation of the Raman lines of both the substances have been studied in order to understand the significance of the changes which are observed in the Raman spectra with the change of temperature and state of these substances.

<div align="center">EXPERIMENTAL</div>

Liquids from Kahlbaum's original packing were used after being re-distilled in vacuum. The technique developed for studying the Raman spectra of substances nearly at the temperature of the liquid oxygen previously by Sirkar and Bishui (1943) was used in the present investigation. The Fuess spectrograph used has a dispersion of about 13 A.U. in the region of 4047 A.U., but as it gives a coma extending up to about 38 cm^{-1} from the centre of the unexposed Rayleigh line on its Stokes side, any weak new Raman lines having frequency shift less than 38 cm^{-1} which might have appeared in the spectra due to the substances in the solid state were masked by this coma and could not be detected. The Raman spectra of the liquids at the room temperature have also been studied by the usual method. The polarisation of the Raman lines due to the liquids was studied by photograph-ing the horizontal and the vertical components of the scattered light simultane-ously with the help of a double image prism. Inspite of the special care taken to solidify the substances slowly in order to obtain a homogeneous transparent mass, the spectrum of the scattered light showed the presence of strong continuous background due to the extraneous light, and therefore, it has not been possible to record all the faint Raman lines in the solid state. The spectrogram due to the solid ethylene chlorhydrin obtained after repeated

trials is not a satisfactory one, because when the liquid is solidified, the solid mass cracks into a number of pieces exhibiting different facets and the whole spectrum is masked by the irregular scattering from these facets. It has, however, been possible to verify the broadening of certain strong lines in the solid state.

TABLE I

n-Propylbromide ($CH_3CH_2CH_2.Br$)

Liquid State			Solid State
At room temp. Present author.	Harkins, & Bowers (1931)	At about −80°C Present author	At about −170°C Present author.
			60 (2) k
			92 (1) k
225 (2) e ; P			227 (1) e, k
317 (8) e, k ; P	312 (2) 459 (2)	317 (1)	308 (2) e, k
568 (10) e, k ; P	563 (1)	568 (3)	v
651 (5) e, k ; P	648 (2)	651 (1)	638 (2) e, k
776 (3) e, k ; P	778 (1)		
848 (3) e, k ; P			
884 (2) e, k ; P			
976 (1) e, k ; P			
1021 (8) e, k ; P	1023 (2) 1143 (2)	1020 (1)	1020 (3) e, k
1228 (3) e, k ; P	1165 (2) 1185 (2)		
1315 (1) k ; P	1229 (2) 1435 (1)		
1462 (5) e, k ; D		1462 (1)	1462 (1) e, k
2850 (3) e, k ; P			2854 (1) e, k
2870 (2) e, k ; P	2896 (2)		
2902 (3) e, k ; P	2933 (2)	2937 (1)	2939 (3) e, k
2937 (3) e, k ; P			
2963 (4) e, k ; P	2965 (2) 2993 (3)	2968 (1)	2961 (2) e, k
3010 (2) e, k ; D		3010 (0)	3005 (1) e, k

TABLE II

Ethylene Chlorhydrin (ClH₂C.CH₂OH),

Liquid State at room temperature		Solid State	
Muzishima *et al* (1940).	Present author	Mizushima *et al* (1940).	At about −170°C Present author.
164 (1b) e	165 (o) e; P		
296 (4) e	295 (1) e; P	311 (o) e,	
396 (5) e, k, i	394 (1b) e, k, P		
476 (4) e, k	475 (2b) e, k; D	471 (o) e,	
662 (10b) e, k (i), f, g.	662 (5) e, k , P	659 (o) e, k, (i), f, g.	660 (2) e, k
750 (7b) e, k, (1)	750 (2) e, k; P		750 (ob) e, k, ?
850 (b) e, (k)	853 (3) e, k; P	849 (3) e, (k)	850 (2) e, k
942 (6b) e, (k) 1	940 (2) e, k; D	939 (3) e, k	
1034 (7) e, k	1032 (2) e, k; P	1036 (3) e, k	
1055 (2) e, k			
1078 (4) e, k		1083 (1) e, k	
		1130 (o) e, k	
		1171 (o) e, k	
1179 (3) e, k			
1245 (5b) e, k	1242 (2) e, k; P	1246 (o) k	
1283 (3) e, k			
1298 (3) e, k			
1379 (1) e, (k)		1387 (o) e, k	
1443 (6) e, k	1430 (3) e, k; D	1424 (2) e, k	
1457 (7) e, k	1458 (3) e, k , D	1451 (2) e, k	1456 (o) e, k
2725 (3b) e, k			
2875 (7) (e) k	2885 (3) e, k , P		2884 (o) k
2925 (6) (e) k, i	2935 (2) e, k; P	2934 (6) e, k, i	2938 (o) k
2962 (10) e, k, i	2960 (5) e, i, k; P	2960 (8) e, k, i	2960 (3) e, k
3011 (8) e, (k) (i)	3010 (3) e, k; D	3013 (5) e, k	3010 (2) k

RESULTS AND DISCUSSION

The spectrograms for *n*-propylbromide at different temperatures are reproduced in Figs. 1 and 2 of Plate XIII. The results obtained are given in Tables

Raman Spectra

Fig. 1. *n* - Propylbromide at about − 170°C
Fig. 2. *n* - Propylbromide at about + 30°C
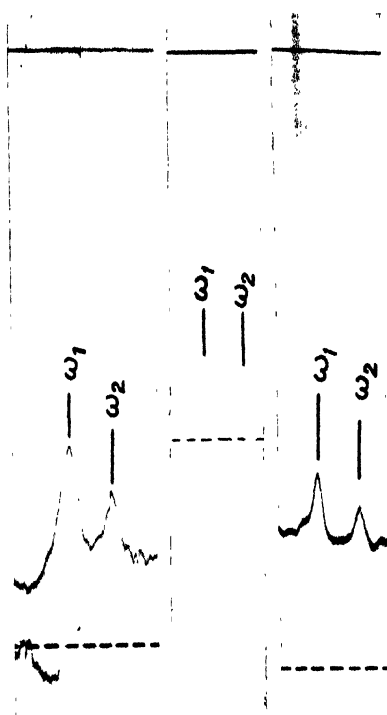
Fig. 3.   Fig. 4.   Fig. 5.

Microphotometric Records of Raman Spectra

Fig. 3   *n* - Propylbromide at + 30°C
Fig. 4.   *n* - Propylbromide at ·· 80°C
Fig. 5.   *n* - Propylbromide dissolved in hexane

v_1 — 568cm⁻ v_2 — 651cm⁻¹

I and II. The first column of each table contains the results reported by some previous workers. The data for the solid at about $-170°C$ obtained in the present investigation are given in the last column. The letters P and D denote polarised and totally depolarised respectively. The approximate visually estimated intensities are given in the parentheses. The microphotometric records of the lines $568\ cm^{-1}$ and $651\ cm^{-1}$ of *n*-propyl bromide in the liquid state at the room temperature, at $-80°C$ and in solution in *n*-hexane are reproduced in figures 3, 4 and 5.

n-propyl bromide.—It can be seen from Table I that the line $568\ cm^{-1}$, which is the most intense line in the Raman spectrum of *n*-propyl bromide in the liquid state, is totally absent in the Raman spectrum due to solid *n*-propylbromide at $-170°C$. Similar phenome was also observed in the case of *n*-propyl chloride by Mizushima *et al* (1940). It is further observed that the ratio $I_{568} : I_{651}$ diminishes only slightly when the liquid is cooled down to about $-80°C$. Hence the disappearance of the line $568\ cm^{-1}$ in the solid state is due almost wholly to the change of state. The disappearance of the corresponding line $649\ cm^{-1}$ of *n*-propylchloride in the solid state has been explained by Mizushima *et al* on the assumption that in the solid state the molecules are all of the "gauche" type while in the liquid state molecules of both gauche and 'trans' configurations are present. Here the name gauche has been given loosely to the configurations in which C-Cl line rotates through an angle of $120°$ from the C-C-C plane and the configuration in which C-C-C-Cl atoms lie in one plane has been called trans. It is further observed that along with the line $568\ cm^{-1}$ and $649\ cm^{-1}$ of *n*-propylbromide and *n*-propylchloride respectively many other Raman lines also disappear when these liquids are frozen. The hypothesis put forward by Mizushima *et al* (1940), therefore, leads to the conclusion that as the C-Cl group rotates through $60°$ from the plane of C-C-C group in propyl chloride, the frequencies of many modes of vibration of the C-C-C group become different from those of the corresponding vibrations of the trans configuration. Since the Cl atom is attached to one end of the molecule, it is difficult to understand how the rotation of C-Cl group can affect the frequency of vibration of the C-C group at the other end. Further, the number of lines below $1100\ cm^{-1}$ due to the different modes of vibrations of the C-C-C-Cl group of *n*-propyl chloride in the solid state is only four and in the liquid state it is about twelve. Hence according to the hypothesis put forward by Mizushima *et al* the gauche configuration gives four Raman lines with frequency shifts below $1100\ cm^{-1}$ and the trans configuration yields eight such lines. This is highly improbable and the explanation does not seem to be correct. In the case of *n*-propyl bromide also similar difficulty arises, the number of corresponding lines in the solid and liquid states being four and nine respectively. Of course, there are two new Raman lines at $60\ cm^{-1}$ and $92\ cm^{-1}$ in the case of solid propyl bromide, but those are not due to any intramolecular vibration of the single molecule but may be due to vibration of strongly associated molecules. It

has also been observed by the present author (Bishui, 1948) that in the case of both 1, 1-dichloro-ethane and 1, 2-dichloro-ethane in the liquid state the number of lines having frequency shifts below 1100 cm^{-1} is ten. Since the former molecule (H_3C-CCl_2H) cannot have any rotational isomer and a single molecule cannot yield more than six lines having frequency shifts below 1100 cm^{-1} we have to make an assumption other than the presence of two rotational isomers in the liquid state in order to explain the presence of a large number of Raman lines having frequencies below 1100 cm^{-1} in the Raman spectrum of 1, 1-dichloro-ethane and 1, 2-dichloro-ethane.

Again if the lines 568 cm^{-1} and 638 cm^{-1} were due to the trans and gauche configurations respectively as assumed by Mizushima *et al*, at -80°C the intensity of the line 568 cm^{-1} ought to have diminished considerably, because in the solid state all molecules are assumed to be of gauche configuration by those authors. Actually, however, the intensity of the line 568 cm^{-1} does not diminish considerably even when the liquid is cooled down to the temperature −80°C. It appears from all these facts that the assumption that in the liquid state two types of single molecules are present is not correct.

An alternative hypothesis can be suggested to explain the observed facts in the case of propyl halides. In the liquid state each molecule of *n*-propyl bromide is surrounded by a large number of similar molecules, but as the arrangement may be expected to be almost random different portions of the surrounding molecules may be adjacent to the different carbon atoms of the central molecule on which our attention is fixed now. Thus the Br atom of a neighbouring molecule may approach very close to a carbon atom of the molecule in question and may form a virtual bond. The frequency of the C-Br valence oscillation in the former molecule will be altered in such a case. The frequencies of vibrations of the C-C-C group will also be changed if a Br atom of a neighbouring molecule becomes attached to one of the carbon atoms and consequently some new Raman lines will appear. The Br atom in C-Br group of some of the molecules, however, may remain free giving thereby the normal C-Br frequency as well as the normal frequencies of the single molecule. The frequency of the C-Br valence oscillation in the methyl-bromide is 594 cm^{-1}. The frequencies of symmetric and anti-symmetric C-Br valence oscillations in CH_2Br_2 are 578 cm^{-1} and 633 cm^{-1} respectively (Trumpy 1934). In the case of *n*-propyl bromide in the liquid state there seems to be two lines due to the C-Br oscillation, the frequencies being 568 cm^{-1} and 651 cm^{-1} respectively. Of these the line 651 cm^{-1} seems to be the normal C-Br valence oscillation and the line 568 cm^{-1} due to the C-Br oscillation in the molecule in which the Br atom has formed a virtual bond with the carbon atom. In the solid state the arrangement of the molecules is regular and therefore instead of having different values as in the liquid state the intermolecular distance will have a particular value in the solid state and consequently the C-Br frequency will not be affected so much as in the liquid state in which the distance between strongly associated molecules mentioned above may be smaller than

those between other free molecules. The frequency of the C-Br valence oscillation in the solid state is none the less smaller than that in the liquid state, the difference being about 17 cm^{-1}. This is due to the influence of the neighbouring molecule on the C-Br bond and this fact definitely shows that in the liquid state if the C-Br group can approach nearer to a carbon atom of the neighbouring molecule the C-Br frequency may diminish still further, and this can explain the presence of the Raman line 568 cm^{-1} in the case of *n*-propyl bromide in the liquid state. In the solid state, therefore, neither strongly associated molecules nor free molecules are present, but the molecules are all loosely associated. From figures 3 and 5 it is seen that on dissolving *n*-propyl bromide in *n*-hexane the intensity of the line 568 cm^{-1} diminishes slightly. The ratio of the intensity of this line with that of 651 cm^{-1} was measured with the help of blackening-log intensity curve both for the pure state and for solution in *n*-hexane. The values of the ratio were found to be 5:2 and 3:2 respectively. These results corroborate the hypothesis that strongly associated molecules are responsible for the presence of the line 568 cm^{-1} in the Raman spectrum of the liquid.

Ethylene Chlorhydrin.—The results for ethylene chlorhydrin are given in Table II. The results reported by Mizushima, Morino and Nakamura (1940) for liquid and solid ethylene chlorhydrin are given in the first and the third column of Table II respectively. Samples of the liquid were taken from different old packings of Merck and Kahlbaum and when examined separately they gave the same Raman lines. Table II, however, shows that the visually estimated relative intensities of the lines 662 cm^{-1} and 750 cm^{-1} observed in the present investigation are not the same as those given by previous authors. The line 750 cm^{-1} is observed to be only about one-third as intense as the line 662 cm^{-1} and the former line is broader than the latter one. The broad and faint lines 394 cm^{-1} and 475 cm^{-1} could not be observed definitely in the spectrograms due to the solid state, but there seemed to be an indication of the presence of a broad line 750 cm^{-1} in the solid state. Thus the disappearance of the line 750 cm^{-1} in the solid state observed by Mizushima *et al* (1940) cannot be confirmed by the results obtained in the present investigation. The line becomes broader in the solid state and is therefore easily masked by the continuous background, but the line does not actually disappear. Hence the conclusions arrived at by those authors from the disappearance of this line in the solid state are not correct. In fact except some minor shifts in the positions of some of the lines and broadening of a few other lines, no other conspicuous change takes place in the Raman spectrum when ethylene chlorhydrin is solidified. In the liquid state the molecules cannot be single but are strongly associated and in the solid state also they remain so. Even in the liquid state the lines 475 cm^{-1}, 940 cm^{-1}, 1430 cm^{-1}, 1458 cm^{-1} and 3010 cm^{-1} are totally depolarised. Hence the molecule has at least one element of symmetry. The single molecule can have only a plane of symmetry. The associated molecule also may have a plane or a two-fold axis of symmetry.

ACKNOWLEDGMEN

The author is indebted to Prof. S. C. Sirkar, D.Sc., F.N.I., for his kind interest and encouragement during the progress of the work and to Prof. M. N. Saha, F.R.S., for kindly allowing him to use the microphotometer and photo-enlarger at the University College of Science, Calcutta.

REFERENCES

Bishui, B. M. 1948), *Ind J. Phys.*, **22**, 319.

Harkins, D , and Bowers, E. (1931), *Phys. Rev* , **38**, 1845.

Mizushima, S., and Morino, Y. (1938', *Proc. Ind. Acad. Sc. of India A.*, **8**, 315.

Mizushima, S., Morino, Y., and Nakamura (1940), *Sci. Papers. Inst. Phys. Chem. Research (Tokyo)*, **37**, 205.

Sirkar, S. C., and Bishui, B. M. (1943), *Proc. Nat. Inst. Sc. of India*, **9**, 287.

Trumpy, B (1934), *Z. f Phys.*, **90**, 133.

ANOMALOUS ABSORPTION OF RaC GAMMA-RAYS

By P. K. SEN CHAUDHARY

ABSTRACT. Absorption coefficient of RaC gamma-rays filtered through more than 19 cms. of lead and up to 27 cms was measured with a Geiger-Müller counter shielded with 1 cm. of lead and placed vertically above the source at a distance of 45 cms. The value of absorption coefficient obtained between 19 and 20 cms. of lead is 0.465 ± 0.04 cm.$^{-1}$ which is practically the same as the present accepted value for RaC gamma-rays in lead but then it gradually decreases to a value as low as 0.307 ± 0.03 cm.$^{-1}$ which is far below the theoretical minimum value about .47 cm.$^{-1}$ for gamma-rays in lead. Due to some uncertainty in the cut off filter thickness this low value may be a little higher. There is a rise again between 24.2 and 27 cms. The two possible causes for the anomaly, e.g., (1) some meson type of radiation such as positron electron system behaving as a neutral electromeson before annihilation and (2) multiple scattering in the forward direction are discussed.

In a recent investigation the author (Sen Chaudhary, 1948) measured the absorption-coefficient of RaC gamma-rays up to 20 cms. thickness of Pb absorber with an unshielded Geiger-Müller counter placed vertically and horizontally at different distances away from the source in order to investigate the nature of secondary effect. When the counter was at a distance of 45 cms. above the source both in vertical and horizontal position, the value of absorption-coefficient between 19 and 20 cms. Pb was found to be 0.41 cm.$^{-1}$ which is much less than the theoretical minimum about 0.47 cm.$^{-1}$ for gamma-rays in lead. From various considerations this low value was attributed to softer positron annihilation radiations. But even after 27.3 cms. lead absorber some excess of counting were obtained and these were suspected to be due to some meson type of radiations. The experiment was therefore carefully repeated and extended for RaC gamma-rays filtered through 19 cms. of lead and up to 27.3 cms.

The experimental arrangement, as shown in Fig. 1, is practically the same as in previous experiment except that the counter was shielded with 1 cm. of lead in order to eliminate softer radiations. As in the first experiment the probable error was too large ; it was repeated again with nearly double amount of radon. The data and experimental results are represented in the tables below and a logarithmic plot of the data of Table I is shown in Fig. 2.

4 CM.

FIG. 1

Pb. THICKNESS IN CM.
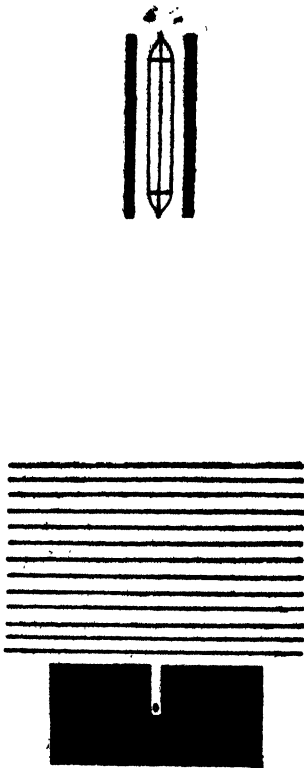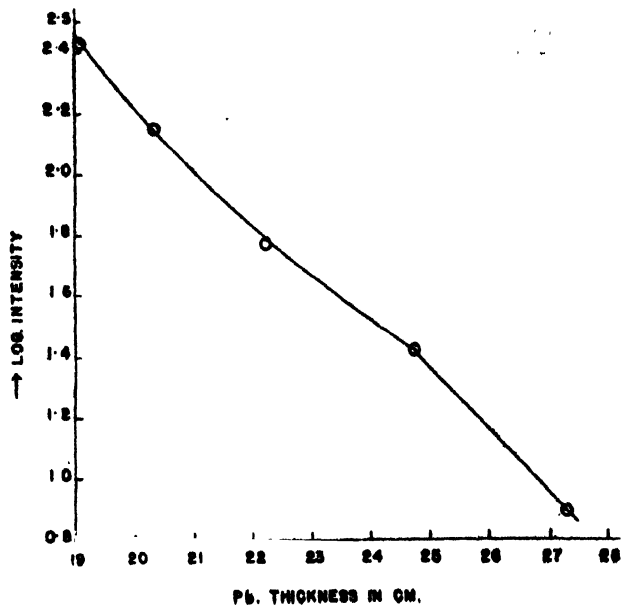
FIG. 2

RESULTS AND DISCUSSIONS

The experimental results show that the absorption-coefficient is 0.465 $\pm$0.04 cm.$^{-1}$ between 19 and 20 cms. which is in agreement with the theoretical value and the present accepted value within the limits of error. But it is very surprising that in both the experiments the absorption-coefficient 0.33 and 0.306 cm.$^{-1}$ between 22.23 and 24.77 cms. is nearly the same and far below the theoretical minimum value 0.47 cm.$^{-1}$ for gamma-rays in lead. Take it to much difference cannot be due to Compton scattering in the forward direction or statistical fluctuation or any other obvious experimental error. To interpret this low value, we are either to assume that the present theories of gamma-ray interaction with matter is inadequate or some new penetrating radiation is emitted by RaC or created by gamma-rays. Since this counter cannot detect neutron therefore if the last alternative is true a positron-electron system behaving as a neutral electromeson before annihilation may be quite possible. But this hypothesis has some drawbacks which has been discussed in detail in previous paper (Sen Chaudhary, 1948). For even if a micro-fraction of the created positrons, with appreciable kinetic energy, capture an electron and form a short-lived unstable system then according to Professor Wheeler and others, it is of atomic dimension and will therefore be ionised in passing

TABLE I

Date 28-2-48.

Amount of Radon	Thickness of Pb absorber in cm.	........No. of counts per 2 minutes........	Average No. of counts	Average intensity	Absorption coefficient cm.⁻¹
Nil	27.31	150 142 132 153 148 135 148 140	143.5±2.7	...	...
150 mc.	27.31	153 148 154 155 146	151.2±1.8	7.7±3.2	0.482±0.17
,,	24.77	175 164 170 170	169.7±2.3	26.2±3.5	0.331±0.10
,,	22.23	205 221 193 198	204.2±6.1	60.7±6.7	0.439±0.05
,,	20.33	248 281 297 283 302 274 270 292 300 287	283.4±5.1	139.9±5.7	0.465±0.04
,,	19.06	384 388 399 402 399 405	396.1±3.4	252.6±4.4	...

TABLE II

Date 12-3-48.

Amount of Radon	Thickness of Pb absorber in cm.	........No. of counts per 2 minutes	Average No. of counts	Average intensity	Absorption coefficient cm.⁻¹
Nil.	Before expt. 27.31 / After expt.	119 123 128 134 142 134 119 144 134 119 142 / 137 138 134 142 140 141 125 150	134.3±2.2		
280 mc.	27.31	155 156 157 148 149 150	152.5±1.6	18.2±2.7	
,,	24.77	183 167 198 193 182 181 185	184.1±3.7	49.8±4.3	0.396±0.07
,,	22.23	224 252 233 221 254 272 221 237 250	242.9±5.9	108.6±6.3	0.307±0.03

through dense matter. Of course it may capture and loose electrons several times before annihilation like alpha-rays. A positron-electron system can behave as a neutral particle of large penetrating power only if the two particles actually come in contact with sufficient kinetic energy and still have some life before annihilation. This is like the K-electron capture by a nucleus and the subsequent gamma-ray emmision. If such particles exist

TABLE III

Thickness of Pb absorber in cm.	Absorption Co-efficient cm.$^{-1}$	
	Expt. 1.	Expt. 2.
27.31		>.81
24.77		
	..41	.41
22.23		
	.48	
20.33		.
	.49	
19.06		

they cannot be detected in a coincidence arrangement unless the counter wall is very thin and the intensity is large.

Again though the experimental value of absorption coefficient between 24.77 and 27.3 cms. is subject to large statistical error still the rise in the value of average absorption coefficient (which is the most probable value) in this region in both the experiments may have some significance. In that case it may have some connection with the controversial existence of Rossi-second maximum which though at a lower thickness but having a different photon source.

In this paper the standard error of the mean is given in both the columns and has been calculated by the method given by Fisher (1941) remembering that standard error of the mean of n random observations is the standard deviation divided by square root of n. Because the standard error of the first two values in experiment 1 is very large due to low intensity therefore the experiment was repeated again with nearly twice the strength of radon for these two values in the second experiment. The standard error has come down to a much lower limit as in Table II.

As the author could not proceed beyond 27.3 cms. of lead due to shortage of lead sheets it has been suspected that the excess of counting even after 27.3 cms. of lead absorber may be due to some scattered photons which escape by the sides of the lead cylinder. But from the fact that a fairly large number of photons are cut out between 24.77 cms. and 27.3 cms. as well as from the comparison of the previous experiment with unshielded counter it can be concluded that the excess of counting after 27.3 cms. is not due to scattered

photons. For any particle which emerges by the sides of the cylinder will have to be scattered through more than $90°$ in order to reach the counter and by such scattering the energy of a 2.4 Mev. photon is reduced to less than 0.5 Mev. and the absorption coefficient of such a photon in lead as calculated by Heitler is of the order of 5 cm.$^{-1}$. Therefore the probability of such a photon entering the counter shielded with 1 cm. of lead is less than one in hundred and as such, even if all the excess countings about 130 per 2 minutes under 27.3 cms. lead absorber in the previous experiment are assumed to be due to scattering, it can give only one or two extra count per 2 mts. in this experiment. We assume that the rate of counting under 27.3 cms. is the background then the experimental values of absorption coefficient under different thickness of absorber are shown in the Table III above. This shows that the value of absorption coefficient between 22.23 cms. and 24.77 cms. is still much below the theoretical minimum and the absorption coefficient between 24.77 cms. and 27.3 cm. becomes abnormally high, greater than 0.81 cm.$^{-1}$.

Finally the probable effect of multiple scattering in the forward direction is considered although there is some apparent agreement with the low value of absorption coefficient obtained by the author with the mass absorption coefficient calculated by Hirchfelder, Magee and Hull (1948), still the meaning of the calculated absorption coefficient which they emphasise is quite different from what we are measuring, as they take into consideration all the scattered radiations. Moreover the nature of the result obtained by us, which is in agreement with theory up to 20 cms. absorber and also the geometry of experimental arrangement, suggest that this investigation has most probably no connection with multiple scattering. As a matter of fact the above mentioned two papers provide theoretical reasons for the apparent increase of absorption coefficient with the increase of absorber thickness as reported by the author in the previous experiment with an unshielded counter held horizontally very near the absorber surface.

Whatever may be the interpretation of this effect, from all these considerations and the fact that the results of this investigation agree with the present accepted value up to 20 cms. of lead absorber beyond which no other experiment has been done as yet, it is highly improbable that the anomalous absorption, which starts after 22.23 cms., is due to statistical fluctuation or any other source of error which the author could not detect though the experiment was repeated twice. If there is any error still this will come out only if the experiment is independently repeated beyond 22 cms. lead absorber in other better equipped laboratories preferably with 1000 millicuries of radon.

through the experimental results and discussions, and to Mr. A. Bhattacharyya, of the Indian Statistical Institute for checking the calculations about mean and errors. My thanks are also, due to Col. Barucha, Superintendent, Tata Memorial Hospital, Bombay, for encouragement.

RADIUM DEPARTMENT,
TATA MEMORIAL HOSPITAL, BOMBAY.

REFERENCES

Fisher, (1941), Statistical methods for Research Workers, p. 113.
Hirchfelder, Magee, Hull, (1948), *Phys. Rev.*, 73, 852, 853.
Sen Chaudhary, (1948), *Ind. Jour. Phys.*, 22, 106.

THE STRUCTURE OF ANTHRAQUINONE
(A QUANTITATIVE X-RAY INVESTIGATION)

By S. N. SEN

Plates XIVA and XIVB

ABSTRACT. Complete structural analysis of anthraquinone crystal has been carried out. It has been proved from X-ray, goniometric and optical studies that anthraquinone does not belong to the orthorhombic class of crystals as was concluded by the earlier workers but it really belongs to the monoclinic class, the correct space group being $C_{2h}^5 P2_1/a$ with two molecules per unit cell. On the basis of the revised space group, it has also been possible to account for a number of observed discrepancies which basis of the orthorhombic hypothesis

Quantitative X-ray investigation has led to a complete determination of the structure of anthraquinone by means of three two-dimensional Fourier syntheses. Precise orientation of the molecules in the crystal and the co-ordinates of the atoms are given. The results obtained show that anthraquinone molecule is planar and centro-symmetrical. The two outer benzene rings are almost regular hexagons, the distance between the carbon atoms being 1.38-1.40 Å ($\pm$ 01 A). The inner benzene ring shows distortion somewhat similar to that in the benzoquinone molecule, the "single" bond C-C distance being 1.50 Å, which is exactly the same as found in benzoquinone. The carbon-oxygen distance in anthraquinone works out as 1.15 Å, which is also almost the same as determined in benzoquinone.

The dominant feature found in the structure of anthraquinone crystal is the grouping of molecules in a zig-zag way in space with the molecular planes in the alternative layers being inclined to one another at an angle of 54°. The minimum intermolecular approach distances are of the order of 3.5 Å, similar to the distances found in other aromatic hydrocarbons.

INTRODUCTION

The structure analysis of anthraquinone is highly interesting, particularly from the point of view of chemists on account of the importance of this compound in organic chemistry. It is interesting whether the valency bonds in the central benzene ring of anthraquinone are similar to those in benzoquinone or are they distorted in a different fashion under influence of the two outer rings. It was also to be seen whether the two outer rings of anthraquinone are distorted under influence of the substitution of oxygen atoms to the central ring or do the outer rings remain regular hexagons just as in the case of anthracene.

Previous attempts to determine the structure of anthraquinone crystal were made by Caspari (1932), Hertel and Romer (1931), Banerjee and Guha (1934-35), but with no conclusive results. All these workers had assumed

the anthraquinone crystal to be orthorhombic after Groth's (1900-19) data. Guha (1938) had also tried to determine the structure of anthraquinone by the 'trial and error' method but without success.

<div align="center">

DETERMINATION OF SPACE-GROUP OF
ANTHRAQUINONE

</div>

On the basis of the space-group $D_{2h}^{13} Pmmn$ as tentatively assumed by Banerjee and Guha (1934-5) for anthraquinone, a determination of structure as projected on (001) plane was carried out by the two-dimensional Fourier summation method (Bragg, 1929) after necessary intensity measurements. After a few trials, satisfactory agreement between the measured and calculated values of structure factors was attained and the Fourier summation also gave a clear electron map. The following peculiar points were, however, noticed during this analysis and were at that time considered to be spurious as they could not be accounted for on the basis of the accepted orthorhombic space group :—

(a) Too many symmetries were obtained in the unit cell which were more than that required by the space-group. These appeared from the observed conditions, namely, for all (hko) reflections, $(h+k)$ and $(h-k)$ are divisible by 4, although these are not necessary space-group conditions.

(b) Intensities of reflections from (hko) and corresponding $(\bar{h}ko)$ planes in certain pairs of such reflections were found to be appreciably different. This is untenable for an orthorhombic crystal where (hko) and $(\bar{h}ko)$ are equivalent planes.

After obtaining the electron map as projected on (001) planes, a second projection was attempted on (010) plane and in order to obtain agreement in corresponding F-values, trials were carried out on the basis of molecular orientation as obtained by magnetic measurements by Banerjee (1938). But the equivalent positions required by the assumed space-group or even any other possible alternative space-group under the orthorhombic system could not be fitted in with the results obtained in the second projection. This led to suspect the correctness of the space-group.

In an attempt to see whether the (001) face is centred or not, a rotation photograph was taken around a diagonal axis [110] and the fundamental translation along that direction was found to be half of the diagonal distance in one photograph, while for a different setting of the crystal for a similar rotation photograph, the fundamental translation was found to be only quarter of the diagonal distance. The difference being surprising, the settings of the crystals were carefully checked up and fresh sets of rotation photographs were taken and it was finally concluded beyond doubt that rotation photographs round [110] and [1̄10] were different and gave the two types of photographs mentioned above. The two rotation photographs are reproduced in Plates XIVA and XIVB. Had the crystal been orthorhombic, the two
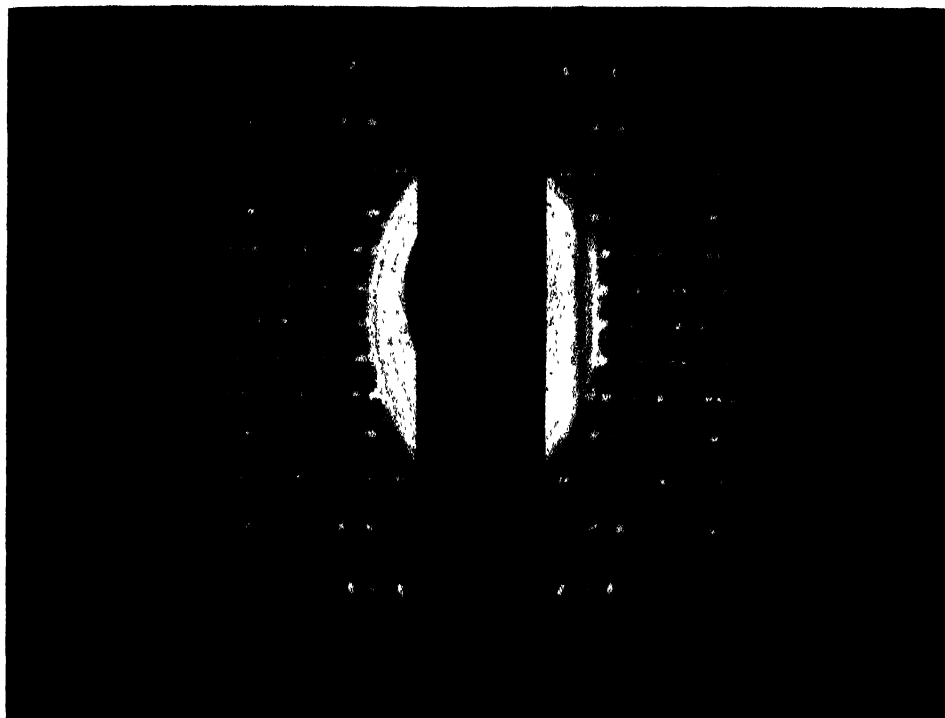
Rotation photograph round [1̄10] on the orthorhombic notation
i.e, round a-axis of monoclinic cell   ($a = 15.85$ A).

Rotation photograph round [110] on the orthorhombi
notation i.e., round c-axis of monoclinic cell ($c = 7.92$ A
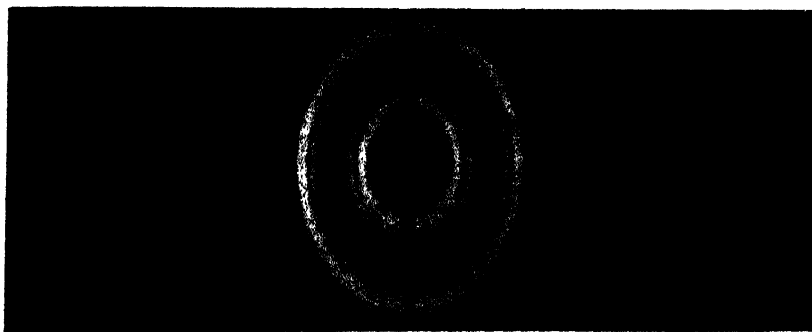
Powder photograph of a mixture of anthraquinone and aluminium.

rotation photographs round the diagonal axes [110] and [1$\bar{1}$0] would have been identical. The striking difference observed is sufficient to prove beyond doubt that the crystal cannot be orthorhombic as concluded by the earlier workers. The elementary translations in these two diagonal directions come out as 15.85Å and 7.92Å respectively, which are more fundamental than the translations 19.68Å and 24.59Å along the directions (a and b) that have been so far assumed to be the axial direction under the orthorhombic system. Taking into consideration the molecular   its already obtained by Fourier projections, it was found that the   ed facts could be well accounted for by the arrangements of molecul   the old ab-plane as shown in Fig. 1 below :—
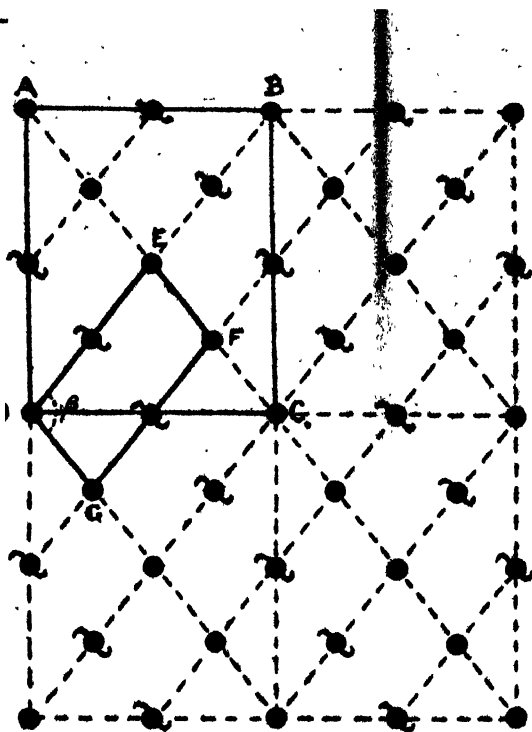
FIG. 1

Molecular net as projected on ab-plane.

ABCD represents the old ab-face of the cell, DEFG is the correct fundamental unit cell (monoclinic) whose elements are a=15.85 Å, b=3.98Å, c=7.92 Å and β=102°/43′, c-axis of the old system being the b-axis of the new system. The pseudo-orthorhombic character of the crystal has been really due to the accidental circumstance that 15.85 is approximately double of 7.92. The arrangement of molecule as shown in Fig. 1 accounts for the confusion of the earlier workers. The molecules represented by the symbol ' ϩ ' have their centres in planes c/2 (referred to old orthorhombic cell) above and below those of the molecules represented by shaded circles.

Goniometric measurements

By careful goniometric measurements of all the faces by a Czapski two-circle theodolite goniometer, the old interfacial angles were re-measured in a large number of crystals: and it was attempted to see whether X-ray evidence is corroborated in the development of crystal faces. A sketch of the anthraquinone crystal with its faces which commonly develop, as observed in the specimens crystallised from benzene, is shown in Fig. 2. The crystallographic data given under Table I (axial ratios being taken from X-ray measurements) revises the old values given by Groth under orthorhombic nomenclatures. It may be mentioned that the observed faces *a, c, m, y* and *z* (*vide* Fig. 2) correspond to *m, m, b, y* and *x* faces of Groth's data respectively and that the faces *b, n,* and *d* recorded by Groth have not been observed at all, while the observed face *z* was not included in Groth's data.
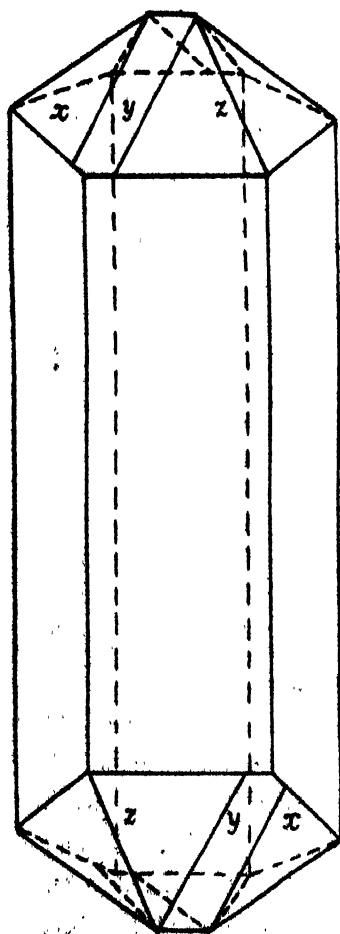
FIG. 2

Anthraquinone crystal with commonly developed faces.
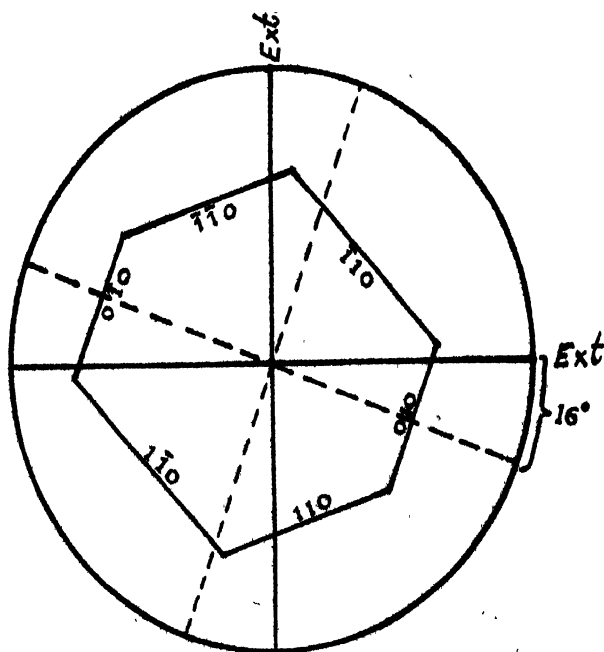
FIG. 2a

Extinction directions in section of anthraquinone crystal crt perpendicular to symmetry axis (old c-axis)

<div align="center">TABLE I</div>

Faces	New Indices	Calculated	Observed
$a:c$	$(100):(001)$	...	$77°17'$
$c:m$	$(001):(\overline{2}01)$	$51°20'$	$51°14'$
$m:a$	$(20\overline{1}):(100)$	$51°22'$	$51°29'$
$a:x$	$(100):(110)$	$75°34'$	$75°40'$
$c:z$	$(001):(011)$	$62°45'$	$62°45'$
$x:z$	$(110):(011)$	$27°36'$	$27°36'$
$y:z$	$(111):(011)$	$12°30'$	$12°37'$

It will be seen that the a- and c-faces of the crystal on the monoclinic nomenclature are the (110) and ($\overline{1}$10) faces of the old orthorhombic system. Had the crystal been orthorhombic, its (110) and ($\overline{1}$10) faces would have been identical planes. It would thus appear difficult to distinguish the new a- and c-faces of the crystal by goniometric measurement. But the existence of the top faces x and z which develop adjacent to the a- and c-faces at angles $75°40'$ and $62°45'$ respectively permit identification of the new a- and c-faces and the corresponding new axes without difficulty. The slight difference of the order of 10 to 15 minutes observed between the interfacial angles $a:m$ and $c:m$ is also found to be fairly consistent in the large number of crystals which have been examined under the goniometer and hence this difference can also be used as confirmation in identifying the a- and c-faces.

Optical measurements

With a view to obtain a further confirmation in respect of the monoclinic nature of the anthraquinone crystal, the optical extinction directions were determined by examining a section of the crystal cut parallel to the symmetry plane (*i.e.*, old 001 plane) under the polarising microscope. It was definitely found that the extinction directions in the ab-plane of the old system of axes make angles of about 16° with the a- and b-axes thus confirming the monoclinic character of the crystal. A number of similar crystal sections were examined under the polarising microscope and the mean deviation of the extinction direction from the old a- and b-axes worked out to be about 16°.

Dutta (1947) has measured the refractive indices of anthraquinone crystal along its principal directions. The relative values of the indices measured by Dutta are in agreement with the structure derived by the author.

Revision of the Space group

The new unit cell contains 2 molecules instead of 8 in the old orthorhombic cell. Thus the previous unit cell being much bigger than the correct fundamental cell, the absent spectra showed symmetries greater than those required by any of the orthorhombic space groups. If (hkl) represents the indices of a plane in the older orthorhombic notation, it can be easily shown that its equivalent indices (HKL) referred to the new monoclinic axes are given by $H = (h+k)/2$, $K = 1$ and $L = (h-k)/4$. The conditions of absent spectra observed in the orthorhombic cell are thus modified as explained below :—

(1) $(h+k)$ and $(h-k)$ divisible by 4 for hko planes reduce to 'H even for HOL' planes'

and (2) (ool) planes halved reduce to (OKO) halved.

These are the absent spectra conditions for the monoclinic space group $C^5_{2h}(P^2_1/a)$, which is, therefore, the space group for anthraquinone.

The monoclinic space group $C^5_{2h}(P^2_1/a)$ requires 4 asymmetric molecules to complete the necessary symmetry but there are only two molecules in the unit cell. Hence if all the halvings found are true halvings, we must ascribe a centre of symmetry to the molecule of anthraquinone, which is the only possible molecular symmetry for this space group. The existence of such centre of symmetry in the anthraquinone molecule is also supported by the dipole moment measurements by Fischer and Rogowski (1939).

Feeble forbidden spots observed in highly over-exposed photograph

In a highly over-exposed Weissenberg photograph about the symmetry axis (old c-axis), 4 or 5 extremely weak reflections were observed, which on identification revealed planes forbidden by the space group $C^5_{2h}(P^2_1/a)$. These planes are $\bar{7}$1o, $\bar{7}$5o, 53o and 35o on the orthorhombic system, which are equivalent to 3o2, 1o3, 1o2 and $\bar{1}$o2 planes respectively on the monoclinic system. Taking these planes into consideration, the space group of anthraquinone can no longer be taken as $C^5_{2h}(P^2_1/a)$ in the strict sense of space group, but has to be taken as C^2_2 in the bispheroidal class. In that case, the molecule does not require any centre of symmetry. But the little deviation from the centro-symmetrical molecule, which would account for these few extremely weak reflections, which are several times weaker than the weakest reflection measured, would be definitely negligible. In fact, these weak reflections will absolutely have no contribution to the electron density maps. Negative result obtained in the dipole measurements (Fischer and Rogowski 1939) also proves that the molecule is at least very nearly centro-symmetrical. So far as the structure is concerned, $C^5_{2h}(P^2_1/a)$ can, therefore, be regarded as at least approximately the correct space group for all practical purposes.

Crystal data

The revised crystal data for anthraquinone are summarised below :—

Anthraquinone : $C_{14}H_8O_2$; melting point 273°C; density, calculated 1.419 (1.419-1.438 given by Groth) ; crystallises in the holohedral class of the monoclinic system, $a=15.85$ Å, $b=3.98$ Å, $c=7.92$ Å, $\beta=102°.7$. Space group, C^5_{2h} (P^2_1/a). Two molecules per unit cell. Molecular symmetry, centre. Volume of the unit cell $=487$ Å^3. Calculated absorption coefficient for Cu K$_\alpha$ rays. $\mu=9.1$ per cm ; Total number of electrons per unit cell$=F(000)=216$.

DETERMINATION OF STRUCTURE FACTORS

Photometry of spots in Weissenberg photographs and relative intensity measurements

The relative intensity measurements were made by Zeiss photoelectric recording photometer. The method followed is briefly described below :—

The Weissenberg photo-film was mounted on the object carriage of the photometer. The dimensions of the spots (Weissenberg photograph) whose intensities were to be measured were generally of the order of 2 m.m. × 1 mm. or smaller. The spot of light of the photometer was adjusted to be much smaller in dimension, about 0.5 mm. × 0.2 mm., and was first adjusted at one end of the spot under measurement. When the motor is started to take a record, the spot of light moves along its width while the transmitted light falls on the photoelectric cell. The current through the photoelectric cell produces deflection of the fibre of a string electrometer. The fibre is illuminated by a lamp and its movement is photographically recorded. The spot under measurement was then displaced along its length through a distance of 0.5 mm., small compared to the length by the lateral movement of the object carriage and the recording was repeated by allowing the spot of light to traverse the reflection spot again along its width. In this way each spot was scanned by the light spot completely by a number of traversals. The photometer was worked with the same sensitivity, that is, with the same range of the electrometer fibre between the "zero" position (direct beam of light falling into the photo-electric cell) and the "maximum blackening" position (beam of light completely cut off). This was done by noticing the movement of the fibre against a graduated scale in the view-finder and fixing its range by adjustment of the aperture through which the light falls into the photo-cell.

The actual intensity corresponding to any spot is not linearly proportional to the deflection of the electrometer fibre of the photometer. To obtain the integrated intensity, therefore, the amplitudes or the ordinates of the photometric curve are to be compared with a standard prepared according to Robinson's (1933) method.

The zero intensity line in the photometric record was drawn for each scanning of the Weissenberg spot. The zero line being taken as the abscissae, ordinates were drawn and measured at intervals of one millimeter. This can be quite easily done by placing a semi-transparent millimeter graph paper on the photo-metric records and reading off the ordinates. Each ordinate was matched with equivalent ordinates of the standard intensity curve, the abscissae corresponding to the latter being proportional to the intensity represented by the ordinate. All these abscissa for all the scannings of the spot were summed up, the net sum giving a relative measure of the integrated intensity.

Reflections at small angles

The spot in the Weissenberg photograph having the smallest angle of diffraction was the 040 reflection. Reflections from planes of larger spacing, *i.e.,* smaller angle of diffraction are obstructed by the lead stop in the Weissenberg camera used to receive and absorb the direct X-ray beam. It was found, as can be seen from the space group condition as well, that 220 and $\overline{2}20$ are the only such planes. It was, therefore, necessary to measure their intensities for inclusion in the Fourier summation. This was done by taking separate oscillation photograph in another camera in which the lead stop used to receive the direct beam was made of such small dimension as to allow the 220 reflection to be photographed. The oscillation ranges were so adjusted that 220 and 260 reflections were recorded in one oscillation photograph and $\overline{2}20$ and $2\overline{6}0$ in another. The relative integrated intensities of these pairs of reflections were measured in the same way as in the case of Weissenberg reflections.

Absolute intensity measurements

In order to calculate the absolute structure factors of the reflecting planes, it is necessary to convert the relative integrated intensities obtained from Weissenberg photographs into absolute scale. For this purpose a powder photograph was taken with a mixture of anthraquinone and aluminium and the intensities of anthraquinone lines were compared with those of aluminium, the latter being absolutely known from the measurements by Brindley (1936). The scattering power and absorption co-efficient of aluminium being much greater than those of anthraquinone, the powder mixture was prepared with 1 part of aluminium and 6 parts of anthraquinone by weight in order that the intensities of reflections and the effective absorption co-efficients for the two ingradients might be comparable. The mixture was crushed into a fine powder in a mortar. The powder was made pasty by a little amount of solution of collodion in ether and formed into a stick by pushing the paste through a capillary tube. A filter of thin nickel foil was used to absorb the Cu-K radiation to avoid confusion among too many lines. The powder

photograph of the mixture is reproduced in plate XIV B. In order to distinguish the aluminium lines from those of the anthraquinone in the photograph, a separate·powder photograph of anthraquinone alone was taken. Relative intensities of the powder lines were measured exactly in the same way as in the Weissenberg photograph but in this case the spot of light was made longer but narrower and each line was scanned by the light spot once. The relative integrated intensities of the different lines are given in Table II below :—

<div align="center">TABLE II</div>

Substance	Reflecting planes		Relative integrated intensity	
Aluminium ...	{	111	11.3	Observed ratio=2.38
	{	200	4 8	Calculated ratio from Brindley's data = 2.22
Anthraquinone ...	{	220	18.6	
	{	040	6.8	

Hence out of the 111 and 200 reflections of aluminium, the former being more intense was considered more reliable and used for final comparison with anthraquinone lines. 3 prominent anthraquinone lines were obtained in the powder photograph, *viz.* (1) 220 plane, *i.e.,* superposition of 220, $\overline{2}20$, $\overline{2}\overline{2}0$ and $2\overline{2}0$ planes ; (2) 040 planes; *i.e.*, superposition of 040 and $0\overline{4}0$ planes and (3) superposition of 440, 260 and their derivatives with negative indices. When the monoclinic nature of the anthraquinone crystal was established, it was known that *hko* and *h̄ko* planes are really different planes except for axial planes and are generally of different intensities. Powder line obtained by superposition of such planes, therefore, could not be made use of for absolute intensity measurements. But the planes 040 and $0\overline{4}0$ being equivalent·planes on the monoclinic system as well, the intensity of this line was used for comparison with the 111 reflection of aluminium. Structure factor for the latter was taken as 8.70 × 4 from Brindley's (1936) measurements. The structure factor of 040 plane thus worked out to be 164.0 and on that basis, the structure factors of other planes have been calculated from their relative intensities in Weissenberg photographs. The details of calculation and questions of absorption and extinction have been discussed in the following section of this chapter.

With a view to checking up the accuracy of the structure factor of 040 plane on which the absolute intensity measurements for all reflections have been based, another powder photograph was taken with a mixture of anthraquinone and rock salt and by similar comparison of intensities, structure

factor of 040 plane worked out to be 166.0 as against 164.0 obtained from comparison with aluminium lines. The agreement happens to be unexpectedly satisfactory. In view of the probable error of $\pm 10\%$ in the intensity measurements and the error for not applying relative absorption corrections, which was comparatively larger in the case of rock salt-mixture, the above agreement appears to be somewhat accidental. Nevertheless, the agreement provides a confirmation that the value of F_{040} obtained from the powder photograph is approximately correct.

Evaluation of Absolute structure factors—Absorption and Extinction effects

(a) *Powder photograph with mixture of anthraquinone and aluminium.*— The integrated intensity for a powder line (neglecting absorption) on cylindrical film is given by :

$$I = \frac{1}{16} \cdot \frac{N^2 e^4 \lambda^3 . l}{\pi m^2 c^4 . r} \cdot \frac{1 + \cos^2 2\theta}{\sin 2\theta . \sin\theta} \cdot p . F^2 . \partial V$$

$$= A . N^2 . \Theta . p . F^2 \partial V.$$

where

$$A = \frac{e^4 . \lambda^3 . l.}{16\pi m^2 c^4 r} = \text{Constant for particular experiment.}$$

$N =$ Number of unit cells per unit volume.

$$\Theta = \frac{1 + \cos^2 2\theta}{\sin 2\theta . \sin\theta}$$

$p =$ Number of equivalent planes.

$F =$ Structure factor.

Thus comparing integrated intensity of an anthraquinone line with that of an aluminium line in the powder photograph, we get

$$\frac{I_A}{I_{A'}} = \frac{N_A^2 . \Theta_A . p_A . F_A^2 . \partial V_A}{N_{A'}^2 . \Theta_{A'} . p_{A'} . F_{A'}^2 \partial V_{A'}}$$

where suffixes A and A' denote corresponding values for the anthraquinone and aluminium lines respectively. As anthraquinone and aluminium were taken in the ratio 6 : 1 by weight for the powder stick,

$$\frac{\partial V_A}{\partial V_{A'}} = 6 . \frac{\rho_{A'}}{\rho_A} = 6 \times \frac{2.7}{1.42} = 11.4,$$

$\rho_{A'}$ and ρ_A being the densities of aluminium and anthraquinone respectively. In the above equation therefore, $I_A/I_{A'}$ being measured and all other factors except F_A being known, the absolute value of F_A can be calculated. F_A for 040 plane thus worked out to be 164.0.

In the above calculation, no allowance has been made for the relative absorption effects for anthraquinone and aluminium in the powder rod,

The relative absorption effect was, however, reduced to minimum by taking the substances in suitable proportion and by using very thin powder rods. The calculated values of linear absorption co-efficients for anthraquinone and aluminium for copper K_α radiation are 9.1 and 131.6 per cm. respectively (calculated from mass absorption co-efficients of different atoms as given in the 'International Tables for the determination of crystal structure'). The proportion of anthraquinone and aluminium in the powder being 11.4 : 1 by volume, the effective absorption co-efficient are 8.4 and 10.6 respectively. The radius of the powder rod used was about 0.025 cm. The approximate probable error in integrated intensities and hence in F-values for 040 reflection of anthraquinone can be calculated from the Table given on page 584 of 'International Table for the determination of cr al structure.' This works out to be roughly +4%, which is small com red to probable limits of experimental error in intensity measurements.

(b) *Weissenberg rotation photograph.*—T appropriate formula for integrated intensity of reflection from a mosaic ideally "imperfect" crystal may be written as :

$$I = \frac{N^2 e^4 \lambda^3}{4 \mu m^2 c^4} \quad \frac{1 + \cos^2 2\theta}{\sin 2\theta}. \quad F^{\bullet} = A.\beta.F^2$$

where $\qquad A = \dfrac{N^2 e^4 \lambda^3}{4 \mu m^2 c^4} \quad$ and $\quad \beta = \dfrac{1 + \cos^2 2\theta}{\sin 2\theta}$

F(040) being determined absolutely from powder photograph, F-values for other reflections have been calculated from relative integrated intensity measurements of reflections in Weissenberg photograph, i.e., from the relation

$$F^2 = \frac{I}{I_{040}} \quad \frac{\beta_{040}}{\beta} \quad F_{040}^2,$$

assuming A, which is equal to $N^2 e^4 \lambda^3 / 4 \mu m^2 c^4$, to be constant for all reflections, But A will be constant only if μ is constant. Variation of μ has, however, been neglected in view of the following considerations :—

The linear absorption co-efficient of anthraquinone (calc. $\mu = 9.1$) being fairly large, care was taken to ensure while taking the Weissenberg photographs that the specimens did not present greatly different paths to the beam in the different reflecting positions. This was done by selecting suitable crystal specimen for the different rotation photographs so as to provide fairly uniform cross-sections parallel to the rotation axes. Further, very small crystals weighing about 0.2 milligram were used to reduce non-uniformity of cross-section to the minimum. Relative absorption corrections were, therefore, not applied. With the small sizes of the crystals used, and further since it was found that the variation of crystal size did not have appreciable influence on intensities, extinction was considered to be small. No attempt has therefore been made to correct for the extinction.

4—1674P—8

Structure factors measured and calculated

The values of the structure factors in absolute units derived from integrated intensity measurements are given under "F measured" in Table III. The indices HKL of planes given in Table III refer to the old orthorhombic cell after Groth. As the Fourier summations were carried out in terms of the orthorhombic cell using the corresponding indices of the planes, these indices have been retained in Table III. Corresponding equivalent indices HKL referred to the new monoclinic axes are obtained from the general relations already given, namely, $H = (h + k)/2$, $K = 1$ and $L = (h - k)/4$. These new indices have also been included under the second column in Table III. Structure factors derived for the orthorhombic cell have, however, been divided by 4 in order to get the same in terms of the monoclinic cell. The latter values are given in Table III.

F (calculated) given under the last column in Table III have been calculated on the basis of co-ordinates of atoms as finally obtained from the electron maps. The values of atomic structure factors for carbon have been taken from Robertson's paper (1935) on the structure of benzoquinone. In the case of benzoquinone, Robertson considered that the existing oxygen f-curve would have to be modified by introducing a large temperature factor, and from the fact that peak value of electron density on the oxygen centre in his analysis was not found to be much higher than that for the carbon atoms, he assumed the average thermal movement of the oxygen atom to be of the same order as that of carbon atom. As such, the carbon f-curve was used by him for oxygen as well, after weighing in the ratio 8 to 6 in the analysis of benzoquinone. In the present analysis on anthraquinone, the peak value of electron density at the oxygen centre is found to be decidedly much higher than those for carbon atoms, actual values being 13.0 per sq. A.U. for oxygen and 7.5 to 9.0 per sq. A.U. for carbon atoms. In view of the uncertainty in the f-curve for oxygen atom, structure factors were separately calculated by using values used by Robertson as well as by those from the measuremants on MgO by Wollan (1930). As the latter gave a better agreement with the observed F-values for most of the reflections, Wollan's values have been preferred and corresponding values of F (calculated) are given in Table III. The general order of agreement between measured and calculated values of F is quite comparable to those obtained for other structures which have been successfully analysed. Considering the uncertainty in the f-curve for oxygen and the fact that contributions of the 16 hydrogen atoms in the new cell (monoclinic) have not been separately accounted for, the discrepancies appear to be well within the limits of experimental error.

The preliminary estimate of the structure

With a view to obtaining the correct signs of the co-efficients $F(hkl)$ of the Fourier series, a preliminary analysis of structure by the trial and error method

TABLE III

Measured and calculated values of structure factor.

hkl (after Groth)	HKL (referred to monoclinic cell)	F measured	F calculated	hkl (after Groth)	HKL (referred to monoclinic cell)	F measured	F calculated
002	020	13	+14	4(24)0	(14)05̄	6	−5
400	201	11	−2	4(2̄4)0	(1̄0)07	6	−6
800	402	20	+21	4(28)0	(16)06̄	5	+7
(12)00	603	25	+23	4(2̄8)0	(1̄2)08	5	+7
(16)00	804	24	+21	620	401	22	+16
(20)00	(10)05	10	+10	6̄20	202	27	+23
040	201	41	+36	660	600	4	−7
080	402̄	27	−14	6̄6̄0	003	13	−13
0(12)0	603̄	49	−33	6(10)0	801̄	15	+18
0(16)0	804̄	12	−11	6(1̄0)0	204	11	+15
0(24)0	(12)06̄	21	−19	6(14)0	(10)02̄	16	−19
220	200	35	+32	6(1̄4)0	4̄05	13	−15
2̄20	001	35	+29	6(18)0	(12)03̄	6	+2
260	401̄	30	−27	6(1̄8)0	6̄06	17	+9
2̄60	2̄02	32	−29	6(22)0	(14)04̄	10	−10
2(10)0	602̄	3	+4	6(26)0	(16)05̄	4	+3
2(1̄0)0	4̄03	14	+14	840	601	55	−40
2(14)0	803̄	26	−18	8̄40	203	54	−39
2(1̄4)0	6̄04	14	−11	880	800	15	−11
2(18)0	(10)04̄	13	+13	8̄8̄0	004	27	−20
2(1̄8)0	8̄05	16	+16	8(16)0	(12)02̄	25	+19
2(22)0	(12)05̄	15	−11	8(1̄6)0	4̄06	31	+24
2(2̄2)0	(1̄0)06	10	−5	8(20)0	(14)03̄	16	+14
2(26)0	(14)06̄	5	−4	8(2̄0)0	6̄07	27	+25
440	400	40	−40	8(24)0	(16)04	7	−8
4̄4̄0	002	40	−39	8(2̄4)0	8̄08	6	−6
480	601̄	26	+25	8(28)0	(1̄0)09	3	−2
4̄8̄0	2̄03	30	+25	(10)20	6̄02	9	−6
4(12)0	802̄	4	+5	(10)60	801	47	−31
4(16)0	(10)03̄	6	0	(10)6̄0	204	44	−31

TABLE III (*contd.*)

Measured and calculated values of structure factor.

hkl (after Groth)	HKL (referred to monoclinic cell)	F measured	F calculated	hkl (after Groth)	HKL (referred to monoclinic cell)	F measured	F calculated
(10)(14)0	(12)0$\bar{1}$	18	+ 8	(22)(10)0	(16)03	4	+ 7
(10)($\overline{14}$)0	$\bar{2}$06	5	− 2	041	21$\bar{1}$	2	− 2
(10)(18)0	(14)0$\bar{2}$	33	+31	042	22$\bar{1}$	10	−11
(10)($\overline{18}$)0	$\bar{4}$07	21	+20	043	23$\bar{1}$	4	− 5
(10)(26)0	(13)0$\bar{4}$	6	− 4	044	24$\bar{1}$	8	− 8
(10)($\overline{26}$)0	809	3	− 3	081	41$\bar{2}$	1	+ 2
(12)40	802	6	− 9	082	42$\bar{2}$	13	+16
(12)80	(10)10	9	+10	083	43$\bar{2}$	5	+ 7
(12)$\bar{8}$0	205	11	+ 11	084	44$\bar{2}$	7	− 3
(12)(16)0	(14)0$\bar{1}$	4	− 4	0(12)1	61$\bar{3}$	7	− 7
(12)($\overline{16}$)0	207	6	−11	0(12)2	62$\bar{3}$	1	0
(12)(24)0	(18)0$\bar{3}$	6	− 7	0(12)4	64$\bar{3}$	3	+ 1
(12)($\overline{24}$)0	609	4	− 7	0(16)2	82$\bar{4}$	2	− 7
(14)20	803	5	− 6	0(16)3	83$\bar{4}$	2	+ 3
(14)$\bar{6}$0	405	6	− 9	0(16)4	84$\bar{4}$	10	+ 7
(14)(10)0	(12)01	9	+ 14	0(20)3	(10)3$\bar{5}$	6	− 8
(14)($\overline{10}$)0	206	6	+14	0(24)1	(12)1$\bar{6}$	3	− 2
(14)(14)0	(14)00	9	− 9	0(24)2	(12)2$\bar{6}$	3	− 5
(14)($\overline{14}$)0	007	5	− 7	0(28)2	(14)2$\bar{7}$	3	+ 5
(14)($\overline{18}$)0	$\bar{2}$08	4	+ 6	401	211	34	−17
(14)(22)0	(18)0$\bar{2}$	6	− 6	402	221	43	+32
(16)($\overline{12}$)0	207	8	− 4	403	23	11	+ 7
(18)20	(10)0$\bar{4}$	24	+18	801	412	9	− 1
(18)$\bar{2}$0	805	28	+26	802	422	5	+ 7
(18)(10)0	(14)02	11	− 4	803	432	21	−10
(18)($\overline{10}$)0	407	7	0	804	442	15	+12
(18)(14)0	(16)01	9	−12	(12)02	623	26	+25
(18)($\overline{14}$)0	208	9	−12	(12)03	633	12	+ 5
(20)(12)0	(16)02	5	− 4	(16)01	814	24	+13
(22)20	(12)05	6	− 6	(20)01	(10)15	19	− 12
(22)$\bar{2}$0	(10)06	5	− 2				

was undertaken. The following points rendered useful guidance to arrive at a tentative structure for the purpose :—

1. Considering the known form of anthracene molecule consisting of three plane hexagonal rings lying in one plane, the anthraquinone molecule derived by adding two oxygen atoms at the central ring of anthracene was also considered to be planar in structure to start with. The probability of such a planar structure of anthraquinone molecule was also supported by the analogous structure of benzoquinone already analysed by Robertson where the planar structure of the benzene ring has not been disturbed by the addition of the two oxygen atoms·

2. The anthraquinone molecule was assumed to be centro-symmetrical as required by the space group condition and also supported by the dipole measurement (Fischer and Rogowski, 1939).

3. In view of the small dimension of 3.68 Å only along c-axis of the old unit cell, it would be difficult to accommodate the molecule in the cell if the molecular plane is very much tilted from the ab-face.

4. Although there are 8 molecules in the pseudo-orthorhombic cell, the real unit cell finally obtained under the monoclinic system contains 2 molecules only, where the second molecule is derived from the first by the symmetry operation. As the molecule has got a pseudo-centre of symmetry, a knowledge of the position of atoms comprising half of one molecule only is sufficient to build up the entire structure. The problem thus gets much simplified as the same reduces to the determination of parameters for 7 carbon atoms and one oxygen atom only.

5. For the preliminary trials, all the three benzene rings of anthraquinone molecule were assumed to be regular hexagons as in the case of anthracene. The dimensions of the rings were also assumed to be similar to those observed in anthracene and benzoquinone.

Taking the above points into consideration, it was then tried to find the x and y co-ordinates of the different atoms in the molecule which would give the calculated structure factors as close a fit with the experimental F values as was possible. After a few trials, the following structure gave sufficiently reasonable agreement to obtain the signs of the F(hko) co-efficients for the Fourier summation.

It was concluded by Banerjee (1938) from his magnetic measurements on this crystal that the molecular plane is tilted about the b-axis from the ab-plane by 30°. This was taken as the starting point for the trial structures for the Fourier projection along the other two axes. The x and y co-ordinates being already known accurately from c-axis projection, the z-co-ordinates for the purpose of trials were calculated from the above tilt of molecular plane about the b-axis.
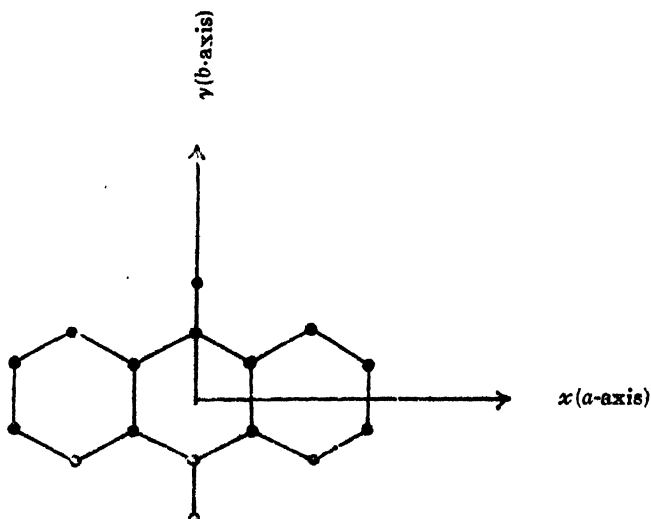
Fourier Summations

Fourier syntheses were carried for projections on the pseudo-orthorhombic planes as they gave much clearer resolutions than the real monoclinic planes. Crystallographic axes, co-ordinates of atoms, molecular orientations, etc., detailed hereafter are as referred to the pseudo-orthorhombic cell ($a = 19.68\text{Å}$, $b = 24.59$ Å and $c = 3.98\text{Å}$) containing 8 molecules of anthraquinone. Corresponding values with reference to the monoclinic cell can easily be calculated from those obtained for this enlarged cell.

A large number of reflecting planes were taken into account in the Fourier projections, particularly along the old c-axis. Contributions from about 180 (hko) planes (*i.e.*, new hol planes) were summed up in the case of c-axis projection as against the maximum of about 150 and 130 planes for one of the projections in the case of anthracene and benzoquinone respectively. Integrated intensities were measured over a wide range, the most intense one having an integrated intensity of about a thousand times that of the weakest. Intensities of a few still weaker reflections were estimated visually from a highly over-exposed photograph and included in the Fourier summation. In the c-axis projection, the Fourier summation was carried out at subdivisions of $a/48$ and $b/48$, which are equivalent to 0.410 Å along a-axis and 0.512 Å along b-axis respectively. For accurate location of the atomic centres, additional summations at closer intervals with axial subdivisions of $a/96$ and $b/96$ round about the atomic centres (*i.e.*, at intervals of 0.205 Å and 0.256 Å along a- and b-axes respectively) were carried out. Axial subdivisions in the projections along a- and b-axes were $b/48$, $c/12$ and $a/48$, $c/12$ respectively, where $c/12 = 0.332$ Å. Closer summations in the regions of the atoms were carried out in these projections also.

Electron maps and atomic co-ordinates

The contour maps were drawn by the graphical interpolation from the summation totals. The maps are reproduced in Figs. 3, 5 and 7. Separate diagrams showing how the molecules are arranged in the projections along the 3 axes are given in Figs. 4, 6 and 8. All the atoms in the molecule are remarkably well resolved in the *c*-axis projection, whereas in the other two projections, atomic centres can hardly be fixed with accuracy owing to considerable overlapping of atoms. *x* and *y* co-ordinates have, therefore been taken from the *c*-axis projection alone, using the other two projections merely as a general check. The accuracy of the co-ordinates is in general 0.01 Å. Direct determination of the *z*-co-ordinates from the *a*- and *b*-axes projections would be
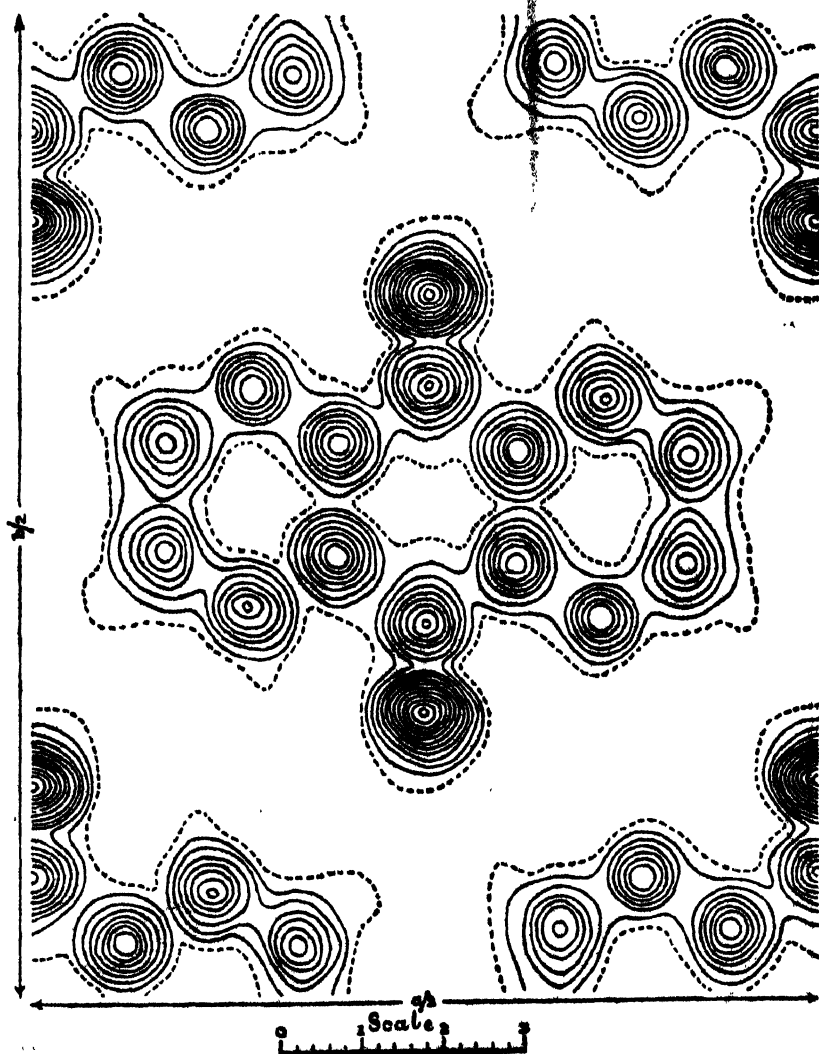
FIG. 3

Projection along the old *c*-axis. Contour lines drawn at intervals of one electron per A², the one electron line being dotted.

unreliable owing to overlapping of atoms. In *b*-axis projection, the molecular plane is found to be tilted from (oo1) plane by 27° degrees about the *b*-axis (30° degrees found by magnetic measurements). The fact that the centres of atoms in one molecule lie approximately on a line in the *b*-axis projection supports the planar structure of the molecule, as has also been found in other allied aromatic compounds. In *a*-axis projection, the oxygen atom and the connecting carbon atom are well resolved, which permit independent evaluation of the co-ordinates for those atoms. In both *a*- and the *c*-axes projections, the oxygen and the adjoining carbon atom and the centre of the molecule lie on the same straight line, which indicates that the oxygen atoms also lie in the plane of the rings. From these considerations, the planar structure of the molecule has been concluded. Deviation from the planar structure,
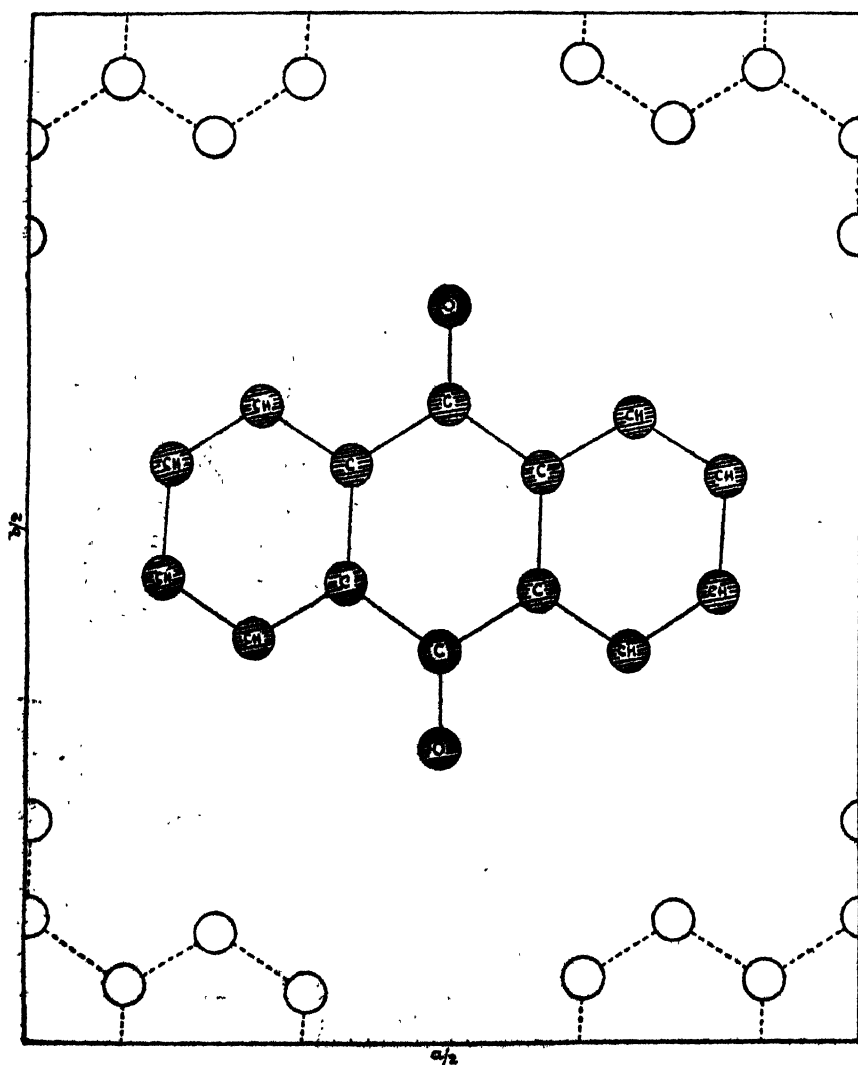
Fig. 4

Showing how the molecules are grouped in *c*-axis projection.

if any, is believed to be negligible. z co-ordinates have, therefore, been worked out from the relation $z = lx + my$, where $l = \tan 27°$ and the constant 'm' is calculated to be 0.0493 from the oxygen co-ordinates assigned independently in the a- and the c-axes projections. The co-ordinates with reference to the orthorhombic cell are given in Table IV. On transformation of the orthorhombic axes of co-ordinates to those of the new monoclinic cell, the final co-ordinates referred to the monoclinic system of axes are obtained from the following relations :—

Scale :
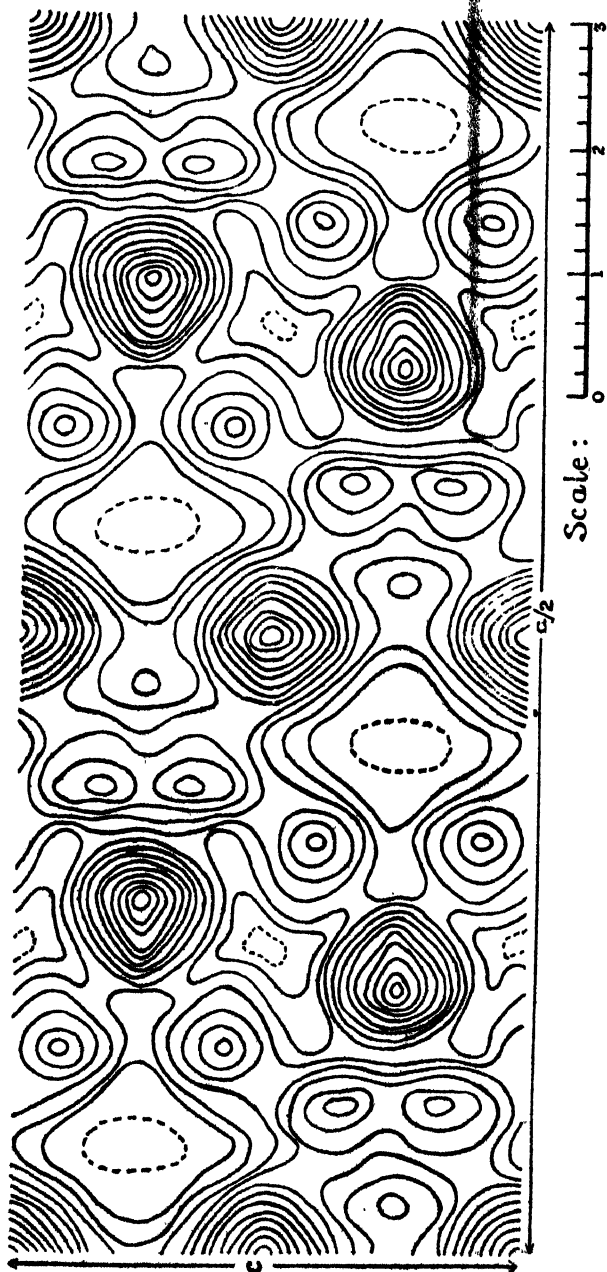
Fig. 5

Projection along the old b-axis. Contour lines drawn at intervals of one electron per the one electron line being dotted.

$$x'/a' = x/a \mp y/b \quad \ldots \qquad \ldots \qquad \ldots \qquad \ldots \quad (i)$$

$$y'/b' = z/c \quad \ldots \qquad \ldots \qquad \ldots \qquad \ldots \quad (ii)$$

$$z'/c' = 2(x/a - y/b) \ldots \qquad \ldots \qquad \ldots \qquad \ldots \quad (iii)$$

$x'y'z'$ and xyz are equivalent co-ordinates on the monoclinic and orthorhombic system and $a'b'c'$ and a, b, c are the corresponding axial lengths of the two cells respectively. The final co-ordinates referred to the monoclinic cell are given in Table V.
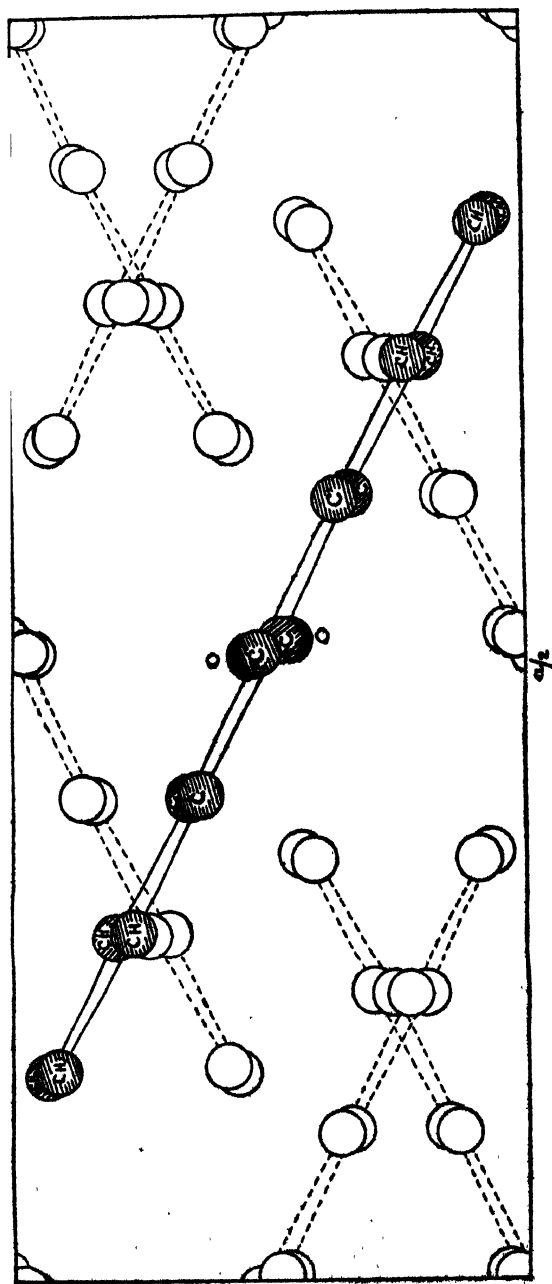
FIG. 6

Showing how the molecules are arranged in projection.

Scale: |____|____|____|
0   1   2   3
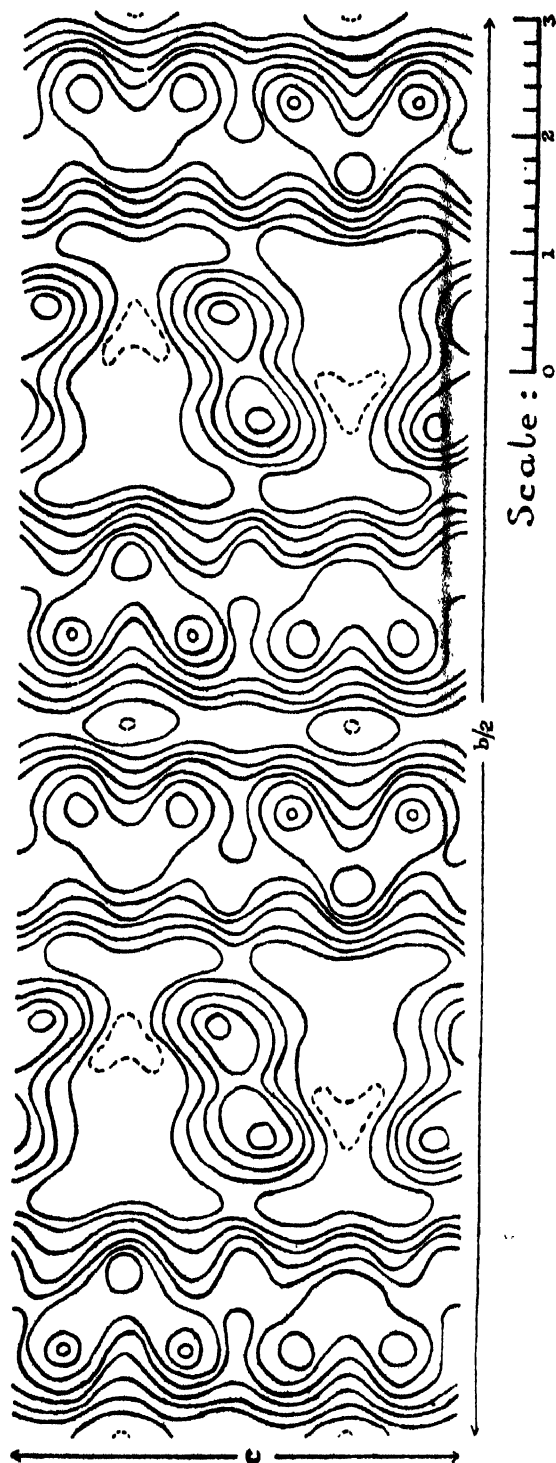
FIG. 7

Projection along the old a-axis. Contour lines drawn at intervals of one electron per A², the one-electron line being dotted.
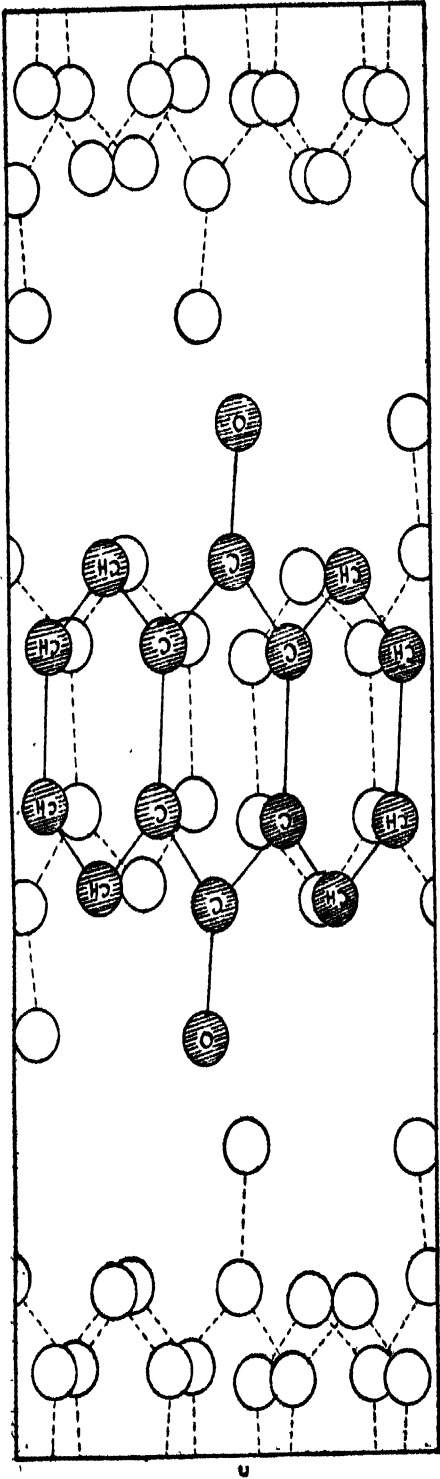
Fig. 8

Showing how the molecules are grouped in a-axis projection.

<div align="center">TABLE IV</div>

Co-ordinates of atoms referred to orthorhombic cell. Molecular centre of symmetry at (ooo) as origin

Atom (*vide* Fig. 9)	xÅ	$(2\pi x/a)°$	yÅ	$(2\pi y/b)°$	zÅ	$(2\pi z/c)°$
A (CH)	−3.253	−59.3	0 765	11.2	−1.634	−147.8
B (CH)	−2.198	−40.2	1.447	21.2	−1 059	− 95.8
C (C)	−1.115	−20.4	0.745	10.9	−0.536	−48.5
D (C)	0.038	0.7	1.476	21.6	0.092	8.3
E (C)	1.164	21.3	0.649	9.5	0.630	57.0
F (CH)	2.236	40.9	1 311	19.2	1.214	109.5
G (CH)	3.308	60.3	0.615	8.8	1.730	156.6
H (O)	0.049	0.9	2.623	38.4	0.155	14.0

<div align="center">TABLE V</div>

Co-ordinates of atoms referred to monoclinic cell. Molecular centre of symmetry at (ooo) as origin

Atom (*vide* Fig. 9)	xÅ	$(2\pi x/a)$	yÅ	$(2\pi y/b)°$	zÅ	$(2\pi z/c)°$
A (CH)	−2.125	−48.3	−1.634	−147.0	−3.111	−141 4
B (CH)	−0.836	−19.0	−1.059	− 95.8	−2.702	−122.8
C (C)	−0.418	− 9.5	−0.536	− 48.5	−1.377	− 62.6
D (C)	0.981	22.3	0.092	8.3	−0.920	− 41.8
E (C)	1.355	30.8	0.630	57.0	0.519	23.6
F (CH)	2.644	60.1	1.214	109 5	0.955	43.4
G (CH)	3.049	69.3	1.730	156.5	2.275	103.4
H (O)	1.729	39.3	0.155	14.0	−1.650	− 75 0

Dimensions and orientation of the molecule

Diagramatic representation of the molecular dimensions together with interatomic distances and valency angles are given in Fig. 9. The distances are probably correct within 0.01 Å with a maximum possible error of ±0.02 Å. The valency angles are expected to be correct within 2°.

The final orientation of the molecules with reference to the crystallographic axes may be described as follows :—

Let us denote the axis passing through the centres of the three rings of anthraquinone as 'long axis' of the molecule and the axis joining the oxygen

atoms and the centre of the molecule as the 'cross axis' of the molecule. Then, the cross axis is very nearly parallel to the b-axis of the pseudo-orthorhombic cell and the position of the molecule is nearly attained by a tilt of the molecular plane about the b-axis so as to make an angle of about 27° with the (001) plane. Tilts about the other axes are of much smaller magnitudes If α, β, γ denote the angles made by the long axis of the molecule with the a, b, c axes respectively and α', β', γ' be the corresponding angles made by the cross axis of the molecule, then these angles as worked out from the structure obtained are :—

$$\alpha = 27°.4 \qquad\qquad \alpha' = 88°.5$$
$$\beta = 91°.2 \qquad\qquad \beta' = 3°.8$$
$$\gamma = 62°.9 \qquad\qquad \gamma' = 86°.4$$
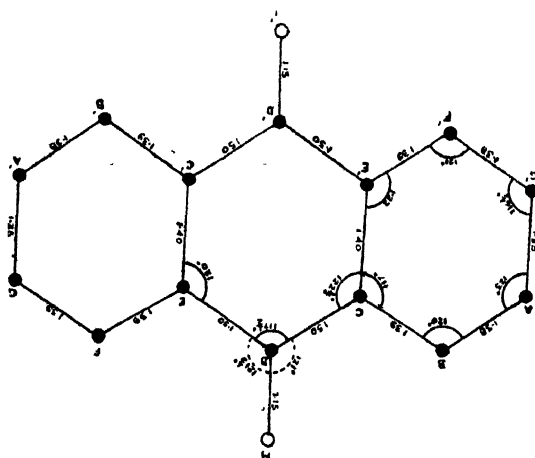
FIG. 9

Dimensions of anthraquinone molecule.

Molecular dimensions

Interatomic distances in A.U.   Valency angles.

Carbon-Carbon : AB = 1.38 ⎱
                 F'G' = 1.38 ⎰   CH–CH $\angle ABC$ = 120°
                 AG' = 1.385 ⎰ (Aromatic) $\angle BCE'$ = 117°
                                                $\angle CE'F$ = 122°

                 BC = 1.39 ⎱ $\angle E'F'G'$ = 121°
                 E'F' = 1.39 ⎰   C–CH $\angle F'G'A$ = 116½°

                 CE' = 1.395   C–G $\angle G'AB$ = 123

                 CD = 1 50 ⎱   C–C $\angle E'CD$ = 122½°
                 DE = 1.50 ⎰ (" single bond ") $\angle CDE$ = 117½°

Carbon-Oxygen : DH = 1.15   C–O $\angle DEC'$ = 120°
                                                $\angle CDH$ = 121°
                                                $\angle EDH$ = 121½°

Arrangement of molecules in the crystal and molecular distances

The dominant feature found in the anthraquinone structure is the grouping of molecules in a zig-zag way in space with the molecular planes in the alternate layers being inclined to one another at an angle of 54°. Molecular planes are inclined at an angle of 27° to the (001) plane. The zig-zag arrangement is best seen by projecting the structure on (010) plane as shown in Fig. 10. The molecules are, however, remarkably well resolved in the
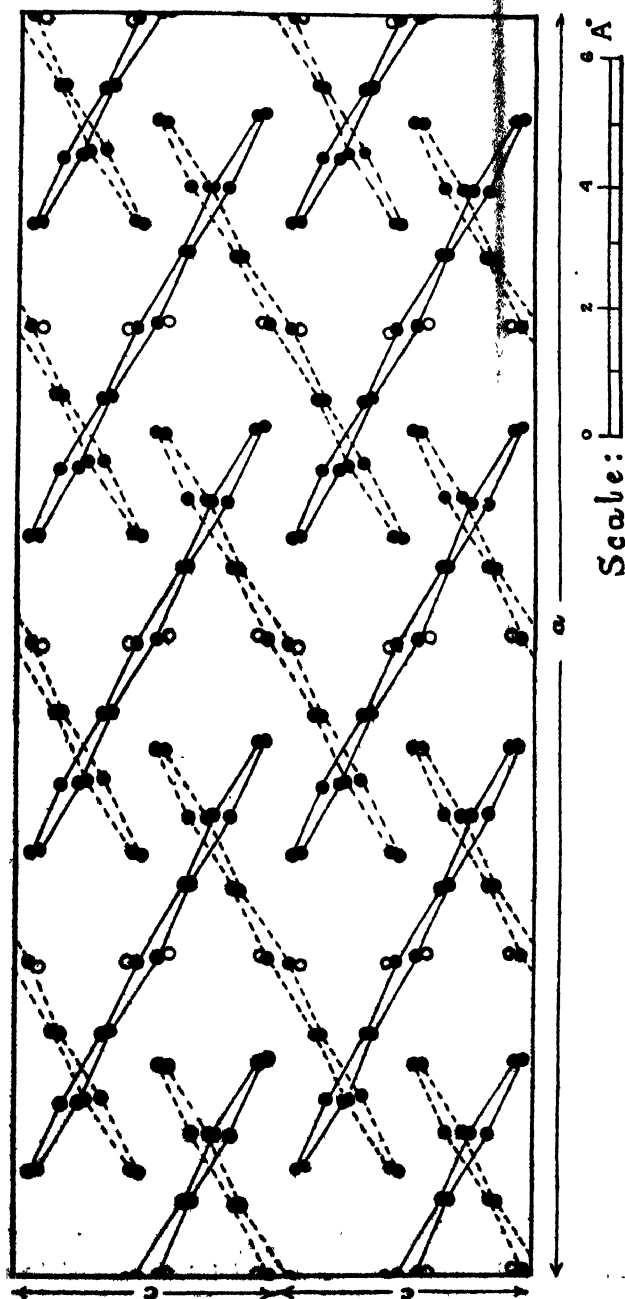
FIG. 10

Projection along old *b*-axis showing 8 molecules. The plane of each molecule is nearly perpendicular to the plane of projection.

projection along the symmetry axis (*i.e.*, old *c*-axis). Such a projection on a smaller scale showing the relations of a group of 32 molecules is shown in Fig. 11. To visualise how the molecules are arranged in space from the diagram (Fig. 11), it is to be imagined that the dotted molecules have their centres in planes $\frac{1}{2}c$ above and below those of the molecules shown with

Scale: E

$\overline{12}\,\mathring{A}$

FIG. 11

Projection along old *c*-axis showing the relation of a group of 32 molecules. The dotted molecules have their centres in planes *c*/2 above and below those of the molecules shown with black atoms.

shaded atoms. All the molecules are tilted from *ab*-plane (plane of the paper) by $27°$ about the *b*-axial direction passing through the centres of the molecule, the tilt of the dotted and shaded molecules being in opposite directions.

The nearest molecular approach occur between two molecules where one is derived from the other by the fundamental translation along *c*-axis ($c = 3.98$ Å). The perpendicular distance between the planes of these two molecules is approximately $3.98 \cos 27° = 3.54$ Å, which is, therefore, the minimum distance of approach between any two molecules. If A, B, C etc. are atoms of the molecule derived by fundamental translation along *c*-axis of the molecule comprised of A, B, C, . . atoms (*vide* Fig. 9), the minimum intermolecular distance between carbon atoms occur between $\bar{A}$ and B; $\bar{B}$ and C; $\bar{C}$ and D and so on. Such distances when worked out range between 3.6 and 3.7 Å. In benzoquinone, corresponding observed distance is 3.45 Å, while in rescorcinol (Robertson, 1936), it is 3.6 Å. Minimum oxygen-oxygen inter-molecular distance in anthraquinone is the same as the fundamental translation of 3.98 Å. In benzoquinone, corresponding observed distance is 3.62 Å. The minimum intermolecular distance obtained in anthraquinone thus agree well with the usual order of such distances observed in other compounds.

Peak values of electron density and electron counts

The observed peak values of electron density for the different atoms in the *c*-axis projection where the atoms are remarkably well resolved are given in Table VI. The values are in general somewhat higher as compared to those observed in anthracene and benzoquinone. The values observed for the carbon atoms in the present case are between 7.5 to 9 electrons per square A.U. (6-7 observed in other structures). The peak values for the carbon atoms are found to gradually fall off as we pass outwards from the centre of the molecule, although one would ordinarily expect higher values for the outer CH groups as compared to the carbon atoms of the inner ring. A slight broadening of the end atoms is also observed. It is interesting to note that such falling off in the peak values of electron density as we pass out from the centre of the molecule, combined with a slight broadening of the structure has also been observed in the case of anthracene and other allied compounds. In anthracene, peak values were found falling gradually from 7 to 5.5 electrons per square A.U. towards the end of the molecule.

In the *c*-axis projection in which each of the atoms is distinctly resolved, electron counting was carried out by the method first used by Bragg (1929). Boundary lines were drawn round each of the atoms comprising half of the molecule as shown in Fig. 12. The appropriate electron densities $\rho(x, y)$ at intervals of $a/96$, $b/96$ were then summed up with appropriate weightage to fractional square near the boundary lines and number of electrons for each of the atoms calculated from the relation $N = \Sigma \rho(x, y) \times ab/96^2$. Results so obtained are given in Table VI. Electron
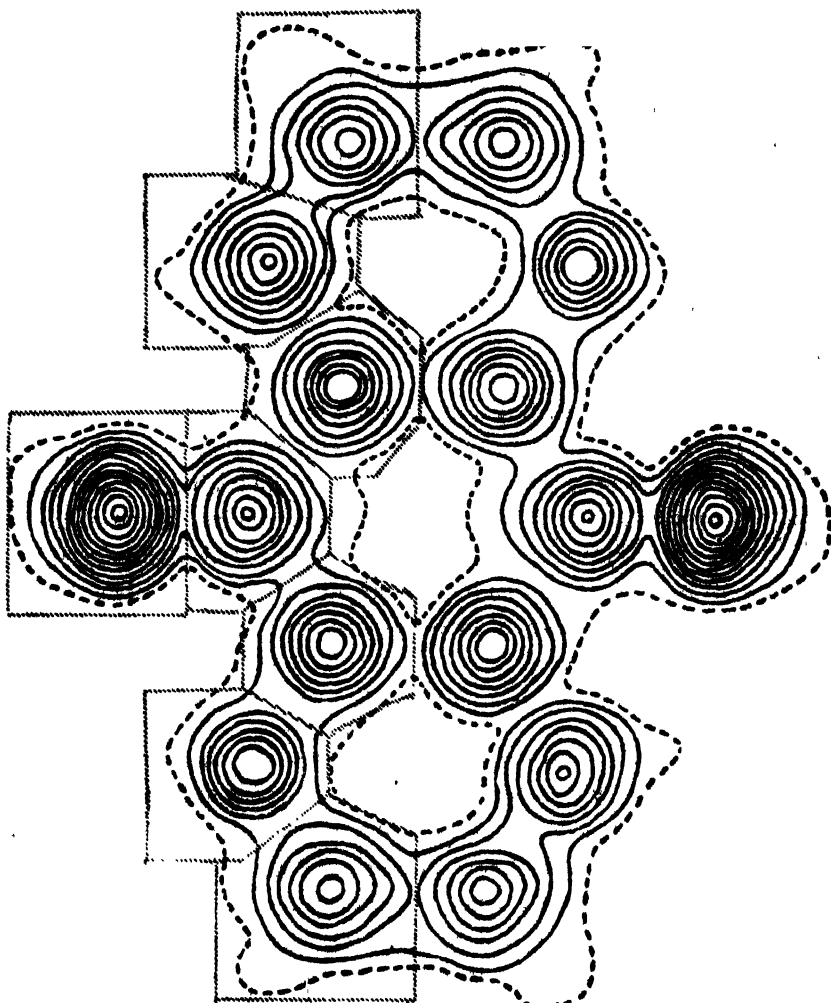
FIG. 12

Electron count in anthraquinone molecule (projection along old c-axis)

TABLE VI

Peak values of electron density : electron counts

	Atom	Peak value per sq. A U	Number of electrons
Carbon :	A (CH)	7.5	6.8
	B (CH)	7.4	5.6
	C (C)	8.8	5.9
	D (C)	9.0	6.0
	E (C)	8.2	5.9
	F (CH)	8.1	6.0
	G (CH)	7.4	6.4
Oxygen :	H (O)	13.0	9.5

count for the oxygen atom gives 9.5 electrons instead of 8 as required by the atomic number. This suggests that the oxygen atoms in anthraquinone have partial ionic character. The discrepancy may also be partly due to inaccuracy in the intensity measurements and to the omission of the still weaker reflections in the Fourier series.

DISCUSSION OF RESULTS

Revision of space group

It will be seen that a wrong assumption of space group for the anthraquinone crystal under the orthorhombic system apparently frustrated all earlier attempts to determine its correct structure. It has now been established beyond doubt that the crystal belongs to the monoclinic system. The space group is found to be $C_{2h}^5 P_1^2/a$. The fact that the crystal developes very few faces has also been partially responsible for the earlier confusion in the classification of the anthraquinone crystal. The revision of the crystal class and the determination of its correct space group fully account for all the observed points which appeared anomalous on the assumption of orthorhombic nature of the crystal. The arrangement of the molecules in the crystal finally obtained clearly explains its pseudo-orthorhombic nature.

It is noteworthy that a few very feeble reflections have been observed in a highly over-exposed Weissenberg photograph which are actually forbidden spectra for the space group $C_{2h}^5 P_1^2/a$ and thus, in the strict sense of space group, anthraquinone has to be classed under the bisphenoidal class with its space group as C_2^2. But the contribution of these few exceedingly feeble reflections towards structure would be so infinitesimally negligible that it can lead to no deviation from the centro-symmetrical structure of the molecule. The space group $C_{2h}^5 P_1^2/a$ has therefore, been assigned to the crystal.

Molecular dimensions and comparison with those of anthracene and benzoquinone

The anthraquinone molecule has been found to be approximately planar. Though none of the three benzene rings in anthraquinone molecule is found to be perfectly regular hexagon, the two outer rings are very nearly regular with carbon to carbon distances varying between 1.38 Å and 1.40 Å. Thus each of these distances lies within the limits 1.39 Å ± .01. Corresponding distances found in anthracene (Robertson, 1933) is 1.41 Å, while in resorcinol (Robertson, 1936) it is 1.39 Å. The valency angles observed in the outer rings are between 117° and 123°. It is, however, difficult to say whether this deviation from 120° for these angles is genuine or only due to experimental error. The outer rings may, therefore, be considered to be regular plane hexagons, within the limits of experimental error, like those of the anthracene molecule. The central ring is, however, definitely distorted like benzoquinone molecule.

The "single" bond carbon to carbon distances in the central ring of anthra-quinone molecule are found to be approximately 1.50 Å which is identically the same value as observed in benzoquinone. One striking difference between the two structures is, however, noticed in the valency angles between the single bonds. In benzoquinone, the angle has the tetrahedral value of 109°½, while in anthraquinone it is found to be 117°. The angle between the single and double bonds was found to be 125° in benzoquinone, but the double bond being absent in anthraquinone molecule, the corresponding valency angle in anthraquinone molecule occurs between a single and a conjugate bond as in the case of hexamethylbenzene (Lonsdale, 1929, or dibenzyl (Robertson, 1934) where these angles are approximately 120°. As would be expected in analogy with the measurements for hexamethylbenzene and dibenzyl, the valency angles between the single and the conjugated bonds of the central ring of the anthraquinone molecule are actually found to be 120°-122°. These angles thus being smaller than corresponding value of 125° observed in benzoquinone, the valency angle between the single bonds in anthraquinone must be proportionately greater than the benzoquinone value of 109°½. This explains the observed value of 117° between the single bonds found in anthraquinone.

The carbon to oxygen distance in anthraquinone is found to be 1.15 Å which is almost the same as that observed in benzoquinone, namely, 1.14 Å. The band spectrum and infra-red absorption spectrum analyses of carbon dioxide vapour give the carbon to oxygen distance as 1.15 Å and 1.16 Å, respectively. In benzoquinone, the carbon to oxygen distance could not be measured directly because the carbon atom to which the oxygen is directly attached remained obscured in all the projections and it also became difficult to locate accurately the position of the centre of the oxygen atom as it appeared slightly elongated in the projection. In anthraquinone, however, both the carbon and oxygen atoms are very well resolved in the projection along the symmetry axis and centres of these atoms could be accurately located. Although a higher value of 1.25 Å has been found for the carbon to oxygen distance in urea (Wyckoff and Corey, 1934), the distance observed in anthraquinone supports the benzoquinone value and those observed in the case of carbon dioxide. The ketonic oxygen in anthraquinone is also thus seen to be rather similar to the oxygen in carbon dioxide.

Chemical formula and the nature of the valency bonds

The alternative structural formula of anthraquinone are given below :—

The outer rings being found to be regular hexagons instead of alternate single and double bond distances, the formula (1) for anthraquinone does not correctly represent the molecule. Formula (2) based on the "centric" formula with unlinked bonds fully supports the observed structure of anthra-quinone molecule.

(1)   (2)
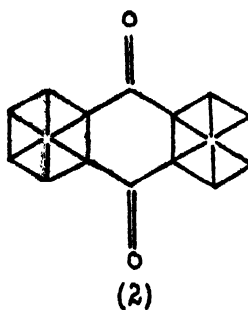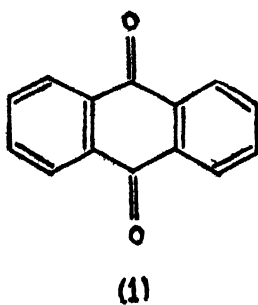
The stability and characteristic aromatic properties of substances have been attributed to a resonance between th different stable valance-bond structures which are termed 'canonical' structures of Pauling analogous to the resonance of benzene between two Kekule structures *viz.*

For anthraquinone, the following four stable valence-bond structures can be formulated :—
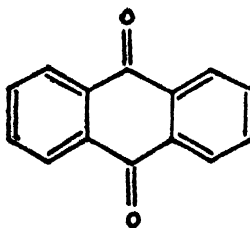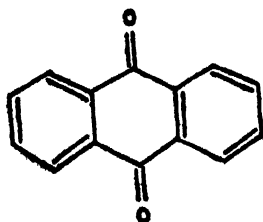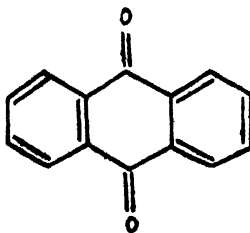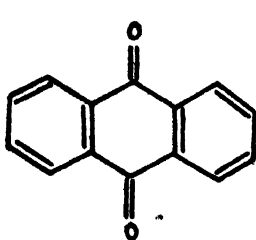
It will be seen that each of the bonds in the outer rings occurs as double bond in two of the above structures and as single bonds in the remaining two structures. That is, each of these may be considered to have 50% double bond character and in accordance with Pauling's curve (1935), such bond

corresponds to an interatomic distance of 1.39 Å. The observed distance agrees well with the above consideration.

ACKNOWLEDGMENTS

I wish to express my grateful thanks to Prof. K. Banerjee, D.Sc., for suggesting the problem and for his many valuable suggestions throughout the progress of the work. My grateful thanks are also due to Prof. S. N. Bose for his keen interest and encouragements throughout this investigation.

METEOROLOGICAL OFFICE
ALIPORE, CALCUTTA.

REFERENCES

Banerjee, K. and Guha, B.C., 1934-35, *Ind. Jour Phys.*, **9**, 288.
Banerjee, S., 1938, *Zcits. fur. Kryst.*, **100(A)**, 316.
Bragg, W.L., 1929, *Proc. Roy Soc.*, **123A**, 537.
Brindley, 1936, *Phil. Mag.*, **21**, 778.
Caspari, 1932, *Proc. Roy. Soc.*, **136A**, 82.
Dutta, M. N., 1947, *Ind. Jour. Phys*, **21**, 303.
Fischer and Rogowski, 1939, *Phys. Zeits.* **40**, 331
Groth, 1906, *Chem. Krist*, **5**, 442.
Guha, B.C., 1938, *Phil. Mag.*, **36**, 213.
Hertel and Romer, 1931, *Zeits. Phys. Chem.*, Bd. **11B**, 90.
Lonsdale, K., 1929, *Proc Roy. Soc.*, **123**, 494.
Pauling, L, Brockway and Beach, 1935, *J Amer. Chem Soc*, **87**, 270
Robertson, J. M., 1933, *Proc. Roy. Soc*, **142**, 674.
Robertson, J. M., 1933, *Proc. Roy. Soc.*, **140**, 79.
Robertson, J. M., 1935, *Proc. Roy. Soc.*, **150**, 106.
Robertson, J. M., 1934 *Proc. Roy. Soc.*, **146**, 473
Robertson, J. M., 1936, *Proc. Roy. Soc.*, **157**, 79.
Robinson, B. W., 1933, *J. Sci. Instr.*, **10**, 233.
Wollan, 1930, *Phys., Rev.*, **36**, 1019.
Wycoff, R. W. and Corey, 1934, *Zeits. Krist.*, **89**, 462.

TOMORROW'S INSTRUMENTS TODAY

RAJ-DER-KAR & CO.

COMMISSARIAT BUILDING

HORNBY ROAD

FORT

BOMBAY

OFFERS

FROM STOCK

GLASS METAL DIFFUSION PUMPS, METAL BOOSTE
PUMPS, OILS AMOILS OCTOILS OCTOIL,
BUTYL SABACATE

MANUFACTURED

BY

DISTILLATION PRODUCTS
(U. S. A.)

SPENCER MICROSCOPE

CENCO HIGHVACS

BESLER EPIDIASCOPE

COMPLETE WITH FILM STRIP ARRANGEMENTS

Telephone 27304
2 Lines

Telegrams
TECHLAB

The following special publications of the Indian Association for the Cultivation of Science, 210, Bowbazar Street, Calcutta, are available at the prices shown against each of them :—

Subject	Author	Price Rs. A. P.
Methods in Scientific Research	... Sir E. J. Russell	0 6 0
The Origin of the Planets	... Sir James H. Jeans	0 6 0
Separation of Isotopes	... Prof. F. W. Aston	0 6 0
Garnets and their Role in Nature	... Sir Lewis L. Fermor	2 8 0
(1) The Royal Botanic Gardens, Kew.	... Sir Arthur Hill	1 8 0
(2) Studies in the Germination of Seeds.	,,	
Interatomic Forces	... Prof. J. E. Lennard-Jones	1 8 0
The Educational Aims and Practices of the California Institute of Technology.	... R. A. Millikan	0 6 0
Active Nitrogen A New Theory.	... Prof. S. K. Mitra	2 8 0
Theory of Valency and the Structure of Chemical Compounds.	... Prof. P. Ray	3 0 0
Petroleum Resources of India	... D. N. Wadia	2 8 0
The Role of the Electrical Double layer in the Electro Chemistry of Colloids.	... J. N. Mukherjee	1 12 0

A discount of 25% is allowed to Booksellers and Agents.

RATES OF ADVERTISEMENTS

Third page of cover	...	...	...	...	Rs. 32, full page
do. do.	...	...	...	...	,, 20, half page
do. do.	...	...	...	...	,, 12, quarter page
Other pages	...	...	...	...	,, 25, full page
do.	...	...	...	...	,, 16, half page
do.	...	...	...	...	,, 10, quarter page

15% Commissions are allowed to *bonafide* publicity agents securing orders for advertisements.

CONTENTS

NOTICE
TO INTENDING AUTHORS

Manuscripts for publication should be sent to Mr. A. N. Banerjee, Assistant Editor, 210, Bowbazar Street, Calcutta.

The manuscript of each paper should contain in the beginning a short abstract of the paper.

All references to published papers should be given in the text by quoting the surname of the authors followed by the year of publication within braces, *e.g.*, Sen (1942). The actual references should be given in a list at the end of the paper according to the following specimen :

Sen, B. K., 1942, Volume rectification of crystals, *Ind. J. Phys.*, **16**, 329.

The references should be arranged alphabetically in the list.

All diagrams should be drawn on thick white paper in Indian ink, and letters and numbers in the diagrams should be written in pencil.

THE GEOMETRY OF EXTRAORDINARY REFRACTION*

By J. B. SETH

ABSTRACT An expression has been deduced connecting the angle of refraction of the extraordinary ray (and of the extraordinary wave normal) in a uni-axial crystal with the angle of incidence and the inclination of the optic axis to the refracting surface The usual special cases given in text books follow from the general expression. The peculiarities in the behaviour of the extraordinary ray at normal incidence but with different inclinations of the optic axis have been derived. Mention has also been made of peculiarities at oblique incidence, the details and data of the general case being left over to another paper

INTRODUCTION

The only method of finding the direction of the extraordinary ray, or of the extra-ordinary wave normal, seems to be with the help of Huygens' construction. An actual geometrical construction in every case, however, cannot be regarded as a really practical method of doing so ; nor can it give quantitatively correct results. It is, therefore, necessary to find some convenient relationship between the angle of incidence and that of the extra-ordinary refraction, *i. e.* the e-ray or the e-wave normal ; some readily applicable expression like Snell's law which holds for the ordinary refraction, namely, that the ratio of the sine of the angle of incidence to that of refraction is a constant, being equal to the ordinary refractive index, μ_o.

Relationships for the extraordinary ray in uni-axial crystals in some simple and special cases, namely, the optic axis in the plane of incidence and either (a) parallel or (b) perpendicular to the refracting surface of the crystal, are found by making use of the pure geometrical properties of an ellipse and are given in all text books dealing with the matter, in connection with the experimental verification of Huygens' construction. In some books, the case of normal incidence, but any inclination of the optic axis, has also been derived, again with the help of pure geometry. The general case, when the optic axis is in any direction whatever and any angle of incidence, does not appear to have been derived, at least, is not given in any of the usual text books.

It, therefore, occurred to the author to investigate the general, or rather the semi-general, case of any angle of incidence and any inclination of the optic axis, only the optic axis remaining in the plane of incidence. This has been done here with the help of co-ordinate geometry. The most general

---

case of the optic axis not being confined to the plane of incidence involves the use of solid geometry and is beyond the scope of the present investigation. The very special case when the optic axis is perpendicular to the plane of incidence does not require any special treatment, for in this case the e-ray obeys all the laws of refraction and therefore its direction is immediately determinable by the application of Snell's law again, the constant being now the extra-ordinary refractive index, μ_e.

From what has preceded, it must be obvious that this paper will deal only with uni-axial crystals. The general case of bi-axials does not fall within our purview. For the sections of the wave surface in a biaxial crystal are not simple curves and the results obtained in this paper are based on the fact that the sections of the extraordinary wave surface in a uni-axial crystal are ellipses in all azimuths but one in which they are circles. In the case of a biaxial crystal as well, the sections of the wave surface by the three principal planes are, in each case, a circle and an ellipse. Of the two rays in these sections, therefore, the one given by the circle will behave like an ordinary ray ; the other given by the ellipse, will behave like the extraordinary ray in a uni-axial. The results obtained in this paper can, therefore, be adapted quite easily to give the direction of the extraordinary ray when the plane of incidence is parallel to one of the three principal sections of the biaxial crystal.

<center>SYMBOLS USED</center>

For the purpose of deriving the relationship wanted, we take the case of a negative uni-axial crystal, like calcite (calcspar), although we shall see that the results obtained in the final working form applies equally to the positive crystals.

Since the case of a uni-axial is only a particular case of a bi-axial, we shall take here that the major and minor semi-axes of the generating ellipse of the spheroid giving the extraordinary wave surface are given by a and c. For the case in hand, that of a negative crystal, the spheroid is oblate and the ordinary and extraordinary wave, or ray, velocities will be given respectively by c and a, taking the velocity of light in vacuo as unity. Thus, $\mu_o = 1/c$, $\mu_e = 1/a$. We take the two axes of reference to be the axis of x and that of z, taking the optic axis, the minor axis, to be the axis of x. Taking O as the point of incidence on the face of the crystal, a line, OX, drawn from O *into* the crystal will be taken as the positive direction of the axis of x. The line, OZ, perpendicular to OX and "above" or on the right side of OX, will be taken as the positive direction for the z-axis. The equation of the generating ellipse is, then,

$$x^2/c^2 + z^2/a^2 = 1 \tag{1}$$

We take the plane of the paper as the plane of incidence, with the optic axis in this plane, and take α as the angle between the optic axis and

the refracting face of the crystal. In Fig. 1, the angle XOT thus $=\alpha$. The angle between the refracted extraordinary ray and the optic axis is taken to be θ, that between the optic axis and the extraordinary wave normal as ϕ. The angle of incidence, *i.e.*, the angle between the incident ray and the normal to the surface at the point of incidence, which is the same as the angle between the incident (plane) wave front and the refracting surface, is, as usual, taken to be i. The angles of refraction for the ordinary ray, the extraordinary ray and the extraordinary wave normal are taken to be r, r', r'', respectively. These are the angles between the normal to the refracting surface and, respectively, the ordinary ray, the e-ray and the normal to the extraordinary refracted (plane) wave front.

We shall find θ (or ϕ) in terms of α and i. θ (or ϕ) being known, r' (or r'') become immediately determined, as is done at the end of the next section after giving the convention regarding signs.

THE SIGN CONVENTION

We shall always consider the incident ray to lie on the left of the normal to the refracting surface and consider i to be positive in this case. In ordinary refraction, the refracted ray always lies on the other side of the normal, *i.e.*, the side of the normal other than that on which the incident ray lies. If, then, the e-ray lies on the right side of the surface normal, r' will be regarded as positive ; if it lies on the left side, r' will be taken as negative. Similarly, if the optic axis lies on the right of the surface normal, α will be taken to be positive ; if it lies on the left, α will be regarded as negative. That is to say, if the straight line to represent the optic axis is drawn from the point of incidence *into* the crystal, then if it lies on the same side of the normal as the incident ray, α will be negative : if it lies on the other side, α will be positive. (As a matter of fact, since the optic axis is taken as the axis of x, the positive direction of which is as, has just been described, the positive and negative signs of α, as given here, follow automatically).

With respect to θ (or ϕ), if this comes out to be positive, it means that the extraordinarily refracted ray lies in the first quadrant, XOZ, whether α be positive or negative. If, on the other hand, θ comes out to be negative then the refracted ray will lie in the fourth quadrant $Z'OX$, if α be positive ; or, when α is negative, then in the second quadrant, ZOX'. By drawing diagrams in all the four cases, it can be verified that the angle of refraction of the e-ray, r', is given by,

$$r' = \theta - \alpha \pm 90° \qquad \qquad \dots \ (2)$$

Both θ and α in the above equation are to be taken with their proper signs. The angle, $90°$, is to be subtracted in only one case, when α is negative and θ positive : in all the other three cases it is to be added.

Similarly, and with similar remarks regarding signs, for the extraordinary wave normal,

$$r'' = \phi - \alpha \pm 90° \qquad \qquad \ldots \ (3)$$

GEOMETRICAL

Fig. 1, represents the plane of incidence. *SOT* is the trace of the refracting surface of the crystal, which is a plane passing through *ST*, perpendicular to the plane of the paper. *OX* is the direction of the optic axis, *O* being the point of incidence. *NON'* is the normal to the surface at *O*. *RO* is the incident ray. A straight line, *OI*, at right angles to *RO*, is the trace of the incident plane wave front, the plane of which is perpendicular to the plane of the paper. *IT*, at right angles to *OI*, is another incident ray. Taking *IT* = unity, and with centre *O*, the appropriate ellipse *SACP* with major and minor axes = 2a and 2c respectively, is drawn so that *OA* = a and *OC* = c. From *T* the tangent, *TP*, to the ellipse, is drawn touching it at *P*. Then *OP* is the extraordinary refracted ray corresponding to the incident
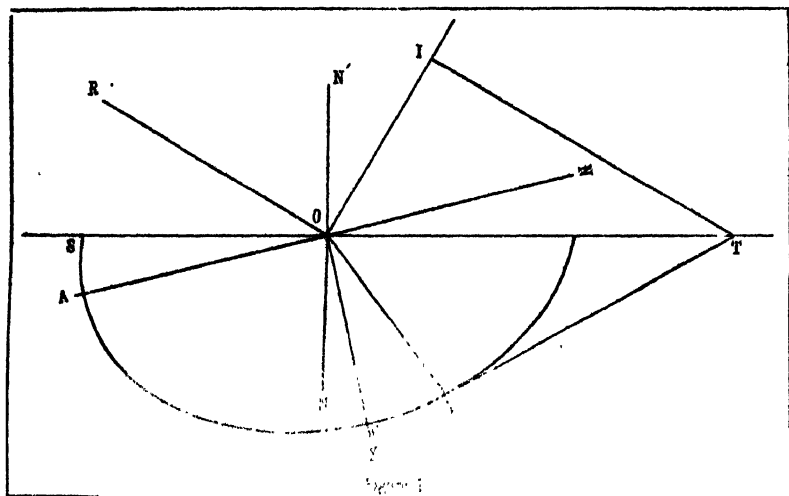
ray, *RO*, and the angle, *POX* = θ, which is to be determined. The angle of refraction itself of the e-ray is *PON* = r'. The angle, *RON'* = the angle, *IOT* = the angle of incidence = i.

Since *IT* = unity, the co-ordinates of *T* are given by, $x = \cos \alpha / \sin i$, $z = \sin \alpha / \sin i$. Let the equation of the tangent, *TP*, be $z = mx + k$. Then, since *TP* passes through *T* and is tangential to the ellipse given by the equation (1), we have,

$$\frac{\sin \alpha}{\sin i} = m\frac{\cos \alpha}{\sin i} + \sqrt{c^2 m^2 + a^2}.$$

This gives a quadratic equation in *m*, namely, $m^2 (\cos^2 \alpha - c^2 \sin^2 i) + m \sin 2\alpha + \sin^2 \alpha - a^2 \sin^2 i = 0$, from which we get,

$$m = \frac{\sin 2\alpha \pm 2 \sin i \sqrt{a^2\cos^2\alpha + c^2\sin^2\alpha - a^2c^2\sin^2 i}}{2(\cos^2\alpha - c^2\sin^2 i)} \qquad \dots \quad (4)$$

This gives the two tangents that can be drawn to the ellipse from the point, T. For our present purpose we want only one of these, the "lower" one in Fig. 1, which, a little consideration will show, is given by the positive value of the radical. In what follows, therefore, we shall retain only the positive sign.

Now the point, P, satisfies the relations.

$$(a) \quad z = mx + k, \ k^2 = c^2 m^2 + a^2 ;$$

$$(b) \quad x^2/c^2 + z^2/a^2 = 1.$$

P is, therefore, given by,

$$x = -mc^2/k ; \ z = a^2/k.$$

Therefore we have

$$\tan \theta \, (= z/x) = -a^2/c^2 m \qquad \dots \quad (5)$$

where m has the value given above (equation 4) with the positive sign before the radical.

THE DIRECTION OF THE EXTRAORDINARY RAY

The direction of the extraordinary ray with respect to the optic axis, namely, θ, has been obtained above (eqn. 5). We give it its final working form by putting a and c in terms of the two refractive indices. Thus putting $c = 1/\mu_0$ and $a = 1/\mu_e$, we get that for any angle α, which the optic axis makes with the refracting surface, the relation between i, the angle of incidence, and θ, the angle which the extraordinary ray makes with the optic axis, is given by,

$$\tan \theta = \frac{-2Q(\mu_0^2\cos^2\alpha - \sin^2 i)}{P \sin^2\alpha + 2 \sin i \sqrt{R}} \qquad \dots \quad (6)$$

where $$P = \mu_0\mu_e ; \ Q = \mu_0/\mu_e ; \text{ and}$$

$$R = \mu_0^2\cos^2\alpha + \mu_e^2\sin^2\alpha - \sin^2 i.$$

It must be remembered that in the above equation α must be taken with the proper sign, namely, positive if the optic axis is inclined towards the right of the surface normal, negative if towards the left. It may also be recalled that we take i to be always positive, *i.e.*, the incident ray towards the left of the surface normal. This only means that in the foregoing expression (and similar expressions which follow) only $\sin 2\alpha$, and no other term, will be affected by the sign of α.

Since the actual angle of refraction, r', is given by $r' = \theta - \alpha \pm 90°$, so that $\theta = r' + \alpha \pm 90°$, and, therefore, $\tan \theta = -\cot (\alpha + r')$, the angle of refraction itself of the extraordinary ray is given by

$$\tan(\alpha + r') = \frac{P \sin 2\alpha + 2 \sin i \sqrt{R}}{2Q(\mu_0^2\cos^2\alpha - \sin^2 i)} \qquad \dots \quad (7)$$

It should be noted that when the right hand side of the equations, 6, 7, 8, 12, come out to be negative, care has to be exercised in selecting the correct angle. For both $\tan(-A)$ and $\tan(180° - A) = -\tan A$, where A is an acute angle.

THE EXTRAORDINARY WAVE NORMAL

Since the equation of the central perpendicular to the tangent, $z = mx + k$, is given by $z = -x/m$, where m is given by equation (4), the angle, ϕ, which the normal to the extraordinary wave front makes with the optic axis will be given by

$$\tan \phi = -\frac{2}{Q} \frac{\mu_0^2\cos^2\alpha - \sin^2 i}{P \sin 2\alpha + 2 \sin i \sqrt{R}},$$

where P, Q, R have the same values as given with equation (6), and, again, α is to be taken with the appropriate sign, i being always regarded as positive.

Thus the relationship between ϕ and θ is,

$$\tan \phi = \frac{1}{Q^2}. \tan \theta \qquad (8)$$

Or, putting θ and ϕ in terms of r' and r'',

$$\tan (\alpha + r'') = Q^2 \tan (\alpha + r') \qquad \ldots \quad (9)$$

It may be mentioned here that very few authors deal specifically with the direction of the extraordinary wave normal.

POSITIVE CRYSTALS

In the foregoing treatment the optic axis, the axis of x, was taken the minor axis of the generating ellipse of which the semi-axes are a and c. That gave the case of the negative crystals. In positive crystals the optic axis is the major axis of the ellipse. Taking this now as the x-axis, we get for $\tan \theta$, where θ is, as before, the angle between the e-ray and the optic axis,

$$\tan \theta = -c^2/a^2 m \qquad \ldots \quad (10)$$

where m is now given by,

$$m = \frac{\sin 2\alpha \pm 2 \sin i \sqrt{c^2\cos^2\alpha + a^2\sin^2\alpha - a^2 c^2\sin^2 i}}{2(\cos^2\alpha - a^2\sin^2 i)} \qquad \ldots \quad (11)$$

On comparing these two expressions, equations (10) and (11), with the corresponding expressions for negative crystals, equations (5) and (4) respectively, we find that they differ from each other only in a and c being interchanged. In view of the fact that now $\mu_0 = 1/a$ and $\mu_e = 1/c$, and that, as before, it is the positive value of the radical which is cognate to the case in hand, the expression for $\tan \theta$ in terms of the refractive indices remains exactly the same as before.

Thus for all uni-axial crystals, whether positive or negative, we have,

$$\tan\theta = -\cot(\alpha + r') = \frac{-2Q(\mu_0{}^2\cos^2\alpha - \sin^2 i)}{P\sin 2\alpha + 2\sin i\sqrt{R}} \tag{12}$$

And, similarly, the angle between the extra-ordinary wave normal and the optic axis is. in all cases of uni-axials, given by equation (8).

THE USUAL SPECIAL CASES

The various special cases usually given in text books and mentioned before are immediately obtained by putting the appropriate values of α or i in the expressions for θ and ϕ (or r' and r''). These are given below.

Case i.—The optic axis parallel to the refracting surface and in the plane of incidence :

Putting $\alpha = 0$ in the expression for $\tan(\alpha + r')$ in equation (7) we get

$$\tan r' = \frac{\mu_e}{\mu_0} \cdot \frac{\sin i}{\sqrt{\mu_0{}^2 - \sin^2 i}} .$$

But $\sin i = \mu_0 \sin r$, and therefore

$$\mu_0 \cos r = \sqrt{\mu_0{}^2 - \sin^2 i}.$$

$$\therefore \qquad \frac{\tan r}{\tan r'} = \frac{\mu_0}{\mu_e}.$$

And since

$$\tan\phi = \frac{\mu_e{}^2}{\mu_0{}^2} \cdot \tan\theta,$$

$$\frac{\tan r}{\tan r''} = \frac{\mu_e}{\mu_0}.$$

Case ii.—The optic axis perpendicular to the refracting surface :

In this case, $\alpha = 90°$. Putting this value in equation (7), we get,

$$\tan(90° + r') = -\cot r' = -\frac{\mu_e}{\mu_0} \cdot \frac{\sqrt{\mu_e{}^2 - \sin^2 i}}{\sin i}$$

or,

$$\tan r' = \frac{\mu_0}{\mu_e} \cdot \frac{\sin i}{\sqrt{\mu_e{}^2 - \sin^2 i}} .$$

So,

$$\tan r'' = \frac{\mu_e}{\mu_0} \cdot \frac{\sin i}{\sqrt{\mu_e{}^2 - \sin^2 i}} .$$

Case iii.—Normal incidence, i.e., any inclination of the optic axis in the plane incidence, but the angle of incidence is zero :

Putting $i = 0$ in the expression for $\tan\theta$ in equation (12), we get

$$\tan\theta = -\cot(\alpha + r') = -\frac{\mu_0{}^2}{\mu_e} \frac{2\mu_0{}^2\cos^2\alpha}{\mu_0\mu_e \sin 2\alpha} .$$

Thus,
$$\tan \theta = -Q^2 . \cot \alpha \qquad \qquad \dots (13)$$

Or,
$$\tan (\alpha + r') = \frac{1}{Q^2} \cot \alpha \qquad \qquad \dots (14)$$

Expanding the left hand side of the equation (14) and collecting terms, we get

$$\tan r' = \frac{\mu_e{}^2 - \mu_0{}^2}{\mu_e{}^2 \tan \alpha + \mu_0{}^2 \cot \alpha} \qquad \qquad \dots (15)$$

For the extra-ordinary wave normal, at normal incidence, we have,

$$\tan \phi = -\cot(\alpha + r'') = \frac{\mu_e{}^2}{\mu_0{}^2} \tan \theta = -\cot \alpha,$$

and therefore,
$$r'' = 0 \qquad \qquad \dots (16)$$

Peculiarities at Normal Incidence

At normal incidence, the extra-ordinary wave front remains parallel to the incident (plane) wave front and, therefore, the extra-ordinary wave normal does not suffer any refraction, so that $r'' = 0$, as given by equation (16). The extra-ordinary ray, however, as is well known, does get refracted even at normal incidence and shows some special peculiarities.

Thus, in the first place, since $\tan \theta = -Q^2 \cot \alpha$, and since α, whether positive or negative, can lie (numerically) only between $0°$ and $90°$, θ and α must always be of opposite signs. This implies that the refracted ray and the refracting surface must always lie on opposite sides of the optic axis. Further insight into the matter is obtained by examining the equation (15). For negative crystals, μ_0 is greater than μ_e. If, then, α is positive, r' must be negative, and *vice versa*. That is to say that in the case of negative crystals, at normal incidence, the refracted extra-ordinary ray and the optic axis lie on opposite sides of the surface normal. In the case of positive crystals, since now it is μ_e which is greater than μ_0, α and r' will always be of the same sign. In other words, in the case of positive crystals, at normal incidence, the e-ray will lie between the surface normal and the optic axis.

When α is $0°$ or $90°$, then, again it is well known and can be easily deduced from the above expressions for θ or r' (equations (6) and (7) which have been combined together in equation (12), the e-ray also does not suffer any refraction, *i.e.*, $r' = 0$. It must, therefore, follow that for some inclination of the optic axis, r' must be a maximum. That this is so, is seen immediately from the curves in Fig. 2, the data for which are given in Table I. These have been worked out for calcite, a negative crystal, and quartz, a positive crystal. For these calculations the refractive indices taken for the two crystals are as given below, Table II, taken from Kaye and Laby's Tables. The angles have been calculated to the nearest minute of arc.

TABLE I

Variation in r' with α (normal incidence)

α	r' (normal incidence) in	
	quartz	calcite
$0°$	$0°$	$0°$
$\pm 10°$	$\pm 0° \ 7'$	$\mp 1° \ 56'$
$\pm 20°$	$\pm 0° \ 13'$	$\mp 3° \ 42'$
$\pm 30°$	$\pm 0° \ 18'$	$\mp 5° \ 7'$
$\pm 40°$	$\pm 0° \ 20'$	$\mp 6° \ 1'$
$\pm 50°$	$\pm 0° \ 20'$	$\mp 6° \ 15'$
$\pm 60°$	$\pm 0° \ 17'$	$\mp 5° \ 42'$
$\pm 70°$	$\pm 0° \ 13'$	$\mp 4° \ 22'$
$\pm 80°$	$\pm 0° \ 7'$	$\mp 2° \ 23'$
$90°$	$0°$	$0°$
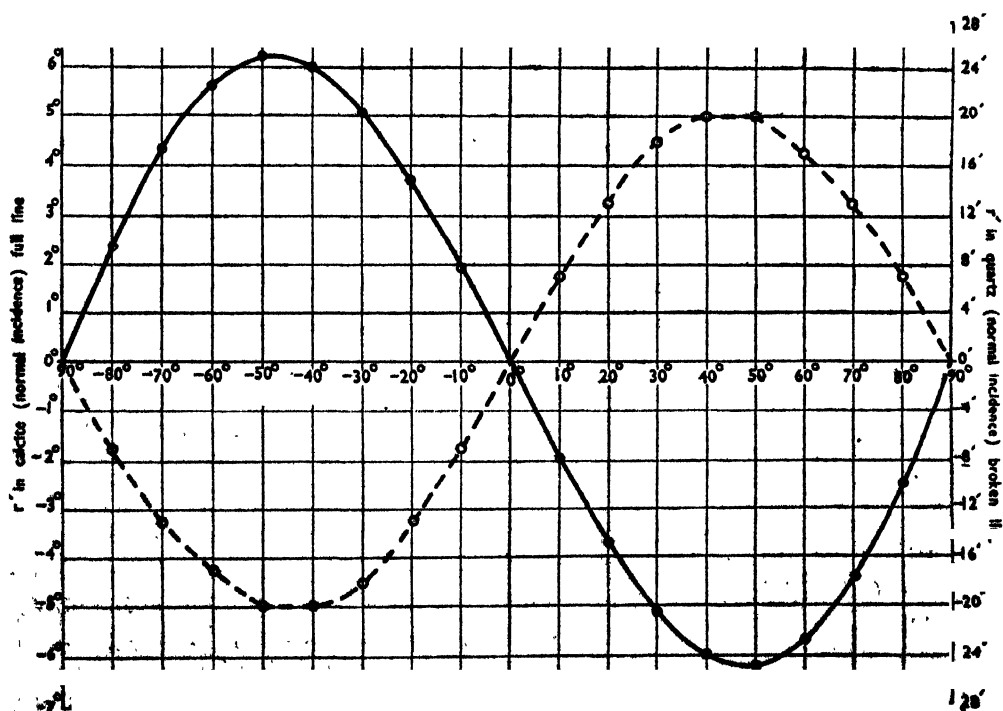
Figure 2

Table II

Refractive indices for λ 5893

Crystal	μ_o	μ_e
Calcite (calcspar)	1.6584	1.4864
Quartz	1.5443	1.5534

The exact angle, α, for which r' will be a maximum can be easily calculated in the usual manner. Thus, since $r' = \theta - \alpha \pm 90°$, $dr'/d\alpha = d\theta/d\alpha - 1$. The maximum r' will, therefore, be obtained when $d\theta = d\alpha$ or $\theta = \alpha$. Putting this value of θ in the expression for $\tan \theta$ (equation 13) and remembering that θ and α are always of opposite signs, we get that the angle, α, which corresponds to the maximum r' is given by

$$\tan \alpha = Q = \mu_e/\mu_o.$$

The corresponding value of r' is $2\alpha - 90°$. The values of α for the maximum r' and the corresponding values of r' for the two crystals taken here are given below, Table III.

Table III

Maximum r' and the appropriate α

Crystal	α to give maximum r'	Corresponding r'
Quartz	$\pm 44° \; 50'$	$\pm 0° \; 20'$
Calcite	$\pm 48° \; 8'$	$\mp 6° \; 16'$

Oblique Incidence.—The case of normal incidence has been given in detail in the preceding section. For other angles of incidence as well, the angle of refraction of the extraordinary ray passes through a maximum for a certain inclination of the optic axis. It is, however, not so easy to calculate this inclination for oblique incidence as it was in the case of normal incidence. For putting $\theta = \alpha$ in the general expression for $\tan \theta$ (equation 6), we get a cubic in $\cos^2 \alpha$ (or $\sin^2 \alpha$). That r' does pass through a maximum for any angle of incidence as α is varied from 0° to 90° can, however, be easily seen by calculating r' for various α's and i's. Such an investigation also reveals a few other peculiarities in the behaviour of the extra-ordinary ray, peculiarities not mentioned in the usual text books.

These peculiarities are (*i*) that for certain angles of incidence and certain inclinations of the optic axis, the extra-ordinary ray lies on the same side of the normal as the incident ray; and (*ii*) that under certain conditions the extra-ordinary ray is refracted away from the normal, *i.e.*, the angle of refraction is greater than the angle of incidence. Since the angle of refraction of the extraordinary ray also is, generally, smaller than the angle of incidence, it follows as a corollary that in the circumstance of peculiarity (*iii*) there must be a certain angle of incidence such that the incident and the refracted rays lie along the same straight line, in other words, there is no refraction even at oblique incidence.

It thus turns out that the extra-ordinary ray transgresses the usual laws of refraction in more ways than what one is led to think from the usual statement that the extraordinary ray, in general, does not obey any of the laws of refraction. So far as the very first of these laws is concerned, which says that the refracted ray lies in the plane of incidence, it is obeyed by the extraordinary ray as well in the cases dealt with in this paper, the optic axis having been taken everywhere to lie in the plane of incidence. The second law of refraction, Snell's law, may for the extra-ordinary ray, when the optic axis lies in the plane of incidence, be considered to be replaced by the rather complicated equation (12).

All these peculiarities are seen to a much more pronounced extent in the case of calcite where the difference of the two refractive indices is a little over 0.17 than with quartz where this difference is nearly 19 times smaller being slightly less than 0.01. The tables and the figure of the previous section exemplify this.

With respect to the extra-ordinary wave normal, *i.e.*, the normal to the extra-ordinary wave front, as has already been stated in section 6, most text books do not specifically give its direction even in the usual special cases. Planck (1935), however, has shown by the application of the boundary conditions to the equations of the electro-magnetic fields, that the extra-ordinary wave normal obeys all the laws of refraction even in the most general case of biaxial crystals, any angle and plane of incidence: It always lies in the plane of incidence; and the ratio of $\sin i$ to $\sin r''$ is equal to the refractive index concerned, *i.e.*, the refractive index of the wave in the direction of the wave normal. The first of these laws does not fall within the purview of the present investigation; but the second law, the modified Snell's law, follows from the equation (8), which will be found to be satisfied by the relation, $\sin i = \mu . \sin r''$, where μ is the wave refractive index in the direction which makes an angle of ϕ with the optic axis and is given by the usual relation,

$$\frac{1}{\mu^2} - \frac{1}{\mu_0^2} = \left(\frac{1}{\mu_e^2} - \frac{1}{\mu_0^2} \right) . \sin^2 \phi$$

It should be noticed, however, that the modified Snell's law cannot give the direction of the wave normal which can be determined only with the help of equation (8).

Full data and details about all these special peculiarities mentioned in this section will be discussed in future.

DEPARTMENT OF PHYSIC
DELHI UNIVERSITY.

REFERENCE

Plank 1035 Treatise on Light. p 1c

A NOTE ON THE THERMODYNAMICS OF THE WET- AND DRY-BULB HYGROMETER*

BY V. S. NANDA AND R. K. KAPUR

ABSTRACT. The paper deals with the thermodynamic study of the wet-and-dry bulb hygrometer as applied to other liquids besides water. Hygroscopic liquids are also included. The theory is found in reasonable accord with experiment.

INTRODUCTION

The present note is concerned with the thermodynamics of the wet-and-dry bulb hygrometer, generalised to apply to liquids other than water. Experiments were performed with different evaporating liquids and also hygroscopic liquids (particularly with strong sulphuric acid) which absorb moisture from the air. The standard theory of the wet- and dry-bulb can easily be extended to cover these cases. The experimental results were found to be in agreement with theory.

In the beginning the generalised formula, known as the psychrometer equation is derived. The symbols relevant for the purpose are the following :—

$L' =$ Latent heat of the liquid at the wet-bulb temperature.

$T =$ Room temperature.

$T' =$ Wet bulb temperature.

$x = e\epsilon/(p - e) =$ Humidity mixing ratio at temperature T.

$x' = e\epsilon/(p - e') =$ Humidity mixing ratio at temperature T'.

$e =$ Vapour pressure at temperature T

where $e' =$ Vapour pressure at temperature T'.

$\epsilon =$ Ratio of densities of vapour and dry air at the same temperature

$C_P =$ Specific heat of dry air at constant pressure.

$C_P' =$ Specific heat of vapour at constant pressure.

$p =$ Total pressure.

When the wet-bulb has reached a constant temperature the heat lost by air in cooling from the dry-bulb to the wet-bulb temperature is utilised in the evaporation of the liquid, the vapour content of the air increasing from the

initial value to a value corresponding to saturation at the wet-bulb temperature. Hence it follows that

$$(C_P + xC'_P)(T - T') = L'(x' - x)$$

Substituting the values of x and x' given above and assuming $xC'_P \ll C_P$ and e', $e \ll p$, we have finally

$$(e' - e) = \frac{C_P p}{L' \epsilon}(T - T') \qquad \dots \quad (1)$$

This is the general equation for all evaporating liquids, substituting $e = o$, which in the present experiments is the case for all evaporating liquids other than water, equation (1) reduces to

$$e' = \frac{C_P p}{L' \epsilon}(T = T') \qquad \dots \quad (2)$$

The case of hygroscopic liquids is now considered. In this case the process is just reversed and the liquid absorbs practically all the water vapour from the air coming in contact with it. Consequently its temperature will rise due to heat of chemical combination and the heat of condensation. The rise in temperature will be proportional to the amount of water vapour present in the air and hence can provide a measure for humidity.

In order to derive, for hygroscopic liquids, a relation corresponding to the equation (1), it is assumed that the air after coming in contact with the hygroscopic liquid is completely robbed of its water vapour contents and acquires the temperature of the liquid. This temperature may be called the "anti-wet-bulb" temperature. In the steady state the heat taken away by the air is equal to the heat of reaction plus the heat of condensation. Heat taken away by one gram of air is $(T' - T)C_P$. If x grams of water vapour be associated with one gram of air, heat liberated is $(H + L')x$. Hence we have

$$(H + L')x = C_P(T' - T)$$

here H denotes the heat of reaction and T' the anti-wet-bulb temperature. Substituting for x the final expression is

$$e = \frac{C_P p(T' - T)}{(H + L')\epsilon} \qquad \dots \quad (3)$$

Thus the expression in the case of hygroscopic liquids comes out to be of the same form as for evaporating liquids. In fact equation (3) can be got directly from (1) by putting $e' = o$ and replacing L' by $(H + L')$.

It is hardly necessary to mention that, the equations derived above hold when the air surrounding the wet-bulb is in a state of sufficient motion. When the air around the wet-bulb is not renewed fast enough, the wet-bulb depression will be less—its full value is obtained when the motion of the air exceeds a certain limiting value. The same applies to the "anti-wet-bulb" rise in temperature. In the experiments performed care was taken that the

full value of depression in the one case and the rise in temperature in the other case are obtained.*

The method of derivation of the psychrometeric equation has been the subject of great controversy and much criticism has been levelled against it. It is not possible to justify, on purely theoretical grounds, what is implied in the above derivations—splitting of the air in two layers, having different properties. In the region just around the wet-bulb the stream lines are parallel to the surface. Beyond this there is the turbulent layer which affects the flow of heat and water-vapour. Alternati methods (Whipple, 1933) of derivation have been proposed, though not wit uch success. We should not however be appalled by the sweeping nature   an assumption, particularly when (as is the case here) we can compare theo with experiment.

EXPERIMENTAL VERIFICATION

The experimental verification equation (3) is first taken up. In this case it was found convenient to use the following arrangement instead of the usual "wick method". The liquid was taken in a thermos flask and its mouth closed by a stopper through which passed a thermometer and two tubes. One of the tubes was kept dipping in the liquid while the other much above its surface. Air from the surface was constantly sucked by connecting the second tube to a suction pump. Fresh air from the atmosphere entered through the first tube. If this process is allowed to run for some time (about half an hour) the liquid attains a steady temperature.

In order to check the working of this arrangement water was tried. The steady temperature in this case was found to nearly coincide with the wet-bulb temperature of the ventilated type of psychrometer.† A feature of this experiment is that it does not require the assumption of two distinct layers in the neighbourhood of the wet-bulb.

Coming back to the case of the hygroscopic liquids we notice that if 'e' is known, the value of H can be found from equation (3). If, however, this equation is used for finding e, H must be determined by a separate experiment. A graph, may be plotted between heat evolved in calories against the weight of water in grams added to a gram molecule of the liquid.

It will be noticed from such a plot that the heat emitted per gram of dissolved water is sensibly independent of the strength of the acid so long as it contains less than twelve grams of water per mol. of the acid. The following is a set of observations taken on a particular day using water and sulphuric acid in turn.

---

* In the case of still air the psychrometeric equation does not retain the simple form (1) but involves some other factors. For a detailed discussion see Glazebrook's Dictionary of Applied Physics' P. 420.

† In this connection it is interesting to note that water in a 'Surahi' (earthen jug) placed in a room is cooled to within 2° of the wet-bulb temperature.

Room temperature = 30.75°C

(1) Depression in wet-bulb = 11.5

Vapour pressure = 10.1 mms.

(2) Rise in anti-wet-bulb = 35°C

H—(heat of solution) = 360 Calories.

Making use of equation (3) we get

Vapour Pressure = 10.8 mms.

The thermos flask method is a universal method—in the respect that any liquid can be used. The psychrometeric method is very limited in its application. It fails in the case of hygroscopic liquids, especially strong sulphuric acid. In fact, the 'wick method' will always fail in these cases. It has been pointed out before that the hygroscopic substance behaves just like a sink for water-vapour present in the air. Consequently it will be diluted continuously and will soon reach the 'non-proportional' region—in which heat evolved is not directly proportional to the amount of water vapour present in the air. It will be seen presently that the psychrometer method has to be rejected in the case of most of the evaporating liquids.
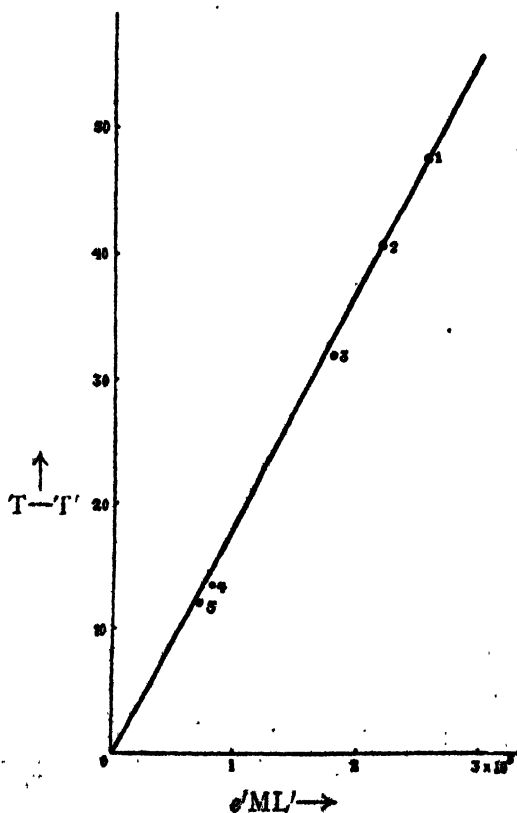
Fig. 1

The experimental verification of equation (2), which is satisfied by all liquids for which $e = o$, is now considered. Substituting $\epsilon = M/M_0$ in we have

$$e'ML' = A(T - T') \qquad \qquad \text{... (4)}$$

where $\qquad A = C_P \, p M_0$

$\qquad \qquad M =$ Molecular weight of the liquid

$\qquad \qquad M_0 =$ Molecular weight of dry air.

It is clear from equation (4) that a plot of $(T - T')$ against $e'ML'$ must be a straight line passing through the origin whose slope is $(1/A)$. The usual psychrometer arrangement was found to fail in the case of liquids with their wet-bulb temperature lower than that of water. The reasons are—

1. Assumption regarding the splitting of air in two distinct layers is no longer valid.

2. The accuracy of observations is considerably marred by the condensation of water vapour present in the air on the wet-bulb. The effect of condensation is to raise the wet-bulb temperature.

In order to get true wet-bulb temperature the thermos flask method, with a slight modification, was used. The air was not allowed to enter the thermos flask directly but was first made to pass through a calcium chloride U-tube and then a sulphuric acid bulb. In this process it was completely dehumidified. Since the absorption of water vapour is accompanied by rise in temperature of the hygroscopic substance, the U-tube and the bulb were cooled by circulating water. The temperature of the incoming air was noted by a thermometer whose bulb was sealed in the tube. The wet-bulb temperature on the other hand was measured by a thermocouple. With the above arrangement acetone, methyl alcohol, ethyl alcohol, acetic acid and butyl alcohol were tried in turn to get the depression in the wet-bulb temperature $(T - T')$. In the graph numerical values of e' and L' have been taken from the 'International Critical Tables' and have been substituted in millimeters and calories respectively. The various points lie approximately on a straight line whose slope is 1.85×10^{-4}. The slope of this line according to theory should be 1.94×10^{-4}. Since theory and experiment are in fair agreement, equation (2) can be taken as correct.

Before concluding it must be mentioned that the liquids used must be free from impurities. The presence of an impurity will change the true wet-bulb temperature. The specimen of ethyl alcohol used in the experiment contained about 4% of water. It will be noticed from the graph that the point representing ethyl alcohol is below the straight line—the depression in the wet-bulb temperature is less that the expected value. Now the wet-bulb temperature of water is known to be higher than for ethyl alcohol. The presence of water in alcohol will, therefore, tend to raise its wet-bulb temperature. This is connected with the depression in wet-bulb temperature of miscible liquids and will be discussed fully in a subsequent paper.

REFERENCE

Whipple, 1933, *Prof. Phys. Soc. Lond.*, **46**, 307.

A NOTE ON BINARY ALLOYS

By K. C. MAZUMDER

ABSTRACT. The binary alloys of some metals like Cu, Ag and Au can be expressed by approximately definite chemical formula and are known as abnormal valency inter metallic compounds. The different phases of these loy systems have definite electron-atom ratios which are generally expressed as 1 4, 3/2, 1/13 and 7/4 for a, β, γ and ϵ phases respectively. They can, however, be expressed more 1 iiformly as 21/15, 21/14. 21/13 and 21/12. This regularity suggests the possibility of thi being extended inside the a-phase also. The a-phase may, then, be composed of several minor phases of electron-atom ratios, 21/16, 21/17, 21/18, 21/19, 21/20, at the boundaries (which there will be discontinuities, however, small, of some physical properties of the all The indications of such discontinuities found in the published data are discussed.

BINARY ALLOYS

It is found from a study of the phase diagrams of the various binary alloy systems, that the intermediate phases do not at once begin to form as soon as small amounts of one metal is added to the other. The parent metal has a capacity to absorb in its own matrix a certain amount of the 2nd metal. The lattice unit will, of course, be distorted but the distortion does not proceed indefinitely ; a stage is soon reached when a new phase with different lattice structure begins to appear. The two alloys existing at the two ends of the phase diagrams and in which the characteristics of the original lattice structures are retained, are called the primary solutions. The extent of these primary solid solutions in the case of the substitutional alloys, in which the atoms of the second metal replace those of the original, will, naturally, depend upon the relative sizes of the two kinds of atoms. From a large number of observations Hume-Rothery concludes that when the atomic diameters are within 14% of each other an extended solid solutions can be expected. It is not, however, always effective ; for instance, the amount of Zn retained in the copper-matrix is much greater than that of Cu in the Zn-matrix though they have mutually favourable size-factors. This type of solid solutions indicate that besides size-factors, the valencies of the solvents and solutes play an important part in determining the amount of a metal which can be taken into solution by other metals. If we examine the intermediate phases, *e. g.*, the binary alloys of Cu, Ag or Au, which are known as the abnormal valence intermetallic compounds (as opposed to the normal valence intermetallic compounds like Mg_3Sb_2, Mg_3Bi_2, Zn_3Sb_2, $MgSe$, $CaTe$, etc.) it will be found that the size-factor alone is insufficient to explain the observed solubilities. The β-phases of the Cu-Zn, Cu-Al and Cu-Sn alloy systems are of the compositions Cu-Zn, Cu_3Al and Cu_5Sn ; thus with the increasing valencies the amounts of the second metals become smaller though they have more or less favourable size factors. It, therefore, becomes quite evident as has, first, been pointed out by Hume-Rothery that the valencies have to be taken into

consideration to understand the extent of mutual solubilities of metals. The one important fact which comes out of the above observations is the following :—The valencies of Cu, Zn, Al and Sn being respectively 1, 2, 3 and 4, the electron-atom ratios of these abnormal valence compounds become identical namely 1.5. A large number of the β-phase abnormal valency intermetallic compounds have been found to yield the same ratio. Further investigations have shown that the other phases of the above type of alloy-systems also have different but constant electron-atom ratios. The γ-phases of Cu-Zn, Cu-Al and Cu-Sn systems have approximately the compositions Cu_5Zn_8, Cu_9Al_4 and $Cu_{31}Sn_8$; with the valencies mentioned above the electron-atom ratio in each case becomes 21:13. The ε-phase of the above systems having approximate compositions $CuZn_3$, Cu_3Sn and Cu_5Al_3 yield an electron-atom ratio 7:4. The end of the α-phase solid solution has 1.4 as its electron-atom ratio. These electron-atom ratios are only approximate, the compositions of these phases being variable within certain limits. These approximate ratios of the abnormal valency intermetallic compounds which are the subject matters of the present note, have been empirically obtained by different workers, including Hume-Rothery, from a large number of obser-vations on various alloy-systems. All phases of each and every alloy system have not been studied or do not yield the exact ratios on account of un-favourable size factors or some other reasons. The ratios obtained from observations agree well with those obtained by theoretical calculations based on quantum mechanics. The average electron-atom ratio of the α-phases of a large number of alloy systems is found to be 1.39 and its theoretical value is 1.36. The corresponding values for the β and γ phases are 1.49 and 2.48 ; 1.59 and 1.54 respectively. These values have been obtained on the assumption that the following are the valency-electrons of the respective metals.

Metals	...	Cu	Ag	Au	Zn	Cd	Hg	Al	In	Ga	Sn	Si	Se	Ni
Valencies	...	1	1	1	2	2	2	3	3	3	4	4	4	0

The electron-atom ratios, it should be noted, determine the crystal structures and the accepted values for the α, β, γ and ε phases are 1.4, 1.5, 21/13 and 7/4 respectively. For the γ-phase besides the ratio, 21/13, the number 13, has been found to be of considerable significance. The γ-brass for instance, has the body-centered cubic structure ; for this structure there are two atoms per unit lattice. If the parameter is given three times its value for the actual unit crystal there will be 27 units in the enlarged lattice and the expected number of atoms in it will be 54. But there has been found a distortion in the lattice, the actual number of atoms being 52 or 4 × 13.

The random values of these ratios can be expressed more uniformly in the following way, retaining the ratio for the γ-phase as it is—21/15, 21/14, 21/13 and 21/12 for the α, β, γ and ε phase respectively. The ratios have now taken very interesting forms ; they are perhaps of more significance in view of the observation regarding the γ-phase. For the same constant numerator the denominator changes by unity from one phase to the next,

i.e., a change of one atom per 21 electrons brings about a change of phase—a change of crystal structure and of many other physical properties. If one starts adding, for instance, Zn to pure Cu, the Cu-lattice retains its own structure till the electron-atom ratio increases (from 1 : 1) to 21 : 15. A rather unstable equilibrium is then reached when for every change of one atom a new phase is developed up to the ratio, 21 : 12. The next and the last ratio, 21 : 11 is not very much different from that for pure zinc namely 21 : 10.5 or 2 : 1. Pronounced phase characteristics very much different from those of Zn will then be absent. A different phase δ or η after ε phase is some time found in some alloy systems but it lacks regularities of the characteristics shown by the earlier phases. It should, of course, be remembered that to decrease the total number of atoms by one, one has to add one Zn-atom for two Cu-atoms removed so as to leave the number of electrons the same.

Turning to the Cu-rich side of the primary solid solution we find the margin very wide ; we can remove 6 Zn-atoms one at a time and add in their places 12 Cu-atoms in 6 equal steps till the electron-atom ratio reaches its pure copper value, namely, 1 : 1. Though the phase characteristics will be determined mostly by copper it is not altogether improbable that some minor phase characteristics may in this range be evident if the regularities in the electron-atom ratios shown above are not merely accidental. The possible electron-atom ratios inside the α-primary solid solutions are 21/16, 21/17, 21/18, 21/19 and 21/20 the corresponding atomic percentage of Zn being 31, 23, 16.5, 10.5 and 5. This is true only when the second metal is divalent. For higher valencies the percentages will be proportionately smaller ; for trivalent metals they will be halves of the above, for quadrivalent, thirds. The last few will not, of course, differ widely from the pure copper ; but one or two near the end of the α-phase may produce minor discontinuities in some properties of the α-alloys. The crystal structure of the Cu-Zn α-alloy which has been investigated by Owen and Pickup (1933) does not show any marked discontinuities in the gradual increase in its parameter ; the points do not either line in a smooth curve. Only a few points in the full range have been examined and accidentally most of these points are situated mostly in the regions of the expected breaks. More systematic work will be necessary to locate the discontinuity, if any, in the lattice dimension. Fairbank (1944) carried out in an exhaustive manner the measurements of the electric resistivities of the Cu-Zn and the Cu-Sn alloys at different temperatures. In the curve for Cu-Zn at 29.3° abs. it will be noticed that the resistivity for the annealed specimen rises to a maximum (conductivity reaching a minimum) near 30 atomic % of Zn. This is exactly the composition giving an electron-atom ratio of 21/16, the next lower one to that for the α-phase. Smith (1930) worked on the same problem previously and carried out measurements of both electrical and thermal conductivities of the Cu-Zn and other alloys. The curve given by him for the conductivity of the Cu-Zn alloys at 20°C (293° abs.) shows a minimum (or maximum for resistivity) at about 40 atomic

percent of Zn—the end of the α-solid solution. Fairbank obtained the alloys from Smith who had these made by the American Brass Company. It can be assumed that the materials used in both these investigations were of the same consistency. In the case of the Cu-Zn alloy system, therefore, a distinct phase does make its appearance at 14.3° abs. The Cu-Sn curve for the annealed specimen at 20.4° abs, has also started drooping before 6 atomic percent of Sn has been added to Cu. It is quite likely that there will also be a maximum long before 13 atomic percent of Sn is added to Cu—this being the expected end of the primary solid solution of the Cu-Sn alloys system. The end of the primary of solid solution of Cu-Sn determined by the X-rays investigation also corresponds to an electron-atom ratio, 1 28 only instead of 1.40, the accepted value for the α-phase. This value is too low to be explained by experimental inaccuracies ; it is, however,. approximately equal to 21/16 the next lower one to 21/15 or 1.40. The Cu-Zn alloy system gives an electron-atom ratio of 1.22 for its α-phase which is equal to 21/17 two steps lower to 21/15. The lower values for the Cu-Sn and the Cu-In α-phases have been attributed by Hume-Rothery to their unfavourable size-factors. Even with the unfavourable size factors the electron-atom ratios are found to belong to the series. For the α-phase of the Cu-Sb alloy it is found to be 1.23 which is again equal to 21/17 instead of 21/15, the usual value for the α-phase. The solubility of Cd is extremely low,—only 1.7 atomic per cent of Cd dissolving in Cu. This gives an electron-atom ratio of 1.02 which is not far from 21/20 (1.05), the last member of the series. From the above discussion it thus appears that the electron-atom ratios for these groups of binary alloy systems, belong to a series, 21/20, 21/19...21/12 ; the first 5 members fall within the α-phase the accepted values for the latter being 21/15. The lower values of the electron concentration for the α-phase of the different alloy systems are approximately equal to one or the other of the above ratios. The electrical conductivity of the Cu-Zn systems at 14°C corresponds to the concentration 21/16 but at 293° abs. it gives the usual value of 21/15.

These minor phases inside the α-phase may be of the nature of the superlattice formation. The electron-atom ratios referred to above and those of the main phases perhaps are responsible for super-lattices. It is, however, suggested that the physical properties of these types of alloys should be more critically studied (within the range of the α-solid solutions) to see if there are any small discontinuities.

RESEARCH LABORATORY
TATA IRON AND STEEL CO., LTD.,
JAMSHEDPORE.

REFERENCES

Fairbank, 1944, *Phys Rev.*, **66**
Owen and Pickup, 1933, *P. R. S.*, **140**.
Smith. C. S.. 1930. *Trans. A. I. M. E. Met. Div.*. **89. 84**.

ROTATIONAL STRUCTURE OF λ 3600 – λ 3200 A. BANDS OF Na₂ *

By S. P. SINHA

* **ABSTRACT.** The λ3432Å (2, 3), λ3450Å (2, 4) and λ3468Å (2, 5) bands of the λ3600 – λ3200 A system of Na₂ have been photographed in the first order of a 21-ft. concave grating with a dispersion of about 1.3 Å per mm and an attempt has been made to study their rotational structure. Each band is found to consist of a single P and a single R branch, characteristic of a $^1\Sigma - ^1\Sigma$ transition. The lower state is known to be a $^1\Sigma_g^+$ state due to $3\,^2S + 3\,^2S$ atoms of sodium. Hence the upper state will be of $^1\Sigma_u^+$ type and is considered, from the results of vibrational analysis, to be due to $3\,^2S + 3\,^2D$ or $3\,^2S + 4\,^2P$ atoms. The values of the molecular constants obtained are :

$$B_3'' = 0.152 \text{ cm}^{-1},\ B_4'' = 0.151 \text{ cm}^{-1},\ B_5'' = 0.151 \text{ cm}^{-1},$$
$$B_2' = 0.103 \text{ cm}^{-1} \text{ and } r'_e = 3.77 \text{ A.}$$

It has not been possible to evaluate α and D from the present data.

INTRODUCTION

Sodium has two systems of bands in the visible, one of which lies in the red and the other in the green region. The rotational structure of the red bands has been studied by Fredrickson (1929) and of the green bands by Smith (1924), Fredrickson and Watson (1927) and by Loomis and Wood (1928). The red bands consist of a single P and a single R branch due to a $^1\Sigma - ^1\Sigma$ transition and the green bands consist of one P one Q and one R branch due to a $^1\Pi - ^1\Sigma$ transition.

Besides the bands in the visible region, Na₂ has a large number of bands in the ultra-violet region which are believed to belong to several systems. Although many attempts have been made at a vibrational analysis of these bands (Pearse and Sinha, 1947; Sinha, 1947, 1948) so far nothing seems to have been done to study their rotational structure. An attempt has, therefore, been made at a rotational analysis of a few bands belonging to the first ultra-violet system of Na₂ which lies between λ3600 and λ3200 A. From this it has been possible to conclude that the bands consist of only two branches and consequently that the upper state is of $^1\Sigma_u^+$ type, the ground state being already known to be $^1\Sigma_g^+$. A rough estimate of the values of B's has also been made. Measurements of the lines and their analysis are given in the following sections.

EXPERIMENTAL

The experimental arrangement was the same as described before (Sinha, 1948a). The bands were photographed in absorption in the first order of a 21-ft. concave grating (dispersion 1.3 Å, per mm.) using a specially built hydrogen discharge tube (Hunter and Pearse, 1936) as source for continuous radiation.

The bands were found to overlap each other and the main concern was to photograph even a few of them without overlapping. For this purpose, a large number of spectra were taken under gradually varying conditions of temperature, pressure and time of exposure. In the spectrograms obtained, at lower temperatures (about 550°C), the overlapping could be avoided to a certain extent, but only few lines corresponding to high J values appeared and it was not even possible to ascertain the band to which they belonged. At higher temperatures (about 800°C), there was so much overlapping that it was impossible to use them for any purpose. At intermediate temperatures (650 to 700°C), the overlapping could be overcome to a certain extent in some regions and the structure could also be traced for these bands from near the heads to fairly high J values.

Three bands, $\lambda 3432$ Å (2, 3), $\lambda 3450$ Å (2, 4) and $\lambda 3468$ Å (2, 5) were found most suitable for studying the rotational structure. They are fairly strong bands of the $\lambda 3600 - \lambda 3200$ Å system and had least overlapping when photographed at about 700°C, maintaining nitrogen at a pressure of about 5 cm. of mercury in the absorption chamber. The time of exposure with an Ilford Special Rapid plate was two to three hours.

The bands were degraded to the red. Using values of B' calculated on the assumption that B_e/ω_e remains constant, it is found that the head is formed by as low as the third or fourth member of the R branch. The low J value lines near the head or the origin are all blended and can be seen resolved only after an interval of 2 to 3 Å on the long wavelength side from the head of the band. Although the spacing between the lines and their intensity changed in a regular manner on passing to higher and higher members, it was not possible to separate the branches by a mere inspection of the spectrum. Supposing the bands to have only two branches, then for molecules like Na_2 having large moment of inertia, there will not be much difference between the intensity of a P line and the corresponding R line; and since the R branch turns off at something like the third member, the J values of the adjacent lines of each branch will not differ by a large number and consequently the neighbouring P and R branch lines will appear equally intense. If the band has also a third branch, i.e., a Q branch, it will appear with somewhat double the intensity of P or R branch. General appearance did not suggest that a Q branch could be present. It may be further noted that the alternation in intensity due to nuclear spin (nuclear spin of $Na = \frac{3}{2}$) is not well marked on the spectrogram. In fact, a reference

to the spectra published by Loomis and Wood (1928) and by Frederickson (1929) also indicates the same thing with regard to the above alternation in intensity of the lines.

ROTATIONAL ANALYSIS

It has not been possible to give a very satisfactory analysis of the rotational structure of the bands investigated in the present work. However, it seems fairly conclusive that the lines associated with each of the three bands investigated here can be classified into only two branches, one P and one R arising from the transitions

$$P(J) = F'(J-1) - F''(J)$$
$$\text{and } R(J) = F'(J+1) - F''(J).$$

This suggests that the bands are due to $^1\Sigma - ^1\Sigma$ transition, and since the ground state is $^1\Sigma_g^+$, the excited state should be of $^1\Sigma_u^+$ type.

An analysis of the rotational structure of these bands is given in Tables I—III. Nearly all the lines measured in this region have been accounted for in these tables. The letter h or d against a line indicates that it was hazy or an unresolved doublet. It was not possible to make any accurate estimate of the intensity of the lines. In general, however, the higher members were somewhat stronger than the lower ones ; the maximum of the intensity corresponded to members higher than those recorded here, as it was not possible to trace the lines right up to them due to overlapping.

Values of $\Delta_2 F$ given in columns $4-7$ of these tables do not appear very satisfactory. Better results could have been obtained by getting rid of the overlapping, if possible, and obtaining a photoghaph at about three times the dispersion used in the present work. The continuum, however, did not seem to have enough intensity to permit of the latter. The details of the analysis are given below, and since this is the only attempt made to study the rotational structure of the Na₂ ultra-violet bands (rotational structure of the corresponding band systems of even other alkali-metal molecules has not been studied), the results might be of some interest.

As stated before, it is not possible to see the band origion or the low member lines of the branches and, hence, it is not easy to assign correct J values to the lines. Advantage, however, has been taken of the consideration that the lower state for these bands is the same as for the green or red bands for which the rotational constants are known with reasonable accuracy. Therefore, having tentatively arranged the lines into branches, $\Delta_2 F''(J)$ which is given by

$$\Delta_2 F''(J) = F''(J+1) - F''(J-1) = R(J-1) - P(J+1)$$

can be computed and compared with those calculated with the help of known constants for the ground state, from the formula

$$\Delta_2 F''(J) = (4J+2)[B''_v + 2D_v''(J^2 + J + 1)\ldots].$$

It may be added that these differences for $V'' = 3, 4$ and 5 with which we are concerned have not been observed in any previous work even for the visible bands and hence the only way to obtain them was with the help of the above formula. From this comparison the arrangement can be checked and correct J values assigned. Although the agreement between the values of $\Delta_2 F''$ (J) obtained in the above two ways (last three columns of Tables I-III) is not very satisfactory, yet any attempt to change the J values of the lines even by unity makes the agreement definitely worse and introduces an error which is much greater than can be allowed for experimental errors.

A rough estimate of the molecular constants can be made as follows :

For the ground state constants :

$$\Delta_2 F''(J) = R(J-1) - P(J+1) = (4J+2)[B'' + 2D''(J^2+J+1)].$$

If we neglect D'' (D'' is about 10^6 times smaller than B''), $\Delta_2 F''$ (J) varies linearly with J, and if J is correctly known B'' can be evaluated. Further, $\Delta_2 F''(J)$ against J will give a straight line, which on extrapolation will intersect $\Delta_2 F''(J) = 0$ for $J = -\frac{1}{2}$, if J values have been correctly assigned (Fig 1). The value of $\Delta_2 F''(J)$ at $J = 0$ gives $2B''$.
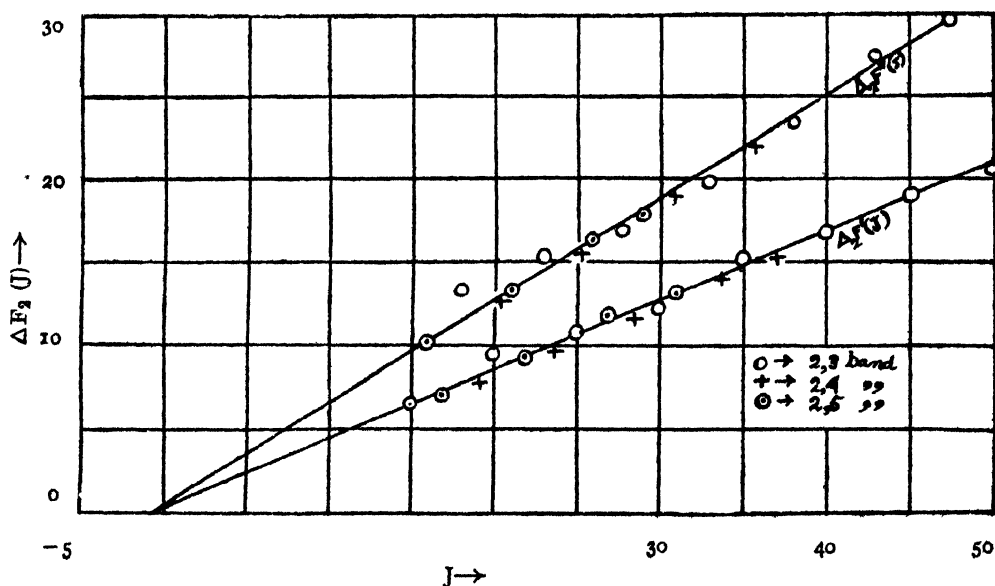
FIG. 1

For the excited state constants :

$$\Delta_2 F'(J) = F'(J+1) - F'(J-1) = R(J) - P(J) = (4J+2)[B' + 2D'(J^2+J+1)].$$

Neglecting D', B' can be calculated from the above equation. Further, as above, $\Delta_2 F'(J)$ varies linearly with J, and extrapolates to o at $J = -\frac{1}{2}$ (lower straight line in Fig. 1). The value of $\Delta_2 F'(J)$ at $J = 0$ gives $2B'$. The values of the constants are given in Table IV.

It may be pointed out that, since the value of B in a given electronic state depends upon the vibrational quantum number, the upper curve in Fig. 1

should really split into three straight lines corresponding to V″= 3, 4 and 5. The measurements are not however, good enough to resolve the differences between the values of B″ for the three bands, and hence a single straight line passing through the mean positions has been drawn.

It also follows from the equation

$$\nu = \nu_0 + (B' + B'')M + (B' - B'' + D' - D'')M^2 + 2(D' + D'')M^3 \ldots,$$

where $\nu_0 = \nu_e + \nu_v$ and is constant for a band,

$$M = J'' + 1 = 1, \ 2, \ldots \text{for R(o), R(1)}, \ldots,$$

and $M = -J'' = -1, -2, \ldots \text{for P(1), P(2)}, \ldots$

TABLE I

Branches and rotational term differences for the λ 3432 Å band of Na₂

J	R (J)	P (J)	Δ₂F′(J)	Δ₂F″(J)	Δ₂F″(calc)	Δ₂F₂(O−C)
14	—	29110.80	—	—	—	—
15	—	09.19	—	—	—	—
16	—	07.16	—	—	—	—
17	29113.43h	05.21	8.22	—	—	—
18	11.73h	03.43	8.30	12.29	11.25	1.04
19	10.04	01.14	8.90	13.21	11.85	1.36
20	08.07	29098.52	9.65	14.15	12.45	1.70
21	05.97	95 89	10.08	14.14	13.05	1.09
22	04.04	94.03	10.01	14.91	13.66	1.25
23	01.89	91.06	10.83	15.43	14.26	1.17
24	29099.45	88.61	10.84	15.49	14.86	0.63
25	96.91	86.40	10.51	15.49	15.46	0 03
26	94.79	83.96	10.83	15.66	16.07	−0.41
27	92.42	81.25	11.17	16 08	16.68	−0.60
28	89 96	78.71	11.25	17.01	17.29	−0.28
29	87.60	75.41	12.19	17 34	17.89	−0.55
30	84.97	72.62	12 35	17.51	18.51	−1.00
31	82.52	70.09	12.43	17.67	19.11	−1.44
32	80.14	67.30	12.84	18.69	19.72	−1.03
33	77.44	63.83	13.61	19.35	20 33	−0.98
34	74.57	60.79	13.87	20.12	20.94	−0.82
35	71.69	57.32	14.67	20.36	21.54	−1.18
36	68.48	54.21	14.27	21.12	22.15	−1.03
37	65.19	50.57h	14.62	22.29	22.76	−0.47
38	62.14	46.19h	15.95	22.13	23.37	−1.24
39	58.93	43.06h	15.87	23.21	23.97	−0 76
40	55.39	38.93h	16 46	24.38	24.57	−0.19
41	51.93h	34.55	17.38	25.57	25.17	0.40
42	48.20h	29.82	18.38	26.57	25.77	0.80
43	44.33h	25.36	19.97	27.73	26.38	1.35
44	40.11h	20.47	19.64	—	26.98	—
45	35.98	—	—	27.98	27.58	0.40
46	31.59	12 13	19.46	28.59	28.19	0.40
47	27.46	07.39	20.07	29.22	28.79	0.43
48	23.08	02.37	20.71	29.46	29.40	0 06
49	18.61	28998.00	20.61	29.96	30.00	−0.04
50	13.81	93.12	20.69	30.54	30.61	−0.07
51	09.10	88.07	21.03	—	—	—
52	04.43	—	—	—	—	—
53	99.50	—	—	—	—	—
54	94.65	—	—	—	—	—
55	89.42	—	—	—	—	—
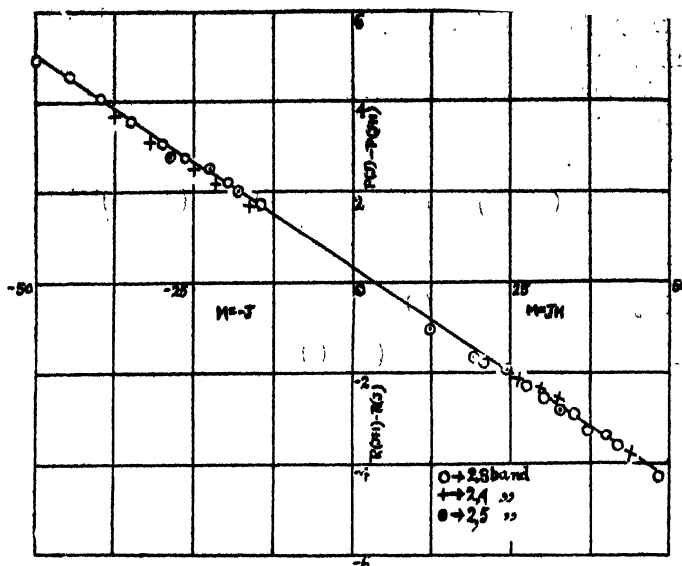
FIG. 2

TABLE II

Branches and rotational term differences for the λ 3450 Å band of Na$_2$

J	R(J)	P(J)	$\Delta_2 F''(J)$	$\Delta_2 F'(J)$	$\Delta_4 F''$ (calc)	$\Delta_2 F''$ (O–C)
15	28968.00h	28959.61	8.39	—	—	—
16	66.74	58.18	8 56	11.16	9.97	1.19
17	65.31	56.84	8.47	11.83	10.57	1.26
18	63.58	54.91	8.67	12.33	11.17	1.16
19	61.74	52.98	8.76	12.36	11.77	0.59
20	59.61	51 22	8.39	12.69	12.38	0.31
21	57.51	49.05	8.46	—	12.98	—
22	56.00	—	—	12.99	13.58	−0.59
23	54.04	44.52	9.52	13.48	14.18	−0.70
24	52.06	42.42	9.64	13.72	14.78	−1.06
25	49.96	40.32	9.64	13.81	15.38	−1.57
26	47.95	38.35	9.70	14.32	15.98	−1.66
27	45.60	35.64	9.96	14.91	16.57	−1.66
28	43.68	33.04	10.54	15.24	17.16	−1.92
29	41.75	30.36	11.39	16.08	17.76	−1.68
30	39.74	27.60	11.86	17.25	18.35	−1.10
31	37.15	24.50	12.65	18.59	18.94	−0.35
32	34.54	21.15	13.39	19.68	19.53	0.15
33	31.95	17.47	14.48	20.16	20.12	0.04
34	29.03	14.38	14.65	20.75	20.71	0.04
35	25.92	11.20	14.72	20.90	21.30	−0.40
36	22.68	08.13	14.55	21.23	21.89	−0.66
37	19.31	04 69	14 62	22.26	22.48	−0.22
38	15.45	00.42	15.03	23.00	23.07	−0.07
39	11.62	28896.31	15.31	23.21	23.65	−0.44
40	08.13	92.24h	15.89	—	—	—
41	04.69	—	—	—	—	—
42	01.34	—	—	—	—	—
43	28897.83	—	—	—	—	—
44	93.48h	—	—	—	—	—
45	88.97h	—	—	—	—	—

Further if we neglect the D' s, the first differences will vary linearly with M. In other words, R(J−1)−R(J) against J+1, and P(J)−P(J+1) against −J will give a single straight line, intersecting M=o and M=1 at 2B″ and 2B′ respectively. (Fig. 2). As pointed out before, in place of three straight lines corresponding to the three values of V″, only one is drawn passing through the mean positions of all the points. The values of B′s calculated from Fig. 2 are also given in Table IV.

TABLE III

Branches and rotational term differences for the λ 3468 Å band of Na₂

J	R (J)	P (J)	$\triangle_2 F'(J)$	$\triangle_2 F''(J)$	$\triangle_2 F''$(calc)	$\triangle_2 F''$(O−C)
13	28813.54d	28808.15	5.49	—	—	—
14	12.39d	06.49	5.90	9.06	8.74	0.32
15	11.05d	04.49	6.56	9.64	9.34	0.30
16	09.64d	02.75	6.89	9.88	9.94	−0.06
17	08.15d	01.17	6.98	10.40	10.54	−0.14
18	06.49d	28799.26	7.23	10 95	11.13	−0.18
19	04.49d	97.20	7.29	11.45	11.73	−0.28
20	02.75d	95.04	7.61	11.95	12.34	−0.39
21	01.17d	92.54	8.63	12.95	12.94	0.01
22	28799.26d	89.80	9.46	13.89	13.54	0.35
23	97.20d	87.06	10.14	14.68	14.14	0.54
24	95.04d	84.58	10 46	15.50	14.74	0.76
25	93.05	81-70	11.35	15.58	15.33	0.25
26	90.73	79 46	11 27	16.28	15.93	0.35
27	88.25	76.72	11.53	16.82	16.52	0.30
28	85.91	73.91	12.00	17.49	17.10	0.39
29	83.35	70.76	12.69	18 19	17.70	0.49
30	80.87	67.80	12.93	18.06	18 29	−0.23
31	78.46	65.29	13.17	18.80	18.88	−0.08
32	75.90	62.07	13.83	—	—	—
33	73.08	—	—	—	—	—
34	69.19	—	—	—	—	—
35	66.12	—	—	—	—	—
36	62.98	—	—	—	—	—

TABLE IV

Values of B″ and B′ for the states of λ3600−λ3200 Å system of Na₂ bands

Method used	B″(cm⁻¹)			B′(cm⁻¹)		
	2, 3 band	2, 4 band	2, 5 baud	2, 3 band	2, 4 band	2, 5 band
From $\triangle_2 F$	0.152	0.151	0.151	0.105	0.102	0.103
From Fig.1		0.15			0.10	
From Fig.2		0.15			0.10	
Loomis & Wood	0.1518	0.1515	0.1510			

Mean value of B′ is 0.103 cm⁻¹ approx. and from this $r_e' = 3.77$ Å. approx.

REFERENCES

Fredrickson, W. R., 1929, *Phys. Rev.*, **34**, 207.
Fredrickson, W. R. and Waston, W. W., 1927, *Phys. Rev.*, **30**, 429.
Hunter, A. and Pearse, R.W. B., 1936, *J. Sci. Inst.* **13**. 403.
Loomis, F. W. and Wood, R. W., 1928, *Phys. Rev.*, **32**, 223,.
Pearse, R. W. B. and Sinha, S. P., 1947, *Nature*, **160**, 159.
Sinha, S. P., 1947, *Proc. Phys. Soc.*, **59**, 610.
Sinha, S. P., 1948, *a Proc. Phys. Soc.* in the press.
Sinha, S. P., 1948, *b Proc. Phys. Soc.*, **60**, 436.
Smith, H. G., 1924, *Proc Roy. Soc. A*, **106**, 400.

THE SPECTRO-CHEMICAL ANALYSIS OF THE BEARING ALLOYS

By M. K. GHOSH and K. C. MAZUMDER

ABSTRACT.—The technique of spectro-chemical analysis of the bearing alloys with copper base has been developed by means of Hilger medium quartz spectrograph. The ranges of the different elements determined are :

  Sn—6.50 to 7.90%,   Pb—3.0 to 3.65%,   Ni—0.70 to 1.0%

The determinations agree well with those found chemically.

INTRODUCTION

The technique of spectro-chemical analysis of the copper base alloys used in the sheet mill as bearing material at Tata has been developed. Its composition is :

 Sn—6.50 to 7.9%,   Pb—3.0 to 3.50%,   Ni—0.70 to 1.0%.

the balance being copper and the trace elements. In the industrial laboratories of different countries the compositions of various copper base alloys are being spectro-chemically determined; but the estimation of such high per cents of both Sn and Pb in an alloy has been rare. From the Bell Telephone Laboratories Jaycox (1945) has published a very comprehensive paper on the "The spectro-chemical analysis of copper base alloys." The percentages of Al, Pb and Sn in the alloys vary from 0.30 to 15.0 ; for some elements it was as high as 40.0. As it is not feasible to determine spectro-chemically such high per cents by arcing and sparking the solid samples directly, the samples have been taken into solutions diluting the latter with copper nitrate. The ranges of different alloying elements have been thereby reduced to 0.01—2.0 % with respect to copper. The spectra have been then obtained by drying the solutions on graphite electrodes and by exciting in the D.C. arc. Besides this additional chemical work there is difficulty in having the same amounts of different solutions dried in the same way on the electrodes. Moreover, the inaccuracy—say in 2.0 % determination will be increased twenty times if the actual percentage is 40.0. The method adopted in the present paper is quite different from the above in as much as the solid samples themselves have been used for sparking even up to 7.8%.

A few papers from the Russian sources have recently been published on the spectro-chemical analysis of the copper base alloys :

(*I*) Spectro-chemical analysis of Pb in brasses, (1945)

(*II*) Spectro-chemical analysis of tin bronzes, (1945)

(*III*) Spectro-chemical analysis of bronzes, (1945)

As only the abstracts of these papers have been published in English or American journals, the methods adopted in or other details of these works are not known to the present authors.

In the Bragg Laboratory, U. K., a large number of gun metal samples were spectro-chemically analysed. Zinc, lead and nickel were determined by the spark method and the trace elements by the D. C. arc technique. They, however, found it more convenient to determine tin *chemically*. The percentage ranges of the elements estimated by the spark method were :

Zn—o.70 to 6.0,   Pb—o.10 to 4.0,   Ni—o.05 to 0.4,   Fe—o.05 to 0.4.

Zinc was used partly to replace tin as a war-measure. In the investigation to be reported the percentage of tin determined is about 7. 8 %. It can be spectro-chemically determined from the same spark spectra used for the estimation of Ni and Pb. There is thus a considerable saving of time if Sn is determined spectro-chemically instead of chemically. Some Fe-lines are also found on the plates which are strong enough to permit the photometric measurements of their blackenings. The percentage of Fe, however, has not been determined for want of suitable standards.

<center>EXPERIMENTAL</center>

Hilger medium quartz spectrograph has been used for photographing the spectra. The following are the conditions for excitation :

Voltage	10,0000
Capacity	.005 μF
Inductance	0.06 or 0.13 mh
Spark gap	2.0 mm.
Upper electrodes	Pointed carbon rods
Lower electrodes	Conical sample with flat top about 2 mm in diameter.

Five standard samples of variable compositions have kindly been prepared by the Tata Metallurgical Department in the small high frequency furnace of the Research Laboratory for this investigation. It became necessary on account of the fact that the variation in the compositions of the alloy made at Tata is not sufficiently large to enable one to draw standard curves properly. The spark spectra of at least four of these standards have been photographed on each plate. With the help of the curves drawn from the spectra of these standards the compositions of the unknown samples have been determined. It is expected that these standards are more segregation-free than the alloys made in the works. They give almost always smooth curves whereas there have been observed occasional variations in the readings obtained for the same unknown samples from different plates which cannot be attributed to experimental error. However, the results obtained for the unknown samples agree very favourably with those estimated chemically. It would have been ideal to re-melt the unknown samples and make fresh rods from them under the same laboratory conditions used for making the standards.

An attempt has been made to improve the accuracy of the results by the emulsion calibration of the photographic plates. The method adopted for this purpose was the one developed by Churchill (1944). This is known as "Two

lines'' method and consists of giving a series of exposures on the photographic plate of the spark spectrum of one representative sample used in the investigation; every thing else remains the same excepting the illumination which is varied. In the present investigation the variation has been effected by gradually changing the time of exposures. Two lines with appropriate blackening containing the range of blackenings to be met within the course of the investigation are selected from these spectra. For comparing the intensities of the spectral lines used for quantitative analysis a non-recording microphotometer has been used. The light from a steady source, a lamp running at a constant voltage, passing through a system of lens and prism, falls on the photographic plate containing the spectra of the various samples. After its passage through the selected spectral lines another system of lenses and a mirror reflect the patch of light on the slit of a photo-cell. The current generated in the photo-cell is measured by a galvanometer. The photographic plate which is placed on a horizontal platform can be given two motions at right angles to each other in the horizontal plane and a rotation about a vertical axis ; with these each and every line belonging to the different spectra photographed on the plate can be placed in the path of the light and their intensity, rather blackening, measured. The photometric readings of these lines for the whole series of spectra are plotted one against the other. The final emulsion curve is prepared from these preliminary curve with the help of an approximate ratio of the intensities of the two lines, if the actual ratio is not known. The intensity ratio of the spectral lines used for percentage determinations is then obtained by referring their photometric readings to the emulsion curve. The correction thus obtained has not been applied to all the plates taken during the investigation but where applied a decided improvement has been noticed. A few results which are very bad, probably due to segregation or other defects have not improved at all, on the contrary some of them have even become worse. The introduction of an auxiliary spark gap in series with the analytical gap, which makes the discharge more violent, has not been found to increase the accuracy of the result whether corrected or not.

RESULTS

Table I contains the results obtained for a few samples of the bearing metals. The samples have been used more than once , the results are concordant and agree well with the chemical determinations[*] The few results which differ considerably from those obtained chemically cannot be ascribed to the experimental errors ; they are perhaps due to segregation or other defects inherent in the samples. It should be remembered that in the chemical analysis, one gets a kind of average effect but in the spectro-chemical analysis, specially when the method of excitation of the

[*] Chemical determinations have been made by Mr. R. C. Dutt, the Chemist of the Research Laboratory.

spectrum by spark is employed only a very small area on the surface of the rod samples is made to emit light. If it happens that a segregate or an inhomogeneity is present on the surface the nature of the light emitted, and consequently the analysis obtained from it, will not be a representative one.

The techniques are still being improved and it is hoped that not only the higher percent of the above elements but also the trace elements present in this kind of alloys will be correctly evaluated from the same spectra.

TABLE I

Sn		Pb		Ni	
Chem.	Sp. Chem.	Chem	Sp. Chem.	Chem.	Sp. Chem,
7.84	7.78	3.63	3.65	0.91	0.93
7.00	7.05	3.08	3.00	0.70	0.70
—	—	3 08	3.00	0.70	0 72
7.00	7 00	3.08	3.05	0.70	0.70
6.93	6.80	3 36	3.36	1.00	0 98
7.09	—	—	—	—	—
6.54	6.58	3.25	3.16	0.88	0.92
6.80	6.70	—	—	1 06	1.05
6.54	6.60	3.25	3.20	0.88	0 92
6.35	6.35	3.15	3.23	0.94	1.00
6.35	6 32	3.15	3.32	0.94	0.98
6.30	8.30	3 46	3 40	0.94	0.92
7.84	7.85	—	—	—	—
7.00	7.00	—	—	—	—
7.00	7.00	—	—	—	—
7.00	7.00	—	—	—	—
6.54 ?	6.54	—	—	—	—
6.54	6.40	—	—	—	—
6.30	6.35	3.46	3.38	0.94	0.92
6.80	6.84	3.22	3.45	1.06	1.10
6.35	6.45	3.15	3.20	0.94	0.94
7.25	7.25	3 15	3.36	1.00	0.97
6.30	6.30	3 46	3.50	0.94	0.95
6.54	6.55	3 25	3.33	0.88	0.87
7 00	7.00	2.98	2.85	0 70	0.70
6.30	6 30	3 46	3 50	0.94	0 92
6.54	6.60	3.25	3.33	0 88	1 02
7.00	6.60	2 98	2 93	0.70	0.73
6.80	6.90	3.22	3 50	1 06	1.10
6.35	6.20	3 15	3.30	0 94	0.95
7.25	7.25	3.15	3.36	1 00	1.02

The bold figures are some of the values which have been corrected by the emulsion calibration curve.

REFERENCES

Churchill, J. R., 1944, Ind. & Eng. Chem, Anal. Ed, 16, 11.
Jaycox, E. K., 1945, J. Opt. Soc. Amer., 35 No. 2.
..   1945, Bull Aca. Sc., U.S.R. Ser. Phys. 9.
...   1945, Bull. Aca. Sc., U.S.R R Ser. Phys., 9.
...   1945, Zavodskays Lal., 11.

PERIODIC OR RHYTHMIC VARIATION OF THE INTENSITY OF SHORT WAVE RADIO SIGNALS

By S. S. BANERJEE AND B. N. SINGH

ABSTRACT. The present communication contains the results of detailed study of periodic or rhythmic types of fading of radio signals which are generally observed during the sun rise and sun set hours. It has been shown by measurement of the angles of arrival of the downcoming waves that such periodic fading may occur due to interference caused by two waves reflected either from one or two different layers of the ionosphere containing required amount of electronic density, when one or both the layers have slow vertical movement, presumbly due to rapid change of electronic density during the transition periods of ionization of the layers. It has been further shown that the development of slow periodic fading occurs due to the approach of maximum usable frequencies between the transmitting and receiving stations, and on such occasions the interference is caused by magneto-ionic components of reflected waves as suggested by Appleton and Beynon. The interference phenomena have been verified by recording the periodic fading of short wave signals transmitted from Delhi on 16 to 41 metre bands at various hours of the day during different months.

INTRODUCTION

Fading observations on short-wave radio signals have been found to be very useful in exploring the conditions of the ionosphere suitable for establishing radio communication between two stations situated apart and also for studying the possibility of diversity reception with spaced aerials as suggested by Banerjee and Mukerjee (1946). According to the mode of formation of various patterns of fading, they have been divided into two main categories, *viz*. (1) random and (2) periodic or rhythmic types. The present communication is concerned with the study of the second type of fading and their application to practical radio communications. For the purpose of explaining the various types of fading, the ionospheric data—recorded by the All India Radio, Delhi, have been used and the angles of arrival of downcoming waves have been measured, the method of which has been described in subsequent section.

THEORETICAL CONSIDERATIONS

The rhythmic or periodic type of variation of received signal, which is fairly regular and occurs mostly during sunrise and sunset hours can be explained to be due to interference fringes caused by either single and double reflections from one layer or two single reflections from two different layers of

the ionosphere containing the required amount of electronic density for the purpose, when one or both the layers are moving up or down very slowly. It should be mentioned, however, that in case the fading pattern is smooth and periodic, there will be, at a time, only two paths of received travelling waves from the ionosphere and the intensity of the waves—should be fairly constant. This has been corroborated by measurement of angles of arrival of the down-coming waves during the observations of fading of signals and by observing the intensity of only one of the rays in the absence of the other. It may be pointed out that such slow movements of the ionospheric layers are difficult to observe by the usual 'pulse method' of measuring the height of the ionospheric layers with cathode ray oscillograph. Calculations show that the rate of movement of the layers for such cases may be of the order of 5 km/hr. whereas, a fairly sensitive instrument for 'pulse method' would measure the height of a layer with an approximation of $\pm$ 10 km/hr. Incidentally, it may be noted that these fringes in fading records indicate the possibility of measuring fairly slow rate of change in height of the ionospheric layers.

The conditions of reflection for different types of fading stated above have been verified generally for 25 and 19 metre bands with vertically polarised waves. The periodic nature of fading, is more often observed either in the morning after ground sun rise, or in the afternoon when the concentrations of electrons in the layers are either increasing or decreasing. It is more pronounced in the afternoon, presumbly due to higher electronic concentra-tions of the layers, permitting double reflections. It may be mentioned that periodic fading has also been observed by Appleton and Beynon (1947), which they have explained to be due to the interference bands caused by magneto-ionic components of the reflected waves. Under such circumstances the frequency of transmission approaches the maximum usable frequencies between transmitting and receiving stations. The periodic patterns of fading under the above conditions have been observed by us. Typical records of periodic fading and discussions thereon have been given in the later section.

PRINCIPLE AND METHOD OF MEASURING THE ANGLE OF ARRIVAL OF DOWNCOMING WAVES

The principle of the method of measuring the angle of arrival of down-coming waves is based on the fact that the intensity of the received signal on a vertical aerial depends on the vertical component of the electric field associated with the downcoming wave and the intensity of the signal received on a frame aerial depends on the horizental component of the magnetic field of the wave. This method of measurement was adopted by Appleton and Barnett (1925) for measuring the angle of arrival of the downcoming waves for medium wave transmission, in the presence of ground wave when the signal was detected by a square-law detector. In the present method employed by us modi-fication has been made for the linear detector used and the absence of ground wave as shown below.

Let E and H be the electric and magnetic vectors respectively, associated with the downcoming radio wave as shown in Fig. 1 and let ϕ be the angle of
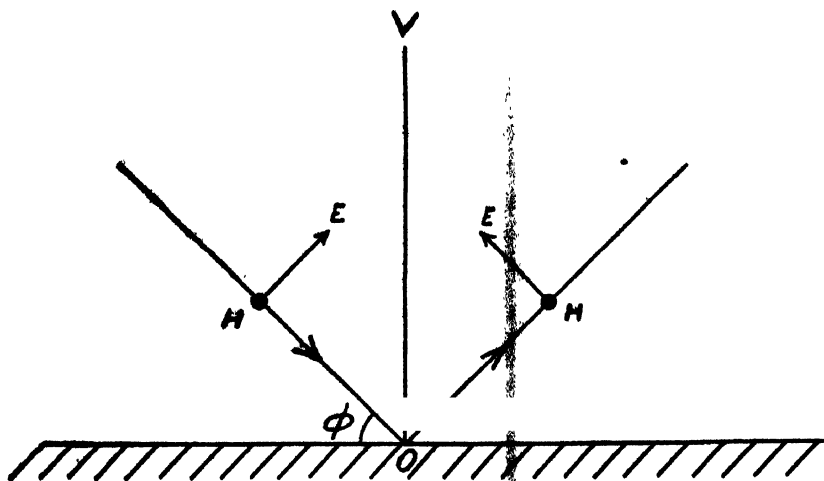
FIG. 1

arrival of the waves, *i.e.*, the angle subtended by the plane of propagation of the wave with the ground. It can be shown that the vertical aerial OV will be acted by an electric field 2E cos ϕ. sin ωt, where ω is the pulsatance of the wave. A frame aerial directed towards the transmitter under the same conditions will be acted by a magnetic field 2H sin ωt.

The instantaneous current flowing through a galvanometer in the second detector circuit of a superhet receiver connected with vertical aerial will therefore be given by 2 α K_vE cos ϕ sin ωt, where α is constant of the detector characteristic and K_v is the constant of the vertical aerial.

The mean current i_v flowing through the galvanometer in the receiver with vertical aerial will, thus, be given by—

$$i_v = 2\alpha\ K_v E \cos \phi \qquad \dots \quad (1)$$

Similarly, it can be shown that the mean current in the galvanometer with a frame serial will be given by—

$$i_f = 2\alpha\ K_f H \qquad \dots \quad (2)$$

where suffix f indicates the corresponding values for frame aerial.

From equations (1) and (2) we get—

$$\frac{i_v}{i_f} = \frac{K_v E \cos \phi}{K_f H} \qquad \dots \quad (3)$$

If the sensitivities of the two receivers are made equal by arranging the two aerials in such a manner that the vertical electric vector from a wave travelling along the ground, without any sky wave gives the same current in both the galvanometers, then, as $E \equiv H$, we have from equation (3),

$$\frac{i_v}{i_f} = \cos \phi \qquad \dots \quad (4)$$

Thus from equation (4), knowing the deflections in the two galvanometers simultaneously, the angle of arrival of the downcoming wave can be determined.

One 5-valve superhet receiver was connected to a vertical aerial and another receiver of the same type was connected to a frame aerial. The sensitivities of the receivers were made equal with the help of a local oscillator kept fairly apart at the same horizontal level as the receiver. The noise level in the receivers was eliminated before starting the observations. The deflections in the sensitive mirror galvanometers were observed simultaneously when a signal was received and the angle of arrival of downcoming wave was calculated. Various fading patterns along with the angles of arrival of the downcoming waves are shown in the following section.

EXPERIMENTAL OBSERVATIONS AND DISCUSSIONS

Typical automatic and visual records of periodic fading on 25 and 19 metre bands from Delhi are shown in Figs 2 to 9. Visual records have been indicated in terms of galvanometer deflections in Figs 5 and 6. During some of these observations angles of arrival of the downcoming waves were measured and the observed results have been explained by the existing electronic concentrations in the ionospheric layers at the hours of observations calculated from ionospheric data obtained from the Research Department, All India Radio, Delhi. For the sake of convenience, a brief summary of results of the above observations is given in Tables I and II. In order to check the results in the above tables, the electronic densities required for reflections of 25 and 19-metre bands for single and double reflections from E and F_1-layers between Delhi (lat. 28°, 35' N, long. 77°, 5'E) and Benares (lat. 25°.16 N. long. 83°.2E) situated at a distance of 678.4 km. over curved surface of the earth along with the angles of radiation, are given in Table III. The electronic densities have been calculated from the well-known relation,

$$\cos^2\beta = 1 - \frac{4\pi N e^2}{m\omega^2}$$

where β = angle of penetration of wave in the ionosphere.

N = electronic density.

e & m = charge and mass of electron respectively.

ω = pulsatance of the wave.

In view of the short wave lengths used in these observations, the collisional frequency of electrons with neutral atoms and molecules has been neglected, and for the sake of simplicity, the ionospheric layers have been ımed to be thin.
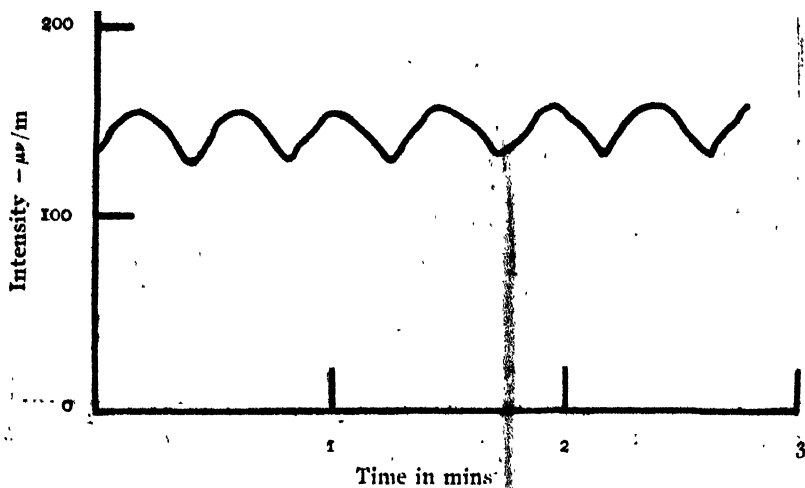
FIG. 2

19m — Delhi.   16 45 Hrs. I S.T., 22.12.46

Time in mins.
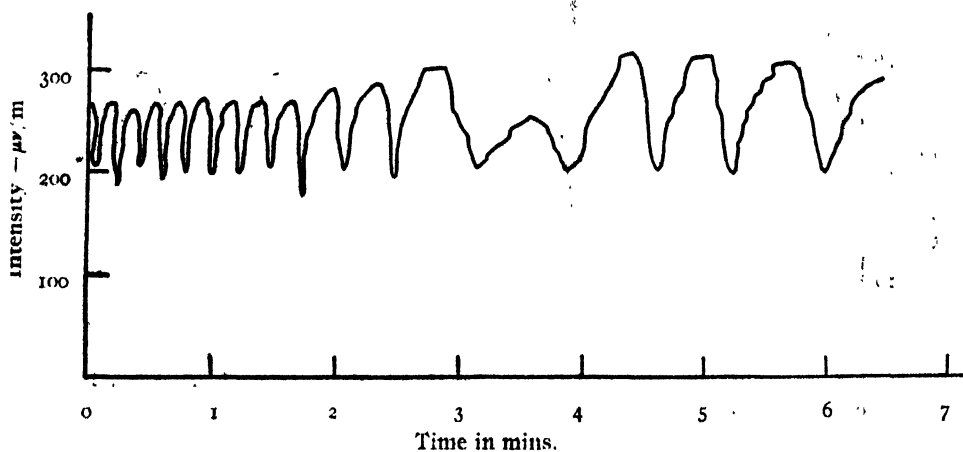
FIG. 3

25m.   Delhi, 09.10 Hrs. I.S.T , 2.5 46

Time in mins.
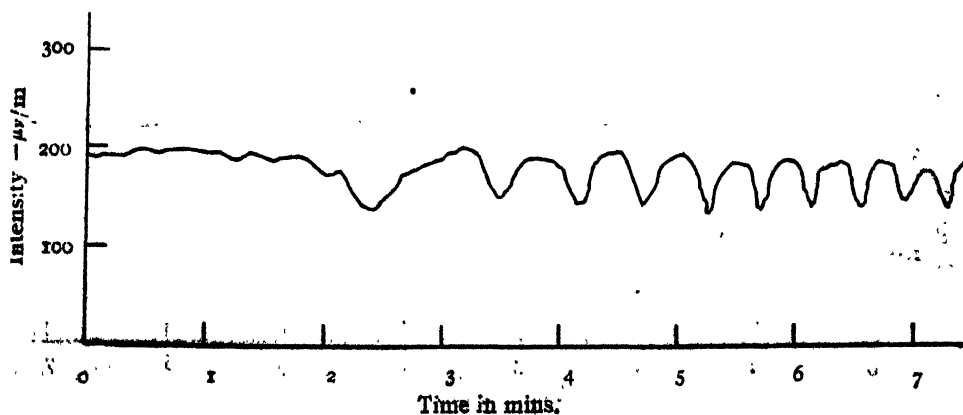
FIG. 4

19m — Delhi, 08.05 Hrs. I.S.T., 6.4.47
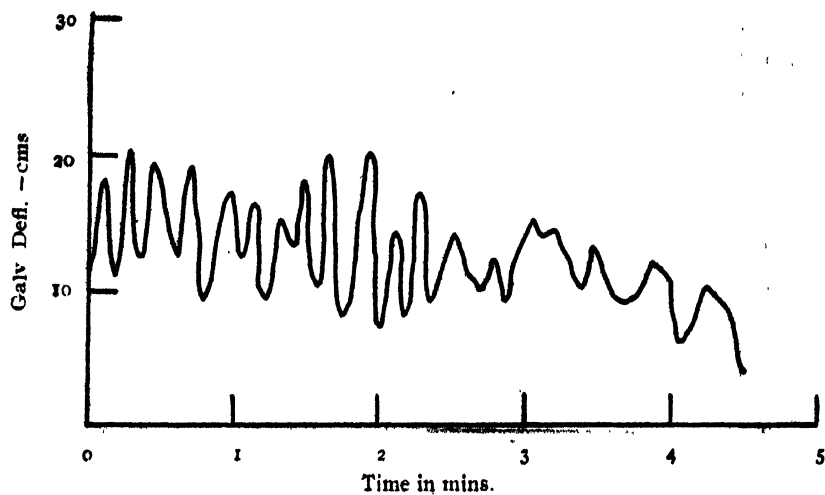
FIG. 5

19m – Delhi, 09.30 Hrs. I.S.T. 30.1.48
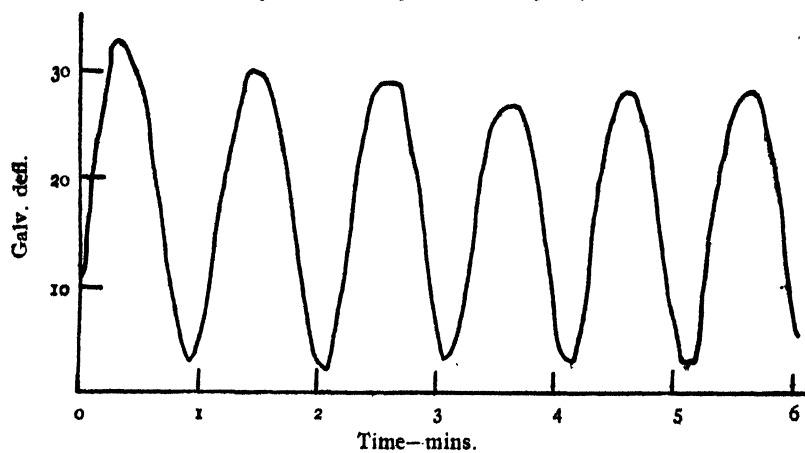
FIG. 6

19m – Delhi, 17.45 Hrs. I.S.T. 10.4.48
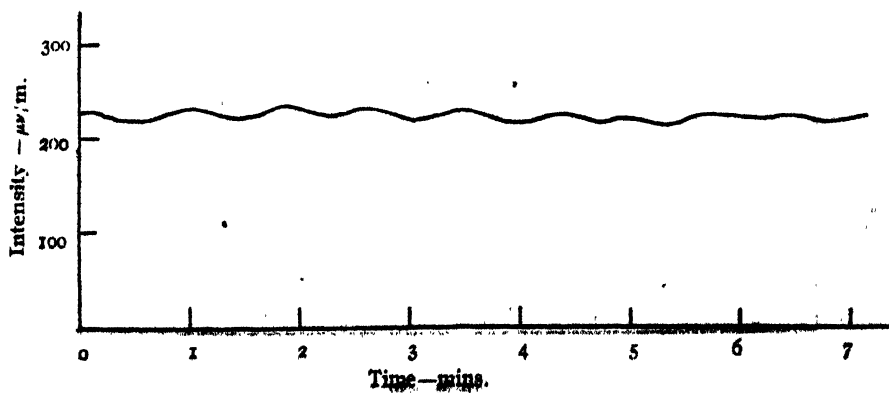
FIG. 7

19m – Delhi, 17.45 Hrs., 12.5.47
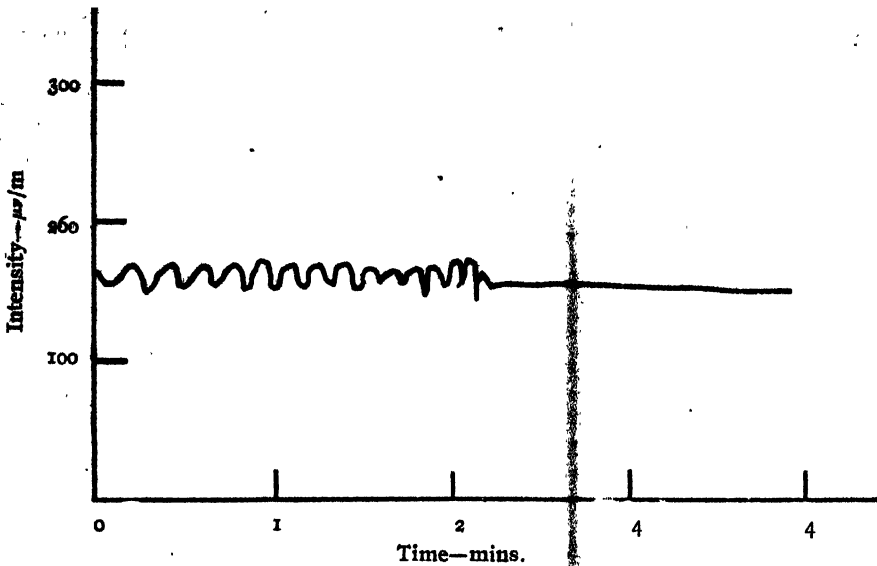
FIG. 8

19m—Delhi, 18.45 Hrs. I.S.T. 12.5.47
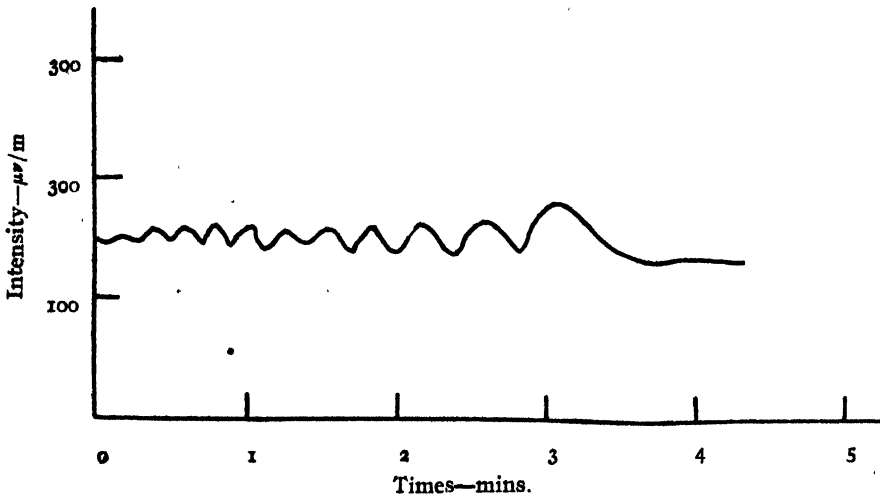
FIG. 9

19m—Delhi, 19.02 Hrs. I.S.T., 12.5.47

It will be observed from Table I that fading pattern under favourable circumstances develops into smooth periodic type as shown in Figs. 2 to 6. It will be seen from the table that this type of fading is obtained when there are only two reflections from either single layer or two different layers of the ionosphere with proper electronic concentration, when one or both the layers have slow vertical movement as described in the previous section.

Figs. 7 and 8 show the automatic records of fading observed on 12-5-47 for prolonged periodic variations of intensities of received signals on 19-metre band from Delhi. The periodic variations on this occasion persisted for

more than one hour during which, however, the periods of variations changed. Simultaneous observations were recorded for the measurement of angles of arrival of the downcoming waves in order to find the layer from which the waves were being reflected. Fig. 9 shows a typical record of fading out of

TABLE I

Fig.	Date	Time in I.S.T	Wave band	Type of fading	Remarks
2	22-12-46	1645 hrs.	19-metre.	Periodic	Single reflection from E (3.1×10^5 electrons/c.c, Single reflection from F_2 (1.5×10^6 electrons/cc.
3	2-5-46	0910 hrs.	25-metre.	Quasi-periodic and periodic.	Single or double reflection from F_2 (1.5×10^6 electrons/c.c).
4	6-4-47	0803 hrs.	19-metre	Random changing to periodic.	Single and double reflections from F_2-layer (2.3×10^6 electrons/c.c).
5	30-1-48	0930 hrs.	19-metre.	Periodic sometimes changing to random.	Single and double reflections from F_2-layer (2.1×10^6 etectrons/c.c).
6	10-4.48	1745 hrs.	19-metre	Smooth periodic with good intensity.	Single and double reflections from F_2-layer (4.5×10^6 electrons/c.c). Predicted value

TABLE II

Fig.	Date	Time in I.S.T.	Wave band	Type of fading	Angles of Arrival of downcoming waves.	Remarks
7	12-5.47	1715 hrs.	19-metre.	Slow periodic	Around 46° or 60°	Single and double reflections from F_2-layer (2.0×10^6 electrons/c.c.) rate of movement of the layer—2.9 km/hr.
8	12-5-47	1845 hrs.	19-metre.	Quick periodic changing to nearly constant intensity.	Atound 42°	Single reflection from F_2 (1.6×10^6 electrons/c.c).
9	12-5-47	1902 hrs.	19-metre.	Periodic. Fading out of signal due to reduction of electronic density.	Around 42°	Single reflection from F_2 (1.2×10^6 electrons/cc) Electronic concentration reduces to 2.0×10^6 electrons/c.c. after 1900 hrs.

TABLE III

Layer and height.	No. of reflections.	Angle of Radiation in degrees.	Required electronic densities for reflection in electrons/c.c.	
			25-metre band	19-metre band
E— 100 km	1	13.7	2.359×10^5 to 2.470×10^5	2.297×10^5 to 2.547×10^5
	2	29.5	2.359×10^5 to 2.714×10^5	7.365×10^5 to 8.158×10^5
F_2— 360 km	1	44.5	1.937×10^5 to 1.665×10^5	1.510×10^6 to 1.673×10^5
	2	63.9	2.359×10^6 to 2.470×16^6	2.297×10^6 to 2.544×10^6

19-metre band signal obtained on the same day near about sun set, caused by reduction of electronic density.

Simultaneous measurements of the angles of arrival of downcoming waves at the time of observation indicated the presence of single and double reflections from F_2-layer as shown in Table II. Fig. 7 shows the periodic pattern obtained when there are single and double reflections from F_2-layer as indicated by the angle of arrival of the downcoming rays as shown in column 6 of Table II. These angles may be compared for single or double reflections from the ionospheric layers with the angles of radiation given in column 3 of Table III. It will be noted from the summary of observation for Fig. 7 that single and double reflections occurred from F_2-layer which might have moved up or down very slowly and the rate of movement of which has also been included in the table. As it has been mentioned previously, that such periodic fading patterns are more pronounced in the morning and afternoon hours, during the transition periods of ionization in the ionospheric layers which might cause slow variations of their equivalent heights.

Figs. 8 and 9 represent clear instance of interference bands produced by magneto-ionic components of reflected waves as suggested by Appleton and Beynon (1947). Observations in columns 6 and 7 of Table II will show that the electronic density at the time of observation was such that the frequency of transmission approached very near the maximum usable frequency between Delhi and Benares. Fig. 8 shows that the periodic patterns in the beginning of the record was due to interference between magneto-ionic components, and the period of which gradually decreased, and subsequently was superposed by interference caused by the Pedersen upper ray and the lower trajectory ray for ordinary component. After this, the ordinary component must have disappeared and then the intensity of the received signal became nearly constant, as the received signal was due to the extra-ordinary component only. Fig. 9 shows the resumption of periodicity in the received signal due to interference

caused by upper and lower trajectory rays of the extra-ordinary component. The sequence of events described above may be attributed to the lowering of electronic density with time as shown in the last column of Table II and evidenced by the disappearance of signal shown in Fig. 9.

SUMMARY AND CONCLUSION

The periodic or rhythmic variations of intensity of short-wave. radio signals which frequently occur during the sun rise and sun set hours, have been recorded for transmissions on 16-to 41-metre bands from Delhi. It has been shown by measuring the angles of arrival of downcoming waves during the time of observation of fading and using the ionspheric data recorded by the All India Radio, Delhi, that such periodic patterns may arise due to interference caused by two waves reflected either from one or two layers of the ionosphere having adequate amount of electronic density, when one or both the layers have slow vertical movement, presumably due to rapid change of concentration of electrons during the transition periods of ionization in the layers. It has been further observed that the periodic type of fading occurs when the electronic density in ionospheric layer is such that the frequency of transmission approaches the maximum usable frequency between the transmitting and receiving stations and the interference is then caused by magneto-ionic components of the radio wave, as shown by Appleton and Beynon.

A part of this paper was read and discussed in the Indian Science Congress held at Patna in January, 1948.

ACKNOWLEDGMENTS

SECTION OF COMMUNICATION
ENGINEERING AND APPLIED PHYSICS,
ENGINEERING COLLEGE,
BENARES HINDU UNIVERSITY.

REFERENCES

Appleton E. V. and Barnett, M.A.F., (1925), *Proc. Roy. Soc. A.*, **109**, 630.
Appleton, E.V. and Beynon, W.J.G., (1947), *Proc. Phys. Soc.*, **89**, 58.
Banerjee, S.S. and Mukerjee, G.C., (1946), *Science and Culture*, **11**, 571.

MULTIPLET SEPARATIONS IN COMPLEX SPECTRA
PART III

(EQUIVALENT f ELECTRON CONFIGURATIONS)

BY V. RAMAKRISHNA RAO

(Received for Publication, July 12, 1948)

ABSTRACT. The separation factors have been calculated for multiplet-terms arising out of equivalent electron configurations of the type f^1 and f^2.

INTRODUCTION

In two previous papers the authors (Rao and Rao, 1948) discussed the applicability to certain known complex spectra of Goudsmit's expressions for mutliplet separations arising from electron configurations of the type d^3, d^4, d^3s and d^3p etc., and it was shown that the expressions could be used to a certain extent to the prediction of the intervals of the deeper set of terms in a spectrum. Goudsmit (1928) made the calculation of the separation factors only in the case of p^n and d^n electron systems, the latter forming the basic configurations for elements like vanadium, and chromium. The rare earth elements involve 'f' type electron-configuration and it would be of interest to derive the expressions for these as well, as they might suggest at least approximate estimates of the magnitudes of the intervals in such spectra, which as yet are not analysed sufficiently.

CALCULATION OF THE SEPARATION FACTORS

The method of deriving the expressions for 'f' electrons is as follows:—

(a) *Systems having one f electron, (f^1)* :—For a single 'f' electron $l = 3$, $m_l = \pm 3$, ± 2, ± 1, 0 and $m_s = \pm \frac{1}{2}$.

Writing down the possible combinations (14 in all) we have :

TABLE I

m_s	m_l	τ/a	M	m_s	m_l	τ/a	M
$\frac{1}{2}$	3	3/2	$3\frac{1}{2}$	$-\frac{1}{2}$	3	$-3/2$	$2\frac{1}{2}$
	2	1	$2\frac{1}{2}$		2	-1	$1\frac{1}{2}$
	1	$\frac{1}{2}$	$1\frac{1}{2}$		1	$-\frac{1}{2}$	$\frac{1}{2}$
	0	0	$\frac{1}{2}$		0	0	$-\frac{1}{2}$
	-1	$-\frac{1}{2}$	$-\frac{1}{2}$		-1	$\frac{1}{2}$	$-1\frac{1}{2}$
	-2	-1	$-1\frac{1}{2}$		-2	1	$-2\frac{1}{2}$
	-3	$-3/2$	$-2\frac{1}{2}$		-3	3/2	$-3\frac{1}{2}$

The second column contains $m_s m_l = \tau/a$. In the third column are given $m_s + m_l = M$. Another table is drawn from the above as follows:

TABLE II

M M_s	$3\frac{1}{2}$	$2\frac{1}{2}$	$1\frac{1}{2}$	$\frac{1}{2}$	$-\frac{1}{2}$	$-1\frac{1}{2}$	$-2\frac{1}{2}$	$-3\frac{1}{2}$
$\frac{1}{2}$	3/2	1	$\frac{1}{2}$	0	$-\frac{1}{2}$	-1	$-3/2$	
$-\frac{1}{2}$		$-3/2$	-1	$-\frac{1}{2}$	0	$\frac{1}{2}$	1	3/2
$\Sigma\tau$	3/2	$-\frac{1}{2}$	$-\frac{1}{2}$	$-\frac{1}{2}$	$-\frac{1}{2}$	$-\frac{1}{2}$	$-\frac{1}{2}$	3/2

which gives the τ sums in a weak field. A similar table is prepared in the case of a strong field as follows: the terms arising out of a single 'f' electron are $^2F_{3\frac{1}{2}}$ and $^2F_{2\frac{1}{2}}$. If we put $^2F_{3\frac{1}{2}} = \tau_1$ and $^2F_{2\frac{1}{2}} = \tau_2$, τ_1 and τ_2 being their separations from a hypothetical level, we have in a strong field :

TABLE III

M J	$3\frac{1}{2}$	$2\frac{1}{2}$	$1\frac{1}{2}$	$\frac{1}{2}$	$-\frac{1}{2}$	$-1\frac{1}{2}$	$-2\frac{1}{2}$	$-3\frac{1}{2}$
$3\frac{1}{2}$	τ_1	τ_1	τ_1	τ_1	τ_1	τ_1	τ_1	τ_1
$2\frac{1}{2}$		τ_2	τ_2	τ_2	τ_2	τ_2	τ_2	
$\Sigma\tau$	τ_1	$\tau_2+\tau_1$	$\tau_2+\tau_1$	$\tau_2+\tau_1$	$\tau_2+\tau_1$	$\tau_2+\tau_1$	$\tau_2+\tau_1$	τ_1

It is easy to see the symmetrical disposition of the $\Sigma\tau$ values about a centre. Equating the corresponding $\Sigma\tau$ values *i.e.*, belonging to the same M we have :

$$\tau_1 = 3/2 \text{ and } \tau_1 + \tau_2 = -\tfrac{1}{2}$$

$$\therefore \tau_2 = -2 \text{ and } \tau_1 - \tau_2 = \tfrac{7}{2}$$

$\tau_1 - \tau_2$ gives the total separation in the ^2F multiplet and is equal to $7/2\, a$.

Applying the Lande interval rule and dividing the separation by the higher of the J-values, we have the separation factor

$$A = (7/2)a. \quad (2/7) = a ;$$

thus for a ^2F in an 'f' configuration we have the total separation $= 7/2\, a$ and the separation factor $A = a$.

(b) "f^2" *configuration*:—In case of the two 'f' electrons the broad principles mentioned above hold and certain new features set in. As before we write down the m_s, m_l values for each electron as follows :

<div align="center">TABLE IV</div>

m_{s_1}	m_{l_1}	m_{s_2}	m_{l_2}	M_S	M_L	M	τ_1/a	τ_2/a	τ/a
½	3	½	3 (x)	1	6	7	3/2	3/2	3
			2		5	6		1	2½
			1		4	5		½	2
			0		3	4		0	1½
			-1		2	3		-½	1
			-2		1	2		-1	½
			-3		0	1		-1½	0
		-½	3	0	6	6		-1½	0
			2		5	5		-1	½
			1		4	4		-½	1
			0		3	3		0	1½
			-1		2	2		½	2
			-2		1	1		1	2½
			-3		0	0		1½	3

Table IV is only a typical portion of an extensive table, setting out all the possible combinations. For each of one type of m_{s_1}, m_{l_1} combination, m_{s_2}, m_{l_2} can have 14 combinations. Among these, however, the combination marked (x) is not allowed by Pauli's exclusion principle, because n, l being the same for the eqvivalent electrons the m_s, m_l values cannot be both identical. Thus writing for different m_l, 3,2,1,0,−1,−2,−3, and also for the negative values of m_{s_1} i.e. −½, we will have 14 × 13 combinations. Of these there will be many combinations which are obtained by mere exchange of places, as in ½ 2, ½ 3; ½ 3, ½ 2, which are not different configurations. In fact we get each combination 2 times. Therefore the net permissible combinations are ½ (14 × 13) = 91. The 13 combinations in the above table are among the permissible ones. Column (2) in Table IV contains

$$M_s = m_{s_1} + m_{s_2}, \quad M_L = m_{l_1} + m_{l_2} \text{ and } M = M_s + M_L.$$

and column (3) gives,

$$\frac{\tau_1}{a} = m_{s_1} \, m_{l_1} \; ; \frac{\tau_2}{a} = m_{s_2} \cdot m_{l_2}$$

and

$$\frac{\tau}{a} = \frac{\tau_1}{a} + \frac{\tau_2}{a}$$

From such a complete table, we form another, similar to Table II, giving sums in strong field. The net result is given below in Table V.

TABLE V

M / M_i	6	5	4	3	2	1	0	−1	−2	−3	−4	−5	−6
1	5/2	2	3	2	3/2	0	−3/2	−2	−3	−2	−5/2		
0	0	0	0	0	0	0	0	0	0	0	0	0	0
−1			−5/2	−2	−3	−2	−3/2	0	3/2	2	3	2	5/2
$\Sigma \tau$	5/2	2	1/2	0	−3/2	−2	−3	−2	−3/2	0	1/2	2	5/2

TABLE VI

M	6	5	4	3	2	1	0	−1	−2	−3	−4	−5	−6
$^3F_4$			$3A_F$	$3A_F$	$3A_F$	$3A_F$	$3A_F$	$3A_F$	$3A_F$	$3A_F$	$3A_F$		
$^3F_3$				$-A_F$	$-A_F$	$-A_F$	$-A_F$	$-A_F$	$-A_F$	$-A_F$			
$^3F_2$					$-4A_F$	$-4A_F$	$-4A_F$	$-4A_F$	$-4A_F$				
$^3P_2$					A_P	A_P	A_P	A_P	A_P				
$^3P_1$						$-A_P$	$-A_P$	$-A_P$					
$^3P_0$							$-A_P$						
$^3H_6$	$5A_H$	$5A_H$	$5A_H$	$5A_H$	$5A_H$	$5A_H$	$5A_H$	$5A_H$	$5A_H$	$5A_H$	$5A_H$	$5A_H$	$5A_H$
$^3H_5$		$-A_H$	$-A_H$	$-A_H$	$-A_H$	$-A_H$	$-A_H$	$-A_H$	$-A_H$	$-A_H$	$-A_H$		
$^3H_4$			$-6A_H$	$-6A_H$	$-6A_H$	$-6A_H$	$-6A_H$	$-6A_H$	$-6A_H$	$-6A_H$	$-6A_H$		
$\Sigma \tau$	$5A_H$	$4A_H$	$3A_F - 2A_H$	$2A_F - 2A_H$	$-2A_F + A_P - 2A_H$	$-2A_F - 2A_H$	$-2A_F - 2A_P - 2A_H$	$-2A_F - 2A_H$	$-2A_F + A_P - 2A_H$	$2A_F - 2A_H$	$3A_F - 2A_H$	$4A_H$	$5A_H$

Taking by corresponding M's we have,

$$5A_H = \tfrac{5}{2}a \quad \text{or} \quad A_H = \tfrac{1}{2}a$$

$$3A_F - 2A_H = \tfrac{1}{2}a \quad \text{or} \quad A_F = \tfrac{1}{2}a \text{ and}$$

$$-2A_F - 2A_H + A_P = -\tfrac{3}{2}a \quad \text{or} \quad A_P = \tfrac{1}{2}a$$

$$i.e. \quad A_H = A_F = A_P = \tfrac{1}{2}a$$

Preparing the $\Sigma\tau$ table for strong field we have for different J values of different multiplets different τ's over a hypothetical level and they will be of the general form as in the case of "f^1" configuration (of the type of $\Sigma\tau_1$ etc.,). Taking these, as before, under corresponding M values and equating, we see that there are more constants to be determined than the available equations. To get over this mathematical difficulty the following simplification is made on the assumption that the Lande-interval rule strictly holds. Illustratively, in the case of $^3P_{2,\,1,\,0}$ we have by Lande-interval rule $^3P_2 - ^3P_1 = 2A_P$ and $^3P_1 - ^3P_0 = A_P$, where A_P is the separation factor and the separation is proportional to the higher J value. If we put $^3P_2$ as having a value A_P and $^3P_1$ a value $-A_P$ then $^3P_2 - ^3P_1 = 2A_P$ proportional to 2 and $^3P_0$ a value $-2A_P$ then $^3P_1 - ^3P_0 = A_P$ which is again proportional to 1. Thus suitably choosing numerical coefficients, we can easily see that there is only one constant A_P to be determined. Thus we can suitably arrange to get only one constant for each multiplet-term and solve the equation easily. It would not be difficult to see that the question of separations does not arise in case of singlets as they are single levels and so we can treat them as zero.

RESULTS

From the above, the total separations for ^3F, ^3P and ^3H are follows :—

$$^3F = 7/2a \qquad ^3P = 3/2a \quad . \quad ^3H = 11/2a$$

The separation factor for each multiplet is $\tfrac{1}{2}a$.

The same method may be adopted for the calculation of the factors for f^3, f^4 etc., configurations, only, the table of permissible combinations would be much more extensive.

ACKNOWLEDGMENTS

REFERENCES

Rao and Rao, (1948), *Ind. Jour. Phy.*, **22**, 4, 173.
Rao and Rao (1948), *Ibid* 189.
Goudsmit, (1928), *Phy. Rev.*, **31**, 946.

TOMORROW'S INSTRUMENTS TODAY

RAJ-DER-KAR & CO.

COMMISSARIAT BUILDING

HORNBY ROAD

FORT

BOMBAY

OFFERS

FROM STOCK

GLASS METAL DIFFUSION PUMPS, METAL BOOSTE
PUMPS, OILS AMOILS OCTOILS OCTOIL,
BUTYL SABACATE

MANUFACTURED

BY

DISTILLATION PRODUCTS
(U. S. A.)

SPENCER MICROSCOPE

CENCO HIGHVACS

BESLER EPIDIASCOPE

COMPLETE WITH FILM STRIP ARRANGEMENTS

Telephone 27304
2 Lines

Telegrams
TECHLAB

The following special publications of the Indian Association for the Cultivation of Science, 210, Bowbazar Street, Calcutta, are available at the prices shown against each of them :—

Subject	Author	Price Rs. A. P.
Methods in Scientific Research	Sir E. J. Russell	0 6 0
The Origin of the Planets	Sir James H. Jeans	0 6 0
Separation of Isotopes	Prof. F. W. Aston	0 6 0
Garnets and their Role in Nature	Sir Lewis L. Fermor	2 8 0
(1) The Royal Botanic Gardens, Kew.	Sir Arthur Hill	1 8 0
(2) Studies in the Germination of Seeds.		
Interatomic Forces	Prof. J. E. Lennard-Jones	1 8 0
The Educational Aims and Practices of the California Institute of Technology.	R. A. Millikan	0 6 0
Active Nitrogen A New Theory.	Prof. S. K. Mitra	2 8 0
Theory of Valency and the Structure of Chemical Compounds.	Prof. P. Ray	3 0 0
Petroleum Resources of India	D. N. Wadia	2 8 0
The Role of the Electrical Double layer in the Electro Chemistry of Colloids.	J. N. Mukherjee	1 12 0

A discount of 25% is allowed to Booksellers and Agents.

RATES OF ADVERTISEMENTS

Third page of cover	...	...	...	...	Rs. 32, full page
do. do.	...	...	...	...	,, 20, half page
do. do.	...	...	...	...	,, 12, quarter page
Other pages	...	...	...	...	,, 25, full page
do.	...	...	...	...	,, 16, half page
do.	...	...	...	...	,, 10, quarter page

15% Commissions are allowed to *bonafide* publicity agents securing orders for advertisements.

CONTENTS

TERM VALUES IN COMPLEX SPECTRA
(COLUMBIUM I & II)

By V. RAMAKRISHNA RAO

ABSTRACT. Term values in the case of d^4 and d^3s configurations of Cb II have been calculated from Ostrofsky's and Bowman's formulæ and compared with experimental data due to Meggers and Humphreys. New formulæ are calculated for d^4s configuration of Cb I and the term values estimated from them are found to agree well with the observed data, the positions of the unidentified terms are also predicted.

INTRODUCTION

In a paper on the theory of complex spectra, Slater (1929) first treated atomic multiplets by the method of wave-mechanics and derived (1) Hund's scheme for multiplet classification directly from theory and (2) energy distances of multiplet terms in atomic spectra arising out of a given electronic configuration. Definite formulæ were calculated for the energy values of certain integrals which could be estimated well enough to permit comparison with experiment. A fairly good agreement was shown from typical examples of spectra due to configurations particularly of equivalent p^2 and d^2 electrons.

Condon and Shortley (1931) applied Slater's method to determine formulæ for the relation between the energies of terms for all two electron and several cases of three electron configurations, and in particular extended Slater's table of values for $a^k(lm_l ; l'm'_l)$ and $b^k(lm_l ; l'm'_l)$ in the case of equivalent f electrons, represented by the spectrum of lanthanum II. Slater's method, however, does not distinguish between terms of the same type occuring more than once in a given configuration, cases of which are very frequent in the more complex spectra ; the method gives only their mean energies. But for this deficiency the Slater-Condon formulæ in terms of their F's and G's are capable of giving a good agreement with experimental observation.

A different method of treatment of the problem of complex spectra was given by Van Vleck (1934) and extended by Serber (1934). Dirac's vector model was employed by them and Serber was able to obtain also the energy differences between similar terms of the same configuration, which could not be done in the Slater derivation.

The purpose of the present paper is to apply the results of the theoretical work outlined above, to check up the energy values of the multiplet-terms arising out of the d^4 and d^3s configurations in Cb II, the d^4s configuration of Cb I, the structure of which was worked out extensively by Megger and Humphrey (1946). This attempt has led to the calculation of expressions for the d^4s configuration which have not been determined before, and to estimate in the above spectra the values of a few terms which are yet to be identified.

RESULTS

Spectrum of Cb II :—Tables I and II embody the results in the spectrum of Cb II for terms due to the d^4 and d^3s electron configurations respectively. The first column in each table contains the configurations, the second the predicted terms. The experimental data as obtained from the analysis of the spectrum are given in the third column. These values are reduced and expressed with respect to the lowest term which is adopted as zero. Further the mean value of a multiplet term alone is given against each ; the individual components cannot be considered here. They involve the question of intervals which were discussed for Cb I and Cb II according to Goudsmit's method, in earlier papers by the author (Rao and Rao, 1948). The fourth column gives the energy values of terms as calculated from the theoretical formulæ quoted in the last column. The formulæ in Table I are due to Ostrofsky (1934) and those mentioned in Table II are taken from Bowman's paper (1941). The derivation of these formulæ was by the methods of Van Vleck and Serber. For the meaning of the parameters $F's$ and $G's$ reference may be made to Condon and Shortley's work. For estimating the numerical values of these parameters in the above formulæ the author adopted the method of Normal equations.

TABLE I

Term values of Cb II

Config.	Term	Obs. value	Cal. value	Formula (Ostrofsky)
d^4				
	^5D	0	-213.2	$6F_0 - 21F_2 - 189F_4$
	^3H	9311.3	9556.6	$6F_0 - 17F_2 - 69F_4$
	^3G	10065.0	10715.4	$6F_0 - 12F_2 - 94F_4$
	^3D	14692.7	12409.0	$6F_0 - 5F_2 - 129F_4$
	^1I	14871.2	14142.0	$6F_0 - 15F_2 - 9F_4$
	Mean value of	16710.1	15716.5	$6F_0 - 5F_2 - 76.5F_4$
	$^3F_+$	20557.7	30773.9	$+\frac{1}{2}(612F_2^2 + 2002F^2_4 - 4860F_2F_4)^{1/2}$
	$^3F_-$	12862.4	659.0	—
	Mean value of	16491.0	15716.5	$6F_0 - 5F_2 - 76.5F_4$
	$^3P_+$	27168.0	2'263.7	$\pm\frac{1}{2}(912F_2 + 38025F^2_4 - 9960F_2F_4)^{1/2}$
	$^3P_-$	5813.7	11169.3	—
	Mean value of	21687.6	20126.5	$6F_0 - 5F_2 - 6.5F_4$
	$^1G_+$	20109.3	25490.2	$\pm\frac{1}{2}(708F_2^2 + 30825F^2_4 - 6420F_2F_4)^{1/2}$
	$^1G_-$	14265.9	11762.8	—
	Mean value of	21139.2	23454.3	$6F_0 + 9F_2 - 76.5F_4$
	$^1D_+$	30539.9	86095.2	$\pm\frac{1}{2}(1296.F^2_2 + 30825F^2_4 - 10440F_2F_4)^{1/2}$
	$^1D_-$	11738.4	-39186.6	—
	Mean value of	—	29204.5	$6F_0 + 10F_2 + 6F_4$
	$^1S_+$	16777.8	42927.6	$\pm\frac{1}{2}(3088F^2_2 + 133200F^2_4 - 20640F_2F_4)^{1/2}$
	$^1S_-$	—	15481.4	—
	^1F	17983.9	18007.5	$6F_0 - 84F_4$

$6F_0 = 23299.5$　　　　$F_2 = 552.7$　　　　$F_4 = 63$

Note —In this and the following tables the suffixes + and − indicate the higher and lower, of two similar terms and the corresponding formulæ must be taken with the respective signs.

TABLE II

Term values of Cb II

Config.	Term	Obs. value	Calc. value	Formulæ (Bowman)
d^4s	^5P	10943.0	8109.6	$F_0-117F_1-\quad -3G_2$
	^3P	11655.2	11842.0	$F_0-117F_1 \quad + G_2$
	^3P	20936.0	18052.0	$F_0-6F_2+12F_4-2G_2$
	^1P	20437.6	19918.2	$F_0-6F_2-12F_4$
	^5F	3540.8	-1050.0	$F_0-15F_2-72F_4-3G_2$
	^3F	1909	2681.2	$F_0-15F_2-72F_4+G_2$
	^3F	25378.	27212.5	$F_0+9F_2-87F_4-2G_2$
	^1F	31762.3	29078.7	$F_0+9F_2-87F_4$
	^3G	15851.1	14998.5	$F_0-11F_2+13F_4-2G_2$
	^1G	16219.0	16861.7	$F^0-11F_2+13F_4$
	^3H	6062.4	18052.0	$F_0-6F_2\cdot12F_4-2G_2$
	^1H	21073.1	19918.2	$F_0\cdot6F_2-12F_4$
	$^3D_+$	—	16025.1	$F_0+5F_2+3F_4-2G_2$
	$^3D_-$	21332.9	20412.3	$\pm\frac{1}{2}(193F^2_2-1650F_2F_4+8325F^2_4)^{\frac{1}{2}}$
	$^1D_+$	—	17891.3	$F_0+5F_2+3F_4$
	$^1D_-$	21332	22278.5	$\pm\frac{1}{2}(193F^2_2-1650F_2F_4+8325F^2_4)^{\frac{1}{2}}$

$F_0=28651.8$ $F_2=1214.2$ $F_4=120.7$ $G_2=933.1$

The following five expressions are taken and equated to their numerical values as found from the experimental data. Then we have

$$^5D = 6F_0 - 21F_2 - 189F_4 = 0$$
$$^3H = 6F_0 - 17F_2 - 69F_4 = 9311.3$$
$$^3G = 6F_0 - 12F_2 - 94F_4 = 10065.3$$
$$^3D = 6F_0 - 5F_2 - 129F_4 = 12092.7$$
$$^1H = 6F_0 - 15F_2 - 9F_4 = 14871.2$$

More equations are taken than there are constants to be determined as the latter are not rigid in their values but are adjustable to give maximum satisfaction to the equations. The procedure of finding the values of these constants, which will give the largest measure of agreement with the numerical values, is as detailed below.

If the coefficients of the three constants are respectively *a*, *b*, and *c*, and *d* is the numerical value of the expression, *i.e.*, the term on the right hand side and *x* is the algebraic sum of the *a*, *b*, *c*, and *d*, then the corresponding values for the five terms for each of the equations are tabulated as below :—

TABLE III

a	*b*	*c*	*d*	*x*
1	− 21	− 189	0	− 209
1	− 17	− 69	9311.3	9226 3
1	− 12	− 91	10065.3	9960.3
1	5	129	12692.7	12559.7
1	− 15	− 9	14871.2	14848.2
5	− 70	− 490	46910 5	46385 5

The formation of *x* is just to indicate the correctness of the operations conducted. For, *x* is equal to the algebraic sum of *a*, *b*, *c*, and *d*. Then each row is multiplied by the value of '*a*' in that row as shown in the following arrangement :—

$$aa \qquad ab \qquad ac \qquad ad \qquad ax$$

(this arrangement is the same as above, for, all *a*'s are taken as unity) Similarly with *b* and *c* as follows .—

TABLE IV

ab	*bb*	*bc*	*bd*	*bx*
	441	3969	− 0	− 4389
	289	1173	− 158292.1	− 156847.1
	144	1128	− 120783 6	− 119523 6
	25	645	− 63463.5	− 62798.5
	225	135	− 223068.0	− 222723.0
− 70	1124	7050	− 565607.2	557503.2

TABLE V

ac	*bc*	*cc*	*cd*	*cx*
		35721	0	39509
		4761	− 642479.7	− 636611.7
		8836	− 946138 2	− 936268.2
		6641	− 1637358.3	− 1620201.3
		81	− 133840.8	− 133633 8
− 490	7050	66040	− 3359817.0	− 3287217.0

The values of the sums of a's etc. are taken as the coefficients of the respective F's and the normal equations are formed:

$$5F_0 - 70F_2 - 490F_4 = 469405$$

$$-70F_0 + 1124F_2 + 7050F_4 = -565607.2$$

$$-490F_0 + 7050F_2 + 66040F_4 = -3359817.0$$

For each constant there is an equation, and solving the three simultaneous equations, the values of the F's are obtained. These values give maximum satisfaction to the equations and are given at the foot of each table. Substituting them in the expressions for the terms the term-values are obtained and given in column 4.

SPECTRUM OF Cb I

Table VI gives similar calculations for the terms in the spectrum of Cb I, arising from the electron configuration d^4s. The theoretical formulæ for this configuration have thus been obtained by the author.

Van Vleck (1934) has shown that in the case of a configuration of the form the energy due to the addition of an s electron to the core a^k, enters in the following manner,

$$W = W(a^k) - \tfrac{1}{2}K_{as}\{k + 2[S(S+1) - S_k(S_k+1) - 3/4]\} - kj_{as} \qquad (1)$$

TABLE VI

Term values of Cb I

Config	Base	Term	Obs. val	Calc val (Ion data)	Cal val (Formulæ)	Formula (author)
d^4s	5D	6D	0	0	-184	$6F_0 - 41F_2 - 189F_4 - 3G_2$
		4D	8311.4	8420	8525	$6F_0 - 21F_2 - 189F_4 + 2G_2$
	3H	4H	10612.1	11520	10984.0	$6F_0 - 17F_2 - 69F_4 - 2G_2$
		2H	16579.6	16572	16210.0	$6F_0 - 17F_2 - 69F_4 + G_2$
	3G	4G	11808.5	12274	11712.5	$6F_0 - 12F_2 - 94F_4 - 2G_2$
		2G	16904.6	17326	16968.5	$6F_0 - 12F_2 - 91F_4 + G_2$
	3F+	4F+	12204.3	18394	20291.9	$6F_0 - 5F_2 - 76.5F_4 - 2G_2$
	3F.	4F.	...		11931.9	$\pm\tfrac{1}{2}(612F_2^2 + 20025F_4^2 - 4860F_2F_4)^{1/2}$
	3F+	2F+	..	23140	25517.9	$6F_0 - 5F_2 - 76.5F_4 + G_2$
	3F.	2F.			17157.0	$\pm\tfrac{1}{2}(612F_2^2 + 20025F_4^2 - 4860F_2F_4)^{1/2}$
	1D	4D	11839.0	14901	12804.1	$6F_0 - 5F_2 - 129F_4 - 2G_2$
		2D	—	10953	18030.1	$6F_0 - 5F_2 - 129F_4 + G_2$
	3P+	4P+	13073.8	18176	19877.5	$6F_0 - 5F_2 - 76.5F_4 - 2G_2$
	3P.	4P.	—	..	12346.3	$\pm\tfrac{1}{2}(912F_2^2 + 38025F_4^2 - 9960F_2F_4)^{1/2}$
	3P+	2P+	.	23288	25103.8	$6F_0 - 5F_2 - 76.5F_4 + G_2$
	3P.	2P.	---		17572.3	$\pm\tfrac{1}{2}(912F_2^2 + 38025F_4^2 - 9960F_2F_4)^{1/2}$
	1I	2I	—		17439.1	$6F_0 + 15F_2 - 9F_4 - G_2$
	1G+	2G+	--	..	26047.6	$6F_0 - 5F_2 - 6.5F_4 - G_2$
	1G.	2G.	—	---	17580.2	$\pm\tfrac{1}{2}(708F_2^2 + 30825F_4^2 - 6120F_2F_4)^{1/2}$
	1F	2F	—	.	19714.9	$6F_0 - 84F_2 - G_2$
	1D+	2D+	-	-	33739.0	$6F_0 + 9F_2 - 76.5F_4 - G_2$
	1D.	2D.	--	—	23856.4	$\pm\tfrac{1}{2}(1296F_2^2 + 30825F_4^2 - 10440F_2F_4)^{1/2}$
	1S+	2S+	..	---	42242.1	$6F_0 + 10F_2 + 6F_4 - G_2$
	1S.	2S.	—	—	17861.7	$\pm\tfrac{1}{2}(3088F_2^2 + 133200F_4^2 - 20040F_2F_4)^{1/2}$

$$F_0 = 26748.9 \qquad F_2 = 466.7 \qquad F_4 = 63 \qquad G_2 = 1742.0 \qquad K_{as} = 1684$$

where   W is the energy of sa^k

W(a^k) the energy of a^k alone

$K_{a\,s}$ the exchange energy between the s electron and core a^k

$_kJ_{a\,s}$ The Coulomb energy

S the resultant spin

S^k The spin of the core $a^{\,k}$. (*i. e.* the base terms)

The core a^k gives rise to a certain set of terms ; if we add an s-electron the multiplicity is changed by ± 1. Thus nd^1 gives $a\,^3D$ terms, besides some more. Addition of an s-electron gives $a\,^6D$ and $a\,^4D$. From a knowledge of the energy of ^5D, we can calculate that of ^6D and/or ^4D, if $K_{a\,s}$ and $J_{a\,s}$ are determined.

$$\text{But} \quad S = S_k \pm \tfrac{1}{2}$$

therefore the difference between ^6D and ^4D is merely given by

$$h\Delta v = 2K_{a\,s}\;(S_k + \tfrac{1}{2}) \qquad \qquad \dots \ (2)$$

The difference between the two terms that arise out of an addition of an s electron to the core is just proportional to $2(S_k + \tfrac{1}{2}) = 2S_k + 1$, *i. e.* the multiplicity of the core terms or the bases on which the two terms are formed. Taking the above case we have

$$\begin{aligned}
^6D - {}^4D = h\Delta v &= 2(K_{a\,s})(S_k + \tfrac{1}{2}) \\
&= (2S_k + 1)K_{a\,s} \\
&= 5K_{a\,s} \qquad \qquad \dots \ (3)
\end{aligned}$$

The difference is equal to 5 times a constant.

Taking again a ^3D of d^4 and the resulting ^1D, ^2D of d's we have

$$^1D - {}^2D = 3K_{a\,s} \qquad \qquad \dots \ (4)$$

Thus the ^4D terms computed from eqns. (3) and (4) are obtained separately and we can get different formulæ for the two similar terms.

Taking from Ostrofsky's formula the energy value of ^6D and substituting this in equation (1) for W (a_k) we have

$$\begin{aligned}
W(^6D) &= W(^5D) - \tfrac{1}{2}K_{a\,s}\{k + 2[S(S + 1) - S_k(S_k + 1) - 3/4]\} + kj_{a\,s} \\
&= W(^5D) - 4K_{a\,s} + kj_{a\,s}
\end{aligned}$$

Similarly

$$W(^4D) = W(^5D) + K_{a\,s} + kj_{a\,s}$$

Subtracting $^6D - {}^4D$ *is* $-5K_{a\,s}$, as previously obtained.

Thus in computing the theoretical formula for the ^6D, it is seen that the formula differs from the base (^5D) only in one respect, it contains an additional term $(-4K_{a\,s})$. (The term $kj_{a\,s}$ is only a Coulomb term affecting only the absolute level but not the relative separation and so can be neglected from consideration).

Similarly the ^{4}D differs only in containing an additional term K_{as}.
The value for the other ^{4}D from ^{3}D base is

$$W(^4D) = W(^3D) - 3K_{as}$$

which is obviously different from the ^{4}D out of the ^{1}D base. The value for
the ^{2}D out of the ^{3}D is $W(^2D) = W(^3D) + o$

Tabulating the results obtained in the above two typical cases :

TABLE VII

Config	base	config	term	formula
d^4	^{3}D	d^3s	^{6}D	$W(^3D) - 4K_{ac} = 6F_0 - 21F_2 - 180F_4 - 4K_{as}$
			a^4D	$W(^3D) + K_{ac} = 6F_0 - 21F_2 - 180F_4 + K_{as}$
	^{1}D		b^4D	$W(^1D) - 3K_{as} = 6F_0 - 5F_2 - 120F_4 - 3K_{as}$
			^{2}D	$W(^1D) - o = 6F_0 - 5F_2 - 120F_4$

This additional term containing the constant K_{as} can in fact be denoted
by the Slater-Condon's G's for it represents the interaction energy between
non-equivalent electrons (d and s). This method can be followed for the
derivation of formulæ for all other terms of d^4s out of all bases given by
the d^4 configuration. In the above method of representation it can be easily
seen that the ^{2}D has apparently the same energy as the base ^{1}D and there
is no symmetrical disposition of the formulæ in that the ^{1}D terms have
different coefficients for the G's. Bowman in his derivation for d^3s has
given the formulæ in this fashion. But a more symmetrical and elegant
method of representation is seen in Condon and Shortley formulæ for the
d^2s etc. It is easy to see that all that matters in the formulas is that ^{6}D and ^{1}D
must differ by 5G. So instead of putting ^{6}D = ^{3}D — 4G and a^4D = ^{3}D + G, we
may put ^{6}D = ^{3}D — 3G and a^4D = ^{3}D + 2G which gives ^{6}D — ^{1}D = — 5G. Similarly
we may put b^4D = ^{3}D — 2G and ^{2}D = ^{3}D + G which gives b^4D — ^{2}D = — 3G. The
advantage of this representation is that similar terms like a^4D and b^4D have
the same coefficient for G's (varying in sign) and no term appears with the
same formula as that of the corresponding base term. It will be relevant to
point out a regularity here namely the sextet formulæ contain as the
coefficient of G, 3 ; the quartet contains 2, and the doublet 1.

The respective formulæ obtained thus are given in the last column of
Table VI against each term. The numerical values of the constants are
determined by the method of normal equations explained earlier, and are
given at the foot of the table and the values of the terms themselves are
shown in column 5.

A different method is also adopted to calculate the term values utilising the experimental data of the analysis of Cb II. The procedure, as mentioned previously, is:

$$^6D - {}^4D = \tfrac{1}{2}K_{as}(S_k + \tfrac{1}{2})$$

from which K_{as} is calculated assuming the observed values of ^6D and ^1D of d^1 s configuration in Cb I. Substituting this value of K_{as} in Van Vleck's equation (1) the values of the terms of d^4 s of Cb I can be determined knowing those of d^1 of Cb II. The value of kj_{as} need not be known for reasons already mentioned. It should be noted that the terms of Cb I which can be calculated by this procedure is limited by the known number of terms of d^1 configuration of Cb II. All terms which could thus be calculated are shown in the same Table VI in column 4. These values provide another check on the theoretical formulae.

A study of the Tables I, II and VI and a comparison of the calculated and observed term values in Cb I and Cb II indicate generally a fairly good agreement. A few exceptions are ^2H, ^1F and ^3F and perhaps ^3P of d^3s configuration of Cb II in which the discrepancies are rather large. It should be noticed that this agreement is approximate and considered as a method for the prediction of unknown terms. It gives us a rough disposition of the region of the multiplets. With this limitation Table VI contains the predicted values of the several terms of Cb I which are yet to be identified. These are expected to be useful in further work on the analysis of the spectrum.

REFERENCES

Bowman D. S., 1941, *Phy. Rev.*, **59**, 386.

Condon and Shortley, 1931 *Phys. Rev.*, **37**, 1025.

Meggers and Humphreys, 1946,*B. S. J.*, **34**, 477.

Ostrofsky, M. 1934, *Phy Rev.*, 46, 604

Rao, V. Ramakrishna and Rao, K. R. 1918, *Ind. J. Phys.*, **22**, 173 and 189.

Serber, 1934, *Phy. Rev.*, **45**, 461.

Slater, 1929, *Ibid*, **34**, 1293.

Van, Vleck J. H., 1934, *Ibid*, **45**, 405.

ANOMALOUS DISPERSION OF DIELECTRIC CONSTANT

By S. K. KULKARNI JATKAR and B. R. YATHIRAJA IYENGAR

ABSTRACT. A new equation based on the ideas of hindered rotation and preferred orientation in quasi-crystalline liquids and solids has been derived in order to quantitatively account for the dispersion and absorption of polar substances. The existing relationships of Debye, Cole and Cole and others have been critically reviewed. The new expression for ϵ' the dielectric constant and ϵ'' the dielectric loss are

$$\epsilon' = \epsilon_\infty + \frac{(\epsilon_0 - \epsilon_\infty)}{1 + \omega^2\tau^2} \quad ; \quad \epsilon'' = \frac{(\epsilon_0 - \epsilon_\infty)\omega\tau}{1 + \omega^2\tau^2}$$

The new equations for dispersion and absorption have been extended to binary solutions of polar components and a general equation has been derived for the dielectric constant and dielectric loss in terms of the relaxation times of the two components.

INTRODUCTION

The phenomenon by which there occurs a marked decrease of the dielectric constant with increasing frequencies of the applied field accompanied by a strong absorption of electric waves is referred to as anomalous dispersion. This effect in liquids was first observed experimentally by Drude (1897). Debye (1929) based his explanation for anomalous dispersion on the idea of the existence of polar molecules. At sufficiently low frequencies when the period of the field is large compared to τ, the time of relaxation of the polar substance, the molecules can follow the field with ease and consequently the material has high static dielectric constant. When the frequency of the field is of a magnitude comparable to relaxation time the dielectric constant falls gradually with increasing frequencies. Finally at very high frequencies, i.e., when the period of the field is very small compared to τ the dipoles reach such a state wherein they do not show any response to the applied field. Thus the polar material here is characterised by a constant high frequency dielectric constant. The extent and the range of dielectric dispersion is a function of the internal forces in the substance such as the viscosity and also depends upon the nature of the dipoles of which the molecules of the substance are constituted.

POLAR LIQUIDS AND SOLIDS

Debye (loc. cit.) was the first to derive a quantitative expression to account for the dispersion and absorption of polar substances. He wrote for the

molecular polarisation in the dispersion region as follows

$$P_{(\omega)} = \frac{(\epsilon - 1)}{(\epsilon + 2)} \frac{M}{d} = \frac{4\pi N}{3}\left(\alpha_E + \frac{\mu^2}{3kt} \frac{1}{1 + i\omega t}\right) \qquad \dots \quad (1)$$

The equation of Debye is based on the validity of the Clausius-Mosotti relationship which has been found to be a failure when applied to concentrated solutions and pure liquids and has got limited application even in the case of dilute solutions. This failure is inherent in the assumption of a spherical cavity in evaluating the internal field and the postulate of a dipole having all possible orientation in space.

It is of interest to note that Debye has derived a formula for the average electric moment of a molecule in solids assuming that the molecule can point with its moment only in two definite directions, the direction of F and the opposite.

The mean moment of a molecule in the direction of F is

$$\bar{m} = \frac{1}{1 + i\omega\tau} \frac{\mu^2 F_0 e^{i\omega t}}{kT} = \frac{1}{1 + i\omega\tau} \frac{\mu^2 F}{kT}$$

The expression on right hand side can be derived in a very simple manner as follows. The general distribution function in a variable field has been given by Debye as

$$f = A\left(1 + \frac{1}{1 + i\omega\tau} \frac{\mu F}{kT} \cos\theta\right) \qquad \dots \quad (2)$$

where θ is the angle 'μ' makes with F. The Boltzmann's distribution function gives for n_1 and n_2 the number of molecules following the two possible orientations one along and the other opposite to the field

$$n_1 = A\left(1 + \frac{\mu F}{kT} \frac{1}{1 + i\omega\tau}\right)$$

$$n_2 = A\left(1 - \frac{\mu F}{kT} \frac{1}{1 + i\omega\tau}\right)$$

obtained by putting $\cos\theta = \pm 1$ in Debye's expression (2)

the mean moment $m = \mu(n_1 - n_2)/(n_1 + n_2)$

$$= \frac{2A(\mu^2 F/kT) \frac{1}{(1 + i\omega\tau)}}{2A}$$

i.e. $\bar{m} = \dfrac{\mu^2 F}{kT} \dfrac{1}{(1 + i\omega\tau)}$

This expression for $\bar{m}$ for solids differs from that derived earlier for the case of gases by a factor $1/3$ since in the former case, only the directions parallel and anti-parallel to the field are considered. Proceeding as before Debye has obtained the same expressions for ϵ' and ϵ'' as for the case of gases. This is because, firstly he has used the same Clausius-Mosotti

relationship $\dfrac{(\epsilon-1)M}{(\epsilon+2)d}$ to hold good and secondly the modified expression for $\bar{m}$ for solids has been eliminated in the initial stages of the derivation by being expressed in terms of $\dfrac{(\epsilon-1)M}{(\epsilon+2)d}$ and hence becomes ineffective to modify the expressions for ϵ' and ϵ''.

THE NEW EQUATION

It has been found by Jatkar, Iyengar and Sathe, (1946) that the polarisation of liquids and solids in a static field is given by

$$(\epsilon-1)M/d = 4\pi N(\alpha_E + \mu^2/kT)$$ instead of the classical expression

$$\frac{(\epsilon-1)}{(\epsilon+2)}\frac{M}{d} = \frac{4\pi N}{3}(\alpha_E + \mu^2/3kT).$$

The former equation has been derived using a new internal field based on the concept of a thin long cylindrical cavity which is in conformity with the anisotropy of the dipole, and also on the consideration of preferred orientation along and opposite to the direction of the applied field. This equation has been found applicable to a large number of polar liquids and solids. Extending the new relationship to the case of a variable field, the polarisation $P_{(\omega)}$ at frequency ω is given by

$$P_{(\omega)} = \frac{(\epsilon-1)M}{d} = 4\pi N\left(\alpha_E + \frac{\mu^2}{kT}\frac{1}{1+i\omega\tau}\right)$$

Defining

$$(\epsilon_\infty-1)M/d = 4\pi N\alpha_E \quad\text{and}\quad (\epsilon_0-1)M/d = 4\pi N\left(\alpha_E + \frac{\mu^2}{kT}\right)$$

we have

$$P_{(\omega)} = M/d\left\{(\epsilon_\infty-1) + \frac{1}{(1+i\omega\tau)}[(\epsilon_0-1)-(\epsilon_\infty-1)]\right\} = \frac{(\epsilon-1)M}{d}$$

whence

$$\epsilon = \epsilon_\infty + \frac{(\epsilon_0-\epsilon_\infty)}{1+i\omega\tau}$$

$$= \epsilon_\infty + \frac{(\epsilon_0-\epsilon_\infty)(1-i\omega\tau)}{1+\omega^2\tau^2}$$

i.e.,

$$\epsilon = \epsilon_\infty + \frac{(\epsilon_0-\epsilon_\infty)}{1+\omega^2\tau^2} - i\omega\tau\frac{(\epsilon_0+\epsilon_\infty)}{1+\omega^2\tau^2}$$

Writing

$$\epsilon = \epsilon' - i\,\epsilon''$$

$$\epsilon' = \frac{(\epsilon_0-\epsilon_\infty)}{1+\omega^2\tau^2} + \epsilon_\infty \quad\text{and}\quad \epsilon'' = \frac{(\epsilon_0-\epsilon_\infty)\omega\tau}{1+\omega^2\tau^2}$$

These expressions are very similar to the classical expressions but for a factor $\dfrac{(\epsilon_0+2)}{(\epsilon_\infty+2)}$ which comes associated with $\omega\tau$ in the latter case. It is note-

worthy that the two expressions are identical when $\frac{(\epsilon_0 + 2)}{(\epsilon_\infty + 2)} = 1$, *i.e.*, when the high frequency dielectric constant does not very much differ from the static dielectric constant.

Wyman's (1936) and Onsager's (1936) expressions for the polarization lead to the same equations for ϵ' and ϵ'' as given by the application of the new equation. For a modified form of Onsager's equation

$$\frac{(\epsilon - 1)}{(\epsilon + 2)} - \frac{(\epsilon_\infty - 1)}{(\epsilon_\infty + 2)} - \beta = q \left\{ \frac{3}{2} \frac{(\epsilon_\infty + 2)}{(\epsilon + 2)} - 1 \right\}$$

where 'q' is an empirical constant; (the case $q = 1$ corresponding to Onsager's equation). Cole (1938) has shown that

$$\epsilon' = \epsilon_\infty + \frac{(\epsilon_0 - \epsilon_\infty)}{1 + Z^2} \quad \text{and} \quad \epsilon'' = \frac{(\epsilon_0 - \epsilon_\infty)}{1 + Z^2} \cdot Z$$

where

$$Z = \frac{\omega\tau}{1 - \delta} \quad [\delta \text{ being a constant} = \frac{1}{3} \cdot \frac{4\pi N\mu^2}{9kT} (\epsilon_\infty + 2) (1 - q)$$

The application of experimental data has shown that 'δ' is indeed small, (*i.e.*, $Z = \omega\tau$) so that the expressions for ϵ' and ϵ'' correspond to the new equation.

The maximum in ϵ'' as well as the maximum slope of the $\epsilon' - \omega$ curve occur at a frequency ω_c the condition for which is given according to (1) Debye's expression as $\omega_c \tau = \frac{(\epsilon_\infty + 2)}{(\epsilon_0 + 2)}$ (2) Onsager's $\omega_c \tau = 1$, (3) the modified Onsager's equation $\frac{\omega_c \tau}{1 - \delta} = 1$ and (4) the new equation $\omega_c \tau = 1$. Thus the relaxation times obtained from the observed values of ω_c are always smaller by a factor $\frac{(\epsilon_\infty + 2)}{(\epsilon_0 + 2)}$ in Debye's case as compared with the correct value calculated from the new equation.

<div align="center">SOLUTIONS</div>

(a) *Nonpolar*:

Since the Clausius-Mosotti expression is considered to be valid for dilute solutions in nonpolar solvents, it is expected that Debye's dispersion equation derived on the basis of this hypothesis should be applicable to measurements in dilute solutions of nonpolar solvents. The extension of Debye's dispersion equation to a binary system has been made by Williams (1934) who has considered a solution in which there are n_2 polar molecules/c.c. each having electronic polarisability $\alpha_{E_2(o)}$ and moment μ_2 dissolved in n_1 mols./c.c. of the

nonpolar solvent each having electronic polarisability $\alpha_{E_1(0)}$ and zero electric moment. Thus the polarisation per c.c. of the mixture

$$P_{12(\omega)} = \frac{(\epsilon_{12} - 1)}{(\epsilon_{12} + 2)} = \frac{4\pi}{3}\left\{\alpha_{E_1(0)}n_1 + \alpha_{E_2(0)}n_2 + \frac{n_2\mu^2}{3kT}\frac{1}{(1 + i\omega\tau_2)}\right\}$$

$$= \frac{(\epsilon_{12(\infty)} - 1)}{(\epsilon_{12(\infty)} + 2)} + \frac{1}{1 + i\omega\tau_2}\left\{\frac{(\epsilon_{12(0)} - 1)}{(\epsilon_{12(0)} + 2)} - \frac{(\epsilon_{12(\infty)} - 1)}{(\epsilon_{12(\infty)} + 2)}\right\}$$

$\epsilon_{12(\infty)}$ = high frequency dielectric constant and $\epsilon_{12(0)}$ = static dielectric constant of solution and τ_2 = relaxation time of the polar solute molecules. Writing $\epsilon_{12} = \epsilon_{12}' - i\epsilon_{12}''$ and separating the real and imaginary parts

$$\epsilon_{12}' = \epsilon_{12(\infty)} + \frac{(\epsilon_{12(0)} - \epsilon_{12(\infty)})}{1 + x^2} - ix\frac{(\epsilon_{12(0)} - \epsilon_{12(\infty)})}{1 + x^2}$$

whence

$$\epsilon_{12} = \epsilon_{12(\infty)} + \frac{(\epsilon_{12(0)} - \epsilon_{12(\infty)})}{1 + x^2} \quad \text{and} \quad \epsilon_{12}'' = \frac{(\epsilon_{12(0)} - \epsilon_{12(\infty)})}{1 + x^2}.x$$

$$\left(x = \omega\tau_2.\frac{(\epsilon_{12(0)} + 2)}{(\epsilon_{12(\infty)} + 2)}\right)$$

These expressions which are very similar to those given by Debye for gases were derived on the basis of Clausius-Mosotti expression for total polarisation. The usage of the correct expression for polarisation $(\epsilon - 1)M/d$ gives expressions for ϵ' and ϵ'' very similar to those derived above except that in the former case the factor $\frac{(\epsilon_{12(\infty)} + 2)}{(\epsilon_{12(0)} + 2)}$ does not occur. In fact in dilute solutions of nonpolar solvents $\epsilon_{12(0)} \simeq \epsilon_{12(\infty)}$ so that the factor $\frac{(\epsilon_{12(\infty)} + 2)}{(\epsilon_{12(0)} + 2)}$ fortuitously becomes unity and hence Debye's expression coincides with the new equation.

(b) *Polar*:

Oncley (1938) has attempted to interpret the dispersion of polar binary solutions using Wyman's (1936) empirical equation for polarisation. No rigorous theoretical treatment of the subject is available in literature. On the basis of the new equation for molecular polarisation $(\epsilon - 1)M/d$, the expression for the molecular polarisation $P_{12(\omega)}$ of the solution at ω frequency can be written as,

$$P_{12(\omega)} = P_{1(\omega)}f_1 + P_{2(\omega)}f_2$$

where $P_{1(\omega)}$ and $P_{2(\omega)}$ are the molecular polarisations of the two polar components at ω frequency.

Now
$$P_{12(\omega)} = \frac{(\epsilon_{12} - 1)}{d_{12}}(M_1f_1 + M_2f_2) = \frac{(\epsilon_1 - 1)M_1f_1}{d_1} + \frac{(\epsilon_2 - 1)M_2f_2}{d_2}.$$

Writing for the sake of simplicity in terms of specific polarisations

$$p_x \left(= \frac{(\epsilon_x - 1)}{d_x} \right)$$

$$p_{12(\omega)} = \frac{(\epsilon_{12} - 1)}{d_{12}} = \frac{(\epsilon_1 - 1)}{d_1} \omega_1 + \frac{(\epsilon_2 - 1)}{d_2} \omega_2 \ ; \ \omega_1 \text{ and } \omega_2$$

being weight fractions.

i.e. $\qquad \epsilon_{12} = 1 + d_{12}\{ p_{1(\omega)} \omega_1 + p_{2(\omega)} \omega_2 \}$

where

$$p_1(\omega) = \frac{(\epsilon_1 - 1)}{d_1} = \frac{(\epsilon_{1(\infty)} - 1)}{d_1} + \frac{1}{1 + i\omega\tau_1} \frac{(\epsilon_{1(0)} - \epsilon_{1(\infty)})}{d_1}$$

and

$$p_2(\omega) = \frac{(\epsilon_2 - 1)}{d_2} = \frac{(\epsilon_{2(\infty)} - 1)}{d_2} + \frac{1}{1 + i\omega\tau_2} \frac{(\epsilon_{2(0)} - \epsilon_{2(\infty)})}{d_2}$$

τ_1 and τ_2 being the relaxation times and $\epsilon_{1(0)}$ and $\epsilon_{2(0)}$ the static dielectric constants of the two polar components. Substituting these values of $p_1(\omega)$ and $p_2(\omega)$ we get

$$\epsilon_{12} = 1 + d_{12}\left\{ \frac{(\epsilon_{1(\infty)} - 1)}{d_1} \omega_1 + \frac{(\epsilon_{2(\infty)} - 1)}{d_2} \omega_2 \right.$$

$$\left. + \frac{(\epsilon_{1(0)} - \epsilon_{1(\infty)})}{1 + i\omega\tau_1} \frac{\omega_1}{d_1} + \frac{(\epsilon_{2(0)} - \epsilon_{2(\infty)})}{1 + i\omega\tau_2} \frac{\omega_2}{d_2} \right\}$$

Since

$$\frac{(\epsilon_{12(\infty)} - 1)}{d_{12}} = \frac{(\epsilon_{1(\infty)} - 1)}{d_1} \omega_1 + \frac{\epsilon_{2(\infty)} - 1}{d_2} \omega_2$$

and

$$\frac{(\epsilon_{2(0)} - \epsilon_{2(\infty)})}{d_2} \omega_2 = \frac{(\epsilon_{12(0)} - \epsilon_{12(\infty)})}{d_{12}} - \frac{(\epsilon_{1(0)} - \epsilon_{1(\infty)})}{d_1} \omega_1$$

$$\epsilon_{12} = \epsilon_{12(\infty)} + \frac{(\epsilon_{12(0)} - \epsilon_{12(\infty)})}{1 + i\omega\tau_2}$$

$$+ d_{12}\left[\frac{(\epsilon_{1(0)} - \epsilon_{1(\infty)})}{d_1} \omega_1 \left\{ \frac{1}{(1 + i\omega\tau_1)} - \frac{1}{(1 + i\omega\tau_2)} \right\} \right]$$

Separating ϵ_{12} into its real and imaginary parts and comparing with

$$\epsilon_{12} = \epsilon_{12}' - i\epsilon_{12}''$$

we get

$$\epsilon_{12}' = \epsilon_{12(\infty)} + \frac{(\epsilon_{12(0)} - \epsilon_{12(\infty)})}{1 + \omega^2\tau_2^2}$$

$$+ \frac{(\epsilon_{1(0)} - \epsilon_{1(\infty)})}{d_1} d_{12}\omega_1 \left\{ \frac{1}{(1 + \omega^2\tau_1^2)} - \frac{1}{(1 + \omega^2\tau_2^2)} \right\}$$

and $\epsilon_{12}'' = \dfrac{(\epsilon_{12(0)} - \epsilon_{12(\infty)})}{1 + \omega^2 \tau_2^2} \omega \tau_2$

$$+ \frac{(\epsilon_{1(0)} - \epsilon_{1(\infty)})}{d_1} d_{12} \omega_1 \left\{ \frac{\omega \tau_1}{(1 + \omega^2 \tau_1^2)} - \frac{\omega \tau_2}{(1 + \omega^2 \tau_2^2)} \right\}$$

For a nonpolar solvent $\epsilon_{1(0)} \simeq \epsilon_{1(\infty)}$ so that the above equations reduce to the expression derived earlier for nonpolar solutions.

MOLECULAR RADIUS

Debye considered the rotation of a molecule amidst its surroundings analogous to a sphere carrying a dipole, rotating in a viscous medium. According to this analogy it is seen that a torque is necessary to rotate the molecule against the inner friction of the medium in which it is suspended. Stokes has calculated that this inner frictional force is given by $\zeta = 8\pi\eta a^3$ where η is the inner friction constant of the surrounding medium in which the sphere of radius ' a ' is rotating. From his considerations of Brownian motion, Debye has deduced that the relaxation times $\tau = \zeta/2kT$. Substituting $8\pi\eta a^3$ for ζ we get

$$\tau = \frac{4\pi\eta a^3}{kT}$$

Thus a knowledge of τ from the observed critical frequency will enable the calculation of ' a ', the radius of the molecule of an assumed spherical shape rotating in a medium of known viscosity η. It is evident that a considerable number of molecules do not fall in conformity with the picture of a rotating sphere. The long zig-zag chain type of molecules which are often met with scoop out a disc-like rather than a spherical cavity when they rotate. It will be thus interesting to investigate the frictional forces in conformity with this picture. In fact, Stokes has dealt with such a two dimensional rotation about an axis and has calculated the frictional torque as $4\pi\eta a^2 h$ where ' a ' is the radius of the disc cavity and ' h ' its thickness. Here ζ is equal to τ/kT corresponding to the case of a rotation in one plane, as has been derived by Debye (1913) in an earlier paper. Thus a knowledge of the thickness ' h ' of a rotating chain enables one to determine ' a ' the radius of the disc. ' a ' then should correspond to half the length of the molecule or any unit thereof which is executing rotation.

DISTRIBUTION OF RELAXATION TIME

In the case of compounds involving complex molecular structure. *e.g.,* the high polymers it was found that there was a considerably broader frequency range of dispersion and absorption together with a smaller maximum value of ϵ'' than predicted by Debye's equation. This discrepancy was thought to be due to the fact, that the polarisation was wrongly assumed to have a single unique relaxation time. Wagner (1913) assumed a distribution

of relaxation time about some probable value and proposed the use of a logarithmic Gaussian distribution. Yager (1936) predicted that ϵ''_{max} is

$<$ by an amount depending upon the density of distribution. Fuoss and Kirkwood (1941) have also deduced an empirical formula to determine the distribution function of relaxation times.

Cole and Cole (1941) gave an expression for the complex dielectric constant

$$\epsilon = \epsilon_\infty + \frac{(\epsilon_0 - \epsilon_\infty)}{1 + (i\omega\tau_0)^{1-\alpha}}$$

by their study of dispersion in the light of the Argand diagram or the complex plane locus. If this ϵ is resolved into its real and imaginary component $\epsilon' - i\epsilon''$ than

$$\epsilon' = \epsilon_r + \frac{(\epsilon_0 - \epsilon_\infty)}{1 + (\omega\tau)^{2(1-\alpha)}} \quad \text{and} \quad \epsilon'' = \frac{(\epsilon_0 - \epsilon_\infty)(\omega\tau)^{1-\alpha}}{1 + (\omega\tau)^{2(1-\alpha)}}$$

Even on this basis the condition at critical frequency ω_c remains the same as calculated on the basis of the new equation for a single τ, viz , $\omega_c\tau = 1$ as can be easily obtained by finding out the $\frac{d\epsilon''}{d\omega}$ and equating it to zero. In fact, the assumption of any distribution co-efficient or parameter does not change the position of the critical frequency but has the effect of changing the shape of the ϵ' and ϵ'' curves.

Cole and Cole (1941) have discussed the representation of dispersion data on the basis of the Argand diagram or complex plane locus in which ϵ'' the imaginary part of the complex dielectric constant is plotted against ϵ' the real part at various frequencies. The locus of such a plot, on the basis of a single relaxation time, has been shown to be a semi-circle with the centre on the ϵ' axis by a consideration of vectors in complex plane. The locus could as well be deduced in a very simple manner from the expressions for ϵ' and ϵ'' by a mere elimination of the frequency factor as follows

$$\epsilon' = \epsilon_\infty + \frac{(\epsilon_0 - \epsilon_\infty)}{1 + x^2} \quad ......(1) \quad \text{and} \quad \epsilon'' = \frac{(\epsilon_0 - \epsilon_\infty)x}{1 + x^2} \quad ......(2) ; \quad x = \omega\tau$$

according to the new equation and is $\omega\tau\frac{(\epsilon_\infty + 2)}{(\epsilon_0 + 2)}$ according to Debye.

From (2) $$\epsilon''^2 = \frac{(\epsilon_0 - \epsilon_\infty)^2}{(1 + x^2)^2} \cdot x^2$$

$$= \frac{(\epsilon_0 - \epsilon_\infty)^2}{(1 + x^2)^2} x^2 + \frac{(\epsilon_0 - \epsilon_\infty)^2}{(1 + x^2)^2} - \frac{(\epsilon_0 - \epsilon_\infty)^2}{(1 + x^2)^2}$$

Using (1) $$\epsilon''^2 = (\epsilon' - \epsilon_\infty)(\epsilon_0 - \epsilon_\infty) - (\epsilon' - \epsilon_\infty)^2$$

i.e., $$\epsilon''^2 = (\epsilon' - \epsilon_\infty)(\epsilon_0 - \epsilon')$$

Geometrically this condition means that the rectangle contained by two segments of a diameter equal to $(\epsilon' - \epsilon_\infty)$ and $(\epsilon_0 - \epsilon')$ equals the square of a chord ϵ'' cutting the diameter perpendicularly. This means that $\epsilon' - \epsilon''$ curve is a semi-circle with centre on the ϵ' axis. Cole and Cole, however, found that experimental data do not justify this semi-circular plot in a number of cases but could be represented by a circular arc characterised by an angle $\alpha\pi/2$ which is a measure of the deviation from the semicircle, being equal to the angle between the ϵ' axis and the radius through ϵ_∞. This circular arc again has been given a theoretical basis by Cole and Cole using complex plane loci. The significance of this angle can be obtained in a very simple way as follows. Considering the circular arc it is seen from figure 1
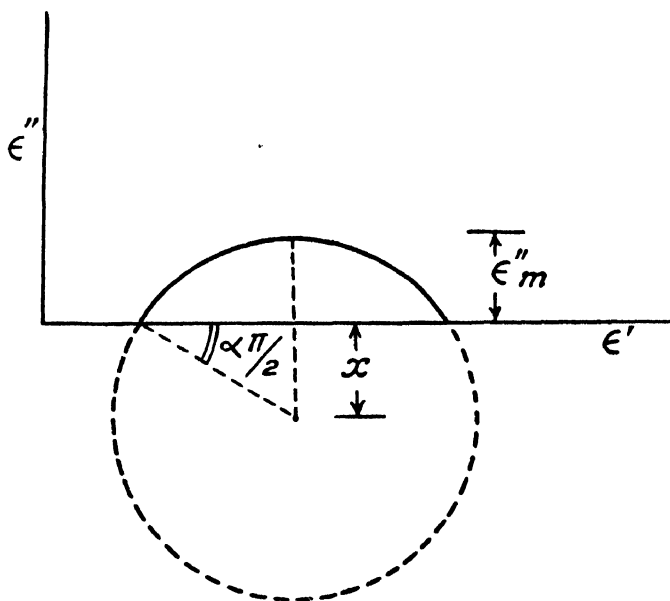
F IG. 1

$$\epsilon''_m(\epsilon''_m + 2x) = \frac{(\epsilon_0 - \epsilon_\infty)^2}{4} \ . \qquad \text{Since } x = \frac{(\epsilon_0 - \epsilon_\infty)}{2} \ \tan \ \alpha\pi/2$$

$$\epsilon''^2_m + (\epsilon_0 - \epsilon_\infty) \tan \ \alpha\pi/2 \ \epsilon''_m - \frac{(\epsilon_0 - \epsilon_\infty)^2}{4} = 0$$

$$\epsilon''_m = \frac{(\epsilon_0 - \epsilon_\infty) \tan \ \alpha\pi/2 \pm (\epsilon_0 - \epsilon_\infty) \sec \ \alpha\pi/2}{2}$$

Discarding the negative solution for ϵ''_m

$$\epsilon''_m = (\epsilon_0 - \epsilon_x) \ (\sec \ \alpha\pi/2 - \tan \ \alpha\pi/2)/2$$

$$= (\epsilon_0 - \epsilon_\infty)k/2$$

' k ' being a constant characteristic of the substance. Thus the parameter ' α ' introduced serves to increase the ϵ''_{max} value which usually falls short of

the value $\dfrac{(\epsilon_0 - \epsilon_\infty)}{2}$ as evaluated on the basis of a single relaxation time. Cole and Cole have given on the basis of their complex plane locus the equation for ϵ''_m as $\epsilon''_m = \frac{1}{2}(\epsilon_0 - \epsilon_\infty) \tan (1-\alpha)\pi/4$

This is identical with the equation derived above since

$$\tan (1-\alpha)\,\frac{\pi}{4} = \frac{(\cos \alpha\pi/4 - \sin \alpha\pi/4)}{\cos \alpha\pi/4 + \sin \alpha\pi/4} = \frac{(1 - 2\cos \alpha\pi/4 \sin \alpha\pi/4)}{(\cos^2 \alpha\pi/4 - \sin^2 \alpha\pi/4)}$$

$$= \frac{(1 - \sin \alpha\pi/2)}{\cos \alpha\pi/2} = (\sec \alpha\pi/2 - \tan \alpha\pi/2)$$

REFERENCES

Cole, R. H., (1938), *J Chem. Phys.*, **6**, 385.

Cole, K. S., and Cole, R. H., (1941), *J. Chem. Phys.*, **9**, 341.

Debye, P. (1913), *Ber. Deut. Phys., Ges.*, **15**, 777.

Debye, P. (1929), " Polar Molecules," pp. 77-108.

Drude, P. (1897), *Z. Phys. Chem.*, **23**, 267.

Fuoss, R. M and Krikwood, J G. (1941), *J Amer. Chem. Soc.*, **63**, 385.

Jatkar, S. K. K , Iyengar, B. R. Y and Sathe. N. V (1946), *J. Ind Inst. Sci.*, **28A**, Part II, 1-15

Oncley, J. L., (1938), *J. Amer. Chem. Soc*, **60**, 1115.

Onsager, L. (1936), *J. Amer. Chem. Soc.*, **58**, 1486.

Wagner K. W. (1913), *Ann. Der. Phys.*, **40**, 817,

Williams, J. W., (1934), *Trans. Farad. Soc,*, **30**, 723.

Wyman, J. (1936), *J. Amer Chem. Soc* , **58**, 1482.

Yager, W. A. (1935), *Physics*, **7**, 434,

THE RAMAN SPECTRA OF ACETYLCHLORIDE, ACETYL-BROMIDE AND ETHYLBROMIDE AT LOW TEMPERATURES

By B. M. BISHUI *

(Received for publication. Aug. 3, 1948)

Plate XV

ABSTRACT. The Raman spectra of acetylchloride, acetylbromide and ethylbromide in the liquid and solid states have been investigated. It has been observed that all the prominent Raman lines of these liquids appear in the case of the solid state. It is concluded therefore that there are no rotational isomers in these liquids. There are, however, two extra lines in the Raman spectrum of each of these substances and it is pointed out that these may be due to formation of associated groups of molecules in the liquid and solid states of these substances.

INTRODUCTION

In continuation of the investigations on the Raman spectra of organic substances in the solid state at low temperatures by the present author and also in collaboration with Sirkar, (1943, 1945, 1946a, 1946b, 1948a, 1948b, 1948c) the Raman spectra of acetylchloride, acetylbromide and ethylbromide have been studied in the solid state at low temperatures. From a systematic investigation of a large number of organic compounds, it has previously been observed that some changes in intensities and frequencies of some of the Raman lines take place, when particular organic liquids are solidified at low temperatures. These changes observed in the case of substituted ethanes have been explained by previous workers (Mizushima et al 1934, 1936, 1938) on the hypothesis that rotation isomers co-exist in the liquid state and molecules of only one configuration are present in the solid state of these compounds. It has been observed by the author (Bishui, 1948b) that there are some difficulties in such an explanation in the case of 1.1—dichloroethane, because although this substance cannot have two stable rotational isomers ; it gives too many Raman lines in the liquid state to be accounted for by the single configuration of the molecule. In order to understand this pheno-menon more clearly the investigation of Raman spectra of a large number of substituted ethane compounds has been undertaken and in the present paper the results obtained in the case of the three compounds mentioned above are discussed. The Raman spectra of these substances in the liquid state have also been studied carefully in order to compare them with those observed in the case of the solid state and the polarisation of the Raman lines due to the liquid state has been studied qualitatively.

* Fellow of the Indian Physical Society.

EXPERIMENTAL

The method for studying the Raman spectra of these substances at low temperatures was the same as that was used by Sirkar and Bishui (1943). The liquids from Kahlbaum's and Merck's original sealed bottles were procured from old stock and redistilled in vacuum. A double walled tube of Pyrex glass containing the distilled liquid was held in a vertical position with its lower portion immersed in the liquid oxygen contained in a transparent Dewar vessel. The solidification of the liquid took place very slowly when the interspace of the double-walled tube was evacuated with a Cenco Hyvac pump. Light from two vertical mercury arcs condensed by two six-inch glass condensers was focussed on the substance from opposite sides.

A Fuess glass spectrograph having the dispersion of 14 Å per m.m. in the region of 4046 Å used in the previous investigations was used in the present investigation also. A blue-violet glass filter was placed in the path of the incident light in order to diminish the continuous background in the blue-green region. The polarisation of the Raman lines due to the liquid state was studied in each case by photographing simultaneously the vertical and the horizontal components of the scattered light with the help of a double image prism. Light from a mercury arc focussed with the help of a condenser was used as the incident light in this case also.

RESULTS AND DISCUSSION

The spectrograms for the liquid and the solid states are reproduced in the Plate XV. The results are given in Tables I, II and III. The first column of each table contains the results reported by some of the previous workers. The data for the solids obtained in the present investigation are given in the last column. The polarisation of the lines is indicated by the letter P and total depolarisation by D. The approximate visually estimated intensities are given in the parenthesis.

Acetyl Chloride. The Raman spectrum of acetyl chloride was studied formerly by Kohlrausch *et al* (1933) and others. The results obtained by the former authors agree fairly well with those obtained in the present investigation. The weak line 236 cm^{-1} reported by them, however, has not been observed in the present investigation. The lines 956 cm^{-1}, 136 cm^{-1}, 1427 cm^{-1}, 2996 cm^{-1} and 3025 cm^{-1} are found to be totally depolarised. This fact suggests that the molecule has an element of symmetry which is evidently a plane of symmetry containing the C, O and Br atoms.

In the solid state at $-170°C$ some of the Raman lines shift a little from their original positions. The line at 596 cm^{-1} due to the C-Cl valence oscillation shifts to 586 cm^{-1} but the line at 356 cm^{-1} due evidently to C-Cl deformation oscillation remains practically in the same position. The line 1810 cm^{-1} due to C=O valence oscillation and the line 2996 cm^{-1} due to the

Fig. 1
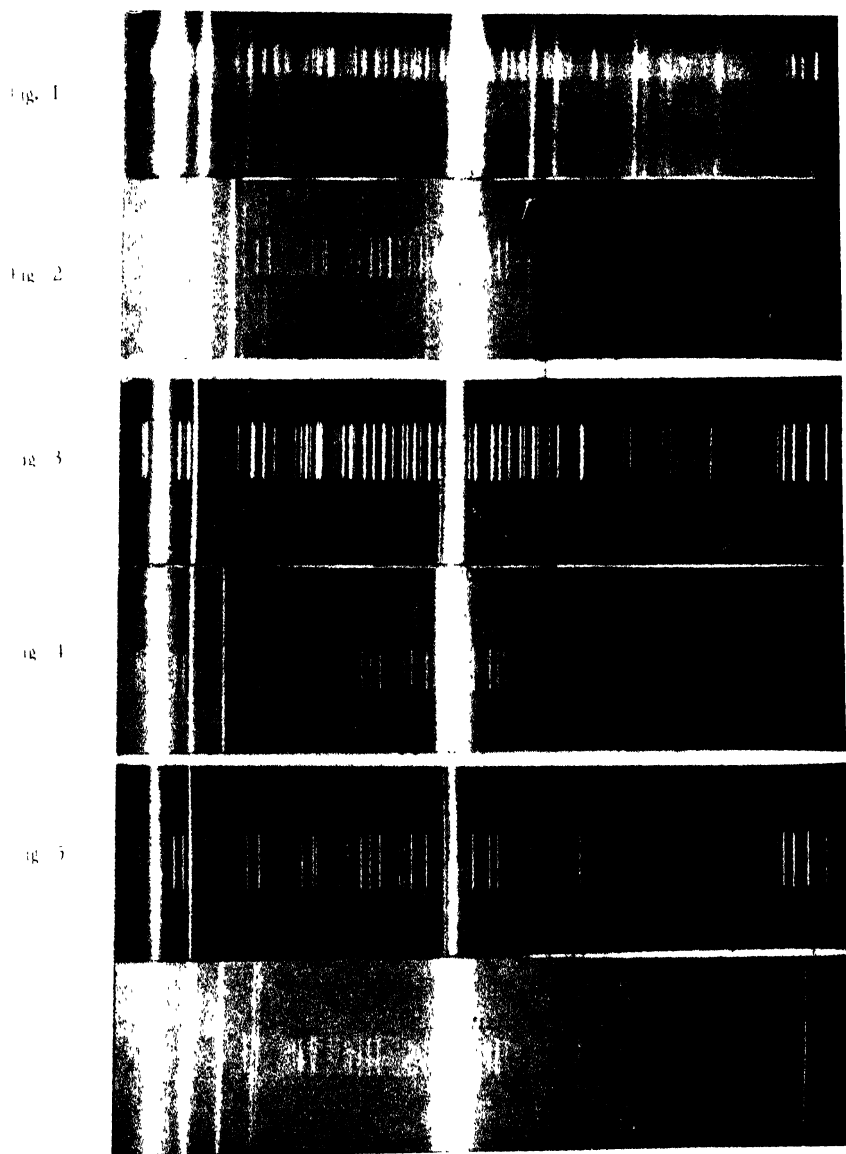
Fig. 2

Fig. 3

Fig. 4

Fig. 5

Raman Spectra

Fig. 1.	Acetylchloride	at about +	32°C
Fig. 2.	"	" " −	170°C
Fig. 3.	Acetylbromide	at about +	32°C
Fig. 4.	"	" " −	170°C
Fig. 5.	Ethylbromide	at about	32°C
Fig. 6.	"	" " -	170°C

TABLE I

Acetyl Chloride H_3CCOCl.

Liquid at room temperature		Solid at about $-170°C$
Kohlrausch *et al* (1933)	Present author	Present author
236 (o) e,		
348 (5) k, f, e, c	354 (3) e, k ; P	356 (1) e, k
434 (12) k, i, g ± f ± e, C	437 (20) e ±, k ; P	430 (5) e, k
590 (10b) k, i, f, e, c.	596 (8b) e ±, k, i ; P	586 (3b) e, k
955 (2) k, e ;	956 (2) e, k ; D	954 (o) e, k
1038 (o) k, e ;	1036 (o) e, k ?	......
1096 (1) k, e,	1102 (1b) e, k ; P	1102 (1) e, k
1328 (o) k, e.	1360 (1) e, k ; D	
1358 (1) k, e	......	
1418 (3) k, e	1427 (1) e, k ; D	1423 (2b) e, k
1793 ± 8 (1b) e,	1810 (6b) e, P	1791 (2) e
2935 (12) q, p, k, i, e	2930 (10) e, i, k ; P	2937 (8) e, k
2991 (2) q, k,	2996 (3) e, k ; D	2986 (3) e, k
3016 (4) k, e	3025 (4) e, k ; D	3025 (5) e, k.

antisymmetric C-H valence oscillation shift respectively to 1794 cm^{-1} and 2986 cm^{-1} in the solid state. No new lines are observed to appear in the neighbourhood of the Rayleigh line at the low temperature. The lines 1036 cm^{-1} and 1360 cm^{-1} are weak in the spectrogram due to the liquid and they are not observed in the case of the solid probably because they are marked by the continuous background which is rather strong in the spectrogram due to the solid. It can thus be seen from Table I that not a single prominent line disappears in the solid state in this case.

The number of Raman lines having frequency shifts below 1200 cm^{-1} is six in the present case but the number of lines in this region due to the vibration of the C-COCl is expected to be five, the sixth line due to C=O valence oscillation being that at 1810 cm^{-1}. Further the CH_3 group is expected to yield only one totally depolarised line due to antisymmetric C-H valence oscillation. Actually such lines at 2996 cm^{-1} and 3025 cm^{-1} are observed in the present case. Hence there are at least two extra lines in the Raman spectrum of acetyl chloride which cannot be accounted for if we assume that the liquid contains only single molecules of a particular configuration. Since no prominent lines disappear when the liquid is frozen,

Table II

Acetylbromide H_3CCOBr.

Liquid at room temperature		Solid at about $-170°C$
Kohlraush *et al* (1934)	Present author	Present author
	246 (1) e, k ?	.. ...
303 (9) k, f, ±e, a	305 (5) c, e, k P	305 (2) e, k
339 (15sb) k, f, ±e, c, b	345 (10) c, e±, k P	340 (5) e, k
555 (8b) k, i, g, f, ±e, c, b, a	560 (8) c, e±, k, i P	555 (4) e, k
944 (o) k, e	950 (2b) e, k ?	
981 (e) k, e	. ....	
1081 (3b) k, f, e	1088 (1b) e, k ; P	1082 (o) e, k
1356 (1) k, e	1360 (3) e, k P	1360 (ob) e, k
1414 (2b) k, e	1425 (3b) e. k ; D	1420 (1b) e, k
1809±10 (2b) e	1820 (4b) e P	1820 (o) e
2931 (6) q, p, k, i, e	2938 (8) e, k, i, P	2934 (5) e, k
2987 (½) k	3000 (3) e, k , D	2982 (3) e, k
3010 (3b) k, e	3015 (3) e, k ; D	3010 (3) e, k

it is evident that the presence of rotational isomers cannot be postulated in the present case. Hence we are left with the explanation that both in the liquid and solid states the molecules of acetyl chloride are in associated state giving rise to extra Raman lines.

Acetylbromide. The Raman spectrum of this liquid was studied previously by Kohlraush *et al* (1934). A comparison of the data given in the first two columns of Table II shows that some of the frequency shifts observed by the present author are a little higher than those observed by the previous authors. The line 246 cm^{-1} observed in the present investigation was not recorded by the previous authors and the line 981 cm^{-1} reported by the previous authors has not been observed in the present investigation. In the solid state at about $-170°C$ some minor changes take place. The frequency of the line at 560 cm^{-1} due to C-Br valence oscillation is lowered a little with the solidification of the substance. The line 1425 cm^{-1} due to C-H deformation vibration undergoes changes both in intensity and in frequency. The frequencies of the lines 345 cm^{-1}, 560 cm^{-1}, 1088 cm^{-1}, 3000 cm^{-1} and 3015 cm^{-1} diminish a little in the solid state but that of the line 1820 cm^{-1} remains unchanged. In this case also there are six Raman lines having frequency shifts below 1200 cm^{-1} and arguments similar to those advanced

TABLE III

Ethylbromide C_2H_5Br.

Liquid at room temperature		Solid at about $-170°C$
Voge (1934)	Present author	Present author
290.5 (3)	296 (3) e, k ; P	300 (o) e, k ?
560.3 (10b)	563 (10) e ±, k ; P	554 (6) e, k
959.4 (2b)	964 (2b) e, k ; P	957 (2) e, k
1062.8 (2)	1056 (2b) e, k ; P	1050 (o) e, k
1214.7 (2)	......	......
1252.9 (2b)	1248 (2) e, k ; P	1248 (1) e, k
1444.0 (2b)	1450 (3b) e, k ; D	1445 (2b) e, k
2867.2 (2)	2870 (2b) e, k ; P	2870 (1b) e, k
2924.4 (4)	2927 (5) e, k ; P	2925 (5) e, k
2969.2 (2d)	2970 (1b) e, k ; P	2968 (2) e, k
......	......	2984 (3) e, k
..	3010 (2b) e, k ; D	3008 (1) e, k

in the case of acetylchloride lead to the conclusion that the molecules are strongly associated in the liquid and solid states and that there are no rotational isomers in the liquid state. In this case also there are several totally depolarised lines in the Raman spectrum of the liquid and therefore the molecule has an element of symmetry.

Ethylbromide. The data given in the first two columns of Table III show that almost all the lines due to the liquid have appeared in the solid state. The liquid was studied formerly by Dadieu, *et al* (1929) and later by Voge (1934). The data reported by the later author have been included in the first column of Table III for comparison. The line 1244.7 cm^{-1}, reported by the later author, has not been observed in the present investigation. The line 3010 cm^{-1} which has been observed by the present author is not reported by any previous workers. The C-Br valence vibration has been diminished and its deformation vibration has been increased in the solid state. The C-C valence vibration has also undergone changes. The C-H valence vibrations have also changed with the solidification of the substance. The line 2970 cm^{-1} has been split up into two lines at 2968 cm^{-1} and 2984 cm^{-1} respectively. The frequency of the C-H deformation vibration diminishes a little in the solid state. The number of lines below 1100 cm^{-1} is four. But the group C-C-Br can yield only three lines in this region. The presence of an

extra line in this case also cannot be explained on the hypothesis of rotational isomers. The origin of this extra line can again be traced to the formation of the associated groups of molecules both in the liquid and solid states. Some of the Raman lines observed in this investigation are totally depolarised and this clearly shows that this molecule possesses an element of symmetry in the liquid state.

REFERENCES

Bishui, B. M. (1948a), *Ind J. Phys.*, **22**, 167.

————— (1948b), *Ind. J. Phys.*, **22**, 319.

————— (1948c), *Ind. J. Phys.*, **22**, 333.

Cleeton, C. E. and Dufford, R. T., (1931). *Phys. Rev.*, **37**, 362.

Dadieu, A. and Kohlraush, K. W. F., (1929), *Wein. Ber.*, **38**, 635.

Kohlraush, K. W. F and Pongratz, A., (1933) *Z. Phys. Chem.* (B)., **22**, 373.

————————————— ——— (1934), *Z. Phys. Chem.* (B). **27**, 176.

Mizushima, S. Morino Y and Higasi, K. (1934). *Phys. Zeit.*, **35**, 905.

————————— Norozi (1936), *Sci. Papers Inst. Phys. Chem. Research* (Tokyo), **29**, 63 and 88.

—————————— (1938a), *Proc. Ind Acad. Sc,*, A. **8**, 315.

Sirkar, S. C. and Bishui B. M. (1943), *Proc. Nat. Inst. Sc. India*, **9**, 287.

——————————— (1945), *Ind. J. Phys.*, **9** 24.

——————————— (1946a), *Ind. J. Phyr.*, **20**, 33.

——————————— (1946b), *Ind. J. Phys.*, **20**, 111.

Voge, H. H. (1931), *Jour. Chem. Phys.*, **2**, 264.

DIELECTRIC CONSTANTS OF PROTEINS

By S. K. KULKANI JATKAR and B. R. YATHIRAJA IYENGAR

ABSTRACT. The dielectric constant data of the aqueous solutions of carboxyhaemoglobin, albumins, zein gliadin, myoglobin etc., have been used to calculate dipole moments from the new equation $(\epsilon - n^2)M/d = \frac{4}{3}\pi N\mu^2/kT$. The moments previously evaluated by Oncley using an empirical equation are systematically higher than that evaluated by the new equation.

Molecular radii of these proteins have been evaluated using the new expression for the dispersion of polar binary mixtures. The identity of Oncley's expression to calculate the critical frequency f_c; $\epsilon'_{12} = \epsilon_{1(0)} + (\epsilon_{12(0)} - \epsilon_{1(0)})/(1 + f^2/f_c^2)$ and hence the molecular radius has been shown to be due to fortuitous coincidence arising out of certain approximations which hold good in dilute aqueous solutions.

The molecular radii (a) evaluated from dispersion data on the basis of the simple picture of the huge molecule as a rotating sphere, and characterised by a single relaxation time are related to the dipole moment (μ) by the relation $\mu = 2a \times e$ (where e is the electronic charge) being actually the moment of a huge dipole with the dipolar distance equal to the diameter of the spherical cavity scooped out by the rotating giant molecule.

INTRODUCTION

The dielectric constants of the aqueous solutions of a number of proteins; carboxyhaemoglobin, albumins, zein, gliadin, myoglobin and etc., have been investigated by a number of workers. Oncley (1938) calculated the dipole moment of the dissolved protein molecules, using a semi empirical relationship based on Wyman's empirical equation. The dispersion data on the proteins have also been utilized to determine the relaxation time by using the theoretical expression of Perrin (1034). The ratios of the axes of an assumed molecular ellipsoid have been derived from Perrin's theory for pseudoglobulin gliadin and other proteins which do not conform to the simple picture of the molecule considered as a rotating sphere.

In the present paper, dipole moments of these protein molecules have been calculated by the application of the new equation $(\epsilon - n^2)M/d = 4\pi N\mu^2/kT$ to the dielectric constant data on aqueous solutions. The moments so obtained have been discussed in relationship with the molecular radius which has been calculated by applying the new relationship to dispersion and absorption data of these proteins.

The case of dispersion of binary mixtures in which both the components are polar is depicted in Fig. 1.
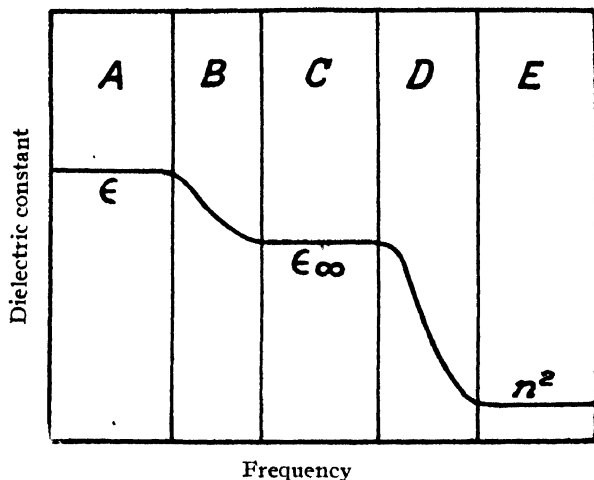
Frequency

FIG. 1

In region 'A' at low frequencies, the orienting torque is sufficient to overcome all frictional forces so that the molecules of both the components are completely oriented. Consequently this region is characterised by a high dielectric constant. In region B the frictional forces of the molecule of higher relaxation time are considerable and the dispersion is characterised by a gradual decline of the dielectric constant. In region C the component of higher relaxation time has completely ceased to respond to the field and thus contributes very little to the dielectric constant although the other component is still completely able to follow the field. Thus in this region the dielectric constant has a constant intermediate value ϵ_∞. The region 'D' which corresponds to the dispersion of the second component of lower relaxation time is characterised by a decline of the dielectric constant. Finally the region E where neither of the two components is orienting, is characterised by a low dielectric constant, equal to the square of refractive index. With this picture in mind and considering that the dispersion of the dissolved protein molecule is completely defined by the region ABC, Oncley (1938) derived an equation :

$$\mu^2 = (p_0 - p_\infty)9kT/4\pi n \tag{1}$$

where p_0 and p_∞, are the polarisations per c.c. of the solution in the low frequency region (region A) and the high frequency region (region C) respectively and n, the number of polar molecules per c.c. being equal to $gN/1000M$ where $g=$ gms. per liter of the solute of molecular weight M.

Using, for polarisation per c.c. an equation of the type $p = (\epsilon - a)/t$, suggested by Wyman (1936) the equation (1) becomes

$$\mu^2 = 9000 \, kTM(\epsilon_0 - \epsilon_\infty)/4\pi Ngb$$

or $$\mu = \alpha\sqrt{M(\epsilon_0 - \epsilon_\infty)g} \quad \text{where} \quad \alpha = \sqrt{\frac{9000 \, kT}{4\pi Nb}}$$

α was evaluated as 2.9 by assuming for glycine the established value of μ in the above equation. With this value of ' α ' the moments of the proteins have been calculated since the factor $(\epsilon_0 - \epsilon_x)/g$ is experimentally observed as the sum of the low frequency and high frequency dielectric increments.

For the dielectric behaviour in the dispersion region (B C in figure 1) Oncley has followed Debye's treatment in its most general form (replacing the D.C.M. polarisation law $\dfrac{(\epsilon - 1)}{(\epsilon + 2)}$ by $\dfrac{\epsilon - a}{b}$ and gets for ϵ' the dielectric constant at γ frequency the expression $\epsilon' = \epsilon_\infty + \dfrac{(\epsilon_0 - \epsilon_\infty)}{1 + \gamma^2/\gamma_c^2}$, γ_c being the critical frequency. The critical frequency is given by $2\pi\gamma_c\tau = 1$ where τ is the relaxation time.

In this paper a simple extension of the new equation

$$\frac{(\epsilon - n^2)M}{d} = \frac{4\pi N\mu^2}{kT}$$

to binary systems has been utilized to calculate the moment. In actual calculations two approximations have been made ; (1) density of solutions $\approx$ density of solvent ≈ 1, as the solutions studied are very dilute ; (2) P_E the electronic polarisation is not taken into account since it becomes absolutely negligible when compared with the enormous values for P_2 the total polarisation of the solute.

TABLE I

	M. W.	$f_2 \times 10^6$	$P_2 \times 10^{-4}$	μ new	μ lit
Myoglobin [Marcy and Wyman (1942)] ...	17000	0 249	333	134	163
Zein [Elliot and Williams (1939)]	40000	2.917	2364	356	400
Gliedin [Entrikin (1941)]	40000	9.365	336	130	177
Carboxyhaemoglobin [Oncley (1938)] ..	68000	3 555	2785	386	470' 500
Albumin (1) ⎫ [Ferry and ⎫ ...	73000	7.993	1275	262	280
Albumin (2) ⎭ Oncley (1938)] ⎭ ...	73000	5.471	3327	422	510
Pseudoglobulin [Ferry and Oncley (1938)] ...	150000	9.919	15230	903	1000' 1200
Edestin [Cohn and Edsall (1935)] ...	300000	...	...	1080*	1400

* Calculated by an approximate relation

$$P_2 = \frac{\Delta\epsilon}{\omega_2} = \frac{4\pi M\mu^2}{kT},$$

$\Delta\epsilon'\omega_2$ being the dielectric increment per gram. This relationship follows from the new relationship applied for solutions

$$p_{12} = \frac{\epsilon_{12} - 1}{d_{12}} = \frac{(\epsilon_1 - 1)\omega_1}{d_1} + p_2\omega_2$$

when the approximation $d_{12} \approx d_1 \approx 1$ and $\omega_1 \approx 1$ is made.

'e' = moments calculated by Cohn's (1935) relationship, $\mu = 4.77 \times 10^{-10}$ $\sqrt{\delta/2.3}$, where δ = dielectric increment per mole. The other values in the column μ_{ui} are calculated by Oncley's equation, $\mu = 2.9 \sqrt{\dfrac{M \Delta \epsilon_i}{g}}$, where, $\dfrac{\Delta \epsilon_i}{g}$ = dielectric increment per gm.

From the observed critical frequencies the relaxation time of the proteins have been calculated by $\tau = \dfrac{1}{2 \pi \gamma_c}$ (this relation being the result of applying the new equation to the dispersion theories). Molecular radii 'a' have been calculated by using Debye's expression $\tau = \dfrac{4 \pi \eta a^3}{kT}$ based on the consideration of the molecule as a sphere rotating in a viscous medium of viscosity η. The results are tabulated in Table I.

TABLE II

Protein			γ_c (m.c.s)	$\tau \times 10^8$	'a' Å	2 $a.c$	μ new
Myoglobin	...	...	...	5.54	2.87	21.3	203	163
Zein	...	...	..	...	30.0	37.5	358	358
Gliadin *	...	...	...	...	43.5	18.4	177	130
Carboxyhaemoglobin		...	...	1.9	8.4	31.1	300	386
Albumin	...	...	..	0.85	19.0	41.1	392	422
Pseudoglobulin	..	...	...	0.24	66.1	62.2	600	900† 800 700

* τ was calculated from the relation $\epsilon' = \epsilon_i + \dfrac{(\epsilon_0 - \epsilon_i)}{1 + \omega^2 \tau^2}$. In other cases $\tau = \dfrac{1}{2 \pi \gamma_i}$.

† With increasing concentration.

DISCUSSION

It is necessary at the very outset to deal with the semi-empirical equation of Oncley which has been widely used to calculate the moment of the proteins. Assuming that the dispersion is defined by the region ABC (Fig. 1) he writes

$$p_2 = \frac{4 \pi N \mu^2}{9kT} \cdot \frac{g}{1000} = \frac{(\epsilon_0 - \epsilon_\infty)}{b}$$

where 'b' is the constant in Wyman's relation $p = \dfrac{(\epsilon - a)}{b}$. A rigorous

application of Wyman's equation to binary system would give

$$\frac{(\epsilon_{12} - a)}{bd_{12}} = \frac{(\epsilon_1 - a)}{bd_1}\omega_1 + p_2\omega_2$$

ω_1 and ω_2 being weight fractions. Since in dilute solutions $d_{12} \simeq d_1 \simeq 1$

$$p_2 = \frac{4\pi N\mu^2}{9kT} = \frac{(\epsilon_{12} - \epsilon_1)}{b}\omega_2 = \frac{(\epsilon_{12} - \epsilon_1)}{b}\frac{g}{1000}$$

This is very nearly the same as Oncley's relation except that he writes ϵ_∞ (corresponding to region C in Fig. 1) in place of ϵ_1 the dielectric constant of solvent. It is found in experiments however that $\epsilon_\infty \simeq \epsilon_1$. Oncley's equation suffers from the disadvantage that it is based on Wyman's relation which is purely empirical.

Similarly in the dispersion case the relation $\epsilon' = \epsilon_x + \dfrac{(\epsilon_0 - \epsilon_x)}{1 + \gamma^2/\gamma_c^2}$ which has been derived again on the basis of Wyman's polarisation as applied to the region of dispersion ABC (Fig. 1), follows only under the assumption $d_{12} \simeq d_1 \simeq 1$ and $\omega_1 \simeq 1$. It is strange that Oncley does not mention this approximation.

An expression for the dispersion of a binary system of two polar components, has been derived in a previous paper on the basis of the new equation $(\epsilon - n^2)M/d = \frac{1}{3}\pi N\mu^2/kT$ which has been found applicable to polar liquids and solids.

According to it ϵ'_{12}, the dielectric constant of the solution at 'ω' frequency is given by

$$\epsilon'_{12} = \epsilon_{12(x)} + \frac{(\epsilon_{1(0)} - \epsilon_{1(x)})}{1 + \omega^2\tau_1^2}\frac{\omega_1}{d_1}d_{12} + \frac{(\epsilon_{2(0)} - \epsilon_{2(\infty)})}{1 + \omega^2\tau_2^2}\frac{\omega_2}{d_2}d_{12}$$

$$= \epsilon_{12(x)} + \frac{(\epsilon_{1(0)} - \epsilon_{1(x)})}{1 + \omega^2\tau_1^2}\frac{\omega_1}{d_1}d_{12} + \frac{d_{12}}{1 + \omega^2\tau_2^2}\frac{(\epsilon_{12(0)} - \epsilon_{12(x)})}{d_{12}}$$

$$- (\epsilon_{1(0)} - \epsilon_{1(\infty)})\frac{\omega_1}{d_1}$$

where τ_1 and τ_2 are the relaxation times and $\epsilon_{1(0)}$ and $\epsilon_{2(0)}$ the static dielectric constants of the components of the binary mixture.

Coming to the specific case of the dispersion of the dilute aqueous solutions of proteins the following approximations could be made—

(1) $\omega\tau_1 \simeq 0$ since in the region in which the measurements are done ω and τ_1 the relaxation time of solvent (water) are individually so small that their product becomes $\ll 1$. $\omega\tau_1$ becomes considerable only at higher frequencies when the dispersion of water starts.

(2) In aqueous dilute solutions $d_{12} \simeq d_1 \simeq 1$ and $\omega_1 \simeq 1$

Making these approximations

$$\epsilon'_{12} = \epsilon_{1(0)} + \frac{(\epsilon_{12(0)} - \epsilon_{1(0)})}{1 + \gamma^2/\gamma_c^2}$$

This equation is identical with the one derived by Oncley, except that in place of $\epsilon_{1(0)}$ he writes ϵ_∞ which is found experimentally very nearly equal to $\epsilon_{1(0)}$. Thus Oncley's expression has fortuitously turned out to be a particular case, involving the above-mentioned approximations, of the most general equation of dispersion obtained by the application of the new equation. In general it is found that the moments calculated by the new equation are of the same order as obtained by Oncley's relationship. The latter values are systematically higher.

The calculations made for pseudoglobulin have to be considered with a certain amount of caution since this was a singular case amongst the proteins which showed marked deviations from the expected linearity of the dielectric constant with concentration in dilute regions. It shows a rapidly declining value of dielectric increment with increasing concentration, Ferry and Oncley actually took an extrapolated value of the increment for calculating the moment. In the case of gliadin, which has been studied in water-alcohol systems, the new equation was applied in the form usually written for a binary system except that for M_1 the molecular weight of the solvent the expression $M_a f_a + M_w f_w$ was used, where M_a, M_w, f_a and f_w are the molecular weights and molefractions of the alcohol and water respectively. It is of interest to note that there has been considerable controversy regarding the value of the molecular weight of gliadin. An ultracentrifugal study of gliadin conducted by Svedberg and Krejci (1935) has revealed that the protein is homogeneous with respect to molecular weight. According to them there is probably a mixture of whole and half molecules of weight 34500 and 17250 at 20°C while at higher temperatures the dissociation into half molecules is complete. The diffusion constants given by Lamm and Polson (1936) reveal a molecular weight of 27000 for the predominant constituent. Arrhenius (1937) estimates the molecular weight as 27000. On the other hand accurate determinations of the amount of certain amino acids in gliadin give a molecular weight 42000, and osmotic pressure measurements in concentrated urea and in water give values ranging from 40000 to 44000. A value of 40000 has been assumed in calculating the moment by the new equation. The assumption of the other value 27000 would reduce the moment by 20 per cent.

No attempts have been made so far to interpret the dipole moments of these proteins on the basis of molecular structure. A globular protein is now best considered as a coiled polypeptide chain. Very little is known as to how these peptides of a large variety of amino acids are arranged with respect to one another. In view of this it is not surprising that the dipole moments have not been quantitatively studied in the light of the structure of the molecules. However, Marcy and Wyman (1942) have attempted to make a comparative study of the structure of the proteins, haemoglobin and myoglobin since both these are made up of 'heme' units. Myoglobin is known to contain one heme while haemoglobin contains 4 hemes. The authors point

out that if there were a considerable degree of stabilization of these heme units with electric moments parallel and pointing in the same direction the polarisation and hence the dielectric increment per gram of haemoglobin should be greater than that of myoglobin. In the limiting case of complete parallel alignment the increase should be four-fold. On the other hand if the 4 units were oriented independently the increment would be the same for both. The experimentally observed fact, *viz.*, that haemoglobin has a dielectric increment twice as great as that of myoglobin suggests that in haemoglobin there is a "partial stabilization" of these units with their electric moments parallel. In this discussion it is obvious that Marcy and Wyman have assumed that the increment of dielectric constant gives a measure of the dipole moment whereas it is the dielectric increment per gram *multiplied by the molecular weight* that gives a measure of the polarisation (and hence of the square of the moment). The moments calculated by the new equation shows that haemoglobin has nearly thrice the moment of myoglobin. This can be explained on the basis of a zigzag arrangement of the 4 hemes

(assuming a mutual tetrahedral angle)

whence if ' m ' is the moment of each heme the resultant of the 4 hemes will be equal to the result of two moments of magnitude 2 m at 71° *i.e.*, 3.1 m. or nearly 3 times the moment of a heme.

In Table II, are recorded the values for the critical frequency γ_c; the time of relaxation $\tau = \dfrac{1}{2\pi\gamma_c}$ and finally the molecular radius ' a ' calculated as $\sqrt[3]{\dfrac{\tau kT}{4\pi\eta}}$ based on the assumption that the molecules are rotating spheres and are characterised by a single unique value of relaxation time. It has been postulated by Perrin that an ellipsoidal molecule could be characterised by at least two relaxation times. The main reason for abandoning the idea of a single relaxation time in favour of multiple times of relaxations seems to be that the calculated curves for dispersion, based on a single τ do not fit in with the experimental data. It may be pointed out here that the data for carboxyhaemoglobin, myoglobin and albumin are calculable on the basis of a single relaxation time. Even in the case of pseudoglobulin the deviation between the theoretical and experimental curves is indeed very small, in fact too small to warrant the abandonment of the postulate of a single unique value of relaxation time. Further, it is to be pointed out that the postulate of two critical frequencies is not justified or confirmed by any marked breaks or irregularities in the dispersion curves which for instance in the case of gliadin and zein are smooth, asymptotic thus characteristic of molecules having a single relaxation time. It has, in fact, been found necessary to calculate

the values of the two critical frequencies by resolving the experimental dispersion curve into two hypothetical dispersion curves. The molecular radii (a) that have been calculated on the basis of the simple picture of the molecule as a rotating sphere and characterised by a single τ show a close relationship with the dipole moment 'μ' previously calculated from static dielectric constants using the new equation. Table II, shows that the product $2a \times e$ (where 'e' =electronic charge) is equal to the dipole moment. Considering the limitations involved in dispersion measurements at the low frequencies, the agreement should be considered very satisfactory. The rather large deviation in gliadin may be due to the fact that the relaxation time which has been calculated in this case by the equation $\epsilon' = \epsilon_\infty + \dfrac{(\epsilon_0 - \epsilon_\infty)}{1 + (2\pi\nu\tau)^2}$

is subject to large errors since ϵ', ϵ_0 and ϵ_∞ are of very nearly the same magnitude so that the factors $(\epsilon' - \epsilon_\infty)$ and $(\epsilon_0 - \epsilon_\infty)$ magnify any small error in measuring ϵ', ϵ_0 and ϵ_∞. The quantity $2a \times e$ is actually the moment of a huge dipole with the dipolar distance equal to the diameter of the spherical cavity scooped out by the rotating molecule. Thus the spherical protein molecule can be considered to be from the electrical point of view, equivalent to a dipole along its diameter.

REFERENCES

Arrhenius, S., (1937), *J. Chem. Phys.*, **5**, 63.

Cohn, E. J., (1935)., *Ann. Rev. Biochem.*, **5**, 106

Cohn, E. J. and Edsall, J. T., (1943), "Proteins Amino acids and Peptide. . A C S Mon. 90.

Elliot, M. A. and Williams, J. W., (1939), *J. Amer. Chem. Soc*, **61**, 718

Eutrikin, P. P, (1941)., *J. Amer. Chem Soc*, **63**, 2127

Ferry, J. D. and Oncley, J. L., (1948), *J. Amer. Chem. Soc.*, **60**, 1123.

Krejci, L. and Svedberg, T., (1935) *J. Amer. Chem Soc.*, **57**, 947.

Lamm, O., and Polson, A., (1936), *Biochem J.*, **30**, 528,

Mercy, H. O. and Wyman, J., (1912), *J. Amer. Chem. Soc.*, **64**, 638

Oncley, J. L., (1938), *J. Amer. Chem. Soc.*, **60**, 1115.

Perrin, F., (1934), *J. Phys. Rad.*, **5**, 497.

Wyman, J., (1936), *J. Amer. Chem. Soc.*, **58**, 1482

THE SPECTRO-CHEMICAL ANALYSIS OF FERROUS ALLOYS WITH THE MEDIUM QUARTZ SPECTROGRAPH

By K. C. MAZUMDER and M. K. GHOSH

ABSTRACT. A preliminary report is given of the spectro-chemical determination of the elements Al, W, V, Mo, Ni, Cr, Cu, Mn and Si found in the ferrous alloys by means of the medium spectrograph. This instrument is not considered to be good enough for this work on account of its low dispersion. The calibration curve obtained for the above elements are given. The curves are regular and smooth, showing that the instrument can possibly be used for carrying out the ferrous alloys analysis.

INTRODUCTORY

The spectro-chemical analysis of the ferrous-alloys is carried out by means of Hilger large quartz Littrow spectrograph or its equivalents of other makes. Iron having a large number of lines the separation of them from one another or from those of the alloying or the impurity elements is only possible by a prism spectrograph of the large Littrow type or a good grating instrument. This has been the custom for the analysis of the ferrous alloys till now. In our attempt to determine quantitatively the aluminium traces occurring in the ferrous alloys, some difficulties in exciting the spectral lines of Al were experienced. It should be mentioned that the importance of the presence of the small traces of Al in controlling the grain of the Fe-alloys is just being realised. The chemical determination of the Al-traces is rather difficult specially in the presence of some of the alloying elements. It has thus become necessary to explore the possibilities of the spectro-chemical determinations of the Al-traces present in the ferrous-alloys. The percentage of the Al present is much less than than 0.1 per cent. varying generally in the neighbourhood of 0.005 per cent. or less. The simple condensed spark method of excitation of the Fe spectrum is not sufficiently strong to bring out the Al-lines from such small percentages. The high voltage A. C. arc or some special types of the condensed spark have been found necessary by the workers in different countries to make the Al-lines appear with sufficient intensities for the photometric work. The partial success realized by these workers is mostly due to the special devices employed for exciting the spectra. In view of the want of these special devices at present in our laboratory we have tried to photograph the spectra with the medium quartz spectrograph and the simple spark method of excitation available. The Al-lines should not only be excited but should also be sufficiently separated from

all possible interfering lines so as to make the photometric observations of their blackenings reliable. Fortunately it has been possible to satisfy both of these conditions in the present investigation and the Al-contents as low as 0.005 per cent. have accurately been determined. It has not been possible to collect or prepare the standard samples from the steel made in the Works and get their contents chemically and accurately determined. Standard samples have been then prepared synthetically by dissolving spectroscopically pure iron in HCl and then converting it into FeCl$_3$ with HNO$_3$. Measured amounts of Al of the same quality dissolved in HCl mixed with HNO$_3$ have been then added to the Fe-solutions. Steps have been taken to keep the solutions just a little acidic. Standard solutions with Al-contents 0.005, 0.01, 0.02, 0.03, 0.05, 0.075, 0.10, 0.15, 0.20, 0.25, 0.30 and 0.50% have in this way been prepared.

EXPERIMENTAL

Hilger medium quartz spectrograph has been used for photographing the spectra. The following are the conditions for excitations:—

Voltage	... ...	8,000 volts.
Capacity	... ...	0.005 μF.
Inductance	... ...	0.25 μH.
Spark gap	... ...	2.0 mm.
Upper electrodes	... ...	Pointed carbon rods.
Lower electrodes	... ...	Graphite rod formed into a cup at the top.

Drillings of the samples to be analysed have been dissolved in HCl and HNO$_3$ and dried. They have again been dissolved in H$_2$O and HCl and filtered. The residue has then been ignited and fused with KHSO$_4$, dissolved in H$_2$O mixed with HCl and added to the original solution. A proportionate amount of KHSO$_4$ has also been added to the standard solutions for making the conditions uniform. Care has been taken to keep the iron and the acid contents of both types of solutions approximately the same. A few drops of these solutions have been taken into the cups formed on the upper end of the lower electrodes and dried by slow heating. For very low percentages of Al a large number of drops is necessary for making the Al-lines sufficiently intense. Only 0.5 minutes pre-sparking has been given to the electrodes and the exposure has been of one minute's duration. The Al-lines 3082.16 and 3961.53 appear clearly on the plates and it has been possible to measure their blackening with photometer. Occasionally the 3092.72 line has also been used for extremely low percentages. But the line 3082.16 is found to give more consistent results. The attached calibration curve (figure 1) is seen to
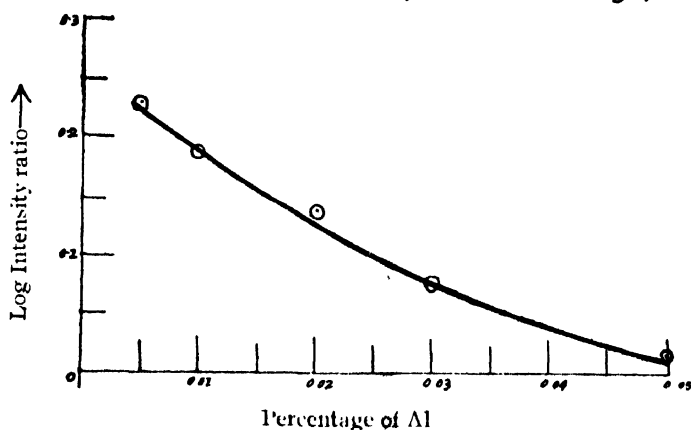
Fig. 1

be very smooth and regular. The agreement with the chemical determinations is satisfactory, but sometime the results differ considerably, the chemical methods yielding higher values. The spectrum of the Al-ppt. obtained by the phosphate method during the chemical determinations has been found to contain the lines of Fe, Mg and Si besides those of Al. The impurity lines are fairly heavy; the higher values obtained chemically may thus be due to the presence of the above elements in the precipitate.

The spectrochemical determinations of W, V, Mo, Ni, Cr, Cu, Mn and Si in the ferrous alloys:—

The successful determination of the Al-traces in the ferrous alloys by the medium quartz spectrograph obviously suggests the possibilities of the spectro-chemical evaluation of the percentages of the above elements as well by the same apparatus. It has also been necessary to try to determine the W-contents by a smaller and more sensitive instruments than the large quartz spectrograph. The simple sparking arrangement at our disposal is not sufficiently powerful for the determination of tungsten less than 2% or so by the large instrument. A prolonged exposure, though brings out the W-line for 0.5% produces so much fogging that the photometric work becomes difficult. The line, 4008.8Å which is generally used for the spectro-chemical work lie in the region where the ordinary plates just begin to be insensitive. The use of the panchromatic plate may ease the situation to a certain extent but that will be an additional complication introduced in the process. The medium quartz spectrograph has, therefore, been tried and the line 2397.1Å of the ionized tungsten appears on the plate even with such lower voltage and an inductance of 0.13 μH in the circuit. The blackening produced by the line is sufficiently strong for the photometric work and for a tungsten content as low as 0.50%. Fig. 2 given below for tungsten shows that the readings are very consistent.

A general search has then been made for suitable lines belonging to the rest of the elements used in the steel making. As mentioned previously the medium spectrograph is not considered to be just the apparatus for the

Percentage of W
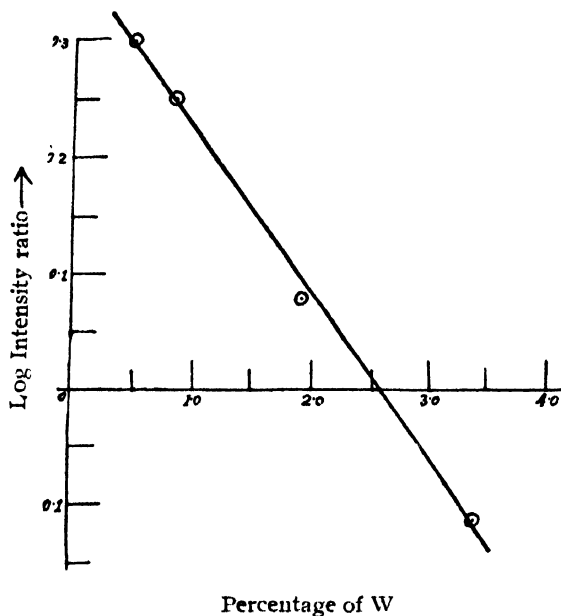
FIG. 2

spectro-chemical analysis of the ferrous alloys on account of the crowding for the lines not only belonging to the iron spectrum but also to those of the rest of the elements present in the sample. Fortunately, however, the short wave-length region of the spectrum appearing on the plate, i.e., the region below 2500Å or so, is not very rich in the spectral lines. On carefully examining this part of the plate lines belonging to the different elements are found which are good enough for the spectro-chemical analysis. For quite a few of the elements there are several lines available, some of which are more or less contaminated by the proximity of the lines belonging to the rest of the ele-

Percentage of N
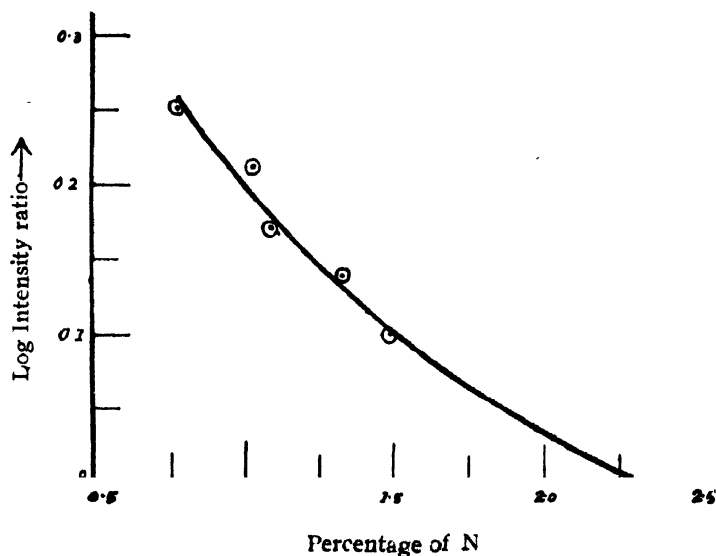
FIG. 3

ments. The particular lines selected should thoroughly be scrutinized with the help of a good wavelength table for all possible contaminations and their magnitudes. Above all, photometric measurements should be carried out on a large number of plates to find out the effects, if any, produced by the contaminating elements; variable percentages of these elements should, of course, be contained in the samples used for producing the spectra. A preliminary survey has been carried out in the way indicated above. The cali-

Percentage of Mn
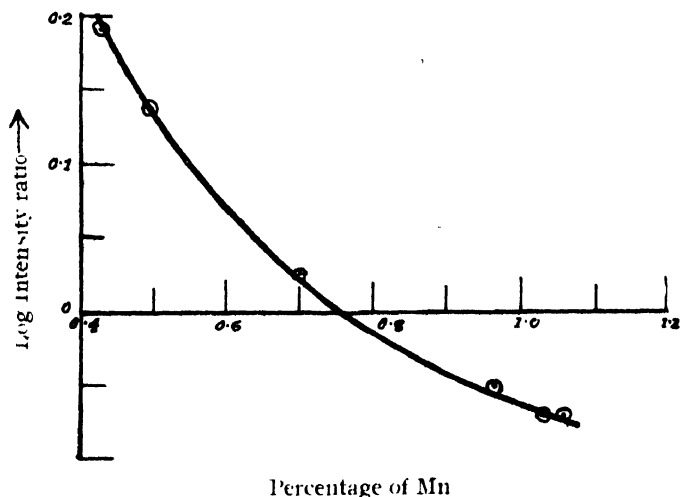
FIG. 4

bration curves for the quantitative determinations of some the elements mentioned are given below. They are very smooth and the results obtained in the few cases tried, check up well with the chemical values. There are, therefore good possibilities for using the medium spectrograph for the quantitative analysis of the ferrous alloys. More work will, however, be necessary to select the most suitable lines for the respective elements and it is being continued.

ACKNOWLEDGMENT

The authors take this opportunity to thank the Tata Iron and Steel, Co., Ltd. and Mr. N. B. Sen, the Chief Chemist, for facilities given for carrying out the investigation.

NEW RESEARCH AND CONTROL LABORATORY
TATA IRON AND STEEL CO., LTD.

REFERENCES

Carlson, C. G., 1942, *J. Am.*, **126**, 101.
Castro, R., 1945, *Met Treatment*, **13**, 19?.
Hartleig, 1939-40, *Arch. Eisentritten Wesen*, **43**, 295
Lab. R. F., 1946, *Blast Furnace and Steel Plant*, **43**, 1509.
Schliessmann, 1940-41, *Arch. Eisentritten Wesen*, **14**, 211.
S. Piers, Fischer, Proctor, 1945, *Ind. and Eng. Chem., Anal Edi.*, **17**, 772.

INFLUENCE OF SERIAL GEISSLER TUBES ON THE PRODUCTION OF JOSHI-EFFECT IN AN OZONISER DISCHARGE

By B. N. PRASAD AND NARENDRA NATH

ABSTRACT. The production of Joshi-effect Δi is studied with and without Geissler type discharge tubes in the low tension (L. T.) line of a chlorine filled ozoniser excited by 5 8 kV of 50 cycles frequency. A double diode coupled inductively with L. T. was the detector. The 100% relative Joshi-effect observed in i_m with neon tube is attributed to the HF's which, according to Joshi, are the chief seats thereof. The sharp reversal of the Joshi-effect from negative to positive and once again to negative in the filtered i_m with neon tube, and the observation of positive effect at large V in i_m with helium tube by mere potential variation have been attributed to simultaneous occurrence of $\mp \Delta i$ in the current. That i at low V is less with the tube than without it and that at large V this order is reversed, are explained by an extension of the relation between V and ozonizer current i due to Joshi.

INTRODUCTION

The present work arose out of Joshi's (1945 *b*) observation of an optical demonstration of the Δi phenomenon, *viz.*, that the luminescence in a Crookes' or Geissler tube coupled with the low tension (L. T.) line of a chlorine filled ozoniser is quenched instantaneously and reversibly on irradiating the latter, to give the negative Joshi-effect $-\Delta i$. Joshi (1943, 1944*b*, 1945*a*) has established that the HF's produced under the discharge constitute a chief seat of the effect $-\Delta i$. The marked potency of the HF's in the electrical obliteration of a nitrogen after-glow (Joshi and Purushotham, 1938) and in the excitation of the luminescence of the above type tubes is known. It appeared, therefore, desirable to study in some detail the comparative production of the Joshi-effect $\mp \Delta i$ with and without the above tubes introduced in the path of the discharge.

EXPERIMENTAL ARRANGEMENT

Chlorine, purified carefully by fractionation over liquid air, was admitted to the annular space of a precleaned and degassed (by repeatedly subjecting to discharge at high potentials and evacuating on the Töpler) ozoniser, at a pressure of 300 mm. Hg. It was excited by a transformer discharge of 50 cycles frequency, and Joshi-effect $\mp \Delta i$ was observed from values of the discharge current in dark (i_b) and when the ozoniser was irradiated with a 220 volt

200 watt incandescent (glass) bulb (i_L). The current i was measured with a double diode 80 connected through a Bell transformer (1:3) with the ozoniser. The general technique and experimental arrangement were essentially as described previously. The relative Joshi-effect %Δi is given by 100 $\Delta i/i_p$. Table I records four series of experiments that were carried out : First, with what is called 'normal' circuit, i.e., when only the ozoniser was excited ; and when, in series with it, a neon, helium, or nitrogen-filled Geissler type tube was introduced between the low tension terminal of the ozoniser and earth (vide Fig. 1). Under each of the four series of experiments mentioned

Fig 1
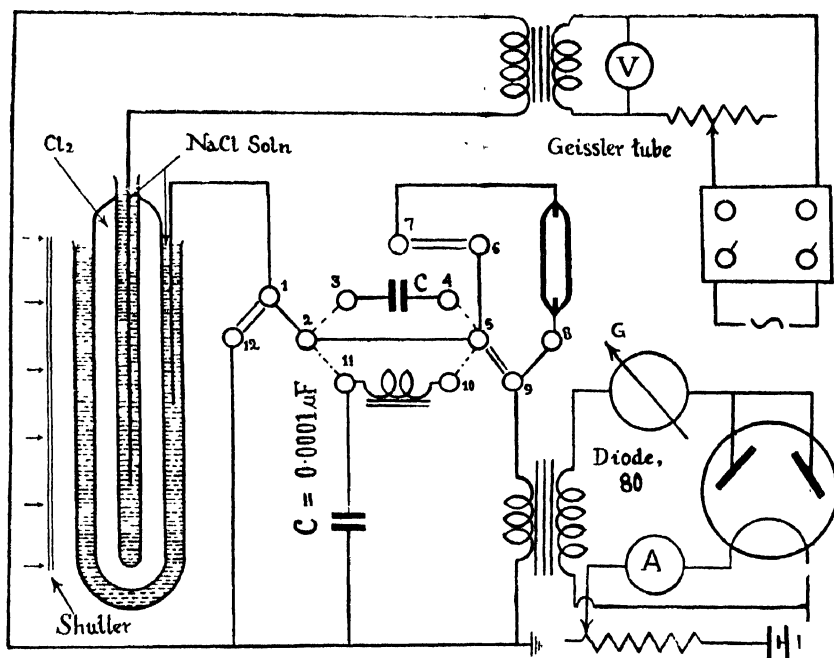
above, i_p, i_1, Δi and %Δi were observed in the high frequency component (i_{nF}), and the low frequency component (i_{LF}) of the discharge current (i_{LT}), in the following manner : In the first series (with 'normal' circuit, i.e., in absence of a Geissler tube in the circuit) the connections 1, 2, 5 and 9 were made (Fig. 1). This gives i_{LT}. The ozoniser was excited in the range 5 to 8 kV ; the corresponding values for i_p, i_1, Δi and %Δi are expressed graphically in Fig. 2. The HF component i_m was next observed by connecting 1, 2, 3, 4, 5 and 9. Lastly, the HF's were filtered out by by-passing through the capacity C, when the detector measured i_{ut}, the connections being 1, 2, 11, 10, 5 and 9 which included an HF choke between 11 and 10 (Fig. 1).

During next part of the work, each of the Geissler tubes mentioned above was introduced in the path of the discharge by connecting 1, 2, 5, 6, 7, 8 and 9. The corresponding i_{nF} and i_{LF} were observed with connections ex-

Table I

Influence of Serial Geissler Tubes on the Comparative Joshi-Effect in Chlorine in the Low and High Frequency Regions of the Discharge Current

kV		Normal			With neon tube			With helium tube		With nitrogen tube	
		$i_{L.r}$	$i_{L.s}$	$i_{H.r}$	$i_{L.r}$	$n.r$	$i_{H.r}$	$i_{H.r}$	$i_{H.r}$	$i_{L.r}$	$i_{H.r}$
5.1	i_D	66	51	18	96	22	3	—	—	52	40
	i_L	44	28	3	86	10	0	—	—	44	35
	Δi	—22	—23	—15	—10	—12	—3	—	—	—8	—5
	$\%\Delta i$	—33	—45	—83	—10	—54	—100	—	—	—15	—12
5.3	i_D	122	75	66	133	60	6	—	—	69	—
	i_L	73	54	29	129	52	0	—	—	49	—
	Δi	—49	—21	—37	—4	—8	—6	—	—	—20	—
	$\%\Delta i$	—40	—28	—56	—3	—13	—100	—	—	—29	—
5.6	i_D	168	92	129	206	78	10	—	—	124	70
	i_L	96	67	100	199	84	0	—	—	102	55
	Δi	—72	—25	—29	—7	+6	—10	—	—	—22	—15
	$\%\Delta i$	—43	—27	—22	—3	+7	—100	—	—	—18	—21
5.9	i_D	230	110	214	289	102	14	195	49	180	—
	i_L	136	75	161	271	106	1	135	20	170	—
	Δi	—94	—35	—53	—18	+4	—13	—60	—29	—10	—
	$\%\Delta i$	—41	—32	—25	—6	+4	—92	—30	—59	—6	—
6.1	i_D	265	120	280	349	157	19	195	49	249	121
	i_L	149	79	224	324	189	2	135	20	234	85
	Δi	—116	—41	—56	—25	+32	—17	—60	—29	—15	—36
	$\%\Delta i$	—44	—35	—20	—7	+20	—89	—30	—59	—6	—29
6.4	i_D	290	131	347	391	202	23	245	94	321	152
	i_L	163	80	264	374	253	3	170	36	299	133
	Δi	—127	—51	—83	—17	+51	—20	—75	—58	—22	—17
	$\%\Delta i$	—44	—39	—24	—4	+25	—87	—31	—62	—7	—11

Table I (contd.)

		Normal			With neon tube			With helium tube		With nitrogen tube	
		$i_{L.T.}$	$i_{L.F.}$	$i_{H.F.}$	$i_{L.T.}$	$i_{L.F.}$	$i_{H.F.}$	$i_{L.T.}$	$i_{H.F.}$	$i_{L.T.}$	$i_{H.F.}$
6.7	i_D	330	142	379	430	207	24	274	119	374	232
	i_L	180	85	286	405	288	3	230	64	339	227
	Δi	−150	−57	−93	−25	+81	−21	−44	−55	−35	−5
	$\%\Delta i$	−45	−40	−25	6	+39	−87	−16	−46	9	2
6.9	i_D	362	153	398	479	223	29	420	156	424	315
	i_L	185	86	316	466	268	3	348	114	378	300
	Δi	−177	−67	−82	−13	+45	−26	−72	−42	−46	−15
	$\%\Delta i$	−49	−44	−21	3	+20	−89	−21	−27	11	5
7.2	i_D	385	165	459	520	202	33	495	184	471	365
	i_L	200	90	345	514	167	3	444	114	405	350
	Δi	−185	−75	−114	−1	−35	−30	−51	−70	−66	−15
	$\%\Delta i$	−48	−45	−27		−17	−90	−10	−37	14	4
7.5	i_D	422	170	509	544	202	35	584	259	499	440
	i_L	220	93	372	539	116	4	542	244	439	390
	Δi	−202	−77	−137	−5	−86	−31	−42	−15	−60	−50
	$\%\Delta i$	−48	−45	−27	0	−42	−88	−7	−6	12	11
7.7	i_D	444	175	539	584	192	39	620	344	539	459
	i_L	226	99	400	567	122	4	610	259	450	417
	Δi	−218	−76	−139	−17	−70	−35	−10	−85	−89	−42
	$\%\Delta i$	−49	−44	−26	3	−36	−89	−2	−25	16	9
8.0	i_D	475	180	579	615	182	43	710	424	570	505
	i_L	243	105	236	355	144	4	680	339	489	464
	Δi	−232	−75	−143	−260	−38	−39	−30	−85	−81	−41
	$\%\Delta i$	−49	−441	−25	42	−21	−90	−4	−20	14	8
8.2	i_D	—	—	—	—	—	—	745	471	—	—
	i_L	—	—	—	—	—	—	760	439	—	—
	Δi	—	—	—	—	—	—	+15	−32	—	—
	$\%\Delta i$	—	—	—	—	—	—	+2	−7	—	—

$i_{L.T.}$—Total current in the low tension line; $i_{L.F.}$ and $i_{H.F.}$—the filtered low and high frequency parts of the current in arbitrary units.

plained already. As illustrative of the generality of these results, one group of data obtained with the neon tube is shown by curves in Figs. 3 to 5.

DISCUSSION

Results in Fig. 2 (*cf.* also Table I) show that for the 'normal' discharge circuit, *i.e.*, when only the chlorine filled ozoniser was excited, the Joshi-


effect sets in above the 'threshold potential' V_m (Joshi, 1929, 1944 *b*) which was 5.1 kV. Above this potential, whilst the net Joshi-effect $-\Delta i$ increases (numerically) progressively upto the largest potential used, *viz.*, 8.2 kV, the relative effect tends to a limiting value of 49%. Due to the small size of the ozoniser used, the energy dissipation in the system was so low that no current could be detected in an aerial within even 3 ft from the ozoniser. On the introduction of a serial and by-pass capacity of 0.0001 μF in the LT line, the results show that relative Joshi-effect $-\%\Delta i$, is a maximum in i_{HF} and least in i_{LF} in 'normal' circuit. This is in accord with Joshi's (1944 *b*, 1945 *a*, 1945 *b*) general result that the HF's represent a chief seat of $-\Delta i$. That $-\%\Delta i$ is intermediate in i_n is due to the circumstance that it contains both HF's and LF's.
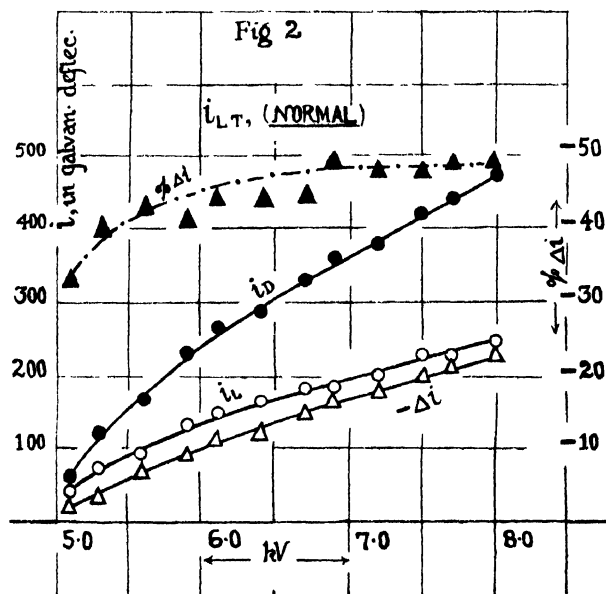
The presence of a Geissler vacuum tube in series with the ozoniser reveals pronounced alterations in the production of the Joshi-effect and also in the potential variation of the conductivity under the discharge, both in light and in dark. It is seen that at low potentials *i* is less with the vacuum tube than without it. At large V, however, the reverse is the case. With the nitrogen and the helium tubes i_{LF} was too small for detection with the available indicators. The corresponding Joshi-effect, however, is markedly

different. With nitrogen there is only $-\Delta i$; its (numerically) maximum value in nitrogen is less than the corresponding value with the neon and helium tubes. Using the latter, i_{LT} shows a negative Joshi-effect of 30% at the 'threshold potential'; which decreases progressively with the applied V to about 4 at 8.0 kV; and remarkably enough, changes sign to give a positive Joshi-effect of 2 to 6%. As is to be expected (*vide supra*), $-\%\Delta i$ is (numerically) larger in i_{HF}, *viz.*, 59. which decreases rapidly with applied V, but does not change sign.

It may be recalled that the 'threshold potential' is located by observation of a rapid increase of current for a small rise of V. Below 5.1 kV, the indicator employed showed but negligible and variable current. This was also the case on the addition of the nitrogen tube. Its substitution by the helium tube increases V_m by about 1.0 kV. The absence of a marked change in i compared with the 'normal.' on the addition of a nitrogen tube and also the decrease of i (especially at low exciting potentials) on the substitution by helium tube are explicable since according to a general result due to Joshi, i depends upon $V-V_m$ (Joshi, 1929, 1939, 1944a, 1945a). The deviations at larger V are considered later. When, however, the neon tube was introduced in the circuit, it was remarkable to observe that even at 1.5 applied kV, whilst the conductivity remained undetectibly low, the neon tube revealed its characteristic luminescence. This remained unaffected on irradiating the chlorine tube. Joshi considers that the proportion of the HF's in the corresponding current is marked near V_m and (unpublished results) that the discharge might start, though comparatively feebly, below V_m. The HF's produced at these low potentials might be responsible for causing the luminescence in the neon tube. The Joshi-effect Δi was, however, detected only near V_m, *i.e.*, at 5.1 kV, near which it is as high as 100%

Fig 3
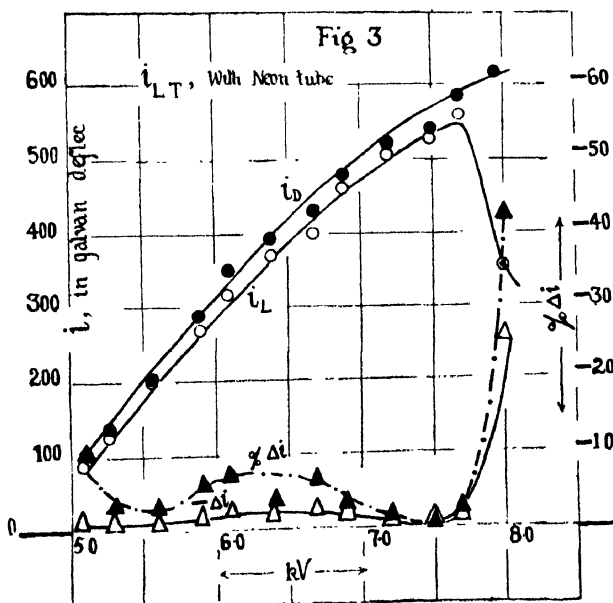
current decrease, using i_{HF} under but ordinary light. The relative Joshi-effect
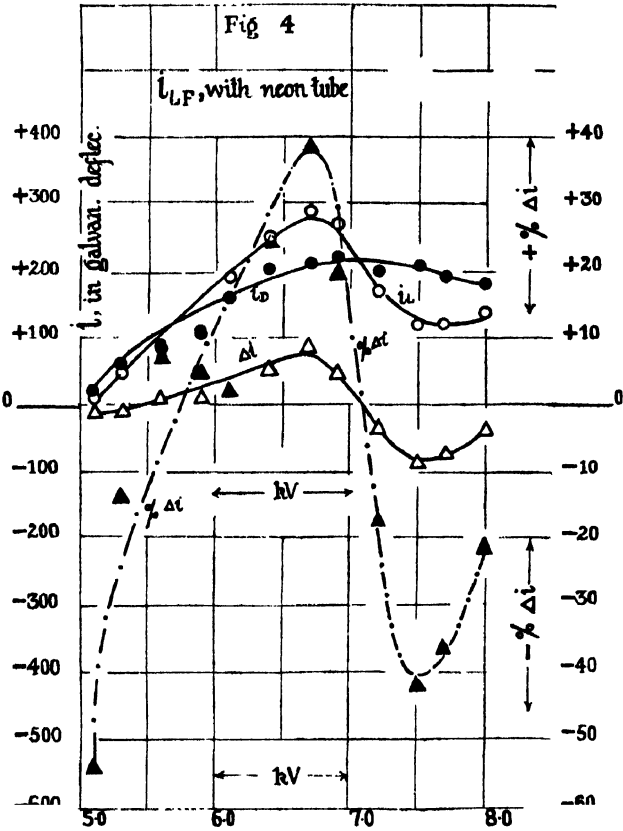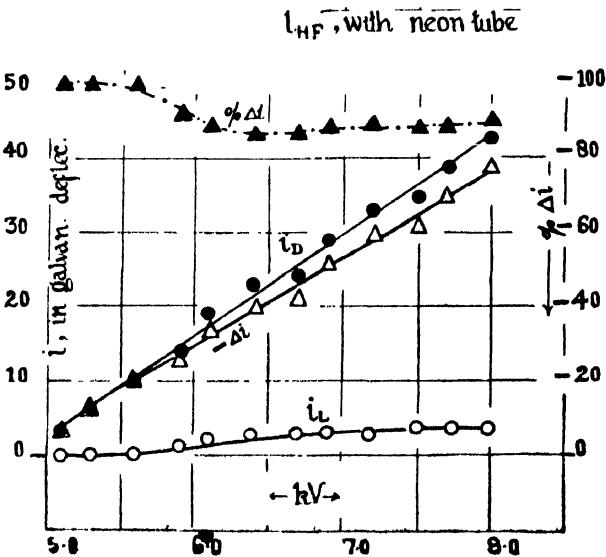$-\%\Delta i$ decreases (numerically) but slightly by increasing V and remains

Fig 4

Fig 5

constant at about 88 over 6.0 to 8.0 kV (Fig. 5). This behaviour differs strikingly from that observed in $i_{l,p}$. Here $\%\Delta i$ is -54 near V_m; and decreases (numerically) rapidly by increasing V and is undetected near 5.7 kV (Fig. 4). A further increase of V initiates a positive Joshi-effect (i.e., a photo-increase of the current $+\Delta i$), which reaches a maximum of 40% at about 6.7 kV. An increase in V hereafter produces not only a precipitous decrease in the $+\%\Delta i$ but a reversal to the negative Joshi-effect of 40%; once again this decreases (numerically) by increasing V. It must be emphasised that the entire sequence of these observations could be reproduced practically any number of time. A reversible inversion by potential increase $+\Delta i \rightleftharpoons -\Delta i$ was observed by Joshi (1947) in Cl_2 under HF — excitation and at low frequencies when the relative surface was increased by introducing powdered wall material in the annular space of the ozoniser. A sharp reversal of positive to negative Joshi-effect (as shown by $\%\Delta i$ versus kV curve in Fig. 4) by mere potential variation was observed (Joshi and Bhutt, 1942; Joshi and Murthy, 1942) in iodine vapour excited by silent discharge and in chlorine under semi-ozoniser excitations (Joshi, 1947). The latter changes were, however, found to be markedly subject to 'ageing.'

The 'ageing' factor had no sensible influence under conditions in the present work. Data for the current $i_{l,r}$ (Fig. 3) show only negative Joshi-effect variable in the range 10 to 40%, the latter increasing suddenly as the applied V is increased above 7.5 kV (vide infra). It may be mentioned at this stage that using i_{nr} and a neon tube which produced a negative Joshi-effect of 88 to 100% near V_m, instantaneously with the irradiation, the luminescence in the neon tube was quenched practically completely and restored equally immediately on shutting off the light. When, however, the neon tube was introduced in the path of i_{l1} the quenching was but partial. Using the i_{l1} the neon luminescence quenched less markedly, corresponding to the negative Joshi-effect. At potentials producing the positive Joshi-effect (Fig. 4) the enhancement in the luminescence was much less than expected from the corresponding $+\%\Delta i$. The Geissler luminescence in the helium and more especially in the nitrogen tube was but slightly affected corresponding to the production of $-\Delta i$. It is suggested that the potency of HF's in exciting the luminescence decreases rapidly in the order neon > helium > nitrogen.

It is instructive to examine curves (of which only one group with neon tube is shown in Figs. 3, 4 and 5, in comparison with the 'normal' in Fig. 2, from Table I) showing the influence of V, on i_n, $i_{l.}$, Δi and $\%\Delta i$ for the $i_{l,r}$, $i_{l,T}$ and i_{nr} lines, obtained with the 'normal' circuit and that containing one of the Geissler tubes employed in this work. It is seen that the influence of V on the various quantities mentioned above, especially the relative Joshi-effect $\%\Delta i$ deviates markedly with latter circuits than the former ('normal'). Thus, e.g., it is seen that with a neon tube, $\%\Delta i$ fluctuates about a small value, except when it rises suddenly from about 0 to 40 within 7.5 to 8.0 kV.

Joshi (1943, 1945*a*, 1945*b*, 1946) has suggested that the conductivity in an ozoniser discharge is a vectorial sum of various frequency currents with relative phase differences; both positive and negative Joshi-effects of different magnitudes may be associated with them. The effect observed with a given detector is the resultant of the $\mp \Delta i$ linked with the frequency bands to which the detector is sensitive. Introduction of a frequency filter cannot initiate a new reaction leading to a $-\Delta i$ or $+\Delta i$ as the case may be. These are presumably present simultaneously in the current structure and its time-delineation under irradiation. The observation of a conspicuous positive effect in the filtered i_{LF} with a serial neon tube is in accord with this view.

ACKNOWLEDGMENT

REFERENCES

Joshi, 1929, *Trans. Faraday Soc.*, **25**, 120.

——— and Purushotham, 1938, *Proc. Indian Sci. Cong.*, Part III, Chem. Soc , p. 48.

— ——, 1939, *Curr. Sci.*, **8**, 548.

——— and Bhatt, 1942, *Proc Ind. Sci. Cong,*, Part III, Chem. Soc., p. 61,

————— and Murthy, 1942, *ibid.*, p. 64.

———, 1943, *B. H. U. Journal*, **8**, 99.

———, 1944 (*a*), *Curr. Sci.*, **13**, 253.

———, 1944 (*b*), *Nature*, **154**, 147.

———, 1945 (*a*), *Curr. Sci.*, **14**, 67.

———, 1945 (*b*), *Proc. Indian Acad. Sci.*, **A22**, 225.

———, 1946, *Curr. Sci*, **15**, 281.

———, 1947, *Curr. Sci.*, **16**, 19.

TOMORROW'S INSTRUMENTS TODAY

RAJ-DER-KAR & CO.

COMMISSARIAT BUILDING

HORNBY ROAD

FORT

BOMBAY

OFFERS

FROM STOCK

GLASS METAL DIFFUSION PUMPS, METAL BOOSTE
PUMPS, OILS AMOILS OCTOILS OCTOIL,
BUTYL SABACATE

MANUFACTURED

By

DISTILLATION PRODUCTS
(U. S. A.)

SPENCER MICROSCOPE

CENCO HIGHVACS

BESLER EPIDIASCOPE

COMPLETE WITH FILM STRIP ARRANGEMENTS

We are now manufacturing :

* Soxhlet Extraction sets of 100cc, 250cc and 1000cc capacity
* B. S. S. Pattern Viscometers
* Kipp's Apparatus of 1 litre and ½ litre capacity
  Petri Dishes of 3″ and 4″ diameter

A N D

ALL TYPES OF GRADUATED GLASSWARE

such as Measuring Flasks, Measuring Cylinders,
Burettes, Pipettes, etc., etc.

Manufactured by :

INDUSTRIAL & ENGINEERING APPARATUS CO., LTD.

CHOTANI ESTATES, PROCTOR ROAD, BOMBAY, 7.

The following special publications of the Indian Association for the Cultivation of Science, 210, Bowbazar Street, Calcutta, are available at the prices shown against each of them :—

Subject	Author	Price
		Rs. A.
Methods in Scientific Research	Sir E. J. Russell	0 6 0
The Origin of the Planets	Sir James H. Jeans	0 6 0
Separation of Isotopes	Prof. F. W. Aston	0 6 0
Garnets and their Role in Nature	Sir Lewis L. Fermor	2 8 0
(1) The Royal Botanic Gardens, Kew.	Sir Arthur Hill	1 8 0
(2) Studies in the Germination of Seeds.		
Interatomic Forces	Prof. J. E. Lennard-Jones	1 8 0
The Educational Aims and Practices of the California Institute of Technology.	R. A. Millikan	0 6 0
Active Nitrogen A New Theory.	Prof. S. K. Mitra	2 8 0
Theory of Valency and the Structure of Chemical Compounds.	Prof. P. Ray	3 0 0
Petroleum Resources of India	D. N. Wadia	2 8 0
The Role of the Electrical Double layer in the Electro Chemistry of Colloids.	J. N. Mukherjee	1 12 0

A discount of 25% is allowed to Booksellers and Agents.

RATES OF ADVERTISEMENTS

Third page of cover	...	...	...	...	Rs. 32, full page
do. do.	...	...	...	...	,, 20, half page
do. do.	...	...	...	...	,, 12, quarter page
Other pages	...	...	...	...	,, 25, full page
do.	...	...	...	...	,, 16, half page
do.	...	...	...	...	,, 10, quarter page

15% Commissions are allowed to *bonafide* publicity agents securing orders for advertisements.

CONTENTS

NOTICE
TO INTENDING AUTHORS

Manuscripts for publication should be sent to Mr. A. N. Banerjee, Assistant Editor, 210, Bowbazar Street, Calcutta.

The manuscript of each paper should contain in the beginning a short abstract of the paper.

All references to published papers should be given in the text by quoting the surname of the authors followed by the year of publication within braces, *e.g.*, Sen (1942). The actual references should be given in a list at the end of the paper according to the following specimen :

Sen, B. K., 1942, Volume rectification of crystals, *Ind. J. Phys.*, **16**, 329.

The references should be arranged alphabetically in the list.

All diagrams should be drawn on thick white paper in Indian ink, and letters and numbers in the diagrams should be written in pencil.

CALCULATION OF THE PIEZO-ELECTRIC CONSTANTS OF α-QUARTZ ON BORN'S THEORY

By BISHAMBHAR DAYAL SAXENA AND KRISHNA
GOPAL SRIVASTAVA

ABSTRACT The relationship between the piezo-electric, dielectric and elastic constants has been obtained on Born's method and it has been shown that by using a generalised system of force-constants, results are obtained which are much nearer the observed values than those obtained on Born's assumption of the validity of Cauchy's relationship. Using only four force-constants, calculations have been made of 17 other constants in approximate agreement with observed values namely 2 piezo-electric constants, 7 elastic constants and 8 Raman and infra-red frequencies. The calculated values of the piezo-electric constants are $\epsilon_{11} = 7.56 \times 10^4$ and $\epsilon_{11} = 3.18 \times 10^4$ (obs. 5.1×10^4 and 1.23×10^4).

INTRODUCTION

The electric moment developed in the crystal due to strain is related to the components of the strain by a general relation of the form $p_i = \epsilon_{kli} u_{kl}$ where p_i are the components of a vector 'p' and u_{kl} are the components of the strain. In α-quartz, which belongs to the point group D_3 there are only two piezo-electric constants given by the equations :—

$$p_x = \epsilon_{11} u_{xx} - u_{yy} + \epsilon_{11} u_{yz} .$$

$$p_y = -\epsilon_{11} u_{xy} - _{11} u_{zx} .$$

$$p_z = 0 \qquad\qquad \dots (1.1)$$

p_x, p_y, p_z, are the components of the electric moment along the axes x, y, z, of the crystal—x being the electric axis, z the optical axis and y the mechanical axis at right angles to both, and ϵ_{11} and ϵ_{11} are the longitudinal and transverse piezo-electric constants. The best values of ϵ_{11} and ϵ_{11} according to Cady (1945) are 5.1×10^4 and 1.23×10^4. In our calculation of the peizo-electric constants we first find the relationship between the piezo-electric, dielectric and elastic constants by following the work of Born and Meyer (1924) on ZnS. We have then obtained the piezo-electric constants by using a generalised force system of valence forces, intra-valence forces and deformation forces.

According to the work of Born, which refers to ionic crystals of the cubic type, Cauchy's relations will hold for piezo-electric crystals (i.e., crystals not possessing a centre of symmetry) provided the piezo-electric forces were not taken into account. This implies, as shown later, that central forces alone are responsible for the elastic equilibrium, which is not true since Cauchy's relations do not hold even for some cubic metals like gold, silver and

tungsten. We have shown that by adopting a more generalised force system for which Cauchy's relations do not hold, results are obtained which are in much better agreement with the observed ones than those obtained by following Born's assumption. There is only a rough agreement and it is likely that the values of force constants chosen and the co-ordinates of atoms in the unit cell are responsible for the discrepancy.

RELATION BETWEEN ELASTIC AND PIEZO-ELECTRIC CONSTANTS

We make use of Born's theory for finding the relation between elastic, dielectric and piezo-electric constants. According to this theory a general homogeneous distortion of the crystal lattice can be represented at the point $\mathbf{r}_k^l$ where k is the basis index and l the cell index by the distortion vector $\mathbf{u}_k^l$ whose Cartesian components are given by —

$$\mathbf{u}_{kx}^l = \mathbf{u}_{kx} + \Sigma u_{xy}{}^r y_k^l.$$

where $\mathbf{u}_{kx}$ corresponds to the inner distortion and $\Sigma u_{xy} y_k^l$ corresponds to the homogeneous distortion of the lattice from the continuous standpoint. The change in the energy density of the homogeneously distorted lattice from its original undistorted configuration can be represented by second order terms in the distortion components—the terms of the first order being absent and those of the higher order can be neglected. If 'U' be the displacement energy, the force on each individual atom Ω_{kx} is given by

$$\Omega_{kx} = -\frac{dU}{d\mathbf{u}_{kx}} \qquad \qquad \ldots \ (2.1)$$

and the stress components are given by

$$K_{xy} = -\frac{dU}{du_{xy}} \qquad \qquad \ldots \ (2.2)$$

As there is no resultant force on the basis in a homogeneous strain $\Sigma_k \Omega_{kx} = 0$. Further, in order to secure equilibrium we must have not only the result of all basis forces vanishing, i. e., $\Sigma \Omega_{kx} = 0$ but for every basis atom,

$$\Omega_{kx} = 0 \qquad \qquad \ldots \ (2.3)$$

Born assumed that for the elastic energy corresponding to a homogeneous distortion, Cauchy's relations are valid. This assumption of Born is not correct because it means that all crystals which are non-piezo-electric must satisfy Cauchy's relatons, which is not the case in many crystals. Therefore in writing the expression for the elastic energy of α-quatz we are not justified in using Cauchy's relationship. Quartz, like zinc sulphide, contains only two basis atoms, silicon and oxygen. For the unit cell of α-quartz in which the horizontal electric axis is taken as the axis of 'x,' we write the displacement energy per unit volume as :—

$$U = \tfrac{1}{2}A(\mathbf{u}_{1x} - \mathbf{u}_{2x})^2 + \tfrac{1}{2}A(\mathbf{u}_{1y} - \mathbf{u}_{2y})^2 + \tfrac{1}{2}B\,\mathbf{u}_{1z} - \mathbf{u}_{2z})^2 + C(\mathbf{u}_{1y} - \mathbf{u}_{2y})\,(\mathbf{u}_{1z} - \mathbf{u}_{2z})$$

$$+ (\mathbf{u}_{1x} - \mathbf{u}_{2x})\,(Du_{xx} + D_1 u_{yy} + Eu_{zz} + Fu_{yz}) + (\mathbf{u}_{1y} - \mathbf{u}_{2y})\,(Gu_{xy} + Hu_{xz})$$

$$+ (\mathbf{u}_{1z} - \mathbf{u}_{2z})\,(Iu_{xy} - Ju_{xz}) + \tfrac{1}{2}R_{11}(u_{xx}^2 + u_{yy}^2) + \tfrac{1}{2}R_{33}u_{zz}^2 + R_{12}u_{xx}u_{yy}$$

$$+ R_{13}u_{zz}(u_{xx} + u_{yy}) + \tfrac{1}{2}R_{31}(u_{yz}^2 + u_{zx}^2) + R_{11}(u_{xx}u_{yz} - u_{yy}u_{yz} + u_{xz}u_{xy})$$

$$+ \tfrac{1}{2}R_{66}u_{xy}^2.$$

$\mathbf{u}_1$, $\mathbf{u}_2$ are the displacement vectors for the two types of atoms and the terms in (R) give the strain energy from the continuum standpoint. A, B, C, D, E, F, G, H, I, J, are the constants whose values are to be determined. All the other terms are absent on account of two-fold symmetry about the 'x' axis.

With the help of the relations (2.1) and (2.3) together with the relation $GC = AI$ and $HC = AJ$, we obtain

$$\mathbf{u}_{1x} - \mathbf{u}_{2x} = -[Du_{xx} + D_1 u_{yy} + Eu_{zz} + Fu_{yz}]A$$

$$\mathbf{u}_{1y} - \mathbf{u}_{2y} = -G/A\,u_{xy} - H/A\,u_{xz}$$

$$\mathbf{u}_{1z} - \mathbf{u}_{2z} = 0 \qquad\qquad \dots \ (2.1)$$

The piezo-electric moment along the 'x' axis is given by

$$p_x = \frac{1}{\Delta}\left(\Sigma_{c_i}\mathbf{u}_{kx} + \Sigma_n u_n\,p_n^0\right)$$

where Δ is the volume of the unit cell and p_n^0 the moment along the y axis in the undeformed condition. The second term vanishes when the cell has no moment in the underformed condition. This is true for α-quartz. In each unit cell there are six oxygen atoms and six silicon atoms which are shared between the two cells. Each silicon atom carries a charge of +4 units and each oxygen atom a charge of −2 units. As the silicons are shared between the two cells, we may assume that in each cell silicon atoms carry a charge of 2 units and oxygen atoms 2 units. Writing $2c = c_k$ and using (2.1) we have

$$p_x = \frac{c_k}{\Delta}\left(\mathbf{u}_{1x} - \mathbf{u}_{2x}\right) = -\frac{c_k}{\Delta}\left(\frac{D}{A}u_{xx} + \frac{D_1}{A}u_{yy} + \frac{E}{A}u_{xy} + \frac{F}{A}u_{yz}\right)$$

$$p_y = \frac{c_k}{\Delta}\left(\mathbf{u}_{1y} - \mathbf{u}_{2y}\right) = -\frac{c_k}{\Delta}\left(\frac{H}{A}u_{xy} + \frac{G}{A}u_{xy}\right)$$

$$p_z = \frac{c_k}{\Delta}\left(\mathbf{u}_{1z} - \mathbf{u}_{2z}\right) = 0 \qquad\qquad \dots \ (2.5)$$

Comparing the above equations with equation (1.1) we find

$$D = -D_1, \quad E = 0, \quad H = -F, \quad G = -D$$

and therefore

$$\epsilon_{11} = -\frac{c_k}{\Delta}\frac{D}{A}, \quad \epsilon_{41} = -\frac{c_k}{\Delta}\frac{F}{A} \qquad\qquad \dots \ (2.6)$$

With the help of the equations (2.2) and (2.4) we get the stress components k_{xx} etc. as

$$K_{xx} = \left(\frac{D^2}{A} - R_{11}\right)u_{x\,x} - \left(\frac{D^2}{A} + R_{12}\right)u_{y\,y} - R_{13}u_{z\,z} + \left(\frac{FD}{A} - R_{14}\right)u_{y\,z}$$

$$K_{xz} = \left(\frac{FD}{A} - R_{11}\right)u_{x\,y} + \left(\frac{F^2}{A} - R_{44}\right)u_{x\,z}$$

If the strain energy is expressed in terms of the elastic constants c_{11}, c_{22}, etc. we get

$$K_{xz} = -c_{11}u_{x\,x} - c_{12}u_{y\,y} - c_{13}u_{z\,z} - c_{14}u_{y\,z}$$

$$K_{xz} = -c_{14}u_{x\,y} - c_{44}u_{x\,z}$$

Comparing the co-efficients in the above equations we get

$$-c_{11} = \frac{D^2}{A} - R_{11} \; ; \; -c_{12} = -\frac{D^2}{A} - R_{12} \; ; \; c_{13} = R_{13} \; ; \; -c_{11} = \frac{FD}{A} - R_{11} \; ;$$

$$-c_{11} = \frac{F^2}{A} - R_{44} \; ; \; c_{33} = R_{33} \; ; \; -c_{44} = \frac{D^2}{A} - R_{16} \qquad \ldots \; (2.7)$$

RELATION BETWEEN DIELECTRIC AND PIEZO-ELECTRIC CONSTANTS

When the crystal is placed in an electric field, an electric moment is produced due to the displacement of the charges parallel to the direction of the field. This moment will be superposed on the moment produced due to the mutual displacement of the atoms if the crystal be distorted. If Ω_k be the force on a single atom 'k' per unit volume then under an electric field 'E', we have

$$\Omega_k = -\frac{c_k}{\Delta}E$$

$$\text{or } \Omega_{1x} = -\frac{c_k}{\Delta}E_x, \quad \Omega_{2x} = \frac{c_k}{\Delta}E_x \qquad \ldots \; (3.1)$$

On application of the field we may assume that although there is a change of polarisation, the crystal is not deformed. The stress components K_{xx}, K_{xy} etc are therefore all zero. Therefore with the help of equations $K_{xx} = K_{yy} = 0$ and $K_{yz} = 0$ together with the relations (2.1), (2.2), (3.1) we get, if we put $\dfrac{c_{44}c_{66} - c^2_{14}}{R_{44}R_{66} - R^2_{14}} = \gamma$,

$$u_{1x} - u_{2x} = \frac{c_k}{\Delta} = \frac{1}{Ay}E_x$$

Similarly with the help of equations $K_{xz}=0$ of $K_{xy}=0$ together with the relations (2.1), (2.2) and (3 1) we get if 'C'=0,

$$u_{1y}-u_{2y}=\frac{c_k}{\Delta}\frac{1}{A\gamma}E_y$$

$$u_{1z}-u_{2z}=\frac{ck}{\Delta}\frac{1}{B}E_z$$

Therefore by the use of equations (2.5) we get

$$p_x=\frac{c_k^2}{\Delta^2}\frac{1}{A\gamma}E_x=\frac{\eta_\perp-1}{4\pi}E_x$$

$$p_y=\frac{c_k^2}{\Delta^2}\frac{1}{A\gamma}E_y=\frac{\eta_\perp-1}{4\pi}E_y$$

$$p_z=\frac{c_k^2}{\Delta^2}\frac{1}{B}E_x=\frac{\eta_{\|}-1}{4\pi}E_z \qquad \dots (3.2)$$

$\eta_\perp$ and $\eta_\|$ are dielectric constants for the free crystal perpendicular and parallel to the optic axis. This will take into account the secondary changes in the polarisation produced by the piezo-electric effect although this secondary effect is very small in quartz. $\eta_\perp$ for α-quartz is 4.5 (Cady *loc. cit.*). As atoms are not point charges, the electronic shell of the atoms will be distorted when the field is applied. Born therefore puts the polarisation $p\frac{\eta_\perp-\eta_0}{4\pi}$ where $\eta_0=n^2$ 'n' being the refractive index. With this modification the equations (3.2) together with (2.6) give

$$\epsilon_{11}^2=\frac{\eta_\perp-\eta_0}{4\pi}\frac{D^2}{A}\gamma$$

$$\epsilon_{41}^2=\frac{\eta_\perp-\eta_0}{4\pi}\frac{E^2}{A}\gamma \qquad \dots (3.3)$$

CALCULATION OF PIEZO-ELECTRIC CONSTANTS

The calculation has been done in two ways :—

1. On Born's asumption :—

If we adopt Cauchy's relations to hold in the expression of the elastic energy we must have $R_{44}=R_{13}$ and $R_{12}=R_{66}$. This enables us to calculate $\frac{D^2}{A}$ and $\frac{E^2}{A}$ from (2.7) and c_{11} and ϵ_{41} from (3.3). We then get

$$\epsilon_{11}^2=\frac{\eta_\perp-\eta_0}{4\pi}\tfrac{1}{2}(c_{12}-c_{66})\gamma$$

$$\epsilon_{41}^2=\frac{\eta_\perp-\eta_0}{4\pi}(c_{13}-c_{44})\gamma$$

Since $\eta_0 = 2.4$, we get $\gamma = -1.272$ and $\epsilon_{11} = 18.5 \times 10^4$ and $\epsilon_{41} = 30.7 \times 10^4$ by using the values of the elastic constants given by Voigt. The expressions for ϵ_{11} and ϵ_{41} given above show that it Cauchy's relations hold *i.e.*, $c_{13} = c_{44}$ and $c_{12} = c_{66}$, both ϵ_{11} and ϵ_{41} would be zero and the crystal would be non-piezo-electric.

2. Using a more generalised force-system :—

If we assume only central forces between the atoms, then as shown below, Cauchy's relations are found to be valid for quartz. The failure of Cauchy's relationship therefore shows that the above assumption regarding the forces between the atoms is not correct and this will be all the more true for quartz which is a valence crystal as is shown by its hardness and the high frequencies of vibrations. We therefore use a more generalised force system. In an earlier paper Saxena (1944) has found the force-constants in quartz from the various Raman frequencies, and with the help of these the elastic constants were calculated from the continuum standpoint. In making these calculations, the structure of the crystal as determined from the X-ray data of Gibbs (1926) was used. If 'K' is the valence force constant of the Si-O bond, 'K_1' and 'K_2' the deformation force constants of the Si-O-Si and O-Si-O angles, and 'K_3' of O O repulsion, we get

$$R_{12} = -\frac{1}{111.2} \left[1.729 \times 10^{-16}K - .2403K_1 - 1.638K_2 + 7.5 \times 10^{-16}K_3 \right] \times 10^{21}$$

$$R_6 \quad \frac{}{111.2} \quad [1.729 \times 10^{-16}K + .241K_1 + 3.314K_2 + 7.5 \times 10^{-16}K_3] \times 10^{21}$$

$$R_{44} = \frac{1}{111.2} \left[2.87 \times 10^{-16}K + .617K_1 + 2.091K_2 + 9.35 \times 10^{-16}K_3 \right] \times 10^{21}$$

$$R_{13} = -\frac{1}{111.2} [2.87 \times 10^{-16}K \quad - 3.344K_2 + 9.35 \times 10^{-16}K_3] \times 10^{21} \quad \ldots \quad (4.2)$$

(The terms C_{11}, C_{12} etc. in the above paper are R_{11}, R_{12} etc. in the terminology of this paper).

We see immediately that if we adopt central forces only *i. e.*, if both K_1 and K_2 are zero in expressions (4.2), we have $R_{12} = R_{66}$ and $R_{13} = R_{44}$ which are Cauchy's relations for quartz class 'D_3'. The expressions (4.2) give

$$R_{66} - R_{12} = \frac{1}{111.2} \left[.481K_1 + 4.952K_2 \right] \times 10^{-24}$$

and

$$R_{44} - R_{13} = \frac{1}{111.2} \left[.627K_1 + 5.438K_2 \right] \times 10^{21} \quad \quad \cdot\cdot \quad (4.3)$$

Thus the relations (4.3) together with (2.2) and (3.3) enable us to calculate the piezo-electric constants ϵ_{11} and ϵ_{41} with the help of only two deformation force-constants K_1 and K_2.

CALCULATIONS

With the help of the Raman frequencies and the infra-red frequencies the author has determined $K_1 = 1.056 \times 10^{-11}$ and $K_2 = 1.315 \times 10^{-11}$ dynes. From (2.7) we then get

$$\frac{D^2}{A} = 2.05 \times 10^{11}, \quad \frac{F^2}{A} = 2.62 \times 10^{11}, \quad \frac{FD}{A} = 2.31 \times 10^{11}$$

This gives $\gamma = .57$ and we get $\epsilon_{11} = 13.2 \times 10^4$ and $\epsilon_{41} = 15.0 \times 10^4$

If, however, we take $K_1 = 1.0 \times 10^{-11}$, $K_2 = .8 \times 10^{-11}$, together with $K = 5.0 \times 10^5$ and $K_3 = -.6 \times 10^5$ dynes, we get a better agreement with the observed and calculated values of the piezo-electric constants while maintaining an approximate agreement between the observed and calculated values of the elastic constant and the Raman and the infra-red frequencies of α-quartz:

(1) Piezo-electric constants : Using (4.3) we get

$$\frac{D^2}{A} = .3725 \times 10^{11} ; \quad \frac{F^2}{A} = .066 \times 10^{11} \text{ and } \gamma = .9198$$

which give on using (3.3)/$\epsilon_{11} = 7.56 \times 10^4$ and $\epsilon_{41} = 3.18 \times 10^4$, the observed values being 5.1×10^4 and 1.23×10^4 respectively.

(2) Elastic constants . Using the formulæ given by the author for calculating the elastic constants of α-quartz in his earlier paper (Saxena, 1944). we get

	c_{11}	c_{12}	c_{33}	c_{13}	c_{14}	c_{14}	c_{66}
calc.	15 0	2.3	13.7	5.4	9.9	2.0	6.3×10^{11}.
obs	8.7	73	10.5	1.4	5.8	1.7	4.0×10^{11}.

It has to be pointed out that the values of R_{11}, R_{12} etc., calculated from (4 2) and from (2 7), using the given values of D^2/A and F^2/A, do not tally. This is due to our insufficient knowledge of force-constants in quartz. For if we take $K = 2.526 \times 10^5$ dynes and $K_3 = -.3238 \times 10^5$ dynes instead of the above values, we find that the two values of R_{11}, R_{12}, R_{13}, R_{14} and $R_{66}(R_{11} - R_{12}/9)$ agree exactly but those of R_{33} and R_{14} do not, and in addition the agreement between the observed and calculated values of Raman frequencies becomes much worse. Even if we disragard the Raman and infra-red frequencies and consider only the elastic constants, we see that four force-constants are not enough for calculating the six elastic constants as the disagreement in the two values of R_{33} and R_{14} is evidently due to this cause. Therefore when we are calculating 17 quantities with only four force-constants, the disagreement between the two calculated values of R_{11}, R_{12} etc., may be expected and it does not in any way vitiate the method of calculating the piezo-electric constants adopted in the paper.

(3) Raman and infra-red frequencies : Using the determinants given by the author in the earlier work (Saxena, 1944, 45) we get

	Raman frequencies				Infra-red frequencies			
calc.	156	256	473	1109	1147	772	479	101
obs.	207	356	466	1984	1111⎱ 1190⎰	800	488	385 ?

As we have calculated 17 different constants (2 piezo-electric, 7 elastic and 8 Raman and infra-red frequencies) with the help of only four force-constants, only a rough agreement between the observed and calculated values can be expected. Moreover, neither the structure of quartz nor the force constants are correctly known, for according to the structure of Gibb's (1926) and Wei (1935) the Si-O distances in quartz have only one value while according to Machatschky (1937) there are two values which differ widely and according to Brill, Hermann and Peters (1942) the two values differ only very slightly. However, it is evident that the values of the piezo-electric constants calculated by using a generalised system of force-constants are much closer to the observed values than those obtained on Born's assumption of the validity of Cauchy's relationship.

There are no calculations of the piezo-electric constants of quartz. Gibbs calculated only the piezo-electric modulus δ_{11} of α-quartz by finding the relative shifts of the centres of gravity of oxygen and silicon atoms for the pressure of one dyne and got a value which is nearly five times too high. We have obtained much better agreement and the discrepancy is most likely due to the uncertainty in the structure of quartz and the values of the force-constants K_1 and K_2.

LONGITUDINAL COEFFICIENT FOR β-QUARTZ

The expression for the displacement energy 'U' immediately enables us to show that ϵ_{11} for β-quartz must be o. For α-quartz the values of the constants in the expression for 'U' are such that E, C, I, and J are all zero while $D = -D_1$. and $H = -F$, $G = -D$. In β-quartz, which possesses a six-fold symmetry, both x and y directions are axes of two-fold symmetry. The energy 'U' should therefore remain unaltered if $(x, y, z,)$ is changed into $(-x, y, -z)$ so that u_{1x}, u_{2x}, u_{xy}, u_{yz} appear with negative signs. This will be possible only when D, G and R_{14} are zero in the expression for 'U'. Hence ϵ_{11} must be zero from (2.6).

DEPARTMENT OF PHYSICS,
UNIVERSITY OF ALLAHABAD.

REFERENCES

Born and Goppert Meyer, 1924, Handbuch der Phy. Bd 24/2, p 636.

Brill, Hermann and Peters, 1942, *Ann. der Phy*, **41**, 233.

Cady, W G., 1945, Piezo-electricity, Mac. Graw Hill Publication, p 415

Gibbs, R. E., 1926, *Proc. Roy. Soc.*, **110**, 443.

Machatschky, 1937, *ibid* **94**, 222.

Saxena, B. D., 1944, *Proc. Ind. Acad. Sc. A.*, **19**, 357.

        1945,   *ibid*   **22**, 379.

Wei, P. H., 1935, *Zs. f. Krys.*, **92**, 356.

PARAMAGNETISM OF SINGLE CRYSTALS OF THE SALTS OF THE IRON GROUP OF ELEMENTS AT LOW TEMPERA-TURES, PART III, SIX CO-ORDINATED IONIC SALTS OF Cu^{++} AND Fe^{++} IONS

By AKSHAYANANDA BOSE

ABSTRACT. In the present part of the paper the *reciprocally related* D-state ions Cu^{++} and Fe^{++} are discussed. The Stark-pattern of such states, under a predominantly cubic crystalline field with a feeble rhombic component, consists of a doublet and a triplet. For 6-co-ordinated Cu^{++} salts the doublet lies lowest, whereas the pattern ie inverted for similar iron salts. But experimentally, the result of this inversion from Cu^{++} to Fe^{++} is not obvious, since, both show large anisotropies and deviations of the effective moments from the *spin only* value. An explanation is attempted to be given of the observed behaviour of Cu^{++} and Fe^{++} salts namely, that in the former the orbital contribution is confined to a single direction in the crystal and in the latter these act *against* the spin in some of the directions and *for* the spin in others. For the Cu^{++} salts from known X-ray data for the crystals a correlation is given between the *ionic* and the *crystalline* moments. The variation with temperature of the angle between the different ionic groups is calculated and an explanation for the change in the orientation of the magnetic axes of the crystal is given on this basis. From these studies, it is plausible to ascribe not only the cubic but also the small rhombic part of the field to the charged particles in the immediate neighbourhood of the paramagnetic ion. Further, it is reasonable to conclude that the disposition of charged atoms about the paramagnetic ion and hence the crystalline field symmetry for a particular ion, is largely decided by the degeneracy of the ion itself. The temperature variation of the moments of the Fe^{++} ion have an apparent similarity to the Co^{++} ions but unlike cobalt all the principal moments tend to *spin only* value at high temperatures showing the relative unimportance of high frequency contributions in Fe^{++}.

INTRODUCTION

In the two earlier parts of the present paper (Bose, 1948), it has been made sufficiently clear how the crystalline electric field theory of Van Vleck (1932), Penney and Schlapp (1932), Görter (1932) and others, has successfully explained the behaviour of the F-state ions Ni^{++} and Co^{++}. It was shown that under a predominant cubic field with a small rhombic field superimposed upon it the ground state of an F-state ion is split up into a singlet and two adjacent triplets. For the Ni^{++} ion the lowest lying level in this Stark-pattern is the singlet when the cubic field potential is positive, whereas, for the same type of field the triplet lies lowest for Co^{++} ion. On the other hand, the situation is exactly reversed with a negative value of the potential. Such an

TABLE I

For Principal Anisotropies of Crystals

CuSO₄(NH₄)₂SO₄, 6H₂O — Monoclinic; $\beta=106°6'$; $a:b:c=0.7433:1:0.4838$

(1) 'b' axis vertical.
(2) 'a' axis vertical, 'b' axis along field

Temp. °K.	Angle** between 'a' axis & x₃ axis = θ	χ₁-χ₃ ×10⁶	χ₁-x₃ ×10⁶
303.1	−61	300.0	63.5
280	−64.7	337.7	117.1
260	−67.0	374.4	161.7
240	−68.3	412.1	200.3
220	−69.1	455.4	238.7
200	−69.8	504.4	239.6
180	−70.3	560.3	322.8
160	−70.8	629.0	373.5
140	−71.1	712.0	431.6
120	−71.1	824.1	502.0
100	−71.1	1013	629.9
92.9	−71.1	1109	698.0
—	—	—	—

CuSO₄K₂SO₄, 6H₂O — Monoclinic; $\beta=104°30'$; $a:b:c=0.7490:1:0.5088$

(1) 'b' axis vertical.
(2) 'a' axis vertical, 'b' axis along field.

Temp. °K	Angle** between 'a' axis & x₂ axis = θ	χ₁-χ₂ ×10⁶	χ₁-x₃ ×10⁶
303.1	−88.0	367.0	74.5
280	−89.4	393.8	81.2
260	−90.3	422.5	88.8
240	−91.2	455.0	97.0
220	−92.0	494.9	108.8
200	−92.6	544.3	125.6
180	−93.1	602.7	142.6
160	−93.5	671.9	160.8
140	−93.8	759.8	181.4
120	−94.0	878.4	206.7
100	−94.0	1052	248.1
90	−94.0	1155	276.4
83.9	−94.0	1226	298.2

CuSO₄, 5H₂O — Triclinic; $a:\beta:\gamma=82°6'. \; 107°26.:102°40'.$ $a:b:c=0.5721:1:0.5554$

Anisotropy values are taken from measurements by Krishnan and Mukherji (1936-38)

Temp. °K	χ₁(=x₃)-x₂ ×10⁶
303.1	275.0
280	290.0
260	306.5
240	327.0
220	352.1
200	383.9
180	423.8
160	471.8
140	535.4
120	615.5
100	717.8
90	782.0
88.7	789.5

FeSO₄(NH₄)₂SO₄, 6H₂O — Monoclinic; $\beta=106°48'$; $a:b:c=0.7466:1:0.4950$

(1) 'b' axis vertical.
(2) (201) plane vertical and 'b' axis horizontal and along the field*

Temp. °K	Angle** between 'a' axis & x₂ axis = θ	χ₁-χ₂ ×10⁶	χ₁-x₃ ×10⁶
303.1	−37	2582	224
280	−37	3091	263
260	−37	3637	313
240	−36.5	4315	372
220	−36	5177	413
200	−36	6267	535
180	−36	7698	658
160	−36	9649	822
140	−35	12330	1039
120	−35	16540	1365
100	−35	22840	1900
90	−35	26290	2270
84.8	−35	29990	2465

FeSO₄K₂SO₄, 6H₂O — Monoclinic; $\beta=104°32'$; $a:b:c=0.7377:1:0.5020$

(1) 'b' axis vertical.
(2) 'a' axis vertical, 'b' axis along the field

Temp. °K	Angle** between 'a' axis & x₂ axis = θ	χ₁-χ₂ ×10⁶	χ₁-x₃ ×10⁶
303.1	−43.8	1841	345.2
280	−43.8	2125	426.0
260	−43.8	2428	515.0
240	−13.8	2788	628.0
220	−43.8	3218	774.0
200	−44.8	3747	938.0
180	−44.8	4422	1164
160	−44.8	5311	1489
140	−44.8	6572	2015
120	−45.8	8612	2566
100	−45.8	11510	3162
90	−45.8	13550	3167
86.3	−45.8	14440	3558

* Angle (001):(201)=64°5'   ** Angle measured in degrees.

inversion of Stark-pattern should generally occur, as was mentioned in the earlier papers, for the "reciprocally related" ions *i. e.*, for those ions in which the incomplete $3d$ shell contains n or $5 + n$, and $5 - n$ or $10 + n$ electrons respectively. The remarkable differences in the magnetic behaviours of such ions are beautifully demonstrated by the six-coordinated salts of Ni^{++} and Co^{++} and also the four-coordinated blue cobalt salts. Thus we should expect similar widely divergent properties in the Cu^{++} and Fe^{+} salts also, in which the numbers of electrons in the $3d$ shells are nine and six, respectively.

With the same experimental techniques as before we studied the monoclinic ammonium and the potassium Tutton salts of Cu^{++} and Fe^{++} and also the triclinic salt $CuSO_4, 5H_2O$. The principal magnetic anisotropies $\chi_1 - \chi_2$ and $\chi_1 - \chi_3$ are given in Table I and the squares of the principal magnetic moments and the mean moments in terms of the Bohr magneton in Table II. Figures 1 − 5 indicate graphically the variations of these quantities with absolute temperature.

TABLE II

For the Gm. Molecular Principal Susceptibilities and the Squares of the Effective Magnetic Moments. (*Corrected for Diamagnetism*)

| Crystal	Crystal suspension & the direction along which the susceptibility is measured, *i.e.*, the direction setting along field	Temp. °K	$\chi_1 \times 10^6$	$\chi_2 \times 10^6$	$\chi_3 \times 10^6$	p^2_1	p^2_2	p^2_3	p^2
$CuSO_4, 5H_2O$	'c' axis vertical, (100) plane at 27°.2, and (110) at 53°.3 to the field. χ measured = χ_1 approx.	295.2	1650	1370	$\chi_1 = \chi_3$	3.923	3.258	$p^2_1 = p^2_3$	3.701
		230.0	2116	1768		3.920	3.277		3.706
		168.8	2871	2422		3.904	3.294		3.701
		88.7	5337	4549		3.814	3.251		3.626
$CuSO_4 NH_4)_2$ $SO_4, 6H_2O$	(001) plane vertical, 'b' axis horizontal and along field	295.9	1709	1397	1628	4.072	3.330	3.881	3.761
		225.0	2289	1850	2063	4.149	3.354	3.740	3.748
		173.6	2910	2328	2571	4.069	3.256	3.595	3.640
		124.9	4124	3333	3642	4.150	3.354	3.664	3.723
		92.9	5554	4445	4856	4.157	3.327	3.634	3.706
$CuSO_4K_2SO_4$ $6H_2O$	'b' axis vertical, χ_1 axis along the field	295.9	1696	1321	1619	4.012	3.149	3.859	3.683
		176.9	2800	2188	2655	3.990	3.117	3.783	3.630
		83.9	5824	4597	5525	3.935	3.107	3.734	3.592
$FeSO_4(NH_4)_2$ $SO_4, 6H_2O$	(201) plane vertical, 'b' axis horizontal & along field	296.8	12893	10189	12662	30.83	24.36	30.28	28.49
		182.5	22162	14670	21522	32.58	21.57	31.63	28.59
		84.8	50227	21137	47762	34.32	14.44	32.62	27.13
$FeSO_4K_2$ $SO_4, 6H_2O$	'a' axis vertical, 'b' axis along field	296.8	12463	10553	12825	29.80	25.23	30.67	28.57
		185.6	19577	15370	20065	29.27	22.98	30.90	27.72
		86.3	41277	26837	44835	28.69	18.65	31.18	26.17

FIG. I
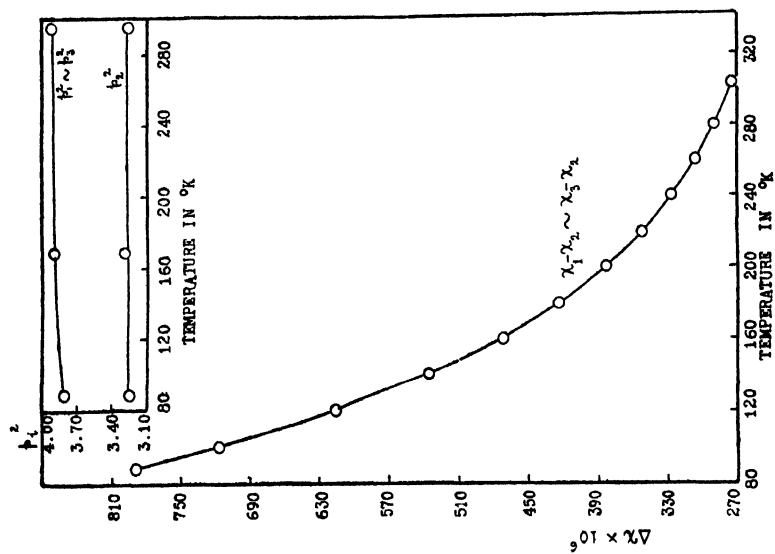
Temperature Variation of. Principal Anisotropies
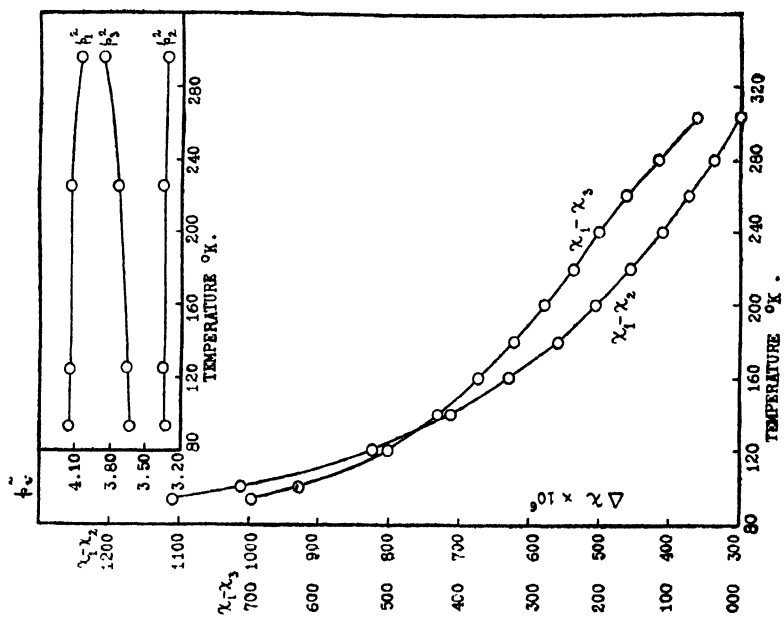and Effective Moments of $CuSO_4$, $5H_2O$.

FIG. 2

Temperature Variation of Principal Anisotropies and
Effective Moments of $CuSO_4(NH_4)_2SO_4$, $6H_2O$

FIG. 3

Temperature Variation of Principal Anisotropies and
Effective Momen of $CuSO_4 \cdot K_2SO_4, 6H_2O$
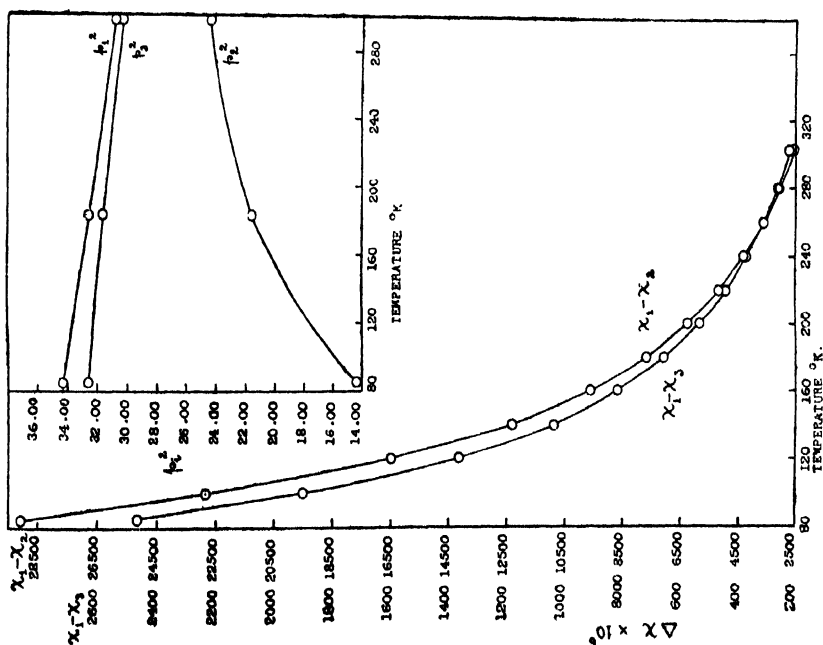
FIG. 4

Temperature Variation of Principal Anisotropies and
Effective Moments of $FeSO_4(NH_4)_2SO_4, 6H_2O$.
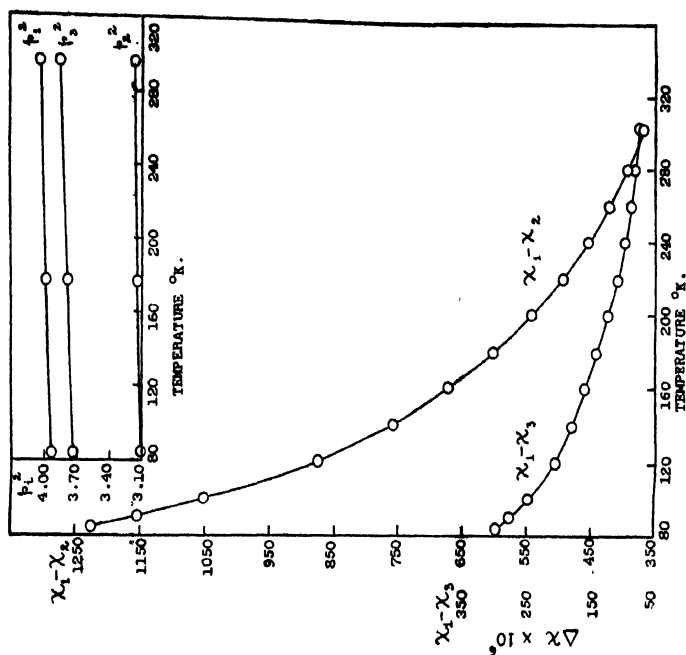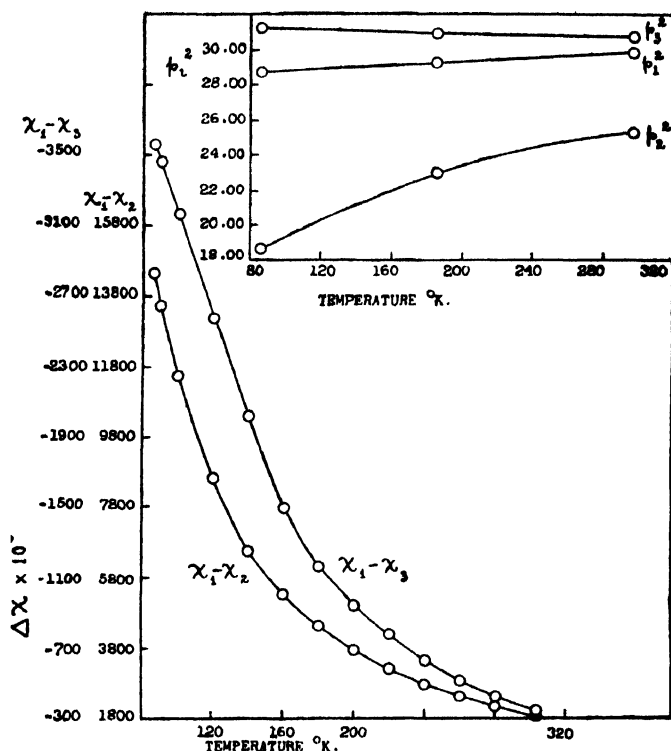
FIG. 5

Temperature Variation of Principal Anisotropies and
Effective Moments of $FeSO_4.K_2SO_4.6H_2O$.

DISCUSSIONS

1. Inversion of Stark-pattern from Cu^{++} to Fe^{++} Salts

It is known that both Cu^{++} and Fe^{++} ions are in the D-state, namely, $3d^9$ $^2D_{5/2}$ and $3d^6$ $^5D_4$ respectively. It has been shown by Bethe (1929) and Van Vleck (1932) that in a predominantly cubic field a D-state splits up into a doublet and a triplet separated to the order of 10^4 cm^{-1}. The small superimposed rhombic field separates the components of the doublet and the triplet by an amount much smaller than the above cubic separation but comparable to kT. Hence, whether the doublet is the lowest lying in the Stark-pattern or the triplet, the population of the upper components of the lowest level will be quite appreciable. Thus, the magnetic behaviour of the D-state ions will not be as simple as that of the F-state ions with singlet lying lowest. Now, the Cu^{++} ion has nine electrons in the $3d$ shell while Fe^{++} has six. Hence, their Stark-patterns in a *given* cubic field will be inverted with respect to each other (Fig. 6) and the difference in the magnetic behaviour of the two ions will depend on whether the doublet or the triplet is the lowest in one or the other. Actually, for a cubic field with positive value of the coefficient D in the expression $V = Ax^2 + By^2 - (A+B)z^2 + D(x^4 + y^4 + z^4)$, the disposition of the patterns will be as given below.

Stark-pattern for Cu^{++} in
a cubic field with +ve D.

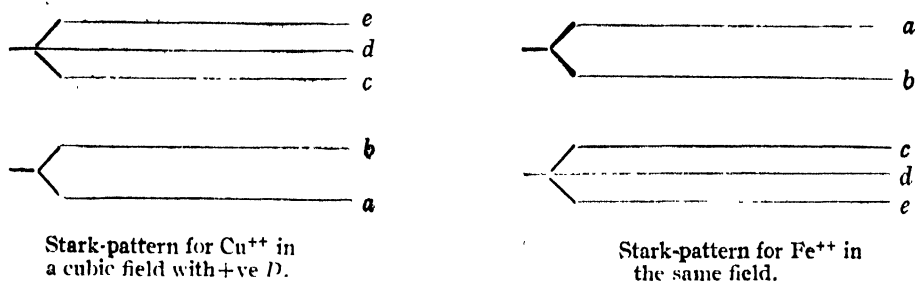Stark-pattern for Fe^{++} in
the same field.

FIG. 6

In the case of Co^{++} and Ni^{++} salts we found (Bose, 1948) that such an inversion in the Stark-pattern is responsible for the striking contrast in the magnetic behaviours of the two salts and arises in the following manner (Van Vleck, *loc. cit.*) as can be readily seen from their respective Stark-patterns. (Fig. 7).
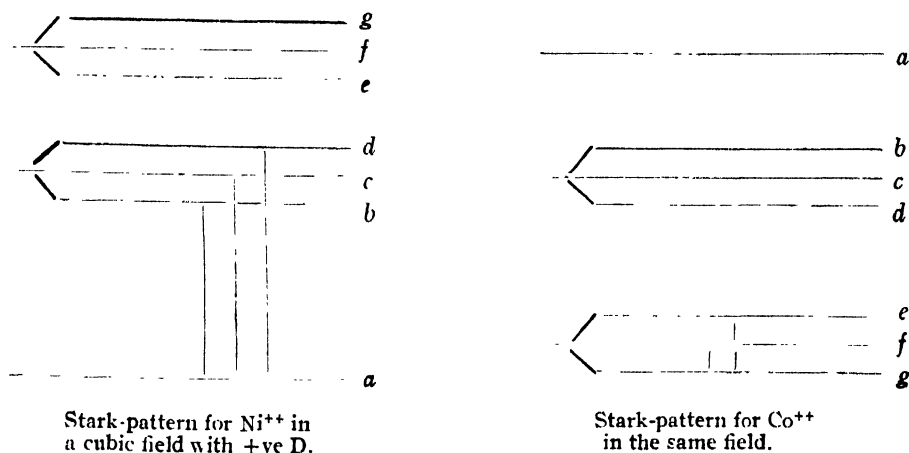

Stark-pattern for Ni^{++} in
a cubic field with +ve D.

Stark-pattern for Co^{++}
in the same field.

FIG. 7

In the case of Ni^{++} in which the ground level is a singlet, the contributions from the orbital moments to the susceptibility will depend inversely on the frequencies v, corresponding to the energy separations $a{\rightarrow}b$, $a{\rightarrow}c$ and $a{\rightarrow}d$, for the different directions of the incident magnetic field in the crystal. In the first place, these frequencies will be large, since they correspond to separations produced by the predominant cubic part of the field. Secondly, they will differ from one another by small amounts, since $\Delta v/v$ will be of the same order as the ratio of the separations produced by the rhombic part of the field to that produced by the cubic part. The results will be that for Ni^{++} salts (1) the contribution from orbital moments to the total effective moment cannot be large ; (2) these contributions will be practically the same along the different crystal directions, thus producing very little anisotropy. On the other hand, when as in Co^{++} the pattern is inverted making triplet level the lowest, the orbital contributions along different directions will be mainly given by the frequencies corresponding to the energy separations $g{\rightarrow}f$ and

$g \rightarrow e$ respectively, due to the rhombic field, which are much smaller than those due to the cubic field. Further, the separations $g \rightarrow f$ and $f \rightarrow e$ will be of comparable magnitudes. Hence we conclude (1) that the contributions from the orbital moments will be large ; (2) that the differences between these contributions along different directions in the crystal, will be comparable to their absolute magnitudes, leading to a very high anisotropy of the order of 25 to 30 % for Co^{++} in comparison with 3 to 4 % only for Ni^{++} salts, all at room temperatures, as is quite well known (Bose, 1948).

On the other hand, Tables I and II show that there is no such marked contrast between the cupric salts and the ferrous salts, in spite of the inversion of the Stark-patterns for the two. In both of them the orbital contributions are found to be large, as is shown by a comparison of the *observed* p^2 values of Cu^{++} and Fe^{++} ions, with the *spin only* values for the two ions, namely 3 and 24 respectively. Both the salts show large anisotropies of the same magnitude, $\Delta p^2 / p^2 = 19$ to 24 % for the different salts at room temperatures.

One would, therefore, be tempted to attribute the negative results of the inversion to the fact that, whether the Stark-pattern is erect or inverted the ground level is a multiplet and hence would correspond to large contributions to orbital moments and to a large anisotropy. But such a simple explanation is vitiated by the interesting fact pointed out by Bethe, (*loc. cit.*) that the doublet is 'non-magnetic' *i. c.*, there can be no orbital contributions involving the frequencies corresponding to the separation of the components of the doublet ; so that the large orbital contributions in Cu^{++} salts cannot arise from the low frequency terms, as it presumably does in Fe^{++} where the ground level is a triplet. So one has to invoke, to explain the orbital contribution in Cu^{++}, the terms depending on the separation between the doublet and the triplet ; and in order to explain the large anisotropy we have further to postulate that it is only the lower of the two levels of the doublet that will be occupied, even at the highest temperature in our measurements ; in other words, to postulate a separation between the two levels of the doublet, much greater than kT even at these temperatures. The latter postulate is plausible, since, the separation produced by the rhombic part of the field, though smaller than that produced by the cubic part, can still be much greater than kT.

Thus, we should expect the orbital contribution in Cu^{++} to be much smaller than in Fe^{++}. But since, the contribution from the spin moments in Cu^{++} is also much smaller than in Fe^{++}, namely in the ratio of $3 : 24$, the ratio of the orbital contribution to the spin contribution is of the same order in both the salts as actually observed. In the ferrous salts, the high anisotropy is due to the orbital contribution being different along different crystal directions—actually adding to the spin contribution along two of the directions, and acting against it along the third. The p^2 value along this direction will, hence, be less than even the *spin only* value of 24. On the other hand, in

cupric salts the high anisotropy is due to the orbital moment being confined to a single direction.

2. *Magnetic Properties of Cupric Salts*

Among the cupric salts studied by us copper sulphate penta-hydrate is the most interesting. The crystal is triclinic and from the X-ray analysis of this crystal made by Beevers and Lipson (1934), we know that it contains two molecules of $CuSO_4. 5H_2O$ in the unit cell. Further, each Cu^{++} ion is surrounded by six oxygen atoms, four of which belong to four water molecules and form a square with the Cu^{++} ion in the centre and each at a distance of 2.0 Å, and the other two oxygen atoms belong to SO_4^{--} ions located centrally above and below the square, each at a distance of 2.4 Å from the Cu^{++} ion. This octahedral arrangement of the oxygen atoms is thus not quite regular but has a tetragonal symmetry, which may be regarded as obtained from a regular arrangement by pulling out the diagonal joining the last two oxygen atoms. Presumably thus, the crystalline field in the neighbourhood of the Cu^{++} ion should also be predominantly cubic in symmetry, with a tetragonal component superposed upon it, the principal axes of the two fields being the same.

As have been shown by Krishnan and Mukherji (1936, 1938), the tetragonal axis of the field, associated individually with the two Cu^{++} ions in the unit cell of the crystal, are nearly perpendicular to each other. Further, denoting the direction of the tetragonal axis of the ion by z and the principal susceptibilities of either ion along this axis and in the plane perpendicular to it by $K_{\parallel}$ and $K_{\perp}$ respectively, and distinguishing the axes of the two ions in the unit cell by subscripts 1 and 2 respectively, they conclude that (1) $K_{\parallel} > K_{\perp}$, (2) the direction in $CuSO_4, 5H_2O$ crystal perpendicular to the $z_1 z_2$ plane, should be one of the principal magnetic axes of the crystal, (3) the exterior and the interior bisectors of the angle between z_1 and z_2 directions should be the other two principal axes, (4) since z_1 and z_2 are nearly at right angles, the susceptibilities along the latter two axes must be nearly equal and of the magnitude $(K_{\parallel} + K_{\perp})/2$, and that along the first axis at right angles to $z_1 z_2$ plane equal to $K_{\perp}$. Denoting the two nearly equal susceptibilities by χ_1 and χ_3 respectively and the third by χ_2

we have

and since

$$\left. \begin{array}{l} \chi_1(\sim \chi_3) = (K_{\parallel} + K_{\perp})/2 \\ \chi_2 = K_{\perp}, \\ K_{\parallel} > K_{\perp}, \\ \chi_1(\sim \chi_3) > \chi_2. \end{array} \right\} \qquad \dots \quad (2)$$

All these various results have been verified by Krishnan and Mukherji. Further, using the data for susceptibility at low temperatures of powdered crystal by de Haas and Görter and from their own measurement of the anisotropy down to liquid air temperature, they conclude that though the squares of principal magnetic moments $p_1^2 (\sim p_3^2)$ and p_2^2 are very different, they are both nearly independent of temperature. In other

words, all the susceptibilities follow the Curie law but with different Curie constants *i.e.* a law of the type

$$\chi_i = \frac{C_i}{T}, \quad i = 2, 3 \,(\sim 1) \qquad \qquad \dots \ (3)$$

$$C_2 = 0.399 \text{ and } C_1 (\sim_3) = 0.486 \;;$$

unlike the usual type of variation

$$\chi_i = \frac{C}{T - \theta_i}, \quad i = 1, 2, 3, \qquad \qquad \dots \ (4)$$

where C is the same but θ's different in different directions.

We have directly measured the absolute susceptibilities at different temperatures down to 80°K along one of the directions in the crystal, namely, the one that sets parallel to the field when the crystal is suspended with '*c*' axis vertical, and using the anisotropy data of Krishnan and Mukherji, calculated the values of $p_1^2 (\sim p_3^2)$ and p_2^2 for the crystal at these temperatures. The data are given in table II and are in agreement with those of Krishnan and Mukherji. The p^2 values also agree with various other authors and are given in Table III, together with p^2 values by the same authors for the two Tutton salts of copper to be discussed later.

TABLE III

p^2 For Various Copper Salts By Different Observers.

Author	$CuSO_4, 5H_2O$		$CuSO_4,(NH_4)_2SO_4,6H_2O$		$CuSO_4,K_2SO_4,6H_2O$	
	Temp.°K	p^2	Temp.°K	p^2	Temp.°K	p^2
da Haas and	290.0	3.705	—	—	—	—
Görter (Leid.	169.4	3.663	—	—	—	—
Comm., 210d	77.47	3.626	—	...	—	—
	14.29	3.505	—	—	—	—
Janes (1935)	—	—	295.7	3.741	296.8	3.729
	—	—	229.8	3.708	205.6	3.696
	—	—	83.3	3.660	82.1	3.657
Reekie	292.2	3.654	292.7	3.720	287.5	3.684
(1939)	80.4	3.632	79.9	3.690	78.6	3.633
	14.78	3.528	14.00	3.648	14.13	3.600
	1.58	2.634	1.60	3.642	1.60	3.579
Present	295.2	3.701	295.9	3.761	295.9	3.683
Author	168.8	3.701	225.0	3.748	176.9	3.630
	88.7	3.626	92.9	3.706	83.9	3.592

We may draw attention here to the interesting result that for the crystal of $CuSO_4, 5H_2O$, p_2^2 conforms roughly to the *spin only* value of 3, whereas the other susceptibility is considerably in excess of it, which shows, in view of the relations (2) between the principal susceptibilities of the *crystal* and the *ion* stated earlier in this section, that the contribution of the orbital moment

is practically confined to one direction, namely, to the tetragonal axis of the crystalline field in the neighbourhood of the ion. Denoting the effective moments of the *ion* by $P_{\parallel}$ $P_{\perp}$, as against the effective moments $p_1(\sim p_3)$ and p_2 of the *crystal*, we have

$$p_1^2(\sim p_3^2) = (P_{\parallel}^2 + P_{\perp}^2)/2 \qquad \dots \quad (5)$$

and

$$p_2^2 = P_{\perp}^2$$

from which we obtain :—

TABLE IV

$CuSO_4, 5H_2O$

$T^\circ K$	295.2	88.7
$P_{\parallel}^2$	4.588	4.377
$P_{\perp}^2$	3.258	3.251

—from which one can see, that the contribution from the orbital moment is considerable and is confined to the direction of the tetragonal axis of the crystalline electric field. The temperature variation of the moment if any, should be also more prominent in this direction as it actually is.

The above results are interesting, since, from the 'non-magnetic' nature of the ground level which is the doublet level, we were already led to the conclusion that the orbital contribution is confined to one direction in the crystal. That when the crystalline field has tetragonal symmetry this direction should be along the tetragonal axis, is indeed to be expected, and can also be explained from direct considerations of the symmetry of the field ; since the orbital moments will be quenched almost completely along directions perpendicular to the tetragonal axis, and if any part of it is conserved it must be along this axial direction only.

In view of the fact that the magnetic anisotropies in the two cupric Tutton salts are nearly the same as in copper sulphate, it is tempting to try whether a similar cubic field with a feeble tetragonal component will also fit the observed data for these two salts. The Tutton salts as already mentioned are monoclinic and contain two Cu^{++} ions in the unit cell. Assuming the field to be tetragonal, the χ_1-axis of the crystal should be evidently the projection of the tetragonal axis of the ion on the (010) plane of the crystal. Denoting the inclination of this tetragonal axis of the ion to the (010) plane by ϕ, we get the following simple relations between the principal magnetic moments of the *crystal* and those of the *ions* :—

$$p_1^2 = P_{\parallel}^2 \cos^2\phi + P_{\perp}^2 \sin^2\phi$$
$$p_2^2 = P_{\perp}^2 \qquad\qquad\qquad \dots \quad (6)$$
$$p_3^2 = P_{\parallel}^2 \sin^2\phi + P_{\perp}^2 \cos^2\phi$$

If the above assumptions, regarding the tetragonal symmetry of the crystal field associated with each Cu^{++} ion, be correct then we should expect $p_2^2 = P_{\perp}^2$, to have practically the *spin only* value of 3. This is actually so as will be seen from below.

TABLE V

Crystal : $CuSO_4$, A_2SO_4, $6H_2O$

	Temp. °K	$P^2_\perp = p_2^2$	$P_\parallel{}^2 = p_1^2 + p_3^2 - p_2^2$
$A = NH_4$ {	295.9	3.330	4.623
	92.9	3.327	4.464
$A = K$ {	295.9	3.149	4.752
	83.9	3.107	4.562

Knowing $P_\perp{}^2$ we can indeed go further and calculated $P_\parallel{}^2$ from the observed values of p_1^2 and p_3^2 using the relation (6), since then $P_{_3}{}^2 + P_\perp{}^2 = p_1^2 + p_3^2$. The values of $P_\parallel{}^2$ so obtained are given in the table above.

These values agree well with the values deduced from the crystal $CuSO_4$, $5H_2O$ and show (1) that the fields in the Tutton salts do have tetragonal symmetry, in spite of the fact, that in the Tutton salts, the Cu^{++} ion is surrounded by six identical oxygens all belonging respectively, to six water molecules, unlike in copper sulphate in which two oxygen atoms are different from the rest and belong to two $SO_4{}^{--}$ groups ; (2) that even the magnitudes of the cubic and the tetragonal parts of the field are the same in the Tutton salts as in copper sulphate. The above conclusions lend strong support to the view expressed by us in our earlier papers (Bose, 1947, 1948), and which has generally been adopted in our discussions, that in addition to the cubic part, the feeble noncubic part of the field also may be due to the immediately neighbouring atoms, and as long as these neighbours are the same and arranged in the same configuration in different crystals, the crystal fields in them also will be the same. These results, have important significance in view of the interesting theorem of Jahn and Teller (1937, 1938), that the asymmetry and the magnitude of the crystalline field are determined ultimately by the degeneracy of the ground state of the paramagnetic ion.

The six oxygens surrounding the Cu^{++} ion will be strongly bound. to the ion and the group as a whole will form a more or less rigid system having tetragonal symmetry. But the binding between two such groups present in the unit cell will be much feebler and hence the two tetragonal axes may, slightly change their relative orientations with change of temperature ; consistent of course with the requirement of the monoclinic symmetry of the crystal, of these Tutton salts, namely, that one of the groups should be the mirror image of the other. In other words, though the crystal fields and therefore, $P_\parallel$ and $P_\perp$ will be practically independent of the temperature, the angle ϕ, which the tetragonal axis makes with the (010) plane, as also its projection on the (010) plane, may change slightly with the temperature. The projection of the tetragonal axis is evidently the χ_1 axis of the crystal, and thus we can readily see how without any change in the crystalline field, either in its magnitude or in its asymmetry, there can be appreciable change in the.

direction of the χ_1 and χ_2 axes of the crystal. The angle ϕ may be calculated from the relation,

$$\frac{p_1 - p_3{}^2}{P_\parallel{}^2 - P_\perp{}^2} = \cos 2\phi \tag{7}$$

and its temperature variation for the two Tutton salts may be seen from the Table VI. We specially emphasise this point, since an explanation of the change of axis in terms of the change in crystalline field, as has been attempted by Jordahl (1934), is not only complicated but requires a large rotation of the rhombic field axes with reference to the axes of the cubic field.

TABLE VI

For the angle ϕ

Crystal: $CuSO_4$, A_2SO_4, $6H_2O$

	Temperature °K	Angle ϕ in degrees
$A = NH_4$ {	295.9	40.8
	92.9	31.3
$A = K$ {	295.0	41.8
	83.0	41.0

Before concluding this section we should refer to some important results obtained by Reekie (1939, vide Table III) on the mean susceptibilities of these three cupric salts at liquid hydrogen and helium temperatures. For all the three salts the effective magnetic moment, corresponding to the mean susceptibility, is practically independent of temperature down to about $14°K$ (as we have also found for each of the three principal moments separately and over a shorter range of temperature). But below this temperature there is a striking contrast in the behaviour of the copper sulphate on one side and the two cupric Tutton salts on the other. Whereas, in copper sulphate the value of p, comes down rapidly at liquid helium temperatures and the trend of the p^2 against T curve suggests that it may reach very low values in the neighbourhood of absolute zero; in the Tutton salts the fall in p, is very slight and its rate is of the same order as at higher temperatures. Presumably, associated with this is the observation of Ashmead (1939) that the specific heat versus temperature curve of copper sulphate shows a large hump in the region of $4°K$, which is completely absent in the corresponding curves of the two cupric Tutton salts. These results do not appear to be explicable on the crystalline field theory, and indeed, at present, on any theory.

3. *Ferrous Salts Versus Cobalt Salts*

As we mentioned in an earlier section, the triplet level in the Stark-pattern of the D-levels of Fe^{++} being lowermost, there should be a large contribution from the orbital moments, and the contributions should be different

along different directions, actually adding to the spin contribution along p_1 and p_3 directions and acting against the spin along p_2 direction. Hence the large anisotropy in the crystals. We further see from the experimental data given in Table II that p_1 and p_3 have nearly the same values which vary little with temperature and they are not much different in the two salts. In cobalt salts (Bose, 1948) all the three p's tend to become temperature-independent at high temperatures, the values being very different from the *spin only* value of $p^2 = 15$. The experimental values for Fe^{++} show that p_1 certainly, and probably also p_1 and p_3 will reach temperature-independent values at high temperatures, and it is not unlikely that those temperature-independent values may all be the same, namely, the *spin only* value corresponding to $p^2 = 24$. If this is so it would mean that high frequency contributions in Fe^{++} are much less than in Co^{++}.

REFERENCES

Ashmead, 1939, *Nature*, 143, 855.

Beevers, C. A. and Lipson, H., 1934, *Proc. Roy. Soc. (A)* 148, 570.

Bethe, H, 1929, *Ann. der Phys.*, 3, 133.

Bose, A., 1947, *Ind. Jour. Phys.* 21, 277.

„ 1948, „ 22, 76, 195 and 276

Görter, C. J., 1932, *Phys. Rev.*, 42, 437.

de Haas and Görter, C. J. *Leiden Comms.* 210d.

Jahn and Teller, 1937, *Proc. Roy. Soc. (A)* 161, 220.

„ „ 1938, „ „ „ 164, 117.

Janes, R. B., 1935, *Phys. Rev.*, 48, 78.

Jordahl, O. M. 1934, *Phys. Rev.*, 45, 87.

Krishnan, K. S, Banerjee, S and Chakravorty. N. C., 1933, *Phil. Trans. Roy. Soc. (A)* 232, 99.

Krishnan, K. S. and Mukherji, A, 1938, *Phil. Trans. Roy Soc. (A)* 237, 135.

„ „ 1936, *Phys Rev.*, 50, 860.

„ „ 1938, „ „ 54, 533

„ „ 1938, „ „ 54, 841.

Penney, W. G. and Schlapp, R., 1932, *Phys. Rev.*, 42, 666.

Reekie, J., 1939, *Proc. Roy. Soc (A)* 173, 367.

Van Vleck, J. H. 1932, The Theory of Electric and Magnetic Susceptibilities (*Oxford*).

„ „ „ 1932, *Phys., Rev.*, 41, 208.

A NEW HORIZONTAL ELECTRON MICROSCOPE

By N. N. DAS GUPTA, M. L. DE, D. L. BHATTACHARYA AND
A. K. CHAUDHURY

Plates XVIA and XVIB

ABSTRACT. A new horizontal electron microscope with several special features has been constructed. The technical details of its construction, power supplies and operation are given in this paper. The microscope can be operated at a maximum electron energy of 80,000 electron volts and is designed for an electron optical magnification of twenty thousand diameters.

INTRODUCTION—HISTORICAL

An electron microscope with several distinctive features has been produced in the University College of Science, Calcutta. It is the aim of this paper to describe these features in detail. However, from the point of view of interest to the reader, a short historical account of the development of the electron microscope up to its present stage will be given, before the technical features of the new microscope are described.

The science of electron optics is of recent origin. Its basis is the fundamental theoretical work on electron lenses by Busch who first showed in 1926, that axially symmetric electric and magnetic fields possess lens characteristics with respect to electron radiation. The practical development of magnetic lenses was carried out by Knoll and Ruska (1931, 1932) in the Technische Hochschule, Berlin. The first electron microscope employing magnetic lenses with pole pieces—the prototype of all modern instruments—was constructed by Ruska in 1934. A cold cathode gas discharge tube was used as the source of electrons, there was no provision for air-lock arrangement for introduction and removal of specimens and the final image formed on a fluorescent screen was photographed through a window by means of an external camera. Marton introduced several improvements in the design of an electron microscope developed by him in the University of Brussels, in 1935. He used a heated filament, air-lock specimen chamber and arrangement for direct recording of electron micrographs on photographic plates introduced into the vacuum. He was also the first to photograph biological specimens with an electron microscope.

Two years later in 1937, the first electron microscope in Britain was constructed by the Metropolitan Vickers Company for Martin, Whelpton and Parnum 137. At about the same time Burton in Canada organised a programme

of research in electron microscopy in the University of Toronto. Two of his graduate students, Prebus and Hillier (1939) built the first electron microscope in America. By 1939 resolving powers better than 100 A° were obtained by Canadian and European workers. (Burton, Hillier and Prebus 1939).

At this stage when the great potentialities of the new microscope was well proved by these successful research instruments, developed primarily in the university laboratories, industry took up further development. The first commercial electron microscope was built at about this time by Siemen's company in Berlin (Borris and Ruska 1939, 1940). The lens coils and the filament of the microscope used current from storage batteries and the coils were water cooled. The high voltage unit consisting of the conventional transformer rectifier system was in a seperate assembly on account of its great bulk and for better shielding of the microscope from sixty cycle electro-magnetic radiation.

Von Ardenne in 1940 published a description of his universal electron microscope developed in the Kaiser Wilhelm Institute, Berlin. It was designed for bright field, dark field and steiio operation. The notable features of this instrument were the arrangement for tilting of the specimen for sterioscopic photography and perfect alignment and also the possibility of direct electronic magnification up to 50,000 diameters.

In 1939 Marton came to U. S. A. and joined the R. C. A laboratories. There he developed the first R. C. A. electron microscope called R. C. A. type A (Marton 1940, Marton, Banca and Bender 1940). A year later R. C. A. announced the development of the first commercial electron microscope in U. S. A, called R. C. A. type B (Zworykin, Hillier, and Vance 1941 a, Hillier and Vance 1941). The chief improvements on its predecessors were (a) combination in a single unit of both the microscope and its power supplies and (b) the use of high frequencies for generation of high voltage and heating of the filament. For stabilisation of the high voltage, feed-back principle was used.

In 1941 various attempts were made to increase the electron energies so as to make possible the examination of thicker specimens with the help of an electron microscope. Müller and Ruska (1941) adopted a Siemens microscope for operation at 220 ckv. Von Ardenne (1941) modified his electron microscope described earlier for operation at 200 ckv. Zworykin, Hillier and Vance (1941b) also reported the construction of a 300 ekv. microscope.

In these cases the microscope body was similar to those already described. Only the electron gun was bui t in two or three stages and the voltage distributed between them by means o fa voltage divider across the high voltage supply for stable operation.

In 1942 Prebus built an electron microscope in the Ohio State University, Columbus, following the design already developed at Toronto. Microscopes
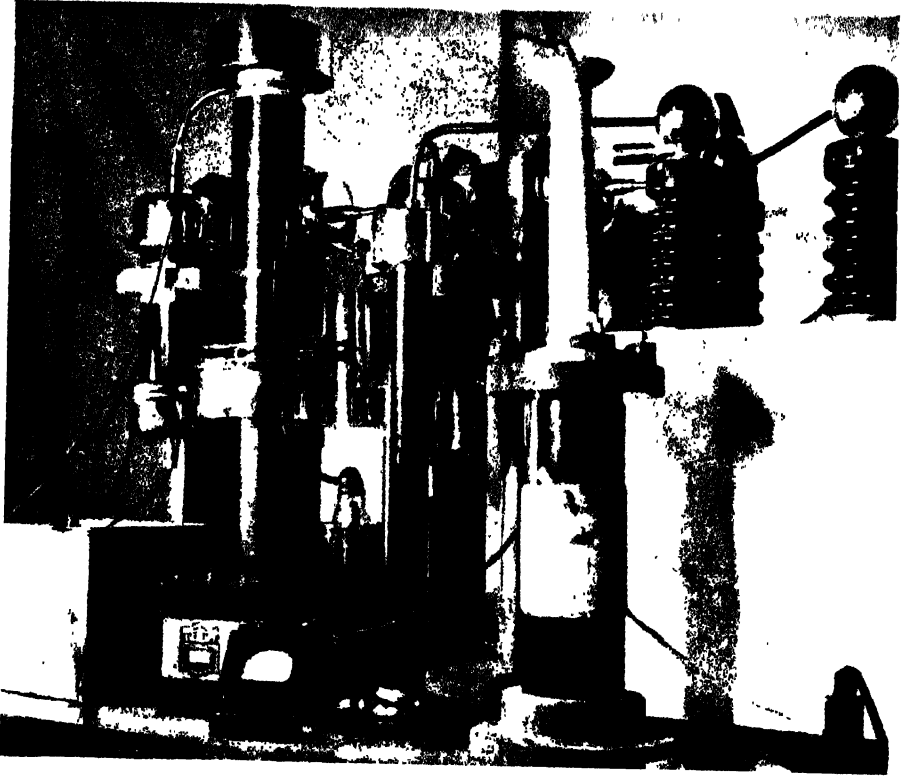
Fig. 8

Photograph of High Frequency Voltage Unit.

based on this design were also installed at the Eastman Kodak Co. and in Columbia Carbon Co., in U.S.A. In the subsequent year R.C.A. announced the development of a small compact electron microscope called R.C.A. console model (Zworykin and Hillier 1943). In this unit the condenser lens was eliminated and the objective and the projector lenses contained in the same magnetic circuit. This extreme simplicity of design had been obtained at the cost of a fixed magnification of only 5000 diameters and an operating voltage of only 30 ckv. The resolution was reported to be better than 100 A°.

In 1945 Marton, now at the University of Stanford, produced an electron microscope employing five lenses and designed for three stage magnification which could be varied from 400—40,000 diameters. This microscope had an intermediate lens in between the usual objective and the projector lenses and was designed for operation at 100 ckv.

During war the research and development of electron microscopes was mostly restricted to U.S.A. However, some work was carried on with great difficulty in Holland, France and Great Britain. Poole developed in 1944 an electron microscope in the Institute of Electron Optics at Delft, Holland whose details have just been published (Poole 1947). This instrument operates at 150 ckv and is a four lens unit. With a distance of only 60 cms between the object and the final image the magnification produced can be varied continuously between 1000 and 80,000 diameters. This instrument has also an arrangement for using 35 mm. film. In 1947 the Metropolitan Vickers Co. in England announced the production of the first commercial electron microscope in England EM3 Model of Metro Vick. (Haine 1947).

The instruments described so far are electromagnetic instruments using electromagnetic type of lenses. The development of electrostatic lenses and of electron microscopes using such lenses has proceeded almost side by side with that of the electromagnetic instruments. Shortly after Busch's original discovery, Davisson and Calbick (1932) in U. S. A. and Brüche and Johannson (1932a) in the A. E. G. laboratories in Berlin successfully developed electrostatic lenses. Brüche and Hagen (1939) and Mahl (1939) designed the first electrostatic microscope of high magnification in the A. E. G. laboratories in Berlin. Boersch (1942) built at the University of Vienna a versatile type of electrostatic electron microscope. This instrument could be easily adapted for taking the usual transmission pictures, electron shadow micrographs as well as diffraction patterns. In 1943 Bachman and Ramo, of the G. E. C. laboratory in U. S. A. developed a three stage electrostatic instrument. With a very simplified design they obtained a resolution 10 times that of the light microscope and an electronic magnification varying from 500-1000 diameters. In France, the Compagnie Generale de Telegraphie sans Fil (C.S.F.) has also produced an electrostatic instrument. Although the electrostatic instruments are simpler to construct, from the point of ultimate performance they have not yet appeared on the market as any serious rival of the electromagnetic instruments.

DESCRIPTION OF THE NEW MICROSCOPE

An illustration of the new electron microscope is given in Plate XVIA, Fig. 1. Fig. 2 shows a section of the complete electron optical system. There are several
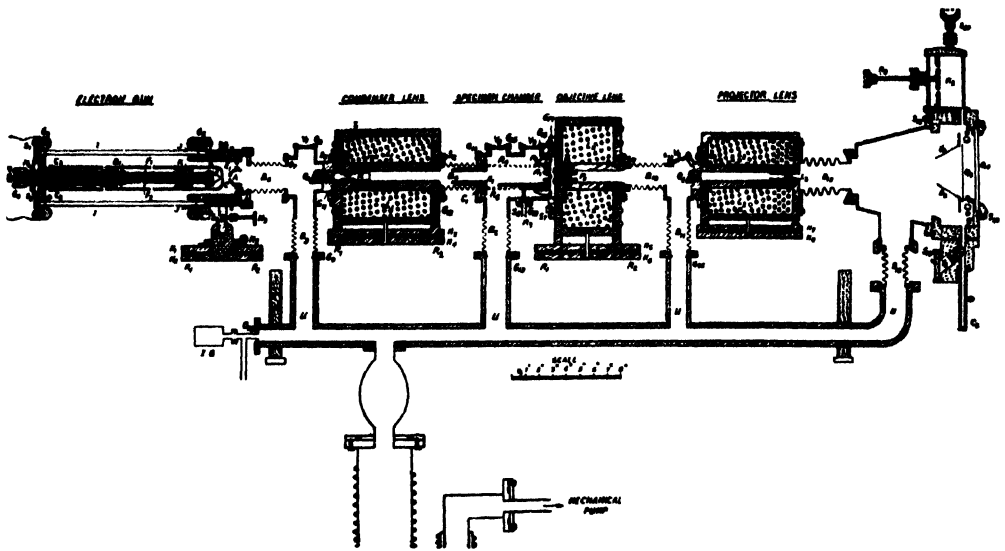

FIG. 2

Sectional Diagram of the New Microscope

features which distinguish this unit from all the instruments described earlier. This instrument is a completely horizontal unit with different elements mounted on two stainless steel rods held in position by brass sleevings which can slide over the steel rods. It is thus possible to dismantle any part of the microscope without disturbing the rest. The distance between any two elements can be varied, it is also possible to interpose an extra element between two of the existing ones if desired. The instrument is thus essentially a research unit, very flexible in design and highly suited for investigations on electron-optical problems. Due to horizontal positioning each microscope element is approachable from all sides and the image formed on the final fluorescent screen can be demonstrated to a number of people simultaneously. The instrument consists of the usual three lenses, the condenser, the objective and projector lenses and is designed for a maximum electronic magnification of twenty thousand diameters.

The electron gun, the condenser, the objective and the projector lenses are supported on separate carriages consisting of pairs of horizontal brass plates H_1 H_2, H_3 H_4, H_5 H_6, and H_7 H_8. Any of the pairs of brass plates can slide together in a horizontal plane perpendicular to the axis of the microscope on a pair of stainless steel guide rods R_1 R_2, fixed to the frame of the instrument. The upper plates H_1, H_3, H_5 and H_7 supporting the microscope elements can also be raised or lowered with respect to the lower plates by a set of screws. These two motions at right angles to the optic axis can be given to any element of the microscope. By means of transmission gear arrangement the operator,

sitting at the control table near the final fluorescent screen, can move any of the lenses or the gun for proper alignment. Each of the three lenses has four levelling screws by means of which the lens may be slightly inclined to the axis so as to allow for any asymmetry of the pole pieces. In addition to lateral motions, the gun can be slightly tilted about horizontal and vertical axes passing through the tip of the filament F, by means of the screws M_3 and M_2 respectively.

The different elements are connected with one another and with the vacuum manifold U by sylphon bellows so that relative movement is possible maintaining the vacuum. The length of the microscope column from the filament tip to the objective is 59 cm. and the length from the objective to the fluorescent screen Q_4 is 79 cms. For evacuating the microscope column an oil diffussion pump and a Cenco Hypervac 20 are used. The mechanical pump is housed in a specially designed underground chamber a little distance away from the microscope in order to reduce noise and vibration. A thermocouple gauge measures the fore-vacuum while the high vacuum within the microscope is indicated by an ionization gauge.

A. Illuminating System

The illuminating system consisting of the electron gun, the primary viewing screen Q_1 and the condenser lens L_1 is shown in the figure 3. The electron gun is a three electrode system consisting of the filament F, cathode shield C and the anode A. The filament consists of a .005 inch diameter tungsten wire bent into hair pin shape. The filament current leads F_1, F_2 consist of a steel cylinder surrounding a steel rod; the two are kept insulated from each other by means of a pyrex tube. The filament is heated by means of a high-frequency (150 kc/s) current and may be maintained at a maximum negative potential of 80 ekv. with respect to the anode which is earthed together with the main body of the microscope. The cathode shield is a cylinder of stainless steel with an 1/8 inch diameter aperture, located just in front of the filament tip. The filament is kept fixed axially within the cathode shield by means of an alsimag cylinder K. For changing the filament, a part of the cathode shield may be unscrewed at C_1. The cathode shield is insulated from the filament and may be suitably biased when it serves as a control grid. The distance between the filament tip and the centre of the shield can be varied by means of the adjusting screw M_1 at the high potential end.

The anode A is a copper hemisphere, drilled axially with an 1/8 inch hole to allow the beam to pass through. The distance between the anode and grid aperture is about 1 inch but may be adjusted by screwing at C_2. The anode is surrounded by a steel shield E_1 which cuts off X-radiation from the anode due to bombardment of high energy electrons. The high voltage insulator I consists of one ft. long pyrex cylinder metallised at the end

to which are soldered steel flanges *J* on either end. The complete filament assembly is held in position by the centering aluminium disc *D*. The whole
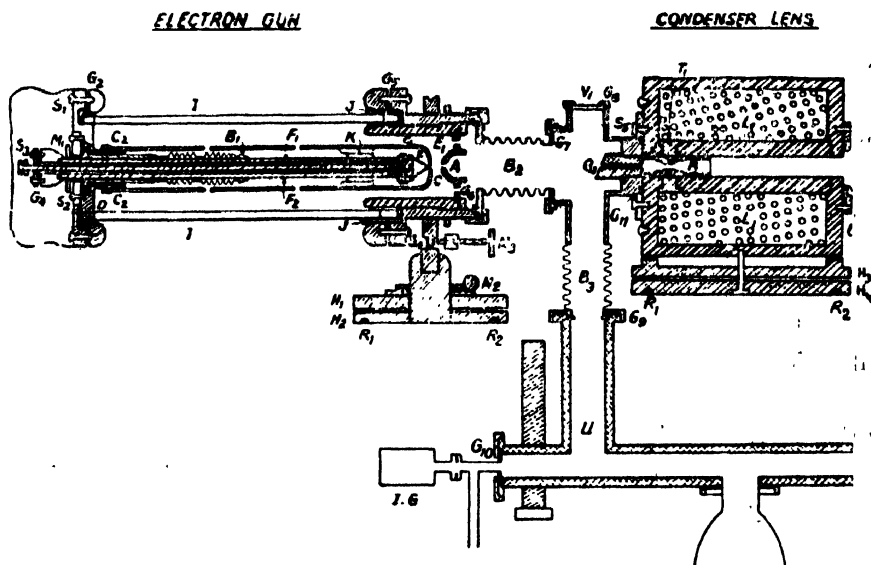

FIG. 3

Illuminating System of the New Microscope.

A anode, B_1-B_3 sylphon bellows, *C* cathode shield, *F* filament, G_1-G_{11} vacuum gaskets, H_1-H_4 brass carriages for movement of the electron gun and condenser lens, *I* metallised pyrex insulator, *J* steel flanges soldered to the insulator, *K* alsimag cylinder, L_1 condenser lens coil, M_1-M_3 adjusting screws for controlling the position of the electron gun, P_1 condenser pole piece, Q_1 primary viewing fluorescent screen, R_1, R_2 rods permitting horizontal motion of the gun and condenser lens, S_1–S_5 gasket tightening screws, T_1 brass spacer in condenser lens, *U* vacuum manifold, V_1 viewing port.

gun assembly is demountable and is made vacuum tight by means of the rubber gaskets $G_1 - G_6$ and gasket tightening screws $S_1 - S_1$. For a change of filament, the filament unit together with the cathode shield can be taken out by unscrewing S_1.

The electron beam after leaving the gun assembly falls on the primary fluorescent screen Q_1 which is a copper rod with an axially drilled hole. This allows the central portion of the beam to pass through and enter the condenser lens L_1. V_1 is a small port for viewing the crosssection of the illuminating beam at this position.

The condenser lens L_1 is also shown in Fig. 3. It consists of a coil housed in an iron cylinder of length $7\frac{1}{4}$ inches, external diameter $6\frac{1}{2}$ inches and internal diameter 5/8 inch. The magnetic circuit is completed through the iron except for a small gap bridged by non-magnetic brass piece T_1, through which the field extends into the vacuum. The field is further concentrated by the insertion of accurately-machined pole pieces P_1 of special design, drilled with a central hole for the passage

of electrons. The coil of the condenser lens is outside the vacuum system ; only the inner hole of 5/8 inch diameter is connected to the vacuum system.

B. Specimen Chamber

. A vertical section of the specimen chamber through the optic axis is shown in Fig. 4. The object stage N is held in position by means of four
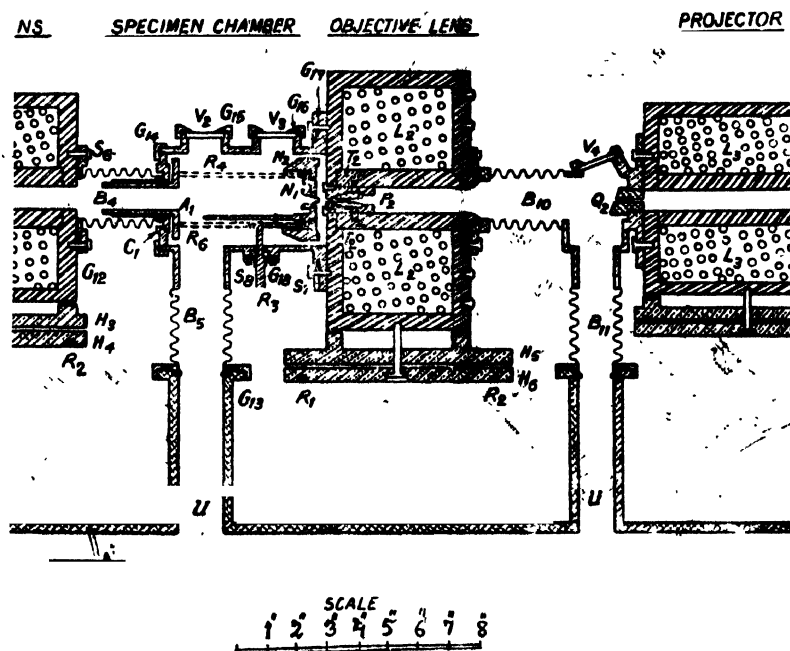

FIG. 4

Objective and Specimen Chamber of the New Microscope.

A_1 brass end piece, B., B_5, B_{10}, B_{11} sylphon connections, C_1 brass cylinder. $G_{12}-G_1'$ vacuum gaskets, H_5, H_6 brass carriage for movement of objective lens, L_2 objective lens coil, N_1, N_2 object stage with the movable part N_1 within the fixed part N_2, P_2 object lens pole piece, Q_2 intermediate viewing screen, R_1, R_2 rods permitting horizontal motion of objective lens, R_3 sterio-motion rod, R_1-R_6 horizontal supporting rods for specimen stage, S_6-S_8 tightening screws, T_2 brass spacer in objective lens, U vacuum manifold, V_2, V_{3}, V_4 viewing ports.

horizontal rods $R_4 - R_7'$, attached to the end piece A_1 which fits tightly into the brass cylinder C_1. For stereophotography the part N_1 of the object stage can be rotated through a small angle within the fixed part N_2. The tilting of the stage for stereography is accomplished by means of the rod R_4 which projects from the lower side of the chamber, through a Wilson seal. Two viewing ports V_2 and V_3 on the upper side of the chamber allow a view of the specimen stage through all operations.

A vertical section of the object chamber perpendicular to optic axis is shown in figure 5. Four hydraulic sylphon bellow $B_6 - B_9$ are
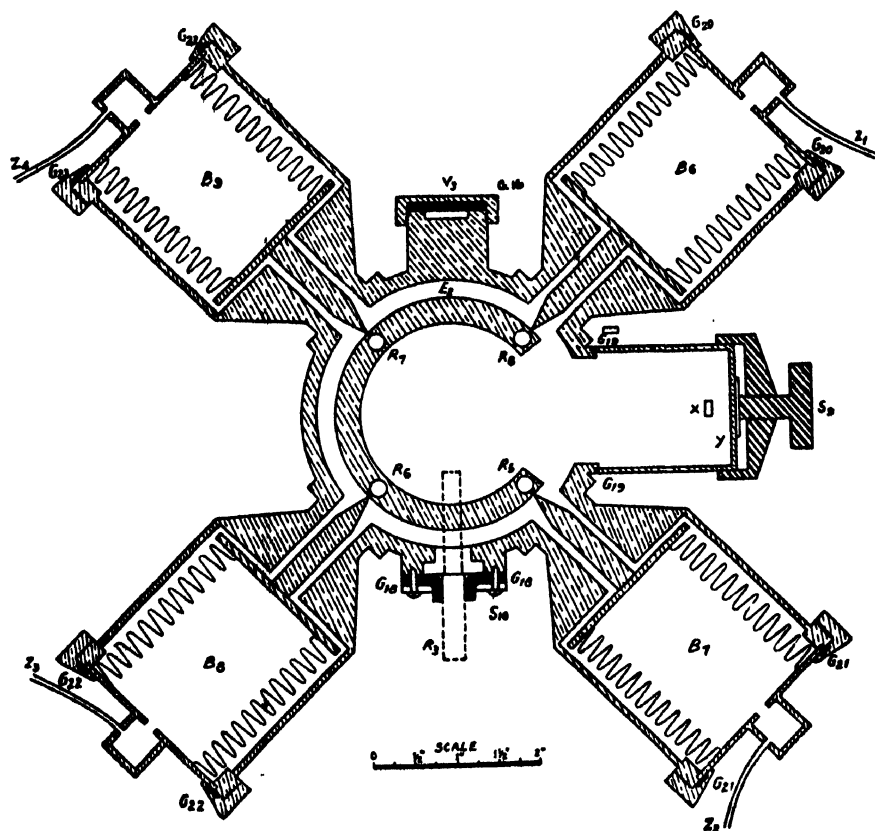
FIG. 5

Mechanism for Movement of Specimen Stage.

B_6-B_9 hydraulically operated sylphon bellows, E_2 brass ring holding the horizontal rods R_4-R_6 together, $G_{18}-G_{23}$ vacuum gaskets, R_3 sterio motion rod, R_4-R_7 horizontal brass supporting rods, S_9 tightening screw for air-lock chamber, V_3 viewing port, X forked handle for removing specimen from stage to air-lock chamber and *vice versa*, Y air-lock chamber, Z_1-Z_4 hydraulic connections from the sylphons to the control panel.

fitted at 90° to each other for moving the object stage in two perpendicular directions at right angles to the optic axis. In normal position the tips of the bellows rest in four accurately drilled holes in a brass ring E_2 fixed to the carrier rods R_4—R_6. The four bellows, slightly compressed, press against each other and help to keep the stage accurately centered and also at a fixed distance relative to the object lens pole piece P_2 (Fig. 4). By compressing and expanding the hydraulic sylphons it is possible to move the stage in a plane perpendicular to the microscope axis and thus explore different parts of the specimen. The fluid from the sylphons B_6 − B_9 passes through small copper tubes Z_1 − Z_4 to a corresponding unit on the control desk. It is thus possible to move the stage while looking at the image on the final fluorescent screen Q_4. The unit on the control desk is provided

with both coarse and fine control adjustments, so that the specimen can be placed accurately in any desired position. The arrangement has no backlash and gives a very smooth motion of the specimen across the field of view.

The specimen change operation is performed with the help of the airlock arrangement shown in Fig. 6 which is a vertical section of the unit. When removing the specimen from the vacuum, a phosphor bronze fork XX holds the bucket W and a 90° rotation of the fork handle from outside releases the bucket from the specimen stage and brings it into the air-lock chamber Y_1. In this position the bucket is pressed from behind by the brass rod R_8 carrying the gasket G_{27}. Half a turn of the nut C_1, presses the gasket G_{27} against the back of the bucket and seals it off from the microscope vacuum. While the bucket is held in this position, air is introduced into the airlock
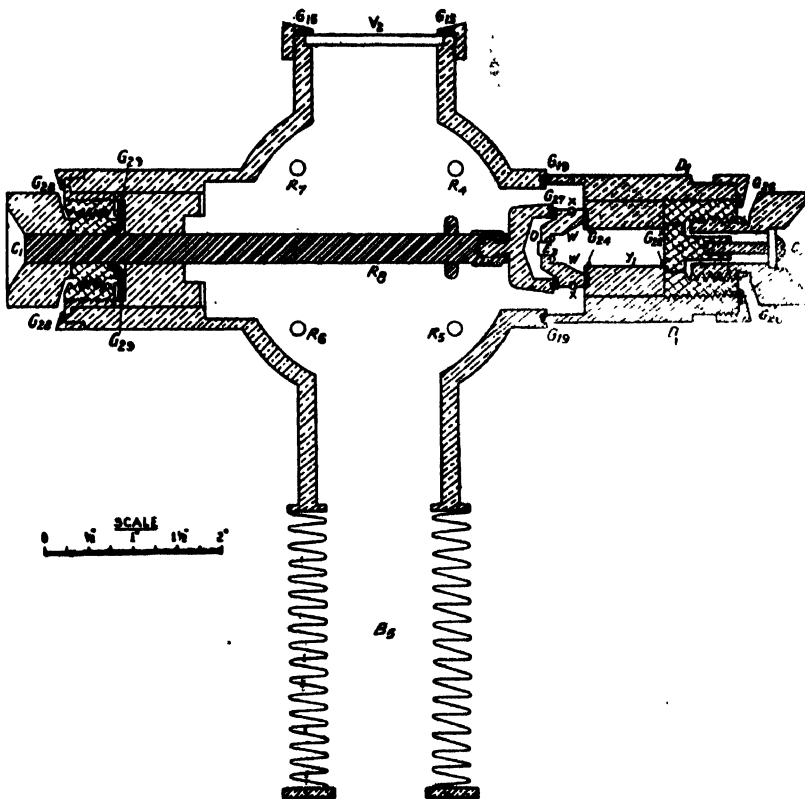

FIG. 6

Vertical Section of the Airlock Chamber at Right Angles to the Optic Axis.

B_8 sylphon connection to the manifold, C_1, C_2 split nuts for closing and opening the airlock chamber, D_1 brass box containing airlock arrangement, E_3 specimen holder, G_{18}, G_{19}, G_{24}, G_{29} vacuum gaskets, O object, R_4-R_7 four brass rods which support the stage and allow it to be moved by the hydraulic stage shifter, R_8 rod for sealing off (by means of gasket G_{27}) the specimen from the microscope vacuum, operating through the Wilson seal G_{29}, V_2 viewing window, W section of the bucket which carries the specimen from the stage to airlock chamber Y_1 or vice versa, Y_1 airlock chamber.

chamber Y_1 by releasing the nut C_2. The specimen holder E_3 is now removed, through the opening made by removal of C_2.

The procedure is reversed for introduction of new specimens into the vacuum system. When a new specimen has been replaced with the bucket in the position shown in Fig. 6, the nut C_2 is locked in first thereby isolating the airlock chamber Y_1 from the external atmosphere by means of gasket G_{25}. The rod R_8 is now pushed back and by means of the fork XX the bucket is replaced in the specimen stage N_1. Once the bucket is held by the specimen stage, it is freed from the fork and can then be moved about by means of hydraulic arrangement described previously. Only the air trapped in the small chamber Y_1 is introduced into the microscope each time a specimen is replaced. This arrangement permits quick replacement of specimens without seriously disturbing internal vacuum.

The whole airlock arrangement is contained in a brass box D_1 which is sealed to the specimen chamber by means of gasket G_{19} and clamping screw S_9 (Fig. 5).

C. Objective Lens

The objective lens L_2 is shown in Fig. 4. This coil is bigger than the condenser lens coil L_1, with an inner diameter 2 inches and outer diameter $7\frac{3}{4}$ inches. The whole coil is shrouded in an iron cylinder except for the brass spacer T_2. This lens contains a specially designed pole piece P_2 of very short focal length. As asymmetry of the pole piece finally limits the resolving power, great care was taken during construction so as to minimise asymmetries as far as possible. The objective lens forms an intermediate image on the intermediate viewing screen Q_2 attached to the projector lens.

D. Projector Lens

The section of the projector lens L_3 together with the photographic unit is shown in Fig. 7. The projector lens coil is similar in construction to that of the condenser coil. The projector pole piece P_3 is inserted at the projector coil end remote from the gun. A copper rod with an axial hole and a coat of fluorescent material is fixed to the other end of the projector lens. This constitutes the intermediate fluorescent screen Q_2.

E. Photographic Unit

Fig. 7 shows a vertical section of the photographic unit through the optic axis. The final image may be obtained either on the flourescent screen Q_4 or intercepted by the photographic plate Q_3. The plate magazine K_2 holds about twenty photographic plates and is demountable for loading in the dark room. The plates are moved forward by a pressure pad, the pressure being maintained by the vacuum. In order to release one plate into

the photochamber the knob R_9 on the back of the photochamber is pulled. One plate then drops on to the carrier bar R_{10}, which can be moved from
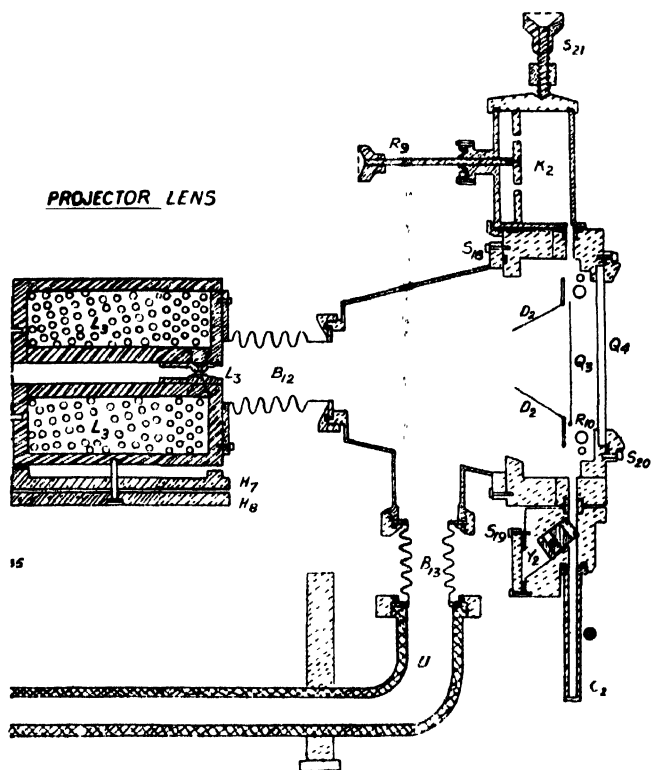

FIG. 7

Vertical Section of the Projector Lens and Photographic Chamber through Optic Axis A_2 terminal aluminium plate, B_{12}, B_{13} sylphon connections to the rest of the microscope, C_2 plate receiver, D_2 adjustable photographic shutter, F_4 pressure pad holding the plates in readiness for dropping one at a time, $G_{37} - G_{50}$ vacuum gaskets, K_2 photographic plate magazine holding about twelve $3\frac{1}{4}'' \times \frac{1}{4}''$ plates, L_3 projector lens coil, R_7 knob for releasing one plate at a time, P_3 projector lens pole piece, Q_2 intermediate flourescent screen, Q_3 photographic plate in position and carried by the carrier bar R_{10}, Q_4 final flourescent screen 6'' diameter, S_{16}, S_{19}–S_{21} gasket tightening screws, U vacuum manifold connection, Y_2 valve interlock into the airlock chamber.

outside and the plate held in any position in the exposure field. Four exposures can be made on a single photographic plate. After the exposure is made the shutter D_2 is closed and the carrier bar lowered until the plate drops into the plate receiver box C_2. The air-lock valve Y_2 is now closed, air introduced into the receiver box and the plates removed for development. By means of a knob it is possible to swing the whole plate carrier and shutter mechanism out of the path of the electron beam so that the total area of the fluorescent screen (5 inches in diameter) can be utilised for visual observation of the micrograph.

The whole photographic unit is mounted on stainless steel guide rods by means of brass sleevings (Fig. 1, Plate XVIA). The unit is connected to the vacuum manifold and the projector lens by means of sylphon bellows B_{12} and B_{13}.

<div align="center">ELECTRONIC CONTROL CIRCUITS</div>

<div align="center">*A. High Voltage Supply for Electron Gun*</div>

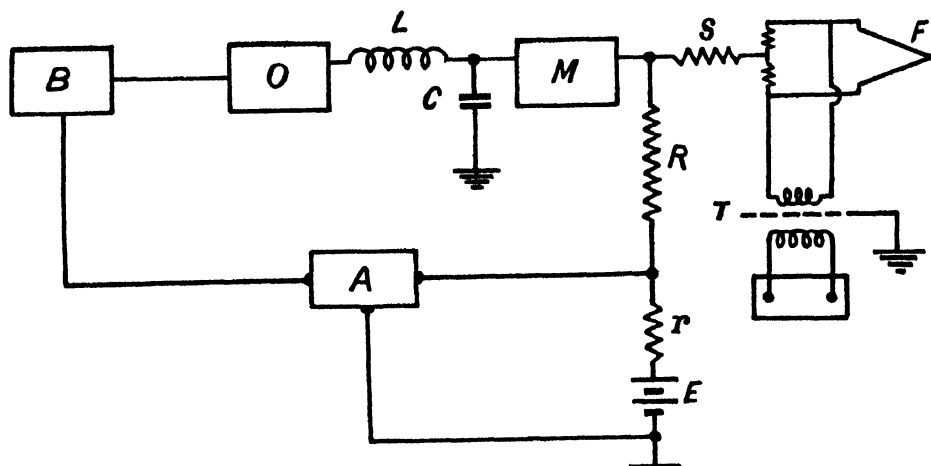Figure 8, Plate XVIB is an illustration of the r.f. high voltage unit. The schematic diagram of the high voltage circuit is shown in Fig. 9.

<div align="center">FIG. 9</div>

<div align="center">Schematic diagram of high voltage generator and regulator</div>

The circuit arrangement follows basically that developed by Hillier and Vance (1941). A high frequency oscillator *O* supplies 500 volts at 50 kc/sec. to the series resonant circuit consisting of *L* and *C* of resonance frequency 50 kc/sec. The resonant circuit, by virtue of its inherent characteristic, steps up the input voltage Q times across the terminals of the condenser *C*, Q being the efficiency factor of the series resonant circuit. Q in our case being about 40, the voltage across *C* is 20 kv at 50 kc/s. This voltage is subsequently quadrupled and rectified by the unit M in the manner first described by Greinacher (1921) and later used by Cockroft and Walton (1932). The unit M incorporates a resistance-capacity network which serves to filter out the ripple content from the output voltage. The output, thus multiplied, rectified and smoothed, is 80 kV negative relative to the ground and is connected to the filament *F* of the microscope through a current limiting resistance S.

The stability of this high voltage is an important consideration for best resolution of the electron microscope. In order that want of sharpness in the final image, due to fluctuations in the high voltage supply alone, will not exceed 10 Å. the maximum permissible variation in the high voltage supply
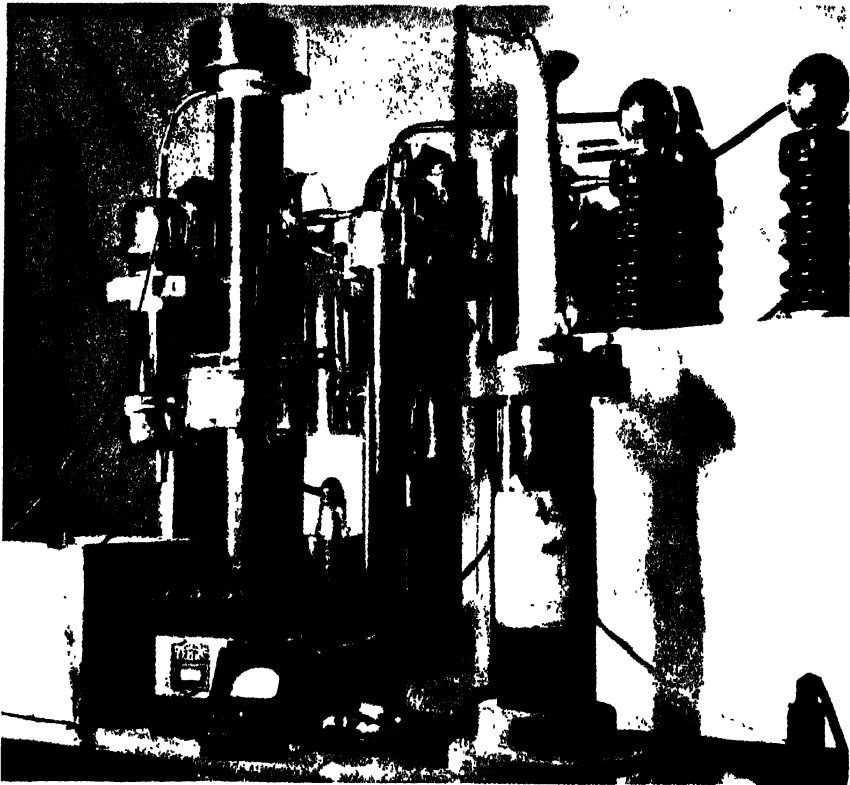
Fig. 8

Photograph of High Frequency Voltage Unit.

is 1 part in 10, 000. This degree of stabilisation is achieved by making use of the principle of inverse feed back. By means of the voltage divider $R + r$ across the high tension generated at M, a part of the output voltage is balanced by the dry battery E and the difference is applied to the direct current amplifier A. Any out of balance voltage due to instability is amplified by A and then supplied to the electronic regulator B which in turn controls the high tension anode input to the oscillator O. This feed-back amplifier arrangement is such that the variation in the oscillator output is in antiphase to those of the rectifier quadrupler unit and is capable of neutralising the original variation in high tension.

The d. c. amplifier A consists of 2 stages, the output variation of which is in the same phase as that of input. This affects the electronic regulator B which acts as a series load to the oscillator tube in O. The electronic regulator B is similar to that used for regulating currents to various lenses (described below).

In addition to the above electronic voltage regulating system the whole a. c. supply is pre-stabilised by a constant voltage transformer of saturable reactor type.

B. Microscope Filament Supply

The filament of an electron microscope usually requires 2-3 amperes at about 2 volts depending on the nature of the filament used. The filament supply has to be maintained at a very high negative voltage with respect to ground and also has to be accurately controllable for varying the intensity of the beam through the microscope. In the present unit, the microscope filament is heated by r. f. current of about 150 kc/s. This reduces the problem of electrostatic shielding and also simplifies that of high voltage insulation. The filament current is supplied by the secondary of a r. f. transformer T through the primary of which passes the r. f. current from an oscillator. The anode voltage of the oscillator is supplied through a variable resistance by means of which the output of the oscillator can be easily regulated thereby controlling the microscope filament current.

The anode circuit of the oscillator is completed through a relay system, operated by the current from the ionisation gauge measuring the vacuum. Whenever the vacuum inside the microscope column falls below the limit, at which it is safe to operate the instrument, the ionisation gauge current becomes excessive and this automatically disconnects the anode voltage. The oscillation ceases at once and the filament of the microscope is thus saved from being burnt off.

C. Current Regulators for Electromagnetic Lenses

In a magnetic electron microscope it is essential to keep the currents through the various lens coils strictly constant. The stabilisation tolerences

of the different current supplies for a resultant image unsharpness of 10 Å. can be computed theoretically (Zworykin, et al 1946) ; the values so obtained for an optimum aperture are as shown below :

Supply	Tolerance $\Delta I / I$
Condenser lens	1.0×10^{-3}
Objective lens	5.5×10^{-5}
Projector lens	1.3×10^{-4}

The three lenses have three separate electronic regulators of the general type shown in figure 10.

A number of 6L6 beam tetrodes connected in parallel serve as the main power tubes driving the magnetising current through the lens coil L in series with a variable resistance R (eventually a number of resistors providing the coarse, medium and fine controls). The voltage drop produced by the load current on passing through the resistor R is compared to that of a dry battery and the difference is applied to the grid of a 6SJ7 tube. The anode voltage of this tube controls the grid excitation of the 6L6 tubes. The circuit is thus essentially a degenerative voltage regulator described by Hunt and Hickman (1939). It maintains a constant voltage across the control resistor R and with constant load, it acts as a good current regulator at very low frequencies. The regulator action is further helped by the screen connection of the 6SJ7 as shown in the Fig. 10. Variation in the current is obtained by variation of R.
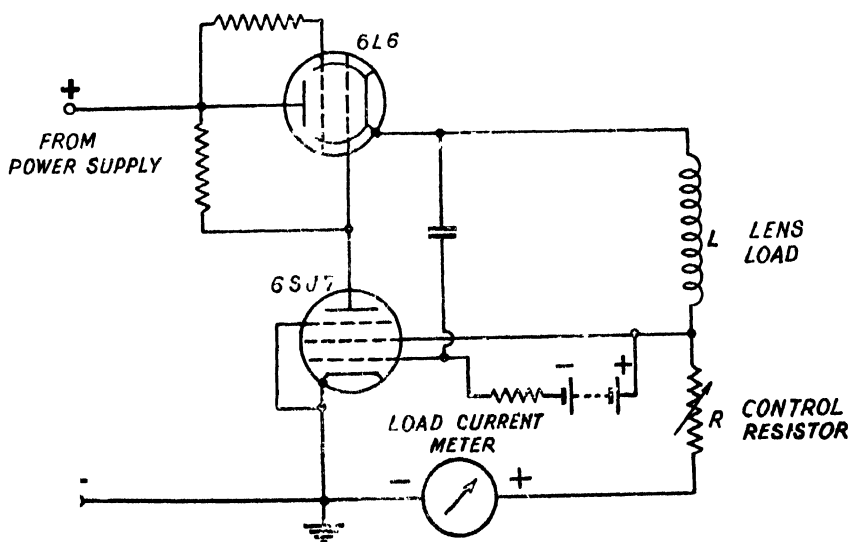

Fig. 10
Circuit diagram of the lens-current regulators

The simple electronic circuit alone is incapable of giving the required degree of stability. The primary a. c. supply is further pre-stabilised by a conventional constant voltage transformer of saturable reactor type.

With this circuit, it has been possible to secure the required order of stability. Slow drifts arising from changes in resistance due to heating or changes in thermionic emission, etc., have been observed, which have been minimised to some extent by using stabilised a. c. voltage to heat the filament of the tubes.

D. *Vacuum Gauge and Relay Circuits*

The electronic circuit also includes a thermocouple and an ionisation gauge for measurement of microscope vacuum. The thermocouple gauge is fitted before the diffusion pump and measures the rough vacuum produced by the mechanical pump. The ionisation gauge is placed after the diffusion pump very close to the microscope filament. It indicates the final vacuum produced at this point.

A relay is fitted in the ionisation gauge circuit which automatically shuts off the high voltage and the heating current of the microscope filament as soon as the pressure inside the microscope becomes more than 3×10^{-4}mm of mercury. Thus the vacuum gauge and the relay system protects the microscope from damage due to accidental failure of the high vacuum as a result of a suddenly developed leak. A second relay is incorporated in the high voltage circuit, which shuts off the high voltage, if for any reason, the current drawn from the high voltage becomes excessive. This relay therefore protects [the components of high voltage circuit in case of an accidental failure of electric insulation.

CONCLUSION

In this preliminary report the constructional details of the new electron microscope have been given.

It will be seen from the introduction, that in every country the electron microscopes were first developed in the university laboratories. It was only after a great deal of experience had been gained, during researches carried out in these laboratories, that it was possible to produce an electron microscope commercially, first in Germany nearly ten years ago and then in U. S. A., and only last year in countries like England, Holland and France. This paper contains an account of the attempt to construct for the first time in a university laboratory in this country an instrument of this type.

advice and guidance in designing the instrument and help in the procurement of parts from U. S. A. Mr. Bert F. Bubb of Stanford University has been of great assistance in the mechanical construction as well as in designing. Apart from the mechanical parts, the complete electronic power system consisting of the high frequency oscillators, both for the microscope filament heating as well as for the rectified 80,000 volt d.c. source for the electron gun, the highly stabilised current supplies for the three electromagnetic lenses, the vacuum gauge and the safety relay systems were built up in our laboratory. Some of the local radio manufacturers particularly Messrs. Indian Radio Institute and India Radio Manufacturing Co. of Calcutta, have helped us by making high Q radio frequency coils and transformers according to our requirements.

The authors are thankful to Mr. B. M. Banerji of this laboratory for some useful suggestions on circuit problems. They are also very much indebted to Prof. M. N. Saha for his constant encouragement and enthusiastic help in this project.

It is a great pleasure to acknowledge with thanks the gift of Rupees 17,500 made by Dr. B. C. Law for the purchase of components for this microscope.

INSTITUTE OF NUCLEAR PHYSICS
      CALCUTTA UNIVERSITY

R E F E R E N C E S

Ardenne, M. v., 1940 Z. Phy, 115, 339.
Ardenne, M. v., 1941, Z. Phys. 177, 657.
Bachman, C. H. and Ramo, S., 1943, J. Appl. Phys., 14, 155.
Boersch, H., 1942, Phys. Z., 43., 515.
Borries, B. v. and Ruska, E., 1939, Naturwiss., 27, 577.
Borries, B. v. and Ruska. E., 1940, Siemens Z., 20, 217.
Brüche, E. and Hagen, E , 1939. Naturwiss., 27, 809.
Brüche, E. and Johannson, H., 1932a, Naturwiss, 20, 353.
Brüche, E. and Johannson, H., 1932b, Ann. d. Phy., 15, 145.
Burton, E. F., Hillier, J. and Prebus, A., 1939, Phys. Rev., 56, 1171.
Busch, H., 1926, Ann d. Phys., 81, 974.
Cockroft, J. D. and Walton, E. T. S., 1032, Proc. Roy. Soc.A, 136. 619.
Davisson, C. J. and Calbick, C. J., 1931, Phys. Rev., 38, 585.
Davisson, C. J. and Calbick, C. J , 1932, Phys. Rev., 42, 580.
Greinacher, H., 1921, Z. Phys., 4, 195.
Haine, M. E., 1947, Engineering, 164, 4249, 20.
Hillier, J. and Vance, A. W , 1941, Proc. Inst. Rad. Eng , 29, 167.
Hunt, F. V. and Hickman, R. W., 1939, Rev. Sci. Instrum., 10, 9
Knoll, M. and Ruska. E. 1931, Z. Techn. Phys., 12, 389.
Knoll, M , and Ruska, E. 1932, Z. Phys., 78, 318.
Mahl, H., 1939, Z. Techn. Phys., 20, 316.
Mahl, H., 1940, Jhrb. der. A. E. G. Forschung, 7, 43.

Martin, L. C., Whelpton, R. V. and Parnum, D. H., 1937, *J Sci. Instrum,* **14**, 14.

Marton, L., 1935, *Bull. Acad Roy. Belg,* **21**, 606.

Marton, L., Banca, M. C. and Bender, J. F., 1940 *R. C. A. Review,* **5**, 232.

Marton, L , 1940, *Phys. Rev.,* **58**, 57.

Marton, L., 1945, *Jour. Appl. Phys ,* **16**, 131.

Müller, H. O. and Ruska, E. 1941, *Koloidzschr., Z,* **96**, 21

Poole, J. B., 1947, *Philips Techn. Rev ,* **9**, 33.

Prebus, A 1942, *Eng. Exp. Sta. News. Columbus,* **14**, 6.

Prebus, A. and Hillier, J., 1939, *Canad. J. Research,* **A17**, 49.

Ruska, E., 1934, *Z. Phys.,* **87**, 580.

Vance, A. W., 1941, *R. C. A. Review,* **5**, 293

Zworykin, V. K., Hillier, J., and Vance, A. W., 1941a, *Elec. Eng.* **60**, 157.

Zworykin, V. K., Hillier, J., and Vance, A. W., 1941b, *Jour. App. Phys ,* **12**, 738.

Zworykin, V. K., Morton, G. A , Ramberg, E. G , Hillier, J., and Vance, A. W., 1946 "Electron optics and the Electron Microscope," John Wiley and Sons, Inc , New York, 214.

Zworykin, V. K , and Hillier, J., 1943, *J. Appl. Phys.,* **14**, 658.

TOMORROW'S INSTRUMENTS TODAY

RAJ-DER-KAR & CO.

COMMISSARIAT BUILDING

HORNBY ROAD

FORT

BOMBAY

OFFERS

FROM STOCK

GLASS METAL DIFFUSION PUMPS, METAL BOOSTE
PUMPS, OILS AMOILS OCTOILS OCTOIL,
BUTYL SABACATE

MANUFACTURED

By

DISTILLATION PRODUCTS
(U. S. A.)

SPENCER MICROSCOPE

CENCO HIGHVACS

BESLER EPIDIASCOPE

COMPLETE WITH FILM STRIP ARRANGEMENTS

We are now manufacturing :

* Soxhlet Extraction sets of 100cc, 250cc and 1000cc capacity
* B. S. S. Pattern Viscometers
* Kipp's Apparatus of 1 litre and ½ litre capacity
  Petri Dishes of 3″ and 2″ diameter

A N D

ALL TYPES OF GRADUATED GLASSWARE

such as Measuring Flasks, Measuring Cylinders, Burettes, Pipettes, etc., etc.

Manufactured by :

INDUSTRIAL & ENGINEERING APPARATUS CO., LTD.

CHOTANI ESTATES, PROCTOR ROAD, BOMBAY, 7.

The following special publications of the Indian Association for the Cultivation of Science, 210, Bowbazar Street, Calcutta, are available at the prices shown against each of them :—

Subject	Author	Price Rs. A.
Methods in Scientific Research	Sir E. J. Russell	0 6 0
The Origin of the Planets	Sir James H. Jeans	0 6 0
Separation of Isotopes	Prof. F. W. Aston	0 6 0
Garnets and their Role in Nature	Sir Lewis L. Fermor	2 8 0
(1) The Royal Botanic Gardens, Kew.	Sir Arthur Hill	1 8 0
(2) Studies in the Germination of Seeds.	,,	
Interatomic Forces	Prof. J. E. Lennard-Jones	1 8
The Educational Aims and Practices of the California Institute of Technology.	R. A. Millikan	0 6 0
Active Nitrogen A New Theory.	Prof. S. K. Mitra	2 8 0
Theory of Valency and the Structure of Chemical Compounds.	Prof. P. Ray	3 0 0
Petroleum Resources of India	D. N. Wadia	2 8 0
The Role of the Electrical Double layer in the Electro Chemistry of Colloids.	J. N. Mukherjee	1 12 0

A discount of 25% is allowed to Booksellers and Agents.

RATES OF ADVERTISEMENTS

Third page of cover	Rs. 32, full page
do. do.	,, 20, half page
do. do.	,, 12, quarter page
Other pages	,, 25, full page
do.	,, 16, half page
do.	,, 10, quarter page

15% Commissions are allowed to *bonafide* publicity agents securing orders for advertisements.

CONTENTS

TO INTENDING AUTHORS

Manuscripts for publication should be sent to Mr. A. N. Banerjee, Assistant Editor, 210, Bowbazar Street, Calcutta.

The manuscript of each paper should contain in the beginning a short abstract of the paper.

All references to published papers should be given in the text by quoting the surname of the authors followed by the year of publication within braces, *e.g.*, Sen (1942). The actual references should be given in a list at the end of the paper according to the following specimen :

Sen, B. K., 1942, Volume rectification of crystals, *Ind. J. Phys.*, **16**, 329.

The references should be arranged alphabetically in the list.

All diagrams should be drawn on thick white paper in Indian ink, and letters and numbers in the diagrams should be written in pencil.

ON THE DISINTEGRATION OF Br⁸⁰ ISOMERS

By S. D. CHATTERJEE * and N. K. SAHA

ABSTRACT. The nuclear isomerism of Br⁸⁰ has been quantitatively studied The β-ray end-points of the isomers have been obtained by the absorption method of Widdowson and Champion. Using neutrons of thermal energy, the end-points of both the isomers happen to be the same viz at 2.02 eMV. When, however, fast neutrons from (Ra + Be) source are used for irradiation, the end-point of the 4.4 hr. isomer remains at 2.02 eMV, whilst that of the 18 mins. isomer shifts to 2.26 eMV. Further the excitation ratio of the two activities of 18 mins: 4.4 hr. period has been studied as a function of the excitation energy of the bromine nucleus as obtained by the bombardment of bromine by (i) slow neutrons, (ii) fast neutrons and (iii) a mixture of fast and slow neutrons. The excitation ratio in the three cases is found to be 2.1, 2.69 and 2.3 respectively, In order to explain these observations an energy level scheme of the Br⁸⁰ and Kr⁸⁰ nuclei has been suggested. According to this a metastable state of ~48 eKV and an excited state of ~0.2 eMV above the ground state are attributed to the Br⁸⁰ nucleus, while an excited state of ~0.5 eMV above the ground level of Kr⁸⁰ appears to fit well with a γ radiation of this energy observed by others

INTRODUCTION

The nuclear isomerism of the Br⁸⁰ characterised by the two half-life periods 18 mins. and 4.4 hrs. has been definitely established by the work of Bothe and Gentner (1937) on the nuclear photo-disintegration of bromine on the one hand and that of Fermi (1935) and his co-workers on the slow neutron capture by bromine on the other. All cases of nuclear isomerism so far obtained may be classified under one of the following heads.

(A) A metastable state decays into the stable ground state, with the emission of electrons and/or γ-rays and X-rays. (B) A metastable state decays into the unstable ground state with the emission of γ-rays and X-rays. The ground state, in its turn undergoes β-transformation and is transmuted into a neighbouring element. (C) Both metastable and ground state undergo β-transformation.

When a nucleus like Br⁸⁰ exhibits two half-life periods, the isomerism must be of either type B or type C. If the nucleus in its ground state is β-active, the isomeric state has choice of either going to the ground state by emission of γ-rays and X-rays or undergoing β-transformation, both processes ought to occur side by side. Actually, however, in all cases so far studied, the probability of one of the processes appears to be negligible compared with that of the other. The early attempts to observe the γ-radiation from

Br-isomers were unsuccessful. Pontecorvo (1938) first pointed out that the γ-rays due to transitions between the isomeric states is largely converted internally in the K or L shell. In the subsequent re-establishment of the shell, the characteristic X-rays of bromine are emitted. Theoretical calculations by Hebb and Uhlenbeck (1938) indicated a large conversion coefficient, which has been qualitatively confirmed by later experiments. Valley and McCreary (1939), have examined the low energy region of the β-spectrum and have photographed with a magnetic spectrograph two lines at 44 ± 1 eKV and 33.5 ± 1 eKV respectively due to K and L internal conversion in bromine of a γ-ray of energy 45 eKV. Siday (1939) has investigated the β-ray spectrum of the same isomer with a Wilson chamber and has confirmed conversion electrons due to a γ-ray of 43 ekV energy. Characteristic X-rays have also been observed in the process and identified as Br-Kα radiation by Abelson (1939), using a bent crystal spectrograph and by Russinow and Yusephovich (1939) from their selective absorption in Se, As, Hg and Pb. The observed γ-radiation showed a simple decay with 4.4 half-life period and must therefore be attributed to the transition of Br^{80} into a lower state of the same nucleus.

It has now been conclusively proved that the lower state of the Br^{80} nucleus is identical with the 18 min. isomer. This has been possible from the actual separation of the genetically related isomers by Segré Halford and Seaborg (1939). The separation is based on the recoil of the bromine nuclei caused by the ejection of an electron in the isomeric transition taking place in an active bromide solution. The separated Br was precipitated as AgBr and was found to decay with 18 mins. half-life period, even though the separation was carried out many hours after the preparation of the active compound. If the precipitation was repeated at intervals of several hours the same lot of active bromine solution being used, the initial activity of the precipitate decreased with a period of 4.4 hrs., the period of the upper state of Br^{80}, as expected. Devault and Libby (1939) also separated the bromine isomers by preparing a bromate solution containing Br^{80} and precipitating silver bromide from it. Immediately after precipitation the solution was found to be nearly inactive, and the authors think it probable that the upper state does not emit β-rays at all but decays to the ground state by emission of a γ-quantum, and that the apparent 4.4 hr. β-decay of Br^{80} is due to the equilibrium between the upper state and its 18 min. β-active product in the ground state. The decay of the nuclei in the ground state would then be partly compensated by the decay of the excited nuclei into the ground state and eventually in the equilibrium state and should show the period of the longer lived component.

It therefore, appears very probable that the nuclear isomerism of Br^{80} is of the type B, that is, there is no β-emission from the metastable state of Br^{80}, but it decays into the ground state through internal conversion and the

β-decay occurs only in the ground state of the nucleus. An importat consequence of this picture would be a single energy limit of the β-ray spectrum of Br^{80}. This fact has been examined by the works of Alichanian, Alichanow and Dzelepow (1938), Snell (1937), Dubridge, Barnes, Buck and Strain (1938), and others. Results obtained by these authors show that the spectral limits of the 18 mins. and 4.4 hrs. isomers obtained under low activation of the nucleus (*e.g.* by slow neutron bombardment of Br^{79}) almost coincide (between 2.00 and 2.02 eMV). The limit of the 18 mins. activity formed under high activation of the nucleus also appears to be the same within the limit of experimental error, although somewhat higher (~ 2.2 eMV) value has also been reported. The results of the various authors together with their methods of analysis and reactions used are collected in Table II. Snell also observed a penetrating γ-ray accompanying the 18 min. isomer, but none with the 4.4 hr. period.

The work of Dubridge *et. al.* mentioned above is particularly interesting in this connection. They obtained the Br^{80} isomers by the bombardment of Se with protons of energy 6.03 eMV, according to the process Se^{80} (p.n) Br^{80}. It was expected that the threshold energy of protons for the initial activation of the long period should lie lower than that for the short period. Actually, however, they found that the short period became observable at a proton energy of 2.9 eMV, while the longer period first came in at 3.1 eMV. A 5 hour bombardment at 3.0 eMV yielded no trace of the 4.4 hrs. period but there was a strong activity of the 18 min. period. This observation suggests that the excitation of the two isomers of Br^{80} depends on the activation of the intermediate nucleus to different energy states, and that for the 4.4 hr. isomer a somewhat higher energy-state is to be excited.

The activation ratio of the two isomers formed in different nuclear reactions (shown in Table III) may not therefore be the same, but may differ considerably according as the resulting nucleus and the energy state in which it is formed. A study of the excitation function of the two isomers would therefore be interesting, as this might reveal the energy states of the resulting nuclei and lead to a proper understanding of the nuclear isomerism of Br^{80} when the energy spectrum of the resulting β-rays is known. The reactions involving simple capture of neutrons in bromine would be particularly useful for the study of the excitation function as here the isomers are directly formed without particle emission. A possible method for this would be to study the spectral limits and the intensity ratio of the 18 mins. to 4.4 hrs. activities as a function of the neutron energy used when direct activation of bromine by a neutron beam is employed. Unfortunately the development of a precise method in this line is essentially concerned with the production of mono-kinetic neutrons, specially in the low energy range. The difficulties in this direction are considerable and progress has been in general slow. Preliminary experiment performed by us show that it is possible to investigate the intensity ratio and

the spectral limits at least under three conditions of activation of bromine, *c. g.* by (*a*) purely slow (thermal) neutrons, (*b*) purely fast neutrons and (*c*) a mixture of slow and fast neutrons. In the following pages an account is given of these experimental works. Different methods employed for the production of radioactive Br^{80} with the various degrees of activation are discussed below. Further a determination of the upper limits of the β-ray spectrum of Br^{80} isomers is made by using the modified absorption method of Widdowson and Champion (1938) and the results are compared with those of the orthodox absorption measurements. These measurements are also made with the slow neutron and the fast neutron activation of Br^{80}. Measurements of excitation ratio of the Br^{80} isomers (18 mins. : 4.4 hrs.) activated by neutrons of the different energies are described below. Finally, attempt is made to construct a disintegration scheme of the Br^{80} isomers which would elucidate the results of our measurements on the ratio of the intensities and the β-spectral limits of the isomers.

PRODUCTION OF RADIOACTIVE Br^{80}

(*a*) *Activation by thermal neutrons.*—The radio-bromines are formed with exceptional readiness by the action of thermal neutrons, the amplification co-efficient of water and paraffin being much greater than unity. The material to be activated was usually taken in the form of an organic liquid, *c. g* ethylene dibromide and placed in the centre of a paraffin block. A Ra + Be source of strength 68 millicuries was used. It was placed within the paraffin block in the vicinity of the material to be irradiated but separated from it by a small paraffin wall. The irradiation was continued for about four half-life periods of decay of the resultant radio-element. The concentration of the radio-element Br^{80} was effected by the well known Szilard and Chalmers' method. Fay and Paneth's electrical method of separation of radiobromine was also tried. A pair of rectangular nickel electrodes (one surface of each being coated with lamp black) was introduced into the vessel containing $C_2H_4Br_2$ to which a drop of HBr solution in water was added. An electric field of $\sim$ 220 volts was maintained between the electrodes during the period of irradiation. The radio-element was collected at the anode. Since Ni was found to be practically inactive for our purpose, the anode plate was directly used for necessary measurement. A simple method due to Sugden was also found useful for the study of radio-bromine. If the ethylene dibromide is activated, the radio-bromine, in whatever form it may be, can largely be removed by immersing suitable metal foils in it. On the other hand, non-metallic surfaces are not activated in this way. Accordingly very thin copper or silver foils, one side of which was covered with cellophane were immersed in ethylene dibromide that had been activated by bombardment with thermal neutrons. The thin foils were then used as a source of Br^{80}.

(*b*) *Activation by fast neutrons.*—When fast neutrons are used for irradiation, the methods described above are not suitable. Organic halogen

compounds like $C_2H_4Br_2$ (containing hydrogen), or solution of inorganic compounds like $NaBrO_4$ in water, which slow down the neutrons, were avoided. In order, therefore, to get thin layers of substance with high specific activity, it was necessary to use compounds having a high percentage of bromine. We started with PBr_7 (PBr_3 dissolved in the requisite amount of Br_2) as the material to be irradiated in a closed double-walled glass vessel (the inner wall being extremely thin). No further concentration of the radio-element was necessary, because the intensity of the activity was adequate for our purpose. It was soon evident, however, that P showed appreciable activity even after 20 hours' irradiation of neutrons, in addition to the usual activities of Br^{80}. It was therefore replaced by hexabromobenzol (C_6Br_6) which was specially prepared for the purpose. The hexabromobenzol formed fine feathery white crystals with m. p. about $315°C$. It was densely packed as layer about 2 mm. thick between two concentric cylinders (the outer of thick paper and the inner of thin cellophane). For irradiation with fast neutron, both the internal and external surfaces were covered with Cd foil of 0.5 mm. thickness, while the (Ra + Be) source, contained in a glass tube was slipped inside. The irradiation was carried out on a tall table in the middle of a room, away from paraffin or water surfaces. The C_6Br_6 cylinder, after irradiation, was used as the source of Br^{80}.

(c) *Activation by resonance neutrons.*—A paraffin block was taken with a ground surface of 20×20 cm. and a height of 15 cms. A hole was drilled into one of the vertical sides about 5 cms. from the top surface. The (Ra + Be) tube was pushed through the hole into the centre of the paraffin block. The material to be irradiated was used as a thin molten layer of C_6Br_6 or simply as the C_6Br_6 cylinder, placed on the top surface of the paraffin block, being wrapped on all sides by sheets of Cd. The material was then activated by resonance neutrons.

(d) *Activation by neutrons of different energies.*—Initially this was attempted by irradiating the C_6Br_6 cylinder with neutrons filtered through varying thickness of paraffin. It resulted in a poor activation of the material, due to the small solid angle subtended by the source at the irradiated material. The sources and the C_6Br_6 cylinder (encased within Cd) were therefore kept close together and then surrounded by water cylinders of gradually varying thickness. Although the arrangement actually produced a mixture of neutrons of different energies at the centre, it gave a rough idea as to how the excitation ratio of Br^{80} isomers changed with increasing thickness of water layer.

DETERMINATION OF THE UPPER LIMITS OF β-RAY SPECTRA OF Br^{80}

For the determination of the end-points of the β-ray spectra, the absorption method has been utilised. It has the advantages of being rapid

and experimentally simple, and of permitting the use of fairly weak sources. Unlike the methods of magnetic focussing and of the expansion chamber, the absorption method gives little information concerning the spectrum itself, but for the naturally occuring radioactive elements it has been found to give satisfactory values of the upper limit. The usual procedure for determining the upper limit from the absorption curve has been to plot the relative ionization or number of counts against thickness of absorber. The limit is then taken as the range corresponding to the point at which the curve becomes flat as estimated by the eye. Having obtained the maximum effective mass-range R in gm/cm^2 of Al, the energy E in eMV is obtained from Feather's formula :

$$R = 0.511E - 0.091$$

which is valid for values of $E > 0.7$ eMV. Thus, from Feather's extrapolation formula the maximum β-ray energy corresponding to the experimentally determined range in gm/cm^2 of Al is obtained.

With strong sources subtending a small solid angle at the detector, the uncertainty introduced by visual extrapolation may not be large. But, with weak sources, such as usually occur with induced radioactive elements, this tailing off is increased ; for, to obtain a sufficient intensity generally a large solid angle must be subtended at the source by the detector, whereupon a very large proportion of the β-rays fail to traverse the absorbing foils in an approximately normal direction. Further, the source itself (specially when chemical concentration cannot be carried out, for short half-life period or other reasons) must be of considerable thickness which introduces further inhomogenity in the β-rays. Moreover, since the weakness of the source introduces large statistical errors, the visual method is less satisfactory. In general, the visual estimate of the upper limit for absorption curves obtained with weak sources is too low. The recent investigations have produced two developments of the absorption method. The first has resulted in the evolution of methods whereby the best use of data obtained with the weakest sources may be made, and the second whereby the absorption curve may be used to provide further information regarding the energy spectrum.

Widdowson and Champion (1938) attempted an empirical solution of the first problem. They showed that the usual method of plotting the logarithm of the intensity against the thickness of the absorber and taking the upper limit of the thickness, at which the resulting linear curve cuts the ordinate corresponding to the background of the measuring apparatus, is open to question. For, it is clear that the β-particles themselves possess a finite upper energy limit and therefore there must be a corresponding upper limit to the absorption curve. This curve, therefore, should not be represented by an exponential function which has no finite upper limit.

On the other hand, they suggested that a curve represented by $Y = \Sigma_n a_n (X_0 - X)^n$, where a_n is a constant and X_0 is the thickness of the absorber corresponding to the upper limit, would appear satisfactory. Now,

the factors producing the absorption curve are very complex and some empirical formula must be adopted. They aimed to produce the simplest formula which would give a correct value for the end point X_0. They found out that a single term of the above polynomial was sufficient, the value of n being determined by the type of source and the arrangement of the apparatus. When the source was separated from the counter by a thin cellophane wall, $n = 4$, gave a satisfactory value for the end point. They also found that a single term of the polynomial with $n = 4$, when applied to the absorption curve gave a correct end point with widely varying radioactive elements.

In the present experiments, the geometrical conditions were closely similar to those adopted by Widdowson and Champion. A single tube-counter of duraluminium, 0.10 mm. wall thickness, 5 cms. long and 1.5 cms. in diameter was used vertically. The activated source consisted of the C_6Br_6 cylinder about 2 mm. thick and placed around the counter. The absorbing material, which was in the form of aluminium tubing, could be placed between the counter and the surrounding source. The solid angle subtended by the counter at a point on the source was as large as $4\pi/5$. The straggling of the β-rays was therefore very large, and for this reason alone some other method than the visual one was necessary in estimating the upper limit from the absorption curve. For the measurement of the β-ray end point of the 18 min. isomer, two exactly similar C_6Br_6 cylinders were taken. One was completely wrapped in Cd foil and irradiated with fast neutron by placing a (Ra + Be) tube in its middle, for 54 mins. While absorption measurement was being carried out with this cylinder, the other was being irradiated (without Cd cover) with the same (Ra + Be) source within a paraffin enclosure. Thus two samples were benig irradiated by fast and slow neutrons alternately while the comparative β-ray spectra were measured.

The β-ray end-point determination of the long life isomer (4.4 hrs.) was carried out by the method of Feather and also that of Widdowson and Champion. In the former case, a strong source of Br^{80} was obtained by the concentration of the radio-element from a large volume of $C_2H_4Br_2$ as has already been described. The absorption measurements were carried out by using flat Al absorber foils with a thin mica window G-M counter. In the second method, the hexabromobenzol cylinder (as used in the case of absorption measurement of the short-life isomer) was used. In both the cases the absorption measurements were started about 3 hours after the stoppage of neutron irradiation, when the intensity of the 18 min. isomer had been reduced to about 0.1 % of its initial value.

EXCITATION RATIO OF THE Br⁸⁰ ISOMERS ACTIVATED BY NEUTRONS OF DIFFERENT ENERGIES.

The mixture proportion of Br^{80} isomers, activated by various sources such as neutrons, protons, deuterons and γ-rays has been investigated by several workers. The first attempt in this line was made by Johnson and

Hamblin (1936). They exposed bromine to the combined action of fast and slow neutrons produced by a (Ra + Be) source and found that the relative initial activity could be expressed as the ratio of the initial activities of 18 min.: 4.4 hrs. = 8 : 3.5. Snell (1937) measured the relative strength of the initial activities under different conditions of activation. Using the reaction Br^{79} (d, p) Br^{80} with deuterons of energy 5 eMV, he found the ratio 2.1 : 1. The ratio became 0.8 : 1, when bombarded with fast (Li + D) neutrons. Soltan and Wertenstein (1938) bombarded bromine with fast neutrons having energies of 14 eMV from the (Li + D) reaction and obtained this ratio as 0.56 : 1.

Dubridge *et. al.* (1938) studied the formation of the isomeric Br^{80} periods, employing the reaction Se^{80} (p, n) Br^{80}. He obtained the threshold voltage of a particular activity by varying the energy of the proton beam. He found that the short period became observable at a proton energy of 2.9 eMV while the longer period first came in at 3.1 eMV. The ratio of the observed activities (after 10 min. bombardment) rose from 78 : 1 at 5.32 eMV to 2000 : 1 at 3.2 eMV. For an infinite bombardment, the ratios would be 6.7 : 1 at 5.3 eMV and 182 : 1 at 3.2 eMV.

Bothe and Gentner (1937) produced the nuclear photo-disintegration of bromine Br^{81} (γ, n) Br^{80} by the action of 17 eMV, γ-rays emitted by (Li + $_1H^1$) reaction. They found the ratio of the initial activities of 18 min. : 4.5 hrs. to be 0.9 : 1. Subsequently, using the 12 eMV, γ-rays emitted by the reaction (B + $_1H^1$), they obtained this ratio to be > 2.6.

In the present set of experiments a (Ra + Be) tube was used as a source of neutrons. The arrangements adopted for the irradiation of the material with varying energy of the neutron beam has been described in a previous section. The time of exposure was about 18 hours and conditions of measurements were indentical. The hexabromobenzol cylinder was exposed to neutron irradiation and put directly over a copper G-M counter (wall-thickness 0.05 mm.) within 1 min. of the cessation of the irradiation. The activity was followed during 7 hours in order to determine exactly the ratio of the two isomers. The counts were recorded at the intervals of 1 min. for the first one hour and subsequently at 5 mins. or 10 mins. intervals. Each experiment was repeated at least 10 times to reduce the statistical errors of the measurement. The average values of particle-counts were then plotted against the corresponding time on a logarithmic scale. The straight line representing the decay of the tail of the 4.4 hr. isomer was produced to meet the Y-axis and thus gave the initial activity of 4.4 hr. isomer. Next, the number of particle counts due to the long lived isomer for a particular time was deduced from the corresponding value shown by the combined decay curve. The fresh points thus obtained were connected by another straight line which obviously shows the 18 min. decay period. The extrapolated ordinate of this straight line at time zero gives the initial activity of the 18 min. isomer.

The ratio of the initial activities of the 18 min and 4.4 hrs. isomers were thus readily obtained. The influence of the third half-life period $T = 36$ hrs. was not evident under our experimental condition.

RESULTS

Our measurements of the absorption of β-particles emitted by Br^{80} (18 min. isomer) when excited by slow and fast neutrons are given in Table I. Y has been recorded as the ratio of the number of counts observed to the number which would have been observed had no absorber been present. Expressing Y in this manner as an intensity ratio allows the combination of results obtained with sources of different initial intensities. In deducing Y, suitable correction has been made for the decay of the source and for the presence of the background count. For the 18 min. isomer, the intensity ratio was taken as the ratio of the number of counts with absorber present for the period 1 to 6 mins. to the number of counts without absorber during the period of 7 to 13.5 mins. This choice gives the intensity ratio of about unity for zero absorber.

TABLE I

Thickness of absorber foils X		Mean Y	
mm.	(gm/cm²)	Br⁸⁰ (18 min) isomer activated by thermal neutrons.	Br⁸⁰ (18 min.) isomer activated by fast neutrons.
0.2	0.054	0.922	0.922
0.5	0.135	0.590	0.656
0.7	0.189	0.452	0.522
1 0	0.270	0.283	0 351
1.2	0.324	0.201	0.254
1.5	0 405	0.113	0.167
2.0	0.540	0.034	0.062

Fig. 1 shows the graph, where $y^{\frac{1}{4}}$ has been plotted against X, in the case of 18 min. isomer. The straight line I corresponds to the case when the 18 min. isomer has been formed by irradiation with thermal neutrons, while the straight line II represents the case when the same isomer has been formed by irradiation with fast neutrons from the (Ra + Be) source. The values of the upper limit are obtained from the intercepts on the X-axis made by the straight lines I and II.

Fig. 2 represents the absorption curve of Br^{80} (4.4 hr.) isomer obtained with a concentrated source and small solid angle conditions as originally attempted by Feather, while the inset figure represents the absorption curve of the same isomer according to the method of Widdowson and Champion.

The upper limits have been converted from gm/cm² to eMV, by making use of Widdowson and Champion's empirical formula

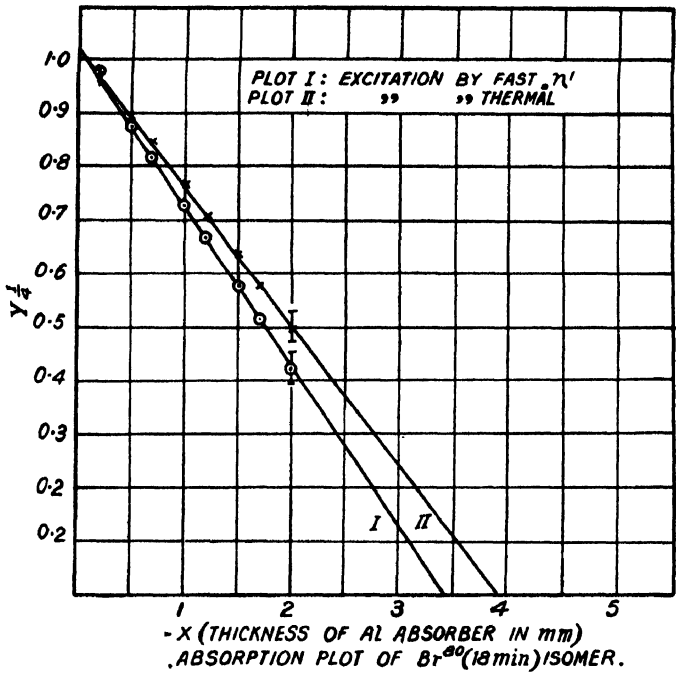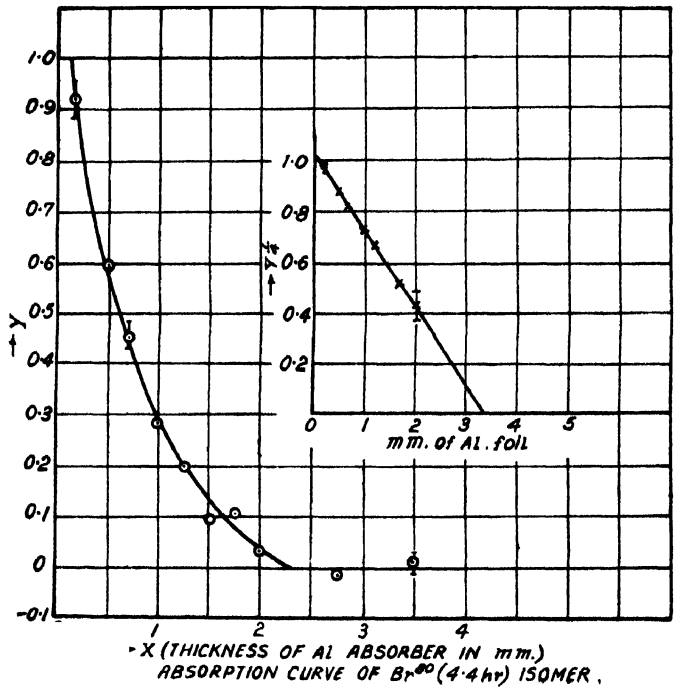$$R = 0.536\,\dot{E} - 0.165. \quad (E > 0.7\ \text{eMV})$$

FIG. 1

FIG. 2

were R is the range of β-rays in gm/cm^2, E=corresponding energy in eMV.

Table II shows the upper limit of the β-rays emitted by Br^{80} isomers as measured by others and ourselves under different experimental conditions.

The result of the decay measurements of both the Br^{80} isomers are shown in Fig. 3. The particle counts have been plotted as the function of time on a logarithmic scale. The lower curve represents the measurements when the activation was made by the bombardment of fast neutrons from a (Ra + Be) source under conditions specified before. The upper curve represents the case when entirely thermal neutrons were employed for necessary activation.

It is evident from these measurements that the initial activity ratio of the isomers 18 min : 4.4 hrs. is 2.69 : 1, when fast neutrons have been employed, which drops down to 2.1 : 1, when thermal neutrons are used instead. For a mixture of fast and thermal neutrons, the ratio was found to be 2.3 : 1.
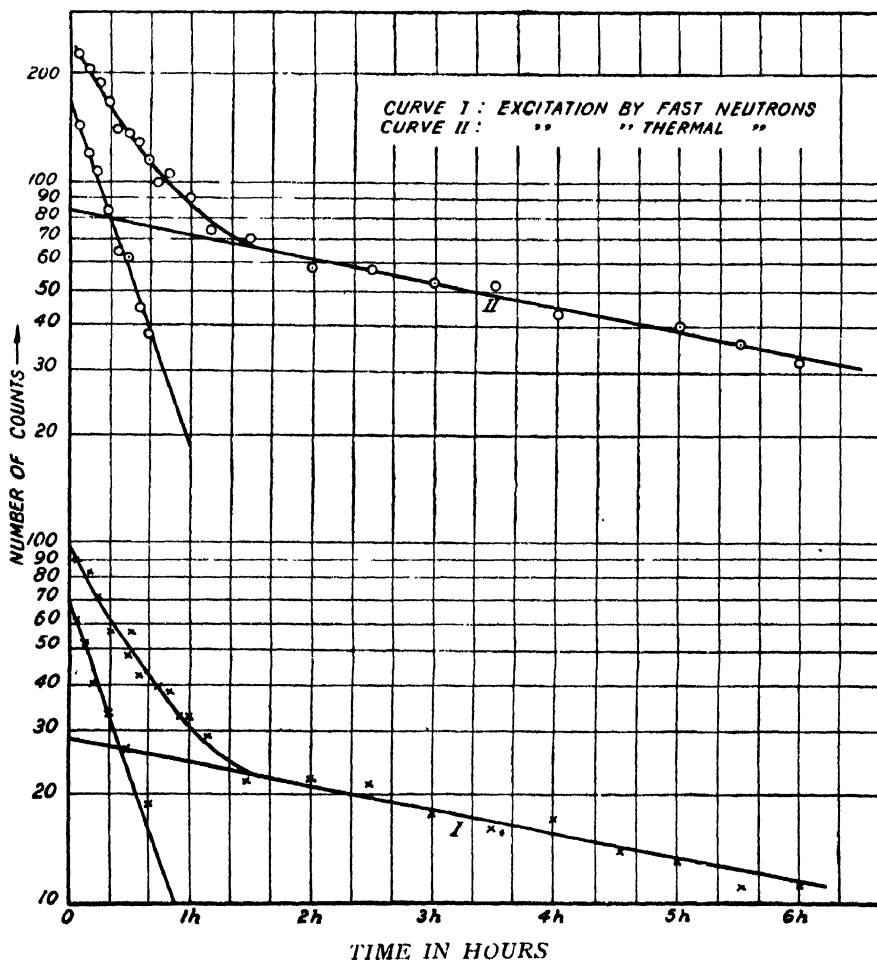

CURVE I : EXCITATION BY FAST NEUTRONS
CURVE II :   ,,   ,, THERMAL ,,

FIG. 3
Decay curve of Radioactive Br^{80} isomers.

Table III shows the value of the initial proportion of the isomers for saturated activation through different productional methods.

TABLE II

Reaction	Half-life	β-upper limit eMV	Method of Measure-ment
Br^{79} (n, γ) Br^{80} (slow neutrons)	18 min. 4.4 hrs.	2.00 2.05	Magnetic analysis (Alichanian and others, 1938)
Br^{79} (d, p) Br^{80} d≈5 eMV	18 min. 4.4 hrs.	2.2 2.0	Absorption method (Snell 1937)
Se^{80} (p, n) Br^{80} p≈5 eMV	18 min. 4.4 hrs.	2.2 2.0	Absorption method (Dubridge and others, 1938)
Same	Same	2.07 1.94	Cloud chamber (same authors)
Br^{79} (n, γ) Br^{80} (Thermal neutrons)	18 mins. 4.4 hrs.	2.03 2.02	Absorption method (Present authors)
Br^{79} (n, γ) Br^{80} Fast neutrons from (Ra+Be) source	18 mins. 4.4 hrs	2.26 2.02	do.

TABLE III

Reaction	Energy of the incident parti-cle eMV	Activity ratio $\dfrac{18 \text{ mins.}}{4.4 \text{ hrs.}}$	Intermediate nucleus	Excitation energy of the int. nucleus	Authors
Br^{79} (n, γ) Br^{80}	$E_n < 8$ (mostly 2)	2 69	Br^{80}	≈11 0	Present authors
	$E_n = 0$	2.1	,,	≈9.0	do.
	$E_n =$ mixture of fast and slow neutrons	2.3	,,	.,	do.
	$E_n = 53$ ev (Resonance)	2.1	,,	≈9.0	do.
	,,	2.18	.,	≈9.0	Fleischmann
	$E_n = 0$	2.0	,,	≈9.0	Soltan & Wertenstein
	$E_n =$ mixture of fast and slow neutrons	2.3	,,	,,	Johnson & Hamblin
Br^{79} (d, p) Br^{80}	$E_d ≈ 5$	2.1	Br^{81}	≈13	Snell
Br^{81} (γ, n) Br^{80}	$E ≈ 17$ $E ≈ 12$	0.9 >2.6	Br^{81} Br^{81}	17 12	Bothe & Gentner do.
Se^{80} (p, n) Br^{80}	$E_p = 4$ $E_p = 3.2$	15	Br^{81} ,,	9 8.2	Dubridge, Buck, Barnes & Strain
Br^{81} (n, 2n) Br^{80}	$E_n ≲ 14$,,	0.6 0.8	Br^{82} ,,	≈22 ,,	Soltan & Wertenstein Snell

DISCUSSION OF THE RESULTS

The results of Bothe and Gentner were obtained when Br^{81} was excited with Li^7 (p,γ) Be^8 γ-rays of energy $E_7 = 17$ eMV, yielding Br^{80} according to the reaction Br^{81} (γ, n) Br^{80}. The initial activation ratio of the isomers observed by them (Table III) was 0.9. On the other hand, when Br^{81} is excited with B^{11} (p, γ) C^{12} — γ-rays of lower energy $E = 12$ eMV, the above ratio rises to ~2.6. Bothe and Gentner have ascribed this shifting of the mixture-proportion to the relative difference in the gain of the 4.4 hour isomer. They concluded that the 4.4 hour isomer requires a stronger stimulation for its origin than that of the 18 min. isomer. In the light of the above view-point, they have attempted to explain the relative yield in the process Se^{80} (p, n) Br^{80} which has been investigated in details by Dubridge, Barnes, Buck and Strain. This reaction, just as in the case of Br^{80}(γ, n) Br^{80} results in the formation of Br^{81} as an intermediate nucleus. In the case of nuclear photo-effect, E (energy of stimulation) $= E\gamma$ simply. In the (p, n) reaction however, $E = N$ (binding energy of a neutron in Br^{81}) $+ E_n$ (K. E. of the neutron). At the threshold of the activation, $E_p = 3$ eMV, we have $E_n = 0$, i.e. $E = N + (E_p - 3) = E_p + 5$, for the binding energy of the neutron in this part of the periodic table is about 8 eMV. An inspection of the results of measurement of these two different kinds of experiments from Table III gives a rather uniform picture, viz., with decreased stimulating energy of Br^{81} nucleus, the mixture proportion 18 min : 4.4 hr. systematically rises from 0.9 at $E = 17$ eMV to 15 at $E = 8$ eMV. They therefore conclude that the 4.5 hr. isomer is a metastable state of excitation of the 18-min. isomer.

Coming to our own results, it may be seen that for $E_n = 0$, the ratio is 2.1 : 1. As the energy of the neutron beam is increased to $E_n = 8$ eMV (the majority having lower energy), the ratio increased to 2.69. Thus the ratio increases with the increase of stimulation energy. Apparently this result goes contrary to Bothe and Gentner's point of view.

The reason for this apparent contradiction appears to be that when the stimulation energy of the intermediate nucleus Br^{80} is increased, the upper state (4.4 hrs.), corresponding to one of the isomeric forms, is destroyed by a competing β-ray transition. On account of the higher stimulation energy of the intermediate nucleus, the final Br^{80} nucleus is pushed to an excited state whose energy is higher than that corresponding to the 4.4 hr. isomer. This excited nucleus decays with the emission of a β-particle with a half life period of 18 mins. This state of affairs may be envisaged by an analysis of the energy-level diagram of Br^{80}.

Fig. 4 represents an energy level diagram of Br^{80} based on the available experimental data. When excited by slow neutron (Fig. 4a), the 18-min. β-rays are associated with a transition from the ground state of Br^{80} to the ground state of Kr^{80}. On the other hand the 4.4 hr. isomer is due to a γ-transition from the metastable state to the ground state of Br^{80}. It has
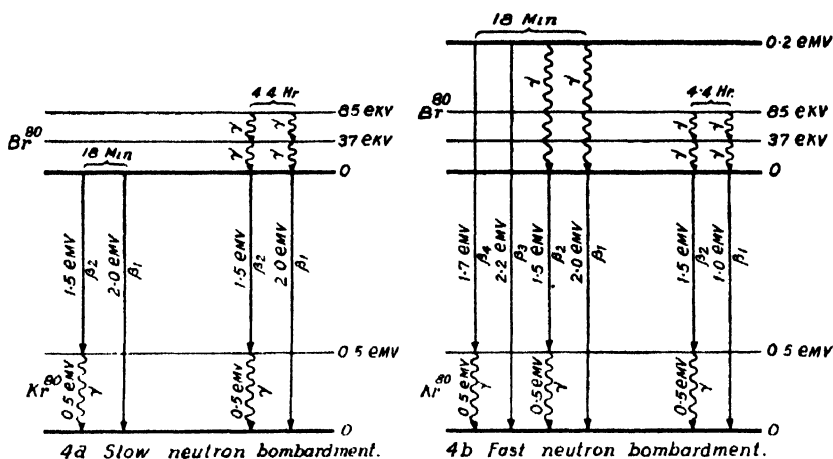
FIG. 4

Energy-levels and β-transition
schemes of Br⁸⁰.

also a fine structure. Grinberg and Roussinow (1940) pointed out that the total excitation energy of the Br⁸⁰ nucleus is 85 eKV leading to a metastable state of this energy. From this level there are transitions to a lower excited level which differs from the upper level by 48 eKV in energy. This transition proceeds by internal conversion only. From this lower excited state, the energy of which exceeds by some 37 eKV that of the ground state of Br⁸⁰, a γ-transition takes place, which is only partially associated with internal conversion. The conversion electrons corresponding to this second transition have been observed by Valley and McCreary. When bombarded by fast neutrons of (Ra + Be), some of the nuclei are pushed to a metastable excited level higher than that associated with the isomeric metastable level. This new level is ∼0.2 eMV above the ground level of Br⁸⁰ (Fig. 4b). From this level, the nucleus falls to the ground state of Kr⁸⁰ with the emission of β-rays by an allowed transition whose end-point energy is ∼2.2 eMV and whose half life happens to be 18 mins. There is another important possibility. From the excited level of Br⁸⁰, the nucleus falls to the ground state of Br⁸⁰ with the emission of γ-rays by an allowed transition. This takes place in such a short time that the β-emission which follows by transition from the resulting ground state of Br⁸⁰ to the ground (or excited) state of Kr⁸⁰ cannot compete with the γ-transition. As a result this emission of β-ray whose end-point energy is 2.0 eMV (or 1.5 eMV) possesses a mean half-life of 18 mins. When the transition is to the excited state of Kr⁸⁰, this β-transition should be followed by a γ-ray quantum of ∼0.5 eMV energy emitted by the excited Kr⁸⁰ nucleus in its transition to the ground state. A γ-ray (∼0 5 eMV) has actually been detected by Snell associated with the 18 min. isomer when produced by high energy deuterons and may be attributed to the above process.

The presence of an excited level of Kr^{80} situated about $\sim$0.5 eMV above its ground level is also supported by another evidence obtained from a critical analysis of the β-spectra of Br^{80}.

As pointed out by Bethe, Hoyle and Peierls (1939) and later by Saha (1939), the Fermi-theory of β-ray spectrum represents the correct law for a single β-disintegration process. But in most cases the observed spectrum is the result of superposition of a number of such elementary Fermi-spectra which correspond to the formation of the final nucleus in a number of "allowed" excited states. This does not alter the upper limit of the complete spectrum, which is due to transition to the ground level of the final nucleus, but the intensity of the low energy electrons is considerably increased compared to that in a single Fermi curve, as is actually obtained.

The β-spectrum of the 18-min. isomer of Br^{80}, when excited by slow neutrons has been obtained by Alichanian, Alichanow and Dzelepow, with the help of a magnetic spectrograph. An analysis of the curve (Fig. 5) shows
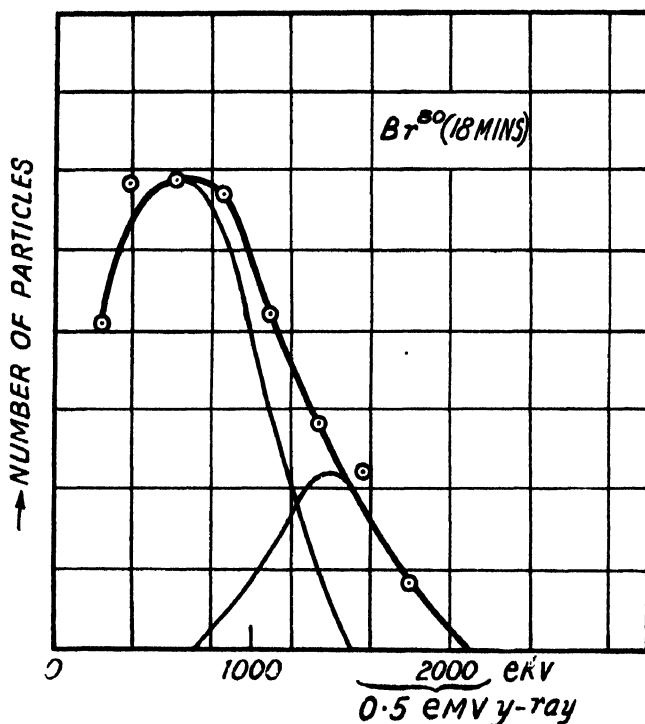

FIG. 5

readily that it is composed of two elementary Fermi spectra, with symmetrical distribution about the maximum. The two spectra have end-points at 2.0 and 1.5 eMV ; thus there must be a γ-ray of $\sim$0.5 eMV. Such a γ-ray has actually been detected by Buck.

It would indeed be interesting to ascertain the resonance neutron-group corresponding the excitation of the $\sim$0.2 eMV nuclear level of Br^{80}. Unfortunately it has not been possible for us to do it yet. From a rough

estimation of the energy-distribution of neutrons from a (Ra + Be) source, it seems probable that the 0.2 eMV level of Br^{80} is excited by the neutrons of ~ 2 eMV energy. This is corroborated by the experiment that the excitation ratio $\dfrac{18 \text{ min.}}{4.4 \text{ hr.}}$ continued to be $\sim 2.5 : 1$, even when the bombarding neutrons were filtered through about 2 cm. of paraffin. The activation ratio decreased when the thickness of the paraffin layer was further increased.

It will be seen, however, from Table III that when Br^{80} is formed according to the process Br^{81} (n, 2n) Br^{80}, by the bombardment of (Li + D) neutrons of energy $E_n \sim 14$ eMV (Soltan and others), the excitation ratio drops down to 0.8. This may be explained as follows : During this process, the intermediate nucleus Br^{82} is formed in a very highly excited state, with a stimulation energy of about 22 eMV, which most probably involves large change in angular momentum of the nucleus. So even after the expulsion of two neutrons, the final nucleus Br^{80} still retains a sufficiently high excitation energy. This extra energy is got rid of by γ-transitions to lower energy levels of Br^{80}. On account of the large difference in the angular momentum, the nucleus does not fall to the ground state of Br^{80}, but to the immediately higher metastable level, thereby enriching the activity of 4.4 hr. period.

REFERENCES

Abelson, 1939, *Phys. Rev.*, **55**, 424.

Alichanian, Alichanow and Dzelepow, 1936. *Phys. Zeit. Sow.*, **10**, 78.

Bethe, Hoyle and Peirls, 1939, *Nature*, **143**, 200.

Bothe and Gentner, 1937, *Zs. Phys.*, **106**, 236.

Dubridge, Barnes. Buck and Strain, 1938, *Phys. Rev.*, **53**, 447.

Devault and Libby, 1939, *Phys. Rev.*, **55**, 322.

Fermi and ors., 1935, *Ric. Scientific.*, **6**, 581.

Grinberg and Roussinow, 1940, *C. R. Acad. U. S. S. R.*, **27**, 649.

Hebb and Uhlenbeck, 1938, *Physica.*, **7**, 605.

Johnson and Hamblin, 1936, *Nature*., **138**, 504.

Pontecorvo, 1938, Rep. of Congress at the Paladi des. De' converts Paris.

Roussinow and Yusephovich, 1939, *Phys. Rev.*, **55**, 979

Saha, 1939, *Trans. Bose Research Inst., Calcutta*, **13**, 159.

Segre, Halford and Seaborg, 1939, *Phys. Rev.*, **55**, 321.

Siday, 1939, *Nature*, **148**, 681.

Snell, 1937, *Phys. Rev.*, **52**, 1007.

Soltan and Wertenstein, 1938, *Nature*, **141**, 76.

Valley and McCreary, 1939, *Phys. Rev.*, **55**, 666.

Widdowson and Champion, 1938, *Proc. Phys. Soc.*, **50**, 185.

THEORY OF CUMULUS CONVECTION.

BY S. MULL AND Y. P. RAO.

ABSTRACT. A new theory of convection based on lateral flow of air into the cloud is discussed, as an alternative to the 'parcel and slice' theories

INTRODUCTION :

The fundamental assumption made in the derivation of equations representing "parcel and slice" method of convection is that the pressure gradient along the vertical is determined by the surrounding air. As this assumption would only be valid in the most initial stage of the growth of the convection clouds, *i.e.*, in the stage when the parcel is isolated and small in dimension and not at the stage when convection is represented by a rising column of cumulus or cumulonimbus, it was thought advisable to examine the problem of cumulus convection to see if a more realistic picture of the growth of the convection clouds could be given, at least qualitatively.

PRESENT IDEAS :

The present ideas about the growth of convection clouds (cumulus and cumulo-nimbus) are represented by the parcel and the slice theories of convection. Whereas, in the first process the parcel of air is assumed to ascend adiabatically with no lateral mixing through an environment at rest, in the second one the environment is allowed to subside in order to preserve mass continuity. The two processes, however, fundamentally depend · upon the principle that a body floating or immersed in a fluid is subjected to an upward directed force equal to the weight of the amount of fluid that the body displaces. The body will rise or sink or remain at the same level depending on whether the force is greater than, less than, or equal to respectively the downward force on the body due to acceleration of gravity. Realising that we are dealing with a parcel of air instead of a fixed body, we may write, following Petterssen (1945), for a parcel of air embedded in an environment in hydrostatic equilibrium

$$\dot{\omega}' = -\alpha' \frac{\partial p'}{\partial z} - g$$

$$0 = -\alpha \frac{\partial p}{\partial z} - g$$

where letters with indices refer to the parcel and letters without indices refer to the environment and where

$\dot{\omega}' =$ vertical acceleration

$\alpha =$ specific volume

$p =$ pressure

$g =$ acceleration of gravity

$z =$ distance along a vertical axis.

If the pressure gradient along the vertical is determined by the surrounding air, then we have

$$\frac{\partial p'}{\partial z} = \frac{\partial p}{\partial z}$$

and therefore

$$\dot{\omega}' = g\,\frac{(\alpha' - \alpha)}{\alpha}$$

or

$$\dot{\omega}' = g\,\frac{(T' - T)}{T}$$

where T is the absolute temperature, which shows that the parcel will be accelerated upward if it is warmer and downwards if it is colder than the environment.

As it is clear, the above derivation is based on the fundamental assumption that the pressure gradient along the vertical is determined by the surrounding air. This assumption would certainly be valid in the most initial stage of cloud formation, since at that stage the parcel is isolated and small in dimension. It is, however, difficult to conceive how the same will hold good during the subsequent stages of cloud growth, where instead of a parcel we have to deal with a rising column, since under such circumstances the pressure difference between any two horizontal levels in the rising column and the surrounding environment cannot be the same.

The slice method as developed by Bjerknes (1938) and Petterssen (1939) computes the excess of heating of the rising column over the surrounding descending air after taking into consideration the modification in temperature due to vertical motion. No attempt is made to explain how the temperature difference results in acceleration or deceleration of the rising air. Presumably it is taken that the acceleration can be derived from the temperature difference as in the parcel method.

It is also assumed in the slice method that there is no net inflow or outflow along the horizontal into the slice under consideration. Temperature ascents inside convective clouds show that in a high percentage of cases, the lapse rate inside the cloud is in excess of the saturated adiabatic rate. This can only be explained on the assumption that there is appreciable lateral flow into the cloud. In situations favourable for convection, the environmental air has a lapse rate in excess of the saturated adiabatic lapse

rate. If there is no immediate and thorough mixing between the air inflowing from the sides at any level and the air coming from below, it is very likely that the air which has newly come from the sides being unsaturated will first cool at dry adiabatic lapse rate. For the above two reasons the lapse rate inside the cloud will definitely be in excess of the saturated adiabatic. The simple picture of a convective cloud fed from below the base with no lateral inflow beyond turbulent mixing with the environment is insufficient to account for the observed lapse rates.

SUGGESTED PICTURE OF CONVECTION IN CUMULUS AND CUMULONIMBUS

(a) Initial Stage :

Let us consider a barotropic atmosphere with horizontal isobaric surfaces. A perturbation in the form of a vertical displacement is applied to the system, the magnitude of the displacement being maximum at C (Fig. 1) and zero at the ground as well as at a higher level E. The displacement also decreases in the horizontal with distance from the vertical $ABCDE$. The pressure surfaces, represented by dotted lines, will consequently be perturbed as shown in Fig. 1, so that at any horizontal level the pressure is higher along the vertical $ABCDE$ than in the surrounding. At the levels A and E, the pressure surface is still horizontal. The above is merely a description of a vertical perturbation.
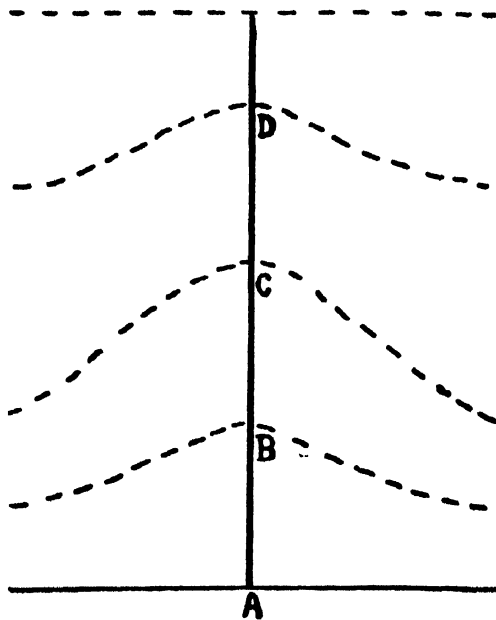

FIG. 1

Owing to the outward pressure gradient at all levels between A and E, air flows out radially and tends to decrease the pressure, its fall at any level being cumulative of the divergence at all levels aloft. This will be a maximum at the ground and as initially the pressure surface was horizontal at the ground, a low pressure will develop at the ground and progressively build upwards. This stage is represented in Fig. 2. Air will then flow
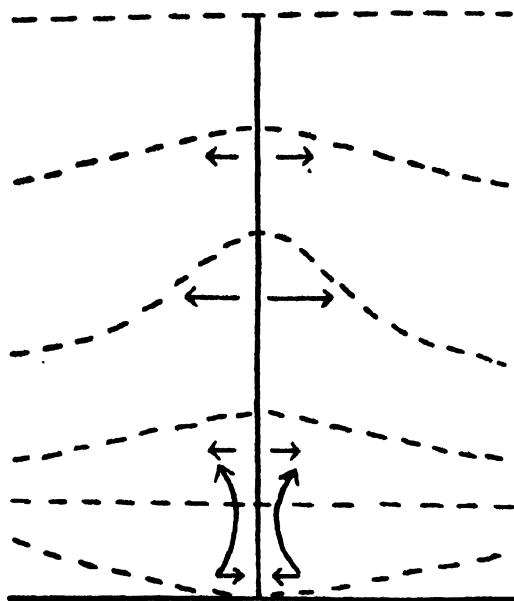

FIG. 2

radially inwards into the low pressure zone and outwards in the high pressure zone aloft. The inflowing air in the lower levels will then set up continuity with the outflowing air aloft in the form of a vertical current or in other words, the air in lower levels will tend to rise.

The rising air will cool either according to dry adiabatic or saturated adiabatic rate depending upon the humidity conditions. If the rising air is denser than the air it replaces (stable stratification), it will counteract the development of low by outflow of air aloft. The perturbation will be damped out in such a case. If on the other hand, the rising air is less dense than the air it replaces (unstable stratification), it will intensify the development of the low pressure below. The radial inflow into the low pressure will therefore increase and feed the rising column.

(b) *Large Cumulus Stage* :

Fig. 3 shows the outline of the cloud, pressure surfaces (broken lines) and air flow (arrow heads) at the stage of a large cumulus. The top of the growing cloud will push upwards the isobaric surfaces and consequently a high pressure will occur immediately above the top of the cloud. Owing to the lower density of the cloud air, the high pressure will change to a low one

some distance below the top of the cloud. The low pressure will intensify from there up to the ground. Air will flow into the low pressure zone of
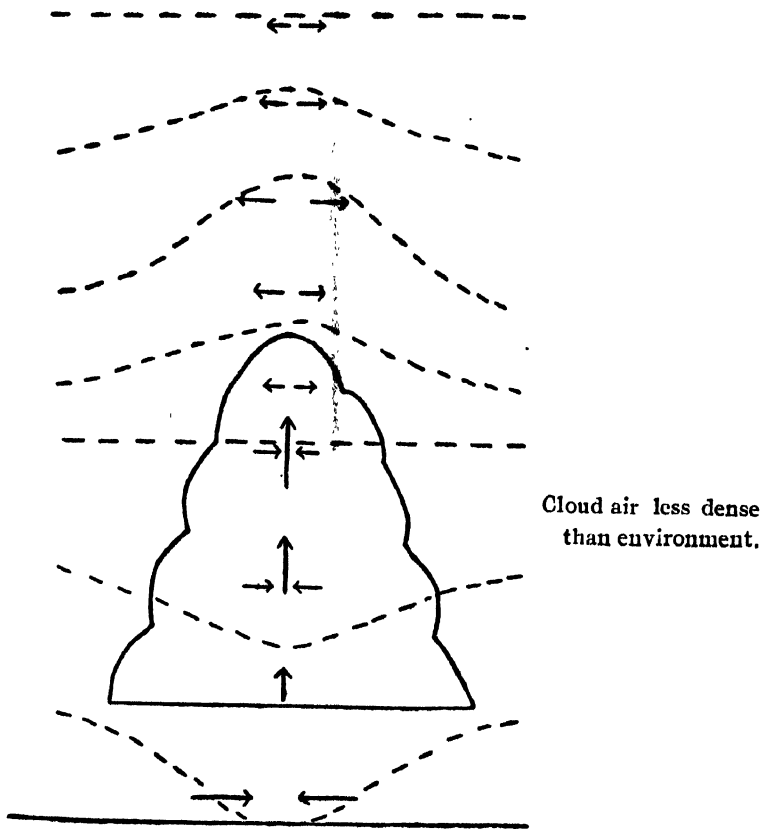

Cloud air less dense than environment.

FIG. 3

the cloud from the sides while there will be some lateral outflow in the shallow high pressure zone in the top part of the cloud. The total convergence of the air into the low pressure zone of the cloud is appreciably greater than the divergence in the top portion of the cloud so that the cloud is still growing. It should be noted that though the top of the cloud forms a high pressure zone, its density is still less than that of the environment and as the cloud grows, the high pressure zone of the cloud is being changed into low pressure. Hence there is no persistent outflow from the top of the cloud and it does not spread out.

(c) *Beginning of Cumulo-nimbus Stage*:

The next stage in the growth of the cloud will be when with further ascent the top portion of the cloud commences to be more dense than the environment. This is shown in Fig. 4. As in the previous stage there is a high pressure zone just at the top of the cloud but due to the higher density of the cloud air (over the environment) the high pressure intensifies below

the top up to the level where the density in the cloud is the same as that of the environment. As a result of this high pressure aloft, the high pressure
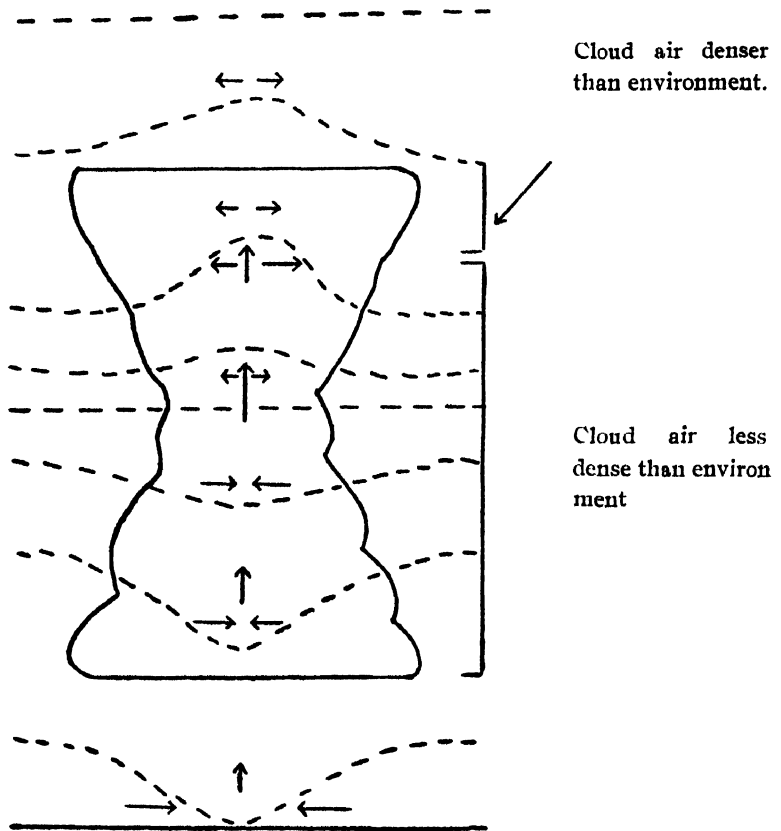

FIG. 4

zone extends down up to some level into that portion of the cloud which is less dense than the environment. Below that level, the low pressure zone builds up. The convergence in the low pressure zone is greater than the divergence in the high pressure portion of the cloud and hence the cloud is still growing. The cloud also spreads out in the high pressure zone unlike in the previous stage, as the high pressure is steadily maintained.

(d) *Fully Grown Cumulo-nimbus*:

At this stage represented in Fig. 5, the pressure right at the top of the cloud is the same as in the environment, as the cloud is no longer growing, and hence no more perturbing the upper pressure surfaces. A high pressure zone builds up below the top and is most intense at the level, S, where the cloud air comes to have the same density as the environment. Below that the cloud air is less dense than the environment and the high pressure zone first diminishes in intensity and finally changes into low pressure zone which attains the maximum intensity at the ground. The convergence in the low pressure zone below and the divergence in the high pressure zone aloft are

in this stage equal so that there is no further growth of the cloud. But the lateral inflow or outflow and the vertical currents do not cease. Thus the

Cloud air denser than environment.
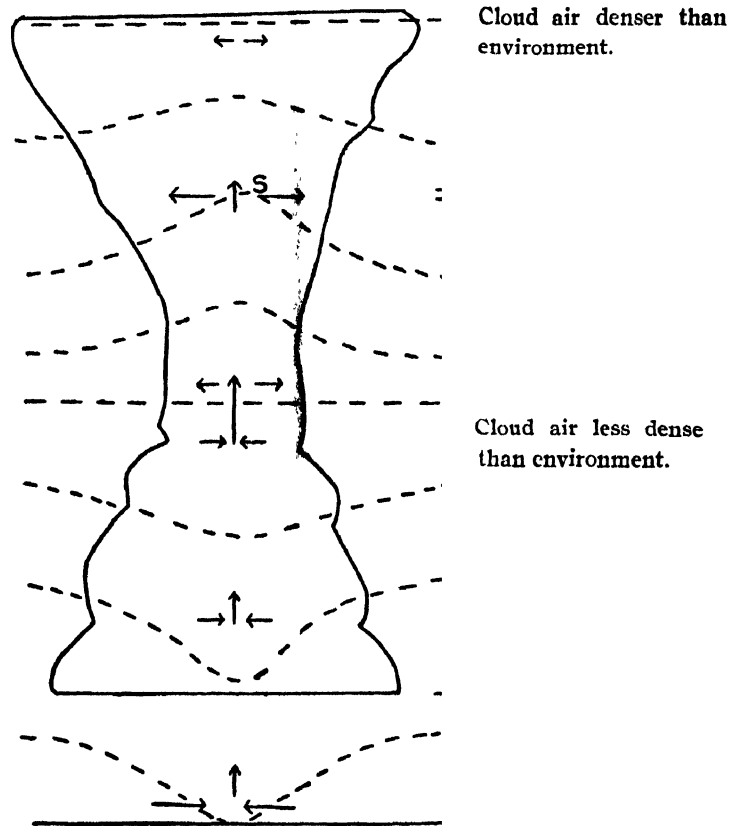
Cloud air less dense than environment.

FIG. 5

fully grown cumulonimbus represents a state of dynamic equilibrium. On this basis it is possible to understand how a cumulonimbus cloud can maintain itself for considerable time without further growth or decay. The low pressure below the cloud is a necessity for causing inflow of air into the cloud. It is also to be noted that the high pressure zone extends from the top of the cloud into a portion of the cloud which is warmer than the environment and hence the outflow compensating the inflow lower down occurs also in a portion of the cloud which is rarer than the environment. Hence the vertical portion which is less dense than the environment, is generally greater than the portion which is denser.

Thus, according to the above discussion, it is possible to conceive purely on theoretical grounds, a stage in the development of the cumulonimbus cloud when the cloud, with its fully grown anvil, can maintain itself without any further growth or decay for hours together. As the cloud represents a system in dynamic equilibrium and as the up currents are stable, it may be expected that the cloud will not break into thunderstorm with the usual

downdraft, squall and precipitation unless an additional mechanism comes into operation. Such an equilibrium stage in the life cycle of cumulonimbus is frequently observed in the tropics, where the cloud persists for a considerable time without any apparent change.

The discussion also clearly reveals how a low pressure occurs below convection clouds at all stages of its growth. This explains the anticlockwise circulation reported in cumulus and cumulonimbus clouds and the low pressure recorded with the passage of such clouds, though the fall of pressure is generally very small.

This paper is restricted to the stages prior to the breakdown of the cloud into a thunderstorm. The mechanism which brings out this change and the resulting circulation are being discussed in a separate paper.

REGIONAL METEOROLOGICAL CENTRE,
NAGPUR.

REFERENCES

Bjerknes, J., (1938), *Quart. Jour. Roy. Met. Soc.*, **64**, 325.
Petterssen, S., (1939), *Geof. Pub. (Oslo)*, **12**, 9.
Petterssen, S., (1945), *Geof. Pub. (Oslo)*, **16**, 10.

APPLICATION OF GAMOW'S THEORY OF α-EMISSION TO (4n + 1) RADIOACTIVE SERIES.*

By SUKUMAR BISWAS AND A. P. PATRO

ABSTRACT. Gamow's theory of α-emission is applied to neptunium (4n+1) series. The values of the assumed "nuclear radius" r_0 are found to vary irregularly as in actinium (4n+3) series. A large drop of r_0 occurs in $_{83}Bi^{213}$ similar to C-products of U, Th and Ac series. A complete calculation of r_0 values for all the members of U, Th and Ac series is also included with their extension to transuranic region using latest experimental values. It has been discussed that the existing theories of α-emission with angular momentum are inadequate in explaining these irregular variations of r_0, specially in the odd radioactive series. It appears that the nuclear charge Z has something to do with the irregularities of r_0.

INTRODUCTION

Gamow's theory of leakage of α-particles through a potential barrier has been applied to three radioactive series known so long. The relation between the disintegration constant λ and decay energy E contains a term r_0 which is referred as "nuclear radius" on the assumption of simplified potential field. This denotes the distance from the centre of the nucleus to the point where the inverse square law of repulsion suddenly changes to a force of attraction as assumed by Gamow. In reality, the fall of potential near the nuclear boundary cannot be so abrupt ; but a calculation of r_0 from the experimentally determined values of λ and E are made to see whether these are consistent. The values of r_0 are in general agreement with the liquid drop model of a nucleus ($r_0 = R. A^{\frac{1}{3}}$) for U, and Th series and less satisfactory for Ac series. But abnormally low values of r_0 are obtained for all the C-products. Since Gamow's work r_0 values have been calculated by Bethe (1937) and by Preston (1946, 1947) for U, Th and Ac series. Recently the missing (4n + 1) radioactive series has been identified by two groups of investigators (Hagemann et al, 1947 and English et al, 1947). Further data have been reported by Seaborg (1948). With these values of E and λ it is worthwhile to observe the consistency of r_0 values for this series. The present work is undertaken with this end in view.

Method of Calculation

The value of r_0 is calculated with experimental values of decay constant λ and disintegration energy E. Various forms of the relations used by different

* Communicated by Prof. M. N. Saha.

investigators have been referred in a previous paper.   Rigorous calculation of transparency factor (Saha, 1944) and Laue's (1929) semi-classical arguments yield the relation

$$\lambda = \frac{v}{r_0} e^{-2K} \qquad \qquad \dots \ (1)$$

where v = velocity of α-particle relative to the product nucleus.

r_0 = radius of the product nucleus.

$$2k = \frac{16\pi e^2 (Z-2)}{hv} (u_0 - \sin u_0 \cos u_0).$$

$$u_0 = \cos^{-1} \left[\frac{r_0}{R} \right]^{\frac{1}{2}} = \cos^{-1} \left[\frac{mv^2 r_0}{4e^2(Z-2)} \right]^{\frac{1}{2}}.$$

Preston (1946, 1947) uses more complex expressions, deduced from complex eigen-function,

$$\lambda = \frac{2v}{r_0} \frac{\mu^2 \tan u_0}{\mu^2 + \tan^2 u_0} e^{-2K} \qquad \qquad \dots \ (2a)$$

$$\mu = -\tan u_0 \tan (\mu k r_0) \qquad \qquad \dots \ (2b)$$

where $\mu = (1 - U/E_a)^{\frac{1}{2}}$

$$k = \frac{2\pi mv}{h} \ .$$

These equations are very sensitive to the small variation in the exponential term, so the additional factor $\dfrac{\mu^2 \tan u_0}{\mu^2 + \tan^2 u_0}$ is not of much consequence.   The values of r_0 calculated from relation (1) are given in Tables I and II.   Preston (1946) remarks that the additional term in (2a) gives a refinement in the value of r_0.   The method adopted for solution of (2a) and (2b) is, however, not referred.   For the comparison of the values of, obtained from the two methods, the latter equations are also used in this work.   Solutions of (2a) and (2b) for r_0 and μ are done here graphically by assuming a new variable $y = \mu k r_0$. Two explicit relations of y and u_0 are used to determine their values graphically.   These come out as

$$y_1 = \frac{\pm (kR) \sin u_0 \cos u_0}{\left[\frac{2v}{\lambda R} \tan u_0 (1 + \tan^2 u_0) e^{-2K} - 1 \right]^{\frac{1}{2}}}$$

$$y_2 = \frac{\mp 1}{\left[\frac{2v}{\lambda R} \tan u_0 (1 + \tan^2 u_0) e^{-2K} - 1 \right]^{\frac{1}{2}}}$$

From the value of u_0, r_0 is calculated, and from r_0 and y, μ is calculated which in turn gives the value of U.

TABLE I

r_0 values for $(4n + 1)$ Neptunium radioactive series.

Nuclei	$E\alpha$ in (Mev)	$v \times 10^{-9}$ cm/sec.	λ sec^{-1}	From relation (1)		From relation (2)	
				$r_0 \times 10^{13}$ cm.	$R \times 10^{13}$ cm.	$r_0 \times 10^{13}$ cm.	$R \times 10^{13}$ cm.
$_{95}Am^{241} \rightarrow _{93}Np^{237}$	5.50	1.661	4.40×10^{-11}	8.93	1.44	9.78	1 58
$_{93}Np^{237} \rightarrow _{91}Pa^{233}$	4 73	1.540	9.78×10^{-15}	9.09	1.48	9.79	1.59
$_{92}U^{233} \rightarrow _{90}Th^{229}$	4.825	1.556	1.37×10^{-13}	9.06	1.48	9.65	1.58
$_{90}Th^{229} \rightarrow _{88}Ra^{225}$	4.85	1.561	3.18×10^{-12}	9.03	1.52	9.67	1.59
$_{89}Ac^{225} \rightarrow _{87}Fr^{221}$	5.801	1.708	$8 00 \times 10^{-7}$	8.68	1.44	9.23	1.53
$_{87}Fr^{221} \rightarrow _{85}At^{217}$	6.31	1.782	2.31×10^{-1}	8.67	1 41	9.34	1.54
$_{85}At^{217} \rightarrow _{83}Bi^{213}$	7.023	1.880	33	8.91	1.49	9.60	1 61
$_{83}Bi^{231} \rightarrow _{81}Tl^{209}$	5 86	1.718	3.15×10^{-6}	7.13	1.20	7 43	1.25
$_{84}Po^{213} \rightarrow _{82}Pb^{209}$	8.336	2.049	1.52×10^{-5}	8.40	1.42	9.10	1.53

TABLE II

r_0 values for Th, U and Ac -series.
(4n) Th-series.

Nuclei	$E\alpha$ in (Mev)	$v \times 10^{-9}$ cm/sec.	λ sec^{-1}	From relation (1)		From relation (2)	
				$r_0 \times 10^{13}$ cm.	$R \times 10^{13}$ cm.	$r_0 \times 10^{13}$ cm.	$R \times 10^{13}$ cm.
$_{96}Cm^{240} \rightarrow$	—	—	2.68×10^{-7}	—	—	—	—
$_{90}Th^{232} \rightarrow _{88}MsTh I^{228}$	3.92	1.400	1.58×10^{-18}	9.90	1.62	10.01	1.64
$_{90}RdTh^{228} \rightarrow _{88}ThX^{224}$	5.420	1.656	9.33×10^{-9} *	9 03	1 49	9.33	1.54
$_{88}ThX^{224} \rightarrow _{86}Tn^{220}$	5.681	1.690	2.2×10^{-6}	8.87	1 47	9.29	1.54
$_{86}Tn^{220} \rightarrow _{84}ThA^{216}$	6.282	1.778	1.27×10^{-2}	8.91	1 49	9.28	1.55
$_{84}ThA^{216} \rightarrow _{82}ThB^{212}$	6.774	1.847	4 39	8.69	1.46	9.12	1.53
$_{83}ThC^{212} \rightarrow _{81}ThC''^{208}$	6.054	1.746	1.75×10^{-5} *	7.07	1.19	7.57	1.28
$_{84}ThC'^{212} \rightarrow _{82}ThD^{208}$	8.776	2.102	2.31×10^{6}	8.65	1.46	9.15	1.54

TABLE II (contd.)

(4n + 2) U-Series

Nuclei	$E\alpha$ in (Mev)	$v \times 10^{-9}$ cm/sec.	λ sec^{-1}	From relation (1)		From relation (2)	
				$r_0 \times 10^{13}$ cm.	$R \times 10^{13}$ cm.	$r_0 \times 10^{13}$ cm.	$R \times 10^{13}$ cm.
$_{94}Pu^{238} \rightarrow _{92}UII^{234}$	5.496	1.669	4.39×10^{-10}	9.54	1.55	9.69	1.57
$_{92}U^{238} \rightarrow _{90}UX_1^{234}$	4.20	1.452	4.87×10^{-18}	9.27	1.46	9.37	1.52
$_{92}UII^{234} \rightarrow _{90}I_0^{230}$	4.76	1.537	8.17×10^{-14}	9.38	1 53	9.26	1.51
$_{90}I_0^{230} \rightarrow _{88}Ra^{226}$	4.66	1.530	2.65×10^{-13}	9.20	1.51	9.26	1.52
$_{88}Ra^{226} \rightarrow _{86}Rn^{222}$	4.791	1.552	$1.35 \times 10^{-11}*$	9.03	1.49	9.29	1.53
$_{86}Rn^{222} \rightarrow _{84}RaA^{218}$	5.486	1 661	2.10×10^{-6}	8.96	1.49	9.28	1.54
$_{84}RaA^{218} \rightarrow _{82}RaB^{214}$	5.998	1.738	3.77×10^{-3}	8.80	1.47	9.14	1.53
$_{83}RaC^{214} \rightarrow _{81}RaC''^{210}$	5.502	1.664	$1.06 \times 10^{-7}*$	7.30	1.27	7.80	1.31
$_{84}RaC^{214} \rightarrow _{82}RaD^{210}$	7.680	1.966	4.62×10^{3}	8.74	1.47	9.34	1.57
$_{83}RaE^{210} \rightarrow _{81}Tl^{206}$	4.87	1.556	1.60×10^{-13}	6.50	1.10	6.63	1.12
$_{84}RaF^{210} \rightarrow _{82}RaG^{206}$	5 303	1.634	5.89×10^{-8}	8.04	1.36	8.27	1.40

TABLE II (contd.)

(4n + 3) Ac-series.

Nuclei	$E\alpha$ in (Mev)	$v \times 10^{-9}$ cm/sec.	λ sec^{-1}	From relation (1)		From relation (2)	
				$r_0 \times 10^{13}$	$R \times 10^{13}$	$r_0 \times 10^{13}$	$R \times 10^{13}$
$_{94}Pu^{239} \rightarrow _{92}U^{235}$	5.137	1.605	$9 28 \times 10^{-12}$	9.52	1.51	10 13	1.64
$_{92}U^{235} \rightarrow _{90}UY^{231}$	4.36	1 479	3.19×10^{-17}	8.97	1.46	9.55	1.56
$_{91}Pa^{231} \rightarrow _{89}Ac^{227}$	5.01	1.586	$5.59 \times 10^{-13}*$	8.38	1.36	8.18	1.34
$_{90}RdAc^{227} \rightarrow _{88}AcX^{223}$	6.049	1.743	$1.02 \times 10^{-7}*$	7.78	1 28	8.56	1.41
$_{88}AcX^{223} \rightarrow _{86}An^{219}$	5.719	1.695	$2.86 \times 10^{-7}*$	8.08	1.34	8.70	1 44
$_{86}An^{219} \rightarrow _{84}AcA^{215}$	6.824	1.854	$0 124 *$	8.20	1 37	8.90	1.45
$_{84}AcA^{215} \rightarrow _{82}AcB^{211}$	7.365	1 925	3.79×10^{2}	8.65	1.45	8 99	1.51
$_{83}AcC^{211} \rightarrow _{81}AcC''^{207}$	6.619	1.825	$4.78 \times 10^{-3}*$	7.65	1.29	7.90	1.33
$_{84}AcC^{211} \rightarrow _{82}AcD^{207}$	7.434	1.934	1.39×10^{3}	8.20	1.39	8 85	1.50

*. Values of λa_0 (partial decay constant for o-group α-particles)

DISCUSSION

A study of the r_0 values for $(4n+1)$ neptunium radio-active series reveals the following features :

Firstly : The values of r_0 do not vary in a regular way as required by the rule $r_0 = R.A^{\frac{1}{3}}$. Such anomaly in r_0 value is predominant in actinium series. In fact the two odd series $(4n+1)$ and $(4n+3)$, behave in an irregular way as regards the r_0 values. On the other hand, two even series Th $(4n)$ and U $(4n+2)$ show nearly regular variation of r_0 values with the exception of C-products. Calculation of r_0 are given by Preston (1946, 1947) for well-known members of U, Th and Ac series. Recently these known series are extended to the transuranic region and some of the experimental data have been revised. So a complete calculation of r_0 values for all the members of U, Th, and Ac series are also included with the latest experimental data. These are given in Table II. The values for $(4n+1)$ series together with those of U, Th and Ac series are given graphically in Fig. 1. The r_0
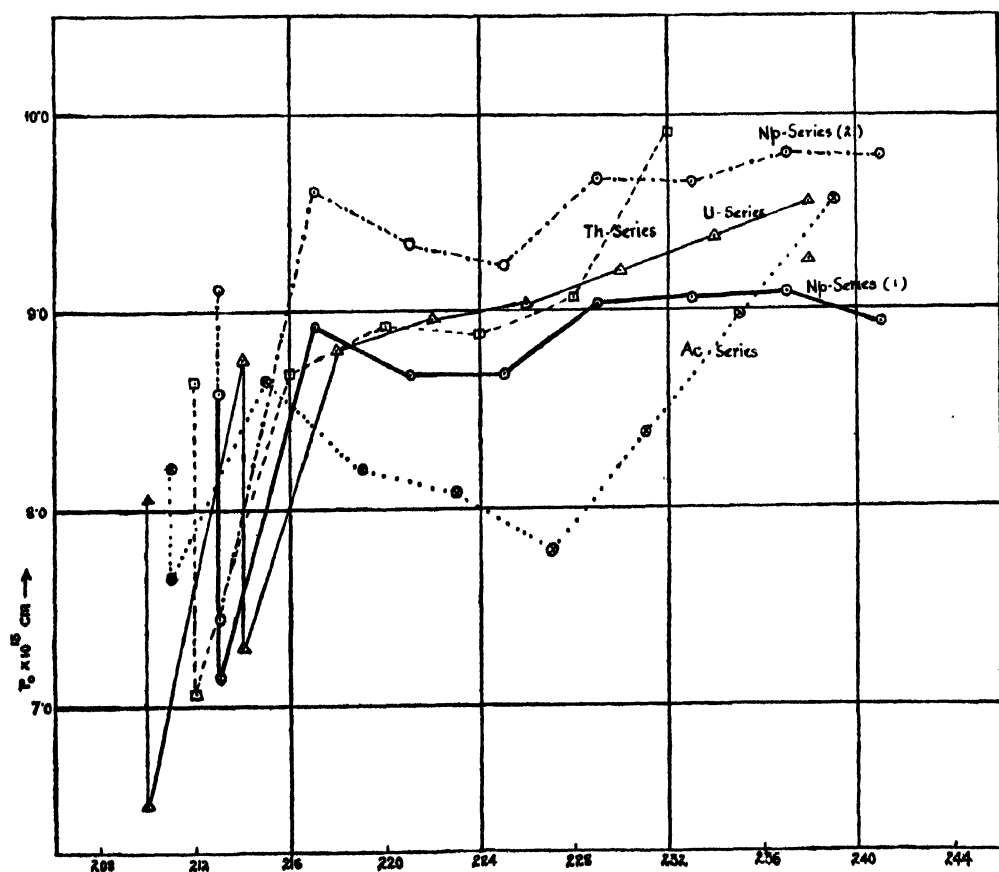
FIG. 1

values of Np series calculated according to both the relations (1) and (2) are plotted on curves. These show that values obtained by relation (2) are higher than the other values by a nearly constant quantity. The plotted values of U, Th and Ac series are those calculated from relation (1). Ac series shows a sharp regular fall to $RdAc^{227}$ and then a rise in r_0 up to AcA. But in Np series the irregularities are not so wide.

Secondly : The value of r_0 for $_{83}Bi^{214} \rightarrow _{81}Tl^{210}$ is abnormally low. Bi^{213} is the corresponding C-product of neptunium series. It has been observed that in U, Th, and Ac series there occurs an abrupt fall in the value of r_0 in $C \rightarrow C''$ disintegrations. The value of r_0 again assumes normal magnitude in $C' \rightarrow D$ disintegrations. Similar phenomena occur also in the $(4n+1)$ radioactive series. It is interesting to note that $_{83}RaE^{210}$ which has been recently observed to be α-active (Broda and Feather, 1947) exhibits an abnormally low value of r_0 in $_{83}RaF^{210} \rightarrow _{81}Tl^{206}$ disintegration. Thus all the α-active isotopes of $_{83}Bi$ show abnormal value of "nuclear radius."

The drop in the values of r_0 for the C-products and the members of the Ac series have been attributed by Gamow (1937) as due to emission of α-particles with angular momentum different from zero $(l \neq 0)$. The effective radius in such a case, as deduced by Gamow (1937) is supposed to follow the relation :

$$r_{eff} = r_0 - \frac{h^2}{4\pi^2 m e^2 (z-2)} \, l(l+1)$$

Allotments of l-values to different α-ray lines are rather arbitrarily made to fit the experimental data. No quantitative treatment on the above line has been found to be satisfactory.

Emission of α-particle with angular momentum $l \neq 0$ has been treated by Preston (1947). Calculations are made by him with the complicated relations for a few α-disintegrations having excited states. The method of calculation is very round about and l values are chosen arbitrarily to give a more or less consistent value of r_0 for different excited states for $ThC - ThC''$ and a few others. On the whole, the problem of emission of α-particle with $l \neq 0$ is at present far from satisfactory.

As in the Ac series, the irregularities in r_0 for the Np series is probably due to emission of α-particles with angular momentum different from zero. The experimental observations on $(4n+1)$ series are rather preliminary. Further investigations are sure to reveal complex α-spectra in many members of $(4n+1)$ radioactive series. A detailed experimental observations are required before any theoretical treatment is attempted. Since the irregularities in r_0 are found with the nuclei with odd mass number and in Bi which is the first member in the even series having odd atomic number it is plausible

that the even-odd property of a nucleus affects the α-emission process to a large extent.

In this connection it may be mentioned that in U and Th series r_0 varies more or less regularly. However, the value of $R = r_0 A^{-\frac{1}{3}}$ is seen to be not a constant but increases from lightest member to heaviest one in the series to the extent of about 15%. The rule $r_0 = R A^{\frac{1}{3}}$ cannot be expected to hold accurately over the whole radioactive series because an increase in Z increases the Coulomb repulsion which tends to decrease the nuclear density, and increase the nuclear radius. The simple rule would hold if the nuclear binding energy contained the only term $E = \alpha A$. But E is given by the expression

$$E = \alpha A - \beta \frac{I^2}{A} - \gamma A^{\frac{2}{3}} - \delta \frac{Z^2}{A^{\frac{1}{3}}}$$

Hence with increasing Z, R the average distance between the nucleons should drift to a higher value. This is actually observed in the value of R calculated from r_0. Present (1940) proposed the following formula for nuclear radius after employing the corrections for $N \neq Z$, surface tension and Coulomb repulsion.

$$r_0 = R.A^{\frac{1}{3}} = R^* A^{\frac{1}{3}} \left[1 + 0.8 \frac{I^2}{A^2} - 0.3 A^{-\frac{1}{3}} + 0.01 \frac{Z^2}{A^{\frac{4}{3}}} \right]$$

In this relation R^* in place of R should be constant for all members in the series. For two extreme members of U series, R varies from 1.55 to 1.36 from $Pu^{238} \rightarrow U \; II^{234}$ to $RaF^{210} \rightarrow RaG^{206}$. With above relation, R^* comes out as 1.48 and 1.35. In case of Th series R for $Th^{232} \rightarrow MsThI^{228}$ is 1.62 and for $ThC'^{212} \rightarrow ThD^{208}$ 1.46. The corresponding values of R^* are 1.55 and 1.40. Thus the proposed relation is far from satisfactory. Although from the very definition of r_0, the relation between r_0 and actual nuclear radius is rather vague, the above relation cannot account for the variation of R along the radioactive series quantitatively.

REFERENCES

Bethe, 1937, *Rev. Mod. Phys.*, **9**, 161.

Broda and Feather, 1947, *Proc. Roy. Soc*, Lond., A., **190**, 20.

English, Cranshaw, Deuners, Harvey, Hincks, Jelley and May, 1947, *Phys. Rev*, **72**, 253,

Gamow, 1937, Structure ot Atomic Nuclei and Nuclear Transformations, (Clarendon Press, Oxford), p 104

Hagemann, Katzin, Studier, Ghiorso, and Seaborg, 1947, *Phys. Rev.*, **72**, 252.

Laue, 1929, *Zeit. f. Physik.*, **52**, 726.

Present, 1940, *Phys. Rev.*, **60**, 28.

Preston, 1946, *Phys. Rev.*, **69**, 535.

Preston, 1947, *Phys. Rev.*, **71**, 865.

Saha, A. K., 1946, *Proc. Nat. Inst. Sc. Ind.*, **10**, 373.

Seaborg, 1948, *Chem. Eng. News.*, **26**, 1902.

ABSORPTION OF ULTRA HIGH FREQUENCY WAVES IN SALT SOLUTIONS

By S. K. CHATTERJEE and B. V. SREEKANTAN

ABSTRACT. Absorption of ultra high frequency electromagnetic waves by aqueous solutions of $MgCl_2$, $CuSO_4$, and KCl has been experimentally studied. Result indicates two absorption peaks for coppersulphate solution but one absorption peak for magnesium chloride and potassium chloride solutions over the frequency range 300 to 500 Mega cycles. Absorption maxima shift towards higher concentration for higher frequencies for all the solutions. The average values for the product of normality at which maximum absorption takes place and corresponding wave length are 11.96, 8.648 and 15.96 for $MgCl_2$, $CuSO_4$ and KCl respectively. The observed relaxation time shows values lower than the theoretical values for all the solutions. Radius of rotor calculated from the observed values of relaxation time for the solutions indicate that the absorption is due to the ionic atmosphere rotating as a whole under high frequency stress.

EXPERIMENTAL

Description of equipments and experimental technique have been published elsewhere (Chatterjee and Sreekantan, 1948). The percentage of absorption
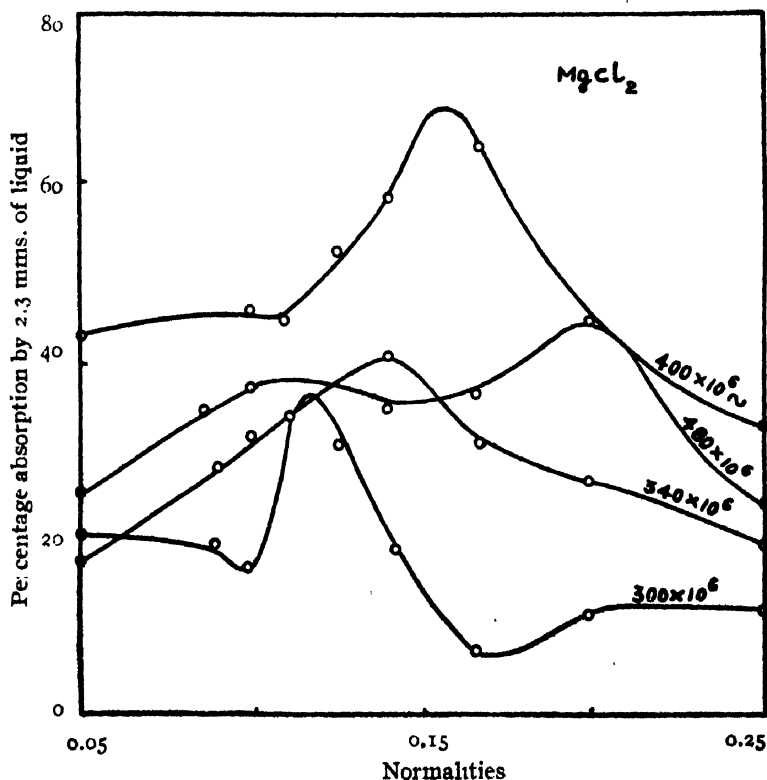

FIG 1

suffered by an electromagnetic wave (300-500 Mc/s) while passing throug
aqueous solutions of magnesium chloride, copper sulphate, and potassiur
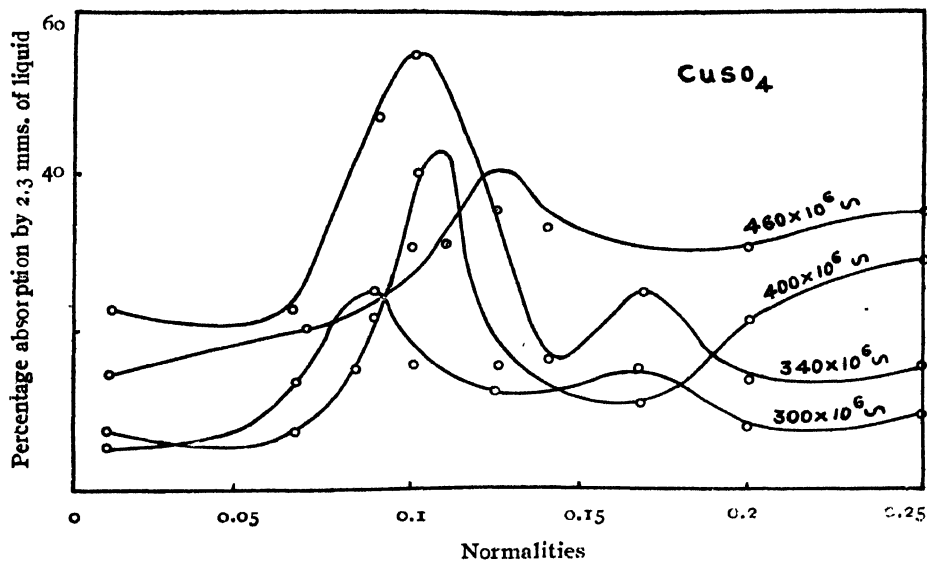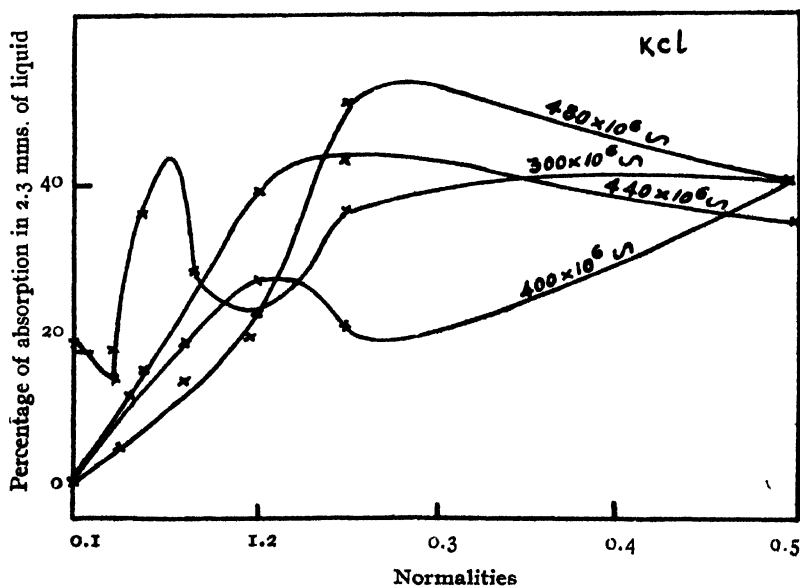chloride of different concentrations is shown in Figs. 1 to 3.

Fig 2

Fig 3

DISCUSSION

From the results of experiment the following facts are significant :—

(1) The absorption peak for all the solutions shifts towards higher concentration with increasing frequencies.

(2) For copper sulphate solution, at all frequencies within the range considered, two distinct peaks separated by a plateau are noticed. It is further observed that the distance between two peaks on the normality axis tends to increase as the frequency of electric stress increases. This shows a similarity with phenomena observed in the case of two tightly coupled circuits where the distance between peaks increases with the coefficient of coupling increasing. In the case of other two solutions only one absorption peak is observed within the frequency range in question.

(3) The product of normality γ^* in gm. equivalent per litre at which absorption maxima occurs and the corresponding wavelength λ maintains an almost constant value, different for different solutions as given in Table I. The average values of the product $\gamma^*.\lambda$ are 11.96, 8.648, and 15.96 for $MgCl_2$, $CuSO_4$, and KCl respectively. It may be mentioned that for copper sulphate solution the values of $\lambda.\gamma^*$ correspond to the first peak.

TABLE I

Frequency in Mc/s.	MgCl₂		CuSO₄		KCl		Average
	γ^+	$\lambda.\gamma^*$	γ^i	$\lambda\ \gamma^*$	γ^*	$\lambda.\gamma^*$	$\lambda.\gamma^*$
300	0.11N	11.00	0.09N	9 00	0.15N	15.00	11.96
340	0.14N	12.31	0 10N	8.82	—	—	(MgCl₂)
400	0.16N	12.00	0.115N	8.626	0.21N	15.75	8.648
460	—	—	0.125N	8.149	—	—	(CuSO₄)
480	0.20N	12.50	—	—	0.27N	16.75	15 96(KCl)

The presence of two peaks in the case of copper sulphate solution needs an explanation. This may be attributed to a random variation in the structure of material or this may be explained on the basis of the existence of two relaxation times. The theoretical relation of Debye and Falkenhagen (1934) gives only one relaxation time Θ given by

$$\Theta = \frac{8.85 \times 10^{-11}}{\Lambda_\infty.\gamma^*}.D_0 \tag{1}$$

corresponding to the existence of one peak only. The existence of one peak is predicted on the Debye's assumption of molecules, spherical in shape rotating in an alternating field. This implies a single region of dispersion and a single relaxation time. The theory of dielectric dispersion has been extended to the case of an ellipsoidal model by Perrin (1934). It has been established that three values of relaxation time are possible in the case of an ellipsoidal

molecule and two values of relaxation time are possible in the case of an ellipsoid of revolution. The experimental curves of copper sulphate solution suggests a complex mode of oscillation which may consist of the rotation of the ellipsoid about the major axis or the oscillation of the major axis itself in an indeterminate plane. In addition to this if we consider that the ellipsoids of revolution are pressed against each other, rotating about or oscillating along the major axis then the viscosity term in the Debye's expression (1929) for relaxation time $\tau = 4\pi\eta a^3/kT$ cannot be evaluated by a macroscopic measurement of viscosity as suggested by Girard and Abadie (1946). The relaxation time observed τ_{obs} crrresponding to the absorption peak (Figs. 1—3) has been calculated from the following relation :—

$$\tau_{obs.} = \frac{1}{\omega_{max.}} \cdot \left(\frac{\epsilon_\infty + 2}{\epsilon_{w=0} + 2}\right) = \frac{1}{2\pi f_{max.}} \cdot \frac{82}{\epsilon_{w=0} + 2}$$

which can be deduced from the Debye's generalised expression (1929) for the dielectric constant

$$c = \epsilon' - j\epsilon''$$

The values of the dielectric constant $\epsilon_{w=0}$ at audio frequencies for different normalities can be calculated from the relation (Falkenhagen, 1934).

$$\epsilon_{w=0} - \epsilon_s = \frac{1.97 \times 10^6 |Z_1 Z_2| \cdot \{|Z_1| + |Z_2|\}^{\frac{1}{2}} \cdot (q\gamma^*)^{\frac{1}{2}}}{2\epsilon^{\frac{1}{2}} \cdot T^{\frac{3}{2}} \cdot \left(1 + \frac{1}{\sqrt{q}}\right)^2}$$

which in the case of different solutions can be reduced to the following experessions.

$$\left(\epsilon_{w=0} - \epsilon_s\right)^{23°C}_{CuSO_4} = 28.95\sqrt{\gamma^*}$$

$$\left(\epsilon_{w=0} - \epsilon_s\right)^{23°C}_{MgCl_2} = 9\,281\sqrt{\gamma^*}$$

$$\left(\epsilon_{w=0} - \epsilon_s\right)^{23°C}_{KCl} = 3.51\sqrt{\gamma^*}$$

where ϵ_s may be taken as 80, the dielectric constant of water at u.h.f. The theoretical values of $\tau_{cal.}$ have been arrived at from the expresison for the ionic relaxation time given in equation (1) where the values of conductivity at infinite dilution Λ_∞ are as follows

$(\Lambda_\infty)MgCl_2 = 110.88, \quad (\Lambda_\infty)CuSO_4 = 113.85, \quad (\Lambda_\infty)KCl = 130.1$

A comparative study of $\tau_{obs.}$ and $\tau_{cal.}$ in the case of the three solutions can be made from Table II.

TABLE II

Frequency in Mc/s.	MgCl₂		CuSO₄		KCl	
	$\tau_{obs.} \times 10^{10}$ secs.	$\tau_{cal.} \times 10^{10}$ secs.	$\tau_{obs.} \times 10^{10}$ secs.	$\tau_{cal.} \times 10^{10}$ secs.	$\tau_{obs.} \times 10^{10}$ secs	$\tau_{cal.} \times 10^{10}$ secs
300	5.114	5.672	4.888	6.913	3.692	5.220
340	4.490	4 561	4.212	6.220	—	—
400	3 806	3 991	3.555	5.411	2 646	3 902
460	—	—	3.076	4.977	—	—
480	3.156	3 193	—	—	2.063	3.245

It will be observed that $\tau_{obs.}$ in each case is lower than $\tau_{cal.}$. This divergence may be due to the complexity of real facts. It may be ascribed to the fact that the value for ionic relaxation time given by equation (1) has been deduced on the assumption of Debye's theory, which is applicable for solutions more dilute than those used in the present investigation.

The occurrence of absorption maxima may be explained due to the rotation of ions or ionic atmosphere as a whole, when the solution is subjected to an ultra high frequency electromagnetic wave. To determine whether it is due to ionic rotation or the rotation of the ionic atmosphere as a whole the radius of the rotor has been calculated from the following relation (Debye, 1929).

where η is the viscosity of the solution. The values of relative viscosity η_r for different solutions at different concentration are given in Table III (Ruby and Kawai, 1926). The volume of the rotor has been calculated using the following relation which holds both for a spherical and an ellipsoidal rotor as shown by Potapenko (1948).

$$\text{Volume } (V) = \frac{\tau kT}{3\eta}$$

The values are given in Table III.

TABLE III

η_r = Relative Viscosity—Viscosity of water = 8.94 millipoises, at 25° C.

Electrolyte	Normality	Relaxation time × 10¹⁰ secs.	η,	$a \times 10^8$ cms.	$v \times 10^{22}$ c.c.	$a, \times 10^8$ cms.	Ionic radius × 10⁸ cms.	
MgCl₂	0.200N	3.156	1.075	4.776	4.474	3.953	0 65	1.81
	0.160N	3.806	1.062	5.075	5.464	4.414	(Mg	(Cl
	0.110N	5.144	1.040	5.633	7.496	5.330	ion)	ion)
CuSO₄	0.125N	3.076	1.072	4.697	4.344	4.380	0.96	
	0 115N	3.555	1.065	4.948	5.578	4.512	(Cu	
	0.090N	4.888	1 050	5.533	7.096	5.101	ion)	
KCl	0.270N	3.245	0.9993	4.896	4.917	5.865	1.33	1.81
	0.210N	3.902	0.9996	5.206	5.910	6.665	(K	(Cl
	0.150N	5.220	1.000	5.736	7.902	7 870	ion)	ion)

In the last column of the above tables value of ionic radii, as given by Pauling (1939), are given for the sake of comparison. It will be observed that the calculated values of radius of the rotor agree more closely with those calculated using the following relation (Falkennagen 1934) for the radius of the ionic atmosphere.

$$a_1 = \frac{4.31 \times 10^{-8}}{\{\gamma \sum \gamma_i Z_i{}^2\}^{\frac{1}{2}}}$$

It may therefore be concluded that the absorption maximum observed in the case of aqueous solutions of electrolytes in the frequency range under consideration (300 to 500 Mc/s) is due to the rotation of the ionic atmosphere as a whole.

ACKNOWLEDGMENT

The authors wish to express their grateful thanks to the Head of the department for the facilities given to carry out the above investigation.

Department of Electrical Communication Engineering,
Indian Institute of Science,
Bangalore.

REFERENCES

Chatterjee, S. and Sreekantan B. V., 1918, *Ind. Jour Phy.*, **22**, 229.

Debye, P. 1929, 'Polar Molecules' Chemical Catalog Co., New York.

Falkenhagen, H., 1934, 'Electrolytes,' p. 213.

Falkenhagen, H., 1934, Electrolytes,' p. 219.

Falkenhagen. H., 1934, 'Electrolytes,' p. 106.

Girard, P. and Abadie 1946, *Trans. Far. Soc.*, **52A**, 'Dielectrics,' 40.

Perrin, J., 1934, *Phys. et Rad*, **5**, 497.

Potapenko and Wheeler, D, 1948, *Rev. Mod. Phy.*, **20**, 143.

Pauling, L. 1939 'Nature of the Chemical Bond and the structure of molecules and crystals,' p. 326.

Ruby, C., and Kawai J., 1926, *Jour. Chem. Soc.*, **48**, 1119

STUDY OF JOSHI-EFFECT IN IODINE VAPOUR IN THE PRESENCE OF POWDERED IODINE UNDER ELECTRICAL DISCHARGE*

INFLUENCE OF DIFFERENT DETECTORS

BY S. N. TEWARI

ABSTRACT. Joshi-effect Δi in iodine is studied in an ozoniser discharge of 50 cycles frequency in the potential range 0.5−2 kV (r. m. s.), the annular space being filled with powdered iodine. Current i was measured with a serially connected vacuo-junction and an oxide rectifier with an inductively and resistively coupled diode, triode and pentode. The 'threshold potential' V_m (viz, 0-95 kV) was independent of the nature of any of the above detectors; for each of these, the relative Joshi-effect $-\%\Delta i$, i. e. $\dfrac{-\Delta i \times 100}{i_D}$ where i_D is the current in dark is maximum near V_m. The observed diminution (numerically) in $-\%\Delta i$ with resistive impedances in the low tension line is attributed to the preferential damping of the H. F. components of i which are found by Joshi to be the chief seat of this phenomenon. The first positive effect $+\Delta i$ has been observed at low applied V with all the detectors. A second positive effect is also observed under heavy resistive inputs with triode and pentode. Based on Joshi's result, that the second positive effect is associated with the H.F's in the grid circuit and that it can be eliminated by (1) shifting the grid bias to higher negative values, (2) by-pass grid capacity, evidence has been adduced to show that this is associated with the external detector circuit; is due to a shift of the grid voltage towards positive by a decrease of the grid current, under irradiation.

INTRODUCTION

Two general results of significance to the elucidation of the above phenomenon, (an instanteneous and reversible photo-variation, usually though not invariably dimunition of the discharge current $-\Delta i$,) have been emphasized by Joshi ; (1) The magnitude of Δi is affected markedly by the nature of the excited solid-gas interface (Joshi, 1943, 1945e, 1947 ; Cherian, 1945) ; and (2) Of the operative conditions, specially the detector employed (Joshi, 1943, 1945a). The present work report result for the Joshi-effect in iodine, excited by an ozoniser discharge under a large surface influence by the introduction of powdered iodine in the discharge space and using a series of current indicators.

EXPERIMENTAL

The general experimental arrangement and the circuit employed are shown in Fig. 1. Alternating potentials of 50 cycles frequency obtained from a rotary

converter worked off 220 volt D.C. mains were applied to a Siemens' glass ozoniser; its annular space was filled with powdered iodine. The deflections of the galvanometer (G) were noted at each applied kV in dark (i_D) and under irradiation (i_L) from a 220 volt, 200 watt incandescent (glass) bulb by manipulating with a shutter, under the following detecting arrangements :

· (a) The low tension electrode was earthed through an appropriately shunted vacuo-junction connected to a reflection galvanometer.

(b) The current i passed through a metal oxide rectifier and a serial galvanometer.

(c) A double diode (83 V) was used as a half-wave rectifier. i was admitted to (1 : 10) Bell transformer ; its secondaries were connected to the plates and the filament through the galvanometer. The input was next tapped from a non-inductive and practically non-capacitative Dubilier resistance R, varied in the range 2-25 kΩ.

(d) Triode (37) was used as an anode bend rectifier in place of the diode used in (c). The secondaries of the Bell transformer were connected to the grid and the cathode through a grid bias battery. As in (c) the input was also tapped from R, varied from 50-500 kΩ.

(e) Pentode (6J7) was used as an anode bend rectifier. The input taken first from the secondaries of the transformer and then across R, varied from 50-500 kΩ, was applied between the control grid and the cathode.

Results of a typical group of experiments made with each of these detectors, for i_D, i_L ; the net Joshi-effect $i_D \sim i_L = \Delta i$; its relative value $\dfrac{100 \times \Delta i}{i_D} = \%\Delta i$ are returned in Table I.

DISCUSSION

During this work the basic significance of the 'threshold potential' V_m (Joshi, 1929, 1939, 1945d, 1946b) as located by observation of an initial rapid increase of i with V was noticed. Despite the widely divergent modes of i measurement (a to e, Fig. I) V_m for the iodine tube used in this work was fairly constant, *viz.*, 0.95 kv. Well below V_m the conductivity is entirely capacitative (Joshi, 1945d) and even intense and short wave irradiations do not produce Δi. Joshi considers that the breakdown of the gas sets in at and even (just) less than V_m Like Paschen potential V_m is a simple linear function of the gas pressure (Joshi, 1946b) and as suggested by Joshi, it is extremely likely that the 'electron affinity' of the excited gas (Joshi, 1939, 1946b) besides its ionisation potential is a chief determinant thereof. In general it is found that the discharge current i (as also the velocity of any associated change) depends principally on V-V_m. The effect of light is to increase V_m (Joshi, 1939, Joshi and Narsimhar, 1940, 1945d). From this Joshi predicted and actually observed a current decrease $-\Delta i$, a consequence at variance with the current theories of photoelectric and discharge reactions.

With all the above modes of detection (*a* to *e*, Fig. 1) a positive Joshi-effect has been observed at low potentials, and the negative Joshi-effect at
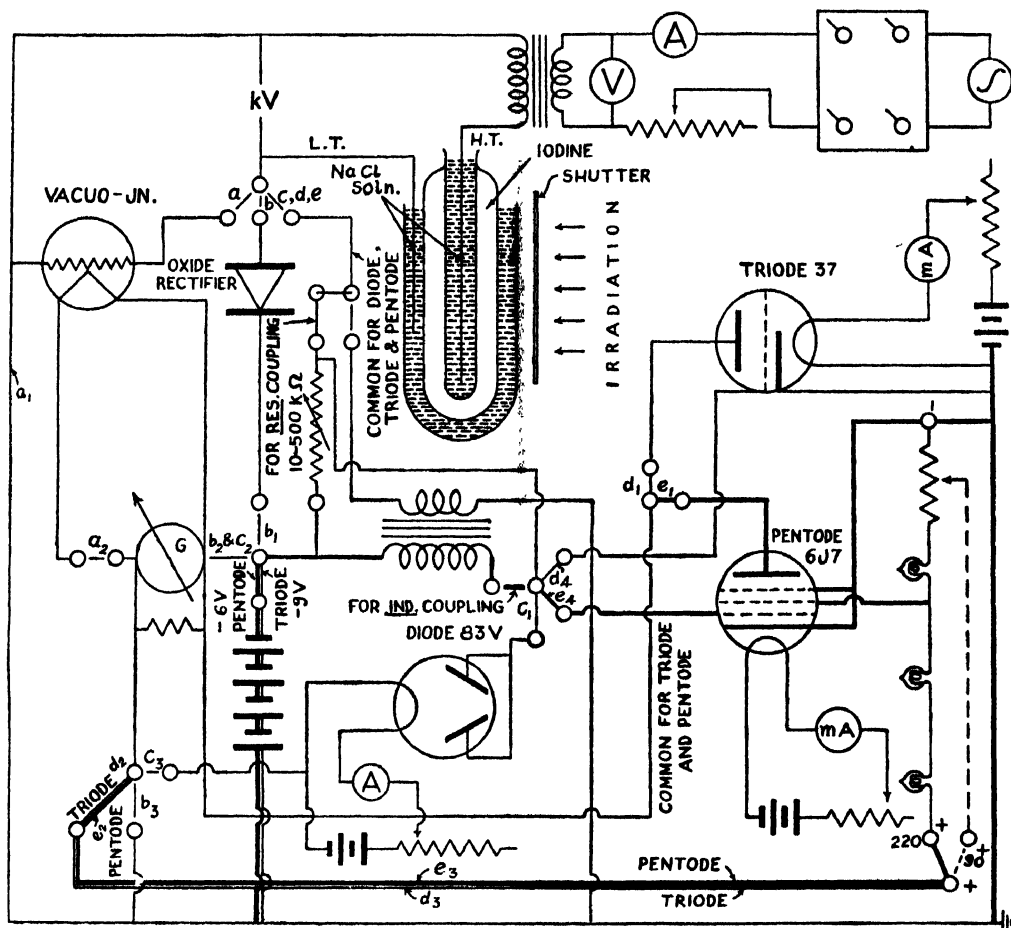
FIG. 1

higher potentials. The transition from the positive to the negative Joshi-effect was found to be repeatedly and reproducibly potential reversible (Joshi, 1943, 1947). A positive Joshi-effect $+\Delta i$ has been observed by Joshi (1943, 1945c, 1947) (*i*) in numerous cases under special coating materials on the annular walls *e.g.*, with KI_3 $+KI$ mixture, vapours of iodine, phosphorus and sulphur; (*ii*) spontaneously after a long 'ageing' at a constant *V* in a semi-ozoniser excitation; and (*iii*) in chlorine under H.F. discharge and also low frequency excitation under increased relative surface by introducing powdered wall material in the discharge space and had generalised that, *inter alia*, a low applied *V* favours $+\Delta i$ Joshi, 1947). The positive effect being shown by all the indicators used in this work suggests that it corresponds to a distinctive photo-reaction under discharge. It is found (unpublished results of Joshi) that V_m decreases under irradiation corresponding to the production of this positive effect as is to be expected from the general result

for the dependence of i on V-V_m. As the exciting potential is increased the positive effect diminishes rapidly. Above V_m over a fairly wide range, the negative Joshi-effect occurs. The limited range of conditions within which only positive effect is observed corresponds perhaps to the comparative rarity of the positive ion emission (Joshi, 1947). A positive Joshi-effect is, however, to be anticipated from the greater probability of the photo-ionisation of the pre-excited particles (Joshi, 1947) under the discharge.

The results in Table I, show that the nature of the detector used affects appreciably the magnitude of the corresponding negative and positive Joshi-effects. Thus, e.g., the -%Δi indicated by the vacuo-junction was 25 at 1.1 kV whereas the oxide rectifier showed a maximum of 33 %. This is significant since the input current was the same. From his oscillographic studies of the Δi phenomenon, Joshi (1943a, 1944, 1944c, 1945d) has shown that "the current i contains a large number of frequencies of varying strengths" (in addition to the supply frequency and its harmonics)—"the vacuo-junction has a low capacity and a negligible inductance, a stable characteristic over a wide range of applied V and frequency of A.C. supply (Joshi, 1945e)". The oxide rectifier on the other hand is a more selective and variable detector (Khastagir, 1934-35). The numerically greater -%Δi, as observed, may, therefore, be attributed to its preferential response to some of the frequencies constituting the discharge current.

Comparing all the detectors in respect of i_D, i_L, $-\Delta i$ and $-$%Δi, it is seen (Table I) that the results obtained with oxide-rectifier, vacuo-junction and diode as detectors are substantially similar. Thus whilst $-$%Δi, which is maximum near V_m but decreases (numerically) thereafter, $-\Delta i$ attains a maximum and then decreases (numerically), i_D and i_L increase progressively. Furthermore, the relative variation in $-\Delta i$ was markedly pronounced with the diode for the same increase in V, e.g., $-\Delta i$ and $-$%Δi were respectively (42, 38) at 0.83 kV; (35, 15) at 1.30 kV; and zero at 1.77 kV and at larger V. The results with triode and pentode form apparently a separate group, e.g., $-\Delta i$ and $-$%Δi attain a maximum near V_m and then decrease (numerically) with V. In the case of resistive coupling, however, the curve $i_D - V$ saturates at higher V and lies below $i_L - V$ curve.

It was significant to observe that the magnitude of both $-\Delta i$ and $-$%Δi with the inductive coupling of the detector diode was higher than when the input was tapped across a non-inductive and practically non-capacitative Dubilier resistance R (Fig. 2); thus, e.g., at $R = 10$ k Ω the maximum $-$%Δi is only 13 at 0.95 kV whereas the inductive coupling records a maximum of -38 at 0.82 kV. The influence of R in suppressing $-$%Δi was markedly uniform under all conditions of excitation. A like inhibition of the negative Joshi-effect was observed by resistive impedances in the case of triode and pentode, where it was further observed that a transition from a negative to an apparently second positive effect occurred as the (resistive) input exceeded

a certain critical value. Thus, *e.g.*, using triode as the current detector and at $R = 300$ kΩ., %Δi changed from -5 to $+18$ as the applied potential increased from 1.09 to 1.90 kV. It must be emphasized, however, that the grid current always showed a higher negative effect.
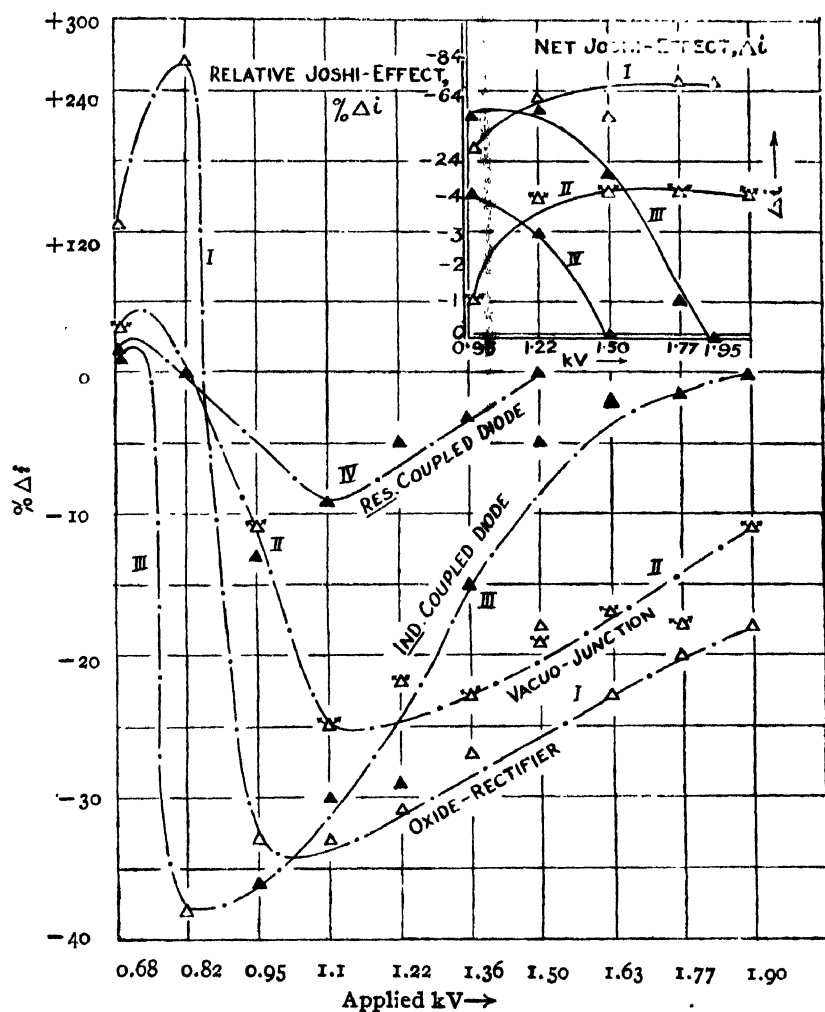

FIG. 2

That $-\%\Delta i$ should be least where the detector was coupled resistively follows from Joshi's theory (Joshi, 1945e). Evidence was adduced previously that the Joshi-effect is caused by a decrease of the amplitudes of H.F. components of i. That R acts likewise, that is, mainly damps the H.F. appeared from the oscillograms of i under various R's; this also follows from the general considerations of an oscillatory discharge of a condenser (such as an ozoniser) in a resistive circuit (Joshi, 1945e). The damping constant of an oscillatory circuit consisting of R, the inductance L and capacity C is given by $R/2L$; the skin-effect arises from the uneven radial distribution of

current in a conductor.   Thus it is obvious that in the inductive coupling the magnitude of $-\%\Delta i$ would be largest due to low (ohmic) resistance in the oscillatory circuit.   On the other hand with the valves coupled resistively and in the vacuo-junction and oxide rectifier an appreciable resistance is introduced;   this increases the damping and also the skin effect, as a consequence a reduction of H.F. oscillations occurs prior to irradiation and therefore, in the corresponding magnitude of $-\%\Delta i$.

Unlike the first, the second positive effect does not originate from a distinctive physical change under the discharge but is associated with the external detector circuit in grid controlled detectors.   It is instructive to consider the following factors in regard to the production of the second positive effect at large resistive inputs.   The anode current depends on the grid
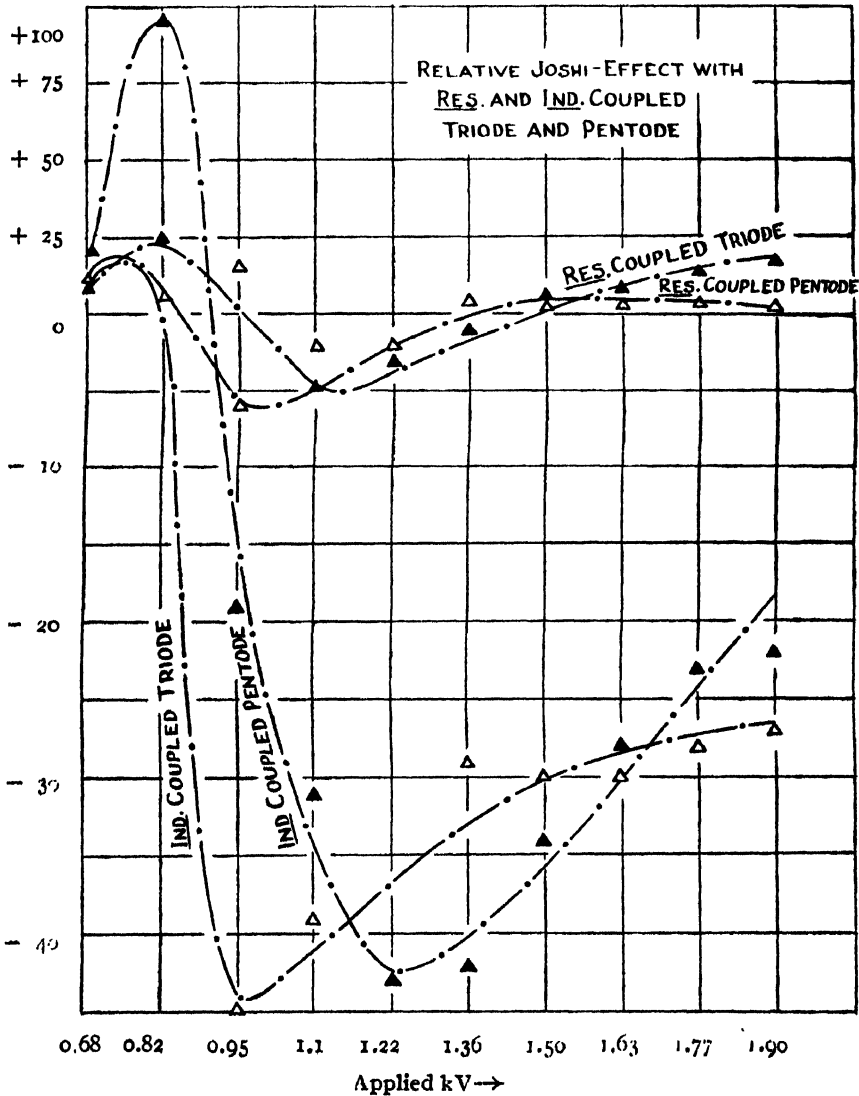
FIG. 3
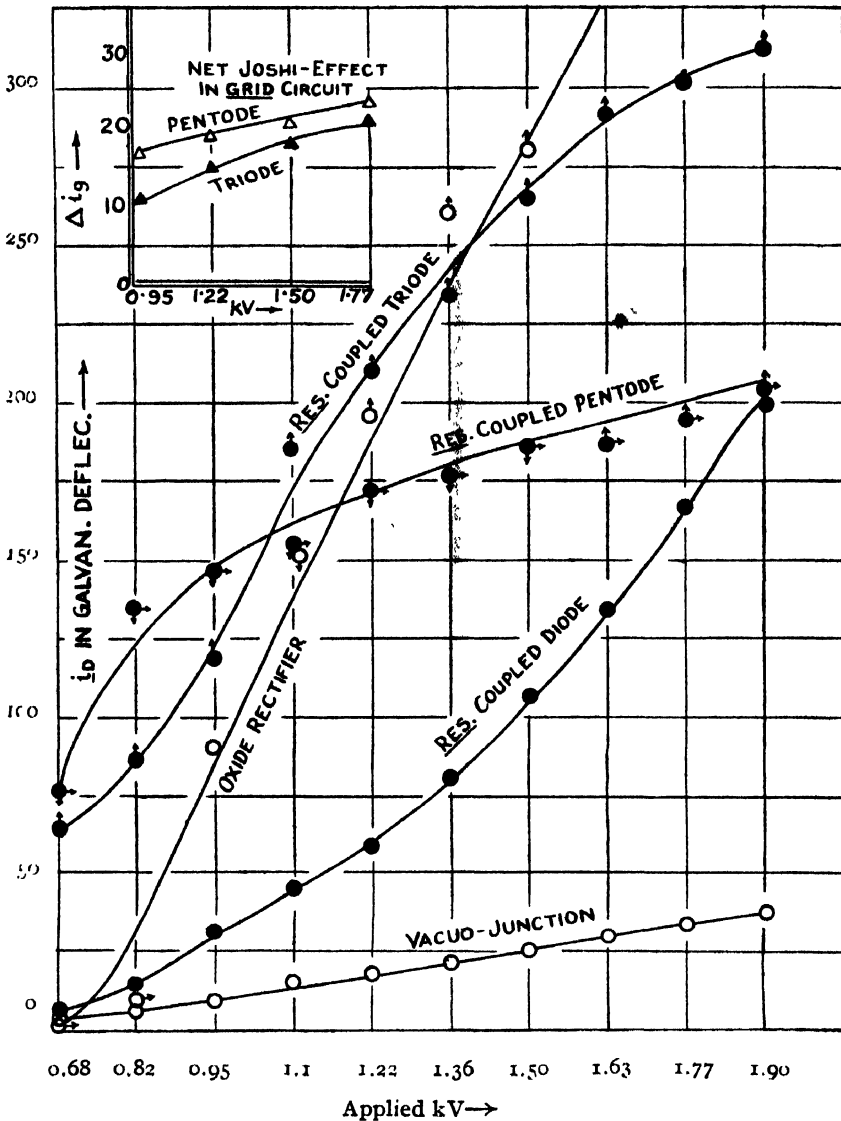
FIG. 4

Current i_D with different detectors

voltage at a constant plate potential; ordinarily in a valve biased for the anode bend rectification, the anode current varies correspondingly with grid voltage. This holds strictly only in the case of weak signals. When, however, a high impedance is present in the grid circuit and the signal strong (as in the inputs studied in this work) a flow of grid current causes an amplitude distortion during positive half of the cycle. If the above impedance (R_g) be purely resistive and i_g the grid current, the grid will be held negative by an additional amount $(R_g \times i_g)$. That this grid shift affects the anode current appreciably is brought out by the characteristic potential-current curves (Fig. 4) where i_D shows a markedly greater increase with low, than

TABLE I

Potential Variation of the Joshi-effect in Iodine (Discharge space packed with powdered iodine)

Applied $\sqrt{kV}$ (rms)	Detector used coupled with L.T.	Oxide rectifier	Vacuo-junction	Double diode 83V		Triode 37		Pentode 6J7	
				Inductively	Resistively	Inductively	Resistively	Inductively	Resistively
0.68	i_D	4	3	25	6	40	64	116	77
	i_L	9	4	29	7	48	70	126	100
	Δi	+ 5	+ 1	+ 4	+ 1	+ 8	+ 6	+ 10	+ 23
	$\% \Delta i$	+ 125	+ 33	+ 16	+ 17	+ 20	+ 9	+ 9	+ 30
0.82	i_D	8	6	110	14	55	87	128	134
	i_L	29	6	68	14	108	109	137	120
	Δi	+ 21	—	− 42	—	+ 53	+ 22	+ 9	− 14
	$\% \Delta i$	+ 263	—	− 38	—	+ 96	+ 25	+ 7	− 10
0.95	i_D	90	9	137	32	210	118	288	146
	i_L	60	8	88	28	170	137	158	137
	Δi	− 30	− 1	− 49	− 4	− 40	+ 19	− 130	− 9
	$\% \Delta i$	− 33	− 11	− 36	− 13	− 19	+ 16	− 45	− 6
1.1	i_D	153	16	162	45	310	185	305	155
	i_L	103	12	114	41	215	176	186	152
	Δi	− 50	− 4	− 48	− 4	− 95	− 9	− 119	− 3
	$\% \Delta i$	− 33	− 25	− 30	− 9	− 31	− 5	− 39	− 2
1.22	i_D	196	18	197	58	405	210	300	172
	i_L	135	14	140	55	230	204	220	169
	Δi	− 61	− 4	− 57	− 3	− 175	− 6	− 80	− 3
	$\% \Delta i$	− 31	− 22	− 29	− 5	− 43	− 3	− 27	− 2

TABLE I (contd.)

Potential Variation of the Joshi-effect in Iodine (Discharge space packed with powdered iodine)

Applied kV (rms)	Detector used coupled with L.T.	Oxide rectifier	Vacuo-junction	Double diode 83V		Triode 37		Pentode 6J7	
				Inductively	Resistively	Inductively	Resistively	Inductively	Resistively
1.36	i_D	253	22	240	80	420	226	323	177
	i_L	190	17	205	78	245	224	230	182
	Δi	− 69	− 5	− 35	− 2	−175	− 2	− 93	+ 5
	$\% \Delta i$	− 27	−23	− 15	− 3	− 42	− 1	− 29	+ 3
1.50	i_D	276	26	267	106	425	235	342	186
	i_L	226	21	253	106	281	250	241	191
	Δi	− 50	− 5	− 14	—	−144	+ 15	−101	+ 5
	$\% \Delta i$	− 18	−19	− 5	—	− 34	+ 6	− 30	+ 3
1.63	i_D	335	32	280	134	425	265	360	187
	i_L	257	25	275	134	308	287	251	192
	Δi	− 78	− 5	− 5	—	−117	+ 22	−109	+ 5
	$\% \Delta i$	− 23	−17	− 2	—	− 28	+ 8	− 30	+ 3
1.77	i_D	356	34	320	166	427	292	363	195
	i_L	286	28	319	166	327	332	263	201
	Δi	− 70	− 6	− 1	—	−100	+ 40	−100	+ 6
	$\% \Delta i$	− 20	−18	—	—	− 23	+ 14	− 28	+ 3
1.90	i_D	393	37	350	200	430	326	373	204
	i_L	323	33	350	200	337	386	273	207
	Δi	− 70	− 4	—	—	− 93	+ 60	−100	+ 3
	$\% \Delta i$	− 18	−11	—	—	− 22	+ 18	− 27	+ 1

at larger V; thus, *e.g.*, with resistively coupled pentode it increased from 77 to 177 as V increased from 0.68 to 1.36 kV whereas it increased only from 177 to 204 with further increase from 1.36 kV to 1.90 kV. The resistively coupled diode, however, increased from 6 to 80 and 80 to 200 over the same range. This differential behaviour of the anode current is due to its suppression by the extra negativity of the grid bias. From his oscillographic studies of the Δi phenomenon Joshi has shown that the input across a resistance consists of a low amplitude L.F. and large amplitude H.F. It follows from above that the grid current is mainly derived from H.F. parts of i. On irradiation, however, the H.F's. are chiefly suppressed and the grid current is reduced. This is equivalent to a grid shift towards positive by $(\Delta i_g \times R_g)$, where $-\Delta i_g$ is the net Joshi-effect in the gird circuit. The resultant anode current i_L will depend on the magnitudes of: (i) the diminution of the signal strength and (ii) the positive grid shift. The observations in the grid circuit (Fig. 4) show that the net Joshi-effect $-\Delta i_g$ increases (numerically) with V (Fig. 4). The other detectors, *viz.*, diode and vacuo-junction, however, show that the net Joshi-effect $-\Delta i$ which measures the total amplitude diminution, attains a maximum near V_m and decreases (numerically) thereafter (Fig. 2). Thus for a given R and large V the positive influence on the anode current of the grid shift exceeds the suppression of the anode current by the decrease under light of the signal strength ; a positive effect should therefore, result as observed. Joshi observed that the second positive effect disappears on increasing (numerically) the grid bias, and that higher the operating voltage, the greater is the increase necessary for the above purpose. This is in accord with the above considerations. That the second positive effect is associated with the H.F's. in the grid circuit was inferred by Joshi in a general result (unpublished) that the introduction of a by-pass grid capacity eliminates it.

REFERENCES

Cherian, 1945, *Proc. Indian Sci. Cong., Phys. Sec.*, III, Abst. 17.
Das Gupta, 1945-46, *Sci. and Cult.*, 11, 318.
Deo and Ghosh, 1946, *Sci. and Cult.*, 12, 17.
Joshi, 1929, *Trans. Faraday Soc.*, 25, 120.
  ,,   1939, *Curr. Sci.*, 8, 548.
  ,,   1943, *B.H.U. Journal*, 8, 99.
  ,,   1943a, Presi. Address, Chem. Sec., Indian Sci. Cong

Joshi, 1946a, *Proc. Indian Sci. Cong., Phys. Sec.,* III, Abst. 26.

,,　1946b, *Curr. Sci.,* **15**, 281.

,,　1947, *Curr. Sci.,* **16**, 19

,,　1944a, *Curr. Sci.,* **13**, 253.

,,　1944b, *ibid.,* **13**, 278.

,,　1944c, *Nature*, **154**, 147.

,,　1945a, *Curr. Sci.,* **14**, 67.

,,　1945b, *ibid.,* **14**, 317.

,,　1945c, *ibid.,* **14**, 175.

,,　1945d, *Proc. Ind. Acad. Sci.,* **A22**, 389.

,,　1945e, *ibid.,* **A22**, 225.

,,　and Deo, 1943, *Nature*, **151**, 561.

,,　and Deo, 1945f, *Curr. Sci.,* **14**, 35.

,,　and Deshmukh, 1941, *Nature*, **147**, 806.

,,　and Lad, 1945, *ibid.,* **A22**, 293.

,,　and Narsimhan, 1940, *ibid.,* **9**, 535.

Khastagir,1934-35, *Indian J. Phys.,* **22**, 355.

Prasad, 1946, *Indian J. Phys.,* **20**, 187.

Prassad and Tewari, 1945, *Curr. Sci.,* **14**, 229.